

KfK 3846  
Juli 1984

# ECOOL 1984

**Proceedings of the Workshop on Electron  
Cooling and Related Applications**

**Editor: H. Poth  
Institut für Kernphysik**

**Kernforschungszentrum Karlsruhe**



KERNFORSCHUNGSZENTRUM KARLSRUHE

Institut für Kernphysik

KfK 3846

PROCEEDINGS OF THE WORKSHOP ON ELECTRON COOLING AND  
RELATED APPLICATIONS

E C O O L 1 9 8 4

Karlsruhe, Federal Republic of Germany,

September 24-26, 1984

Editor: H. Poth



Kernforschungszentrum Karlsruhe GmbH, Karlsruhe

Als Manuskript vervielfältigt  
Für diesen Bericht behalten wir uns alle Rechte vor

Kernforschungszentrum Karlsruhe GmbH  
ISSN 0303-4003

## Preface

This workshop was meant to condense all present knowledge on electron cooling, experiments and theory, sound understanding and wild speculation. Personally, I am convinced that the electron cooling technique in storage rings will provide a plethora of application exceeding by far its primary use as a phase space compression technique. Indeed, it may pave the way of novel experimentation methods for particle, nuclear and atomic physics. At the moment where traditional nuclear and atomic physics research looks for new possibilities, the application of this technique in dedicated storage rings could have a considerable impetus on new developments. It was one of the main goals of this workshop to stimulate and support these new directions.

At a workshop many speculations and ideas may emerge, which later may turn out to be unrealistic. However, they could also trigger new developments so far not considered and hopefully the talks and discussions at this meeting had provided some premises for this.

Electron cooling was invented by G. Budker in Novosibirsk and many applications were anticipated already by him and his colleagues. Although the major amount of work in this field has been done in his laboratory, today the community working theoretically and experimentally on electron cooling has increased considerably.

As it will be apparent from these proceedings worldwide over a dozen of institutes have electron cooling projects. The Kernforschungszentrum Karlsruhe itself is committed to this field since the first ICE experiments and is at present developing jointly with CERN the electron cooler for LEAR.

There are still many interesting aspects to be studied which are within the possibilities of university institutes. It would be fortunate, if part of the research could develop along these lines.

We hope that this workshop has helped to promote the case of electron cooling and encouraged further developments in this new accelerator technique.

It is the appropriate place here to thank my colleagues from the international advisory committee for the firm engagement in preparing and carrying out this workshop. The help of the local organizing committee, the secretaries of the Institut für Kernphysik Mrs. U. Diehl and Mrs. V. Lallemand and the office of public relations of the Kernforschungszentrum Karlsruhe is warmly acknowledged. In particular, I would like to thank the Kernforschungszentrum Karlsruhe for its generous support of this meeting.

H. Poth

ECOOL 84

Workshop on Electron Cooling and Related Applications

September 24-26, 1984

International Advisory  
Committee:

F. Mills, Fermilab,  
Batavia, Ill.

D. Möhl, CERN, Genève

H. Poth, KfK, Karlsruhe

A.N. Skrinsky, INP,  
Novosibirsk

Local Organizing Committee:  
(Institut für Kernphysik)

A. Citron

C. Habfast

L. Hütten

H. Poth

A. Wolf

## CONTENTS

|  |     |
|--|-----|
| - Introduction to the theory of electron cooling   | 1   |
| A. Sørenson  |     |
| - Realistic calculations concerning electron cooling<br>in storage rings   | 21  |
| A. Wolf  |     |
| - Ultra relativistic electron cooling to improve the<br>luminosity and lifetime of pp colliders  | 41  |
| D. Cline   |     |
| - Review of electron cooling experiments   | 45  |
| H. Poth  |     |
| - Study of fast electron cooling   | 71  |
| V. Parkhomchuk   |     |
| - Electron cooling at very low velocities  | 85  |
| H. Herr  |     |
| - The LEAR electron cooler   | 93  |
| H. Häsleroth, C.E. Hill, J.-L. Vallet, C. Habfast, L. Hütten,<br>H. Poth, A. Wolf<br>presented by C.E. Hill  |     |
| - Some performance predictions for the IUCF Cooler   | 109 |
| R.E. Pollock   |     |
| - European Cooler Storage Rings  | 123 |
| S. Martin  |     |
| - Electron cooling project at INS  | 127 |
| T. Tanabe, M. Sekiguchi, K. Sato, A. Noda, M. Kodaira,<br>M. Takanaka, J. Tanaka, M. Tsujikawa, T. Honma, T. Katayama,<br>A. Mizobuchi and Y. Hirao<br>presented by T. Tanabe              |     |
| - The Heidelberg Heavy Ion Test Storage Ring (TSR)   | 137 |
| D. Fick, D. Habs, E. Jaeschke, D. Krämer, V. Metag, R. Neumann,<br>B. Povh, R. Repnow, U. Schmidt-Rohr, R. Schuch, D. Schwalm,<br>E. Steffens and C.A. Wiedner<br>presented by E. Jaeschke |     |
| - Intermediate energy electron cooling   | 143 |
| F. Mills (copy of transparencies; manuscript not received)   |     |

|  |     |
|--|-----|
| - High Energy electron cooling at related diagnostics  | 155 |
| M. Biagini, U. Bizzarri, R. Calabrese, M. Conte, S. Guiducci,<br>F. Petrucci, L. Picardi, C. Ronsivalle, C. Salvetti, M. Savri ,<br>S. Scrimaglio, S. Tazzari, L. Tecchio and A. Vignati |     |
| presented by L. Tecchio  |     |
| - Relativistic electron cooling and intrabeam scattering   | 173 |
| A.G. Ruggiero  |     |
| - Construction of a 3 MeV Amp re-Intensity recirculating<br>electron beam system: A Progress Report  | 185 |
| M. Sundquist and J. Adney  |     |
| presented by M. Sundquist  |     |
| - High efficiency recovery of an Amp re-Intensity 3 MeV<br>electron beam   | 197 |
| D. Larson, F. Mills, F. Cole   |     |
| presented by D. Larson   |     |
| - Diagnostics for electron and ion beam in electron cooling  | 219 |
| P. M ller-Petersen   |     |
| - Computational calculation of electron trajectories   | 233 |
| M. Sedlacek  |     |
| - Proposal for hollow cathode electron gun for electron<br>cooling   | 245 |
| F. Krienen and W. Herrmannsfeldt   |     |
| presented by F. Krienen  |     |
| - Energy recovering of the electron beam in electron<br>cooling devices  | 253 |
| I.N. Meshkov, A.N. Sharapa and A.V. Shemjakin  |     |
| presented by D. Pestrikov  |     |
| - An ultra-high vacuum system for coolers  | 267 |
| M. Brouet, M. Giradini, A. Poncet, A. Wolf, L. H tten,<br>H. Poth and C. Habfast   |     |
| presented by A. Poncet   |     |
| - Equilibrium properties of stored and cooled beams with<br>internal targets   |     |
| H.O. Meyer (written contribution not submitted, no copies<br>of transparencies available)  |     |
| - Ordering effects in Coulomb relaxation of a cold beam  | 275 |
| N.S. Dikansky and D. Pestrikov   |     |
| presented by D. Pestrikov  |     |

|   |     |
|---|-----|
| - A comparison between electron cooling and stochastic cooling                      | 293 |
| D. Möhl   |     |
| - Cooling of heavy ion beams  | 303 |
| B. Franzke  |     |
| - Storing and electron cooling of polarized ions                                    | 313 |
| E. Steffens   |     |
| - Lattice design for cooler rings   | 325 |
| D. Johnson (copies of transparencies)   |     |
| - Lattice design of TARN II cooler ring mode  | 343 |
| A. Noda, N. Takahashi, T. Tanabe, T. Katayama, Y. Hirao,<br>and M. Takanaka         |     |
| presented by A. Noda  |     |
| - New possibilities with electron cooling in atomic<br>nuclear and particle physics | 361 |
| K. Kilian (copies of transparencies)  |     |
| - Electron capture  | 379 |
| M. Bell   |     |
| - Laser induced electron capture and related physics                                | 387 |
| R. Neumann  |     |
| - Dielectronic recombination measurements in a single<br>pass experiment            | 401 |
| S. Datz, P.F. Dittner, P.D. Miller and P.L. Pepmiller<br>presented by S. Datz       |     |
| - An Ion beam lamp for monochromatic X-rays   | 413 |
| H. Pilkuhn and H. Poth<br>presented by H. Pilkuhn                                   |     |
| - Thomas peak measurement in beam recirculation ring                                | 415 |
| I. Ktayama  |     |
| Papers submitted and not orally presented:  |     |
| - Electron cooling antiprotons to thermal energies in a<br>penning trap             | 419 |
| W. Kells, G. Gabrielse and K. Helmerson   |     |
| - CRYRING, a small storage and acceleration ring for heavy<br>ions                  | 429 |
| C.J. Herrlander and A. Bárány   |     |
| - List of participants  | 439 |

## INTRODUCTION TO THE THEORY OF ELECTRON COOLING

Allan H. Sørensen  
CERN, Geneva, Switzerland

### PRELUDE

Electron cooling is one of the phase space compression methods which may be applied to a charged particle beam in order to improve its emittances and momentum spread. Besides providing the possibility of obtaining higher beam quality as such, beam cooling is essential for accumulation purposes and for the counterbalancing of various heating processes, e.g., rest-gas multiple scattering. By performing a transformation to the so-called particle frame (PF) which moves along the ring with the average particle velocity the reductions in question are seen to correspond to reductions in rms velocities and, thereby, to a lowering of what might be called the beam temperature; hence the term beam "cooling".

Various cooling techniques have been proposed, for excellent reviews see ref.s 1-2. Due to Liouville's theorem, a suitable dissipative force is in general needed to obtain a compression of the volume occupied by the beam in phase space. In electron-positron storage rings this force is provided as the beam particles undergo emission of synchrotron radiation in their passage of, e.g., bending magnetic fields. For heavier particles the radiation mode is clearly suppressed, and other methods have been invented. Among these stochastic cooling has demonstrated its powerfulness in the CERN antiproton accumulation project. However, as opposed to radiation and other cooling techniques, the stochastic is not based on the presence of a dissipative force but rather on the simple observation that if each individual beam particle could be tracked and guided separately in its motion throughout the ring by a suitable sensitive and fast electronical pick-up and correction system then a zero-emittance beam could be created simply by bringing each single particle onto the ideal particle path.

In electron cooling a dissipative force is introduced via Coulomb interactions between the circulating particle beam and a co-streaming cold

dense beam of electrons. In the traditional design, fig.1, the electrons are kept cold as they are renewed continuously, the electron gas acts as a cold reservoir, and the ions are cooled down to the level of the low electron temperature. At ultrarelativistic beam energies other set-up's are necessary<sup>3</sup>. In fig.1 we have indicated the presence of a longitudinal magnetic field, which is applied throughout the electron path in order to guide and confine the electron stream. The presence of this field appears to be of major importance to the basic cooling process as we shall see below.

Among other beam cooling methods, we may mention the so-called laser cooling technique<sup>4</sup> which has been proposed for atomic beams but which has not yet been tested experimentally.

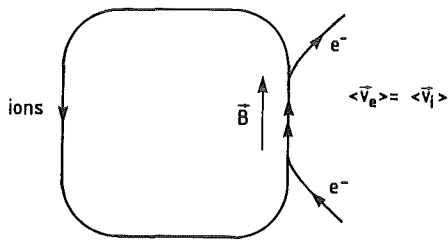


Fig. 1. Typical low and medium energy electron cooling set-up. Relevant initial PF velocities and temperatures are indicated.

$$\text{PF: } \langle v_e^2 \rangle \leq \langle v_i^2 \rangle$$

$$\therefore T_e \leq (m/M) T_i \ll T_i$$

In the pages to follow we shall discuss the theory of the basic electron cooling process. In order to have a clear picture in mind we shall assume a very idealized situation and neglect, e.g.,

- ion beam beta- and synchrotron oscillations
- ion beam instabilities
- electron beam space charge phenomena

and ion beam blow-up and intensity-loss mechanisms such as

- intrabeam scattering
- rest gas multiple and single scattering
- recombination or similar effects changing the charge state of the ions

All these topics will be treated in other contributions to the workshop<sup>5</sup>. In our discussion we shall stick to the particle frame, where we assume the electron gas to be spatially homogeneous, and we shall not consider effects of finite dimensions of the cooling region.

A cooling process is characterized by two parameters, namely the final ion-beam temperature and the cooling time, which constitutes a measure of the time it takes to reach the equilibrium. In the present discussion we shall mainly consider the latter parameter since the final ion beam temperature in general is determined by a balance between cooling and the various heating processes, which are neglected here, and not by the equilibrium with the cold electron reservoir. On the other hand, the latter situation of course gives a lower limit for the obtainable temperature. The cooling time is fixed by the cooling (drag or friction) force, and a determination of this quantity is therefore the aim of the present report.

The main points to be emphasized are:

- 1) The combined effect of the "flattened" electron velocity distribution, fig.2, which is set up due to the acceleration of the electrons in the electron gun<sup>6</sup>, and the longitudinal magnetic field, fig.1. The latter tends to some extend to freeze the transverse degrees of freedom of the electrons and this fact together with the extremely low longitudinal electron temperature leads to the introduction of an essentially zero-temperature electron gas. Consequently, the effectiveness of the electron cooling is enhanced and a situation, generally known as supercooling<sup>6</sup>, is approached.
- 2) The complementarity of a conventional binary encounter model and a continuum (dielectric) description for the ion-electron gas interaction. Whereas the former, which is simple to evaluate, fails in the supercooling regime the latter becomes excessively accurate here, but is on the other hand in general lengthy to evaluate. It will be shown how the two models may be combined into a single easy evaluable expression for the drag force.

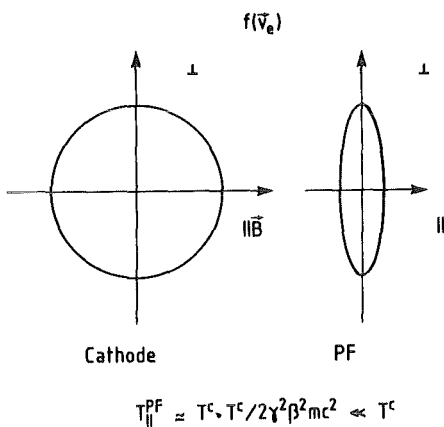


Fig. 2. The flattened electron velocity distribution. The reduction of the longitudinal ms velocities following acceleration to a mean drift velocity  $v_0$  is expressed in terms of the reduction of the longitudinal temperature from the cathode value. The usual definitions  $\beta=v_0/c$  and  $\gamma^2 = 1-\beta^{-2}$  apply.

The discussion below will closely follow that given in ref.7, and this publication should therefore be consulted for further details.

### BINARY ENCOUNTER MODEL

In the usually applied binary encounter model the ion-electron gas interaction is treated as a series of independent two-body collisions. Correspondingly, the drag force  $\vec{F}$  is obtained by summing up the momentum transfers to the individual electrons.

B=0

It is instructive first to consider the case of vanishing magnetic field strength. In the rest frame of an ion of PF-velocity  $\vec{v}_i$  an electron of PF-velocity  $\vec{v}_e$ , corresponding to a relative electron-ion velocity  $\vec{w} = \vec{v}_e - \vec{v}_i$ , is scattered by the heavy projectile through an angle  $\theta$  and thereby acquires a velocity  $\vec{w}'$ , where  $w' = w$ . Within a time  $dt$ , the average momentum transfer to the ion is

$$-d\vec{p} = (dn w dt) \sigma(\theta, w) d\Omega (\vec{w}' - \vec{w})m \quad (1)$$

where  $\sigma(\theta, w)$  denotes the differential scattering cross section,  $d\Omega$  the solid angle into which the electrons of mass  $m$  are scattered, and  $dn = nf(\vec{v}_e)d^3\vec{v}_e$  the number of electrons per unit volume with velocity within  $d^3\vec{v}_e$  around  $\vec{v}_e$ ,  $n$  being the homogeneous spatial electron density and  $f(\vec{v}_e)$  the velocity distribution. The drag force is obtained by integrating eq.(1) over scattering angle and relative velocity, i.e.,

$$\vec{F} = mnJ d^3\vec{v}_e f(\vec{v}_e) w \sigma_{tr}(w) \vec{w}, \quad (2)$$

where the quantity  $\sigma_{tr}$  is defined by the relation

$$\sigma_{tr} = \int_0^\pi (1-\cos\theta) \sigma(\theta, w) 2\pi \sin\theta d\theta \quad (3)$$

and known as the transport cross section.

To compute  $\sigma_{tr}$  an explicit expression for the differential cross section  $\sigma$  is needed. For a pure Coulomb field, the usual Rutherford formula applies which contains the scaling  $\propto \sin^{-4}\theta/2$ . As is well-known, this behaviour leads to a logarithmic divergence at small angles in eq.(3). To avoid that problem the lower limit of  $\theta$ -integration is substituted by a suitable but non-zero  $\theta_{min}$ . The physical justification for such a procedure is to be found in the fact that the scattering problem in question is not a pure two-body one but rather, the remaining "field" or "back-ground" electrons tend to screen off the ion-(test)electron interaction potential at large distances. By simply cutting the interaction off beyond a suitable

distance  $\lambda$ , known as the screening length, a minimal scattering angle is obtained through the relation  $\tan\theta/2=d/2\rho$ , connecting the scattering angle to the impact parameter  $\rho$ , as

$$\theta_{\min} \sim d/\lambda , \quad d = 2|Z|e^2/mw^2 \quad (4)$$

where  $Ze$  is the projectile charge. With this approximation we may write the cooling force as

$$\vec{F} = Z^2 \frac{4\pi ne^4}{m} \int d^3v_e L f(\vec{v}_e) \frac{\vec{w}}{w^3} , \quad L = \log(2\lambda/d) \quad (5)$$

where  $L$  is known as the "Coulomb logarithm".

At this stage mention should be made of the so-called Coulomb analogy, which is often quoted in the literature on electron cooling<sup>2</sup>. In eq.(5), the variation with velocity of the parameter  $L$ , being of logarithmic nature, is slow. To lowest order the Coulomb logarithm may therefore be taken outside the integral. With the replacements  $(\vec{v}_i, \vec{v}_e, f(\vec{v}_e)) \rightarrow (R, r, \rho(r))$ , the equation (5) for the force is then seen to be completely identical in shape to the formula determining the electrostatic field at position  $\vec{R}$  from a charge distribution  $\rho(\vec{r})$ . This analogy, which implies that the use of, e.g., Gauss' theorem is valid to a good approximation, makes the determination of cooling forces and corresponding slowing down times fairly easy in many cases. As an example, for an isotropic Maxwellian distribution  $f(\vec{v}_e)$  the force is velocity proportional for low values of  $v_i$ . For high values of  $v_i$  the distribution function in eq.(5) may of course be replaced by a  $\delta$ -function and for  $\vec{F}$  we therefore obtain the result

$$F = -Z^2 \frac{4\pi ne^4}{m} L \begin{cases} v_i^{-2} & , v_i > v \\ \frac{4}{3\sqrt{\pi}} \frac{v_i}{v^3} & , v_i < v \end{cases} \quad (6)$$

where  $v$  denotes the two-dimensional rms electron velocity.

With the expression for the force available, eq.(5), we may determine a cooling time according to the relation  $\tau^{-1} = -v_i^{-1} dv_i/dt = -F/Mv_i$ . Let us at this one occasion quote the result as it will be encountered in the laboratory. Taking into account time-dilation and Lorentz contraction in the transformation from PF to the laboratory system we get for a Maxwellian distribution  $f(\vec{v}_e)$  with eq.(6) the result

$$\tau_L = Z^{-2} \frac{\gamma^2}{\eta} \frac{mM}{e^4} \frac{1}{\ln L} \cdot \begin{cases} \frac{1}{4\pi} v_i^3 & , v_i > v \\ \frac{3}{4\sqrt{2\pi}} \left(\frac{T}{m}\right)^{3/2} & , v_i < v \end{cases} \quad (7)$$

where  $n_L$  denotes the electron spatial density as measured in the laboratory,  $\eta$  the fraction of the ion storage ring occupied by the cooling electron beam and  $T$  the electron beam temperature which is connected to the two-dimensional rms electron velocity through the relation  $T=1/2mv^2$ . Note the scaling with the Lorentz- $\gamma$  which as usual is defined as  $\gamma^2=(1-v_0^2/c^2)^{-1}$  for a beam of drift velocity  $v_0$ . This scaling makes the electron cooling in the traditional design very unfavourable at ultrarelativistic energies. In the literature  $\tau_L$  is often expressed in terms of angular divergences rather than in terms of the PF-velocities  $v_i, v$ . In this case a scaling with  $\gamma^5$  is encountered.

When the flattened electron velocity distribution, fig.2, is introduced some changes appear for  $v_i < v$  in eq.s (6-7). For low ion velocities transverse to  $z$ , the beam axis,  $F$  is increased by a factor of  $3\pi/4 \approx 2.4$  with respect to the Maxwellian case whereas for longitudinal velocities the force tends to a constant as  $v_i$  approaches zero. The latter behaviour appears to be unphysical since also  $F_z$  decreases  $\propto v_i$  at (now very) low velocities when the assumption of a constant Coulomb logarithm is abandoned. The overall behaviour of the cooling force for vanishing magnetic field strength is illustrated in fig.3 for proton cooling in an electron gas with a completely collapsed Maxwellian velocity distribution.

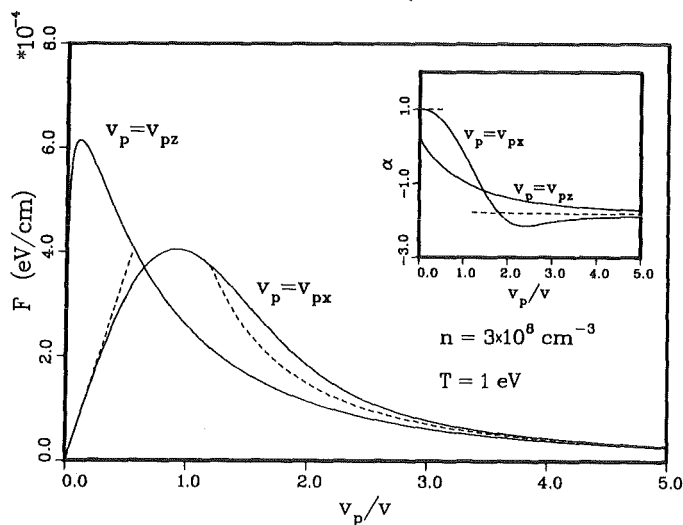


Fig. 3. Drag force on proton in flattened electron gas as a function of projectile velocity. Dashed curves give asymptotic behaviour. The insert shows the local power as determined by the relation  $F \propto v_p^\alpha$ .

In applying the above binary encounter scheme one is faced with some problems. First, a suitable measure for the screening length  $\lambda$  needs to be introduced in eq.(5). Clearly, screening is due to collective electron-electron interactions and  $\lambda$  cannot be estimated within a binary approach. Instead the Boltzmann equation governing the evolution in phase space of the electron gas, considered as a continuous fluid, should be applied. At low velocities,  $v_i < v$ , an interaction potential somewhat similar to the exponentially screened Debye-Hückel potential, as it is encountered for an isotropic Maxwellian electron velocity distribution, is expected, i.e., for the screening length we have

$$\lambda \approx \lambda_D \equiv v/\sqrt{2}\omega_p , \quad v_i < v , \quad (8a)$$

where as usual  $\omega_p$  denotes the plasma frequency of the electron gas,  $\omega_p^2 = 4\pi n e^2/m$ . At high velocities,  $v_i > v$ , the Debye-length  $\lambda_D$  does no longer constitute a measure of the screening length since the projectile in this case travels a distance long compared with  $\lambda_D$  during the time  $\sim \omega_p^{-1}$  it takes to set up the polarization fields in the electron fluid. To determine  $\lambda$ , arguments are needed, which appear to be fairly suspect within the binary treatment: In distant collisions collective (electron density) oscillations are excited at frequency  $\omega_p$ . Hence no energy transfers take place in case the collision time, which is roughly  $\rho/v_i$ , is higher than  $\omega_p^{-1}$ , i.e., a dynamical screening is introduced at

$$\lambda \approx \lambda_a \equiv v_i/\omega_p , \quad v_i > v , \quad (8b)$$

where  $\lambda_a$  is known as the adiabatic screening distance. The two formulae (8) fit smoothly each other for  $v_i \sim v$ .

Besides the question of screening a second problem is faced with the binary encounter model, namely, if one can be sure that collective plasma oscillations do not contribute significantly to  $\vec{F}$ . Indeed, the arguments given above to derive eq.(8b) were completely dependent on the occurrence of the excitation of such oscillations. The answer to this serious problem will be postponed until we take up the discussion of the dielectric treatment.

### B>0

Let us now turn to the question of the influence of the magnetic field  $\vec{B}$ , cf. fig.1. According to the above discussion, the longest collision times are of order  $\sim \omega_p^{-1}$ . Hence for the magnetic field to influence the cooling process it will in general be required that the

cyclotron frequency of the electrons,  $\omega_c = eB/mc$ , be in excess of the plasma frequency,  $\omega_c > \omega_p$ . However, a full binary treatment is not simple for finite field strengths due to the spiralling motion of the electrons. Instead the recipiy has been to attempt to construct  $\vec{F}$  as a suitable combination of the expressions obtained in the two opposite extremes of vanishing and infinite magnetic field strength.

In the limit  $B \rightarrow \infty$  all times and lengths are long compared with  $\omega_c^{-1}$  and the Larmor radius of the electrons,  $r_L = v/\omega_c$ , respectively. (The heavy ion, on the other hand, will be assumed unaffected by the magnetic field due to the large ion-electron mass ratio.) In this situation the electron is pinned to a fixed position in transverse directions and therefore only the component of the momentum transfer parallel to  $\vec{B}$  is associated with an energy transfer. Further on, with the flattened electron velocity distribution, fig.2, the electron is initially at rest in the longitudinal direction. The combined effect is then that the electron gas appears to be completely cold,  $T=0$ . Consequently, the drag force should show a velocity-dependence similar to the high velocity part of eq.(6), i.e.,

$$F^{B \rightarrow \infty} \propto -L \hat{v}_i v_i^{-2}. \quad (9)$$

Clearly, for low projectile velocities the cooling force is then enhanced by a very large factor  $\sim (v/v_i)^3$ .

An explicit formula for  $\vec{F}$  may be obtained by application of a simple perturbation scheme, the so-called impulse approximation<sup>7</sup>, where the heavy projectile during a collision is assumed to travel along the unperturbed trajectory and where the energy transfer to an electron (at rest) is computed as  $\Delta E = \Delta p^2/2m$  with the momentum transfer  $\Delta p$  determined as the integral over time of the Coulomb force between the two objects. Since the average of  $\Delta p$  over all collisions is zero by symmetry the impulse approximation can only give an answer to the energy-loss rate which is the projection of  $\vec{F}$  along the projectile velocity,  $dE/dt = \vec{F} \cdot \vec{v}_i / m v_i$ , and we may therefore only derive the expression for the force for the symmetric cases, namely,

$$F^{B \rightarrow \infty} = -Z^2 \frac{2\pi n e^4}{mv_i^2} \left\{ \begin{array}{l} L, \quad \vec{v}_i \perp \vec{B} \\ 0, \quad \vec{v}_i \parallel \vec{B} \end{array} \right\}, \quad L \approx \log(2\lambda/d). \quad (10)$$

To find the full expression for  $\vec{F}$  requires much more intensive work<sup>6,8</sup>.

In order to determine how the results for the cooling force obtained in the two opposite extremes  $B=0$  and  $B \rightarrow \infty$  should be combined to give a

reasonable estimate for  $\vec{F}$  for the case of finite magnetic field strengths, consider the collision time. If a given ion-electron collision lasts only for a short time as compared with the cyclotron period of electron motion  $\omega_c^{-1}$ , the collision will be essentially unaffected by the magnetic field and the force obtained for  $B=0$  may be applied. On the other hand, for collisions which last over many Larmor periods the result obtained for  $B \rightarrow \infty$  is expected to hold. Consequently, with the collision time given as  $\sim \rho/w$  the region of impact parameters  $\rho$  is split into two with a dividing distance of

$$\rho_{\text{div}} \sim w/\omega_c \sim v/\omega_c \equiv r_L , \quad (11)$$

where we have used the substitution  $w \sim \max\{v, v_i\} = v$  for  $v_i < v$ . With eq.s (6) and (9) we may therefore quote the approximate result

$$F \propto \log \left( \frac{r_L}{d} \right) \left\{ \begin{array}{ll} x & , \quad x < 1 \\ x^{-2} & , \quad x > 1 \end{array} \right\} + \log \left( \frac{\lambda}{r_L} \right) x^{-2} \quad (12)$$

For  $x \equiv v_i/v < 1$  the supercooling regime is reached where the drag force is enhanced considerably over the force for the case of vanishing magnetic field strength.

Having obtained the cooling force in the above - fairly simple way it remains once again to discuss the problems encountered within the binary encounter model. As to the screening length, the best guess will be to apply the adiabatic screening length  $\lambda_a = v_i/\omega_p$  at all projectile velocities since the distant-collision contribution has been taken to correspond to the limit  $B \rightarrow \infty$  where the only relevant electron velocity,  $v_{ez}$ , vanishes with the flattened distribution. Another more severe problem has to do with the relative magnitude of the two logarithms appearing in eq.(12). Typically, the fast collision logarithm is of order 10 whereas the slow collision logarithm may be as small as 1-2. Due to the abrupt cutting procedure applied at  $r_L$ , as well as at the screening length  $\lambda$ , the result for each part of the force can only be assumed reliable to within accuracies  $\sim 1/L$ . However, this immediately implies that the slow collision contribution, and in the supercooling regime thereby the total force, is extremely poorly determined. Besides, the question whether collective plasma oscillations may give significant contributions to the drag still remains open.

### DIELECTRIC DESCRIPTION

Since the number of electrons in a sphere with radius equal to the screening length is very large,

$$n\lambda^3 \gg 1 , \quad (13)$$

typical values being  $10^3$ - $10^5$ , a binary collision model does not appear to be the natural means by which to treat distant encounters. Instead, a continuum description of the electron gas should be applied<sup>9</sup>. Clearly, such a model contains all collective phenomena, e.g., plasma oscillations and screening. Further on, in a proper treatment the drag force for finite magnetic field strengths may be determined without any dubious splitting of the impact parameter region.

In the continuum - or dielectric description the drag force on a penetrating ion is due to the dielectric response as it polarizes the electron fluid since, by the neglect of space charge, no force is acting on the projectile from the undisturbed gas, i.e.,

$$\vec{F}(\vec{r}_i(t)) = Ze\vec{E}_{ind}(\vec{r}_i(t)) = Ze[\vec{E}_{tot} - \vec{E}_o]_{\vec{r}} = \vec{r}_i(t) \quad (14)$$

Here,  $\vec{E}_{tot}$ ,  $\vec{E}_{ind}$ , and  $\vec{E}_o$  denote the total, the induced, and the source field, respectively. The equation is conveniently expressed in terms of Fourier transforms of the potentials as

$$\vec{F} = -Ze \left\{ \frac{\partial}{\partial \vec{r}} \frac{1}{(2\pi)^4} \int d^3k d\omega e^{i(\vec{k}\vec{r} + \omega t)} [V_{tot}(\vec{k}, \omega) - V_o(\vec{k}, \omega)] \right\}_{\vec{r}=\vec{r}_i(t)}. \quad (15)$$

Introducing a dielectric function  $\epsilon$  through the relation

$$V_{tot}(\vec{k}, \omega) = V_o(\vec{k}, \omega)/\epsilon(\vec{k}, \omega) \quad (16)$$

and expressing the potential  $V_o$  in terms of the charge density  $q_o$  of the source via the Poisson equation we get with  $\vec{r}_i = \vec{v}_i t$  the result

$$\vec{F} = -\frac{Zei}{(2\pi)^4} \int d^3k d\omega e^{i(\vec{k}\vec{v}_i + \omega)t} \frac{4\pi q_o(\vec{k}, \omega)}{k^2} \left[ \frac{1}{\epsilon(\vec{k}, \omega)} - 1 \right]. \quad (17)$$

Finally, since  $q_o(\vec{r}_i(t)) = Ze\delta(\vec{r} - \vec{v}_i t)$  implies that  $q_o(\vec{k}, \omega) = 2\pi Ze\delta(\vec{k}\vec{v}_i + \omega)$ , eq.(17) may be rewritten as

$$\vec{F} = -Z^2 \frac{e^2 i}{2\pi^2} \int d^3 k \frac{\vec{k}}{k^2} \left[ \frac{1}{\epsilon(\vec{k}, -\vec{k}v_i)} - 1 \right] = \frac{Z^2 e^2}{2\pi^2} \int d^3 k \frac{\vec{k}}{k^2} \text{Im} \frac{1}{\epsilon(\vec{k}, -\vec{k}v_i)}, \quad (18)$$

where the last step follows since the force is a real quantity. In eq.(18), the complete information on the response of the plasma to any disturbance, including screening properties, is contained in  $\epsilon$ .

To compute the dielectric function we consider the collisionless Boltzmann equation governing the time evolution of the electronical phase space distribution  $\rho(\vec{k}, \vec{v}_e, t)$ . Letting  $\rho_0$  denote the distribution for the undisturbed gas and  $\rho_1 = \rho - \rho_0$  the corresponding change introduced by the external electric field of the penetrating charged particle, we may write the Boltzmann equation as

$$\frac{d\rho_1}{dt} \underset{\substack{\text{perturbed} \\ \text{orbits}}}{=} -\frac{e}{m} \frac{\partial V^{\text{tot}}}{\partial \vec{r}} \frac{\partial \rho_0}{\partial \vec{v}_e} \quad (19)$$

where  $\rho_0$  is assumed homogeneous in configuration space. In the limit of weak perturbation it is sufficient to integrate eq.(19) along unperturbed trajectories, a procedure which corresponds to the usual linearization of the Boltzmann equation. By Fourier transforming and by relating the induced charge density  $\rho_1(\vec{k}, \omega) = \int d^3 \vec{v}_e \rho_1(\vec{k}, \vec{v}_e, \omega)$  to the induced potential  $V(1-\epsilon)$ , an expression for the dielectric function may be obtained.

B=0

In the case of vanishing magnetic field strength the unperturbed trajectories are straight lines and the expression for the dielectric function is simple to obtain as

$$\epsilon(\vec{k}, \omega) = 1 - \lim_{\tau \rightarrow \infty} \frac{\omega_p^2}{k^2} \int d^3 \vec{v}_e \frac{i k \partial f_0 / \partial u}{i(ku + \omega) + 1/\tau}, \quad u = \vec{v}_e \cdot \vec{k} / k, \quad (20)$$

where  $f_0 = \rho_0/n$  and where the quantity  $1/\tau$  appearing in the denominator derives from a collisional damping term introduced into the Boltzmann equation,  $(\partial \rho / \partial t)_{\text{coll}} = -\rho_1 / \tau$ . An infinitesimal damping is necessary to ensure the proper interpretation of integrals like the one in eq.(20), which otherwise would contain poles on the path of integration. Note that the perturbation approach used in solving the Boltzmann equation breaks down at  $k_{\max} \sim \max\{v^2, v_i^2\} m/e^2 \sim 1/d$  where the induced density equals the unperturbed one.

As an example, let us determine the drag force for high projectile velocities or, equivalently, in the case of an electron gas at rest. Being

one of the simplest cases in which to compute  $F$  we shall go through it in some detail in order to demonstrate explicitly the steps involved in evaluations of the drag force according to eq.(18). Inserting  $f_0 = \delta(\vec{v}_e)$  into eq.(20), we obtain for the dielectric function

$$\epsilon(\vec{k}, \omega) = 1 - \lim_{\tau \rightarrow \infty} \frac{\omega_p^2}{(\omega - i/\tau)^2}. \quad (21)$$

With  $\omega = -\vec{k}\vec{v}_i = -kv_i \cos\theta$ , this equation reduces to  $\epsilon = 1 - (k\lambda_a \cos\theta)^{-2}$ , and this shows that the field around a projectile of high velocity  $v_i > v$  is screened out at distances of the order of the adiabatic cut-off length  $\lambda_a$ . This result was already applied in our discussion of the binary-collision model, eq.(8b). For symmetry reasons the drag force is directed along  $\vec{v}_i$ ,  $\vec{F} = F\hat{v}_i$ , and eq.(18) reads

$$\begin{aligned} F &= -\frac{Z^2 e^2 i}{2\pi^2} \int d^3 k \frac{\vec{k}\vec{v}_i}{k^2 v_i} \left[ \frac{1}{\epsilon(\vec{k}, -\vec{k}\vec{v}_i)} - 1 \right] \\ &= -\frac{Z^2 e^2}{\pi v_i^2} \int_0^\infty \frac{dk}{k} \int_{-kv_i}^{kv_i} d\omega \omega \operatorname{Im} \left[ \frac{1}{\epsilon(\omega)} - 1 \right]. \end{aligned} \quad (22)$$

The integral receives contributions only from regions where  $\operatorname{Re}\epsilon = 0$ , corresponding to  $\omega^2 = \omega_p^2$ , and therefore eq.(22) may be rewritten as

$$F = -\frac{Z^2 e^2}{\pi v_i^2} \int_{\lambda_a^{-1}}^\infty \frac{dk}{k} \int_{-\infty}^\infty d\omega \omega \operatorname{Im} \left[ \frac{1}{\epsilon(\omega)} - 1 \right] \quad (23)$$

Since the function  $\epsilon^{-1}(\omega)$  is analytical below the real axis in the complex  $\omega$  plane, the  $\omega$ -integration in eq.(23) may, with the imaginary part taken outside, be performed along a large semi-circle in the lower half-plane. From the asymptotic behaviour  $\epsilon^{-1} \sim (\omega_p/\omega)^2$  for  $\omega \rightarrow \infty$ , one then immediately obtains

$$F = -Z^2 \frac{\omega_p^2 e^2}{v_i^2} \cdot \log(k_{\max} \lambda_a) = -Z^2 \frac{4\pi n e^4}{mv_i^2} \cdot \log(k_{\max} \lambda_a) \quad (24)$$

At this stage it should once again be stressed that screening is built into the dielectric description by definition. This is also clear from eq.(24) where no artificial cut-off at small  $k$ -values, corresponding to large impact parameters, was needed to bring  $\lambda_a$  into the argument of the logarithm. As is typical for this type of consideration, a logarithmic

divergence appears instead at large  $k$  since the dielectric description becomes inadequate for  $k > \max\{v^2, v_i^2\}m/e^2$ . Such  $k$  values correspond to very close collisions, where the force may safely be determined from a binary-encounter treatment. This leads to an effective minimum impact parameter equal to  $d/2 \approx e^2/mv_i^2$ . For insertion into eq.(24), we shall therefore use  $k_{\max} \sim 1/d$ , the exact choice being immaterial since the divergence appears underneath a large logarithm. The expression (6) from the binary-collision calculation is then retrieved.

Also for the case of low velocities, which may be worked through in a similar way, all the above remarks hold, the screening length appears to be the Debye length applied already in eq.(8a), and the binary result is retrieved by introducing  $k_{\max} \sim 1/d$ . Hence, for the case of vanishing magnetic field strength we may in general conclude that the binary encounter model and the dielectric description give the same answer to the cooling force provided suitable cut-off's are introduced in both approaches in order to prevent the force from diverging logarithmically.

### B>0

As for the binary model let us treat the case of infinite magnetic field strength as an introduction to a discussion of the influence of a finite magnetic field.

For  $B \rightarrow \infty$ , the electrons are pinned to their positions in transverse space leading to a one-dimensional Boltzmann equation. With  $\rho_0 \propto n\delta(v_{ez})$  it is then very simple to determine the dielectric function as

$$\epsilon(\vec{k}, \omega) = 1 - \lim_{\tau \rightarrow \infty} \left( \frac{k_z}{k} \right)^2 \left( \frac{\omega_p}{\omega - i/\tau} \right)^2 , \quad (25)$$

cf. also ref.10. For the drag force the result is in turn

$$F = -Z^2 \frac{2\pi n e^4}{mv_i^2} \begin{cases} \log(2\lambda_a \cdot k_{\max})^{-1} & , \vec{v}_i \perp \vec{B} \\ 1 & , \vec{v}_i \parallel \vec{B} \end{cases} . \quad (26)$$

We note that the screening length is  $\lambda_a$  as expected. Further on, with  $k_{\max} \sim 1/d$  the binary result eq.(10) is retrieved as for the case with  $B=0$  except for longitudinal velocities where the force is not exactly zero but only down with  $1/L \sim 0.1$  with respect to the transverse case. This contribution which is completely due to collective excitations turns out to be of more importance for  $0 < B < \infty$ .

For finite magnetic field strengths the dielectric function is somewhat lengthy to determine since the unperturbed orbits now are electron

helices. A derivation is given in ref.7 but let us here only quote the result as it applies for a fully flattened electron velocity distribution,

$$\epsilon(\vec{k}, \omega) = 1 + \lim_{\tau \rightarrow \infty} \frac{\omega_p^2}{k^2} e^{-\mu} \sum_{n=-\infty}^{\infty} I_n(\mu) \left[ \frac{2n\omega_c/v^2}{\omega+n\omega_c-i/\tau} - \frac{k_z^2}{(\omega+n\omega_c-i/\tau)^2} \right], \quad (27)$$

$$\mu = \frac{1}{2}(k_{\perp}v/\omega_c)^2,$$

where  $I_n$  denotes a modified Bessel function of order  $n$ .

The simplest case to treat for  $0 < B < \infty$  is that of an electron gas at rest,  $T=0$ . Here eq.(27) reduces to

$$\epsilon(\vec{k}, \omega) = 1 - \lim_{\tau \rightarrow \infty} \frac{\omega_p^2}{k^2} \left[ \frac{k_z^2}{(\omega-i/\tau)^2} + \frac{k_{\perp}^2}{(\omega-i/\tau)^2 - \omega_c^2} \right] \quad (28)$$

The contribution to the integral for the force, eq.(18), comes from poles in  $\text{Im}\epsilon^{-1}$ , corresponding to vanishing  $\text{Re}\epsilon$ . These will be situated at  $\omega = -\vec{k}v_i = \pm\omega_p$  (up to a trigonometric factor) and very close to  $\pm\omega_c$ , where we recall that we assume  $\omega_c \gg \omega_p$ . The result for the drag force is shown in fig.4 before the final integration over  $\log k$  for projectiles with purely transverse and purely longitudinal velocities. We show the integrands  $I_1$  and  $I_z$  from which the force is obtainable as

$$F_{1,z} = -Z^2 \frac{4\pi n e^4}{mv_{\perp}^2} \int_{-\infty}^{\infty} d(\log \kappa) I_{1,z}, \quad \kappa \equiv \begin{cases} kr_1 & , v_i = v_{i\perp} \\ k_{\perp}r_1 & , v_i = v_{iz} \end{cases} \quad (29)$$

where  $r_1 = v_i/\omega_c$ . Note that  $\lambda_a$  and  $r_1$  are the only lengths in the present problem (especially,  $r_L=0$ ). In the binary collision treatment  $r_1$  enters as the impact parameter,  $\rho$ , at which the separation between fast and slow collisions is introduced. Correspondingly, in fig.4 an abrupt change in  $I$  appears around  $\kappa=1$ . For  $\kappa>1$  the dashed level  $I=1$  valid for binary scattering in a Coulomb field for  $B=0$  (and for  $\rho \gg d$ ) is quickly reached. For  $\kappa<1$ , only the plasma pole contributes. However, the plasma-pole contribution is in general not restricted to  $\kappa<1$ , as is observed from the figure. For transverse velocities, this resonance yields half of the force at large  $\kappa$ .

Since  $\kappa<1$  corresponds to distances  $\gtrsim r_1$ , we may attribute contributions from this region to slow collisions. In the simple binary calculations these are treated as if the magnetic field was of infinite strength, in which case the  $I$ -levels would be  $I_1=1/2$ ,  $I_z=0$ . For transverse velocities this is reproduced in the dielectric treatment down to the

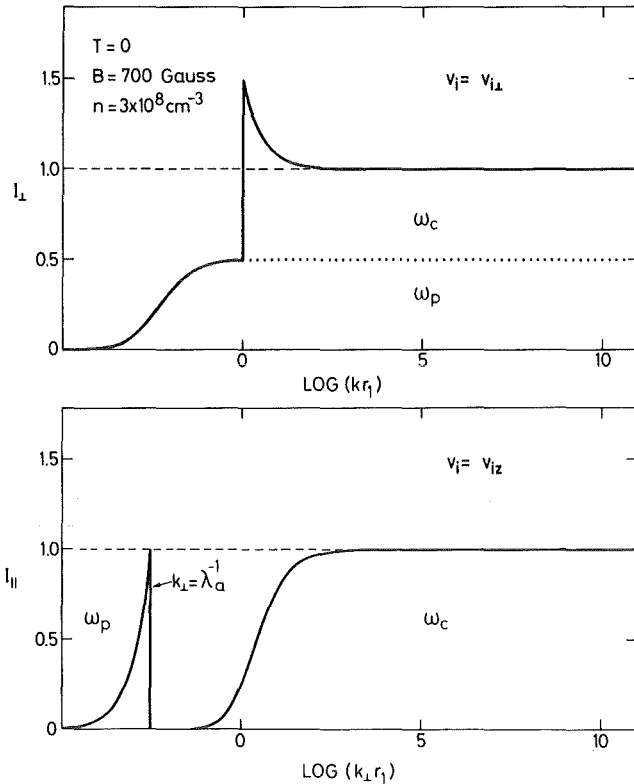


Fig. 4. Drag force in electron gas at rest. The plasma and cyclotron contributions are identified.

region around the inverse of the adiabatic screening distance  $k \sim \lambda_a^{-1} = \omega_p / v_i$  where  $I_{\perp}$  falls off. For longitudinal velocities, however, there is a difference due to the occurrence of the  $\omega_p$ -spike. The figure further shows the presence of the abovementioned simple logarithmic divergence at large  $k$ . Performing the integration over  $\log k$  in eq.(29) we obtain with an accuracy of  $1/\log(k_{\max})$  the same result for the drag as in the simple binary model.

In the general case with finite transverse temperature the dielectric function for the perfectly flattened electron gas in a longitudinal magnetic field is given by eq.(27). With this  $\epsilon$  the contributions to the force, eq.(18), come from poles situated at

$$\omega \approx \pm \omega_p \quad \omega \approx \pm n \omega_c \quad , \quad n = 1, 2, 3, \dots \quad (30)$$

where the cyclotron resonances contribute only to fast collisions. The result for the drag force for a low velocity projectiles moving parallel to  $B$  is shown in fig.5 before the final integration over  $\log k$  for an electron temperature of  $T=1 \text{ eV}$ . The quantity  $I_z$  is defined as in eq.(29) except for the change  $v_i \rightarrow v$  in the definition of  $\kappa$ , hence  $k$  is measured in units of

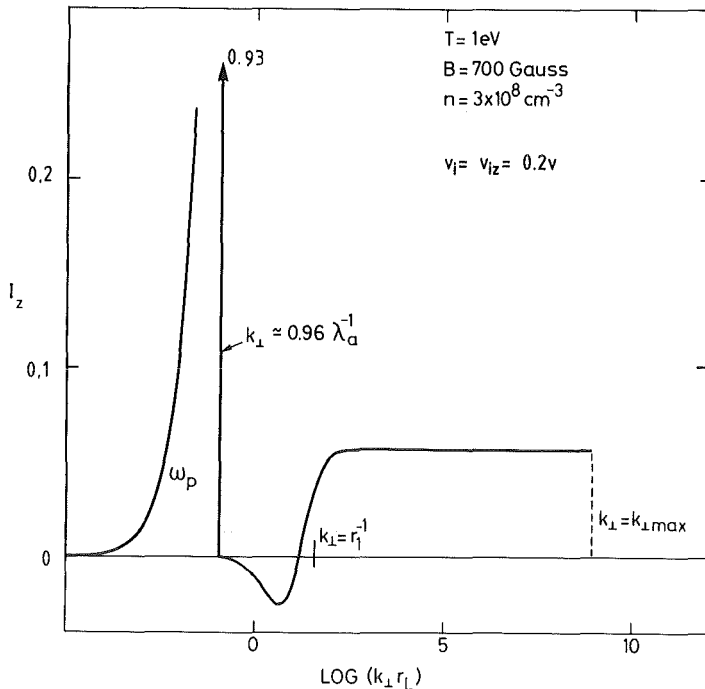


Fig. 5. Drag on ion of longitudinal velocity in flattened electron gas. The contribution for  $\log(k_{\perp}r_L) > 0$  is solely due to  $\omega_c$ -poles. The cut-off at  $k_{\max} = 1/d$  is indicated for  $Z = 1$ .

the inverse of the Larmor radius  $r_L^{-1} = \omega_c/v$ . As for the electron gas at rest, the contributions from the plasma pole and the cyclotron poles are well separated. The latter changes abruptly at  $k \sim r_1^{-1}$  above which a steady level, reproducible by binary calculations for  $B=0$ , quickly is reached. On the other hand, the very large yield from the  $\omega_p$ -resonance cannot be accounted for in binary considerations, which therefore appear insufficient.

Comparing with fig.4 it should be stressed that the abrupt change for the finite temperature gas, fig.5, still appears around  $k \sim r_1^{-1}$  and not at  $k \sim r_L^{-1}$  as was assumed in the binary model, cf. eq.s (11-12). Further on we note that for  $k_{\perp} < r_1^{-1}$  only minor changes have appeared with respect to fig.4, i.e., the plasma-pole spike is only weakly affected by the finite temperature and the screening length is still  $\lambda_a$ . For  $k_{\perp} > r_1^{-1}$  a huge reduction has appeared.

In fig.6 we show in the same units  $\log(kr_L)$  versus  $I_{\perp}$  for low velocity ions moving transverse to the magnetic field. Again at  $k = r_1^{-1}$  an abrupt decrease in  $I_{\perp}$  is observed. This corresponds to the entry of the first set of cyclotron resonances, and each time a new set has to be included with increasing  $k$ , similar drops are observed. The plasma-pole term is shown dotted in this region,  $k > r_1^{-1}$ . At large  $k$ -values the

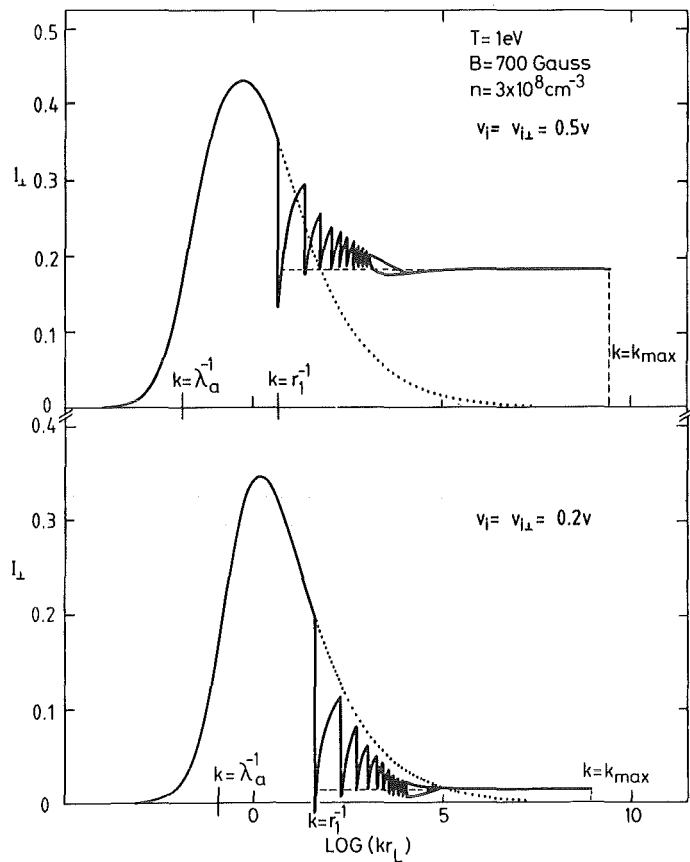


Fig. 6. Drag on ion of transverse velocity in flattened electron gas. Only the plasma pole contributes for  $k < r_1^{-1}$ .

excursions of the integrand  $I_1$  are damped, and a constant level is reached. As in fig.s 4-5 this level may be reproduced by binary calculations for  $B=0$  and  $\rho \gg d$ . In the figure we have further indicated the cut-off at  $k_{\max} = 1/d$ .

By comparing also fig.6 to the case of an electron gas at rest, fig.4, we note again that the changes appearing for  $k < r_1^{-1}$ , where  $I_1$  in fig.4 reaches a maximum of  $I_1 = 1/2$ , are much less drastic than those appearing for  $k > r_1^{-1}$  and that  $\lambda_a$  is a suitable measure of the screening length in the flattened electron gas when confined by a longitudinal magnetic field.

To summarize, in a full dielectric description no artificial splitting of the impact parameter or, equivalently, the  $k$ -region is introduced and screening is naturally included such as to provide a smooth fade-off of the  $I$ -spectrum against small  $k$ -values. Only at large  $k$  is a divergence encountered. In the limits  $B=0, \infty$  the cut-off at  $k_{\max} \sim 1/d$ , introduced by simple binary arguments, causes uncertainties of order  $\sim 1/L \sim 10\%$  in the drag force. In the present case with finite values for both the magnetic field strength and the electron temperature this

uncertainty is, however, strongly suppressed in the supercooling region due to the dominance of the plasma-pole term.

Although we have now established a very accurate way of computing the drag force at the troublesome low velocities, one serious complication needs still to be discussed, namely the effort necessary to evaluate the force numerically. While it is fairly simple to determine the plasma-pole contribution, it requires in general rather extensive calculations to determine the yield from the cyclotron resonances, especially since a very large number may contribute to the force at large  $k$ . However, the study of fig.s 4-6 leads to the following suggestion for a simple prescription for obtaining a fairly accurate value for the cooling force: Compute the plasma-pole term  $\vec{I}^{p1}$  for the magnetic field strength in question, truncate it at  $k=r_1^{-1}$ , and integrate over  $\log k$  to obtain the force contribution  $\vec{F}^{p1}$ . To this, add  $\vec{F}^b$ , the binary result for the drag force for  $B=0$  but cut-off at a maximal impact parameter of  $\rho=r_1$ , i.e.

$$\vec{F} = \vec{F}^{p1} + \vec{F}^b = -Z^2 \frac{4\pi n e^4}{m v_i^2} \int_{-\infty}^{\log(r_1^{-1})} d(\log k) \vec{I}^{p1} + \vec{F}^b . \quad (31)$$

Expressions for  $\vec{I}^{p1}$  are given in ref.11, see also ref.7 where another normalization has been used.

The above simple prescription, eq.(31), contains a splitting of the drag force into two parts as was also the case in the the binary model. However, whereas the force computed in the latter case easily attains errors of  $\sim 100\%$ , the force computed according to eq.(31) agrees in all cases with the correct one obtained in a full dielectric treatment to within  $\sim 10\%$ . The dividing distance is  $r_1=v_i/\omega_c$  rather than  $r_L$ . It should further be stressed that the contribution from distant encounters, the plasma-pole term, is calculated at the finite magnetic field strength in question, and not as in the binary model for  $B=\infty$ , since some reduction appears, cf. fig.s 4-6.

In fig.7 we show the plasma-pole contribution  $F^{p1}(v_i)$  in units of  $-4\pi n Z^2 e^4 / m v_i^2$  for both purely transverse and purely longitudinal projectile velocities, where  $\vec{F}^{p1}$  clearly is (anti)parallel to  $\vec{v}_i$ . For the longitudinal case the simple binary treatment gives vanishing drag in slow collisions. On the contrary, we find as aforementioned for  $F^{p1}$  a significant contribution due to the occurrence of the plasma spike in fig.5. In the case of an infinite magnetic field strength the dielectric level for  $v_i \parallel \vec{B}$  was  $1/2$ , cf. eq.(26). For not too low projectile velocities this level is also found for the case of  $0 < B < \infty$ , as is clear from fig.7. The contribution  $F^{p1}$  is confined to the region of impact parameters  $\lambda_a = v_i/\omega_p > \rho \geq r_1 = v_i/\omega_c$

which is independent of the electron temperature. However, when the latter parameter rises from zero to values corresponding to a  $r_L$  which enters deeply into the above interval,  $F^{pl}$  drops off. In the figure we have marked the velocity  $v_a \equiv v_{wp}/\omega_c$  below which  $\lambda_a$  becomes smaller than  $r_L$ . Clearly, this value is a measure for the velocities where  $F^{pl}$  becomes significantly different from the results computed in the limit  $B \rightarrow \infty$ . For  $v_i < v_a$  the curve falls off  $\propto v_i^{2/3}$  for the longitudinal case; note that in the present units  $F^b$  falls off  $\propto v_i^3$  in the low velocity region.

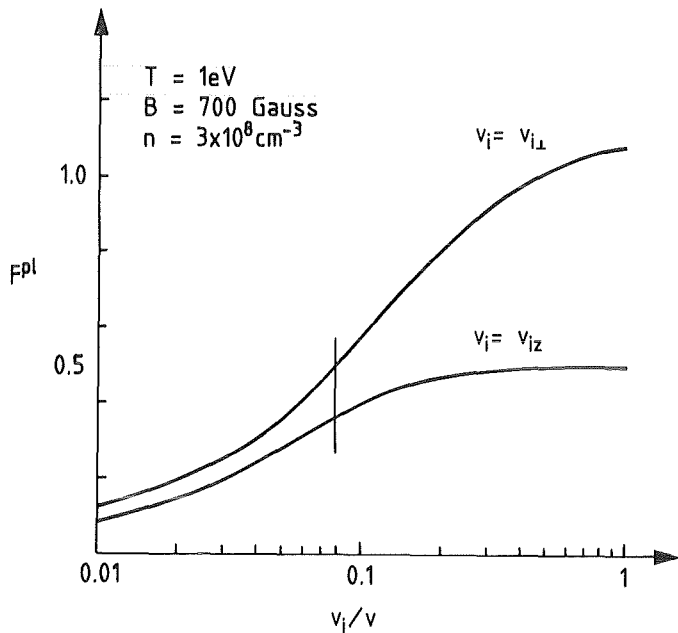


Fig. 7. Plasma-pole contribution to the drag. The velocity  $v_a$  is marked by a verticle bar.

#### CONCLUDING REMARKS

The discussion above demonstrates how the two complementary models, the binary encounter and the dielectric description, may be combined into one to give very reliable and easily computable expressions for the electron cooling friction force. All the considerations above were performed for a fully collapsed Maxwellian electron velocity distribution,  $f \propto \delta(v_{ez})$ . This makes the plasma-pole contribution to the force, fig. 7, to diverge at vanishing projectile velocity. This unphysical behaviour is prevented by introducing some finite longitudinal electron temperature, partly from a not complete collapse, cf. fig. 2, partly from imperfections in the experimental set-up. Below the longitudinal rms electron velocity the force will fall off towards zero. As to the absolute minimum of the

final temperature of the ion beam as it is obtained from the equilibrium with the electron reservoir alone we may refer to discussions given elsewhere. For the case of a completely flattened electron gas and vanishing magnetic field strength the final transverse ion temperature is  $T/2$  whereas the longitudinal typically is 2-3 orders of magnitude smaller<sup>7</sup>. When a magnetic field is introduced, the ion temperature is reduced further towards the level of the longitudinal electron temperature<sup>6</sup>.

#### REFERENCES

1. A.N. Skrinskii and V.V. Parkhomchuk, Sov.J.Nucl.Part.Sci. 12 (1981) 223
2. F.T. Cole and F.E. Mills, Ann.Rev.Nucl.Part.Sci. 31 (1981) 295
3. D. Cline, these proceedings and references therein
4. P.J. Channell, J.Appl.Phys. 52 (1981) 3791
5. See, e.g., A. Wolf, these proceedings
6. Y.S. Derbenev and A.N. Skrinsky, Part.Acc. 8 (1978) 235; see also Y.S. Derbenev and I. Meshkov, Studies on Electron Cooling of Heavy Particle Beams, CERN 77-08 (1977)
7. A.H. Sørensen and E. Bonderup, Nucl.Instr.Meth. 215 (1983) 27
8. M. Bell, Part.Acc. 10 (1980) 101
9. For electron cooling a continuum description was first adapted by M.N. Rosenbluth in a couple of unpublished notes (1977), Ion Cooling by Electrons in a Strong Magnetic Field, and Magnetic Cooling Equations
10. Y.S. Derbenev and A.N. Skrinskii in Physics Reviews, Vol. 3, Ed. I.M. Khalatnikov (Harwood Academic Press, 1981) 165
11. A.H. Sørensen, Proc. Beam Cooling Workshop, Univ. of Wisconsin-Madison, Sept.9-11, 1982.

## REALISTIC CALCULATIONS CONCERNING ELECTRON COOLING IN STORAGE RINGS

A. Wolf

CERN, Geneva, Switzerland

### 1. INTRODUCTION

For experimental projects which rely on the cooling of a stored ion beam by means of electrons, it is of great interest to predict the efficiency of the electron cooling process under realistic conditions. This talk is based on work done during the preparation of the electron cooling device for the Low-Energy Antiproton Ring (LEAR) at CERN. Its purpose is to follow the line from the cooling force, experienced by an ion in the electron beam, to the properties of a stored, cooled ion *beam*, and their time dependence. In this sense, it complements the preceding contribution [1] to this conference.

In the following, the situation of cooling slightly relativistic ions with an electrostatically generated electron beam will be considered. Specifically relativistic effects will not be discussed. However, the properties and the spatial structure of the electron beam will be dealt with, as will the specific properties of the ion motion. The oscillatory character of the ion motion implies that, instead of the primary cooling force, a 'cooling rate' (which will be defined below) is relevant for the damping. Such cooling rates can be obtained by analytical methods in simple cases, or by numerical calculation.

Based on a summary of the 'kinetics of electron cooling' as first discussed by Derbenev and Skrinskij [2], both possibilities will be outlined. Numerically calculated cooling rates, in particular, are an important intermediate result in a computer simulation of the electron cooling process.

Single-particle simulation of electron cooling was first attempted by M. Bell [3]. We have tried to develop this approach. Results obtained with the computer code in preparation [4] will be presented at the end of this talk.

### 2. THE CONDITIONS OF ELECTRON COOLING

#### 2.1 Space dimensions

The friction experienced by an ion in an electron beam is determined by the Coulomb interaction with the surrounding electrons. Let us consider the range of distances around an ion in which the interactions relevant to the friction force take place. As has been discussed by A. Sørensen [1], at this conference, three lengths are of particular importance to the theory of friction in a magnetized electron gas.

- i) The collision diameter

$$d_0 = |Z| e^2 / (m w^2),$$

below which the momentum transfer in binary collisions has its maximum kinematically allowed value.

ii) The adiabatic collision limit

$$r_1 = w_a/\omega_c ;$$

for electrons at a distance greater than  $r_1$ , the velocity spread transverse to the magnetic field ceases to influence the friction force. This happens because the electric field of the ion is changing in time in an adiabatic manner with respect to the electron cyclotron motion.

iii) The screening distance

$$\lambda = w_a/\omega_{pl} ;$$

beyond this distance the effective field of the ion, as compared with the Coulomb field is strongly reduced by screening.

In these expressions (valid in the beam rest-frame),  $w$  describes the relative velocity between an ion (charge  $Ze$ ) and electrons of a selected velocity group; in the 'adiabatic' relative velocity  $w_a$ , the electron motion transverse to the magnetic field is ignored. For the most frequent, typical collisions we may approximate the relative velocity by its average over the electron velocity distribution:

$$w \approx \max(v_p, \Delta_\perp) , \\ w_a \approx \max(v_p, \Delta_\parallel) ,$$

where  $\Delta_\perp$  and  $\Delta_\parallel$  denote the electron velocity spread in directions transverse and longitudinal to the magnetic field. External parameters enter via the cyclotron frequency  $\omega_c$  (determined by the magnetic field strength), and the plasma frequency  $\omega_{pl}$  (determined by the electron density).

In a single-pass, magnetically confined electron beam, as used for electron cooling at moderate energies, the following conditions are met:

- i) the electron velocity distribution is longitudinally flattened ( $\Delta_\parallel/\Delta_\perp \ll 1$ );
- ii) the cyclotron frequency is large compared with the plasma frequency ( $\omega_c \gg \omega_{pl}$ ), which is necessary for magnetic confinement at low transverse energies.

For parameters typical of this situation and single-charged ions, Fig. 1 shows the relevant distances for varying ion velocity  $v_p$  in the beam rest-frame. This velocity is given relative to the beam velocity  $v_0 = \beta c$  and is plotted on the horizontal axis. The friction force is produced by interaction of the ion with electrons in the range between  $d_0$  and  $\lambda$ . This range is subdivided by  $r_1$ .

At low ion velocities  $v_p < \Delta_\perp$ , the adiabatic collisions with electrons at a distance  $x > r_1$  give rise to the dominant contribution to the cooling force ('magnetic cooling force'). Compared with fast collisions ( $x < r_1$ ) at the same ion velocity, this contribution is larger by roughly a factor of  $(\Delta_\perp/w_a)^3$ . The maximum value of this ratio follows from the compression of the electron velocity distribution by acceleration, which can be calculated as

$$\Delta_\parallel/\Delta_\perp = (\Delta_\perp/v_0)/(4\gamma) \approx 10^{-3}$$

where  $\gamma = 1/\sqrt{1-\beta^2}$ . Thus the cooling force can be up to  $10^9$  times higher than expected when adiabatic collisions are disregarded ('supercooling').

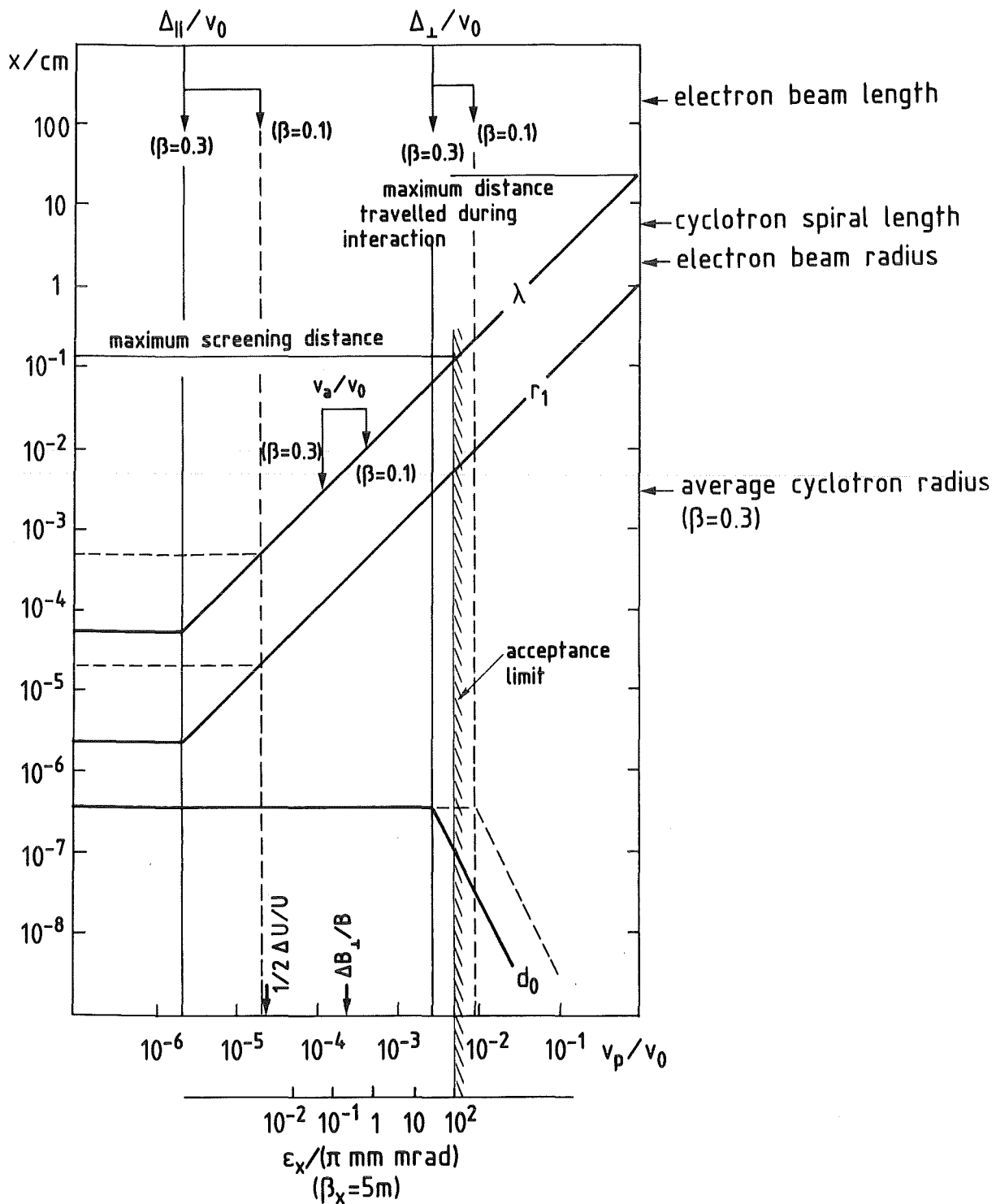


**Fig. 1** Space dimensions relevant to electron cooling for varying ion velocity in the electron beam rest-frame. The parameters correspond to an electron beam of 2.54 cm radius, at a perveance of  $0.5 \times 10^{-6} \text{ AV}^{-3/2}$ , at a cyclotron spiral length of 6.3 cm and at a cathode temperature of 1100 °C.

The horizontal axis in Fig. 1 represents emittances or momentum deviations in a storage ring, independent of the beam velocity (powers of  $\gamma$  neglected). Also the relevant distances as functions of  $v_p/v_0$  are quite independent of the working energy of the storage ring under certain, technically favourable conditions. These conditions are realized if the electron beam device is operated with a constant permeance  $P = I/U^{3/2}$  and with a constant electron cyclotron spiral length  $\lambda_c = 2\pi v_0/\omega_c$ . Both  $\omega_c$  and  $\omega_{pl}$  are proportional to  $v_0$  in this case; therefore, the ratios  $v_p/\omega_c$  and  $v_p/\omega_{pl}$ , which give the relevant distances, remain constant for a given value of  $v_p/v_0$ , if  $v_0$  is varied. Consequently, the positions of the diagonal lines in Fig. 1 are independent of the beam velocity and are in fact determined by the basic electron-gun design criteria,  $P$  and  $\lambda_c$ .

From this point of view, the following conclusion, to be drawn from Fig. 1, is valid quite generally for electron cooling at relativistically moderate energies. It is seen that screening limits the interaction range to below 1 mm, which is still small compared with the usual electron beam diameter and with the range over which the electron beam properties may change radially. Note that in a storage ring the acceptance limits the range of  $v_p/v_0$  to below approximately  $5 \times 10^{-3}$ ; this specifies the maximum screening length  $\lambda$ . Considering the longitudinal dimensions of the electron beam, we state that the interaction time for electron-ion encounters is approximately given by

$$\tau = x/v_p ;$$

thus, the distance travelled along the beam by both particles during their interaction is

$$\ell = x/(v_p/v_0) .$$

The intercept of the diagonal line for  $\lambda$  with the vertical axis at  $v_p/v_0 = 1$  gives the maximum occurring distance  $\ell$ , at least for  $v_p > \Delta_{||}$ . This maximum is of the order of 20 cm; therefore, the distance travelled during interaction remains small compared with both the usual electron beam length  $L$  and the distance over which we expect external conditions such as the magnetic field to change by significant amounts. Consequently, the assumption of an homogeneous and infinitely extended electron gas for the cooling force calculation seems reasonable with respect to both the transverse and the longitudinal direction. On the other hand, we have stated the critical lengths and we have made clear their dependence on external parameters.

## 2.2 The lowest effective ion velocity

In practice, the minimum value of the adiabatic relative velocity between electrons and ions is determined by technical imperfections rather than by the longitudinal velocity spread of the electrons,  $\Delta_{||}$ . Whereas  $\Delta_{||}/v_0$  is of the order of  $10^{-6}$  for  $\beta = 0.3$ , the usual high-voltage fluctuations are  $\Delta U/U \approx 5 \times 10^{-5}$ , and the magnetic field direction is constant over the electron beam length within  $\Delta B_z/B \approx 2 \times 10^{-4}$  only. Both imperfections set a lower limit to the velocity of the ions in the relevant reference frame for the microscopic interaction. The limits are indicated in Fig. 1. The probability of rest-frame velocities much below these values is strongly reduced. In the remaining velocity range, the statistical velocity spread  $\Delta_{||}$  is small compared with the ion velocity, so that a completely flattened velocity distribution of the electrons can be assumed for microscopic calculations.

The variation of  $\Delta_{\perp}/v_0$  and of  $\Delta_{\parallel}/v_0$  with the beam velocity is also indicated in Fig. 1; values are shown for  $\beta = 0.3$  and  $\beta = 0.1$ . In particular,  $\Delta_{\parallel}/v_0$  changes strongly with  $v_0$ . Therefore, the longitudinal temperature itself will start to influence the microscopic interaction at very low beam energies below  $\beta = 0.1$ .

### 2.3 Electron beam properties

We will briefly summarize the general conditions encountered in the electron beam of a real cooling device. The flattening of the velocity distribution has already been mentioned. The relaxation of the flattened distribution to Maxwellian equilibrium proceeds slowly compared with the time needed by the electron beam to reach the cooling region. Furthermore, it seems to be suppressed by the magnetic guiding field [5].

In any magnetically confined electron beam, the transverse and longitudinal velocities vary with the radial distance  $r$  from the beam centre owing to the electric field associated with the space-charge. For low perveances ( $P \leq 10^{-6} \text{ A V}^{-3/2}$ ), the potential in the beam is given by

$$U = U_0 + (r/R)^2 U_R ,$$

where  $eU_0$  is the energy in the centre,  $R$  is the beam radius, and

$$U_R = \{I/A\} \times 30 \text{ V}/(\beta\gamma)$$

is the space-charge potential. For varying  $U_0$  but constant perveance and  $\gamma \approx 1$ ,  $U_R/U_0$  remains constant. The transverse velocity due to the rotational drift motion in the crossed magnetic and space-charge fields is given by

$$v_\theta = r \omega_c (\omega_{pl}/\omega_c)^2 .$$

For constant perveance and cyclotron spiral length, also  $v_\theta/v_0$  does not vary with the beam velocity.

In addition to these unavoidable velocity variations, the transverse energy due to focusing errors will in general increase with the radial position in the electron beam. For example, estimates for the Initial Cooling Experiment (ICE) electron cooler [6] indicate that the transverse energy induced by external fields reached 10 times the thermal energy, at the beam edge.

From the statement of these electron beam properties, it can be concluded that the average relative velocity between an ion and the electron will depend not only on the ion velocity, but also on its position in the electron beam. The friction force is therefore a function of the positional ion coordinates as well.

### 2.4 Electron velocity distribution

Except for low beam velocities  $\beta < 0.1$ , we find it satisfactory to use a completely flattened electron velocity distribution of the form

$$f(\vec{v}_e) = \delta(v_{e\parallel}) f_{\perp}(\vec{v}_{e\perp}) ,$$

with the beam axis, which is assumed parallel to the magnetic field, as the longitudinal reference direction (Fig. 2). This has been justified above by considering the usual high-voltage stability and magnetic field angle variations, which are expected to be more than one order of magnitude larger than the expected longitudinal velocity spread of the electrons. The assumption of a completely flattened distribution strongly reduces the effort required when calculating the cooling force.

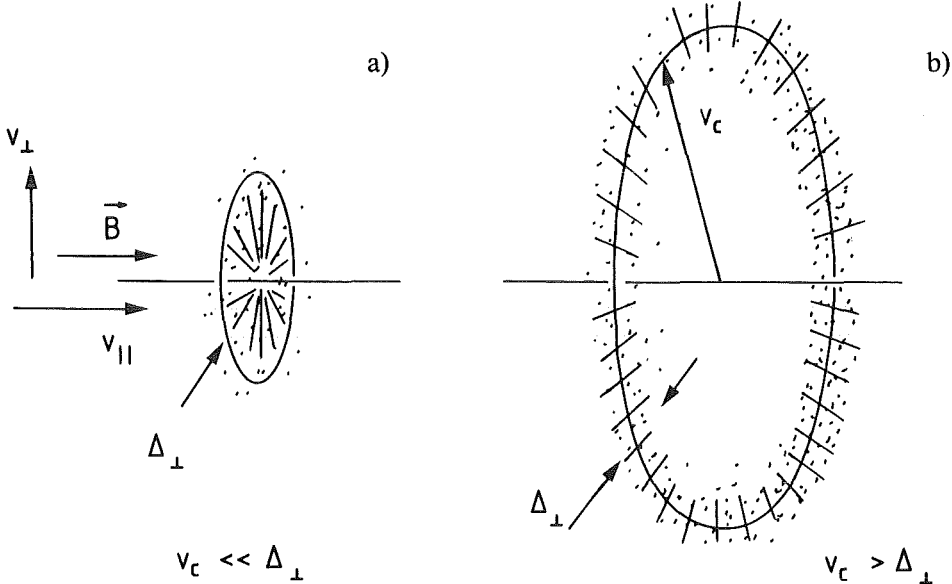


**Fig. 2** Effective electron velocity distributions in a magnetic field with vanishing longitudinal width and dominated by thermal motion ( $v_c \ll \Delta_{\perp}$ ) or by coherent motion from imperfections of the electron optics ( $v_c > \Delta_{\perp}$ ).

The transverse electron velocity is affected by the thermal speed of the electrons at the emitter and by eventual transverse fields during acceleration, which excite a coherent cyclotron motion of the electrons. By considering the equations of motion in the longitudinal magnetic field, one finds that it is reasonable to superimpose the thermal velocities on the coherent motion. This yields the following distribution function:

$$f_{\perp}(\vec{v}_{e_{\perp}}) = f_{\text{th}}(\vec{v}_{e_{\perp}} - \vec{v}_c),$$

where  $\vec{v}_c$  varies along the beam length  $s$ :

$$\vec{v}_c = v_c \begin{pmatrix} \cos [(2\pi/\lambda_c)s + \phi_c] \\ \sin [(2\pi/\lambda_c)s + \phi_c] \end{pmatrix}.$$

$f_{\text{th}}$  is the two-dimensional Maxwell distribution. Within a binary calculation of the cooling force, the average over a longitudinal distance  $\Delta s \gg \lambda_c$  can already be performed on the electron velocity distribution. The result is

$$f_{\perp,\text{av}}(\vec{v}_{e_{\perp}}) = (\pi \Delta_{\perp}^2)^{-1} \exp [-(v_{e_{\perp}}^2 - v_c^2)/\Delta_{\perp}^2] \cdot I_0(2v_{e_{\perp}}v_c/\Delta_{\perp}^2) \exp (-2v_{e_{\perp}}v_c/\Delta_{\perp}^2),$$

with the modified Bessel function  $I_0$ . For  $v_c \geq \Delta_\perp$ , this represents a ring-shaped distribution in velocity space, with the ring radius given by the velocity  $v_c$  caused by focusing errors; the ring is smeared out over a width of about  $\Delta_\perp$  by the thermal motion (Fig. 2b).

For a cooling-force calculation which takes into account collective effects, the averaging over the phase of the coherent motion does not seem adequate if already performed on the distribution function [4].

### 3. FRICTION FORCE AND COOLING RATES

#### 3.1 Magnetic cooling force

In Fig. 1 we can easily situate the velocity  $\Delta_\perp \omega_{pl}/\omega_c = v_a$  (as used by Sørensen [1]). Around and below this ion velocity, it becomes important to take into account the finite value of the magnetic field strength, instead of assuming that this value is infinite. In the frequently quoted result for the magnetic cooling force, as first derived by Derbenev and Skrinskij [7], an infinite field strength is assumed when considering the binary electron-ion interaction. The deviations of these simple expressions from the result of refined calculations have been demonstrated by Sørensen at this conference.

The velocity  $v_a$  lies well within the interesting range of ion velocities ( $v_a/v_0 \approx 10^{-4}$ ). In our calculations on electron cooling we therefore avoid the standard expressions for the magnetic cooling force and compute the friction caused by slow collisions as the plasma pole contribution [8] of the dielectric treatment for finite magnetic field. We determine this contribution by numerical integration and tabulate the results for selected values of the independent parameters  $v_p/\Delta_\perp$ ,  $v_{p_\perp}/v_{p_\parallel}$ , and  $\omega_c/\omega_{pl}$ . To find the cooling force for any given parameters, linear interpolation is performed. A graph of the plasma pole contribution as a function of  $v_p$  can be seen in Fig. 7 of Sørensen's paper [1].

For the magnetic cooling force, the flattened Maxwell distribution of width  $\Delta_\perp$  is assumed in our calculations. No way was found to perform the dielectric calculation with reasonable effort when the coherent motion of the electrons, due to focusing errors, is to be included in the distribution function.

#### 3.2 Non-magnetic cooling force

The friction from close collisions ('non-magnetic cooling force') is the dominant contribution to the cooling force at high ion velocities  $v_p > \Delta_\perp$ . In its calculation, we do take into account the focusing errors by using the effective velocity distribution  $f_{\perp,av}(\vec{v}_{e_\perp})$  given above. The Coulomb logarithm

$$L_c = \ln(r_1/d_0)$$

being large in the interesting velocity range (see Fig. 1), its variation over the electron velocity distribution is neglected. The Coulomb analogy is used to find the cooling force from the potential

$$\phi \propto \int d^2v_{e_\perp} f_{\perp,av}(\vec{v}_{e_\perp}) |\vec{v}_p - \vec{v}_{e_\perp}|^{-1},$$

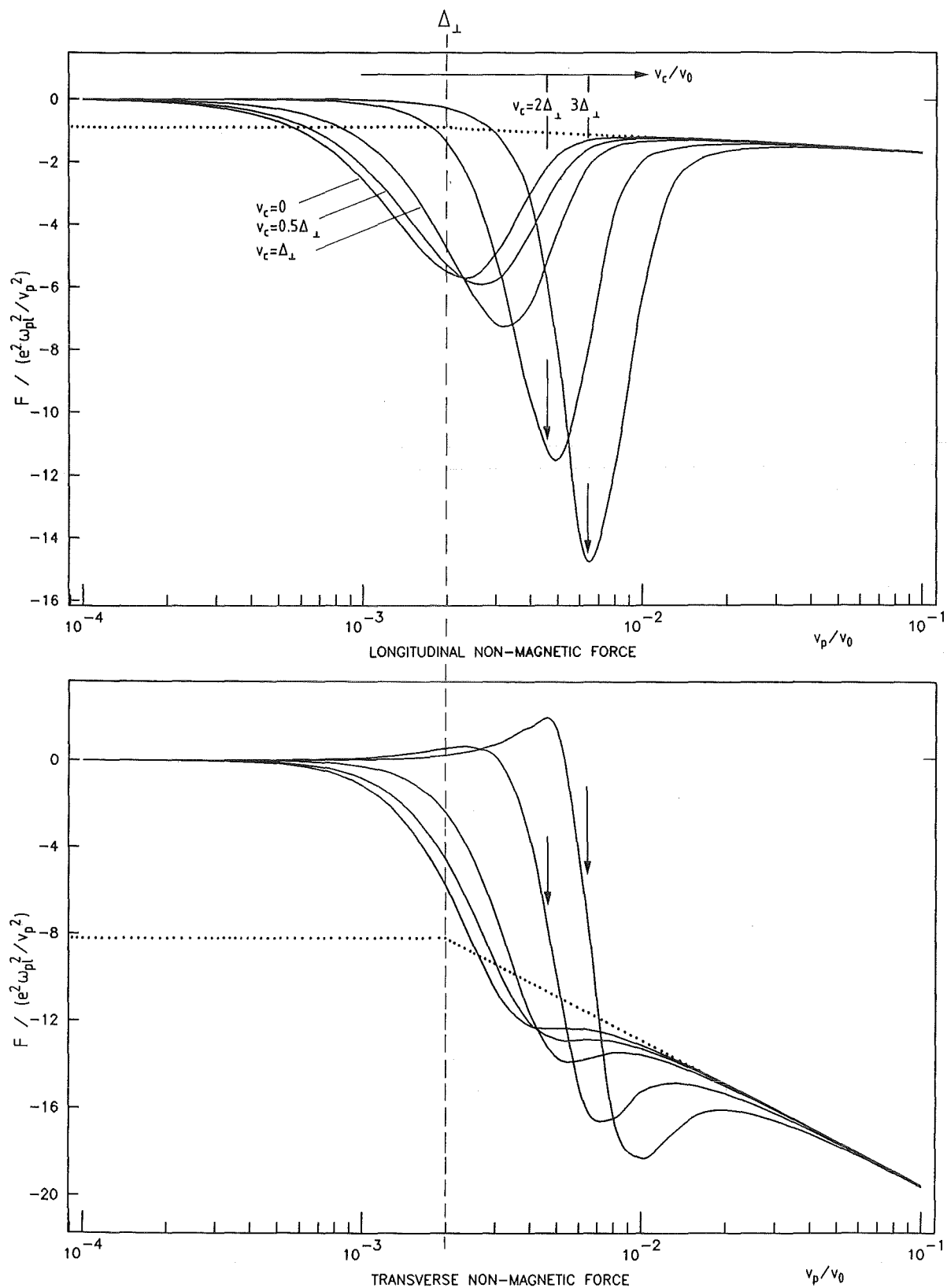


**Fig. 3** Velocity dependence of the 'non-magnetic' cooling force for a flattened distribution and imperfect electron optics. The ion moves almost transverse in the electron beam rest-frame ( $85^\circ$  to the longitudinal axis).

which is computed numerically. The force components are

$$F_{\parallel} = - \partial\phi/\partial v_{p_{\parallel}}, \quad F_{\perp} = - \partial\phi/\partial v_{p_{\perp}}.$$

Again, they are tabulated for computer simulation.

Figure 3 shows the force components for an ion moving in an almost transverse direction in the rest frame of the electrons. As a function of  $v_p/v_0$ , the normalized force is shown for some values of the coherent cyclotron velocity  $v_c$ , including  $v_c = 0$ . In an isotropic velocity distribution, the longitudinal force should be small compared to the transverse component for the assumed ion direction. However, as an effect of the flattening of the distribution, the longitudinal component is enhanced around  $v_p = \Delta_{\perp}$  even if  $v_c = 0$ . The peak in the longitudinal component and the corresponding dispersion-like variation in the transverse force move to higher values if  $v_c$  is increasing, and lie near  $v_c$  for  $v_c > \Delta_{\perp}$ . It can be seen that the influence of focusing errors differs from that of the transverse temperature; it leads to a relatively sharp structure in the cooling force and can, in particular, change the sign of the transverse component for  $v_c/\Delta_{\perp} > 1$  and  $v_p < v_c$ , so that the ion is accelerated by the electrons.

### 3.3 Cooling rates in a storage ring

We shall now try to follow the motion of an ion under the influence of electron cooling in a storage ring. In the absence of forces of statistical origin, this motion is characterized by three invariants which represent the amplitude of the betatron oscillations in the transverse direction and the longitudinal momentum deviation of the ion from a nominal value (or, in the case of a bunched beam, the amplitude of the synchrotron oscillations). If these invariants are chosen with the dimension of an action, their averages over all ions are a measure for the invariant emittances of the beam.

We are interested in the changes of these constants of motion caused by friction in the electron beam and by scattering processes in general. During the revolutions of an ion, each position on the ring circumference is passed with varying position and velocity coordinates. For the betatron oscillations, the transverse position in one (say, the horizontal) direction is given at a point  $s$  in the longitudinal direction by

$$x_b = \sqrt{\epsilon_x \beta_x(s)} \cos [\mu_x(s) + \phi_x],$$

with the periodic lattice function  $\beta_x(s) = \beta_x(s+C)$  and the related phase function  $\mu_x(s) = \mu_x(s+C) - Q_x$ . The constant of motion will be denoted by  $\epsilon_x (\epsilon_z, \epsilon_s)$  for the horizontal (vertical, longitudinal) direction;  $C$  is the storage ring circumference. The transverse velocity follows from

$$x'_b = dx_b/ds = v_x/v_0.$$

The cooling force acts during a time  $\Delta t$  when the ion passes the electron cooler, and is a function of its coordinates  $x_b$  and  $x'_b$  in the electron beam. It will change the momentum  $\vec{p}$  of the ion and also the constant of motion by

$$\Delta\epsilon_x = \Delta t \vec{F} \cdot \partial\epsilon_x/\partial\vec{p}.$$

More precisely, the average of the right-hand side over the electron beam length  $L$  gives the change of  $\epsilon_x$  following one passage. But the variation of  $x_b$  and  $x'_b$  over that distance can be neglected if  $\beta_x(s) \gg L$ , which is frequently true. Then it is sufficient to make the calculation with fixed ion coordinates for a single passage. The average of  $\Delta\epsilon_x$  over many passages is in practice equivalent to its average over the phases of the oscillatory motion [2], since one position on the ring circumference is passed with all phases in the course of time, the storage ring being tuned off low-order resonances. Denoting by angular brackets the average over phases and over the electron beam length, we obtain the following cooling rate for a circulating ion with revolution frequency  $f_{rev}$ :

$$\dot{\epsilon}_x = \langle \Delta\epsilon_x \rangle f_{rev} = \langle \vec{F} \cdot \partial\epsilon_x / \partial\vec{p} \rangle \Delta t f_{rev}.$$

For the example of a betatron oscillation in one transverse direction, we have (neglecting here the derivative of the lattice function)

$$\partial\epsilon_x / \partial p_x \propto v_x;$$

consequently, the cooling rate is proportional to the *average power* of the cooling force [2],

$$\dot{\epsilon}_x = A \langle F_x v_x \rangle,$$

where the factor  $A$  depends on the lattice function at the cooling device. In an approximation for small oscillations, we can finally linearize the functional dependence of  $\vec{F}$  on the position and velocity of the ion. In our example, this gives the simple expression

$$\dot{\epsilon}_x \approx A (\partial F_x / \partial v_x)|_0 \langle v_x^2 \rangle = -\epsilon_x / \tau_x,$$

which defines the constant cooling time  $\tau_x$ . The derivative is to be taken at the equilibrium coordinates of the oscillation.

### 3.4 Consequences of velocity detuning

Cooling and heating of small oscillations can be understood with this formula and the typical dependence of the cooling force on the ion velocity  $v_x$  for a selected space direction, as sketched in Fig. 4. In the upper diagram, the average velocity  $\bar{v}_e$  of the electrons is well tuned to the average  $\langle v_x \rangle$  of the ion velocity during the oscillation. Here, the slope  $(\partial F_x / \partial v_x)|_0$  is negative, and cooling takes place according to the steepness of the function  $F_x(v_x)$  at  $v_x = \bar{v}_e$ . Standard electron-cooling damping times are calculated from this slope.

However, for a detuning  $|\langle v_x \rangle - \bar{v}_e|$  which is larger than the electron velocity spread  $\Delta$  (Fig. 4b), the slope is positive; the oscillation amplitude will grow until it reaches the magnitude of the detuning. This shows that angular misalignment and, for a bunched beam, longitudinal velocity detuning, will blow up the ion beam [2]. In particular, these effects must be considered when one tries to reach very low beam divergencies, utilizing the strong magnetic cooling force. Then,  $\Delta$  can be as low as the longitudinal velocity spread of the electrons. Randomly varying misalignment and detuning will not necessarily result in ion beam blow-up but in reduced cooling performance, as discussed by Derbenev and Skrinskij [7] for the adiabatic cooling force.

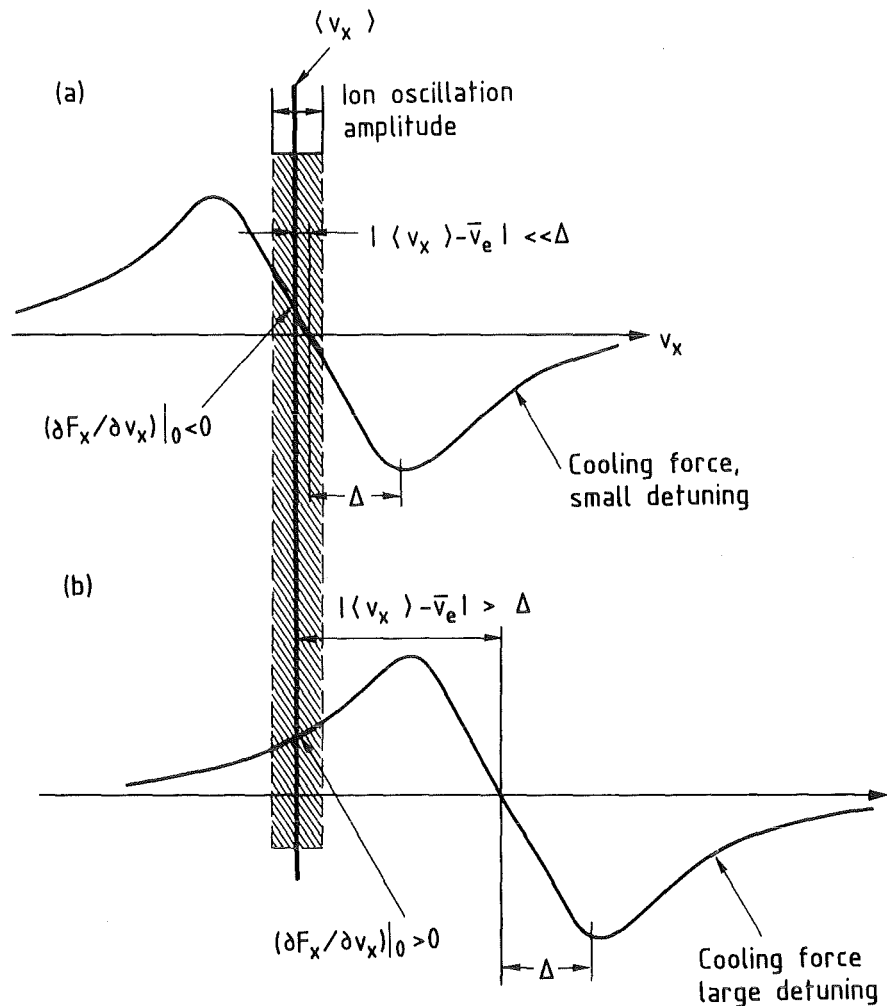


**Fig. 4** Damping and excitation of small oscillations by the cooling force.

### 3.5 Coupling of degrees of freedom

Using the linear approximation of the cooling force, we now discuss the consequences of the coupling between horizontal and longitudinal ion coordinates in a storage ring. Taking into account this coupling, the horizontal ion coordinates are

$$\begin{aligned} x &= x_b + D(s)\delta, \\ x' &= x'_b + D'(s)\delta, \end{aligned}$$

with the dispersion function  $D(s)$ , its derivative  $D'(s)$  and the relative momentum deviation  $\delta$ . The horizontal constant of motion is still calculated using  $x_b, x'_b$ :

$$\epsilon_x = (x - D\delta)^2/\beta_x + (x' - D'\delta)^2\beta_x$$

(again neglecting  $d\beta_x/ds$ , which gives no additional terms in linear approximation). Now  $\partial\epsilon_x/\partial\delta \neq 0$ , so that the longitudinal force component  $F_{\parallel}$  also acts on  $\epsilon_x$ . Retaining only the terms with a non-zero average over the oscillation phases, we have

$$\dot{\epsilon}_x = A[(\partial F_x/\partial v_x)|_0 \langle x_b'^2 \rangle - D'(\partial F_{\parallel}/\partial v_x)|_0 \langle x_b'^2 \rangle - D(\partial F_{\parallel}/\partial x)|_0 \langle x_b^2 \rangle].$$

It is seen that a derivative of the dispersion function or a gradient of the electron beam properties produces coupling terms. As discussed by Derbenev and Skrinskij [2], complementary coupling terms occur if the cooling of longitudinal synchrotron oscillations is considered in the same situation.

#### 4. NUMERICAL CALCULATIONS

##### 4.1 Cooling rates for arbitrary amplitudes

In the two preceding sections, we assumed the dependence of the cooling force on the ion coordinates to be linear over the entire range of the oscillatory motion. The results for the cooling rates were simplified to a large extent by the cancellation of coupling terms during the averaging. The remaining terms can be gathered in the form of a constant cooling time  $\tau_x$  by expressing the results as

$$\dot{\epsilon}_x = -\epsilon_x/\tau_x.$$

We observe an exponential approach to an equilibrium emittance  $\epsilon_{x,eq}$ , if there is a constant emittance blow-up rate  $R_x$  from scattering processes [2]:

$$\begin{aligned}\epsilon_x(t) &= \epsilon_{x,eq} + (\epsilon_{x,0} - \epsilon_{x,eq}) \exp(-t/\tau_x), \\ \epsilon_{x,eq} &= R_x \tau_x.\end{aligned}$$

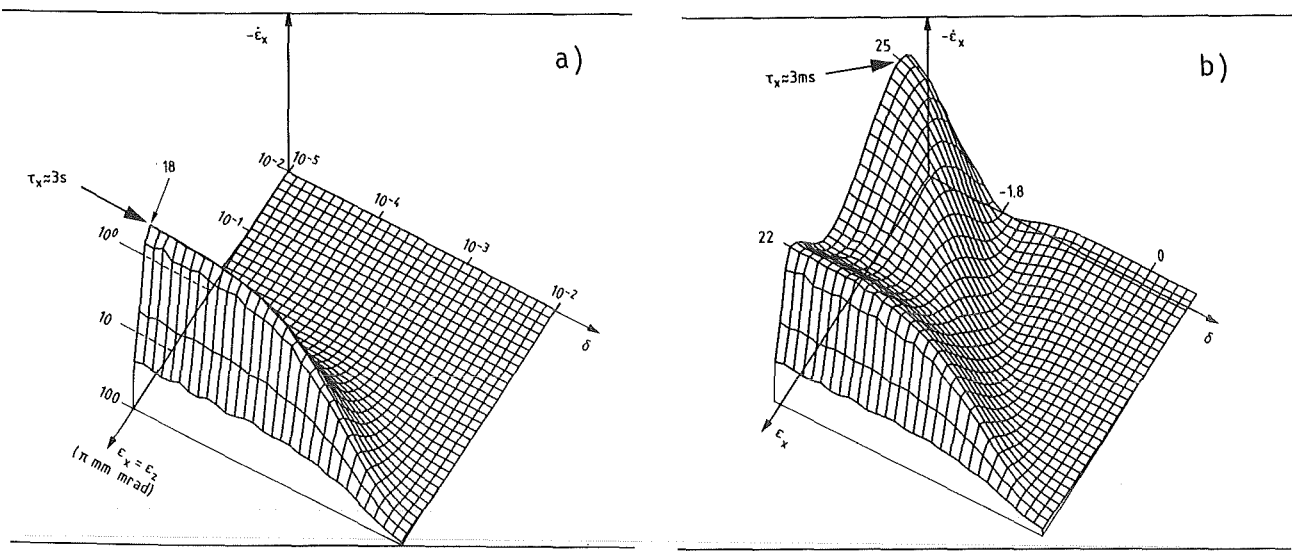
For large oscillation amplitudes, the linear approximation is no longer applicable. However, we can perform the averaging numerically and calculate the emittance change for single passages of an ion through the cooling section. Here it is possible to take into account all the details of the cooling force, electron beam structure, and ion motion as discussed above. The calculation is repeated with the same values of the constants of motion but with varying phases. For obtaining the average emittance changes, we have to vary two phases for a coasting beam, three for a bunched beam.

A simple betatron phase advance [3] is performed with different horizontal and vertical tunes far from low-order resonances. A convergence check on the three results  $\dot{\epsilon}_x$ ,  $\dot{\epsilon}_z$ , and  $\dot{\epsilon}_s$  (5% precision) controls the total number of revolutions ( $10^2$  to  $10^3$ ).

Figure 5 shows results from such a calculation for a coasting beam, assuming the conditions of the half perveance gun in the ICE ring [6] with protons at  $\beta = 0.3$  (46 MeV). To reduce the number of independent variables for this presentation, equal horizontal and vertical action constants  $\epsilon_x = \epsilon_z$  are assumed. In a logarithmic scale,  $\epsilon_x$  and the momentum deviation  $\delta$  are plotted along the axes of the horizontal plane. The vertical axis of the diagram represents the cooling rate  $-\dot{\epsilon}_x$  in a linear scale.

Close collisions only

Close + distant collisions

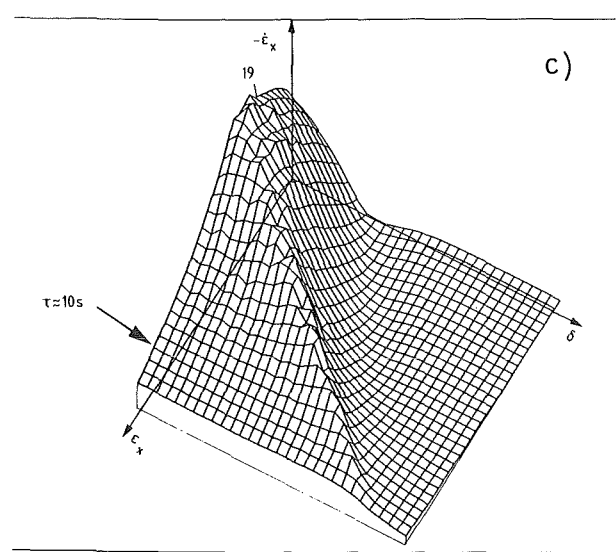


HORIZONTAL EMITTANCE CHANGE

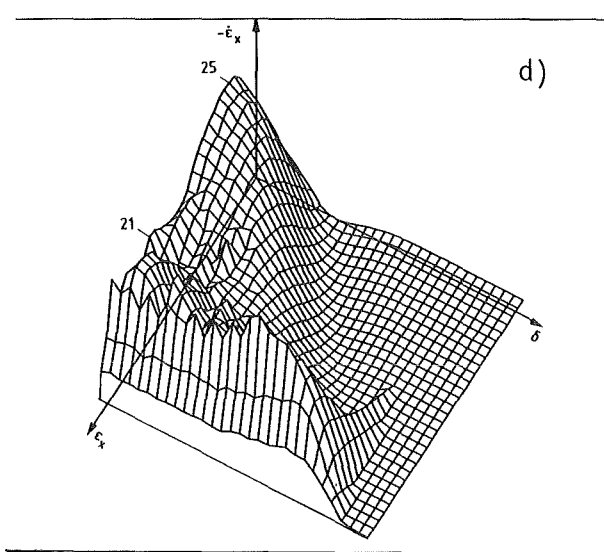
HORIZONTAL EMITTANCE CHANGE

Radial variation of electron beam properties included

Dispersion function at the cooler included  
 $D = 9.6 \text{ m}$     $D' = 0$



HORIZONTAL EMITTANCE CHANGE



HORIZONTAL EMITTANCE CHANGE

**Fig. 5** Numerically calculated cooling rates (discussed in the text). Some significant values of  $-\dot{\epsilon}_x$  (in  $\pi \text{ mm} \cdot \text{mrad s}^{-1}$ ) are indicated by numbers.

In Fig. 5, graphs (a) and (b), a homogeneous electron beam without focusing errors but with the flattened thermal distribution for a cathode temperature of 1300 K is assumed. The dispersion function at the cooler is set to 0. Figure 5a shows the cooling rate neglecting adiabatic collisions; it drops proportionally to  $\epsilon_x$  at  $\epsilon_x = 10\pi \text{ mm}\cdot\text{mrad}$  and below, and is reduced for large momentum deviation. In Fig. 5b, adiabatic collisions are allowed for; they lead to a drastic decrease of the cooling time  $\tau_x = -\dot{\epsilon}_x/\epsilon_x$ , as marked. The anisotropy of the adiabatic collisions manifests itself by the excitation of betatron oscillations for a certain ratio of momentum spread and emittance, so that a valley with  $-\dot{\epsilon}_x < 0$  can be seen.

Graphs (c) and (d) show how Fig. 5b changes if more details of electron and ion motion are taken into account. Figure 5c demonstrates the reduction of the cooling rate by the systematic variation of the electron beam properties over its cross-section, as described in Section 2.3. Figure 5d, on the other hand, shows the influence of a dispersion at the cooler, but for a homogeneous electron beam. The cooling rate is not influenced strongly by the ring dispersion alone. However, additional horizontal cooling occurs if the horizontal betatron oscillation crosses the beam edge. More coupling effects occur if the conditions of graphs (c) and (d) apply simultaneously, as in the real case. The influence of technical imperfections on the cooling rate can be taken into account by varying related parameters during the averaging procedure. In the simulations described below, this has been practiced for magnetic field angle and high-voltage fluctuations.

#### 4.2 Simulation of beam cooling

For the simulation of beam cooling we represent the ion ensemble by a sample of particle coordinates, set up randomly according to a distribution function. In principle, the time evolution of the particle distribution under the influence of electron cooling can be found from the momentum changes in the cooler, as calculated for each ion during each passage through the electron beam. By repeating this calculation for many revolutions of the ions, we can simulate the cooling-down of a hot ion beam after injection into a storage ring, or the reaction to specific disturbances of the ion beam in the presence of electron cooling. The most typical advantage of this simulation would be to display details of the shape of the ion beam distribution function. However, particular care is needed to avoid artefacts if such details are to be trusted.

Beam cooling being a slow process with respect to the period of the circular ion motion, the time interval over which we want to carry on the simulation represents millions of revolutions in the storage ring. Therefore, the essential step which makes the calculations feasible is to reduce the number of single-passage calculations. One easy method for arriving at a lower number of computed turns was outlined by M. Bell [3] but it required artificial limits to the cooling force. The approach to an equilibrium state could not be simulated with this method.

A procedure we find more transparent works explicitly with the slow rates of change for the action constants of each ion. These single-particle cooling rates  $\dot{\epsilon}$  were calculated above by averaging over  $10^2$  to  $10^3$  revolutions. We consider these rates approximately fixed over a time interval  $T$  for which about 50 ms proved to be an adequate choice. With the cooling rates obtained, we perform the linear extrapolation

$$\epsilon(t + T) = \epsilon(t) + \dot{\epsilon}T$$

for each ion and each space direction  $x, z, s$ . The time interval must be small enough to satisfy  $|\dot{\epsilon}T| \ll \epsilon$ . The given interval was adequate if the magnetic field angle variations and high-voltage fluctuations relevant in practice were taken into account in the rate calculation.

We note that, with the single-particle cooling rates, we have determined the phase-averaged [2] Fokker-Planck coefficients for friction due to electron cooling. By introducing corresponding coefficients for other scattering processes in the storage ring, we can also describe their influence on the ion beam, and simulate the approach to an equilibrium. In general, an emittance growth is accompanied by an essential particle diffusion, which can be taken into account as a fluctuation in the rates  $\dot{\epsilon}$  when the particle action constants are reset after the time interval  $T$ .

For the scattering on the residual gas the Fokker-Planck coefficients for the emittance change and its fluctuation are easily determined (see, for example, Ref. 2). The intrabeam scattering of the ions is harder to describe in this framework; at present we apply beam growth rates as calculated for Maxwellian distributions by Piwinski [9].

The computer simulation code which employs the method sketched above, will be described in more detail elsewhere [4]. Here we present some results for a coasting ion beam obtained with parameters corresponding to the ICE storage ring at 46 MeV operating with electron cooling at 'half perveance' [6]. A computer listing of the parameters is reproduced in Fig. 6. In Fig. 7, the coordinates of the 100 sample protons are indicated by dots in pairs of frames which represent the ion beam state every 0.5 s. The lower frame of each pair shows the beam cross-section. In the upper frame, the correlation between the horizontal coordinate and the momentum deviation of the protons is displayed. The lines in this frame show the dispersion of the storage ring at the cooling section (straight) and the space-charge velocity profile of the electrons (parabola).

By averaging the action constants of the protons, the beam emittances  $E_x, E_z$  and the momentum spread  $\sigma_p$  are found as a function of the time after the injection of a hot proton beam (Fig. 8). These curves can be compared with the ICE results [6]. It is found that the initial cooling-down times agree well with the observations. Also the equilibrium momentum spread is in good agreement, but the transverse beam divergence found experimentally is higher by a factor of 4. However, some excitation modes of betatron oscillations, such as fluctuations of the magnetic guiding field of the storage ring, could not be included in the simulation. In view of these uncertainties, the agreement seems quite satisfactory.

## 5. CONCLUSIONS

We have discussed the process of electron cooling from the aspect of its practical realization. The present status of theory allows for a well-founded calculation of the friction force on ions in an electron beam. We have shown how, from the friction force, the cooling rates for ions and the evolution of an ion beam can be computed. In these calculations, attention must be paid to the electron beam structure and to technical imperfections which finally limit the cooling efficiency. The consequences of technical imperfections can be studied with the computer simulation. Scattering processes leading to beam blow-up in a storage ring can be included. With these possibilities, the calculations may find an application for the study of experiments with stored particle beams, as, for example, with an internal target at LEAR.

#### RING PARAMETERS

|                       |             |            |          |
|-----------------------|-------------|------------|----------|
| RING MOMENTUM         | 299.60      | MEV/C      | (PMEVC ) |
| RING CIRCUMFERENCE    | 74.380      | METER      | (CIRCUM) |
| TRANSITION GAMMA      | 1.3000      |            | (GAMTR ) |
| BETATRON TUNE HOR     | 10.700      | RADIANS    | (QH )    |
| BETATRON TUNE VERT    | 7.3000      | RADIANS    | (QV )    |
| ACCEPTANCE HOR        | 75.000      | PI MM MRAD | (ACCEPH) |
| ACCEPTANCE VERT       | 30.000      | PI MM MRAD | (ACCEPV) |
| MOMENTUM ACCEPTANCE   | 1.8000      | 1/1000     | (ACCEPP) |
| NUMBER OF STORED IONS | 1.00000E+08 |            | (PSTORD) |
| RESIDUAL GAS PRESSURE | 1.00000E-09 | TORR N2    | (PTORR ) |

#### DEVICES / LATTICE PARAMETERS

##### ELECTRON COOLER

|                           |        |       |          |
|---------------------------|--------|-------|----------|
| POSITION ON CIRCUMFERENCE | 0.     | METER | (POSITN) |
| BETATRON PHASE HOR        | 0.     | RAD   | (PHASEH) |
| BETATRON PHASE VERT       | 0.     | RAD   | (PHASEV) |
| BETA FUNCTION HOR         | 3.0000 | METER | (BETAH ) |
| BETA FUNCTION VERT        | 11.000 | METER | (BETAV ) |
| DERIV. OF BETA HOR        | 0.     |       | (ALPHAH) |
| DERIV. OF BETA VERT       | 0.     |       | (ALPHAV) |
| DISPERSION FUNCTION       | 5.7000 | METER | (DISFCT) |

#### ELECTRON COOLING PARAMETERS

|                             |             |            |          |
|-----------------------------|-------------|------------|----------|
| BEAM RADIUS                 | 25.400      | MM         | (ERADI ) |
| BEAM LENGTH                 | 3.0000      | METER      | (ELEN )  |
| CENTER MOMENTUM DETUNING    | 0.          | 1/1000     | (EDTUNE) |
| PERVEANCE                   | .31500      | MICROPERVS | (EPERV ) |
| MAGNETIC FIELD              | 500.00      | GAUSS      | (EBGAUS) |
| CATHODE TEMPERATURE         | .12000      | EV         | (ETMPEV) |
| FLATTENING FACTOR           | 30.000      |            | (EFLATT) |
| TRANSV. ENERGY AT CENTER    | 3.00000E-02 | EV         | (ETRCEN) |
| TRANSV. ENERGY AT PERIPHERY | 1.0000      | EV         | (ETROUT) |
| BEAM DISPLACEMENT HOR       | 0.          | MM         | (EDSPLH) |
| BEAM DISPLACEMENT VERT      | 0.          | MM         | (EDSPLV) |
| BEAM ANGLE HOR              | 0.          | MRAD       | (EANGH ) |
| BEAM ANGLE VERT             | 0.          | MRAD       | (EANGV ) |
| ANGLE VARIATION ALONG BEAM  | .30000      | MRAD RMS   | (EARMS ) |
| ACCELERATION VOLTAGE NOISE  | 5.00000E-02 | 1/1000 RMS | (ENOISE) |

#### CALCULATED PARAMETERS

|                        |             |            |  |
|------------------------|-------------|------------|--|
| REVOLUTION FREQUENCY   | 1.22600E+06 | 1/SEC      |  |
| ELECTRON BEAM ENERGY   | 25418.      | EV         |  |
| ELECTRON BEAM CURRENT  | 1.2765      | AMP        |  |
| P.F. ELECTRON DENSITY  | 4.10643E+13 | 1/CUB.MET. |  |
| SPACE CHARGE POTENTIAL | 125.81      | VOLT       |  |
| CYC.FREQ/PLASMA FREQ.  | 23.173      |            |  |
| CYC.FREQ/TWIST FREQ.   | 983.02      |            |  |

Fig. 6 Parameter set for the simulation of proton beam cooling at JCE.

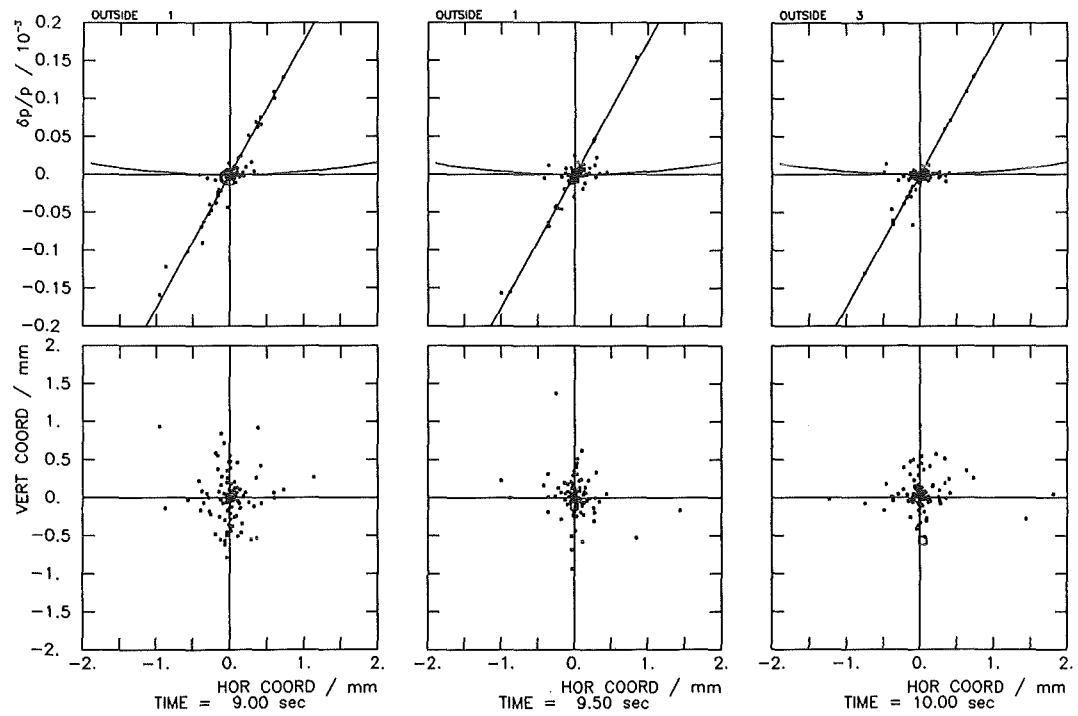
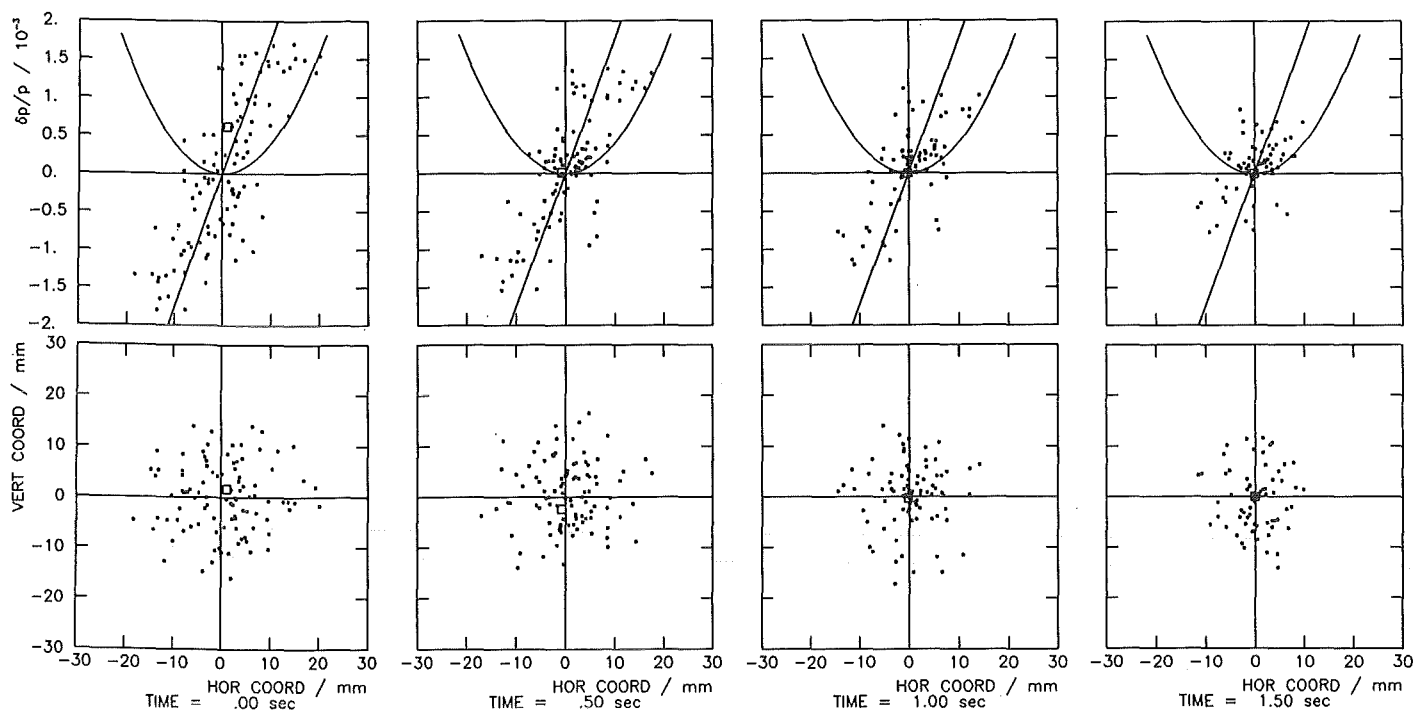


**Fig. 7** Proton coordinates during the simulation of cooling down a hot proton beam (explained in the text).

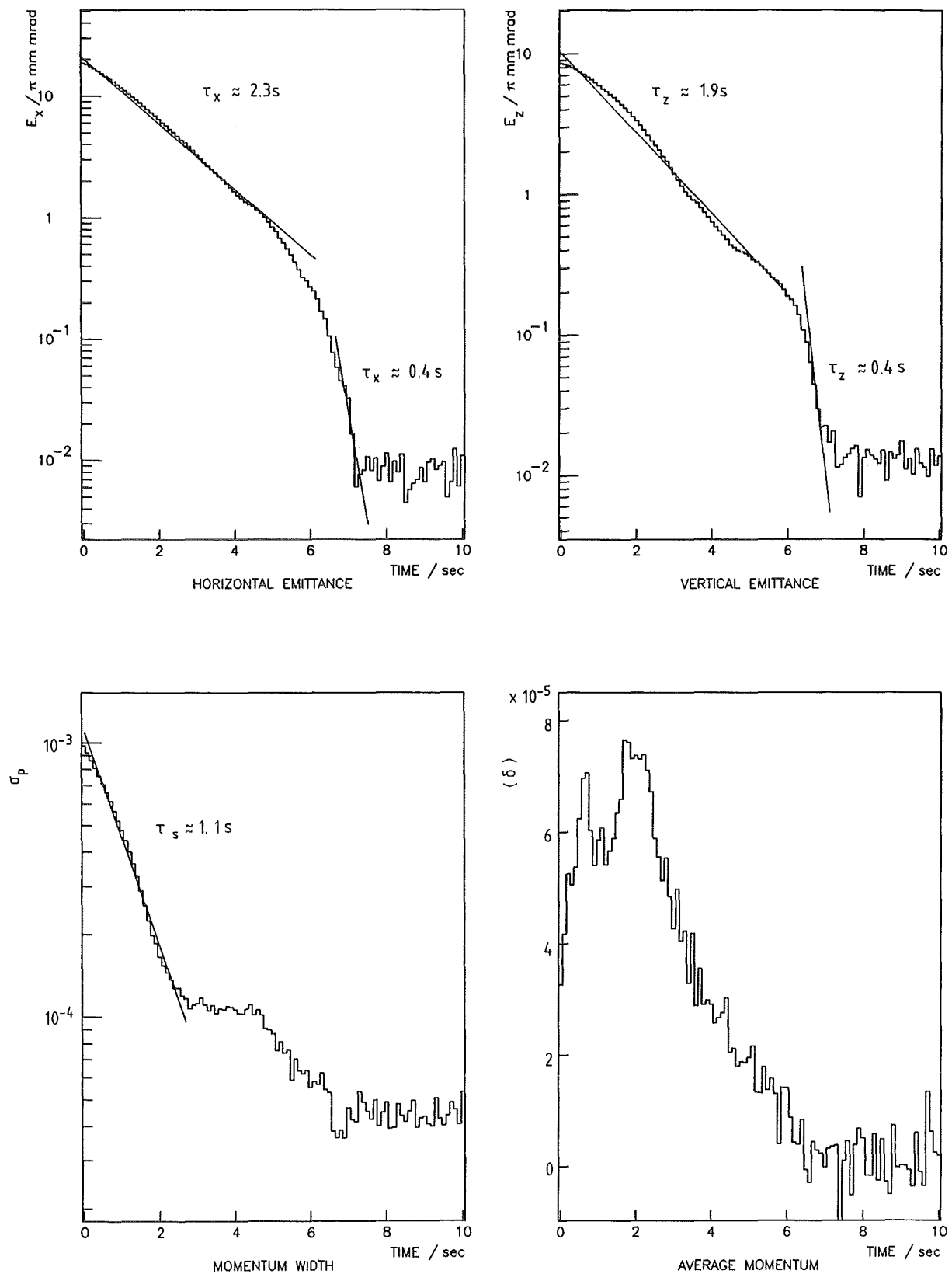


Fig. 8 Time dependence of averaged proton beam properties during simulation. The emittances contain 63.2% of the beam particles for a Maxwellian beam profile.

#### REFERENCES

- [1] A.H. Sørensen, Introduction to the theory of electron cooling, these proceedings.
- [2] Ya.S. Derbenev and A.N. Skrinskij, Part. Acc. **8** (1977) 1.
- [3] M. Bell, CERN EP Internal report 79-10 (1979).
- [4] H. Poth, A.H. Sørensen and A. Wolf, Simulating electron cooling of ion beams, in preparation.
- [5] V.I. Kudelainen, V.A. Lebedev, I.N. Meshkov, V.V. Parkhomchuk and B.N. Sukhina, Preprint INP (Novosibirsk) 82-78 (1982).
- [6] M. Bell, J. Chaney, H. Herr, F. Krienen, P. Møller-Petersen and G. Petrucci, Nucl. Instrum. Methods **190** (1981) 237.
- [7] Ya.S. Derbenev and A.N. Skrinskij, Part. Acc. **8** (1978) 235.
- [8] A.H. Sørensen and E. Bonderup, Nucl. Instrum. Methods **215** (1983) 27.
- [9] A. Piwinski, Proc. 9<sup>th</sup> Int. Conf. on High-Energy Accelerators, Stanford, 1974 (US Atomic Energy Commission, Washington, 1974), p. 405.



Ultra Relativistic Electron Cooling to Improve the Luminosity  
and Lifetime of  $\bar{p}p$  Colliders\*

David B. Cline

Physics Department  
University of Wisconsin  
Madison, WI 53706 U.S.A.

Electron cooling techniques can be divided up into three energy regions of the electron beam and the corresponding proton or antiproton beams that are being cooled:

1. [10-300] KeV to cool low energy beams in low energy storage rings or to help with the accumulation of decelerated antiprotons.
2. [1/2-10] MeV to cool intermediate energy protons or antiprotons in storage rings or to improve the emittance of antiproton sources.<sup>1</sup>
3. [greater than 200 MeV] to cool antiprotons or protons in high energy storage rings such as the SppS or FNAL TeV  $\bar{p}p$  collider.

The use of high energy cooling techniques has been discussed for sometime but there are no plans for the construction of such devices. Nevertheless these techniques could find a useful purpose in a few years after the  $\bar{p}p$  collider at FNAL is operating. High Energy Electron

---

\*Invited talk at the Karlsruhe Electron Cooling Workshop (E Cool 84).

cooling may also be important to cool heavy ions to improve the luminosity and lifetime in heavy ion colliding beam machines.

In this note we review the progress in these cooling calculations during the past few years. The luminosity of a high energy  $\bar{p}p$  collider is given by:

$$L = 5.6 \times 10^{22} \frac{(\Delta\nu)_{\max}}{\beta^*} N_{\bar{p}} \text{ cm}^{-2} \text{ sec}^{-1}$$

where  $N_{\bar{p}}$  is the total number of  $\bar{p}$  in the storage ring,  $\beta^*$  is the  $\beta$  at the collision point and  $(\Delta\nu)_{\max}$  is the beam-beam tune shift. The goal of high energy beam cooling is to increase  $(\Delta\nu)_{\max}$  by an order of magnitude thus gaining an order of magnitude in the luminosity. A secondary goal is to reduce the effects of intrabeam scattering-heating effects that decrease the luminosity lifetime. It may also be possible to increase the luminosity of ep machines like HERA by cooling the proton beam down to the same emittance as the electron beam.

The possible success of high energy electron cooling was reported in references 2 through 5 given here. The most recent calculations indicate that these are two possible solutions for the cooling device:

1. A medium energy storage ring of energy 200-500 MeV with specially designed wigglers.<sup>5</sup>
2. A very high intensity electron linac (see the report of A. Ruggerio in reference 3).

Skrinsky has proposed the use of a magnetic field in the cooling straight section to stimulate fast electron cooling in the same was as is observed in low energy electron cooling.<sup>4</sup>

Further information on the possibility of usefulness of high energy cooling can be found in the report of Ruggerio.<sup>6</sup>

References

1. See the report by Del Larson at this meeting.
2. Papers by C. Rubbia, D. Berley, M. Month, and A. Ruggerio, The Workshop on High Luminosity Antiproton-Proton Collision, LBL, 1978.
3. Proceedings of the Workshop on High Energy Electron Cooling, held at Madison, Wisconsin, Edited by D. Cline, 1979.
4. Proceedings of the Beam Cooling Workshop, held at Madison, Wisconsin, 1982.
5. D. Cline, A. Garren, H. Herr, F. Mills, C. Rubbia, A. Ruggerio, and D. Young. IEEE Trans. Nucl. Sciences Vol. NS-26, 3, 3472 (1980).
6. A. Ruggerio, report to this conference.

REVIEW OF ELECTRON COOLING EXPERIMENTS

H. Poth<sup>\*)</sup>

Kernforschungszentrum Karlsruhe

Institut für Kernphysik

Karlsruhe

Federal Republic of Germany

ABSTRACT

The principal results of electron cooling experiments in Novosibirsk, CERN, and Fermilab will be reviewed. In these three laboratories cooling experiments were performed with stored protons at 1.5, 35, 46, 65, 85, 114, and 200 MeV. Transverse and longitudinal cooling times were measured under various conditions, and equilibrium beam properties were determined. The cooling of coasting and bunched beams was studied, and the stacking and accumulation of successive proton pulses were attempted.

1. INTRODUCTION

The use of an electron beam to compress the phase-space density of a stored proton beam was suggested by G. Budker in 1966 [1]. The first experiments began in the early seventies at the Institute for Nuclear Physics

---

<sup>\*)</sup> Visitor at CERN, Geneva, Switzerland.

(INP) in Novosibirsk [2]. The goal was to demonstrate the usefulness of this method to increase the phase-space density of stored beams and, if successful, to apply it to antiproton accumulation and the generation of intense antiproton beams for high-energy physics. Somewhat later electron cooling experiments were started with similar intentions at CERN and at Fermilab.

It turned out that stochastic cooling was more suitable for mastering this task at the required high beam energies. However, the detailed experimental studies, together with a good understanding of the dynamics involved, yielded many valuable results for the application of this method to a wide range of accelerator projects. Although it will still be used to cool antiprotons, its major application is found in cooler rings for light and heavy ions at medium energies.

In this paper we try to summarize the most important results from the first experimental studies in the three laboratories: INP in Novosibirsk, CERN, and Fermilab.

A glossary of symbols used throughout the text is found at the end of the paper.

## 2. THE COOLER RINGS

The electron cooling experiments were performed at the NAP-M ring in Novosibirsk, the Initial Cooling Experiment (ICE) ring at CERN, and the Fermilab cooler ring. All studies were done with stored proton beams in the energy range between 1.5 MeV and 200 MeV and beam intensities from  $10^6$  to  $10^9$  circulating particles. In Table 1 the basic parameters of the storage rings are summarized and in Fig. 1 the machine layout is shown.

Table 1  
Parameters of the electron cooling storage rings

|   | NAP-M               | ICE                | Fermilab            |
|---|---------------------|--------------------|---------------------|
| Circumference [m]                                 | 47                  | 74                 | 135                 |
| Operation energy [MeV]                            | 1.5-85              | 46                 | 114, 200            |
| Stored beam intensity                             | $10^6$ - $10^8$     | $10^6$ - $10^9$    | $5 \times 10^6$     |
| Average ring vacuum [Torr]                        | $5 \times 10^{-10}$ | $2 \times 10^{-9}$ | $1 \times 10^{-10}$ |
| Hor. and vert. acceptance [ $\pi$ mm mrad]        | 400, 200            | 80, 40             | 40, 20              |
| Longitudinal acceptance [%]                       | $\pm 1$             | $\pm 0.25$         | $\pm 1$             |
| Fraction of cooling section of ring circumference | 0.02                | 0.04               | 0.037               |
| Working point $Q_H$ , $Q_V$                       | 1.24, 1.34          | 1.71, 1.16         | 3.57, 5.57          |
| Average hor. $\beta$ -function [m]                | 6                   | 18                 |                     |
| $\beta_H$ in cooling section [m]                  | 5.2                 | 3                  | 25                  |
| $\beta_V$ in cooling section [m]                  | 5.2                 | 11                 | 40                  |
| Dispersion in cooling section [m]                 | 6                   | 5.7                | 0.1                 |
| Beam lifetime without cooling [s]                 | 1500 <sup>*)</sup>  | 200                | 60-100              |
| Transition $\gamma_t$                             | 1.2                 | 1.3                | 3.6                 |
| Reference   | 3                   | 4                  | 5                   |

\*) At 65 MeV.

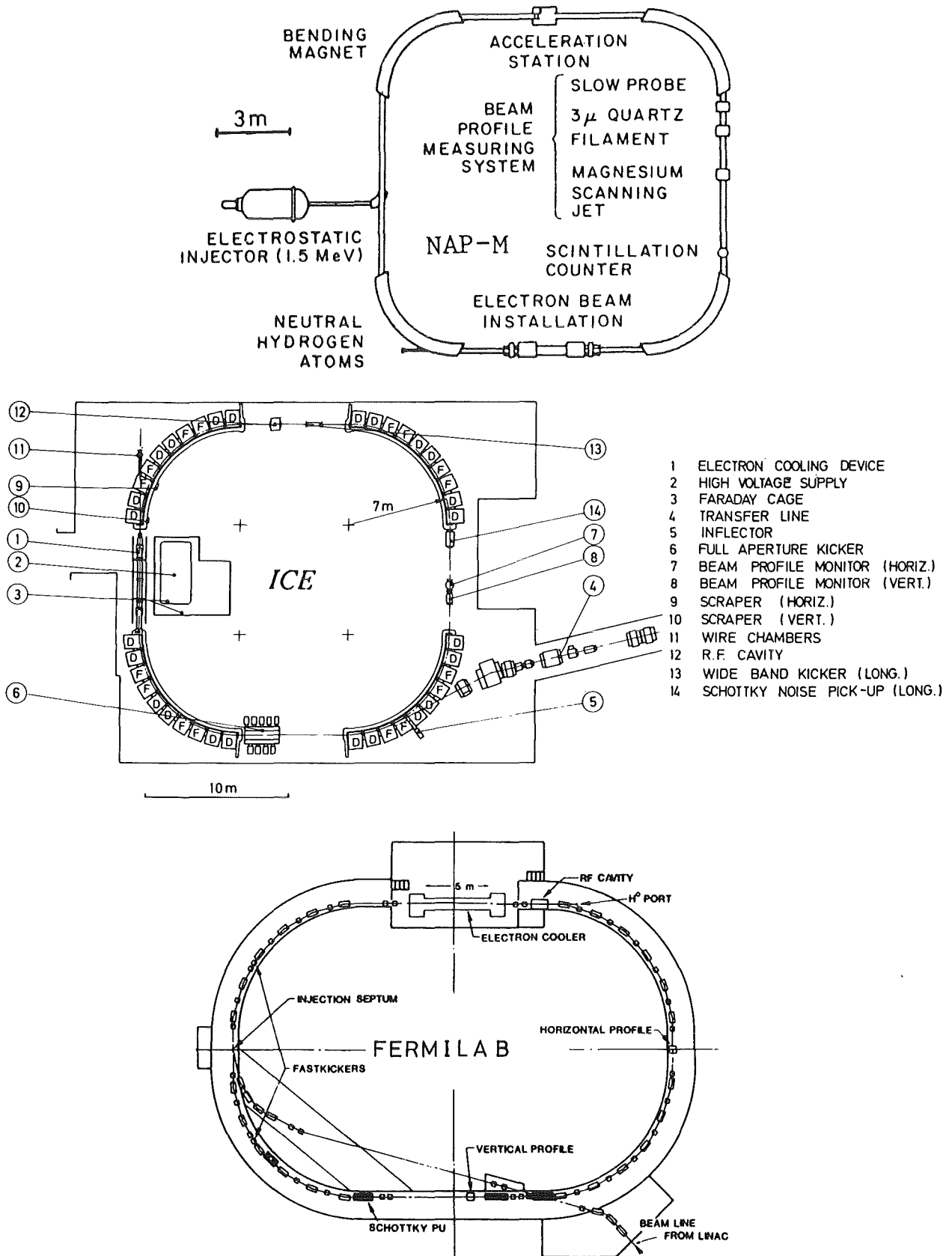


Fig. 1 The storage rings for studying electron cooling.

### 3. THE ELECTRON COOLING DEVICES

The electron cooling devices of the first-generation experiments had many common features, although there were some basic differences.

Electrons were emitted from a hot thermocathode on negative high potential, and accelerated through a ring anode structure to the desired energy which they reached when entering the long drift region. Solenoidal and toroidal magnetic fields transported the electron beam through the cooling region to the collector. There the electrons were decelerated to a few thousand volts and re-collected. Whilst in Novosibirsk and at CERN the electron gun consisted of a flat cathode immersed in the solenoidal field, Fermilab used a spherical cathode and converging geometry. Also the collector designs were quite different. Whilst Novosibirsk and Fermilab used a geometry similar to the electron gun, in ICE a rapid electron deceleration in a tapering magnetic field with radial deflection was applied. In Table 2 the basic parameters of the cooling devices are summarized. The experiments were performed under various conditions and Table 2 shows some typical values. The cooling at the highest energies was done at Fermilab, whilst the group in Novosibirsk studied the process at a variety of energies under many different conditions. At CERN intensive studies were done at 300 MeV/c with a large proton beam at high intensity.

In Fig. 2 schematic drawings of the electron cooling devices are shown.

Table 2

Electron cooler parameters

|   | NAP-M          | ICE                       | Fermilab       |
|---|----------------|---------------------------|----------------|
| Cathode diameter [cm]                       | 1, 2           | 5                         | 10             |
| Beam diameter [cm]                          | 1, 2           | 5                         | 5              |
| Electron energy [keV]                       | 0.7-46         | 26                        | 62, 111        |
| Electron current [A]                        | 0.1-0.8        | 0.6, 1.3, 2.2             | 0.5-3          |
| Electron density [ $10^8 \text{ cm}^{-3}$ ] | 0.09-3.7       | 0.2, 0.4, 0.8             | 0.1-0.6        |
| Magnetic field [kG]                         | 1              | 0.5                       | 0.7, 0.93      |
| Toroidal angle [°]                          | 45             | 30                        | 90             |
| Length of cooling section [m]               | 1              | 3                         | 5              |
| Gun-collector voltage [kV]                  | ~ 1            | ~ 1.2                     | ~ 1            |
| Electron current losses                     | $\leq 10^{-4}$ | $\sim 2.5 \times 10^{-2}$ | $\leq 10^{-4}$ |
| References                                  | 3              | 4                         | 5              |

|                      |                       |
|----------------------|-----------------------|
| 1 ELECTRON GUN       | 6 COLLECTOR           |
| 2 GUN SOLENOID       | 7 ION PUMP            |
| 3 TOROID             | 8 CORRECTION DIPOLE   |
| 4 CENTRAL SOLENOID   | 9 Ti SUBLIMATION PUMP |
| 5 COLLECTOR SOLENOID | 10 MICROWAVE ANTENNA  |

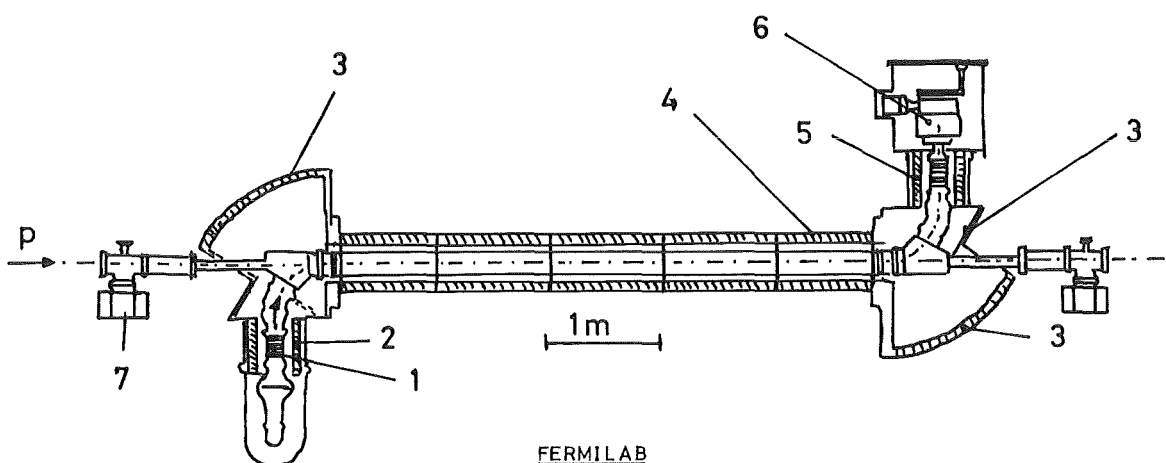
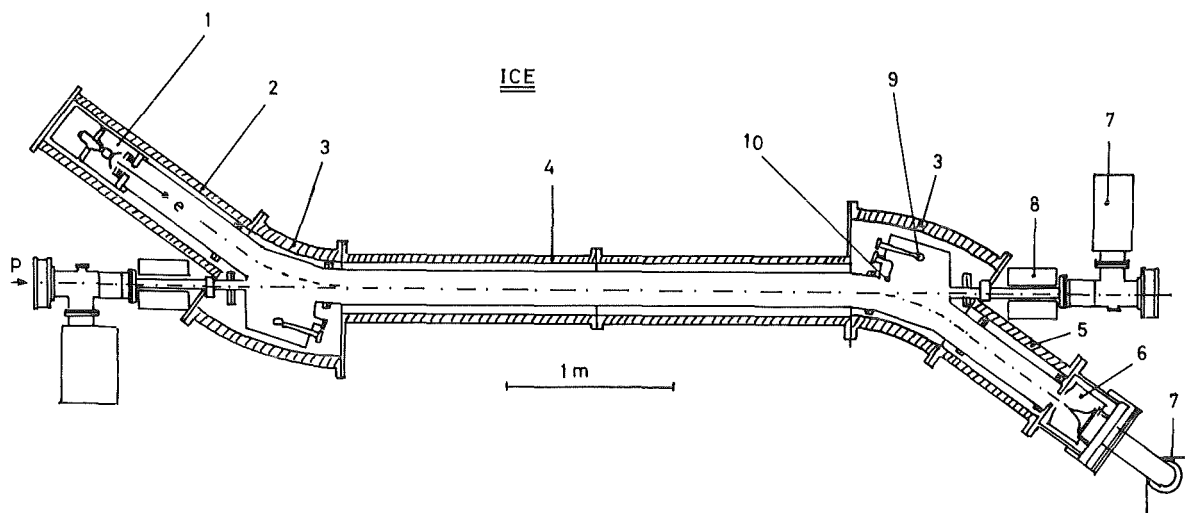
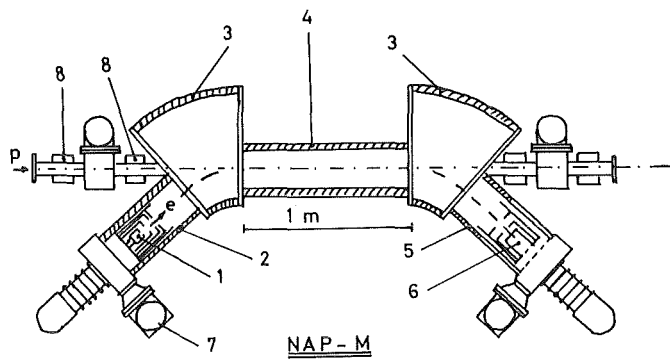


Fig. 2 The electron cooling devices.

#### 4. COOLING FORCES AND COOLING TIMES (pedestrian view)

Naïvely, electron cooling can be considered in the rest frame of the electrons as a moderation (energy loss) of a proton beam in a free electron gas. The cooling (friction) force  $F$  is given by the proton energy loss  $dE/dx = -F$  and scales, for large proton velocities  $v$ , as  $F \sim v^{-2}$ . For frozen electrons it would diverge for  $v \rightarrow 0$ . However, the electrons have a finite temperature [velocity distribution  $f(\vec{v}_e)$ ], which leads to a linear decrease of the frictional force for ion velocities smaller than the average electron velocity. The frictional force is hence to be averaged over the electron velocity distribution:

$$\vec{F} \propto \int f(\vec{v}_e) (\vec{v}_e - \vec{v}) |\vec{v}_e - \vec{v}|^{-3} d^3 \vec{v}_e .$$

Moreover, electrons are magnetized by the longitudinal magnetic field.

Owing to the electrostatic acceleration of the electrons to their nominal energy, the longitudinal electron velocity spread is much smaller than the transverse one. The effect of the longitudinal magnetic field is to transform the transverse electron motion into rotations about the magnetic field lines. For distant collisions (large impact parameters, small ion velocities), the protons interact essentially with 'electron discs' whose size is determined by the gyroradius  $\varrho$ . Since the longitudinal electron velocity is very small, many encounters take place during the passage of the proton through the electron beam. This effect gives rise to an additional frictional force, the magnetic force, which leads to an enhancement of the cooling force at small proton velocities. The onset of the linear decrease now only starts at the point where the proton velocity becomes smaller than the longitudinal velocity spread of the electrons. Derbenev and Skrinsky [6] considered this effect in detail and derived the non-magnetic  $F^0$  and magnetic  $F^M$  forces. In view of the following discussion

of experimental results, a short summary of their calculations is given. For proton velocities larger than the transverse electron velocity spread  $\Delta_{e_T}$ , they give:

$$I. \quad v > \Delta_{e_T} \quad \vec{F}^0 \propto -\vec{v}|v^{-3}| \rightarrow |\vec{F}^0| \propto -v^{-2},$$

and, for small proton velocities:

$$II. \quad v \ll \Delta_{e_T} \quad \vec{F}^0 \propto -\vec{v}\Delta_{e_T}^{-3} \rightarrow |\vec{F}^0| \propto -|v|.$$

In this domain the magnetic cooling force behaves as

$$II.a) \quad v \gg \Delta_{e_L}$$

$$\vec{F}_T^m \propto -(v_T^2 - 2v_L^2)v^{-5}\vec{v}_T \rightarrow |\vec{F}_T^m| \propto -v^{-2},$$

$$F_L^m \propto -v_T^2 v_L v^{-5} \rightarrow F_L^m \propto -v_L^{-4}.$$

$$b) \quad v < \Delta_{e_L}$$

$$\vec{F}^m \propto -\vec{v}\Delta_{e_L}^{-3} \rightarrow |\vec{F}^m| \propto -|v|.$$

The cooling time  $\tau$  is related to the force through  $\tau \propto v/F$ . Thus we can distinguish the following domains of cooling. For large proton velocities  $v > \Delta_{e_T}$  (hot proton beam), the cooling time increases as  $\tau \propto v^3$ ; for betatron amplitude cooling, for instance, that means that it increases with the third power of the proton beam divergence. If only the non-magnetic force would act, the cooling time would become constant for  $v < \Delta_{e_T}$  (exponential damping). However, for small proton velocities the magnetic force becomes important, which leads to a further decrease of cooling times for proton velocities decreasing below  $\Delta_{e_T}$ :

$$\Delta_{e_L} < v < \Delta_{e_T} \quad \tau \propto -v^3 \dots v^5$$

This effect is called superfast cooling (faster than exponential). Only when the proton velocity reaches values smaller than  $\Delta_{e_L}$  does the cooling time become constant:

$$v < \Delta_{e_L} \quad \tau = \text{constant}.$$

Another interesting effect appears in case II(a). If there the longitudinal proton velocity  $v_L$  is larger by a factor  $\sqrt{2}$  than the transverse velocity, the transverse magnetic cooling force is positive and leads to heating until  $v_T = \sqrt{2} v_L$ .

A simple formula for electron cooling times was given some time ago [3] and is frequently used:

$$\tau_e = k(\eta L r_p r_e j_e)^{-1} \cdot e \beta \gamma^3 (T_T/mc^2)^{3/2}, \quad (1)$$

where  $k = 0.6$  is used for a spherical Maxwellian electron velocity distribution and  $k = 0.16$  for a flattened distribution. The quantity  $T_T$  is the sum of the proton and the transverse electron temperatures. It is easily seen that this formula gives the right scaling for large proton velocities  $v \gg \Delta_{e_T}$  as  $T_{\text{proton}} \propto v^2$  and hence  $\tau \propto v^3$ . However, it neglects completely the magnetization effect since it gives a constant cooling time for

$$\Delta_{e_L} < v < \Delta_{e_T}.$$

## 5. EXPERIMENTAL RESULTS

### 5.1 Determination of cooling rates

#### a) Transverse cooling

Intensive measurements were performed to determine the transverse cooling rates and betatron amplitude damping decrements. Their dependence on the various parameters (transverse and longitudinal proton velocities,

transverse and longitudinal electron temperature, etc.) were investigated. Two different techniques were used. In one method the damping of the betatron amplitude of an initially hot (large emittance) beam for different settings of the electron cooling device was measured. This was achieved by observing the beam profiles at given time intervals. The other way was to excite betatron oscillations by a transverse kick of the beam and follow the damping of this coherent oscillation again through observation of beam profiles. In Fig. 3 the data are summarized by plotting the measured cooling times against the betatron amplitude (3a) and against transverse velocity differences between the electron and the

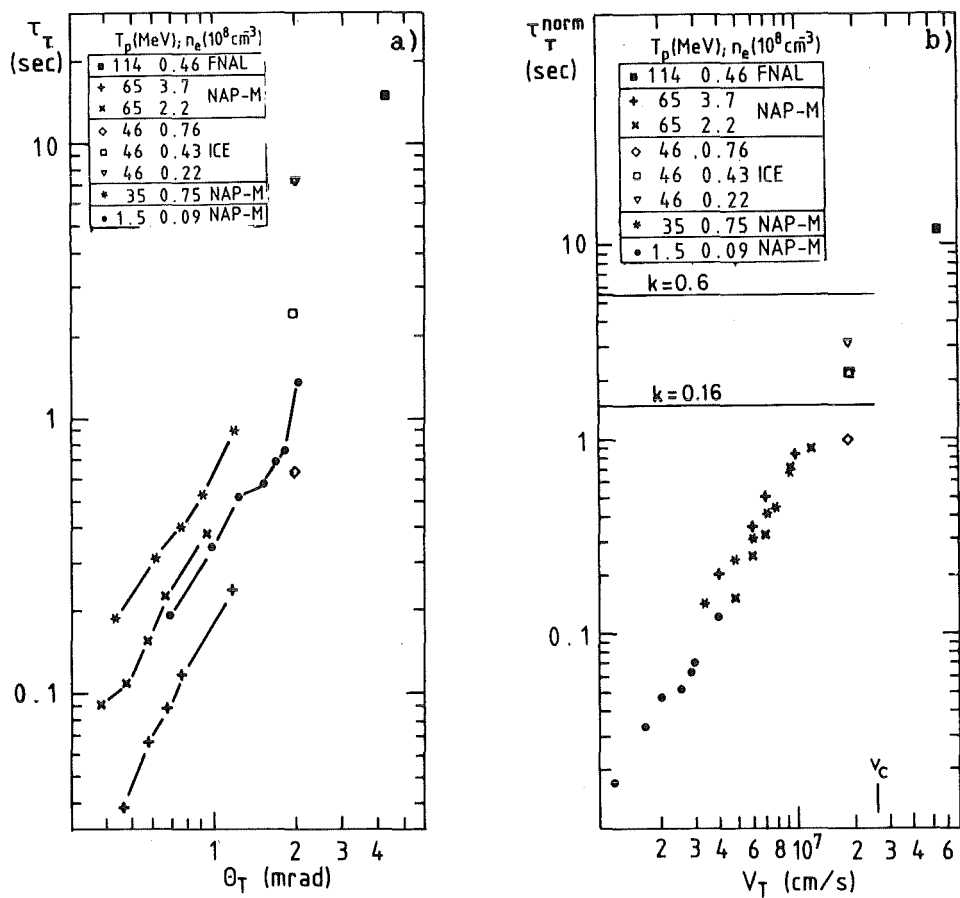


Fig. 3 Transverse cooling times: a) unnormalized cooling times plotted against betatron amplitude of beam; b) cooling times normalized to  $n_e = 10^8 \text{ cm}^{-3}$  and  $\eta = 0.02$  plotted against transverse beam velocity;  $v_c$  indicates the transverse electron velocity for a transverse electron temperature of 0.2 eV. Also shown are the cooling times calculated from formula (1) for  $T_T = T_{e_T}$  and  $L = 10$ .

proton beam (3b). In the latter case the cooling times are normalized to an electron density of  $n_e = 10^8 \text{ cm}^{-3}$  and a cooling section of  $\eta = 2\%$  of the ring circumference. One notes a very clear scaling of the cooling times with the transverse velocity.

The Novosibirsk group derived a semi-empirical formula (independent of beam energy) which reproduces the measurements very well [7]:

$$\tau_T = \frac{1}{66r_p r_e c^4 \eta n_e} (\alpha_0^2 v_0^2 + v_T^2 + 11v_L^2) \sqrt{v_C^2 + v_T^2 + v_L^2} .$$

One denotes two regimes of cooling. For a hot proton beam ( $v_T \gg v_C$ ), i.e. the domain of the non-magnetic cooling force, the cooling time scales as  $\tau_T \propto v_T^3$ ; on the other hand, for  $v_T \ll v_C$ , the transverse cooling time scales as  $\tau_T \approx 10^{-6} v_T^2$  (for  $v_T \geq v_L$ ). This is due to the onset of the magnetic force. Otherwise, one would expect that the cooling time would remain constant for  $v_T < v_C$  as the simple formula (1) predicts. The rapid decreasing of cooling times for small betatron amplitudes is frequently referred to as superfast cooling [8].

#### b) Momentum cooling

Similar to the measurement of the transverse cooling times, the longitudinal cooling was investigated. Three methods were applied. In the first one the proton beam was accelerated (decelerated) by increasing (decreasing) the electron energy, and the rate of proton beam energy change was measured. From this the longitudinal frictional force,  $F_L$ , and in turn the longitudinal cooling time  $\tau_L$ , was determined. Another method consisted in employing a longitudinal beam blow-up and making a subsequent observation of the cooling by measuring continuously the widths of the frequency spread of the circulating beam. In the third method a

radio frequency slightly different from the actual revolution frequency of the beam was applied. Then the electron energy was changed and by that means the protons were accelerated and finally captured in the RF bucket. The time needed to accelerate the protons to be captured is a measure for the longitudinal frictional force.

The results of the different measurements are summarized in Fig. 4, where in (a) the longitudinal force and in (b) the longitudinal cooling time are plotted against the longitudinal velocity difference.

Again a formula was derived [7] which describes the data rather well:

$$F_L = \frac{1}{12\pi r_e^2 n_e \eta m_e c^4} \left[ \left( \frac{\alpha_0^2}{4} v_0^2 + v_T^2 + v_L^2 \right) \left( \frac{v_c^2}{4} + v_T^2 + v_L^2 \right) \right]^{-1/2} .$$

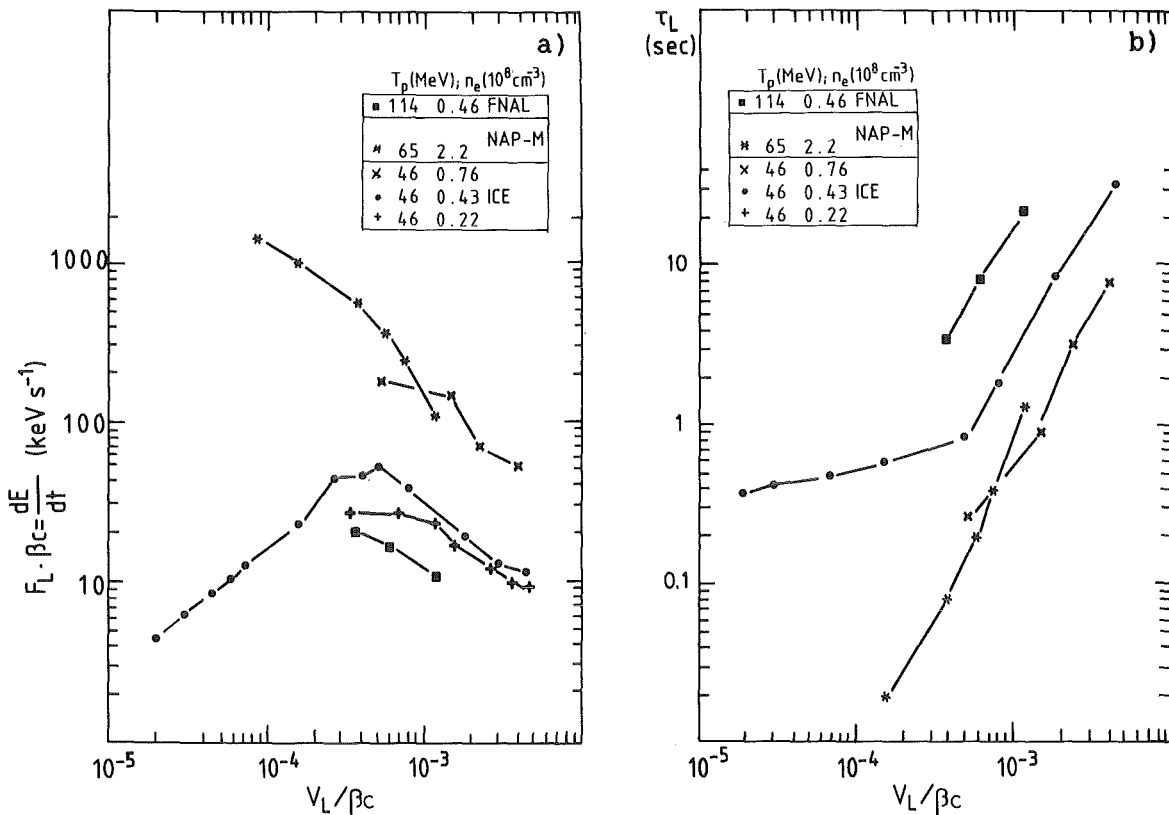


Fig. 4 Longitudinal cooling: a) Longitudinal drag force plotted against longitudinal electron-proton velocity difference divided by the beam velocity; b) Longitudinal cooling times plotted against the longitudinal electron-proton velocity difference divided by the beam velocity.

Again one denotes two regimes of cooling. For  $v_L \gg v_c$  the force decreases with  $v_L^{-2}$  and the cooling time scales as  $\tau_L \sim v_L^3$ . In contrast for  $v_L \ll v_c$  the force depends linearly on  $v_L$  and hence the cooling time is constant. Whether this regime is reached depends very strongly on imperfections due to misalignment or magnetic field errors characterized by  $\alpha_0$ .

The measurements can be summarized as follows. Cooling was investigated over a wide range of electron-proton velocity differences. The scaling of cooling times agrees well with theoretical predictions when magnetization is included. Deviations from the ideal situation have to be accounted for by correction terms. One can consider the basic prediction of the theory as confirmed. A detailed description of the evolution of beam properties in the presence of electron cooling has, however, to take into account lattice parameters, electron beam properties, imperfections, and other beam heating effects.

From the semi-empirical formula for cooling times one may, however, conclude the following for scaling cooling times with beam energy. For the same velocities and electron density, and negligible misalignment, the cooling time is constant at all energies, since

$$\tau \propto n_e^{-1} (\alpha_0^2 v_0^2 + v^2) \sqrt{v_c^2 + v^2} .$$

Expressing the velocities as  $v_0 = \beta c$  and  $v = \theta \beta c$  one finds

$$\tau \propto n_e^{-1} \beta^3 c^3 (\alpha_0^2 + \theta^2) \sqrt{\theta_e^2 e_T^2 + \theta^2} ,$$

which means

$$\tau \propto \begin{cases} \beta^3 \theta^3 & \text{for } \theta \gg \theta_{e_T} \\ \beta^3 \theta^2 & \text{for } \theta_{e_T} \ll \theta \end{cases} \quad \text{and fixed } \theta_{e_T}$$

For electron guns operating in constant perveance mode ( $I = P V^{3/2} \propto \beta^3 P$ ) the electron density scales as  $n_e = j_e / e \beta c \sim \beta^2 P$ . Hence the cooling times for constant electron and proton angles increase linearly with  $\beta$ :

$$\tau (\text{constant perveance}) \propto \beta (\alpha_0^2 + \theta^2) \sqrt{\theta_{e_T}^2 + \theta^2} .$$

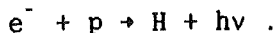
Since transverse electron temperature is essentially given by the cathode temperature, it is practically independent of the electron energy, i.e.  $v_c = \text{constant}$  and  $\theta_{e_T} \propto \beta^{-1}$ . Taking this into account one can state that the scaling of cooling times for constant perveance guns is

$$\tau (\text{constant perveance}) \propto \begin{cases} \text{const.}, \theta \ll \theta_{e_T}, \alpha_0 \ll \theta, \\ \beta, \theta \gg \theta_{e_T}. \end{cases}$$

In other words, for constant and small proton velocities in the rest frame, the cooling time is independent of  $\beta$  as the transverse electron temperature is fixed. For highly relativistic beams, one has to take into account also the dependence on  $\gamma$ , which was neglected here. The operation of a constant perveance gun has another advantage. The tune shift produced by the electrons is  $\Delta\nu = 0.5 \beta * r_p n_e \beta^{-2} \gamma^{-3}$ . Since  $n_e \sim \beta^2$  for constant perveance, the tune shift experienced by the proton beam is independent of the operation energy of the storage ring for  $\gamma \sim 1$ .

## 5.2 Measurement of the recombination rate

During the electron cooling, radiative capture of electrons by the protons takes place and hydrogen atoms are formed:



The hydrogen atoms leave the storage ring and can be detected. They represent an excellent non-destructive diagnostics means to monitor the cooling

process. The capture rate has been calculated by various authors [3, 9-11]. For a cooled beam it is, apart from other influencing factors, determined by the transverse electron energy. The capture rate for a longitudinal, cold electron beam  $T_{e_L} \ll T_{e_T}$  (flattened electron velocity distribution) is roughly a factor of  $\pi/2$  higher [10, 11] than for an electron beam with an isotropic velocity distribution of Maxwellian form ( $T_{e_L} = T_{e_T}$ ). Hence by measuring the hydrogen rate the average electron temperature can be determined. It is given by

$$R_H = \alpha_r n_e n N_p \gamma^{-2} .$$

The recombination coefficient is linked to the electron temperature. We use here the simplified relation given by Ref. 10:

$$\alpha_r = \begin{cases} 3.79 T_{e_T}^{-0.678} & \text{for Maxwellian distribution} \\ 7.88 T_{e_T}^{-0.645} & \text{for flattened distribution} \end{cases} \times 10^{-13} \text{ cm}^3 \text{ s}^{-1}$$

This relation is plotted in Fig. 5. Experimentally, recombination coefficients in the range  $0.8-2.3 \times 10^{-12} \text{ cm}^3 \text{ s}^{-1}$  were found in ICE and

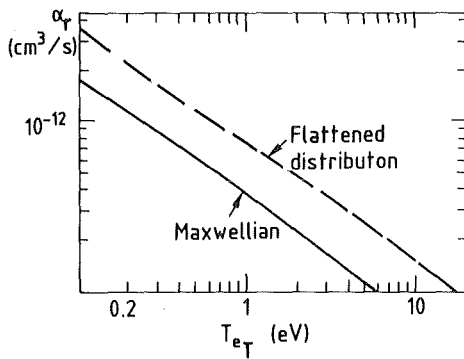


Fig. 5 Recombination coefficient of radiative electron capture plotted against electron temperature. Dashed line: flattened distribution. Solid line: Maxwellian electron velocity distribution.

at Novosibirsk, pointing to electron temperatures of 0.15-1 eV, in agreement with the observed cooling rates. It should be noted that a recombination coefficient of  $10^{-12} \text{ cm}^3 \text{ s}^{-1}$  corresponds to a recombination time constant of

$$\tau_{\text{rec}} = 3 \times 10^5 \text{ s} \text{ (for } \eta = 0.02 \text{ and } n_e = 10^8 \text{ cm}^{-3} \text{)} .$$

This has to be compared with cooling times of the order of 1 s, which shows that beam losses due to the radiative capture of cooling electrons by cooled protons are completely negligible. Since the cooling time decreases with A/Z and the recombination with  $z^{-1}$  (Z is the charge of the fully stripped ion) the recombination time can always be kept nearly a factor of  $10^3$  larger than the cooling time.

### 5.3 Equilibrium beam properties

The determination of equilibrium emittance and momentum spread provides information about the cooling force at small electron-proton velocities. In particular, the contribution of the magnetic force can be evaluated. Moreover, it is of practical interest as it shows which beam properties can be achieved under realistic conditions.

In practice, thermal equilibrium between the electron and the proton beam ( $T_e = T_p$ ) was rarely reached since other effects such as intrabeam scattering and machine imperfections led to beam heating. The equilibrium was then rather determined by the balance between the heating process and the cooling.

In the cooling experiments the beam sizes were measured with beam profile monitors and by the divergence from the spot size of the neutral hydrogen beam resulting from electron capture by protons in the electron cooler emerging from the cooling straight section. The equilibrium beam

momentum spread was determined from the Schottky noise induced in a pick-up by the coasting beam. Analysis of this signal in frequency gave characteristic peaks at revolution frequency and at higher harmonics. The widths of the peaks are related to the momentum spread through  $\Delta p/p = (\Delta f/f)\eta^*$ . Another method of determining the momentum spread was to kick out a part of the circulating beam and to measure the time until the void was filled up again.

The lowest beam sizes found in ICE were 2.3 mm (FWHM) with a divergence of 0.2 mrad for  $10^8$  circulating protons. In Novosibirsk a divergence of even 30  $\mu$ rad was found under favourable conditions. The lowest momentum spread measured in ICE was  $4 \times 10^{-5}$  for a proton intensity of  $8 \times 10^6$ . The equilibrium momentum spread depends, however, strongly on the number of stored protons as intrabeam scattering [12] tends to blow up the beam. There are several theoretical attempts to find the equilibrium between intrabeam scattering and cooling as a function of beam intensity [13-15]. For low beam intensity a new effect was observed in Novosibirsk, where the Schottky signal nearly disappeared, indicating an ordering effect in the proton beam [16].

#### 5.4 Cooling of bunched beams

Although most of the cooling experiments were performed with coasting proton beams, the cooling of bunched proton beams was successfully demonstrated in all three laboratories. After careful matching of the radio frequency to the electron-gun high voltage, cooling was observed and similar cooling times were found. Figures 6 and 7 show the frequency spectrum of the Schottky pick-up and the pulsed neutral hydrogen production of a cooled bunched beam.

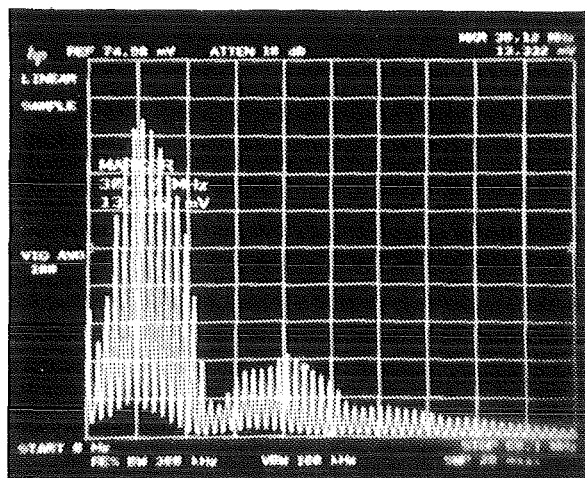


Fig. 6 Frequency spectrum (0-60 MHz) from Schottky pick-up electrode for a bunched cooled proton beam in ICE (bunched with first harmonics of revolution frequency, radio frequency voltage  $V_{RF} = 10$  V).

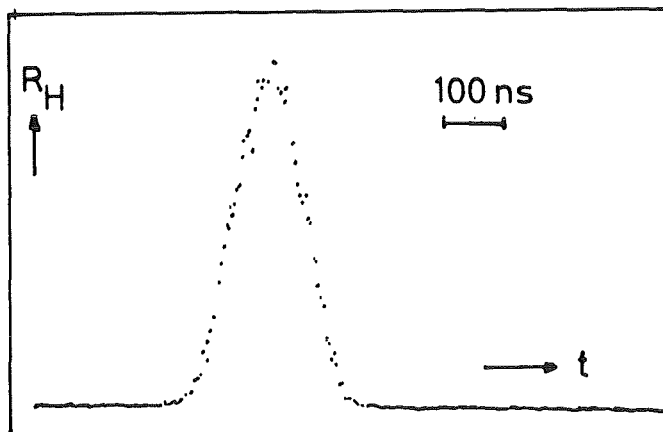


Fig. 7 Hydrogen formation rate as a function of the time difference to the RF signal for a bunched beam in ICE.

##### 5.5 Stacking and accumulation

The successful cooling of bunched beams allowed for attempts to be made to stack and accumulate successive proton pulses. This was studied at Fermilab and in ICE. In the latter case protons were captured in a RF bucket at the first harmonics of the revolution frequency. The RF voltage of about 10 V provided a bunching factor of 0.4. A new pulse was then injected into the remaining empty space, cooled and transferred to the bucket

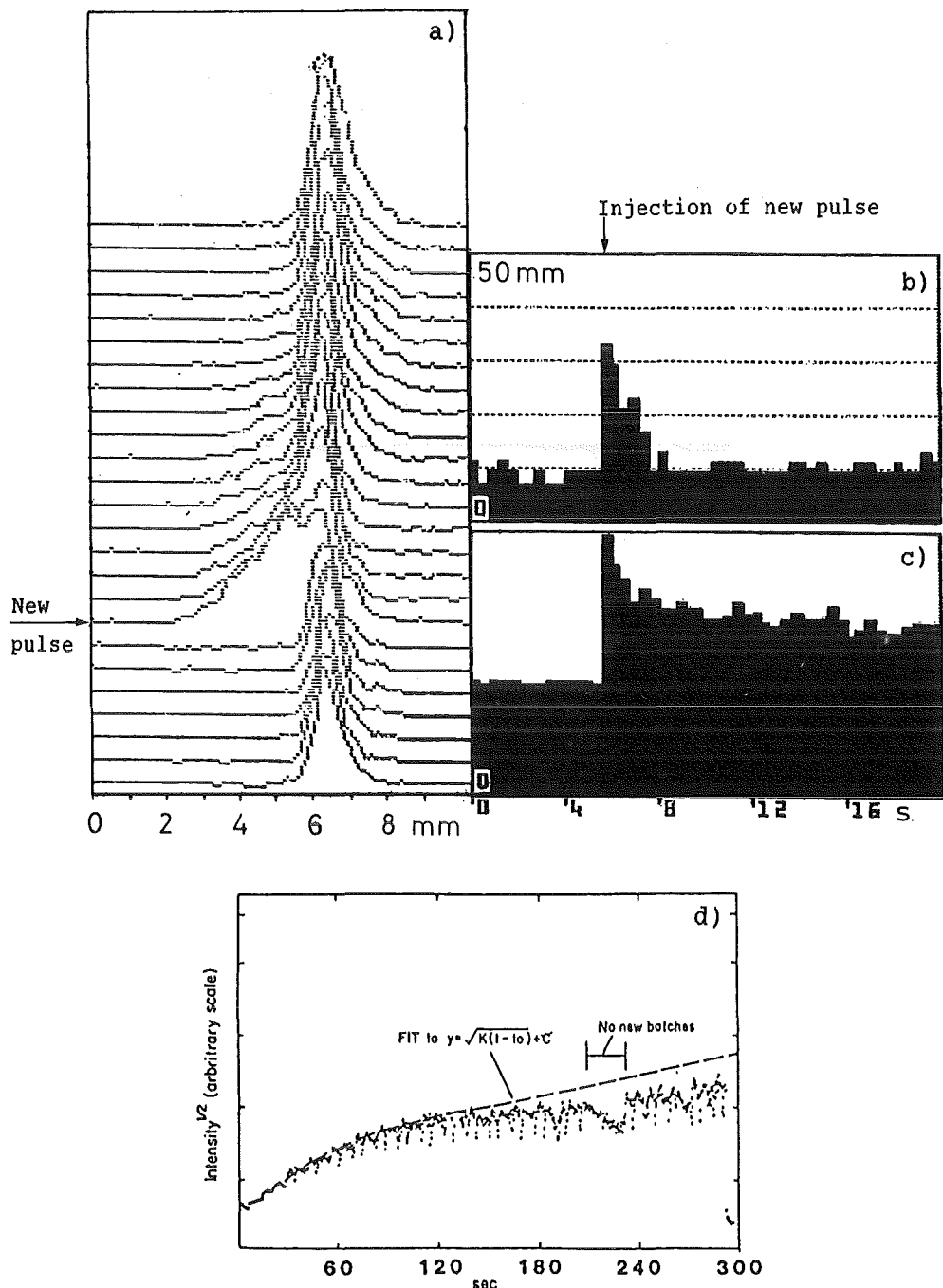


Fig. 8 a) Horizontal beam profiles of 800 ms time intervals; b) horizontal beam width and c) stored beam intensity, both plotted against time, showing stacking of a proton pulse in ICE; d) accumulation for beam injected every 5 s in the Fermilab cooler ring.

(Fig. 8). This was repeated several times. In this way the stored beam intensity was increased by roughly a factor of 20. The maximum beam intensity accumulated was  $2 \times 10^9$  protons, corresponding to 0.5 mA.

### 5.6 Instabilities

Instabilities of the stored cooled proton beams were observed in all three experimental studies. The reasons for the instabilities are not all completely understood. In ICE two major instabilities were encountered. One appeared during stacking and accumulation, and was intensity-dependent. Its threshold was around  $2 \times 10^9$  stored protons and its appearance led to a rapid beam loss. The other one appeared when operating ICE above transition and set in when the beam became cooler. It manifested itself in a self-bunching clearly visible in the Schottky frequency spectrum (Fig. 9) and in a pulsed hydrogen atom rate (Fig. 10). Bunches of 5 ns

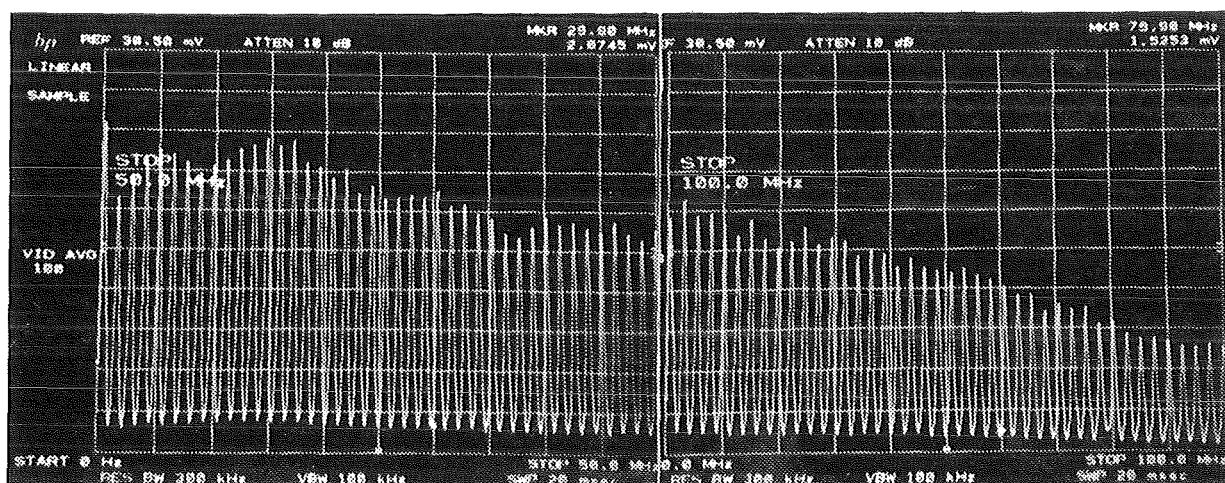


Fig. 9 Schottky frequency spectrum (0-100 MHz) of a self-bunched beam observed in ICE, when operating above transition ( $\gamma_t \approx 0.93$ ).

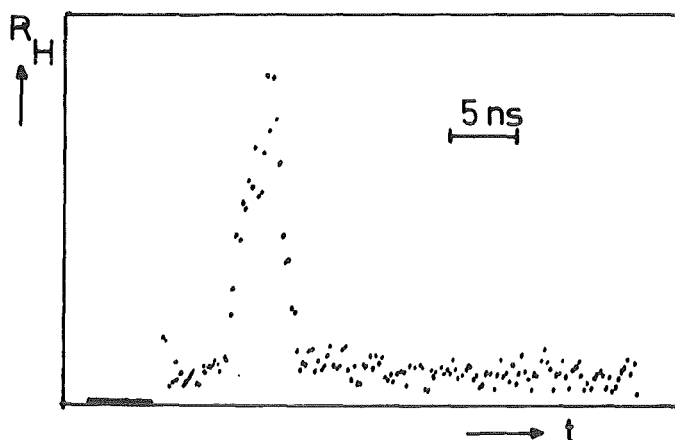


Fig. 10 Hydrogen rate as a function of time difference between a pick-up and a scintillator signal for a self-bunched proton beam in ICE.

length containing about 7% of the beam intensity were observed. The observations pointed to the negative mass or the microwave instability.

Summary

In the first experiments the dynamics of electron cooling and its dependence on the various parameters were studied in detail, leading to a good understanding of the process. There is a rather satisfactory agreement between theory and experiment.

The measurements were performed with proton beams in the energy range 1.5 MeV to 200 MeV, corresponding to beam velocities between 0.05c and 0.57c. There is an agreement between the data at all energies when the different conditions are taken into account.

The principal results show that the cooling of large emittance beams ( $\theta > \theta_{e_T}$ ) gives cooling times ( $\propto \theta^3$ ) between a few seconds and few tens of seconds. Cooling of small emittance beams ( $\theta_p < \theta_{e_T}$ ) is considerably enhanced by the magnetic cooling force, resulting in cooling times much below one second.

For low-intensity beams ( $10^6$ - $10^7$  stored protons) equilibrium divergences of the order of  $10^{-6}$ - $10^{-5}$  rad have been achieved. A relation between beam intensity and equilibrium momentum spread due to the counteracting of cooling and intra-beam scattering was experimentally established.

The technology for producing a high-quality electron beam for cooling can be considered as established for beam energies between a few hundred electron-volts and 100 keV. Electron cooling devices aiming at the MeV range are under study.

GLOSSARY

|                |   |
|----------------|---|
| $r_e$          | classical electron radius   |
| $r_p$          | classical proton radius   |
| $c$            | speed of light  |
| $n_e$          | electron density  |
| $\eta$         | ratio of cooling section length to ring circumference                         |
| $\eta^*$       | $\gamma_t^{-2} - \gamma^{-2}$   |
| $\beta$        | fraction of speed of light  |
| $\gamma$       | $= (1 - \beta^2)^{1/2}$   |
| $\gamma_t$     | transition energy $\gamma$ value  |
| $v_0$          | average velocity of the matched beams ( $= \beta c$ )                         |
| $v_c$          | transverse electron velocity (cyclotron velocity)                             |
| $v_T$          | transverse proton velocity  |
| $v_L$          | longitudinal proton velocity      } in the frame moving with $v_0$            |
| $\tau_T$       | transverse (betatron) cooling time  |
| $\tau_L$       | longitudinal (momentum) cooling time  |
| $\tau_{rec}$   | beam lifetime with respect to electron-proton recombination losses            |
| $F_L$          | longitudinal frictional (drag) force  |
| $F_T$          | transverse frictional force   |
| $m_e$          | mass of the electron  |
| $T_{e_T}$      | transverse electron temperature = $m_e \beta^2 \gamma^2 c^2 \theta_{e_T}^2$   |
| $\theta_{e_T}$ | $= v_c / \beta c$   |
| $T_{e_L}$      | longitudinal electron temperature   |
| $\theta$       | proton transverse angle = $v_T / \beta c$                                     |
| $\beta^*$      | average beta function of the storage ring                                     |
| $\Delta\nu$    | tune shift caused by the electron beam  |
| $\alpha_0$     | constant to account for magnetic field alignment error in the electron cooler |

P      perveance of electron gun  
e      elementary electric charge  
 $\Delta_{e_T}$     transverse electron velocity spread  
 $\Delta_{e_L}$     longitudinal electron velocity spread  
L      Coulomb logarithm  
 $j_e$     electron beam current density ( $= n_e \beta c e$ )

References

- 1) G.I. Budker, Proc. Int. Symposium on Electron and Positron Storage Rings, Saclay, 1966 (PUF, Paris, 1967), p. II-1-1.
- 2) G.I. Budker et al., Part. Accelerators 7 (1976) 197.
- 3) G.I. Budker and A.N. Skrinsky, Sov. Phys. Usp. 21 (1978) 277; Ya. Derbenev and I. Meshkov, CERN 77-08 (1977).
- 4) M. Bell et al., Nucl. Instrum. Methods 190 (1981) 237 and Phys. Lett. 87B (1979) 275.
- 5) R. Forster et al., IEEE Trans. Nucl. Sci. NS-28 (1981) 2386 and T. Ellison et al., IEEE Trans. Nucl. Sci. NS-30 (1983) 2636.
- 6) Ya.S. Derbenev and A.N. Skrinsky, Part. Accelerators 8 (1978) 235.
- 7) N.S. Dikansky et al., The study of fast electron cooling, INP Novosibirsk Preprint 79-56 (1979); V.V. Parkhomchuk et al., Measurement of momentum cooling rates with electron cooling at NAP-M, INP Novosibirsk Preprint 78-81 (1978).
- 8) V.V. Parkhomchuk, Physics of fast electron cooling, this workshop.
- 9) L. Spitzer, Physics of fully ionized gases (Interscience, NY, 1956).
- 10) M. Bell and J.S. Bell, Part. Accelerators 12 (1982) 49.
- 11) R. Neumann et al., Z. Phys. A313 (1983) 253.
- 12) A. Piwinski, Proc. 9th Int. conf. on High energy Accelerators, Stanford, 1974 (US Atomic Energy Commission, Washington, 1974), p. 405; J.D. Bjorken and S.K. Mtingwa, Part. Accelerators 13 (1983) 115.
- 13) A. Ruggiero, Relativistic electron cooling and intrabeam scattering, this workshop.
- 14) A. Wolf, Realistic calculations concerning electron cooling in storage rings, this workshop.

- 15) H. Herr, Electron cooling at low energies, this workshop.
- 16) D.V. Pestrikov, Coulomb relaxation in a cold proton beam, this workshop.

PHYSICS OF FAST ELECTRON COOLING

V.V.Parkhomchuk

Institute of Nuclear Physics,  
630090 Novosibirsk, USSR

Electron cooling of a beam of heavy charged particles is based on a Coulomb interaction between the electrons and the beam particles (Ref. 1). As a result of the heat exchange between the electrons and the particles, the cooling takes place until the effective temperatures become equal in the rest frame:

$$\mathcal{V}_s^2 = \mathcal{V}_e^2 \cdot \frac{m}{M} \quad (1)$$

where  $\mathcal{V}_s$ ,  $\mathcal{V}_e$ ,  $M$  and  $m$  are the velocities and the masses of a particle and an electron, respectively. The velocity spread of the electrons is determined by the cathode temperature and by a perturbing action of electromagnetic fields forming the electron beam. Therefore of this, a minimum achievable temperature of the electron beam has first been assumed to be close to the cathode temperature of the electron gun. However, the situation change dramatically because of the presence of the longitudinal magnetic field used to guide the electrons and because of decrease longitudinal-velocity spread of electron motion after electrostatic acceleration. In this case, the far-action character of the Coulomb field dictates the interaction of a particle with a Larmor circle slowly drifting along the magnetic field rather than with a rapidly travelling electron (Ref. 2). Fast cooling

down to very low temperatures can occur as a result. The NAP-M (Ref. 3) experiments have demonstrated the possibility of cooling a 65 MeV beam down to a temperature of 1 (K) for 50 ms.

Let us calculate the friction force under the condition that the velocity of particle motion is much larger in comparison with that of thermal motion of Larmor circles. If the magnetic field is rather strong, the electrons travel only along the magnetic field force lines under the action of the field of a particle. Let the particles move in electron gas at an angle  $\theta$  towards the magnetic field and have passed the  $\xi$ -long path at the moment of calculation of the friction force. Assuming that the particle mass  $M$  is fairly large and its velocity changes slightly for single through the cooling section, we write the equations of electron motion as follows:

$$\ddot{x} = \frac{eq}{m} \frac{x - x_i}{((x - x_i)^2 + (y - y_i)^2 + (z - z_i)^2)^{3/2}}$$
$$y = \text{const}$$
$$z = \text{const} \quad (2)$$

where  $x_i = v \cdot t \cos \theta$ ,  $y_i = v t \sin \theta$ ,  $z_i = 0$  are the coordinates of the particle;  $e$  and  $q$  are the charges of the electron and particles, respectively;  $t$  is chosen in such a way that at  $t = 0$  the particle is at the beginning of the coordinates, the  $X$ -coordinate being directed along the magnetic field whereas the particle velocity  $\vec{v}$  lying in the  $X-Y$  plane. In a first approximation, the electron displacement can be written in the form

$$\dot{X} = \int_{-t_0}^t \ddot{X} dt \rightarrow \Delta X = \int_{-t_0}^0 \dot{X} dt.$$

Under the assumption that the electron displacement  $\Delta X$  are small as compared with the distance to the particle, the expressions for the force caused of the electron displacement are of the form

$$F_I = -3 e q n_e \int \frac{\Delta X X Y}{r^5} dx dy dz$$

$$F_{II} = -e q n_e \int \Delta X \left( \frac{1}{r^3} - \frac{3 X^2}{r^5} \right) dx dy dz$$

All these calculations are most convenient to be made in the cylindrical system of coordinates with the axis along a particle trajectory; Having made simple but cumbersome calculations, we obtain the friction force in the form

$$F_I = -\frac{2\pi e^2 q^2 n_e}{m} L_c \frac{(v_I^2 - v_{II}^2) v_I}{r^5}$$

$$F_{II} = -\frac{2\pi e^2 q^2 n_e}{m} L_c 2 \frac{v_I^2 v_{II}}{r^5} \quad (3)$$

where  $L_c$  is the Coulomb logarithm of collisions,  $L_c = \ln(\rho_{MAX}/\rho_{MIN})$  and  $\rho_{MAX}$  and  $\rho_{MIN}$  are the maximum and minimum impact parameters. With the electron-electron interaction neglected and with the electron distribution assumed to be rather uniform, we may assume that  $\rho_{MAX}$  is determined by the length path which the particle transits during its presence in the electron flux  $\Delta t$ ;  $\rho_{MAX} = r \cdot \Delta t$  and  $\rho_{MIN}$  is determined by the applicability condition for the calculation in first approximation: the electron displacement,  $e q / m v^2$ , should be small in comparison with the impact parameter  $\rho$ :  $\rho \gg \rho_{MIN} = |e q / m v^2|$ .

Of interest is to estimate the magnitude of the friction force at low particle velocities, when there is no possibility of using the first approximation. In this case, the characteristic velocities are determined by the equality of the maximum and minimum impact parameters,  $\rho_{\max} = \rho_{\min}$ :

$$v_{th} = \left( \frac{eq}{m \Delta t} \right)^{1/3} \quad (4)$$

Figure 1 shows the computational values of the frictional force when the particle moves across the magnetic field. It is seen that at the particle velocity  $v \ll v_{th}$  the force grows linearly with the velocity whereas at  $v \gg v_{th}$  it begins decreasing and is determined by the expression (3).

In this ( $v \ll v_{th}$ ) region, a substantial difference emerges in the kinetics of the negatively and positively charged particles. A positively charged particle, flying into the electron beam, attracts the nearest electron which oscillates all the time in the vicinity of the particle along the magnetic field force line, thereby leading to a strong perturbation of the transverse motion of the particle. Figure 2 demonstrates a comparative picture of the collisions between the positive and negative charged particles and an electron (in rest frame of the particle). The time of interaction of the electron with the repelling particle is determined by the electron longitudinal-velocity spread,  $\gamma = \rho/v_e$ . Upon slow motion of a particle with velocity  $v$ , the momentum acquired by the electron during collision, is approximately  $m v$  and hence, the energy lost by the particle is roughly  $m v^2/2$ . The momentum, transferred to the particle and associated with

the thermal motion of the electrons, is  $m\mathcal{V}_e$ ; therefore, the balance of the energy and heat losses because of the electron motion is established under the condition of temperature equality:

$$\frac{m\mathcal{V}_s^2}{2} = \frac{(m\mathcal{V}_e)^2}{2M} \rightarrow \mathcal{V}_s^2 = \mathcal{V}_e^2 \frac{m}{M} \quad (5)$$

Upon motion across the magnetic field the particle attracting the electron is capable of confining it if the velocity of drift motion of the electron in the particle field is higher than the longitudinal velocity of electron motion:

$$\frac{q}{M\rho^2}c > \mathcal{V}_e \rightarrow \rho^2 < \frac{qc}{\mathcal{V}_e H} \quad (6)$$

In the process of this cooperative motion a strong modulation of the transverse momentum of the particle takes place because the frequency of drift motion  $\Omega_d = e^2 c / (\rho^3 H)$  is small:

$$\Delta P_\perp = \frac{e^2}{\rho^2 \Omega_d} = \frac{e \rho H}{c} \quad (7)$$

The balance condition of the energy losses and the diffusion connected with the kicks described above in the transverse direction leads in this case, to the equilibrium condition in the form

$$m\mathcal{V}_s^2 = \frac{(\Delta P_\perp)^2}{M} = \frac{e^2 \rho^2 H^2}{M c^2} \quad (8)$$

When accelerating the electron beam to a fairly high energy, the longitudinal electron temperature is determined by the mutual repulsion of the electrons and is equal to

(Ref. 3,4)

$$\frac{m v_e^2}{2} = e^2 n_e^{1/3} \rightarrow v_e = \sqrt{\frac{2 e^2 n_e^{1/3}}{m}} \quad (9)$$

Using the above expression, we can write down the stationary value of the particle velocity, transverse to the magnetic field, as follows:

$$v_s^2 = v_e^2 \frac{m}{M} \sqrt{\frac{H^2}{8 n_e m c^2}} \quad (10)$$

It is clear that as the magnetic field  $H$  grows, the equilibrium temperature of the positively charged particles elevates at  $1 \ll \sqrt{H^2/(8 n_e m c^2)} \ll M/m$ . With further increase of the magnetic field,  $\sqrt{H^2/(8 n_e m c^2)} \gg M/m$ , the drift frequency becomes lower than the frequency of particle oscillations in the electron field,  $\Omega = \sqrt{e^2 / (\rho^2 M)}$ . Under these conditions the energy variation upon collision is compared with the kinetic energy of the longitudinal electron motion:

$$\Delta P = \frac{e^2}{\rho^2 \Omega} = \sqrt{\frac{e^2}{\rho} M} \rightarrow \Delta E = \frac{e^2}{\rho} \approx \frac{m v_e^2}{2} \quad (11)$$

and the energy balance equation upon collisions leads to the equality of the transverse particle velocities to the longitudinal spread of the electron velocities:

$$v_s^2 = v_e^2 = \frac{2 e^2 n_e^{1/3}}{m} \quad (12)$$

Figure 3 shows the time variation of the velocities of a proton during its interaction with the electron beam for the case of a strong magnetic field. This dynamics has been obtained using the computer simulation of the process. It is seen that the velocity component is established close to

$\sqrt{2e'n_e^{1/3}/M}$  along the magnetic field, while the transverse velocities are considerably higher and are approximately equal to  $v_t = \sqrt{2e'n_e^{1/3}/m}$ , according to equation (12). In the repulsion case (e.g., cooling of antiprotons by electrons), all three velocity components are cooled down to  $v_s = \sqrt{2e'n_e^{1/3}/M}$ . The computational results concerning the transverse-velocity spread of a proton at different magnetic fields and of the transverse electron velocities are presented in Fig. 4. In our computations the magnitude of the electron longitudinal-velocity scatter is equal to  $v_e = \sqrt{2e'n_e^{1/3}/m}$ . It is seen that with increasing the magnetic field the equilibrium spread of the proton velocities first reduces because of the magnetization of the transverse electron motion and then increases as the transverse diffusion increases. The experimental values of the equilibrium spread of velocity, which have been obtained in the NAP-M experiments, are in good agreement with the computational values.

Fast electron cooling enables one to obtain extremely low temperatures of heavy-particle beams, thereby offering the possibility of revealing interesting peculiarities in the properties of the cooled beams. As has previously been mentioned (Ref. 5), an interaction between the beam particles gives rise to suppressing the noises in the beam. The distribution of the particle density over the storage ring orbit can be written as follows:

$$P(\theta, t) = \sum_{k=1}^N \delta(\theta - \theta_k(t)) = \sum_{k=1}^N \frac{A_k}{2\pi} \exp(i k \theta) \quad (13)$$

where  $N$  is the number of particles and  $A_k$  is the amplitude

de of a  $K$ -harmonic of density. If the particle motion is not correlated, there is no difficulty in seeing that  $\langle A_k \rangle = 0$ ,  $\langle A_k^2 \rangle = N$ . Dispersion of  $\langle A_k^2 \rangle$  i.e. the noise powers in the beam, which are induced at the pick-up electrodes, are equal, with an interaction between the beam particles taken into account, to

$$\langle A_k^2 \rangle = \frac{N \cdot N_{th}}{N + N_{th}} = \begin{cases} N, & N \ll N_{th} \\ N_{th} = \frac{\pi R_0 (\Delta \omega)^2}{e^2 w_0 w_p' Z}, & N \gg N_{th} \end{cases} \quad (14)$$

where  $R_0$  is the storage ring radius,  $Z = \ln(\alpha_k/\alpha_0)/\gamma^2 V_0$  is the chamber impedance with respect to the proton beam, and  $\Delta \omega$  is the revolution frequency spread:  $\Delta \omega = w_p' \Delta p$  and  $\Delta p$  - momentum spread.

Figure 5 demonstrates the noise power  $W$  of the proton beam versus the proton current  $J_p$  upon cooling and without it. It is seen that after cooling the noise power reduces by two orders of magnitude and change slightly with increasing the proton current to  $10 \mu\text{A}$ . The Schottky noise in the beam after its strong cooling is converted to a thermal one proportional to the temperature of proton beam:  $(\Delta \omega) \propto (\Delta p)^2$ . This permits one to restore, without difficulty, the longitudinal momentum spread of the proton beam using the data available (Fig. 6). For  $J_p < 10 \mu\text{A}$ , the longitudinal-momentum spread is  $\Delta p/p = 1.1 \div 1.2 \cdot 10^{-6}$ . This corresponds to a  $1^\circ\text{K}$  longitudinal temperature. This value is good accordance with the estimation (9):  $k e^2 n_e^{1/3} \approx 1^\circ\text{K}$ . However, strange in these results is a slight growth of the momentum spread with increasing the proton current. Under the cooling conditions for the NAP-M proton beam, the transverse-velocity <sup>spread</sup>~~sputter~~ is

much higher as compared with a longitudinal one:  $\Delta p/p \approx 15 \cdot 10^{-6}$ . As a consequence, this should give rise to heating of the longitudinal degrees of freedom because of the intrabeam particle scattering. Independent longitudinal-cooling rate measurements have shown that the time of cooling constitutes  $\tau_u = 10$  msec, and estimation of the rate of heating of the longitudinal degree by intrabeam scattering gives the equilibrium longitudinal momentum spread, at a  $10 \mu\text{A}$  proton beam, equal to

$$\frac{\Delta P_u}{P} = \sqrt{\frac{d}{dt} \left( \frac{\Delta P_u}{P} \right)^2 \cdot \frac{\tau_u}{2}} \approx 10^{-4}$$
$$\frac{d}{dt} \left( \frac{\Delta P_u}{P} \right)^2 = \frac{\gamma \gamma_p^2 N L_e C}{\gamma^3 \beta^3 R_o^3 (\Delta P_u/P)^3}$$

Such a substantial difference between the experimentally measured longitudinal-moment spread and that expected from the intrabeam scattering effect may be accounted for only by a strong suppression of the intrabeam scattering caused by a mutual correlation of the particles in the proton beam. If the particles are equally spaced and do not close in small distance at their cooperative thermal motion, it is natural that the energy transfer from the transverse to longitudinal motion does not occur. Of course, the strong noise suppression in the low-frequency region does not imply a simultaneous appearance of the particle ordering at short distances since the latter requires additional conditions. The observed phenomena connected with the particle ordering in the cooled beam are of great interest and need further investigations.

Allowing the obtaining of very cold charge particle beams, fast electron cooling opens new prospects in the experimental field of elementary particle physics.

References

1. Budker G.I. "Effective method for damping the particle oscillations in proton and antiproton storage rings" Atommaya Energia, 1967, vol. 22, N 5, p. 346-348.
2. Derbenev Ya.S. and Skrinsky A.N. "Magnetization effects in electron cooling", Fizika Plazmy, 1978, vol. 4, No. 3, p. 492-500.
3. Derbenev Ya.S., Dikansky N.S. et al. "Status report on electron cooling". In: Proc. of the 8th National Conf. on Charged Particle Accelerators (Protvino, 1982). Dubna, 1983, vol. 2, p. 242-249.
4. Kudelainen V.I., Lebedev V.I. et al. "Temperature relaxation in a magnetized electron flux". Soviet ZhETF, 1982, vol 82, No. 6, p. 2056-2064.
5. Parkhomchuk V.V. and Pestrikov D.V. "Thermal noises of the intense flux in a storage ring. Soviet ZhETF, 1980, vol. 50, No. 7, p. 1411-1418.

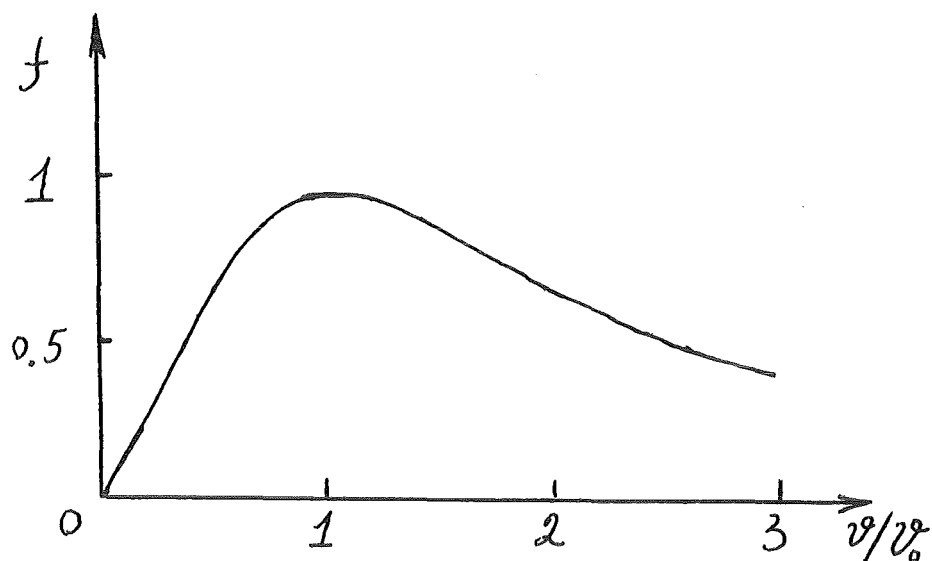


Fig. 1. The frictional force for the particle moving across the magnetic field with small velocity  $v$ .  $f$  and  $v_0$  mean respectively  $f = F_f / \left( \frac{2\pi n_e e^4}{m v_0^2} \right)$ .  
 $v_0 = 2 \sqrt[3]{e^2 / (m \Delta t)}$ ,  $\Delta t$  - time of particle interaction with electron beam.

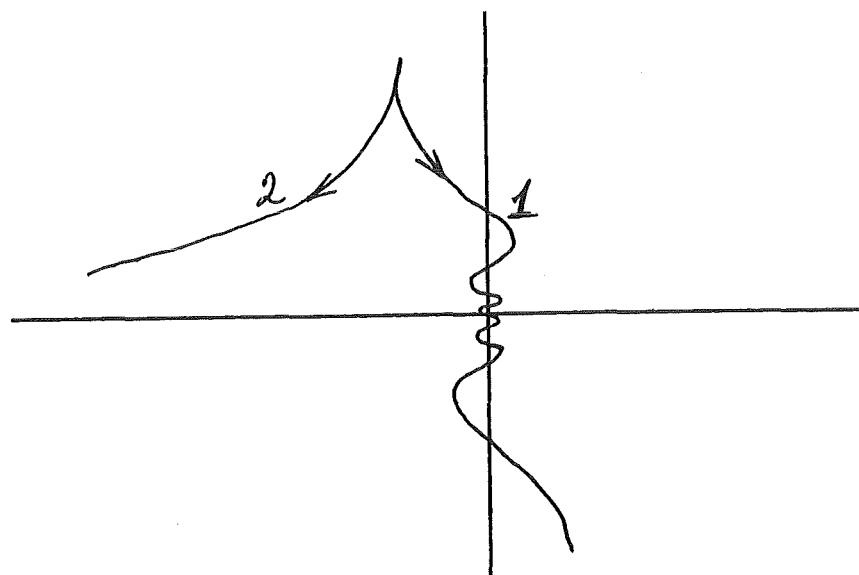


Fig. 2. A comparative picture of collisions between the positive (1) and negative (2) charged particles with electron (in the rest frame system of particles).

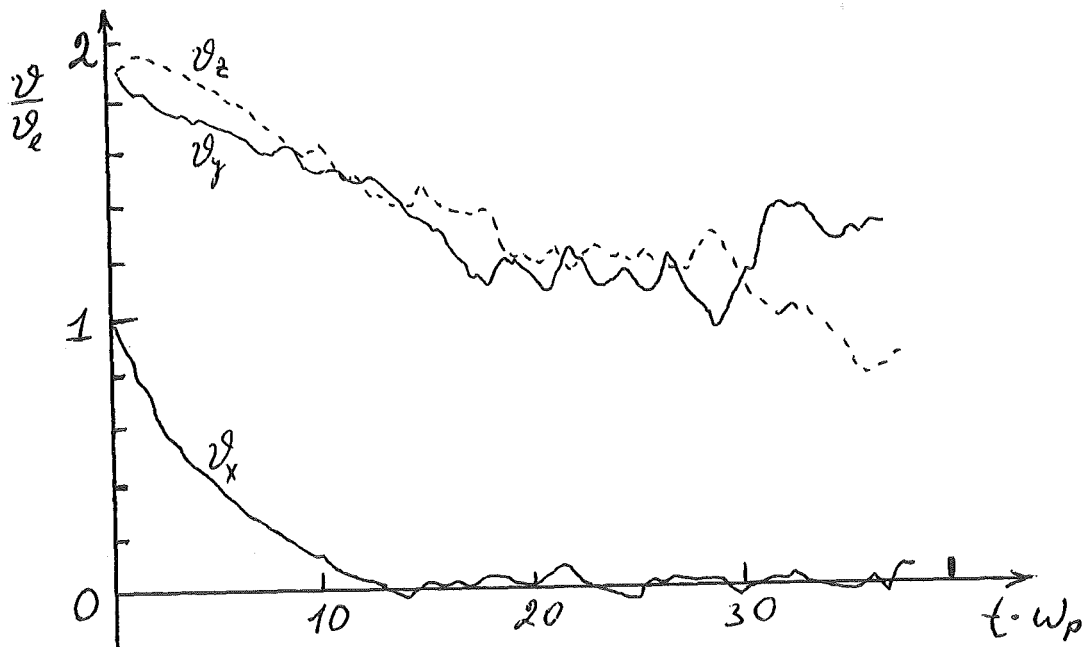


Fig. 2. The time variation of velocities of a proton during int cooling in strong magnetic field. The symbols  $v_e$  and  $\omega_p$  mean  $v_e = \sqrt{2e^2 n_e^{1/3} / m}$ ,  $\omega_p = \sqrt{4\pi e^2 n_e m / M^2}$ .

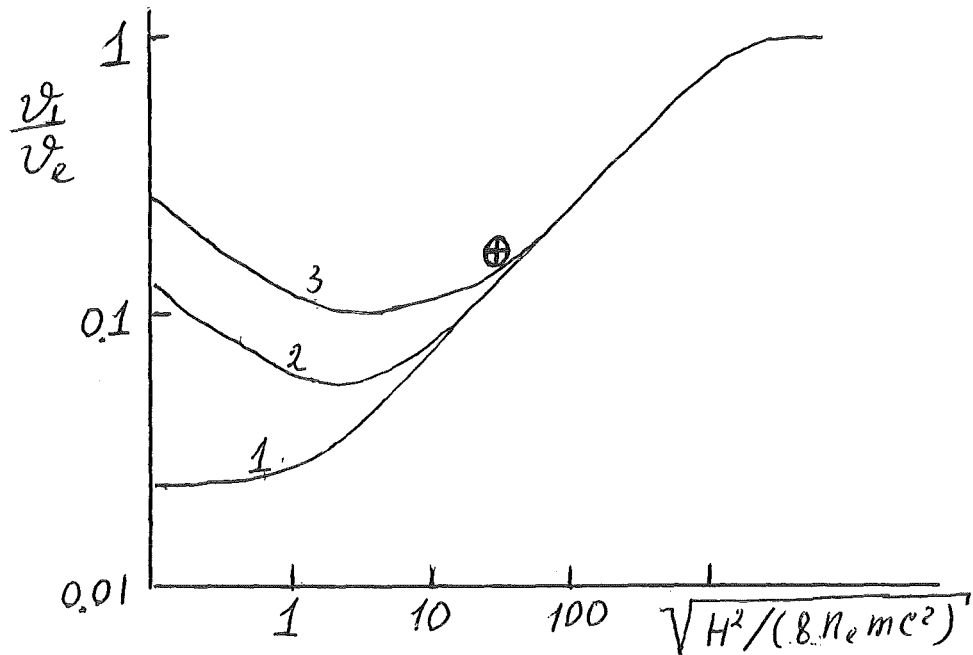


Fig. 4. The proton transfer velocity spread versus the magnetic field and the transfer electron velocity. 1 -  $v_t/v_e = 0$ , 2 -  $v_t/v_e = 8$ , 3 -  $v_t/v_e = 16$   
 Ⓢ - experimental value obtained at the NAP-II.

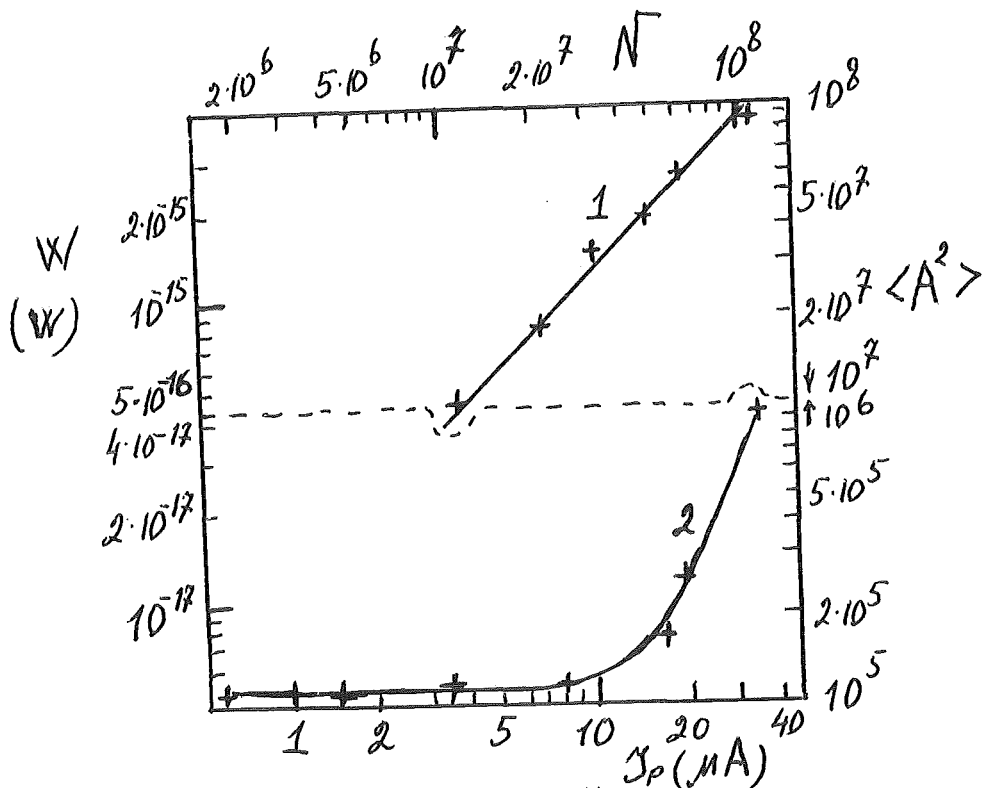


Fig. 5. The noise power  $W$  versus proton beam current  $J_p$ . Energy of protons 65 MeV, the electron beam current 0.3 A. 1 - normal beam, 2 - cooled beam.

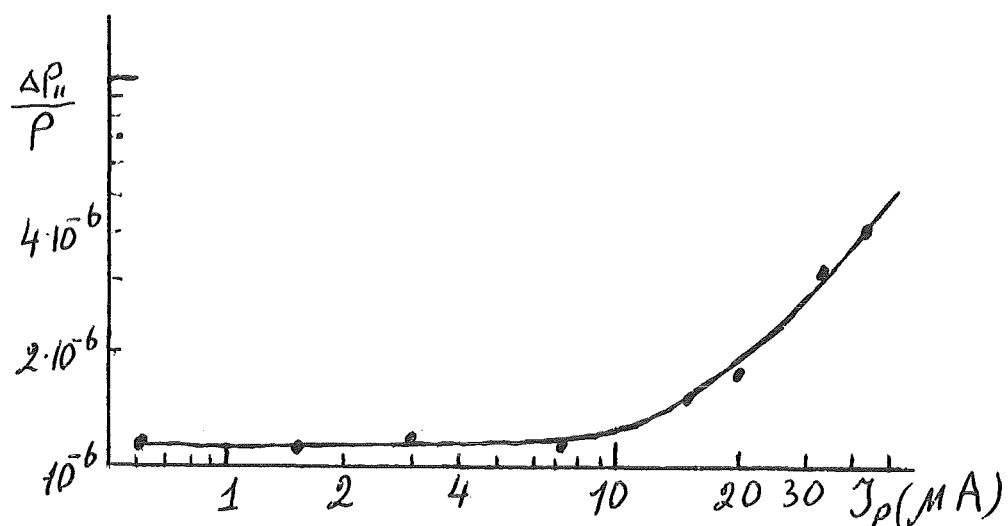
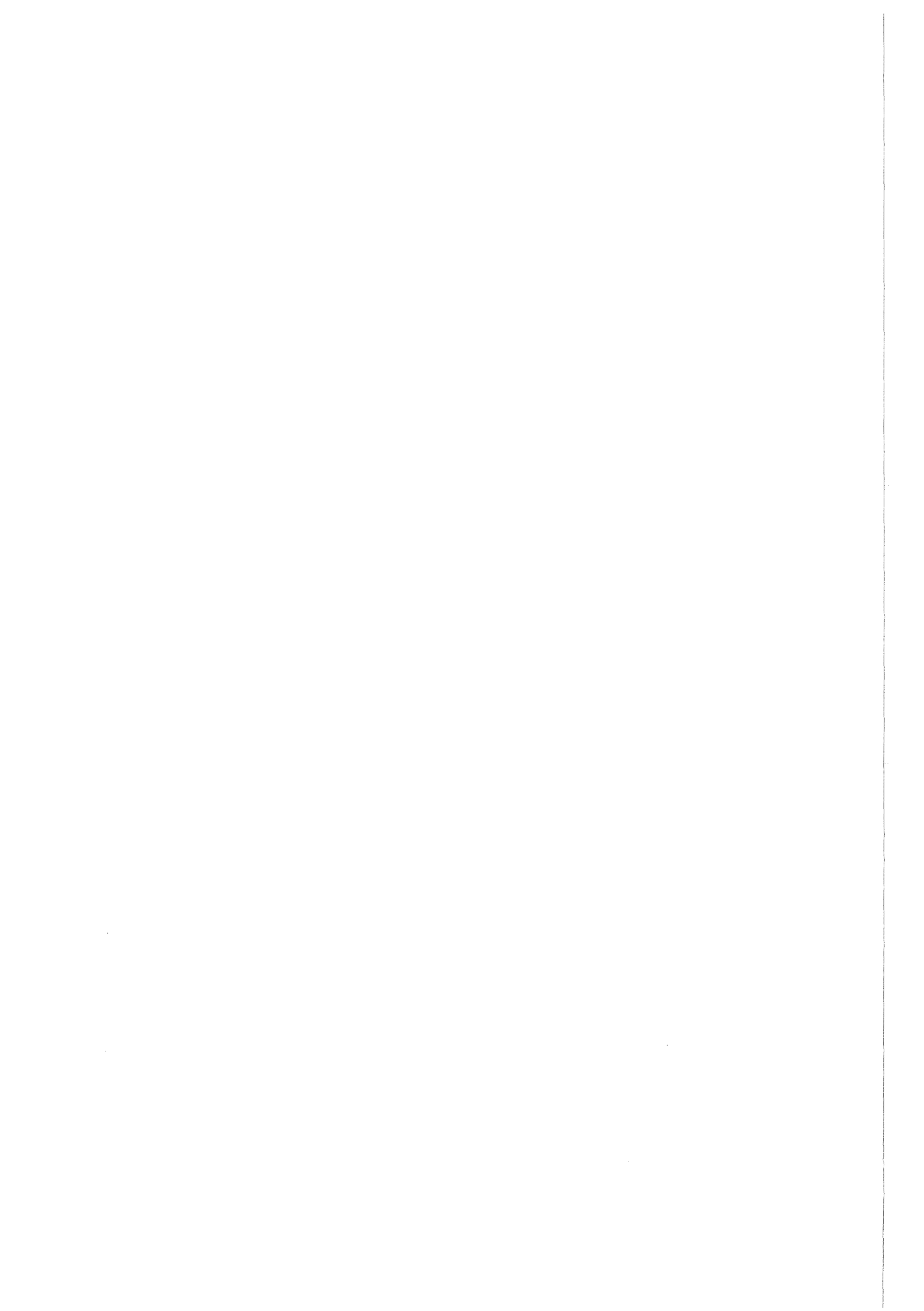


Fig. 6. The momentum spread of proton beam versus current  $J_p$ .



ELECTRON COOLING AT VERY LOW VELOCITIES

Heiner Herr  
CERN, EP Division, Geneva, Switzerland

A B S T R A C T

Due to the  $\beta^4 \gamma^5$  dependence of the cooling time electron cooling seems to be very suitable for cooling of particles with very low velocities, for example ions below  $\sim 10$  MeV/n. However, the velocity spread in the electron beam created by the heated cathode set some limits. A possible construction of a small electron gun for very low velocities is presented here together with some measurements of the beam properties.

INTRODUCTION

Electron cooling at very low velocities was investigated for a small deceleration ring (ELENA)<sup>1</sup> which should decelerate 5 MeV antiprotons from LEAR down to  $\sim 200$  keV for different experiments<sup>2-8</sup>. As the electron beam, having the same velocity as 200 keV antiprotons, has a kinetic energy as low as 110 eV, a small electron gun was constructed to study the beam properties in the range between 100 eV and 3 keV. The results of the studies might also be interesting for the cooling of ions below  $\sim 10$  MeV/n in the storage rings for light or heavy ions presently being under discussion.

COOLING TIME AT LOW VELOCITIES

The strong velocity dependence of electron cooling seems to favour the application at low energies as the cooling time is given by:

$$\tau = 0.16 \frac{\beta^4 \gamma^5 e (\theta_e^2 + \theta_i^2)^{3/2}}{r_p r_e \eta L_c j} \cdot \frac{A}{Z^2}$$

with  $\beta$  and  $\gamma$  being the usual kinematical factors,  $e$  the electron charge [Cb],  $\theta_{e,i}$  the divergence of the electron resp. ion beam,  $r_e$ ,  $r_p$  [m] the "classical particle radius" of the electron resp. proton,  $\eta$  the ratio between the length of the cooling straight section and the circumference of the storage ring,  $L_c$  the Coulomb logarithm,  $j$  [A/m<sup>2</sup>] the current density of the electron beam and -in the case of ions-  $A$  the atomic number and  $Z$  the charge state.

While the divergence of the ion beam can be adjusted by the focusing properties of the storage ring, the divergence of the electrons is given by the temperature of the cathode and the gun construction.

As it seems to be quite reasonable to have a cooling time for 200 MeV protons in the order of 1 sec<sup>9</sup> one could deduce from the above formula a cooling time of  $\sim 10^{-4}$  sec for 2 MeV protons! Unfortunately however, this is not realistic. The reason is the minimum transverse divergence of the electron beam which is given by the cathode temperature. This temperature is for example for a Ba-Sr-Oxide cathode in the order of 0.1 eV ( $\sim 800^\circ\text{C}$ ). As the temperature of the beam is given for one plane by

$$T = 1/2 mc^2 \beta^2 \gamma^2 \theta^2$$

the beam divergence increases while the velocity  $\beta c$  is decreasing.

In contrary to the longitudinal plane the divergence in the transverse directions stays unchanged by the electrostatic acceleration of the electron beam, which means that:

The  $\beta^4$  dependence of cooling is counteracted by a  $1/\beta^3$  dependence due to the transverse divergence of the electron beam.

If the electron gun has a constant perveance another velocity dependence is given by the relation between beam current  $I$  and acceleration voltage  $U$ : as  $I \sim U^{3/2}$  and  $U \sim \beta^2$  one finds:

The  $\beta^4$  dependence of cooling is counteracted in a gun with constant perveance by  $1/\beta^3$  due to the dependence on the current.

Both effects give an overall dependence of the cooling time of

$$\tau \sim 1/\beta^2 !$$

It might be therefore desirable to increase the electron current at lower energies by increasing the perveance of the gun either mechanically by moving the anode or electrically by changing the potential of an intermediate electrode. However this is only possible within certain limits because this increases the velocity spread in the electron beam due to space charge. If this spread becomes too big, cooling becomes less effective or will even stop, because the frictional force between electrons and ions decreases above a certain value by  $1/v^2$  with  $v$  being the electron-ion velocity difference. The velocity spread in the electron beam due to space charge is given by <sup>10</sup>:

$$\Delta U = 4.8 \times 10^4 \frac{I_e}{\pi \sqrt{U_B}} \quad (I_e [\text{A}], U_B [\text{V}])$$

$$\frac{\Delta U}{U} = \frac{4.8 \times 10^4}{\pi} \cdot \frac{I}{U^{3/2}} = \text{const.} \times \text{perveance}$$

which means that the permissible velocity spread set a limit for the perveance.

In the experiments at Novosibirsk<sup>11</sup> the velocity spread was  $1-2 \times 10^{-3}$ , at CERN<sup>12</sup>  $\sim 4-7 \times 10^{-3}$ , which gives an idea about the order of magnitude for  $\Delta U/U$ .

Another possibility to shorten the cooling time could be an increase of the current density  $j$  of the electron beam which means making the beam smaller while keeping the total current constant. In this case, however, one has to make also the ion beam in the cooling section of the storage ring smaller. For constant emittance this can only be done by making the focusing function  $\beta_c$  of the cooling ring smaller which causes bigger divergences of the ion beam. The bigger divergence has as consequence that the maximum possible length of the cooling section gets shorter and, as it can be seen from the cooling time formula, the cooling time gets longer with the third power of the divergence if  $\theta_i > \theta_e$ . Furthermore cooling stops when

$$\theta_i \sim \theta_e \sqrt{m_e/M_i}$$

Another effect which has to be watched while increasing the current density is the tune shift  $\Delta Q$  in the storage ring due to the electron beam, which is given in the case of protons by

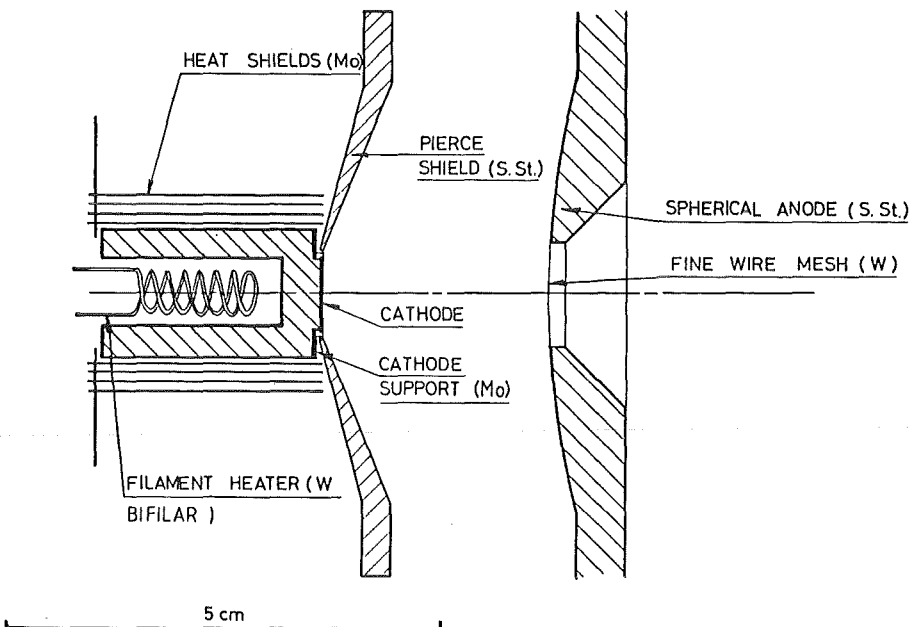
$$\Delta Q = \frac{r_p \beta_c}{2ec} \cdot \frac{1/j}{\beta^3 \gamma^3}$$

It should be pointed out that this tune shift is in the non-relativistic region independent of the energy when the electron beam is accelerated by a gun with constant perveance because of the above shown dependence of  $j \sim \beta^3$ .

#### STUDY OF AN ELECTRON GUN FOR LOW VELOCITY BEAMS

Studies of electron guns working around 1 kV can be found in the literature<sup>13</sup>. Already there is pointed out the importance of a vacuum below  $10^{-8}$  Torr and of the very precise alignment between the edge of the pierce shield and the edge of the cathode. Also the effects of the transverse velocity of the beam due to the heated cathode are discussed<sup>14</sup>.

To study the properties of an electron beam at even lower velocities, a small gun was built for tests between 100 V and 3 kV. The construction of this gun is shown in Fig. 1.



To get a sufficient "cold" (parallel) beam for electron cooling, one has to compensate the defocusing effect of the aperture in the acceleration electrode. This can be achieved either by a concave cathode or a resonance optics<sup>15</sup>. The concave cathode creates a converging beam which is then made parallel by the defocusing action of the anode aperture. For the resonance optics the fact is used that the electron beam is guided by a longitudinal magnetic field. The electrons, diverging by the defocusing effect of a first anode start to spiral around the field lines. After a turn of 180° (or an uneven multiple of this) the now converging electrons are passing a second anode which makes the beam parallel by its defocusing action. The voltage on both anodes and the magnetic fields must have obviously a fixed relationship.

As it can be seen from Fig. 1 a third method was used for our test gun: electrons were accelerated by a simple tungsten grid having a mesh size of 0.5 mm and a wire thickness of 32  $\mu$ . The mean defocusing angle by the opening of the grid is<sup>16,17</sup>,

$$\theta \sim r/3d$$

where  $r$  is half the mesh size and  $d$  the cathode-anode distance. The

resulting divergence of the electrons passing the grid is in the velocity region of the gun smaller than the divergence due to the cathode temperature. This construction allows to choose the magnetic field strength independently of the beam energy.

The following table summarizes the gun parameters:

|          |
|----------|
| GUN DATA |
|----------|

|  |                             |                        |
|--|-----------------------------|------------------------|
| Gun voltage  | 116 V                       | 2.8 kV                 |
| Ion energy   | 200 keV/n                   | 5 MeV/n                |
| Gun current  | 160 $\mu$ A                 | 28 mA                  |
| Beam divergence $\theta_t$<br>due to cathode temperature   | $3 \times 10^{-2}$ rad      | $6 \times 10^{-3}$ rad |
| Expected cooling time for<br>1.1 m cooling length in ELENA | 3.3 sec                     | 0.14 sec               |
| Cathode diameter   | 1 cm                        |                        |
| Distance cathode-mesh                                      | $\sim 3.2$ cm               |                        |
| Mesh size  | $0.5 \times 0.5$ mm         |                        |
| Wire thickness   | 32 $\mu$                    |                        |
| Material   | Tungsten                    |                        |
| Divergence by mesh openings                                | $\sim 3 \times 10^{-3}$ rad |                        |
| Vacuum   | $3-7 \times 10^{-9}$ Torr   |                        |
| Magnetic field of solenoid                                 | 50 - 200 Gauss              |                        |

Due to the above discussed limits of current and current density and the relatively low acceleration voltage, the total power in the electron beam is so low that no energy recuperation is needed and the gun can be powered by a standard photomultiplier supply which has excellent voltage stability.

In respect to a later application in a small storage ring for protons or antiprotons the strength of the solenoidal magnetic field was limited to 200 Gauss. As the longitudinal magnetic field causes a coupling of the horizontal and vertical motion of the stored particles in the ring, strong fields can change considerably the tune of the storage ring. This effect is of course less critical for ions.

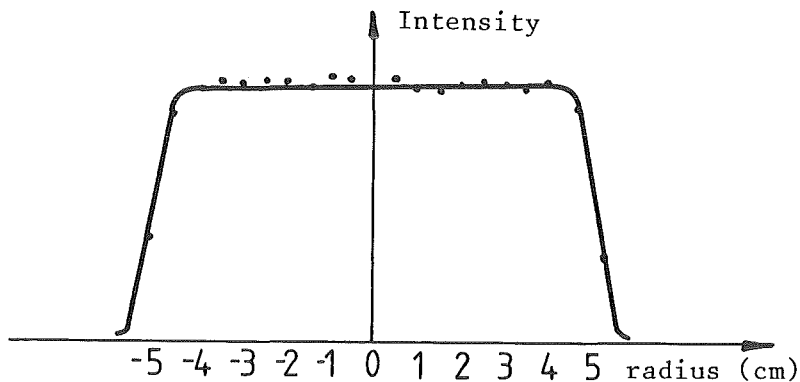
To achieve a sufficient homogeneity ( $< 10^{-3}$ ) of such a low magnetic field the set-up has to be shielded carefully against the earth magnetic field and other stray-fields.

It also turned out that the design of the filament for heating the cathode is very critical. Obviously the beam is most sensitive near the cathode where fields in the 100 m Gauss region, which are easily reached by standard heater designs, can deform the beam considerably.

Therefore the magnetic field of several filament configurations was measured and the heater was tested in the gun. The final solution is shown in Fig. 1: a longitudinal bifilar wound tungsten filament is placed in a thick walled molybdenum cylinder which guides the heat to the cathode. With this set-up the field on the cathode was less than 10 m Gauss at full heater current.

To study the beam properties the intensity distribution of the electron beam was measured in a distance of 30-40 cm from the gun. As probe a 0.2 mm thick shielded tungsten wire mounted opposite to the beam direction could be moved perpendicular to the beam in both transverse directions. The charge captured by the wire was measured as a function of the position.

Fig. 2 shows the measured intensity distribution for an electron beam of 200 eV. It shows a very homogeneous distribution over the full beam cross-section. Measurements were made over the full operating range of the gun giving similar results as shown here.



#### CONCLUSION

The above study shows that a design for an electron cooling device for low velocities has not only to take into account the properties of the particles to be cooled but also the parameters of the storage ring to achieve the best cooling results. The construction is facilitated by the fact that the acceleration voltages are relatively low and the power in the electron beam small. The device needs however a proper shielding

against the earth magnetic field and a careful filament design when the magnetic guiding field has to be kept low to avoid coupling effects in the storage ring. The results of the test gun shows that even with low fields a homogenous intensity distribution can be achieved with reasonable beam currents. As electron cooling was tested up to now only down to 820 eV ( $\sim$  1.5 MeV protons)<sup>11</sup>, it would be interesting to study electron cooling with such a device in a storage ring below 800 eV down to 110 eV corresponding to 200 keV protons or antiprotons.

REFERENCES

- 1) H. Herr  
Proc. of the 3rd International School of Physics of Exotic Atoms, Erice 1982, New-York: Plenum (1984), p 659
- 2) G. Audi et al  
CERN/PSCC/81-84/PSCC/P52 (1981)
- 3) "ASTERIX Collaboration" (PS171)  
CERN/PSCC/82-43/PSCC/M114 (1982)
- 4) G. Piragino  
CERN/PSCC/82-48/PSCC/M116 (1982)
- 5) S. Polikanov  
CERN/PSCC/82-50/PSCC/M118 (1982)
- 6) L. Tauscher  
CERN/PSCC/82-49/PSCC/M117 (1982)
- 7) T. Bressani et al  
CERN/PSCC/82-69/PSCC/M128 (1982)
- 8) J. Saudinos  
CERN/PSCC/82-67/PSCC/M127 (1982)
- 9) H. Herr  
CELSIUS Note 83-2, Uppsala Sweden (1983)
- 10) V. Ardenne  
Tabellen der Elektronenphysik, Deutscher Verlag der Wissenschaften, Berlin 1956
- 11) N.S. Dikansky et al  
The study of fast electron cooling, Preprint Novosibirsk, USSR
- 12) M. Bell et al  
Electron cooling in ICE at CERN, Nucl. Inst. Meth. 190(1981), p 237
- 13) C.C. Cutler et al  
Proc. IRE (1955), p 299
- 14) H. Boersch  
Zeitschrift für Physik 139 (1954), p 115
- 15) J.R. Pierce  
Bell System Technical Journal 30 (1951), p 825
- 16) C. Rubbia  
CERN/EP 77-2
- 17) J.L. Verster  
Philips Res. Repts. 18 (1963), p 465



## THE LEAR ELECTRON COOLER

H. Haseroth, C.E. Hill, J.-L. Vallet  
CERN, Geneva, Switzerland  
C. Habfast, L. Hütten, H. Poth, A. Wolf  
Institut für Kernphysik, Kernforschungszentrum  
Karlsruhe, West Germany

### 1. Introduction

A powerful technique for rapidly improving the characteristics of low energy beams and for considerably increasing their phase space density has been demonstrated using cold electron beams for cooling. Although it seems that the main use of this method will be the cooling of non-relativistic ions, cooling of protons and antiprotons at very high energies, using synchrotron radiative cooling of stored electrons, can be contemplated.

A high rate of phase space compression independent of intensity is the main advantage of electron cooling which enables the accumulation and stacking of "hot" beams and compensates beam blow-up due to residual gas and intra-beam scattering. With the attainment of high phase space densities, loss-free deceleration to very low energies is conceivable, as is the possibility of operation of thin internal targets at these energies.

Thus, with the understanding of the cooling process obtained from experimental work (1-3), electron cooling can be considered as a valid accelerator technique complementing stochastic cooling.

In the following, the application of electron cooling to LEAR and its technological problems will be discussed.

## 2. Electron Cooling Applied to LEAR

During internal target operation, the compensation of beam blow-up due to the repeated passage of the beam through the target will result in an enormous gain in efficiency and beam characteristics. This is by far the strongest justification for the use of electron cooling in LEAR. At lower energies, where the degradation is much more apparent, good and efficient cooling is even more important. The high energy resolution, high luminosity and small interaction region that can be obtained by a combination of electron cooling and internal targets is a further advantage, especially for experiments at momenta below 300 MeV/c. At these energies external antiproton beams are plagued by low efficiency and bad resolution.

In the stretcher mode, the use of electron cooling could also be of advantage during low energy operation and would be an efficient complement to stochastic cooling. LEAR operation down to 100 MeV/c would be aided by the small emittances and low momentum spreads attainable with electron cooling. Furthermore, lower momenta could possibly be reached by further deceleration.

A detailed study of the compatibility of simultaneous electron cooling and ultra-slow extraction has not been carried out as the electron cooling is only envisaged to be operational, possibly intermittently, before extraction. Actually only transverse cooling is needed during the extraction process.

Electron cooling will also be of importance in the  $H^-/\bar{p}$  co-rotating beam mode to decrease the  $H^-$  losses and to increase the formation of  $p-\bar{p}$  atoms.

## 3. The Cooler

The electron cooling equipment for LEAR is shown in Fig. 1. In actual fact it is a modified version of the ICE experimental equipment which has been improved and adapted to the stringent requirements of LEAR (4).

Electrons from a 2" dispenser cathode (operating at 1350°K) are accelerated in a graded five electrode accelerating structure towards the grounded drift space. The potentials on the accelerating structure are defined by tappings on a 1 M $\Omega$  "bleeder" resistor which enables the electrode potentials to be maintained inspite of small leakage currents to the electrodes, and also enables changes in gun perveance to be made easily. A solenoidal field prevents beam blow-up and the positioning of the cathode within the uniform field region of the gun solenoid ensures that the conditions for immersed flow can be met. Thus, the electron beam retains its original diameter of about 5 cm with what is practically a homogeneous density distribution. Toroidal sections adapt the gun solenoidal field, and hence the electron beam, into the axial cooling section and out again into the collector solenoid. By this means the electron beam is brought into interaction with the antiprotons. At the end of the collector solenoid the electrons are rapidly decelerated in a strongly decreasing magnetic field to an energy of a few KeV and distributed over the cooled collector pot. Up to 99.5% of the electron beam current is recovered in this way. Modelling of the gun and collector regions were performed using the SLAC 226 (5) trajectory program (Figs. 2 and 3). In principle, the electron gun and collector are those used in ICE but some minor modifications were necessary.

The initial project envisages that the cooler will work with electron energies between 2.5 and 40 KeV ( $\beta = 0.1 - 0.36$ ) with space charge limited emission. As the cooler length in LEAR is only 1.5 m (a factor of two lower than ICE), considerable attention has been paid to the quality of the electron beam and in particular to the uniformity of the magnetic fields inside the cooling section (6). Special correction coils have been made to reduce end effects to an acceptable level and additional trim coils are to be provided to reduce field variations to about  $2 \times 10^{-4}$  rad for fine adjustment of the electron beam.

The longitudinal temperature of the electron beam is essentially defined by the stability of the high voltage applied to the electron gun and calculations have shown that a stability of  $5 \times 10^{-5}$  is desirable (7).

A redesign of the old vacuum system proved to be necessary to meet the demanding requirement of the LEAR vacuum system (8).

Operation of the electron cooler during beam studies and performance test away from LEAR is carried out with the help of a computerized control system which has been designed (9) to be capable of being linked to the LEAR serial highway after final installation (Fig. 5). Furthermore, the old but improved ICE diagnostic equipment will be re-used and additional measuring facilities are envisaged.

#### 4. Design Values and Expected Performance

The table below gives details of the main design parameters:

|                                |   |                     |                |
|--------------------------------|---|---------------------|----------------|
| Electron energy                | : | 2.5 - 40            | KeV            |
| Equivalent $\bar{p}$ -momentum | : | 100 - 370           | MeV/c          |
| Electron current               | : | $< = 5$             | Amp.           |
| Electron beam diameter         | : | 5(2)                | cm ("")        |
| Transverse e temperature       | : | $< = 0.2$           | eV             |
| Longitudinal e energy spread   | : | $5 \times 10^{-5}$  | (40 KeV)       |
| Electron recovery efficiency   | : | 99                  | %              |
| Magnetic field                 | : | $< = 1.5$           | kGauss         |
| Vacuum, cold cathode           | : | $5 \times 10^{-12}$ | Torr (N equiv) |
| Vacuum, hot cathode            | : | $1 \times 10^{-11}$ | Torr (N equiv) |
| Transverse cooling time        | : | $< = 2$             | s              |
| Longitudinal cooling time      | : | $< = 1$             | s              |

At first, the intention is to operate the cooler where it is most needed, that is at low energies. Depending on the prehistory of the injected beam it might only be necessary to cool at working energy. However, cooling could also be applied at the higher energy.

Although, as stated earlier, it is not envisaged to use electron cooling during ultra-slow extraction, the fast cooling times available could be of benefit if LEAR were operated on a cycle time of less than 1000 seconds. ICE experience indicates that a e-fold emittance cooling time of the order of 2-5 s is achievable at 300 MeV/c with momentum cooling faster by a factor of about 4. This should give equilibrium emittances around 1  $\pi$  mm mrad and momentum spreads around  $10^{-4}$ . Cooling times for a constant perveance gun, the easiest to operate during deceleration, increase as  $\beta$  for constant betatron angles. However, it could be possible to change the perveance to meet specific requirements.

The exact performance during internal target operation depends strongly on the experimental and target conditions during the experiment. It is clear, however, that very short cooling times will be needed for operation at the lowest energies and careful selection of operating parameters will be needed. Scanning with high accuracy around the nominal momentum could be carried out by acceleration and deceleration with the electron beam. The actual antiproton momentum will then be accurately known from the electron gun voltage.

Co-rotating  $H^-$  and  $\bar{p}$  beams can be cooled simultaneously by the electron beam. Although the  $H^-$  beam will strip rapidly if the energy differences between  $H^-$ , antiprotons or electrons exceeds 0.75 eV ( $H^-$  neutralization threshold), the losses drop dramatically if the beams are cooled to less than  $10^{-4}$  in momentum spread and matched to  $10^{-3}$  in velocity. Fast cooling rates with electron cooling will enable these conditions to be met quickly and the equalisation of velocities would considerably increase the  $p-\bar{p}$  formation rates.

## 5. Technical Problems

Initial trial operation of the gun and collector after it had been dismantled from ICE indicated that modifications inside these units would be needed to improve their ability to withstand the severe LEAR bakeout requirements. Modifications to metal/ceramic joints both inside and out of the vacuum have been successfully carried out. Certain inaccessible vacuum seals in the collector have been modified to facilitate assembly and maintenance.

The controls, power supplies and Faraday cages needed to operate the cooler were completely rebuilt to conform to the different safety standards demanded for operational equipment as compared to those required for an experimental device, and to the requirements of computer control (Fig. 4). At the same time advantage was taken to rationalize the power supplies and controls. A CAMAC crate at electron gun potential performs all interfacing for command and acquisition of parameters. This crate is connected to the ground level CAMAC and the computer by means of a fibre optic serial branch. All status and interlock functions are passed between ground and the various potential levels by "hard wired" fibre optic links to ensure safety in the event of a computer failure. Power supplies, including the gun/collector bias supply, were made fully programmable.

Considerable effort was expended to protect all electronics equipment from the effects of high voltage discharges by heavy filtering, Zener type protection, isolation amplifiers and the reduction of voltage excursions which could occur on components at different potentials inside the Faraday cages. Supplies of different types to gun and collector were rigorously segregated according to their function or destination.

The 40 kV 200 mA power supply intended for the electron gun is still a source of concern. The present unit has problems in

attaining the stability requirements and its ripple at low voltage is too high. A new power supply is under consideration.

Reduction of the 3 meter 2 part cooling colenoid to a single 1.5 meter unit required certain mechanical modifications to enable it to be adapted to the toroids. A full programme of magnetic measurements has been carried out and the results are shown in Fig. 5. From this data, a number of permanent correction coils were manufactured and installed. Further measurements demonstrated the effectiveness of these coils as serious errors were reduced to the order of  $10^{-4}$  on the beam axis.

The problems of the vacuum system are the subject of another presentation at this Workshop (8).

## 6. Diagnostics

To optimize the beam properties and achieve satisfactory cooling performance, it is essential to have adequate diagnostic systems both for use on a test stand and in the operational environment. This does not means that all the diagnostics are applicable to each situation (10).

An effective, but crude, method of partially optimizing the beam is to monitor the electron loss current. However, a minimal loss current may not necessarily correspond to an optimal beam for cooling. The detection of microwave radiation emitted by the electrons spiralling in the solenoidal field proved very useful in ICE whilst trying to minimize the transverse electron temperature. The antennae and detection system for this technique will be further improved and installed for routine monitoring.

Backscatter of laser light sent head-on into the beam will give a sensitive, non destructive measuremet of the electron density and of the longitudinal electron temperature. A powerful pulsed far-red or infra-red laser is needed, but the optical analysis is simple. Background is suppressed by the Doppler shift in the backscattered light and by pulsing the laser. This method could work over a wide range of electron energies and, although the photon count rates would be low (order 1 Hz), this would not be an insurmountable problem. Development of this system is under way for use on the test stand.

---

Positional pick-up electrodes (item 3 in Fig. 2) in the gun, cooler and collector solenoids are being installed to enable the beam to be steered accurately into the cooling region and enable fine adjustment of the electron beam relative to the antiprotons. The collector pick-up will aid the optimization of the collection efficiency.

The optical radiation produced by the excitation of background gas molecules after interaction with the electron beam will be explored using position sensitive micro-channel plates to try to monitor the electron density distribution in the beam. If needed, additional gas could be injected to enhance the effect.

Cooling performance will be studied initially in LEAR with protons (LEAR polarities reversed) by studying the formation of neutral hydrogen atoms. The neutral beam distribution leaving the LEAR straight section will be monitored with multiwire proportional chambers and their formation rate with scintillators. This would enable beam emittances to be measured and the neutral production rate gives a measurement of the transverse electron temperature.

This diagnostic facility will be lost when cooling antiprotons but H<sup>-</sup> could be used instead to give indications as to the cooling performance.

#### 7. Present Status

The gun and collector are being studied in an experimental set-up using the gun, short drift space and collector inside the gun solenoid in a vertical position. All the controls are installed and are connected to a local control computer.

---

Vacuum test with both hot and cold cathodes have demonstrated that the vacuum requirements of LEAR can be attained by the use of non-evaporable getter (NEG) pumps between gun, collector and the cooling region (11).

Without an electron beam the high voltage sections have been formed up to maximum operating voltage without undue difficulty or surprises. Reliable operation with an electron beam has been achieved up to 31.6 kV and 800 mA electron current with 5.8% electron loss. During these tests the gun operates at one quarter of its nominal perveance.

After magnetic measurements, installation of correction coils and remeasurement, the magnet assembly is being surveyed to obtain the external mechanical reference point needed for future assembly work.

The cooling section with its toroidal transitions and pick-up stations is being reassembled after initial vacuum tests and minor modifications. The remaining pick-ups and their electronics are under construction.

#### 8. Future Ideas

Increasing the gun high voltage to 100 kV (630 MeV/c) would be possible but would require improvements to both gun and

collector and an upgraded high-voltage power supply. All other parts of the cooler would remain the same. Although the improvements are basically of a technical nature (components), the need to improve considerably the electron recovery efficiency at 100 kV will probably require a redesign of the collector. Additionally, the replacement of the bleeder by separate power supplies for each anode in the electron gun is being studied. Thus, electron cooling at antiproton injection energy would be possible.

The operation of the cooler below 3 kV would be straightforward. If LEAR can operate below 100 MeV/c, then the electron cooler could be used there. Cooling at 53 MeV/c has been demonstrated at Novosibirsk.

#### 9. Planning

End 1984 - First test of the complete cooler as shown in Fig. 1.

1985 - Laboratory testing of the cooler, operation of diagnostics.

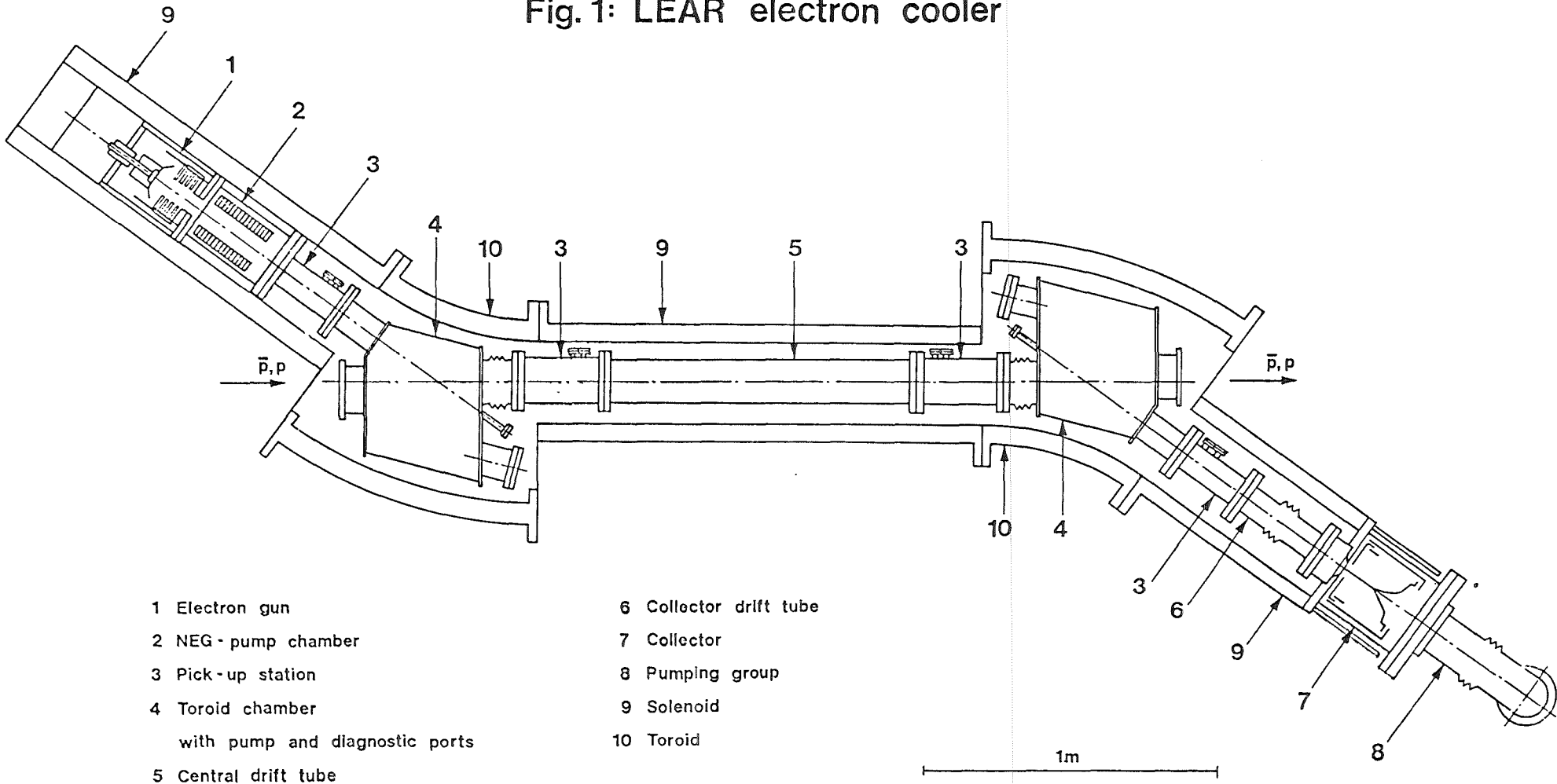
1986 - Installation in LEAR and testing with proton and H<sup>-</sup> beams during the ACOL shutdown.

9. References

- (1) G.I. Budker, N.S. Dikansky, V.I. Kudelainen, I.N. Meshkov, V.V. Parchomchuk, D.V. Pestrikov, A.N. Skrinsky, B.N. Sukhina. Part. Accel., 7; 197 (1976) and I. Derbenev, I. Meshkov: "Studies on electron cooling of heavy particle beams made by the VAAP-NAP group at Novosibairsk" CERN 77-08.
- (2) M. Bell, J. Chaney, H. Herr, F. Krienen, P. Moeller-Petersen, G. Petrucci: "Electron Cooling in ICE at CERN", Nucl. Instrum. and Methods, 190: 237 (1981).
- (3) R. Forster, T. Hardek, D.E. Johnson, W. Kells, V. Kerner, H. Lai, A.J. Lennox, F. Mills, Y. Miyahara, L. Oleksuik, R. Peters, T. Rhoades, D. Young, P.M. Melutyre: "Electron Cooling Experiments at Fermilab", IEEE Trans. Nucl. Sci., NS28:2386 (1981).
- (4) H. Haseroth, C.E. Hill, H. Poth, P. Moeller-Petersen: On the use of the ICE gun of electron cooling in LEAR", CERN /PS/LR Note 80-7 (1980)
- (5) W.B. Herrmannsfeldt: "Electron Trajectory Program", SLAC-226 (1979).
- (6) A. Wolf, L. Hütten, H. Poth: "Magnetic Measurements in the Electron Cooling Device for LEAR", CERN-EP 84-01 (1984).
- (7) H. Poth: "High voltage stability requirements for the electron cooler", CERN/PS/DL/LEAR/Note 81-2 (1981).
- (8) A. Poncet: "Ultra-high vacuum systems for coolers", this workshop.
- (9) U. Tallgren: Private communication.
- (10) P. Moeller-Petersen: "Diagnostics for electron/ion beam cooling", this workshop.
- (11) M. Brouet, M. Girardini, L. Hütten, A. Poncet, H. Poth, A. Wolf: "Ultra-high vacuum test measurements on LEAR electron cooler". To be published.

Fig. 1: LEAR electron cooler

-104-



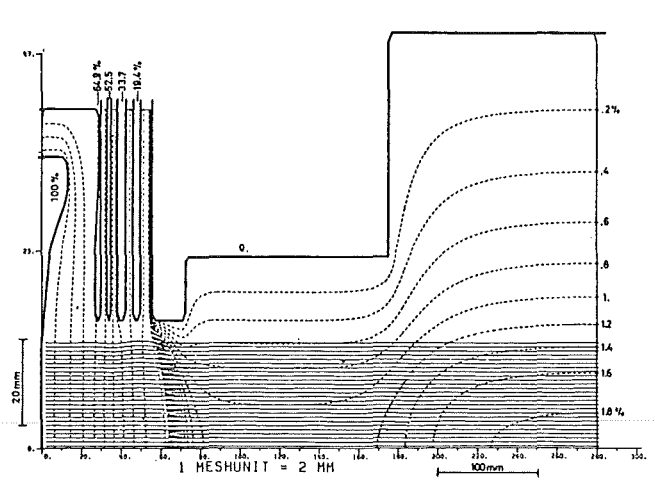


Fig. 2 - The LEAR Electron Gun. Calculated electron trajectories (full), and electric potential lines (dashed) in a constant longitudinal magnetic field. Potentials are given in percent of the cathode high voltage.

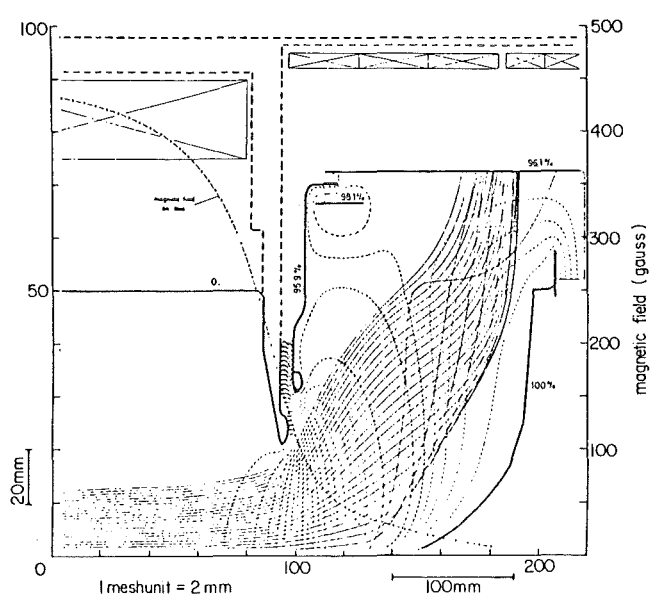
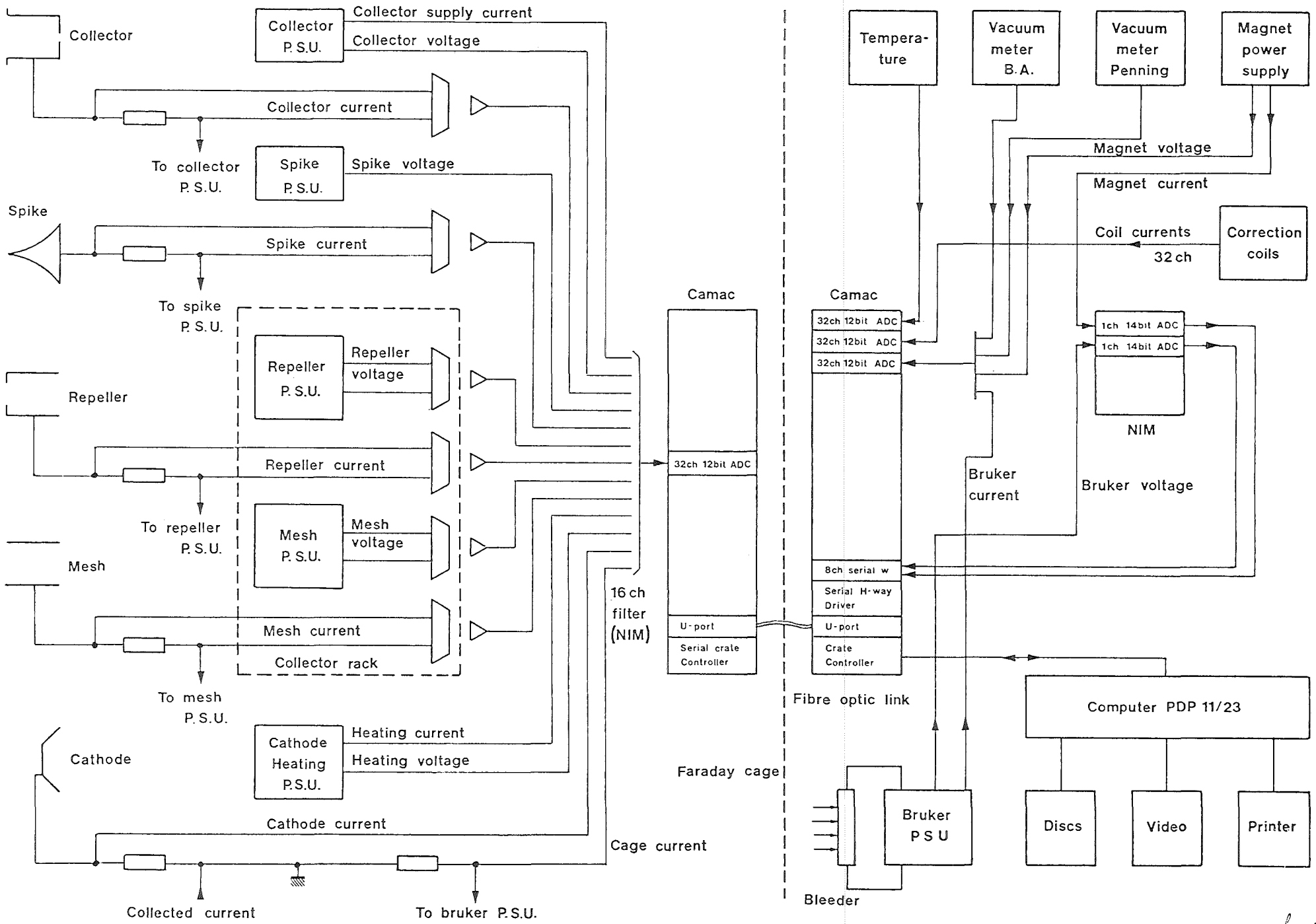


Fig. 3 - The LEAR Electron Collector. Calculated electron trajectories (full), electric potential lines (dashed, percentage of cathode high voltage) and the magnetic field on the axis (dashed-dotted).

FIG 4. Electron cooling monitoring system



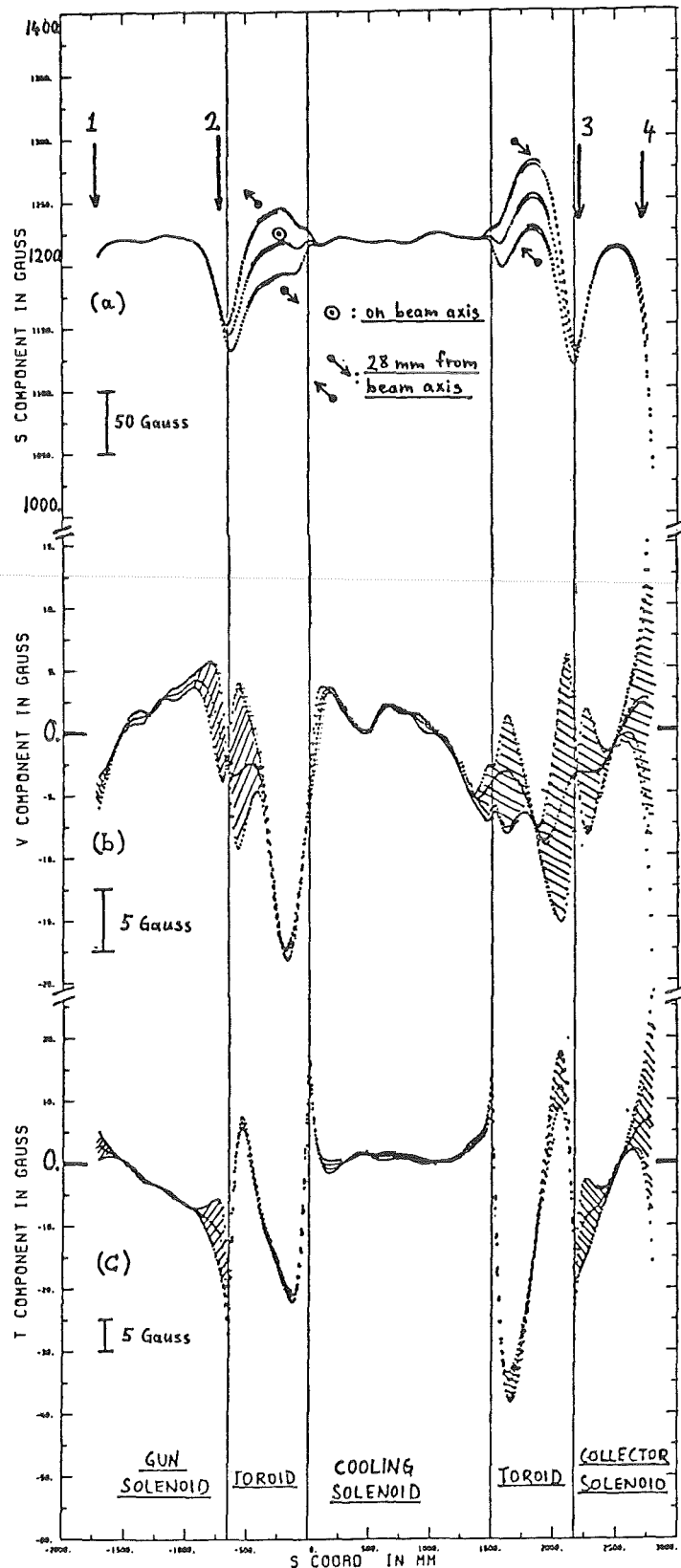
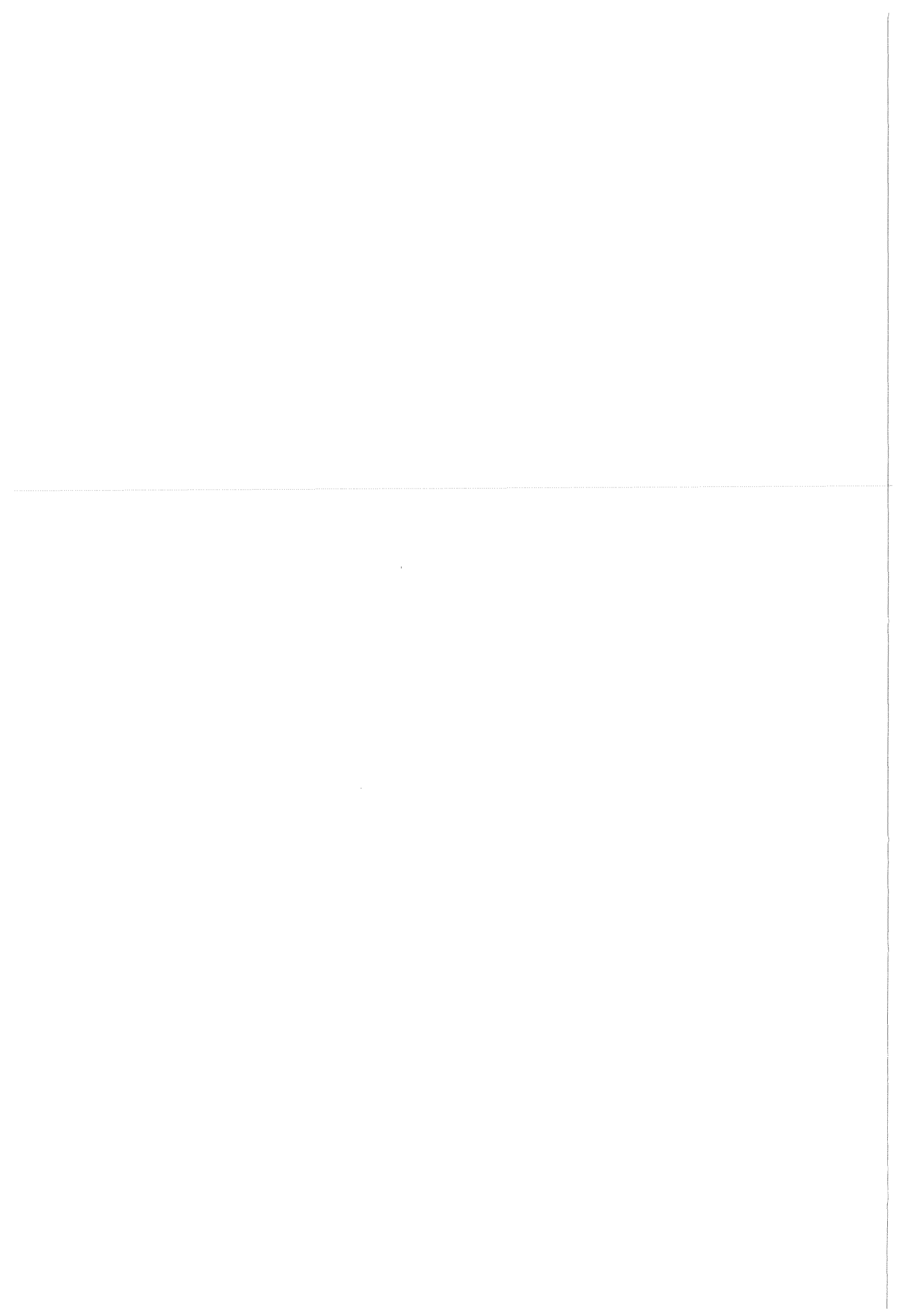


Fig. 5 Magnetic field components along the electron beam:  
 a) Longitudinal component;  
 b) Transverse component perpendicular to the bending plane of the toroids;  
 c) Transverse component in the bending plane of the toroids.



Some Performance Predictions for The IUCF Cooler \*

Robert E. Pollock  
Physics Department, Indiana University, and IUCF

Abstract

Factors influencing the performance of a storage ring with electron cooling and internal targets are reviewed from the standpoint of the implications for facility design. The emittance of the stored beam, at intensities useful for nuclear physics applications, is estimated to be on the order of  $0.1\pi \text{ mm-mrad}$ , limited by intrabeam scattering. The dispersion-matching technique, for obtaining higher resolution in scattering experiments with magnetic spectrometers, appears to be limited in usefulness by the manner in which a high resolving power waist increases the transverse beam heating by intrabeam scattering, and therefore the equilibrium emittance. Resolution of order 10 keV, obtained by dispersion-matching, appears possible only for proton beam energies below about 100 MeV. At higher energies the cooled beam momentum resolution must be better than the resolution goal of the experiment.

---

\* This work was supported by the U.S. National Science Foundation under grants NSF PHY 81-14339 and 82-11347.

### Introduction

A storage ring with electron cooling is under construction at the Indiana University Cyclotron Facility (IUCF). This "Cooler" is designed for use in intermediate energy nuclear physics experiments employing light ions incident on ultrathin internal targets. The design range of velocity and magnetic rigidity corresponds to protons of kinetic energy  $12 \leq T_p \leq 500$  MeV. Other light ions which are presently available from the IUCF cyclotrons, including deuterons, helium and lithium ions, will also be accommodated. The Cooler is expected to retain hydrogen beam polarization transverse to the bend plane.

The ring can function as a synchrotron to adjust the stored beam energy after accumulation. Because the average current transferred to the Cooler during periodic refills will be much less than the cyclotron output current, the Cooler will normally operate in combination with more conventional cyclotron experiments, stealing beam intermittently, of particle type and energy determined by the other user, and then adjusting the stored beam energy to the value required by the Cooler user.

The project began construction in 1983 and is scheduled for startup in 1987.

The properties of the electron cooling force determine the performance of a storage ring in which beam heating caused by passage of the beam through an internal target, and by other disturbances such as intrabeam scattering, is balanced by the interaction with an intense cold electron beam. In this report, the status of our understanding of some phenomena affecting the performance, and the implications for the Cooler design, are reviewed. The intent is to provide an update of information which appeared in the original Cooler proposal<sup>1</sup> some four years ago. A companion paper<sup>2</sup> gives more detail of the present Cooler design.

### Relation Between Beam Emittance and Beam Intensity

Emittance is a more useful measure of the transverse beam quality than is beam temperature. The temperature (a measure of velocity spread) changes from point to point around the ring due to compression and expansion by the confining strong-focussing lenses, while the emittance (a measure of phase space area for a given transverse dimension) is quasi-invariant, being changed slowly over the course of many orbit periods by microscopic processes such as particle-particle scattering which circumvent the Liouvillean constraint of constant phase space density (constant "brightness").

We discuss in the following subsections, and summarize in Figure 1, a number of physical phenomena which act to constrain the beam emittance and intensity. The curves are evaluated for protons in the IUCF Cooler at five energies spanning the operating range.

#### a) Emittance Upper Bound

It is useful to examine the beam emittance in the absence of a target. The ring acceptance forms an absolute upper bound to the phase space volume of the stored beam, and is an economic limit related to magnet apertures. In the IUCF Cooler, ring tunes have differing acceptances over a factor of two range. The beam emittance, however, must be smaller than the acceptance by a factor chosen to give a long storage lifetime. This factor is determined by the tails of the distribution. For electron machines, in which the tails are generated by synchrotron radiation, the factor is of order ten. For the IUCF Cooler, a study<sup>3</sup> of the effect of finite acceptance on the lifetime against scattering on residual gas, has shown that a 90% emittance of  $6\pi$  mm-mrad in an acceptance of  $25\pi$  leads to a loss rate which is larger by a factor of about two compared to the loss rate of a beam of zero emittance. We take this emittance value of  $6\pi$  as a practical upper bound.

b) Emittance Lower Bound

One lower bound to the stored beam emittance comes from the finite temperature of the electron beam. If the beam were otherwise undisturbed, a thermal equilibrium would be established between the electron beam and the stored ion beam. More correctly, the temperature of the cooled ion beam in the electron region of the ring would come into equilibrium with the electron beam. The temperature elsewhere in the ring can be found using the invariance of the emittance with azimuth, in conjunction with the known azimuthal dependence of the lattice parameters.

The relation between transverse beam temperature at a waist and beam emittance is simply expressed in terms of the aperture function<sup>4</sup>  $\beta_x$ :

$$\epsilon_x = \pi \beta_x \theta_x^2; \text{ where: } 1/2 kT_x = (\Delta p_x)^2 / 2m = 1/2 mc^2 \beta^2 \gamma^2 \theta_x^2.$$

The energy dependence appears because the emittance is defined in terms of an angle, through the momentum ratio  $\theta_x = (\Delta p_x / p)$ , and  $p = mc\beta\gamma$ . Figure 1 shows the result for an aperture function of  $\beta_x = \beta_y = 6.5$  m, and an assumed equilibrium temperature of 0.2 eV at all electron energies. Except at the lowest stored currents, other phenomena set the lower bound.

The ion beam must be smaller in diameter than the electron beam to avoid the strongly non-linear electrostatic defocussing forces outside the electron beam boundary. For a given emittance, the minimum ion beam size is obtained if the aperture functions  $\beta_x$  &  $\beta_y$  are equal to half the length of the electron beam cooling region. This choice gives the minimum electron beam power for a fixed current density.

The fastest cooling of the tails of the ion beam is obtained if the angle spread of an ion beam of emittance equal to ring acceptance is comparable to the angle spread of the electron beam, because the transverse cooling time involves a factor<sup>5</sup>  $(\theta_e^2 + \theta_i^2)^{3/2}$ . This leads to a second relation

which is equivalent to an energy-dependent bound on the aperture function at the cooling waist. The IUCF Cooler has been designed with a variable  $\beta_x, \beta_y$  in the cooling region for optimum performance over a range of ion velocities.

The cooling rate has a plateau over a range of ion beam emittances which is equal to the ratio of ion mass to electron mass. Ideally, the cooling region  $\beta_x$  is adjusted so that this range overlaps the acceptance on the high end, so that the tails of the beam distribution will cool rapidly, and the emittance corresponding to equilibrium temperature on the low end.

Equating temperatures is an oversimplification because the effects of the confining magnetic field on the cooling interaction make possible an ion temperature which is substantially below the electron temperature<sup>6</sup>.

c) Stored Current Upper Bound

So far the discussion has been essentially independent of ion beam intensity. A storage ring has a number of instabilities that can set upper bounds to the stored intensity. A discussion of these phenomena is outside the scope of this paper. We show in Figure 1 a single example for the IUCF Cooler, the transverse resistive wall instability<sup>7</sup> (TRWI). If the assumption is made that the cooling force provides the only stabilizing mechanism, and that the wall impedance is that of a smooth stainless steel vacuum chamber of uniform cross section, the emittance-independent current limit shown on the right of Figure 1 is obtained.

It is clear that there could be electron beam - ion beam interactions or other effects which could set in between the highest<sup>8</sup> ion current of a few times  $10^{15}$  ions/second which has been observed with electron cooling in use, and the TRWI stability limit which is nearly two orders of magnitude higher. This is a question which can only be settled by further tests with a working cooler ring.

d) Tune Shift Limit

In addition to collective effects of the beam interacting with its environment, there is an interaction of individual particles within the beam with the electromagnetic field due to all the other particles of the beam. One of the familiar consequences is a defocussing force on the beam surface that is not present on the axis of the beam and which leads to an incoherent tune shift that must be small to avoid loss at tune resonances. This tune shift forms an emittance- and energy-dependent intensity limit as indicated in Figure 1. In the construction of Figure 1, the assumption is made that residual lattice coupling effects will lead to equality between the two transverse emittances. This leads to a linear relation between intensity and emittance for a given incoherent tune shift. A maximum allowable tune shift of 0.1 is assumed.

In the absence of a target or other heating mechanism, the tune shift limit might be expected to manifest itself by a beam loss if cooling were applied at intensities where this limit was reached before equilibrium could be established. The presence of a controlled heat source such as a target of variable thickness in the ring will allow the exploration of the onset of this limiting mechanism.

e) Intrabeam Scattering Limit

There is an additional and important relation between intensity and emittance which arises from the intrabeam scattering (IBS)<sup>9</sup> of individual beam particles from one another. The rate depends on the six-dimensional beam brightness, on the properties of the lattice, and on the shape of the equilibrium distributions in phase space. With the assumptions of a flattened velocity distribution and of a heating rate by the IBS mechanism which is

balanced by electron cooling, a relation can be obtained giving emittance varying as the 0.4 power of the beam intensity. A similar dependence emerges from a full computer simulation<sup>10</sup>. The position of the curve on Figure 1 makes clear that this mechanism may be expected to set a lower bound for emittance of about  $0.1\pi \text{ mm-mrad}$  for intensities of order  $10^{16} \text{ s}^{-1}$  at energies above 100 MeV in the IUCF Cooler.

The theory of intrabeam scattering has been tested in the regime of moderate particle density and high temperature where it sets an important limit to the luminosity lifetime of colliding particle beams. It should be noted that the assumption of two-body collisions which is central to the IBS theory in its present form may require modification for very cold dense beams where there are many particles within an interaction distance and where the timescale of the IBS collision is long enough that the sudden collision approximation begins to break down. The analogy can be drawn with the cooling interaction which has required important corrections for adiabatic collisions in the magnetic confining field<sup>11</sup>. The measured Novosibirsk beam sizes<sup>6</sup> imply an emittance lower by an order of magnitude than the IBS curve shown in Figure 1, which may indicate a disagreement with the IBS theory in its present form.

#### f) Target Effects

When a target is placed in the ring, its thickness must be small enough that the cooling force can make up for the rate of energy transfer to target electrons. The thickness limit<sup>3</sup> is on the order of  $10^{16} \text{ electrons/cm}^2$ . Nuclear target densities which are consistent with the above limit have a transverse heating rate by multiple small-angle scattering by the target nuclei which is comparable to the heating predicted by the standard IBS theory, except for targets of large atomic number Z, where the equilibrium emittance is largely determined by the target.

g) Summary of the Emittance-Intensity Relations

The various limiting phenomena discussed above and summarized in Figure 1 define the boundaries of a region in intensity-emittance space within which the stored beam must be located. One can describe some of the operations performed on the beam in terms of the motion of a point representing the beam within this bounded region. For example, the incident beam has the properties of the injection accelerator and can be represented by a point on the figure. The IUCF cyclotron beam has a moderately small emittance and low peak intensity and appears on the left of the figure. The stacking of beam in the Cooler leads to an increase in emittance as the stored intensity is raised, shifting the point representing the stored beam progressively toward the upper right on the figure as stacking proceeds.

Different stacking methods affect the emittance by differing amounts. Transverse stacking gives a direct increase in emittance which limits its usefulness, while for longitudinal stacking the effects are indirect (eg through cumulative kicker perturbations). Stripping injection causes a slow growth in emittance from multiple traversals of the stripping material.

After stacking is completed, the electron cooling lowers the stored beam emittance until an equilibrium is established which is appropriate to the beam energy, stacked intensity, and the amount of target material in the path of the beam. Experimental data-taking may then begin. After some time, the loss of intensity from interactions with the target gives an unacceptable event rate and refilling is called for. The emittance should improve only slightly as the experiment proceeds because the target heating prevents the beam from following the constant brightness contour given by IBS alone.

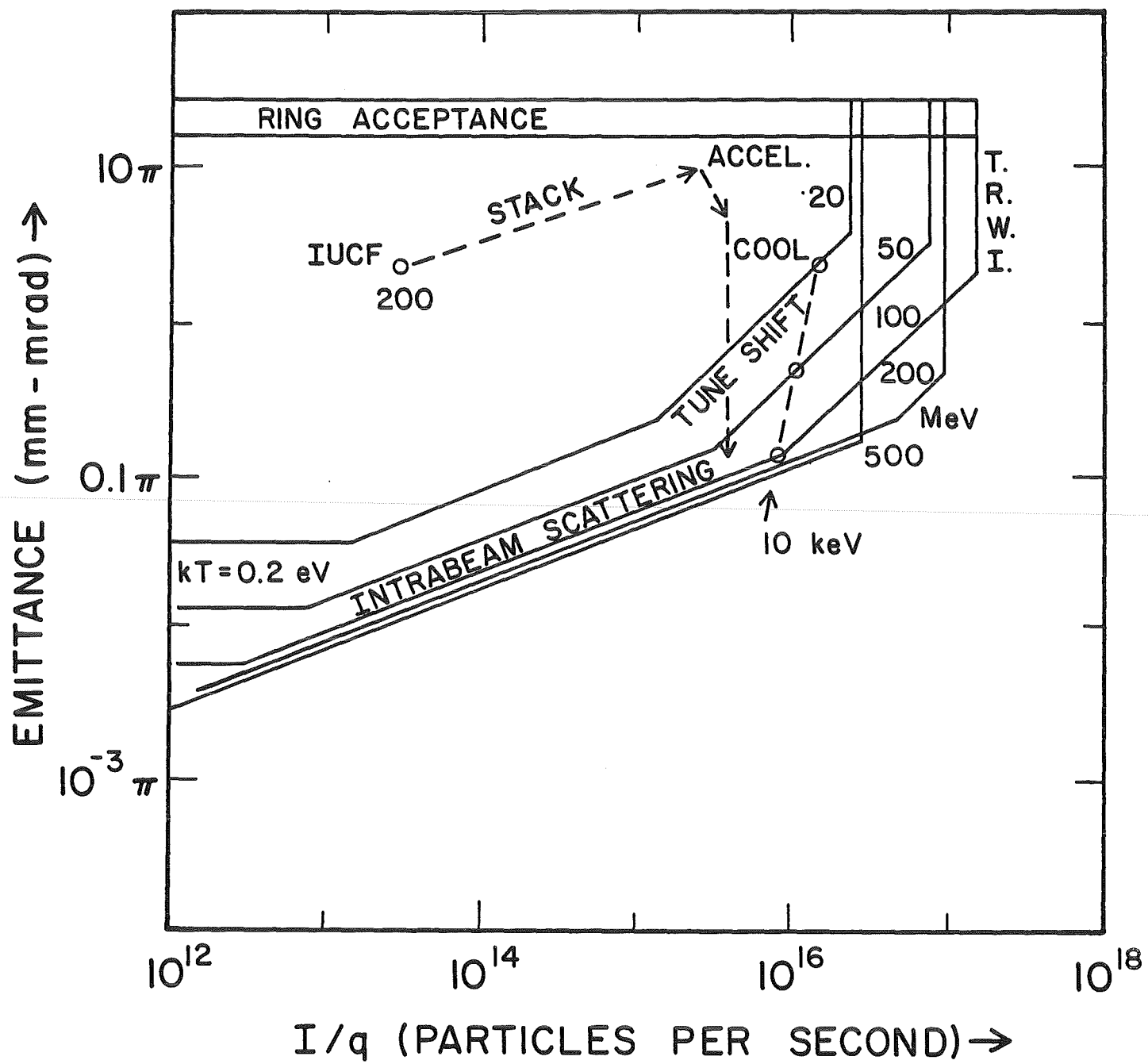


Figure 1. The relation between beam intensity and beam emittance as estimated for the IUCF Cooler. The lines are bounds for an allowed region of emittance for several proton energies. The physical phenomena and design characteristics which generate the bounds are discussed in the text.

Implications for an Optimal Lattice Design

Given the relation between emittance and intensity as described in the previous section, what are some of the implications for the design of a storage ring for electron cooling? One immediate consequence has to do with the usefulness of the dispersion-matching technique<sup>12</sup> which improves the resolution of a spectrograph experiment by making the overall resolution in excitation energy independent to first order of the beam momentum spread.

The first order resolution with a properly matched system will be given by the ratio of dispersion  $\eta$  ( $\eta = p \cdot dx/dp$ ) to beam size:

$$p/\Delta p = \eta/x = \eta/2(\beta_x \cdot \epsilon_x/\pi)^{1/2}$$

The ring dispersion is matched to that of the spectrograph, so for high resolution the beam size itself must be small, either through a small emittance  $\epsilon_x$  or small value of  $\beta_x$ , the aperture function at the target, or both. Using the results summarized in Figure 1, and the properties of a high resolution spectrograph nearing completion at IUCF, we conclude that the highest intensity of beam for which it will be possible to obtain at least 10 keV resolution in a dispersion-matched mode, (ie. independent of the momentum spectrum of the stored beam), is as shown by the dashed line in Figure 1. This intensity is high enough for most nuclear experiments only for energies below 100 MeV. At higher energies, the slow variation of the intrabeam scattering-determined equilibrium emittance with intensity, implies that an unacceptably low intensity must be employed to achieve the required emittance.

Attempts to reduce the value of  $\beta_x$  run into at least three problems. The first problem is with chromaticity correction for the long straight section which is required by the size of the spectrograph. A smaller  $\beta_x$  at the target leads to a larger  $\beta_x$  at the lattice quadrupoles at the end of the straight section.

The hexapole strength required to cancel the chromaticity is not strongly dependent on the  $\beta_x$  at the quadrupoles, but higher order effects enter as  $\beta_x^{3/2}$  and lead to containment problems that show up in particle tracking for target  $\beta_x \approx 0.3$  m.

A second difficulty arises from the coupling, through the presence of dispersion, of energy changes, caused by beam collisions with target electrons, to the transverse x coordinate. A beam energy change in the target causes a shift in the equilibrium orbit, if dispersion is non-zero, which results in an increase in emittance because the beam particle begins to perform betatron oscillations about the new equilibrium orbit of amplitude given by  $\Delta x = \eta \cdot \Delta p/p$ , where  $\eta$  is the dispersion and  $\Delta p/p$  is the fractional change in the longitudinal momentum component caused by the collision. The area of the phase space ellipse traced out by an individual particle after such an event is  $\epsilon_x = \pi(\Delta x)^2/\beta_x = \pi \cdot (\eta^2/\beta) \cdot (\Delta p/p)^2$ . The transverse heating rate by the random walk increase in emittance induced by a succession of such collisions is proportional to the same resolving power parameter  $(\eta^2/\beta)^{1/2}$  which appears in the expression for the resolution. Thus there is a mechanism for increasing the equilibrium beam emittance which grows if the lattice is modified to try to improve the resolution.

The emittance change caused by the above mechanism can be sufficient to lead to a loss of beam after a single electron knockon ("δ-ray") event if the resulting emittance exceeds the acceptance of the ring. In the IUCF Cooler, this can be the principal loss mode<sup>3</sup> for targets placed at dispersed waists. It should be noted that both heating and loss effects described above work in the opposite direction to the transverse heating by multiple-scattering from target nuclei, which is minimized by reducing the aperture function at the target. The optimal lattice would require a target Z-dependent tune.

A third difficulty arises from the nature of the IBS process. The heating of the beam is driven by a term which also involves the parameter ( $\eta^2/\beta$ ), so that even if the target were too thin to heat the beam, the IBS would give rise to a larger emittance if the lattice were modified to try to increase the resolving power. For the IBS mechanism there is a threshold value for ( $\eta^2/\beta$ ) below which a scattering exchange of momentum from a transverse direction into the longitudinal direction leads to transverse cooling and above which the dispersion-coupling results in heating in the dispersed plane.

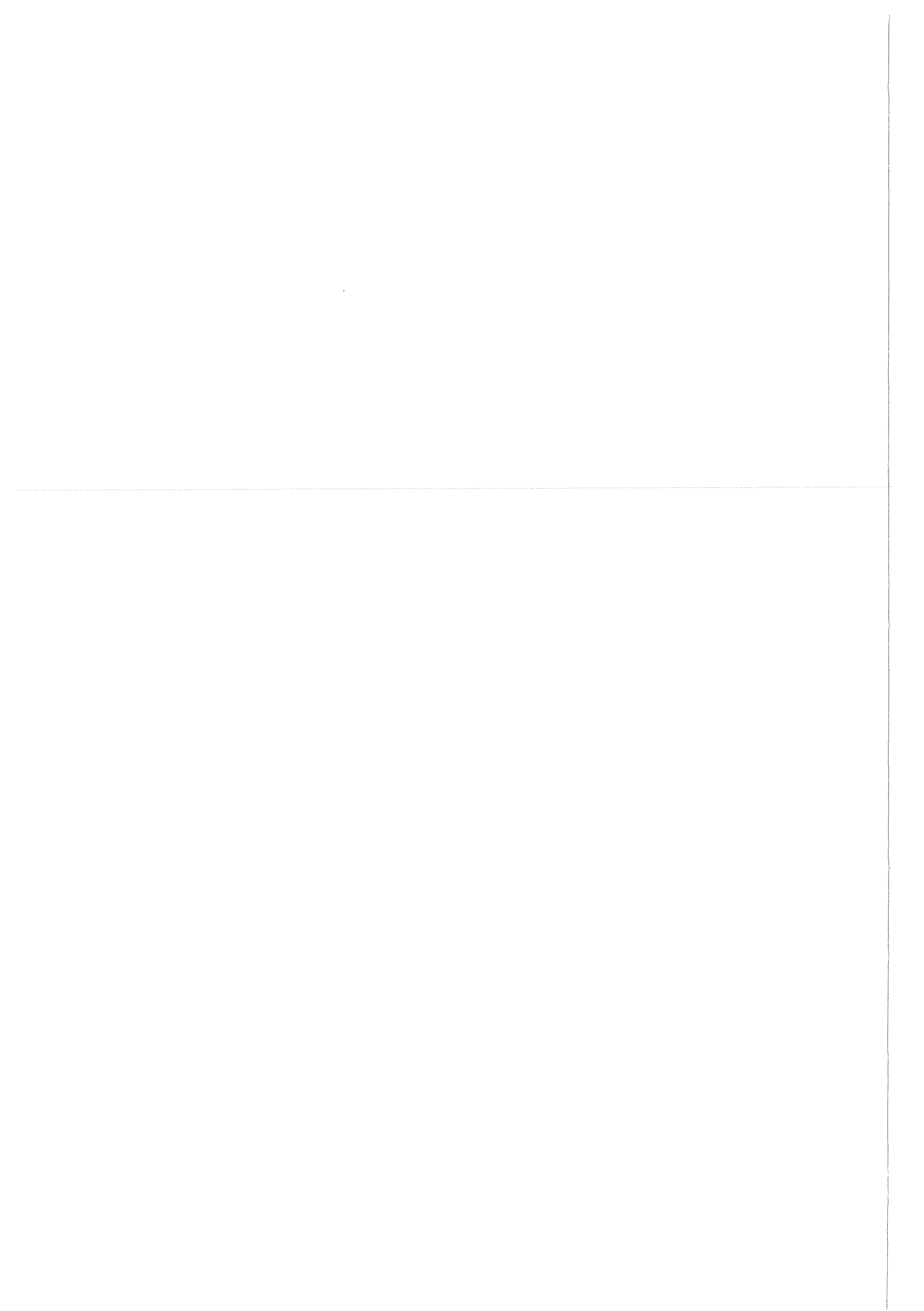
Detailed calculations are needed to find the optimum behaviour as a result of the interplay of these three mechanisms with target heating phenomena. It appears to be the case, however, that the usefulness of the dispersion-matching technique is limited to the lower end of the operating energy range of the IUCF Cooler and that over most of the range, it will be the narrowness of the energy spread of the stored beam which must be relied upon to obtain good resolution. Had we known this some years ago, the design strategy for our Cooler might have been altered. In particular it would have been preferable to have a lower resolving power at more of the waists set aside for experimental targets to reduce the loss rates.

#### Acknowledgement

A group of approximately 40 people is at work on the IUCF Cooler project. In many cases, important design concepts have emerged from group discussions. It is impractical to give detailed recognition to the work of each individual in this short note. Nevertheless the author is very conscious of the fact that he is representing the efforts of many colleagues when asked to report on our common endeavors.

References

1. "IUCF Cooler-Tripler, A Proposal for an Advanced Light Ion Physics Facility", IUCF Internal Report 1980.
2. R.E. Pollock, Status Report on the IUCF Cooler, Proceedings of the IUCF Cooler Workshop, October 1984 (to be published, A.I.P. Conf. Proc.)
3. H.-O. Meyer, op. cit. (to be published)
4. E. Courant & H. Snyder, Annals of Physics 3 (1958) 1
5. Ya.S. Derbenev & A.N. Skrinsky, Particle Accelerators 8 (1978) 235
6. A.N. Skrinskii & V.V. Parkhomchuk, Sov. J. Part. Nucl. 12 (1981) 239
7. V.K. Neal & A.M. Sessler, Rev. Sci. Instr. 32 (1961) 276; L.J. Laslett, V.K. Neal, & A.M. Sessler, Rev. Sci. Instr. 36 (1965) 424
8. M. Bell et al, Nucl. Instr. Meth. 190 (1983) 249
9. J.D. Bjorken & S.K. Mtingwa, Particle Accelerators 13 (1983) 115
10. H. Herr, Proc. Heidelberg Workshop on Cooling in Heavy Ion Rings 1984
11. A.H. Sorensen & E. Bonderup, Nucl. Instr. Meth. 215 (1983) 27
12. S.A. Martin et al, Nucl. Instr. Meth. 214 (1983) 281



EUROPEAN COOLER STORAGE RINGS  
=====

(S. Martin, KFA-Juelich)

A review of european cooler storage rings is given. The existing storage rings at CERN AA (1) and LEAR (2) are discussed. A few general requirements on the design of accumulator storage rings are discussed at the example of the approved new antiproton accumulator ACOL (3) at CERN. The basic ideas of the cooler storage rings at rings at CELSIUS, Uppsala (4), ESR at the GSI Darmstadt (5), the Heavy Ion Cooling Experiment at the MPI Heidelberg (6), and the COSY ring at the KFA-Juelich (7) are given. New cooler storage rings for heavy ions are proposed at Aarhus and Stockholm (8).

The history of the storage rings for antiprotons at CERN has been discussed by K. Johnson (9).

The ACOL-AA-combination demonstrates a few general features of cooler rings from the designers point of view (10): The transverse acceptance of the ACOL is larger by a factor 2.2 than in the AA, because of the stronger focusing. The 4 straight sections are dispersion free. The increase in momentum acceptance is done by bunch rotation followed by adiabatic debunching using 2 high Q cavities ( $U*T=750$  KV). The stochastic precooling in ACOL will be done within 2.4 sec first transverse then longitudinal (frequency between 1 and 3 GHz). Because of the higher intensity the cooling in the AA will be improved (core cooling 4-8 GHz, momentum cooling 2-4 GHz, stack tail cooling 1-2 GHz).

The LEAR operation has demonstrated the feasibility of a few very important features for the other cooling rings in discussion: The small dispersion in magnets and straight sections is good for stochastic cooling (very high transition causes good "mixing") and for all kind of "...transverse gymnastic of coasting beams" (11) and favorizes the ultra slow extraction process.

The CELSIUS ring will be buildt by a cooperation of different laboratories (Gustav-Werner-Institut Uppsala, CERN, Studsvik, Royal Inst. of Techn. Stockholm). The lattice of CELSIUS is a modified version of the ICE (12) ring. The horizontal and vertical acceptances are 50 resp. 150  $\pi*mm*mr$ . A 9.6 m long straight section houses the 100 KeV electron gun. This allows to do cooling of protons up to 185 MeV. The maximum energy is 520 MeV in the first and 1300 MeV in a later stage. A preliminary calculation of H. Herr (13) shows that for  $10^{11}$  particles in the ring a momentum spread of about  $3 \times 10^{-4}$  is expected.

The experimental background for the ESR (5) is given by proposed experiments with fully stripped very heavy ions, by accumulation of secondary beams (large acceptance), by experiments to study the e-capture cross section, and the ion-photon interaction. The request for very low energies of naked heavy ions led to a study on the feasibility decelerating the beam from the maximum energy of 560 MeV/A for U(92+) down to 10 MeV/A. For experimental reasons multicharge operation needs to be possible, e.g. U(87+) until U(92+). The large acceptance of 530 resp. 160  $\pi*mm*mr$  allows inflight experiments using crossing beams. The variability of the optics of the ring is done by maintaining the different periods with different tunes together. In this way high and low dispersion modes are possible.

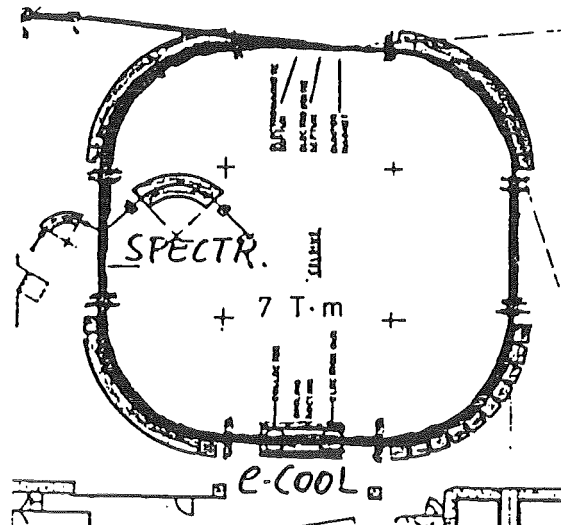
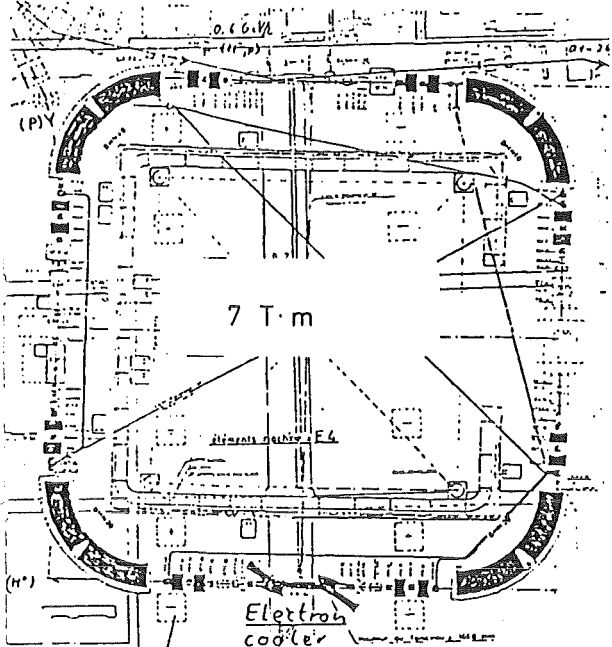
The Heidelberg Heavy Ion Cooling Experiment (6) is an accelerator experiment to study problems related to the cooling of heavy ions, to measure e-capture during cooling, to study the multiple charge mode and the behaviour of internal jet targets. The lattice is not completely frozen but at least 4 straight sections should leave space for injection, cooling and 2 experimental areas. The adjustment of the beam properties to the experiment is realized by changing the tune in the different periodes of the ring.

The Aarhus ring is designed for highly charged heavy ions injected from the Aarhus EN tandem. The physics program are studies of the ion-ion, the electron-ion, and the light-ion interaction. The laser cooling will be studied (14). The CRY ring at the Institute of Physics, Stockholm, has in this stage of discussion a similar lattice as the Aarhus ring, but the injector is a CRYEBIS source followed by a RFQ accelerator (15).

The combined synchrotron-cooler-ring COSY is proposed to perform proton and light ion physics at energies between 100 and 1500 MeV (16). The ring has the two functions of a storage ring and an accelerator. Acceleration from 45 MeV protons up to the bending limit of 10 Tm will be possible. Two 35 m long straight sections maintain the beam to the shape as it is requested by the experiment as well as by the electron cooler. The tune shift in the straight sections is always  $2\pi$ , so it will in 0'th order not be seen by the rest of the ring. The injectors will be the existing Juelich cyclotron and in a later stage the 1100 MeV SNQ LINAC (17).

References:

- (1) Design study of a Proton-Antiproton colliding beam facility. CERN/PS/AA 78-3, 1978
- (2) P. Lefevre, D. Moehl, G. Plass: The CERN low energy antiproton ring project. Proc. of the 11th International Conference on High Energy Accelerators, Geneva 1980
- (3) E.J.N. Wilson (Editor): Design study of an Antiproton Collector for the Antiproton Accumulator (ACOL). CERN 83-10, Geneva 1983
- (4) A. Johansson: CELSIUS - Cooling with Electrons and Storing of Ions from the Uppsala Synchrocyclotron. Report at the Workshop on the Physics with Heavy Ion Cooler Rings, Max-Planck-Institut für Kernphysik, Heidelberg, May 1984
- (5) B. Franzke, H. Eickhoff, B. Franczak, B. Langenbeck: Zwischenbericht zur Planung des Experimentier-Speicherringes (ESR) der GSI. GSI-SIS-INT/84-5, Darmstadt, August 1984
- (6) E. Jaeschke: Study on a Heidelberg Heavy Ion Cooler Ring. Report at the Workshop on the Physics with Heavy Ion Cooler Rings, Max-Planck-Institut für Kernphysik, Heidelberg, May 1984
- (7) S. Martin: Design Criteria for the Cooler Synchrotron COSY. Report at the Workshop on the Physics with Heavy Ion Cooler Rings, Max-Planck-Institut für Kernphysik, Heidelberg, May 1984
- (8) A. Steensgaard: private communication at this conference
- (9) K. Johnson: Opening Address to the CERN Accelerator School Antiprotons for Colliding Beam Facilities, CERN 84-15
- (10) S. van der Meer: A short description of ACOL. CERN note, PS/AA/ACOL Note 84-4
- (11) P. Lefevre: LEAR, lecture given at the CERN Accelerator School Antiprotons for Colliding Beam Facilities. CERN 84-15
- (12) M. Bell et al. Nucl. Instr. Meth. 190 (1981), p. 237
- (13) H. Herr: Limits on the final energy spread in the ring. Contribution to the Workshop on the physics program at CELSIUS, Uppsala, November 1983
- (14) O. Poulsen: Laser cooling of fast accelerated ion beams. Contribution to the Workshop on the physics program at CELSIUS, Uppsala, November 1983
- (15) C.J. Herrlander: private communication, June 1984
- (16) Arbeitsgruppe COSY: Studie zum Bau eines kombinierten Kühler-Synchrotron-Rings an der KFA. JüL-Spez-242, Febr. 1984, KFA Jülich
- (17) KFA Jülich GmbH: SNQ Project Proposal for a Spallation Neutron Source, KFA Jülich, December 1984



ESR Darmstadt

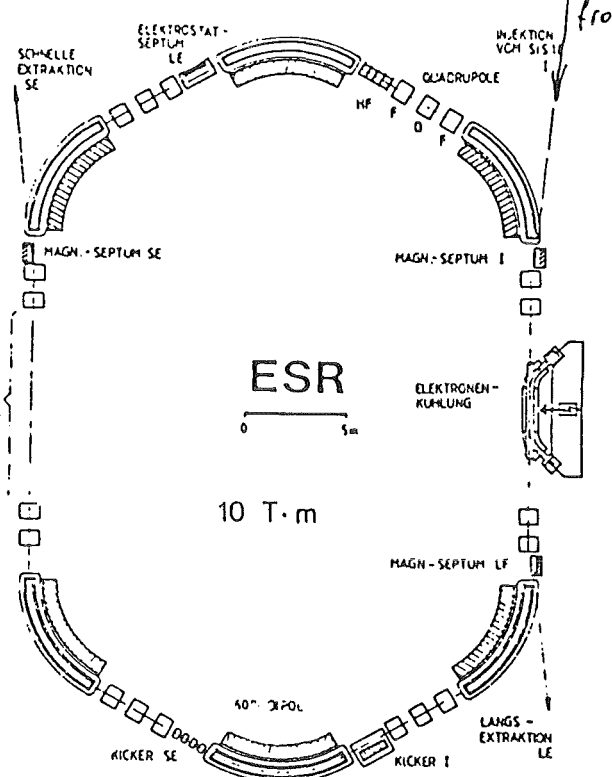
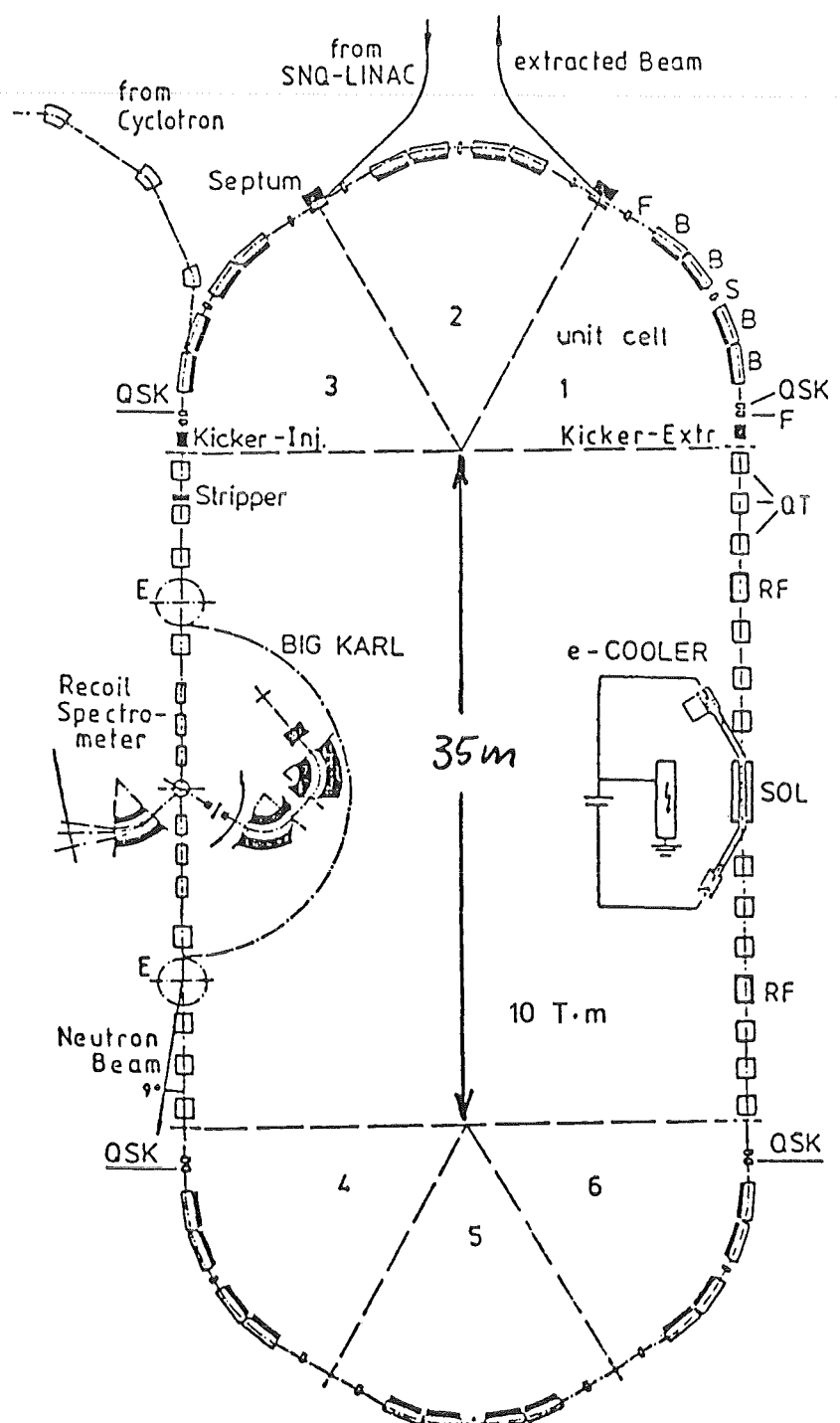
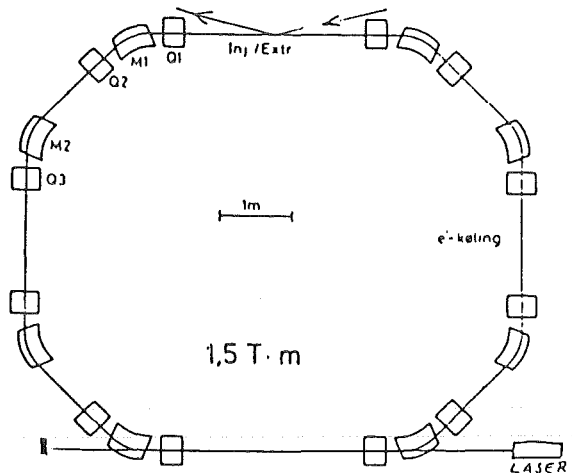


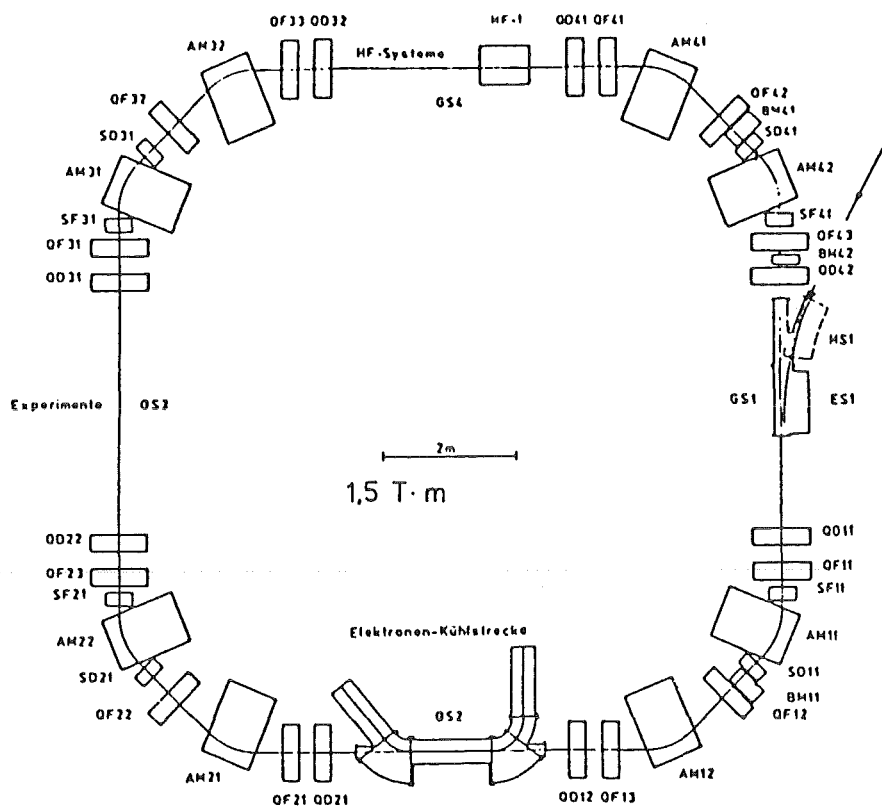
Fig.1: The cooler rings  
LEAR, CELSIUS,  
ESR and COSY



AARHUS



TSR Heidelberg



CRY RING Stockholm

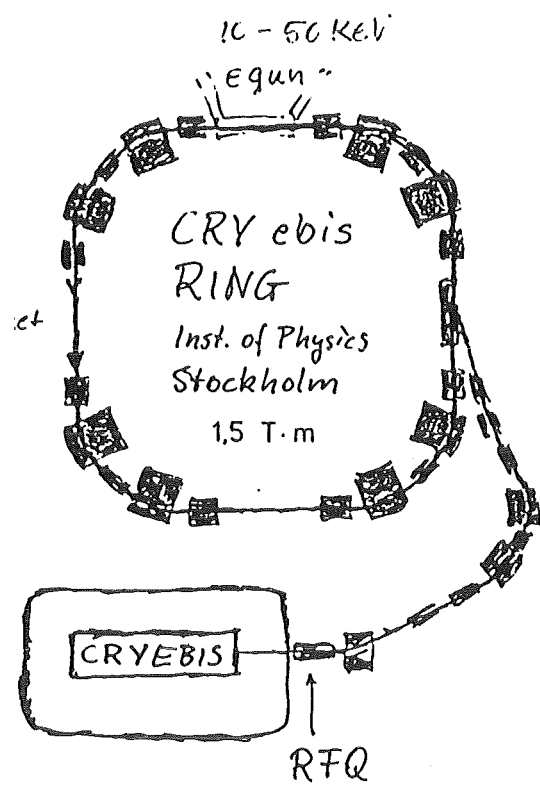


Fig.2: The cooler rings at  
Aarhus, Heidelberg and  
Stockholm

ELECTRON COOLING PROJECT AT INS

T. Tanabe, M. Sekiguchi, K. Sato, A. Noda, M. Kodaira,

M. Takanaka, J. Tanaka, H. Tsujikawa, T. Honma,

T. Katayama, A. Mizobuchi and Y. Hirao

Institute for Nuclear Study, University of Tokyo,

Tanashi, Tokyo, Japan

INTRODUCTION

Recently, much interest has been focused on the cooling of ion beams by cold electrons as a very powerful technique complementing the stochastic cooling. At the INS, a project of electron cooling has started at the beginning of this year (1984).

Since 1978, we have studied accelerator technologies for the accumulation and stochastic cooling of ion beams<sup>1)</sup> by using a storage ring, TARN<sup>2)</sup>. After completion of these experiments at the end of this year, we intend to shut down the machine and to construct a newly extended ring, TARN II, by using the most components of the present TARN and by adding some new elements. The main purpose in the TARN II is the study of accelerator technologies concerning synchrotron acceleration, beam cooling, slow extraction and so on. Such a study will open possibilities for further accelerator ring developments. Nuclear physics research will also be studied in parallel with the machine studies. The discussion for the physics experiments has just begun.

THE RING

The layout of the TARN II is shown in Fig. 1 together with the TARN and the beam line from the injector cyclotron. It consists of a ring of 75 m circumference with hexagonal layout. The maximum size

is limited by the dimensions of the existing building for the ring, which are about 26 meters by 30 meters. The magnet lattice consists of 24 dipoles and 18 quadrupole singlet magnets which are all made of laminated steel plates. The layout of the ring offers six straight sections as shown in Fig. 1. These are used for electron cooling, stochastic cooling, injection, extraction, RF equipment and internal target station.

The main parameters of the ring are listed in Table 1, although the final design parameters have not yet been fixed. The maximum energy is 1.3 GeV for proton, while it is 450 MeV/A for ions with  $Q/A=1/2$ . The rising time of the magnet system up to fully excited level is 0.75 sec and the repetition rate is less than 1/2 Hz, which depends on the operation mode. The RF system is operated from 0.76 MHz to 7.50 MHz in harmonic number of 2, which cover the frequency range required for the acceleration of all ions up to full energies. The operating vacuum pressure is lower than  $10^{-10}$  Torr.

#### THE MODES OF OPERATION

The ring can be operated in two modes, depending on the aim of experiments. The mode I and II are relating mainly to the use of external and internal target experiments, respectively. In the mode I, ions are accelerated and then extracted in an ordinary synchrotron acceleration mode with rise time of 0.75 sec and repetition frequency of about 1/2 Hz. In the mode II, on the other hand, ions are cooled after acceleration with sufficiently long flat-top time. The lattice parameters are also different for these modes in spite of the same magnet system. This is because large acceptance is needed for the mode I in order to obtain high intensity beam. Also for the mode II, special attention has to be paid for the design of the lattice: 1) At the long straight section which installs the electron cooling device,

the dispersion function has to be zero. 2) At another straight section in which the internal target is set, amplitude function should be small. An example of the optics parameters studied for the mode II is listed in Table 2. The lattice design for these modes is described in detail by Noda<sup>3)</sup>.

#### THE INJECTOR

The injector of the ring, for the time being, is the existing SF cyclotron with  $K=68$ <sup>4)</sup>. The cyclotron can supply with fully or partially stripped ions from proton to neon. These ions are injected into the ring after completely stripped in a thin foil. Typical ion beams from the cyclotron are listed in Table 3. Their energies are high enough to obtain fully stripped ion beams. For the mode I, the number of ions injected into the ring by multi-turn injection is estimated to be about  $10^9$  for light ions and  $10^7$  for heavy ions. For the mode II, on the other hand, the numbers are less than those of the mode I by a factor of 10, because the acceptance for the mode II is limited inevitably due to the strong constraint to the lattice structure as described above. The peak current of the cyclotron is not so high. In the future, ion beams will be injected also from a LINAC system with energies of about 3 MeV/A. In this case, the intensity is expected to increase by two orders of magnitude. The first stage of the LINAC system, RF-Q LINAC with energies of 800 keV/A, is now being constructed.

#### THE ELECTRON COOLING SYSTEM

The main parameters of the electron cooling device are listed in Table 4, which are still preliminary at the present stage. The electron cooling device is designed to cool the ions from  $H^+$  to  $Ne^{10+}$ , up to 200 MeV/A, which is limited by the electron energy of

120 keV. This electron energy seems to be the upper limit from the high voltage holding capability of the gun and the collector in our geometry. The electron energy is variable from 12 to 120 keV with a maximum current density of  $0.5 \text{ A/cm}^2$ . The length of the interaction region between electron and ion is limited by rather short length (4 m) of the straight section. Therefore, in order to shorten the cooling time, it is indispensable to increase the electron current density. As the beam size at the cooling section after acceleration is mostly less than 50 mm, the cathode diameter is taken to be 50 mm. Maximum solenoid field of 1.2 kG is strong enough to attain the minimum electron temperature. Gun optics consists of Pierce type electrode and resonance focussing electrodes. In order to avoid unwanted transversal oscillation of electron beam, we choose a flat cathode rather than a spherical one. In this case, the cathode is immersed in the uniform solenoidal field. The design of the electron gun and collector is currently being studied by computer simulation with the help of the SLAC program<sup>5)</sup>. An example of electron trajectories in the region of the electron gun is shown in Fig. 2. The cooling time estimated by a simple formula for the transversal component is about 8 sec for 200 MeV proton and 2 sec for 200 MeV/A  $^{20}\text{Ne}^{10+}$ . If we use an internal target, a luminosity of around  $10^{30} \text{ cm}^{-2} \cdot \text{sec}^{-1}$  is expected for proton, assuming some reasonable conditions. A preliminary layout of the electron cooling device is shown in Fig. 3. Its shape is so-called U-scheme, in which electrons are injected and ejected over the beam line of the ring. This type was chosen by the engineering considerations and the boundary condition of the building.

The electron cooling device has some harmful effects on the synchrotron orbit, especially for low-energy ions during acceleration. The first one of these effects is the orbit

deformation mainly due to the toroidal field. The second one is the coupling between horizontal and vertical motions in the solenoidal field. And the third one is the tune shift of beam caused by the space charge of electrons. The last effect seems to be serious for low energy ions. Therefore, we intend to suppress the electron current density during injection and acceleration, by the control of gun anode voltage.

#### TIME SCHEDULE

The design and construction work of the TARN II and the electron cooling device has started this year. In 1986, an electron beam will be produced and its properties will be studied in the test. As the ring will be completed in 1986, the electron cooling device is scheduled to be installed in the ring also in the same year. The beam cooling test is expected to begin in 1987.

We would like to thank members of the computer section for the use of the FACOM-380R computer. The electron cooling project was supported by the Grant for Scientific Research of the Ministry of Education, Science and Culture.

#### References:

- 1) T. Katayama, Proc. of the Xth Int. Conf. on Cyclotron and their Applications, (East Lansing, 1984)
- 2) Y. Hirao et al., IEEE Trans. NS-26 (1979) 3730.
- 3) A. Noda et al., Contributed paper to this Workshop.
- 4) Y. Hirao et al., Proc. of the 7th Int. Conf. on Cyclotrons and their Applications (Birkhäuser, Basel, 1975), p. 103.
- 5) W. B. Herrmansfeldt, SLAC Report 226 (1979).

Table 1. TARN II Parameters

|  |                   |                        |
|--|-------------------|------------------------|
| Maximum beam energy                          | proton            | 1300 MeV               |
|  | ions with Q/A=1/2 | 450 MeV/A              |
| Circumference                                |                   | 75.60 m                |
| Average radius                               |                   | 12.03 m                |
| Radius of curvature                          |                   | 3.820 m                |
| Focusing structure                           |                   | FBDBFO                 |
| Length of long straight section              |                   | 4 m                    |
| Superperiodicity for mode I                  |                   | 6                      |
| " for mode II                                |                   | 3                      |
| Betatron tune value $\nu_x/\nu_y$ for mode I |                   | 1.75/1.75              |
| " for mode II                                |                   | 1.75/1.25              |
| Useful aperture                              |                   | 50x200 mm <sup>2</sup> |
| Transition $\gamma$ for mode I               |                   | 1.86                   |
| for mode II                                  |                   | 2.97                   |
| Rising time of magnet                        |                   | 750 ms                 |
| Repetition rate                              |                   | $\leq 1/2$ Hz          |
| Maximum field of dipole magnets              |                   | 18 kG                  |
| Maximum gradient of quadrupole magnets       |                   | 70 kG/m                |
| Revolution frequency                         |                   | 0.38 - 3.75 MHz        |
| Acceleration frequency                       |                   | 0.76 - 7.50 MHz        |
| Harmonic number                              |                   | 2                      |
| Maximum RF voltage                           |                   | 6 kV                   |
| Vacuum pressure                              |                   | $10^{-11}$ Torr        |

Table 2. Horizontal(x) and vertical(y) radial aperture function  
and dispersion for the mode II of the TARN II

| Station | $\beta_x$ (m) | $\beta_y$ (m) | $\eta$ (m) |
|---------|---------------|---------------|------------|
| Cooling | 36            | 19            | 0          |
| Target  | 1.6           | 2.7           | 4.8        |

Table 3. Typical ion beams from SF cyclotron

|              | $H^+$ | ${}^6 Li^{2+}$ | ${}^{11} B^{3+}$ | ${}^{12} C^{4+}$ | ${}^{14} N^{4+}$ | ${}^{16} O^{5+}$ | ${}^{20} Ne^{6+}$ |
|--------------|-------|----------------|------------------|------------------|------------------|------------------|-------------------|
| T(MeV/A)     | 20    | 7.6            | 5.1              | 7.6              | 5.5              | 6.6              | 5.8               |
| I(e $\mu$ A) | 100   | 14             | 9                | 15               | 17               | 5                | 12                |

Table 4. Electron cooling parameters

|                                  |  |                       |
|----------------------------------|--|-----------------------|
| Maximum working energy           | ions   | 200 MeV/A             |
|                                  | electrons                                    | 120 keV               |
| Cooled ions                      | $H^+$ - ${}^{20} Ne^{10+}$                   |                       |
| Gun optics                       | Pierce type + resonance focussing electrodes |                       |
| Length of interaction region     |  | 1.6 m                 |
| Maximum electron current density |  | 0.5 A/cm <sup>2</sup> |
| Cathode diameter                 |  | 50 mm                 |
| Maximum current                  |  | 10 A                  |
| Maximum solenoid field           |  | 1200 G                |

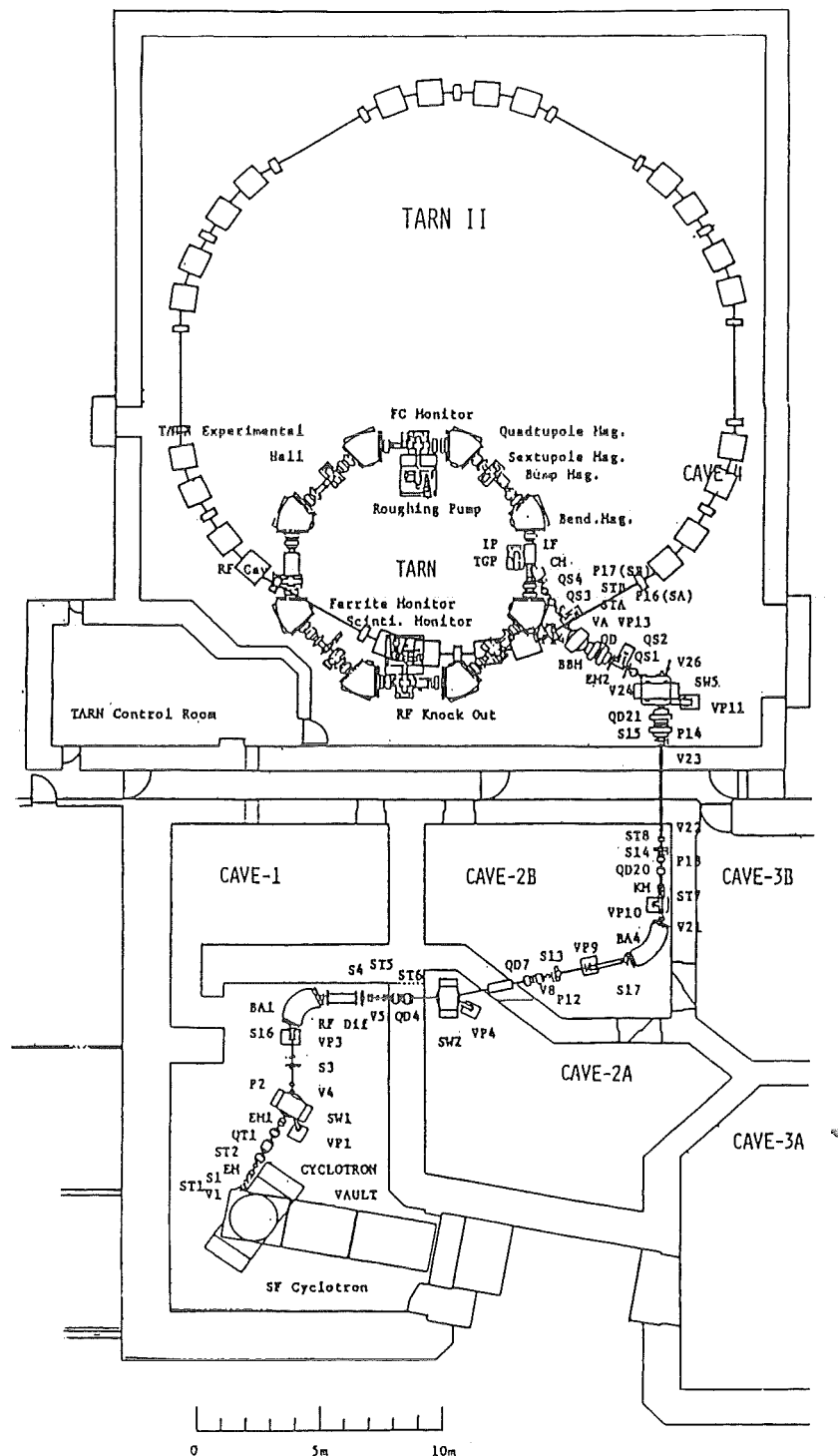


Fig. 1 Layout of TARN II

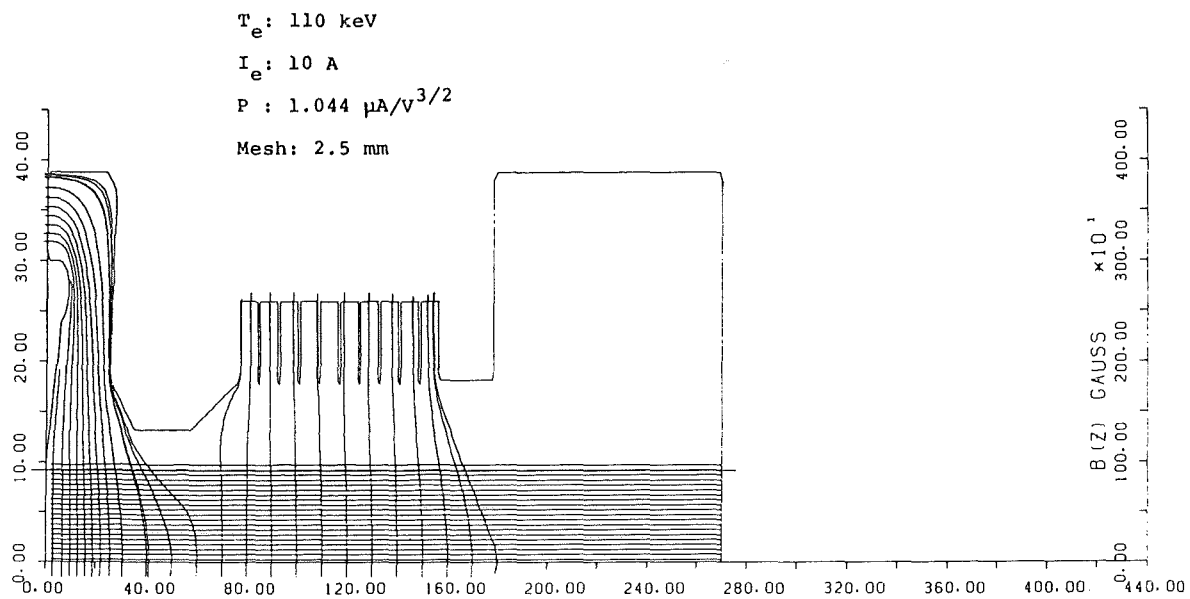


Fig. 2 Calculated electron trajectories in gun.

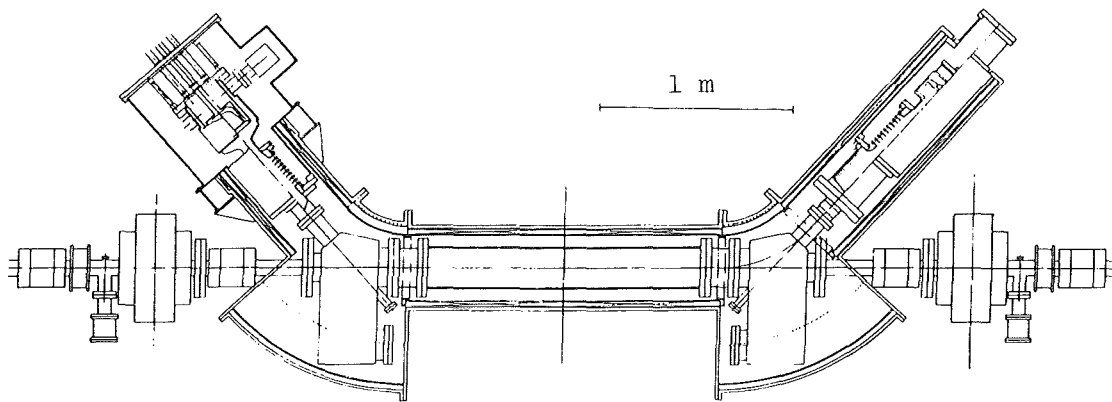
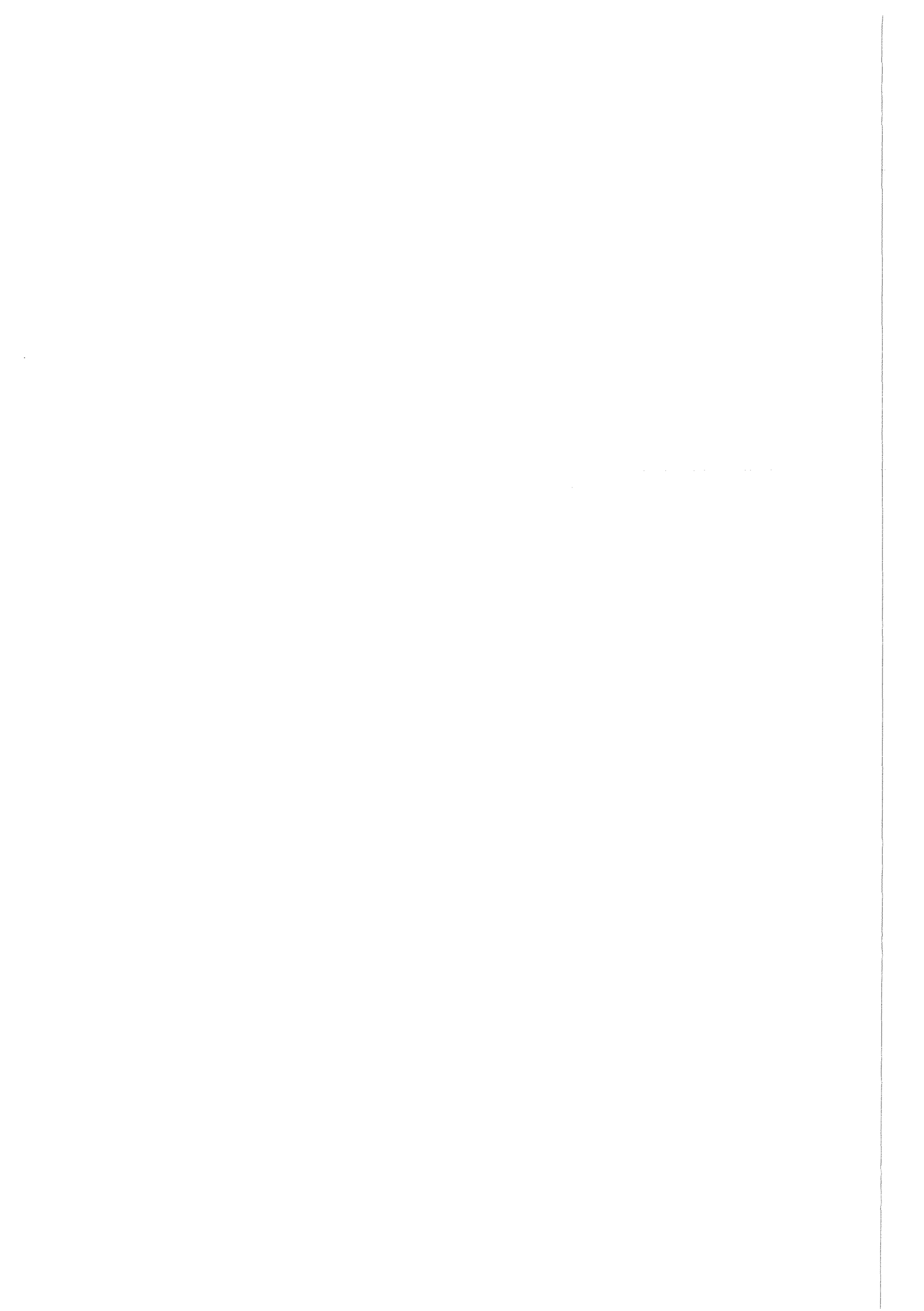


Fig. 3 Layout of the electron cooling device.



THE HEIDELBERG HEAVY ION TEST STORAGE RING (TSR)

D. Fick, D. Habs, E. Jaeschke, D. Krämer, V. Metag, R. Neumann,  
B. Povh, R. Repnow, U. Schmidt-Rohr, R. Schuch, D. Schwalm,  
E. Steffens and C.A. Wiedner

Max-Planck-Institut für Kernphysik, Postfach 10 39 80, D-6900 Heidelberg

The Heidelberg Heavy Ion Storage Ring TSR is an experimental facility under construction at the Heidelberg MP-Tandem Postaccelerator Combination. The TSR is built in close cooperation with the GSI Darmstadt and working groups of the Physics Institutes of the Universities of Heidelberg, Gießen, and Marburg.

The main purpose of its construction is to study many still open questions related to stochastic and electron cooling of heavy ions [1] as well as questions connected with the operation and usage of larger facilities as for example the ESR at GSI [2]. Furthermore it will be valuable research instrument for a large variety of atomic physics experiments especially investigating the interaction of free electrons and photons with fully or partially stripped heavy ions. It will also enable the entry into experimental techniques completely new for nuclear physics.

The TSR is matched to the magnetic beam rigidities of the injecting postaccelerator which are typically  $B \times p = 1.1 \text{ TM}$  ( $^{12}\text{C}^{6+}$  15 MeV/u,  $^{127}\text{J}^{47+}$  8 MeV/u). As an experimental machine the TSR must have a high degree of flexibility to allow the operation in quite different modes. The most far reaching requirement is that of a multi-chargestate operation; that is the simultaneous storage of heavy ions with equal momentum but different charge states that have been formed in various processes in the ring. As for light ions like  $^{16}\text{O}$  still two charge states have to be stored in the TSR, a momentum acceptance of  $\Delta p/p = 0.0625$  is required; a value that corresponds to seven simultaneously stored charge states for  $^{127}\text{J}$ -ions with  $47+$  as the mean one.

Table I lists the basic parameters of the TSR while Fig. 1 shows a layout of the ring with its main components. The ring is designed in fourfold symmetry for a maximum magnetic rigidity of  $B \times p = 1.5 \text{ TM}$ ; its circumference is 35.28 m. The deflection is accomplished by eight 45 deg. magnets with parallel endfaces constructed as laminated C-type magnets. Always two bending magnets (AMX1 and AMX2) with a horizontal focussing quadrupole (QFX2) for dispersion adjustment inbetween form the center of a focussing period, which is completed on both sides by the quadrupole doublets QDX1, QFX1 and QFX3, QDX2 as well as by the halves of the large straight sections GSX. One focussing period is so of the structure FP = ODFBOFOBFDO. In the main operation mode of the TSR two antisymmetric focussing periods (FF, -FP) form one of the two superperiods. Fig. 2a shows the envelope functions  $(\epsilon_H \beta_H)^{1/2}$  and  $(\epsilon_V \beta_V)^{1/2}$  with  $\epsilon = 1 \pi \text{ mm mrad}$  for one superperiod; Fig. 2a shows the dispersion function D. Both diagrams have been calculated with the program MIRKO [3]. The dispersion is equal to zero in two straight sections (GS2 and GS4) and is  $D = 1.24 \text{ m}$  in the remaining two (GS1 and GS3). The elements of the injection system are located in GS1, while the electron cooling takes place in GS2. The straight section GS3 has space for further experimental equipment, while the RF-systems can be found in GS4.

Table I: Basic parameters of the TSR

|   |   |
|---|---|
| Magnetic rigidity                                     | $B \times p_{(\max)} = 1.5 \text{ Tm}$  |
| Specific momentum (max)                               |   |
| at $q/A = 0.5$  | $p = 0.255 \text{ GeV/c}$   |
| Circumference   | $C = 35.28 \text{ m}$   |
| Mean radius   | $R = 5.62 \text{ m}$  |
| Number of stored particles                            | $N \leq 10^{10}$  |
| Long straight sections                                | $4 \times 3.5 \text{ m}$  |
| Short straight sections per sector                    | $2 \times 0.6 \text{ m}$  |
| Focussingperiod                                       | FP = ODFBOFOBOFDO   |
| Number of superperiods                                | $S = 2; 2 \times (\text{FP}, -\text{FP})$ main mode   |
| Betatron tune   | $Q_H = 2.25, Q_V = 1.30$  |
| Transitionenergy                                      | $\gamma_{tr} = 3.07$  |
| Natural Chromaticity                                  | $Q' = -5.5, Q = -4.2$   |
| Acceptance (maximum values)                           | $A_H = 550 \pi \text{ mm mrad}$<br>$A_V = 100 \pi \text{ mm mrad}$<br>$\Delta p/p = \pm 0.0625$ |
| Acceptance used (Multiturn-Injection and RF-Stacking) | $A_H = 200 \pi \text{ mm mrad}$<br>$A_V = 50 \pi \text{ mm mrad}$<br>$\Delta p/p = \pm 0.03$    |
| Vacuumsystem  | $p < 10^{-11} \text{ Torr (N}_2 \text{ equivalent)}$  |

Fig. 3 shows single particle orbits differing in momentum by steps of  $\Delta p/p = 0.02$  from the momentum of the nominal particle. The orbits shown thus correspond to those of different charge states around  $^{127}\text{J}^{47+}$  as the central ion.

For injection into the TSR two stacking methods in combination will be employed: multturnstacking into the horizontal betatron phasespace followed by RF-stacking into momentum space. In order to store  $10^{10}$  particles at least for light ions, pulse operated sputter sources have to be used at the MP-Tandem [4] similar to the practice at the Brookhaven Tandem Injector for the AGS. Taking into account transmission-, stripper- and bunching efficiencies the equivalent of injected turns to reach  $10^{10}$  stored particles ranges from 100 for  $^{12}\text{C}$  to 5000 for  $^{58}\text{Ni}$ . This seems only possible with the excellent longitudinal and transversal beam quality of a Tandem-Postaccelerator combination.

- [1] Experimente mit gespeicherten Schwerionen, ein Memorandum MPI H 1985 V1
- [2] B. Franzke, H. Eickhoff, B. Franczak and B. Langenbeck, Zwischenbericht zur Planung des Experimentierspeicherrings ESR, GSI/SIS/Int./84-5
- [3] B. Franczak, MIRKO - An interactive Computerprogram for Ion Optical Systems, GSI Scientific Report (1980) 260
- [4] P. Thieberger, Nucl.Instr.Meth. 220 (1984) 45

Figure Captions

Fig. 1 Layout of the main components of the TSR and the Injection. The abbreviations have the following meaning: AM bending magnet; QF,QD quadrupole; SF,SD sextupole; BM bumpmagnet; MS,ES magnetic and electrostatic septum; GS straight section; KM correction dipole.

Fig. 2 a) Envelope functions as computed by program MIRKO [3] for one superperiod.  
b) Dispersion function for one superperiod.

Fig. 3 Single particle orbits for particles with different momenta corresponding to charge states  $44^+$  to  $50^+ 1^{27}J$ .

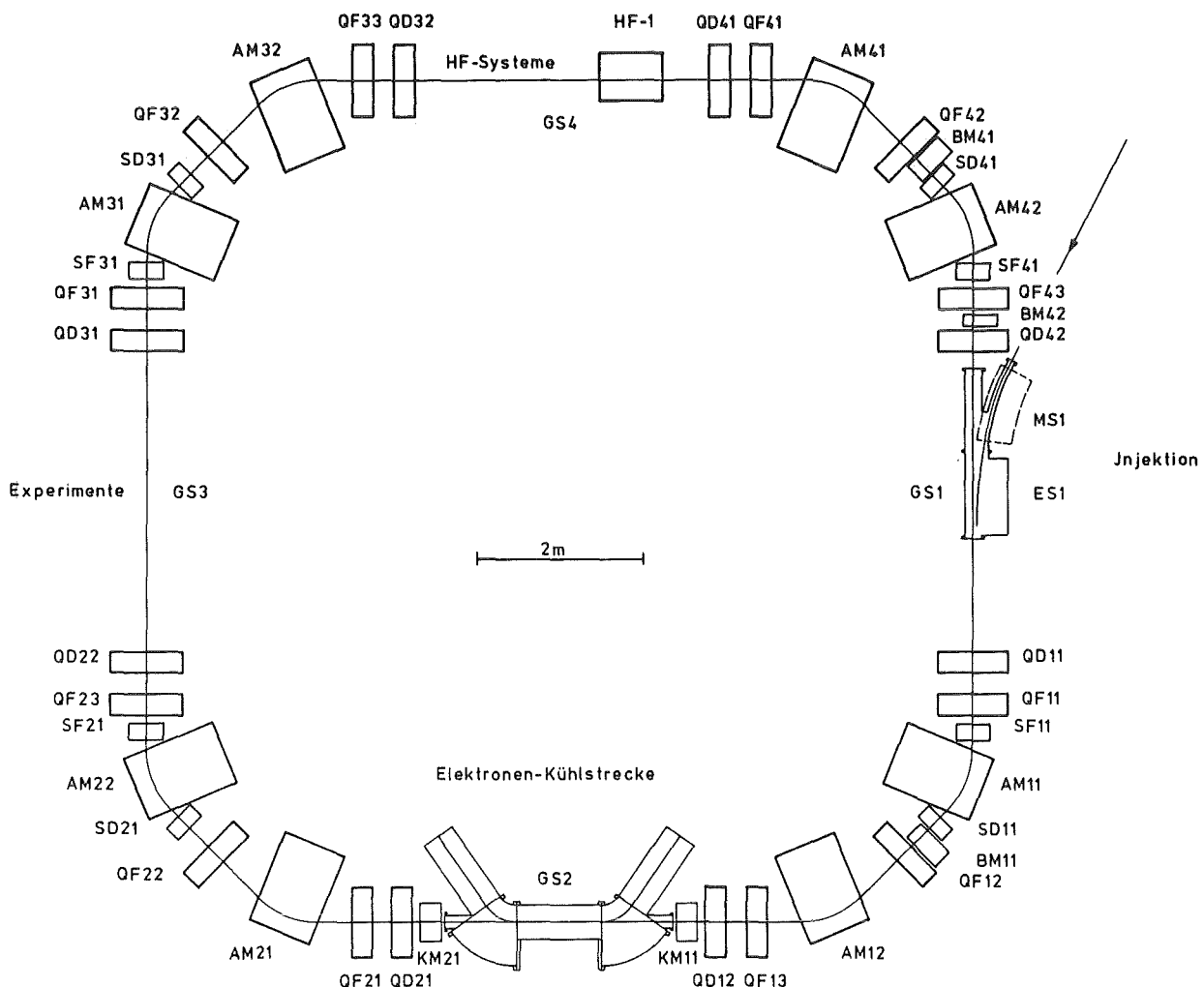


Fig. 1

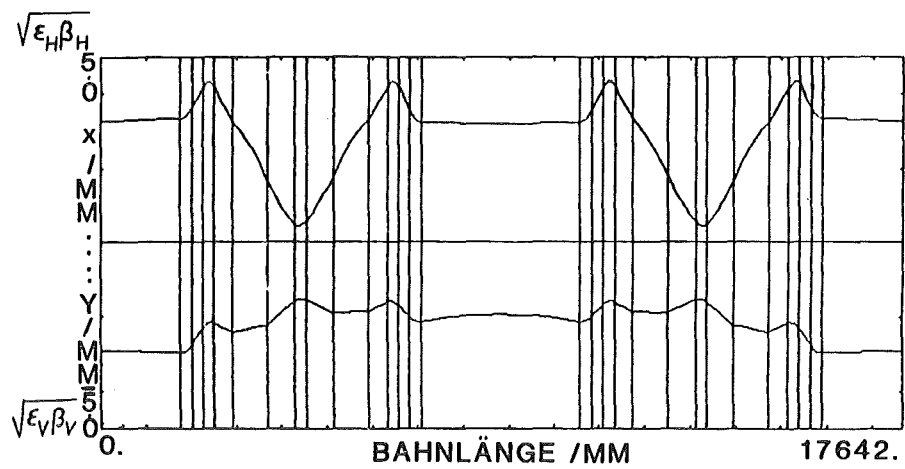


Fig. 2

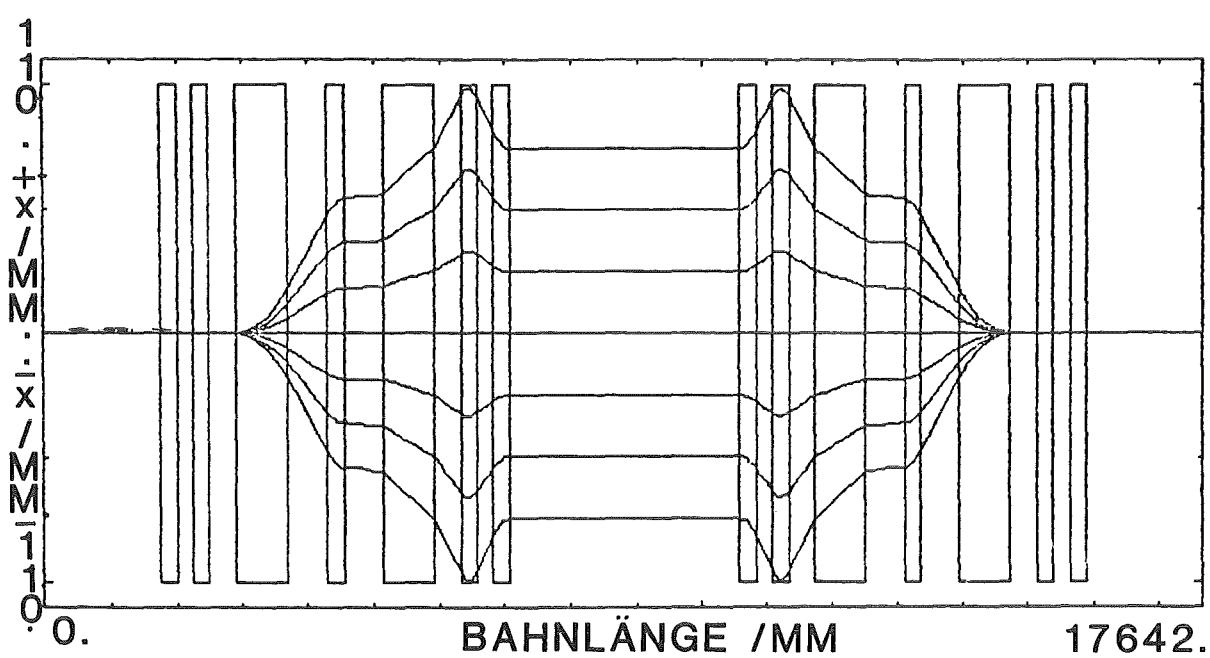


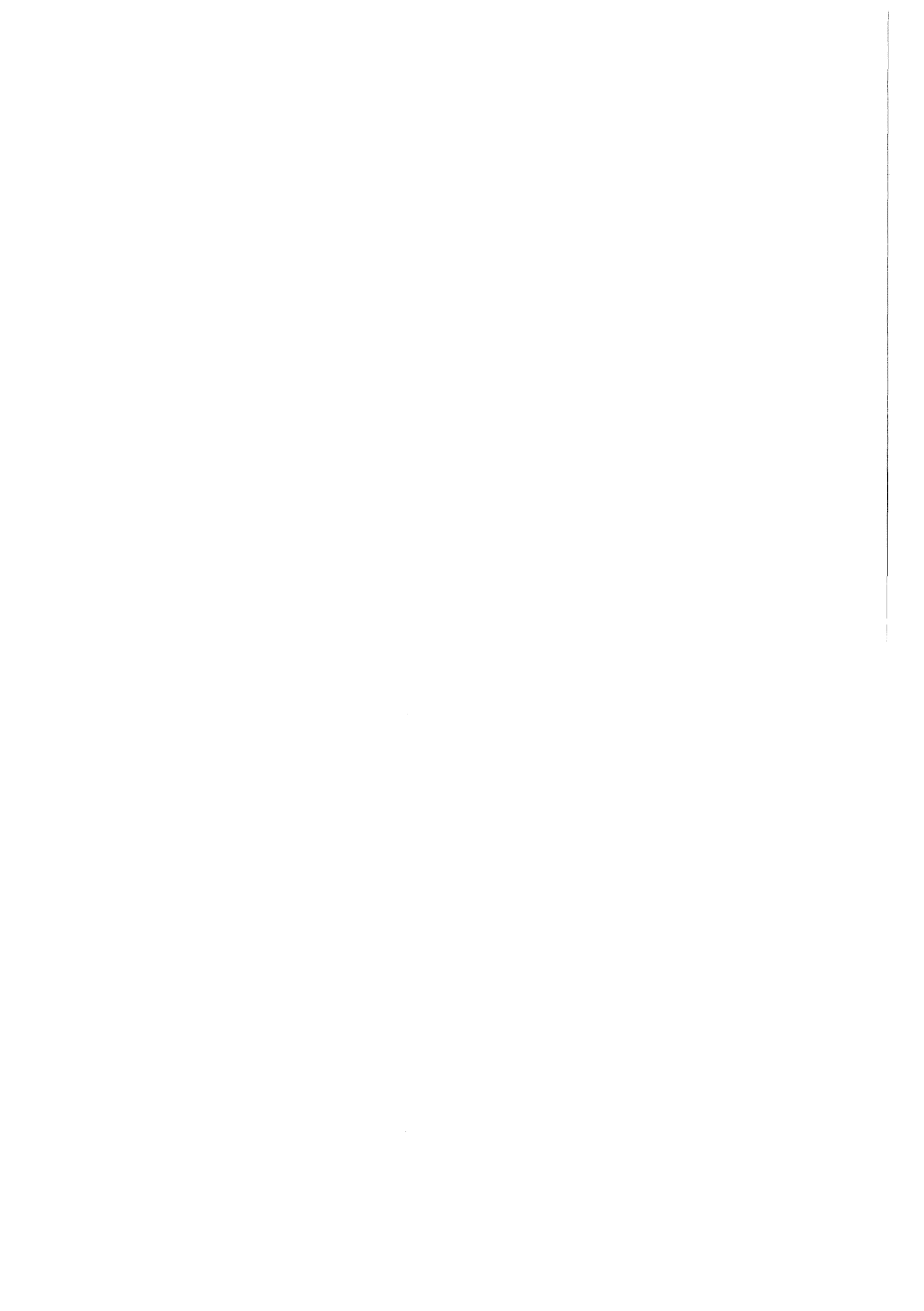
Fig. 3

INTERMEDIATE ENERGY ELECTRON COOLING

F. Mills

Fermi National Laboratory, Batavia, Ill.

(Copy of transparencies)



INTERMEDIATE ENERGY ELECTRON COOLING

Requires: Pelletron (Van de Graff)

technology

Efficient collection

Patience

May yield: A means to reduce emittance  
and energy spread of beams  
for colliders.

A means to achieve rapid  
collection of antiprotons.

Work by:

Fermilab

University of Wisconsin

National Electrostatics Corp.

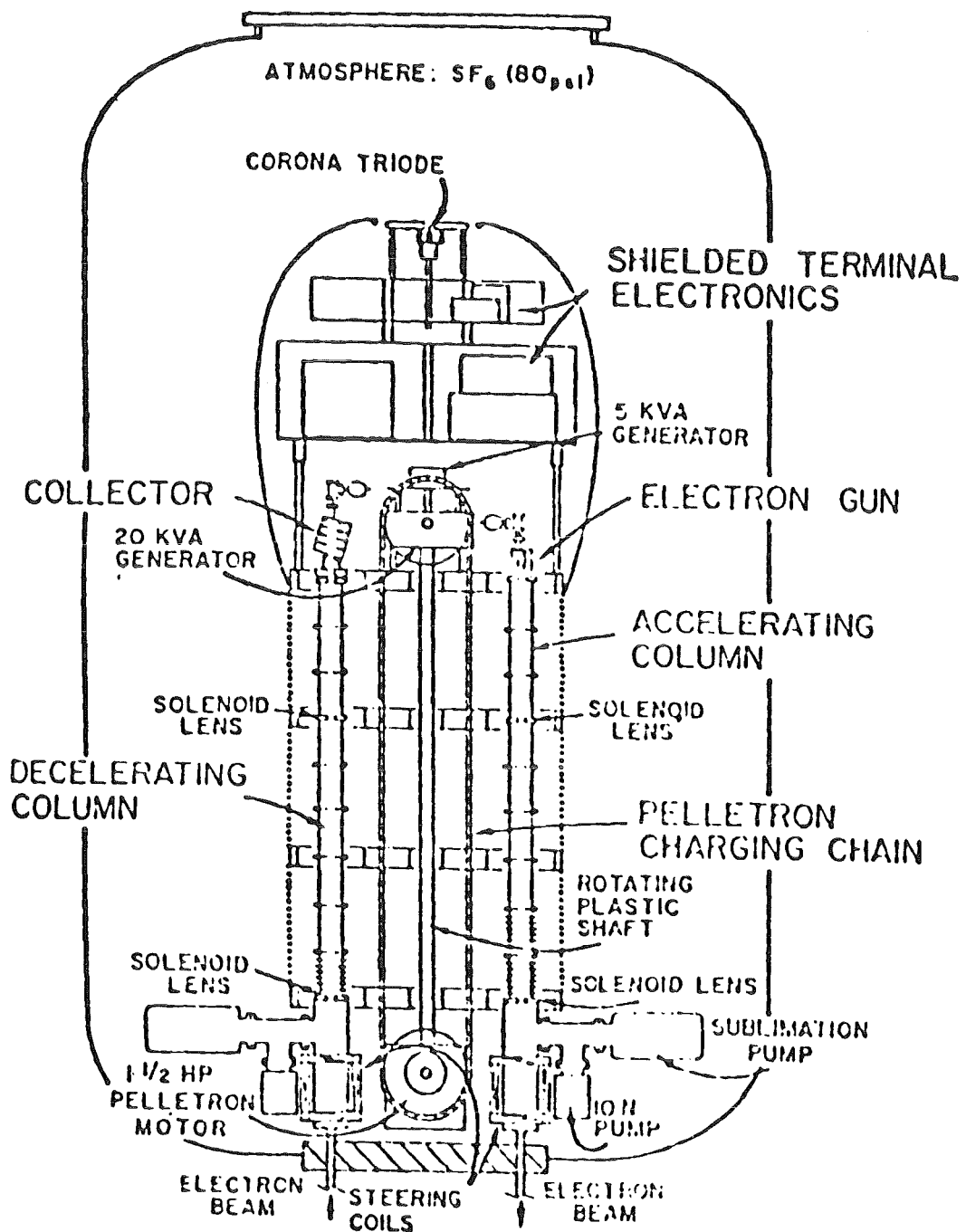
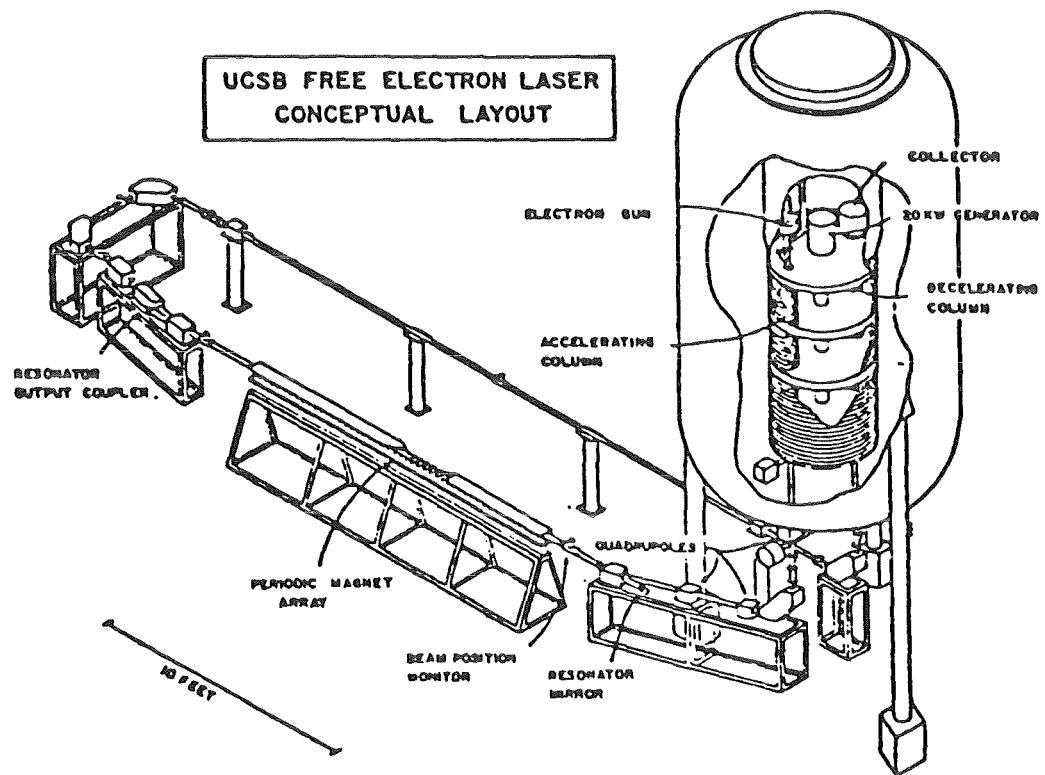
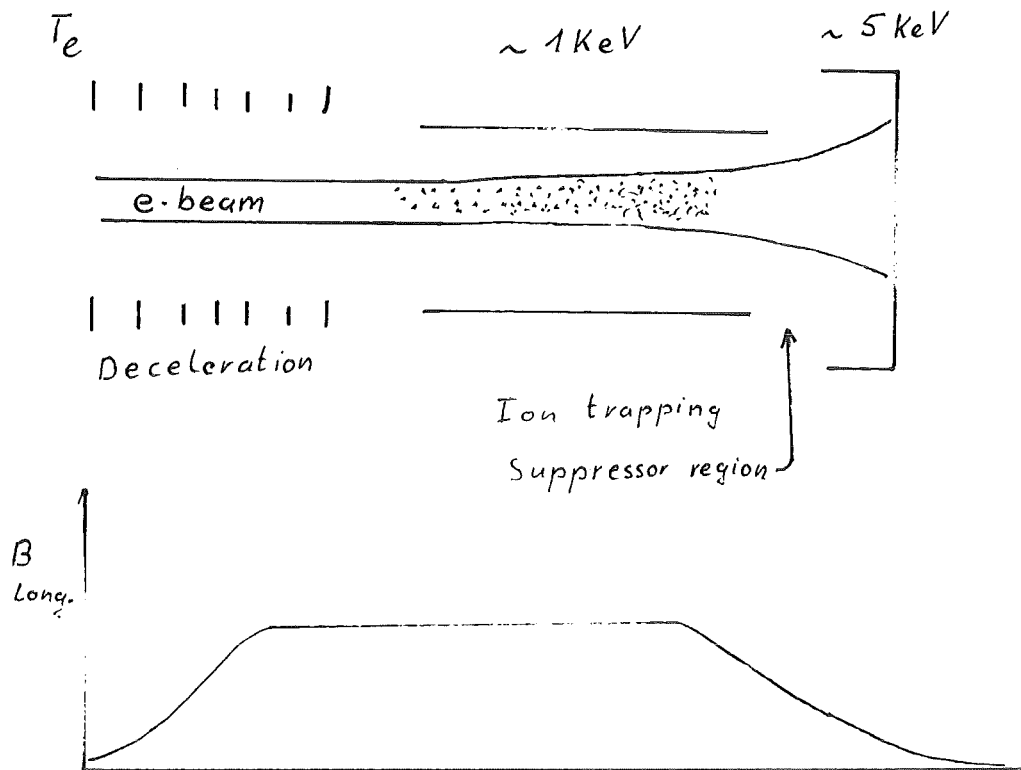


Fig. 1 3 MV Pelletron Accelerator for Free Electron Laser Recirculating Electron Beam (after Elias and Ramian, Ref. 2).



COLLECTOR



Ions are trapped longitudinally by electric fields, transversely by magnetic field, neutralize the e-beam space charge at low e velocity. Secondary electrons are pushed back into collector by electric field. Gyromotion of electrons can be kept acceptably small.

- 147 -

SOME PARAMETERS

$$\gamma = 10$$

$$T_e \sim 0.1 - 0.2 \text{ eV}$$

$$I = 5 \text{ A}$$

$$\text{Beam radius} = 5 \text{ mm}$$

$$\Theta_e \approx 50 \text{ urad}$$

$$B_0 \approx 10 \text{ m}$$

$$\epsilon_p = 1.2 \cdot 10^{-6} \text{ m}$$

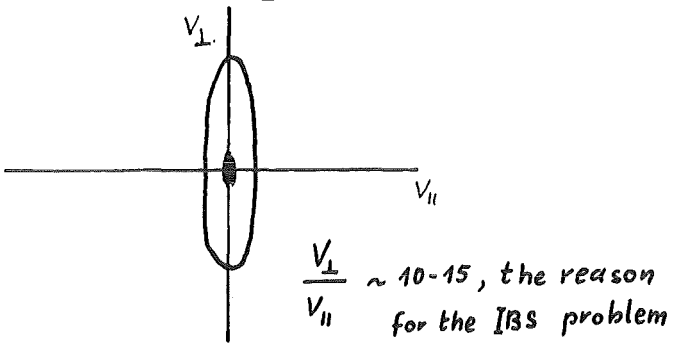
$$\Theta_p = .3 \cdot 10^{-3} \text{ rad} \gg \Theta_e \text{ for any applic}$$

$B = 0$ , all cooling is non adiabatic

$$F \propto 1/\Theta_p^2$$

## COOLING AN ACCUMULATED BEAM

The main reason would be to reduce the momentum spread, which is increasing due to intrabeam scattering (IBS).



To cool  $v_{\perp}$

$$T = \frac{\beta^3 \gamma^5 \Theta_p^3}{12\pi n_e c L \eta r_0 r_p}$$

$$\sim 2 \times 10^4 \text{ sec}$$

$$\eta \sim \frac{12}{470} = .025$$

$$L \sim 15$$

$$n_e \sim 1.3 \cdot 10^9 \text{ cm}^{-3}$$

But the the core is cooled much faster.

The equilibrium and cooling in the presence of IBS needs more study.

## SPACE CHARGE SPREADING

Due to space charge the beam will spread from a waist. In the previous example the beam would grow to ~1.5 times its radius and to an angle of 0.5 mrad in 10 meters.

Then a 12m cooling region may need one or two refocussings. Solenoid lenses are the easiest method.

D. Larson has written a program which includes finite emittance in the equation as well as space charge. This is not expected to be important except in very small waist sizes. The electron "B" is about 100m.

This is independent of  $B_t$  so space charge spreading can be avoided. If we take:

$$\dot{p}/p = \frac{2.5 \cdot 10^{-3}}{2 \text{ sec}} = 1.25 \text{ Hz}$$

Then for the previous parameters:

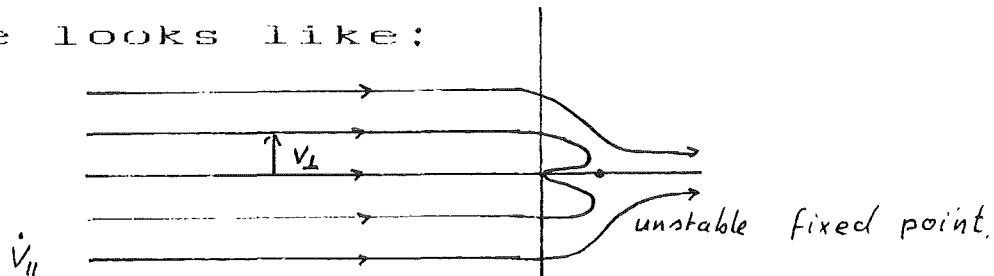
$$\xi \sim 10^{-6} \text{ m}$$

This requires a lot of stochastic pre-cooling but this can be done in the dilute unaccumulated state. For a momentum aperture of 2% 20-30 sec would be available.

Overall, the conclusion is that collection and final cooling would work better at lower  $\gamma$ , but may possibly have some applicability at Fermilab.

## ACCUMULATION

Here the electrostatic analogy is useful. If a  $\vec{p}$  beam is swept in momentum at a rate  $\dot{p}/p$  (for example by phase displacement) then the  $v_{\parallel}, v_{\perp}$  plane looks like:



The question of what  $v_{\perp}$  is trapped is

done by Gauss' theorem (what is the radius of the flux bundle that ends on the charge?). If  $F = -k/v^2$  from the "point charge" a beam, then:

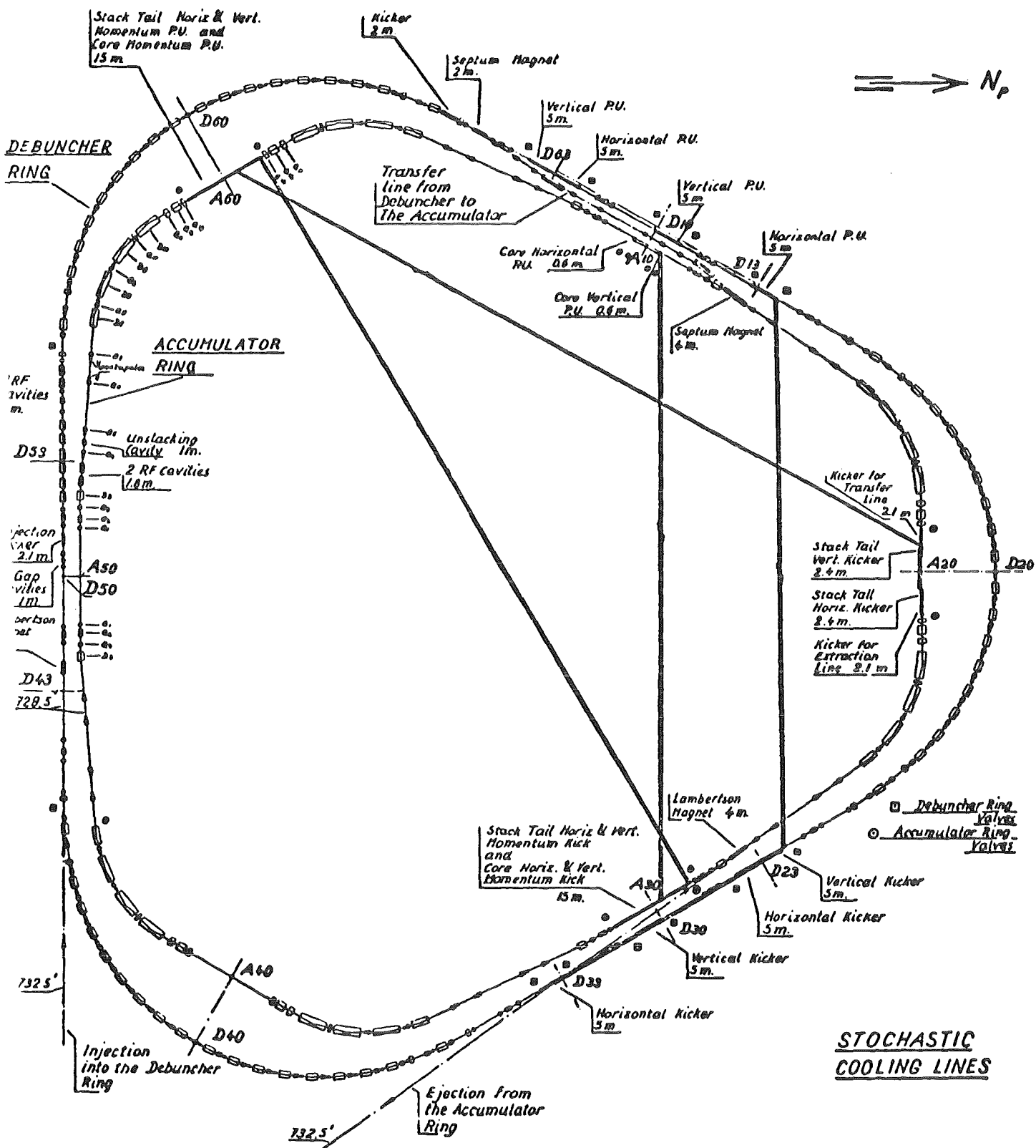
$$v_{\perp}^2 = 4k/v_{\parallel}$$

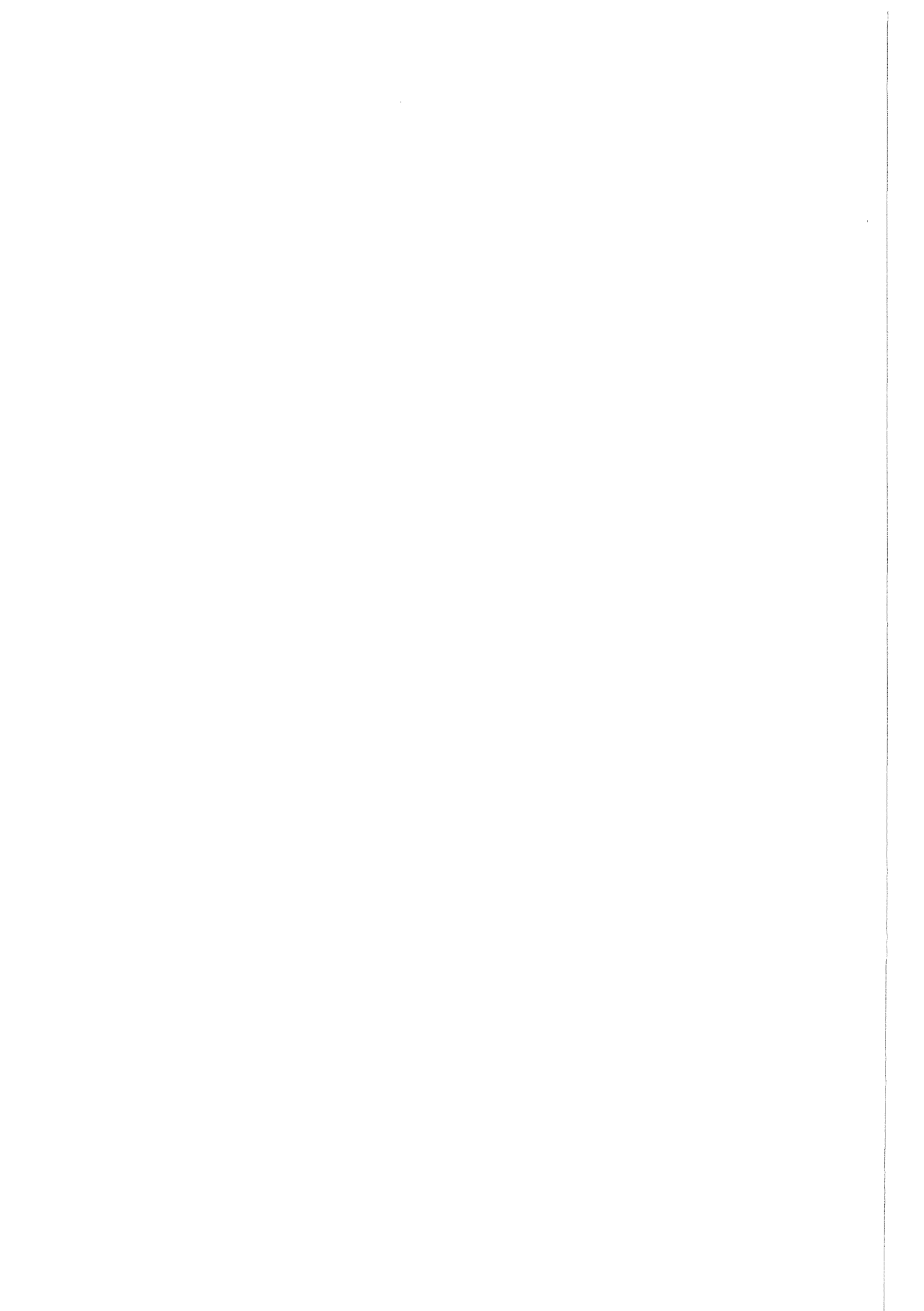
Matching the e-beam radius to the ion beam radius yields (in other notation)

$$\dot{p}/p \quad \xi_{x_2} = \frac{8\pi r_p r_e L \eta I/e}{(\beta\gamma)^4}$$

STATUS

- 1982 - Measured emittance of e-beam  
(Santa Barbara). Found no beam  
blow-up at 2.5 MeV beam.
- 1984 - Construction of components for  
test of recirculation with high  
efficiency recovery.
- Jan. 1985 - Bench test of gun + collecto
- March 1985 - Test recirculation at 2.5  
to 3 MeV with currents of  
100  $\mu$ A to 4-5 A.





HIGH ENERGY ELECTRON COOLING AND RELATED DIAGNOSTICS.

Presented by L.Tecchio.

M.Biagini <sup>1)</sup>, U.Bizzarri <sup>2)</sup>, R.Calabrese <sup>3)</sup>, M.Conte <sup>4)</sup>, S.Guiducci <sup>1)</sup>, F.Petrucci <sup>3)</sup>,  
L.Picardi <sup>2)</sup>, C.Ronsivalle <sup>2)</sup>, C.Salvetti <sup>5)</sup>, M.Savrié <sup>3)</sup>, R.Scrimaglio <sup>1)</sup>, S.Tazzari <sup>1)</sup>,  
L.Tecchio <sup>5)</sup> and A.Vignati <sup>2)</sup>.

1) Laboratori Nazionali di Frascati - Frascati.

2) ENEA Centro Ricerche Energetiche di Frascati - Frascati.

3) Istituto di Fisica dell'Università - Ferrara.

Istituto Nazionale di Fisica Nucleare - Sezione di Bologna.

4) Dipartimento di Fisica dell'Università - Genova.

Istituto Nazionale di Fisica Nucleare - Sezione di Genova.

5) Istituto di Fisica Superiore dell'Università - Torino.

Istituto Nazionale di Fisica Nucleare - Sezione di Torino.

Presented to the " Workshop on Electron Cooling and Related Applications,  
Karlsruhe , Germany , 24 - 26 september 1984.

## 1 - Introduction.

The possibility to transform LEAR in  $\bar{p}$ -p collider or in Super LEAR (1,2) represents a very promising facility to study antiproton-proton collisions, to answer some fundamental questions of the present-day physics. In fact, the good quality and the high intensity make the  $\bar{p}$ -p cooled beams a unique tool for performing fine spectroscopy, and several problems, otherwise not solved, may find a solution.

In order to perform the proposed(2) physics program, a high luminosity ( $L > 10^{30} \text{ cm}^{-2} \text{s}^{-1}$ ) machine is required. In this sense, stochastic and high energy electron cooling could be used to increase furthermore the luminosity and improve the resolution. In fact, being the antiproton tune shift ( $\Delta\nu$ ) at fixed intensity inversely proportional to the size of the proton beam, a strong electron cooling can be used to reach a very small transverse beam size and, at the same time, to avoid a rapid beam decay, due to beam-beam interaction. Since the luminosity is directly proportional to the tune shift, to increase the  $\Delta\nu$  means to increase the luminosity of the same factor.

In this report we present a project of high energy electron cooling for LEAR, operating as minicollider between 0.6 and 2.0 GeV/c, in order to improve the beam qualities and increase luminosity. The increase of electron beam energy for application to Super LEAR is also taken into account. Experimental results from tests on a prototype of the electron cooling device are presented and the feasibility of the project is demonstrated. Finally we discuss about the non-destructive methods of diagnostics to measure the electron beam characteristics (density, longitudinal and transversal temperatures) in a high energy electron cooling device.

## 2 - High energy electron cooling device.

In order to obtain a fast cooling of the (anti)proton in the (Super)LEAR  $\bar{p}$ -p collider, we have been proposing (3) to realize an electron beam which characteristics are as follows :

|                                       |                                 |
|---------------------------------------|---------------------------------|
| Beam Energy                           | 0.1 - 1 MeV                     |
| Electron Current                      | 10 A (at 1 MeV)                 |
| Beam Diameter                         | 3 cm                            |
| Momentum Spread                       | $< 10^{-3}$                     |
| Electron Beam Transversal Temperature | $\lesssim 0.5 \text{ eV}$       |
| Collector Voltage                     | 0-10 KV                         |
| Magnetic Field                        | 3 KG max                        |
| Drift Region Length                   | 1.5 m                           |
| Vacuum in the Drift Region            | $\approx 10^{-12} \text{ Torr}$ |

The power to the device is supplied by a high voltage electrostatic generator. For electric insulation reasons, the generator will be contained in a SF6 tank at a pressure of 8 atmospheres.

## 2.1 - High voltage generator.

Among several types of high voltage generators, we have chosen the Cockcroft-Walton one, as it can be built in different stages with relative easiness. A symmetrical cascade Cockcroft-Walton generator has been built at the Centro Ricerche Energetiche dell'ENEA di Frascati. It consists of 25 stages, 40 KV each, driven by a 15 KHz - 20 KV oscillator of 2 KW power. The nominal voltage is 1 MV. The generator supplies a total current of about 5 mA, corresponding to a total output power of 5 KW. The high voltage generator has been tested in air up to 350 KV, giving very promising results. The measured ripple was of the order of  $10^{-4}$ .

## 2.2 - Electron gun and energy recovery system.

The electron gun uses a reserve cathode, heated at 1050 °C and produces a 10 A, 7 cm<sup>2</sup> beam at 1 MeV. As the electron beam must have a temperature less than 0.5 eV, the first electrodes have to be designed with a classic immersed flow Pierce geometry, followed by standard "resonant optics", aimed to minimizing the electron spiral. This gun brings the electrons to about 130 KeV; the acceleration up to 1 MeV is accomplished by a further accelerating tube. At the end of this tube a diverging lens effect exists, which has to be compensated by an appropriate graduation of the electron field. After having left the gun, the electron beam is bent to superpose itself with the (anti)proton beam. The bending is accomplished by means of a toroidal and a dipole magnetic field. The cooling occurs in the 1.5 m long drift region. In order to avoid an electron dump of the order of 10 MW and to save the installed power, a very efficient recovery of the electron energy is needed. The energy recovery system consists of a decelerating tube, whose optics is the same of the accelerating one, where the electrons are decelerated down to about 30 KeV. The further energy decrease can take place according to existing successful methods. We consider sufficient to use a single plate collector, operating at 2 KV, expecting thus an energy dissipation of the order of 20 KW. In this way, we think to minimize the relative current losses around  $10^{-4}$ .

A sketch of the apparatus is shown in Fig. 1.

In order to compensate the space charge effect, the electrons, from cathode to collector, must be immersed in an axial magnetic field of 3 KG max. The whole apparatus will have to match its vacuum to the severe LEAR vacuum condition ( $\approx 10^{-12}$  Torr).

## 2.3 - Beam optics.

In order to compensate the space charge effect, a Pierce geometry electron gun has been conceived. The Pierce region is composed of 4 electrodes. The anode is located at 7 cm from the cathode and activated at 50 KV. The last two electrodes are at distances of 10.5 cm and 14.6 cm, where potentials of 80.5 KV and 130 KV are respectively applied. The electrodes shape has been studied in an electrolytic tank and by computer.

The accelerating tube consists of a column of 30 stainless-steel annular electrodes (4 mm thick) spaced (2.5 cm) by ceramic rings. The electrodes are polarized through a resistive voltage divider, made of a spiral of resistances wrapped around the tube and protected by guard rings.

Fig. 2 shows the electric region; the resonant optics condition is imposed to the section I , II and III . Setting different voltages on the anode of the gun and/or short-circuiting the sections II and III , it is possible to operate the device in a wide energy range and to conserve an electron temperature of the order of 0.3 eV at the end of the accelerating tube, as computed in Fig. 3 .

### 3 - Electron beam prototype.

In order to study the feasibility of the project, a prototype (Fig. 4) of the device has been built in the Centro Ricerche Energetiche dell'ENEA di Frascati, whose aims are to test the proposed accelerating methods, the beam optics and the electron energy recovery system(4).

The apparatus consists of a pulsed (20÷60 KeV , 2  $\mu$ s) electron gun, a drift region 1 m long and a depressed collector for electron energy recovery.

To provide a low rest frame temperature ( $T < 1$  eV ), the electron gun has been designed with a classic immersed flow Pierce geometry. It produces a 5 A ,  $7\text{cm}^2$  beam at 60 KeV. The defocusing lens action of the anode causes the electron to spiral, resulting in the undulation. This undulation is cancelled by a resonant focusing system of three electrodes. Fig. 5 shows how the electric field varies along the accelerating region. An efficient recovery of the electron energy is accomplished by the depressed collector. In the collector, electrons are decelerated in a magnetic field before being collected. One difficulty in maximizing the collection efficiency is given by the secondary emission from the collector surface. In our stainless-steel collector, the secondary electron rate is estimated to be of the order of 1% of the primary electrons. In principle, they contribute mainly to current losses, in fact our prototype collector was conceived disregarding the secondary emissions. The electrons travel in an uniform solenoidal magnetic field (1 KG max) in order to avoid the divergence produced by space charge forces. In the gun and in the collector regions the coils are about 50 cm diameter, while a coil of about 20 cm diameter is installed in the drift region.

The adiabatic matching between the coils is realized with an uniformity less than  $10^{-3}$  , sufficient not to perturb the electron beam . Each of these elements are powered separately. With the cathode at operation temperature (1500 °C), a pressure of  $10^{-7}$  Torr was measured close to the cathode.

#### 3.1 - Experimental results.

In the experiment we have detected the emitted( $I_e, I_g$ ) and collected ( $I_c$ ) currents through three Rogosky torus  $T_1, T_2$  and  $T_3$  as shown in Fig. 6 . The measurements were made with 0.5÷1 % accuracy. which is considered sufficient at this level. In fact , being secondary electrons rate in the collector of the same order of magnitude, no more precision is required. Experiments were performed in two steps. In the first step , we studied the beam performance where the current was limited by reducing cathode temperature. The beam energies were ranging from 20 to 55 KeV and currents limited in the range 0.2÷0.4 A.

In a second time, we studied beam performance with currents in the range 0.8÷4.0 A in space charge limited operation.

Experiments at beam energies in the range 20÷55 KeV have been performed.

Fig. 7 shows the emitted electron currents at different beam energies; the Child's law behaviour is verified. Setting a depression of 3 KV on the collector we studied the electron energy recovery. The ratio between the current loss ( $I_e - I_c$ ) and the emitted current ( $I_e$ ) represents the fractional value ( $I_L$ ) of current lost during the energy recovery process. The measured values of  $I_L$ , at different beam energies are shown in Fig. 8. We attribute the losses to secondary electrons emitted from the collector walls, as explained before. Since the power lost is in general dissipated as heat in the collector, it is preferred to collect the current at a collector potential as low as possible. In order to minimize the power losses, energy recovery measurements at different collector voltages have been made. The results are shown in Fig. 9. The obtained collection efficiency (about the 98% of the involved power is recuperated) is sufficient to assure a good operation in the energy range of our interest.

#### 4 - Electron beam diagnostics.

Beam position and electron temperatures are very important informations to be picked-up. As in the first stage of our work no electron - (anti)proton beam matching is foreseen, methods based upon cooling and correlated phenomena cannot be considered at the moment.

A first low-current diagnostic, not necessitating energy recovery, can be used for testing optics tuning, alignements and magnetic field uniformity.

Diagnostic at full intensity require application of a non-destructive method.

Two method seem very promising : the microwave detection for measuring the electron transversal temperature and the detection of laser light scattered from the electron beam for measuring the longitudinal electron temperature.

##### 4.1 - Microwave detection.

The method consists on the detection of the radiation field of the electrons spiralling in the solenoidal field. In fact, the power radiated by an electron in a solenoidal magnetic field is (5) :

$$P = \frac{4}{3} \frac{r_e e}{c} \gamma^4 \omega_c^2 T_{\perp}$$

where  $\omega_c = \frac{e B}{m}$

Since the drift section acts as a waveguide, an antenna located in the toroid allows to detect the radiation emitted by the electrons. The calculated powers to be measured are shown in table I, where we take :

$$B = 1 \text{ KG} \quad (\omega_c = 18 \text{ GHz rad} ; v = 2.8 \text{ GHz}) \text{ and } T = 0.5 \text{ eV} .$$

The power radiation to be detected is of the order of nWatt. With an adequate antenna it is possible to reach a sensitivity to measure  $T \lesssim 0.5 \text{ eV}$ .

TABLE I

| E (MeV) | $n_e \times 10^{11}*$ | P/v (nW/GHz) | P (nW) |
|---------|-----------------------|--------------|--------|
| 0.1     | 5.6                   | 0.11         | 0.3    |
| 0.5     | 3.6                   | 0.5          | 1.4    |
| 0.7     | 3.4                   | 0.98         | 2.7    |
| 1.0     | 3.2                   | 2.2          | 6.3    |

\*non-relativistic approximation.

#### 4.2 - Laser light scattering.

The scattering of laser light from an electron beam can be used to determine the beam density and the electron longitudinal temperature (6) .

We discuss here the possibility of measuring the longitudinal electron temperature ( $T_{\parallel}$  or  $\Delta p/p$ ) from the spectrum of scattered light . The measure of the beam density is not discussed, being a direct consequence of the former experiments. In order to detect the scattered light in the visible spectrum, or around the visible range, we think to use two different laser beam (Nd and  $\text{CO}_2$  ), as incident radiation. The choice of the laser depend on the electron beam energy .

The measure of the longitudinal temperature can be carried out, in principle, by means of the apparatus shown in Fig. 10. The laser (Nd or  $\text{CO}_2$  ) is focused and aligned parallel to the incoming electron beam in the 1.5 m straight section. The laser can be displaced parallel such that it can illuminate the beam cross-section. The back-scattered light is collected by the same injection optics, but split off from the laser path by a specially coated mirror and directed to the monochromator, travelling across an appropriate optical system consisting of lenses and filters. The monochromator has a resolution of the order of 0.5 Å, fulfilling completely our requirements.

In our case laser energies of 3 Joule/pulse (Nd,  $\lambda_0 = 1.06 \mu\text{m}$ ) and 32 Joule/pulse ( $\text{CO}_2$ ,  $\lambda_0 = 10.6 \mu\text{m}$ ) are taken into account.

The expected rates of scattered photons are :

$$\begin{aligned} N_{\text{ph}} &= 3.4 \times 10^3 \text{ photons/pulse} && \text{for Nd laser} \\ N_{\text{ph}} &= 6.0 \times 10^5 \text{ photons/pulse} && \text{for } \text{CO}_2 \text{ laser} \end{aligned}$$

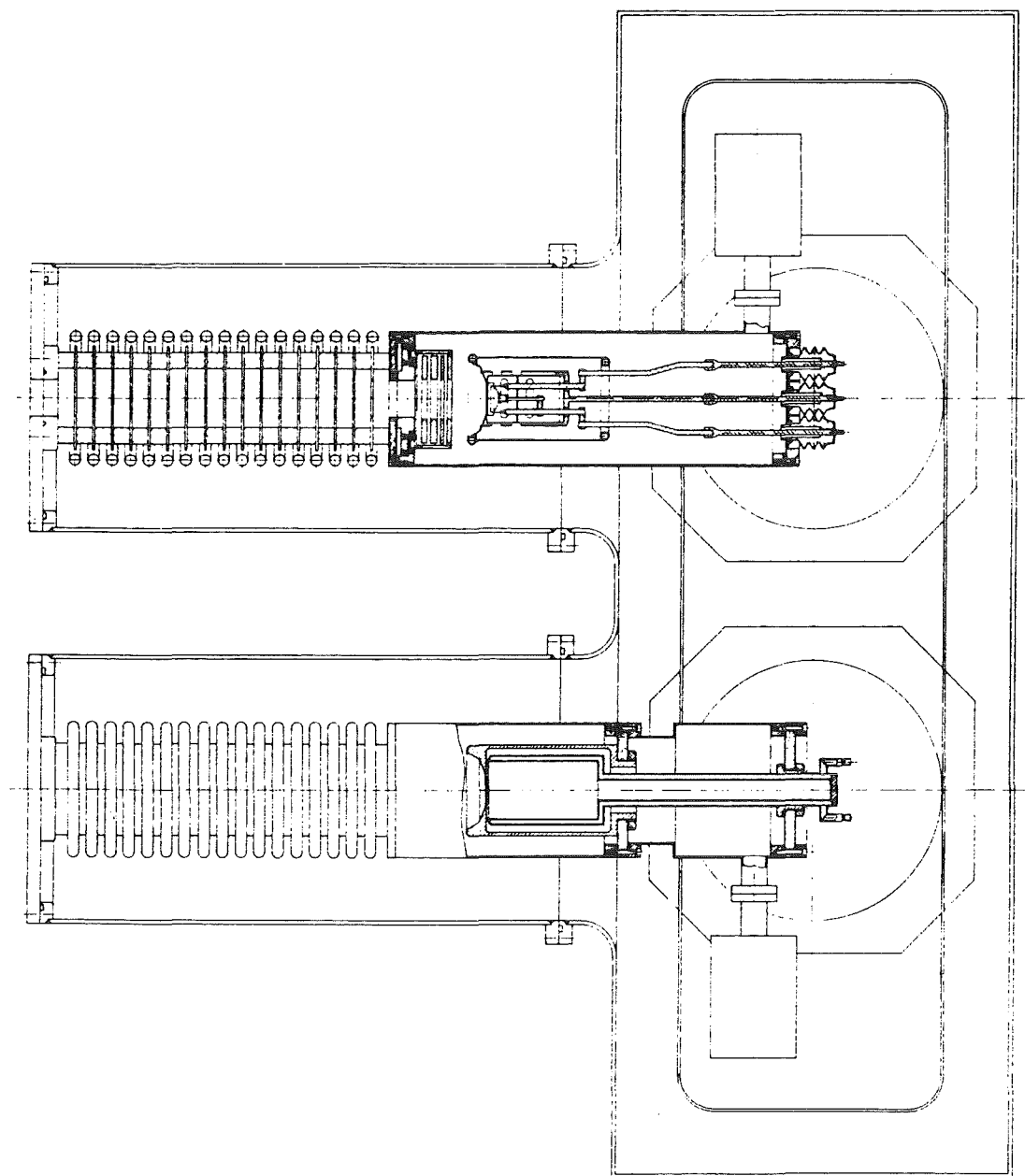
assuming a total transmission efficiency, along the optical path, of the order of 10 % . The expected momentum spread resolutions are ranging from  $10^{-4}$  to  $10^{-5}$  . Fig. 11 shows the corresponding longitudinal temperatures : we can observe that the resolution ( $T \approx 10^{-4} \text{ to } 10^{-6} \text{ eV}$ ) are good enough to allow precise measurements.

REFERENCES.

- 1 - W.Hardt,L.Hoffman,P.Lefèvre,D.Mohl,G.Plass and D.Simon;Conceptual study of a facility for low energy antiproton experiments,CERN/PS/DL/Note 79-1; Design study of a facility for experiments with low energy antiprotons (LEAR),Ed. G.Plass,CERN PS/DL 80-7 .
- 2 - P.Dalpiaz,Proceeding of the Joint CERN-KfK Workshop on Physics with Cooled Low Energetic Antiprotons, March 19-21,1979, Ed. H.Poth (1979),p. 111 .
- 3 - U.Bizzarri et al. ;Il Nuovo Cimento 73A, 425 (1983) .
- 4 - U.Bizzarri et al. ;Experimental Study of Beam Optics and Energy Recovery for a High Energy Electron Cooling Device, submitted to Il Nuovo Cimento.
- 5 - C.Rubbia; Microwave Radiation from the Transverse Temperature;CERN EP 77-4,1977.
- 6 - L.Tecchio et al. ;Diagnostic with a Laser Beam in Electron Cooling Experiment; to be published in Il Nuovo Cimento.

FIGURE CAPTIONS.

- Fig. 1 - Sketch of the high energy electron cooling apparatus.  
Fig. 2 - Electric field behaviour along the accelerating region.  
Fig. 3 - Computed transversal electron temperature.  
Fig. 4 - Prototype of the electron cooling device.  
Fig. 5 - Electric field along the accelerating region,for 60 KeV electron beam.  
Fig. 6 - Electric scheme of the electron cooling device.  
Fig. 7 - Emitted electron currents in space charge limited operation.  
Fig. 8 - Current losses at different beam energies. The collector depression is set at 3 KV .  
Fig. 9 - Collector voltages for total electrons recovery,at different beam energies.  
Fig. 10 - A sketch of the apparatus for longitudinal temperature measurement.  
Fig. 11 - Longitudinal temperature resolutions at different beam energies.



*Section AA*

FIG. 1

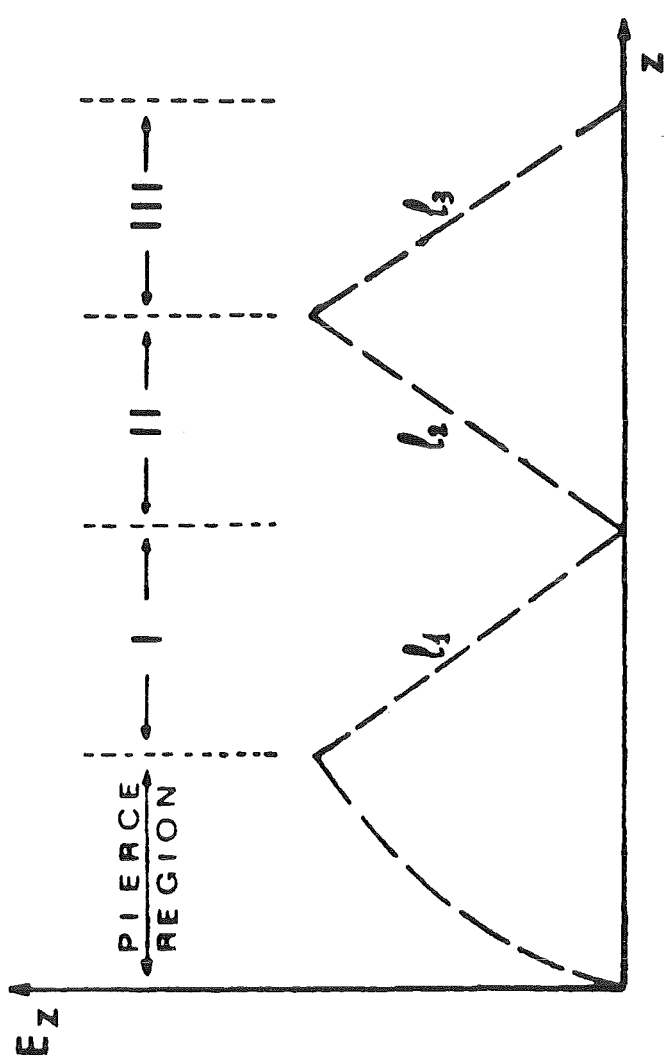


FIG: 2

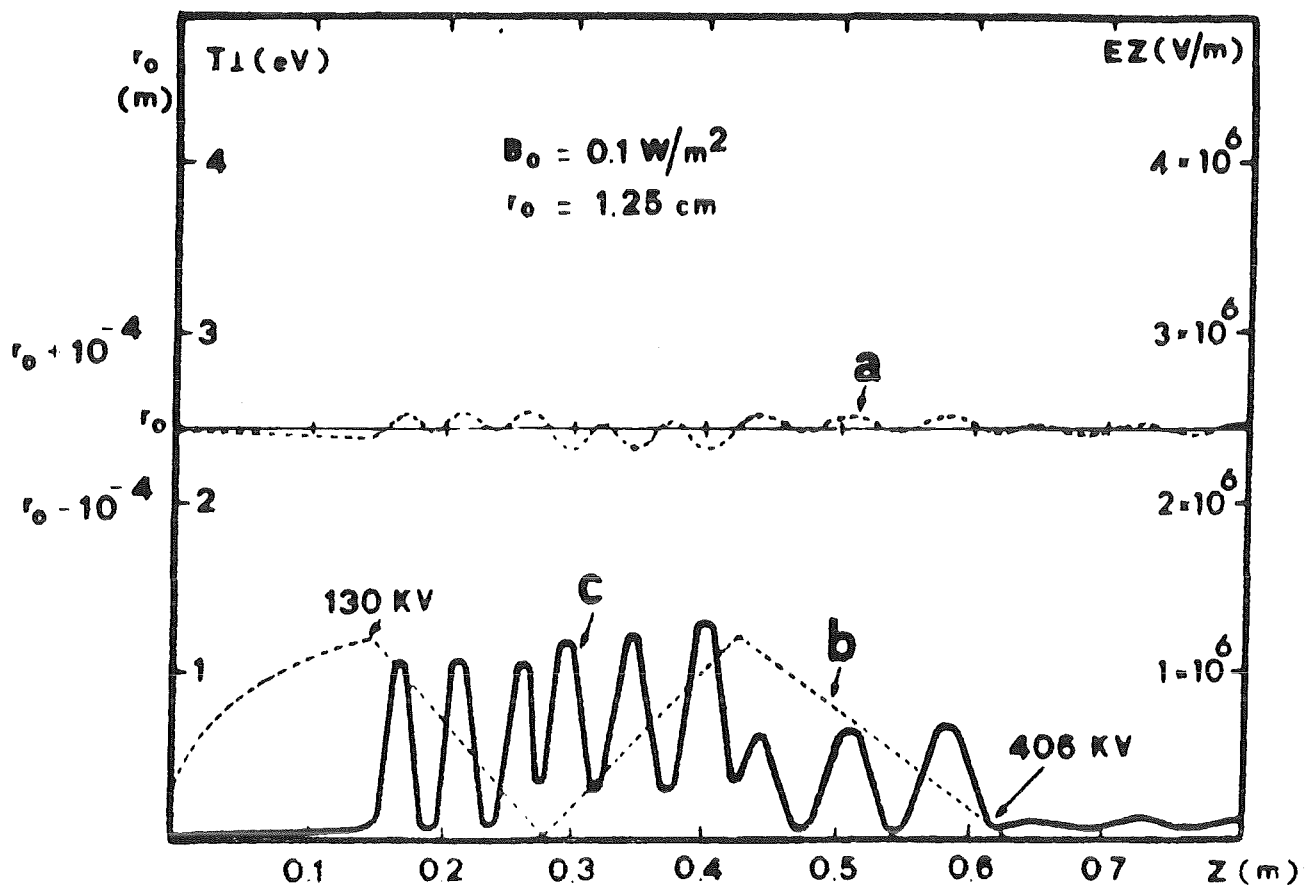


FIG. 3 - a) electron orbit

b) electric field along the gun and

accelerating tube

c) electron temperature

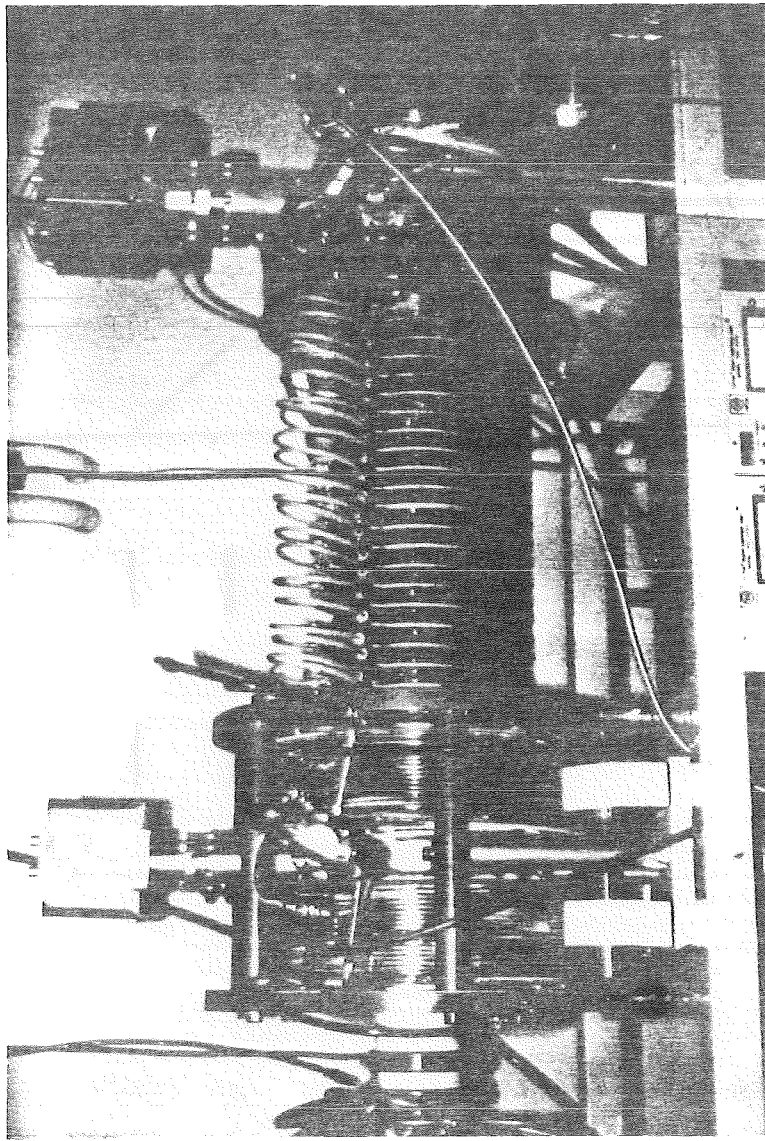


FIG. 4

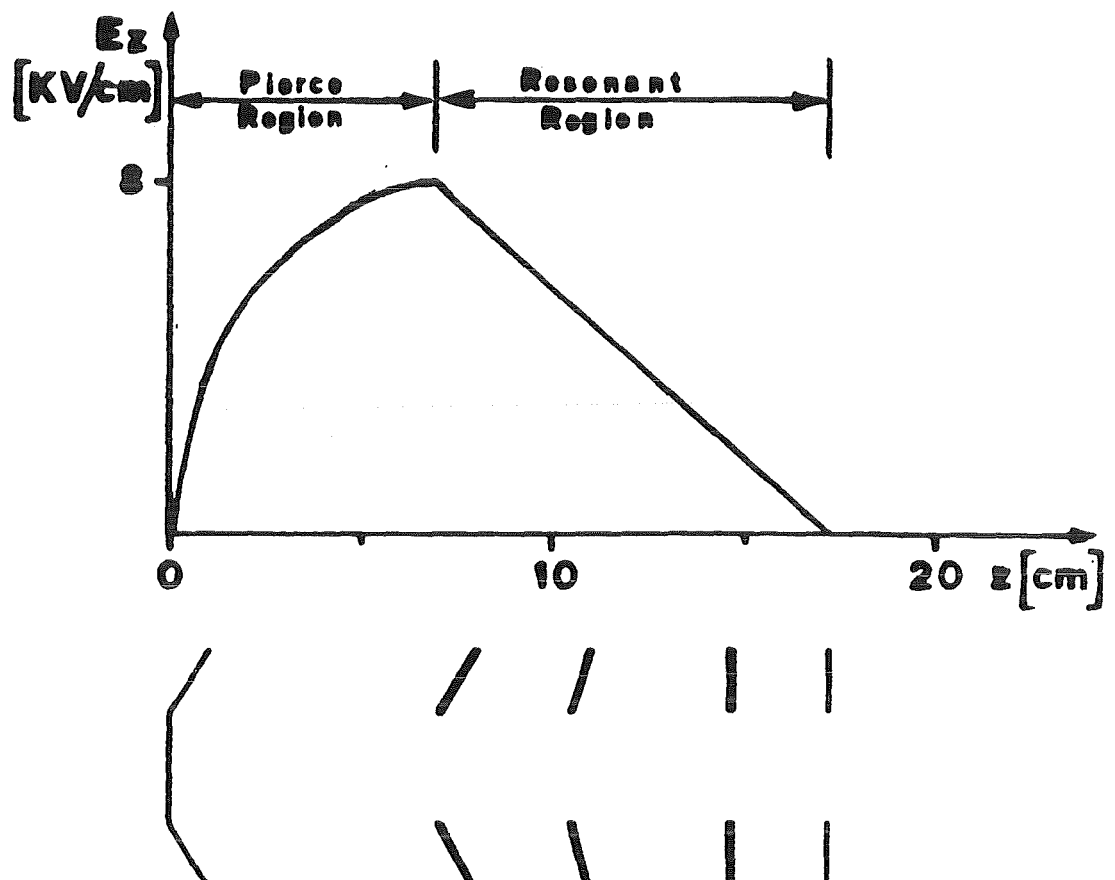


FIG. 5

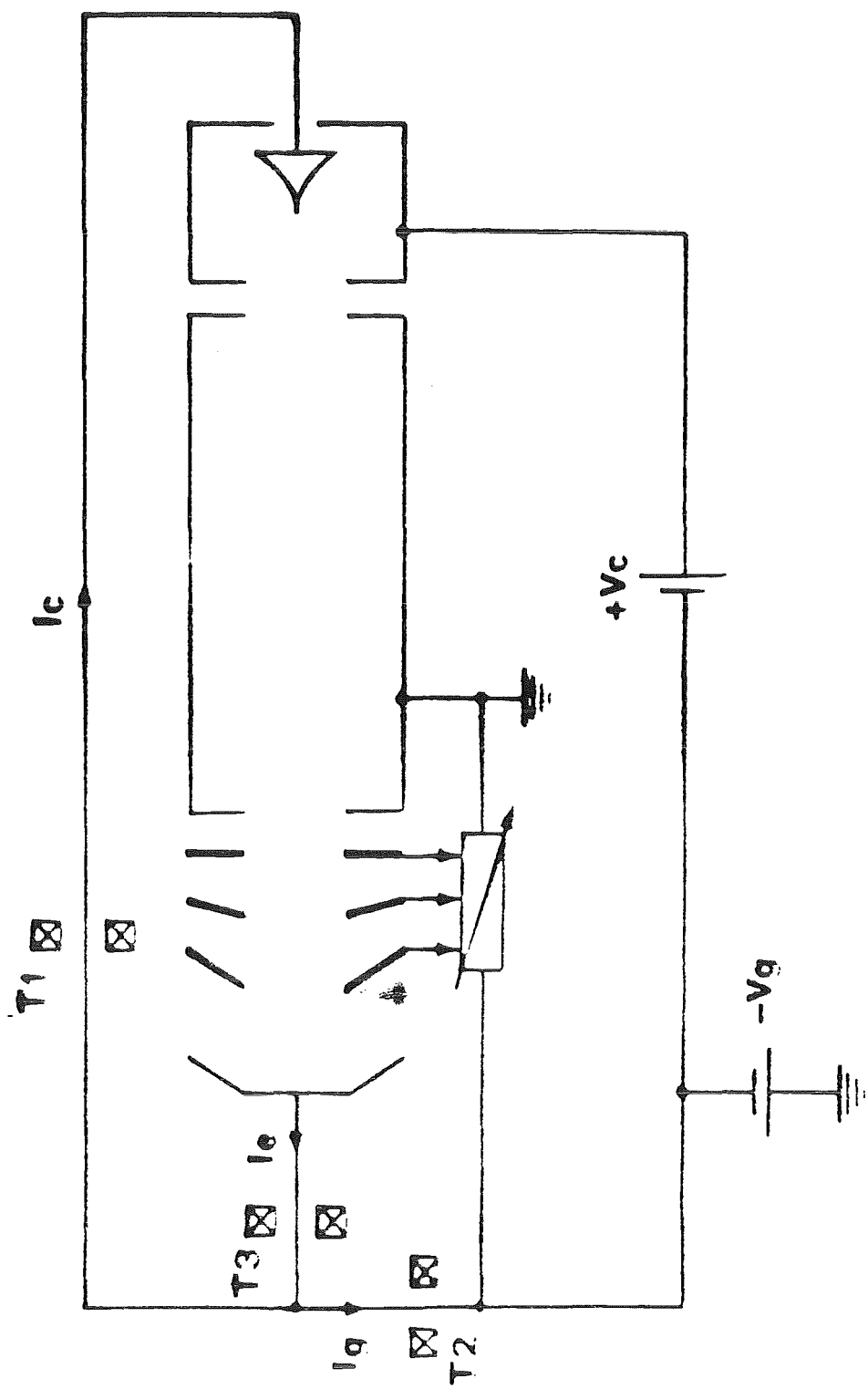


FIG. 6

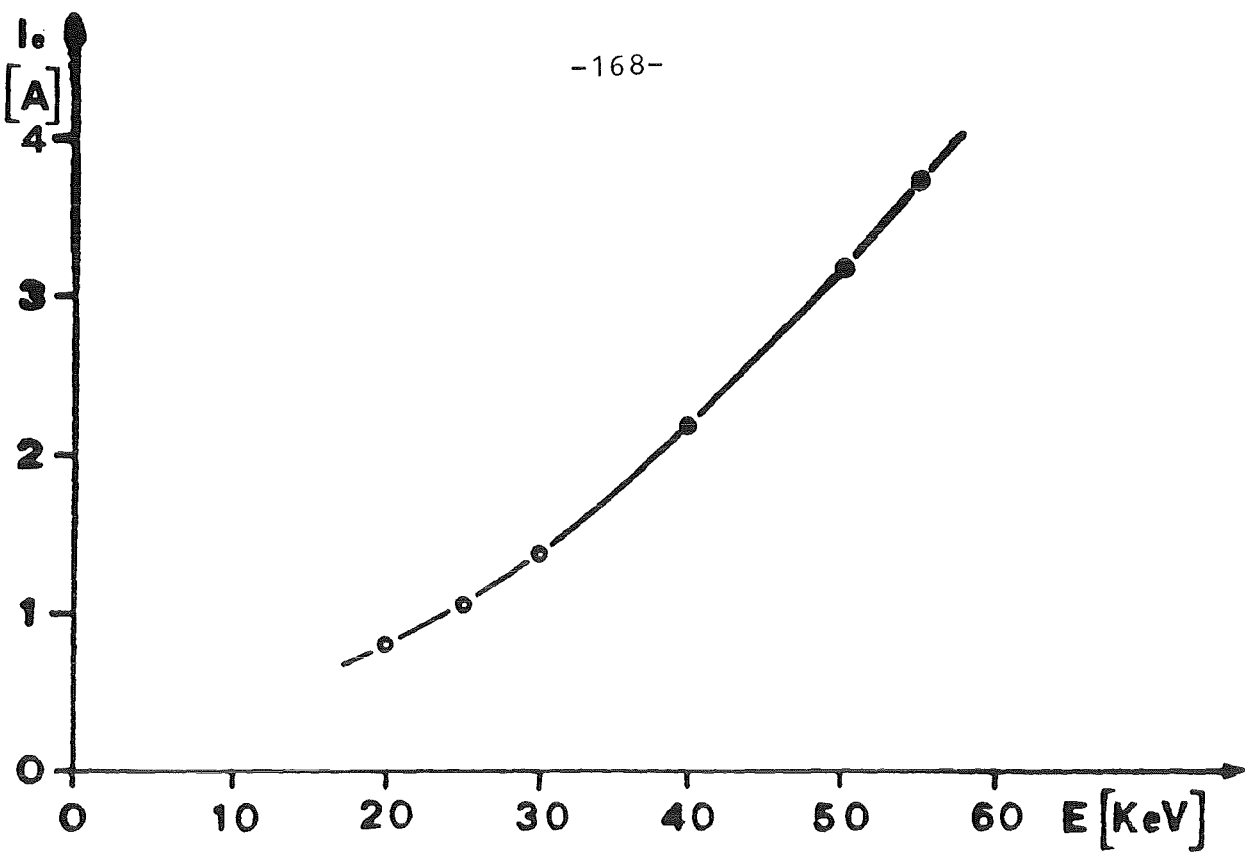


FIG. 7

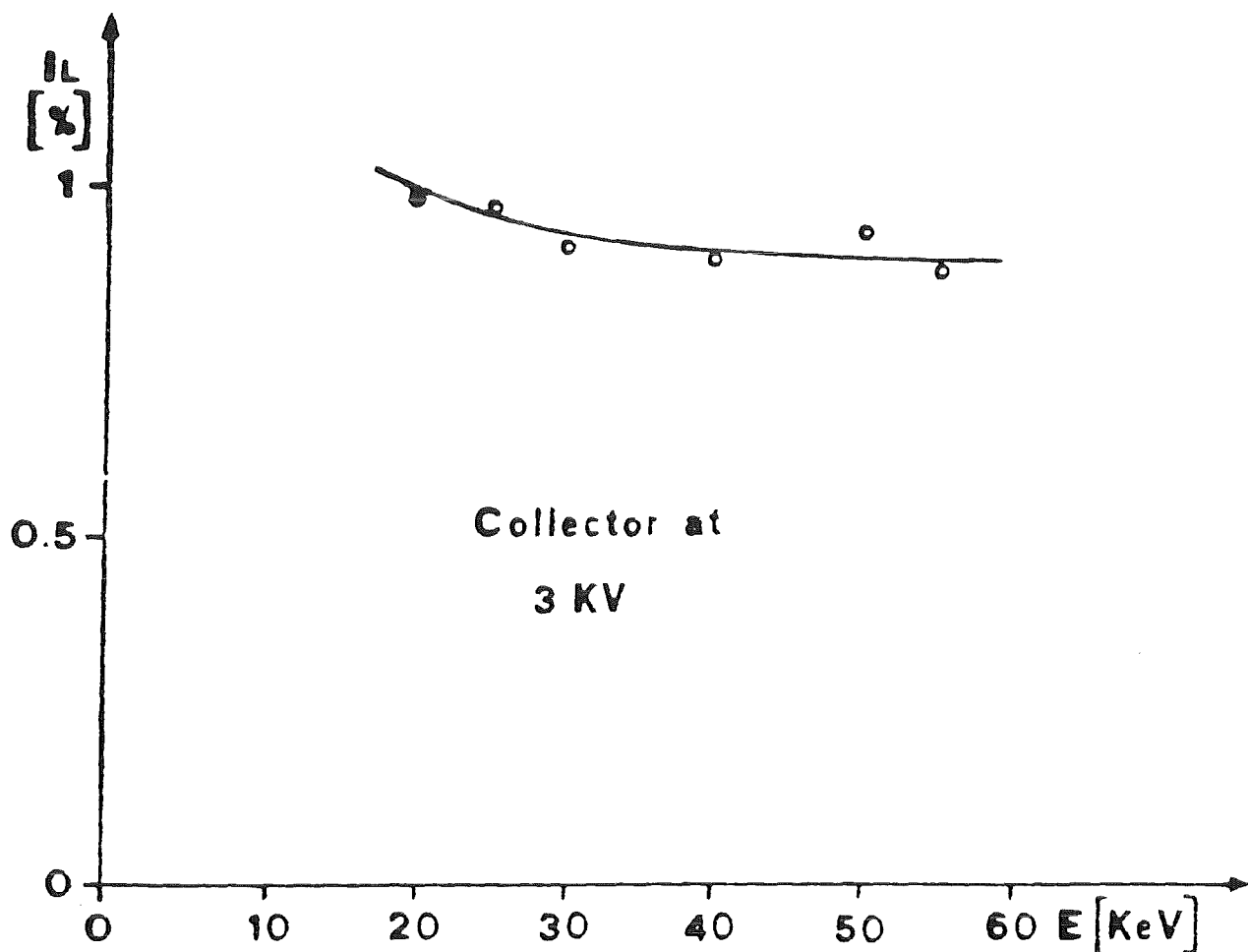


FIG. 8

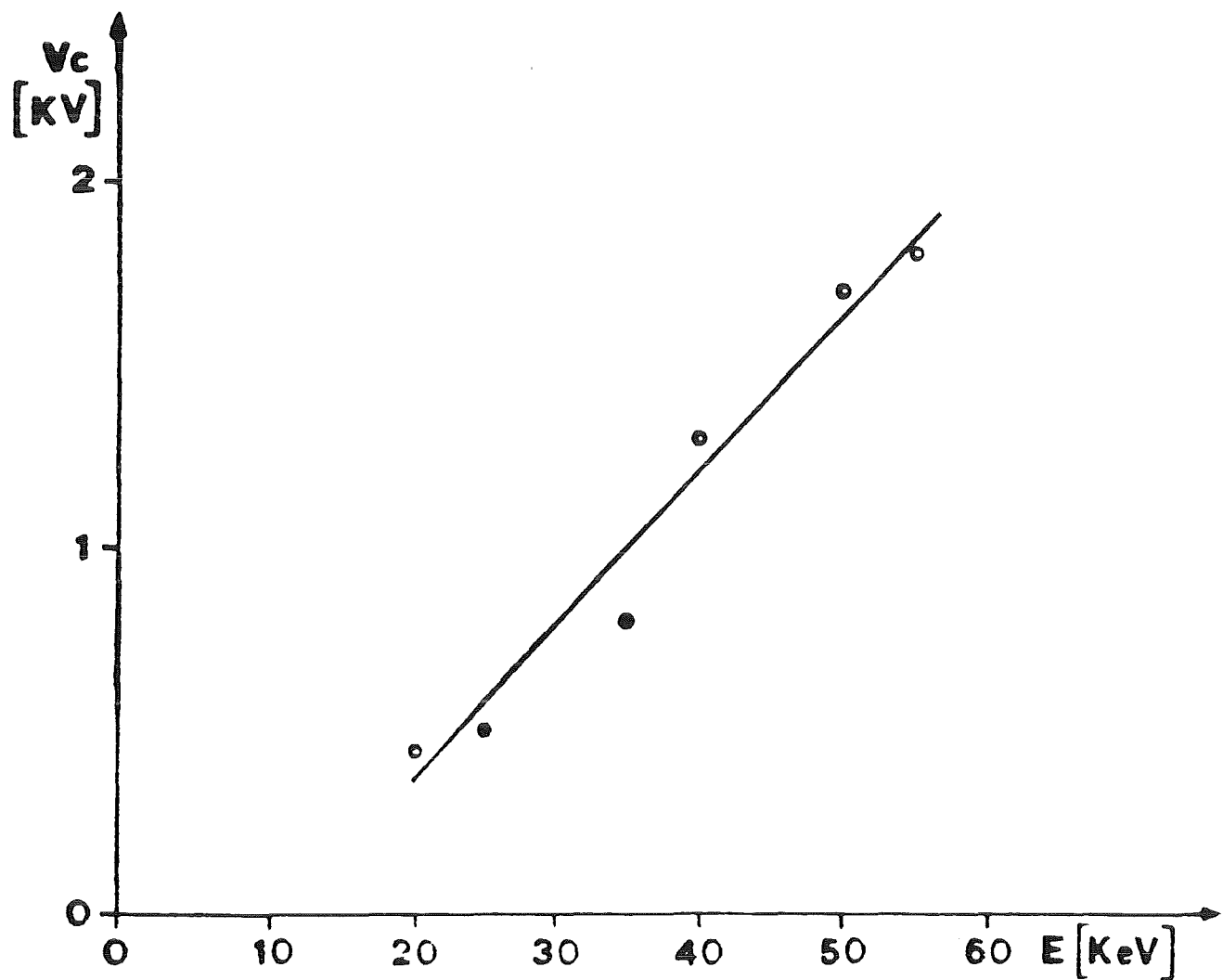


FIG. 9

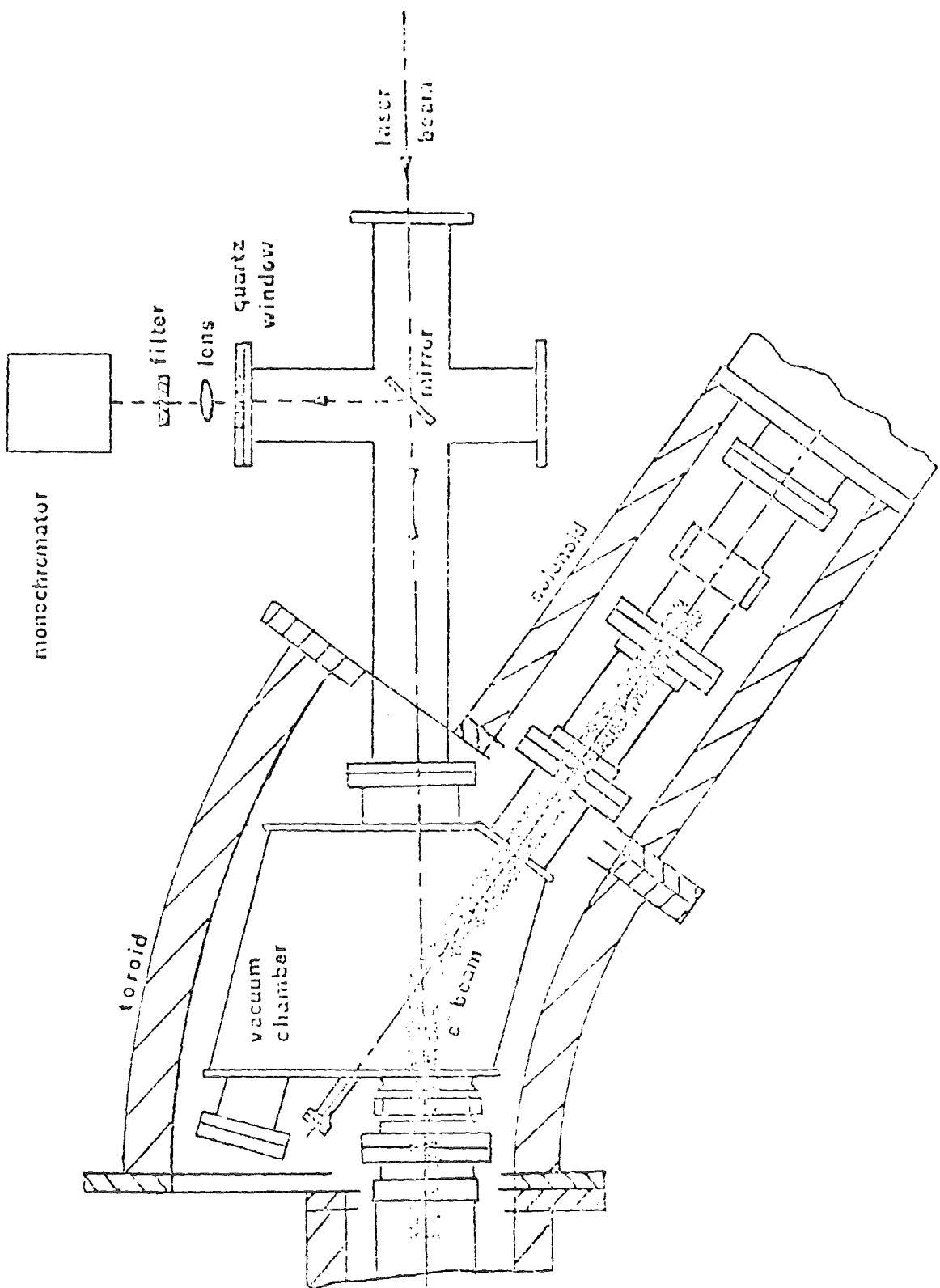


FIG. 10

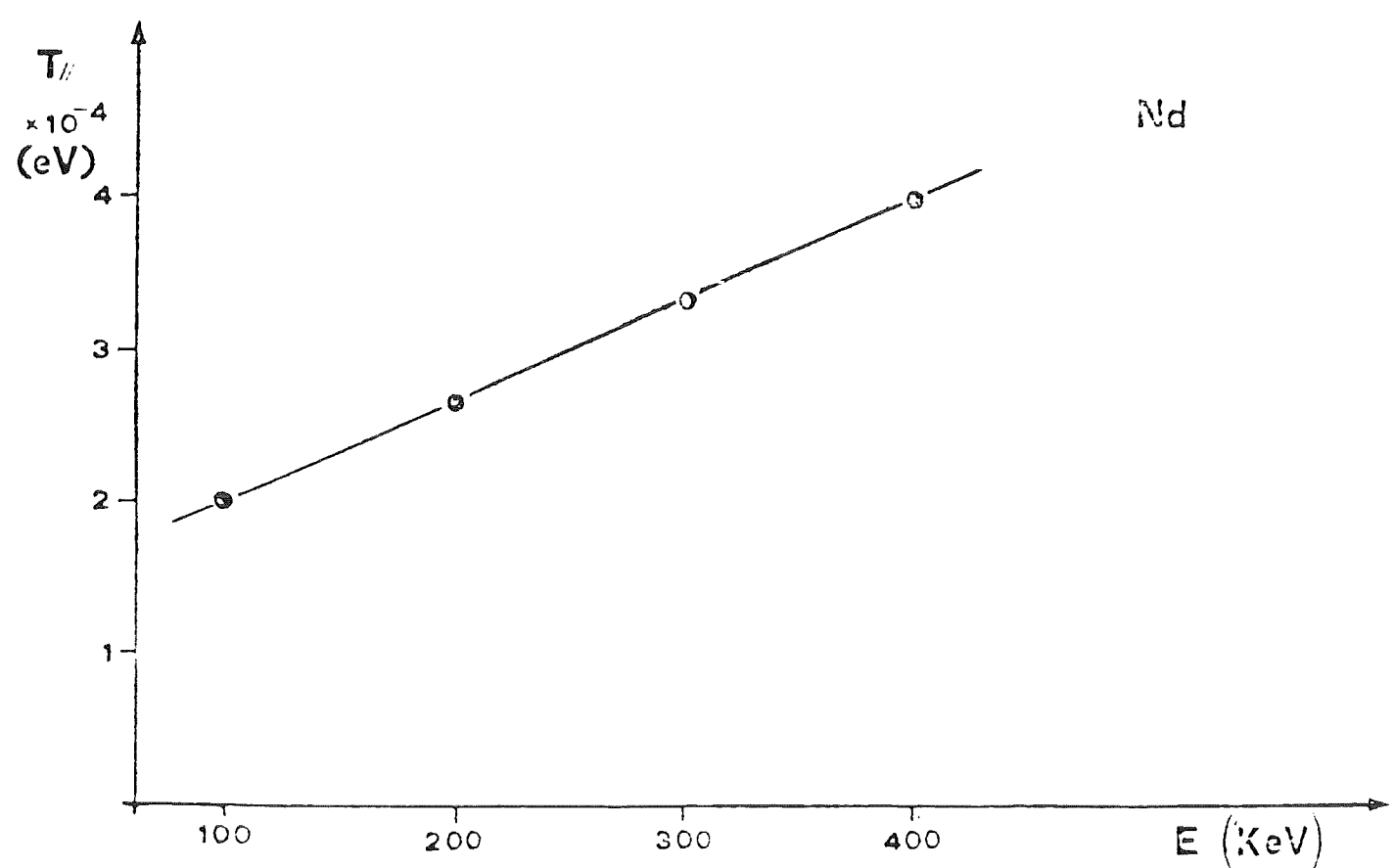
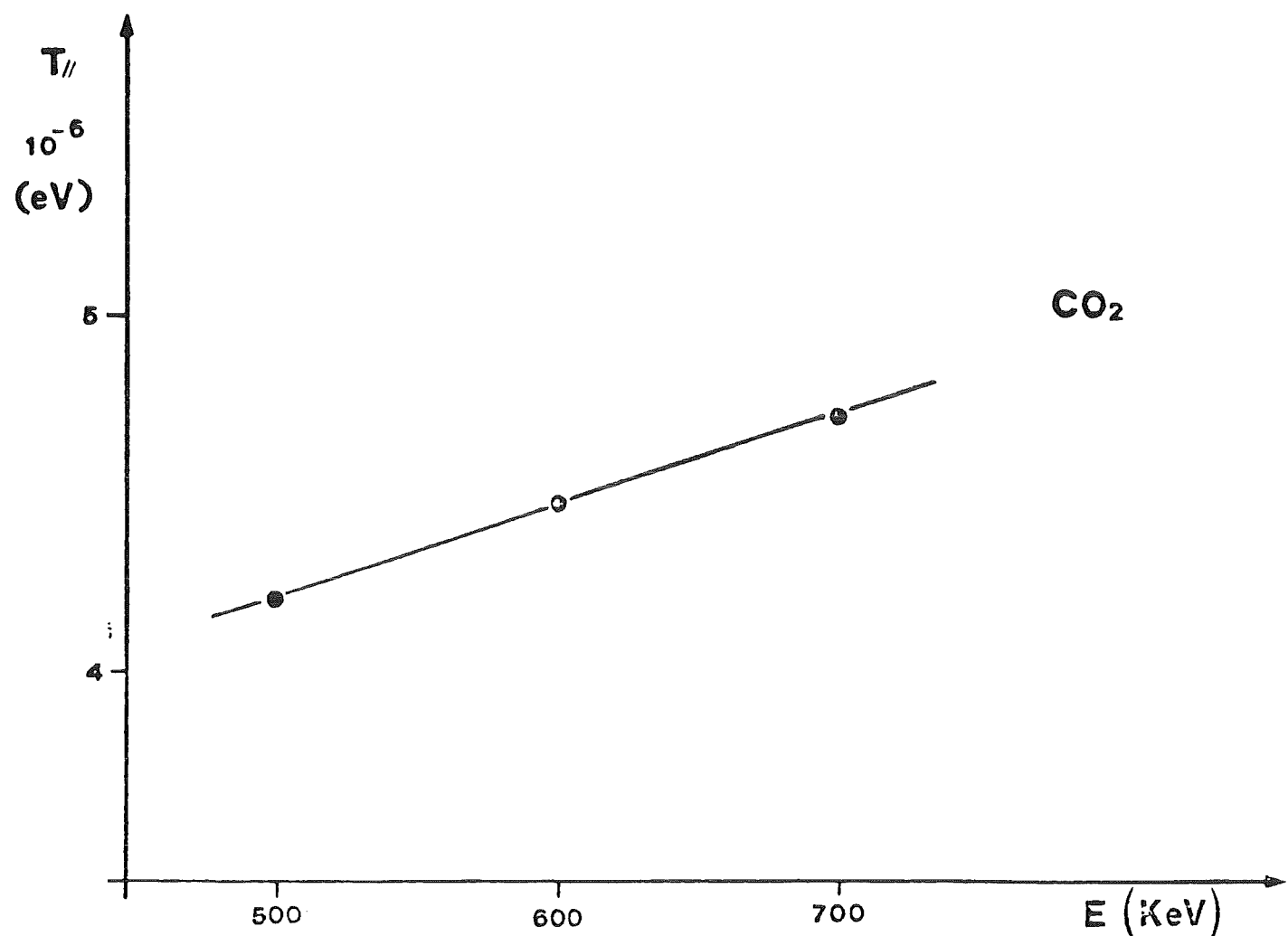


FIG. 11



## RELATIVISTIC ELECTRON COOLING AND INTRABEAM SCATTERING

A.G. Ruggiero

Fermilab, P.O. Box 500, Batavia, IL 60510

### Introduction

In this paper we discuss two issues one of which concerning the usefulness of relativistic electron cooling for large hadron colliders, and the other the limit on the performance of this from intrabeam scattering. The background we have chosen for our analysis is made specifically for proton-antiproton colliders, not just as workable examples but primarily, as we shall see later, for reasons of need, though our results apply to a proton-proton collider as well.

By relativistic electron cooling we do not mean only the instance when  $\beta=1$  for both beams but also the case where the electron beam is made of bunches circulating in a storage ring. In this configuration originally proposed by C. Rubbia<sup>1</sup> very high electron current densities can be reached. In Fig. 1 we show a possible proton-antiproton collider with two electron storage rings, one for cooling of the protons and the other for cooling of the antiprotons. It is well known that electron cooling is independent of the sign of the particle charge, but the two beams have to move in the same direction of the electron bunches to which they have also to match in velocity. We consider three examples; the collider in CERN ( $Spp\bar{S}$ ), at Fermilab (Tev I) and a possible Superconducting Super Collider ( $p\bar{p}$  SSC). The first is already operating,<sup>2</sup> the second is in construction<sup>3</sup> and the third just a possibility.<sup>4</sup> In Table I we give the comparison of the performance for these three colliders. We can make the following remarks: (i) the emittance values assumed or measured are about the same; (ii) the beam-beam tune-shift per crossing in the  $Spp\bar{S}$  turned out to be larger<sup>5</sup> than what it was thought to be allowed for beam stability; a value of  $\Delta\nu = 0.005$  seems to be now reachable, though what really seems to count is the total tune spread in each beam, rather than the shift itself; (iii) the number of antiprotons required is too large; there is definitively the need to find a method to reduce the filling time without reducing the performance; (iv) intrabeam scattering was found in the  $Spp\bar{S}$  to be a serious limitation to the luminosity lifetime<sup>6</sup> and it is expected to play an important role also in the other two colliders. In Figs. 2 and 3 which have been taken from ref. 6, we show the effect of intrabeam scattering in the  $Spp\bar{S}$  collider.

### Performance of Proton-Antiproton Colliders

The performance of the collider is measured by the luminosity  $L$  and the beam-beam tune-shift per crossing  $\Delta\nu_{BB}$ . For crossing at very small angle  $\alpha$  (total)

$$L = \frac{N_p N_{\bar{p}} B f_{rev}}{4\pi\sigma^2 f} \quad (1)$$

and

$$\Delta\nu_{BB} = \frac{3N_p r_p}{\pi\epsilon_N(1+f)} \quad (2)$$

where  $N_p$  and  $N_{\bar{p}}$  are the number of protons and antiprotons per bunch,  $B$  the total number of bunches per beam,  $f_{rev}$  the revolution frequency,  $\sigma$  the rms cross-section of the beam at the collision point,  $\epsilon_N$  the normalized beam emittance for 95% of the population,  $r_p = 1.535 \times 10^{-18} \text{ m}$  and

$$f = \sqrt{1+p^2} \quad \text{with} \quad p = \alpha\sigma_e/2\sigma \quad (3)$$

and  $\sigma_e$  the rms bunch length.

Let us make the reduction of the number of antiprotons to be our goal. It is then seen from eq. (1) the  $N_{\bar{p}}$  can be lowered if also  $\sigma^2$ , that is the emittance  $\epsilon_N$ , is also reduced. For obvious reasons it is important to reduce the emittance of both beams since it is usually assumed the two beams have the same emittance to start with. Inspection of eq. (2) then shows one has also to lower the number of protons per bunch, if we require to maintain the value of  $\Delta\nu_{BB}$  within an acceptable limit. For instance if it is possible to find a method to reduce the emittance by a factor of four, the product  $N_p N_{\bar{p}}$  can also be reduced by the same factor; we can allow both  $N_p$  and  $N_{\bar{p}}$  to change by a common factor which in this case is two. It turns out that the tune-shift  $\Delta\nu_{BB}$  and the betatron phase space density  $N/\epsilon_N$  (a parameter which is important to estimate the intrabeam scattering) are both increased also by a factor of two. An example is worked out in Table II following the same criteria for the three colliders. In this table we give the beam-beam tune-shift, versus the emittance, as well as the number of particles per bunch  $N$  and the density  $N/\epsilon_N$  which we both take equal to one unit for the reference case of  $\epsilon_N = 24\pi \text{ mm-mrad}$ . As the emittance decreases the beam-beam tune-shift increases beyond what it is believed to be an acceptable value. Clearly the design of a proton-antiproton collider is limited by the allowable beam-beam tune-shift and as a consequence it is not possible to reduce the total number of antiproton required for a given luminosity figure.

#### The Need for Relativistic Electron Cooling

It has been found that in the electron-positron storage rings one can allow a much larger beam-beam tune-shift, typically an order of magnitude larger than the one accepted as a limit for hadron colliders. It is believed<sup>7</sup> that the main reason for this is that the electrons betatron and synchrotron trajectories are strongly damped by the synchrotron radiation effects, a mechanism which is quite

negligible for hadrons at least for energies up to 20 TeV. If it is possible to find a damping mechanism also for the protons (antiprotons), fast enough like the synchrotron radiation effects for the electron beams, it should be possible to raise the beam-beam tune-shift by an order of magnitude also for these beams. As one can see from Table II, this could allow 10 times less beam intensity in the Sp $\bar{p}$ S, or 20 times less in the Tev I and 50 times less in the p $\bar{p}$ -SSC, with an equivalent shortening of the antiproton production period and unchanged luminosity performance. It has often been suggested that relativistic electron cooling is the method to create a damping mechanism for protons and antiprotons. We want to investigate this method here again, but use different emphasize as by now it will be obvious to the reader. We will not just be content to preserve the initial beam dimensions with electron cooling against diffusion processes (gas scattering, power supply ripples, rf noise...) to lengthen the beam lifetime, but we will look to the possibility of employing electron cooling first to reduce the beam dimensions, and second to provide a fast damping effect with the purpose of minimizing the number of antiprotons.

#### Intrabeam Scattering

As we have already pointed out, the betatron phase space density will increase and we expect a limit to the effectiveness of the electron cooling caused by intrabeam scattering. This phenomena has been investigated theoretically in a couple of papers<sup>8,9</sup> and it is rather well understood. Several computer codes have been written to estimate diffusion coefficients for a particular beam circulating in a storage ring with assigned lattice. For the Tevatron I project we have made use of a computer code we have obtained from CERN.<sup>10</sup> For the case the beam energy is well above the ring transition energy it is usually found that the energy and radial betatron oscillations are antidamped whereas the vertical motion is damped though at rather slow rate. We take into account the fact that non-linearities in the storage ring, like the beam-beam interaction itself, cause non-linear coupling between the two transverse modes of oscillations difficult to cure; as a consequence the beam will preserve at anytime its "roundness" also in presence of intrabeam scattering, therefore we will denote with  $\epsilon$  the common value of the emittances in the two planes. From the computer code, using the lattice proper for Tevatron I, we have derived the following approximate, empirical formula for the diffusion rates due to intrabeam scattering

$$D_\beta = \frac{d\epsilon}{dt} \approx \frac{A_x I_p}{\delta \epsilon \gamma^3} \quad (4)$$

and

$$D_p = \frac{d\delta}{dt} \approx \frac{A_p I_p}{\delta \epsilon \gamma^2} \quad (5)$$

where  $\epsilon$  ( $= \sigma^2/\beta$ ) is the actual rms emittance and  $\delta$  the rms momentum spread ( $\delta p/p$ ).

$$I_p = \frac{N_p e \beta c}{\sqrt{2\pi} \sigma_e} \quad (6)$$

is the peak bunch current. If time is given in hours, the emittance in meter-radians and the current in Ampere then

$$A_x = 0.13 \times 10^{-13} \text{ m}^2 / (\text{hour} \times \text{Amp})$$

$$A_p = 0.49 \times 10^{-12} \text{ m} / (\text{hour} \times \text{Amp})$$

These values and parametric dependence with  $\delta$ ,  $\epsilon$  and  $\gamma$  are about correct for beam parameters which corresponds to Tevatron I and, likely, also to the SpS. They may not be a representation of the intrabeam scattering effects in the p-p-SSC.

#### The Theory of Relativistic Electron Cooling

The theory of relativistic electron cooling has already been established.<sup>11</sup> It consists mainly of the so-called thermodinamical equations which give the time evolution of the dimensions of both beams (electrons and protons or antiprotons) as they interact with each other. For simplicity in this note we shall make the following approximations: (i) The dimensions of the electron beam are determined only by the synchrotron radiation effects, that is the quantum fluctuation and the radiation damping are of considerably large contribution than the effects from interacting with the hadron beam. Also intrabeam scattering in the electron beam will be ignored compared to the quantum fluctuation. (ii) On the other hand intrabeam scattering will determine the proton beam dimensions more than any other cause, as it is given in equilibrium with coooling effects when interacting with the electron beam.

The following equations then apply to the electron beam

$$\frac{d\epsilon_e}{dt} = Q_\beta - \frac{2}{\tau} \epsilon_e \quad (7a)$$

$$\frac{d\delta_e}{dt} = Q_p - \frac{2}{\tau} \delta_e \quad (7b)$$

where  $Q_\beta$  and  $Q_p$  are the diffusion coefficents due to quantum fluctuations and  $\tau$  is the synchrotron radiation damping time which we assumed here to be the same for both the rms emittance  $\epsilon_e$  and the rms momentum spread  $\delta_e$ . Eqs. (7a and 7b) admits the following equilibrium values

$$\epsilon_e = \frac{1}{2} \tau Q_\beta \quad (8a)$$

$$\bar{\delta}_e = \frac{1}{2} \tau Q_p \quad (8b)$$

The following equations apply to the proton or antiproton beam<sup>11</sup>

$$\frac{d\epsilon_p}{dt} = D_\beta - \frac{k_p \epsilon_p / \epsilon_e}{(\frac{\epsilon_p}{\beta_{p^*}} + \frac{\epsilon_e}{\beta_{e^*}})^{3/2}} \quad (9a)$$

$$\frac{d\delta_p}{dt} = D_p - \frac{k_p \beta^2 \gamma^2 \delta_p / 2 \epsilon_e}{(\frac{\epsilon_p}{\beta_{p^*}} + \frac{\epsilon_e}{\beta_{e^*}})^{3/2}} \quad (9b)$$

where  $D_\beta$  and  $D_p$  are given by eqs. (4 and 5), and

$$k_p = \frac{8r_e r_p I_e L_C n_p}{2^{3/2} e \beta^4 \gamma^5 \beta_{e^*}} \quad (10)$$

$$\begin{aligned} r_e &= 2.818 \times 10^{-15} \text{ m} \\ r_p &= 1.535 \times 10^{-18} \text{ m} \end{aligned}$$

$I_e$  is the peak current of the electron bunch defined by an equation similar to (6). It is obviously required that the two beams have bunches with the same rms length,  $\sigma_e$ .  $L_C \sim 15$  is the Coulomb logarithm and  $n_p$  is the ratio of the length over which the two beams interact and the circumference of the hadron storage ring. Finally  $\beta_{p^*}$  and  $\beta_{e^*}$  are the values of the amplitude lattice functions, in the two rings in the section where the two beams travel together, they are assumed to be the same in both planes. An approximation has been at the denominator of the r.h. side of both eqs. (9a and b) where we have neglected a term  $(\delta_e^2 + \delta_p^2)/\gamma^2$  compared to the emittance contribution  $(\epsilon_p/\beta_{p^*} + \epsilon_e/\beta_{e^*})$ .

#### Search for the Equilibrium

An equilibrium is found by letting the r.h. side of eqs. (9a and b) to vanish identically and by taking into account the equilibrium values (8a and b) for the electron beam. We have

$$\frac{A_x I_p}{\delta_p \epsilon_p \gamma^3} = \frac{k_p \bar{\epsilon}_e / \bar{\epsilon}_e}{(\frac{\epsilon_e}{\beta_e^*} + \frac{\epsilon_e}{\beta_p^*})^{3/2}} \quad (11a)$$

$$\frac{A_p I_p}{\delta_p \epsilon_p^2} = \frac{k_p \beta^2 \gamma^2 \delta_p / 2 \bar{\epsilon}_e}{(\frac{\epsilon_p}{\beta_p^*} + \frac{\epsilon_e}{\beta_e^*})^{3/2}} \quad (11b)$$

By taking the ratio side by side of these equations we obtain

$$\delta_p = \frac{2 \epsilon_p}{\beta^2 \gamma} \frac{A_p}{A_x} \quad (12)$$

For the particular application we have chosen this would yield a very small value, in proximity of  $10^{-8}$ , which we do not believe can be sustained for instance against microwave instability. Therefore we shall assume that the equilibrium value of  $\delta_p$  is the result of microwave stability rather than intrabeam scattering and electron cooling. As a consequence we shall ignore the second equation (11b) and solve the first (11a) for  $\epsilon_p$ .

Indeed it is well known from experimental observations on electron storage rings that the microwave stability criterion holds despite the presence of synchrotron radiation effects; therefore this should be even more true for an hadron beam in presence of electron cooling.

In Table III we give general parameters for the electron storage ring for each of the case considered. We have chosen strong focussing lattice to reduce the equilibrium emittance. Moreover we have assumed full coupling between the two modes of oscillations so that the electron beam is also "round" to match the "roundness" of the hadron beam. We have taken a bending field of 10 Kgauss and the circumference fraction for cooling  $\eta_p = 0.0015$ . The expected momentum spread  $\delta_p$  for the hadron team are given in Table I.

#### Results and Discussions

From eq. (11a) we obtain

$$\epsilon_p^2 = 0.0021 \frac{\beta^4 \gamma^2}{\delta_p} \left( \frac{I_p}{I_e} \right) \beta_e^* \epsilon_e \left( \frac{\bar{\epsilon}_e}{\beta_e^*} + \frac{\epsilon_p}{\beta_p^*} \right)^{3/2} \quad (13)$$

For an efficient cooling it is required that  $\bar{\epsilon}_e \beta_e^* > \epsilon_p \beta_p^*$ . Let us define

$$f_o = \frac{\bar{\epsilon}_e \beta_e^*}{\epsilon_p \beta_p^*} > 1 \quad (14)$$

then

$$\epsilon_p^2 = 0.0021 \frac{\beta^4 \gamma^2}{\sigma_p} \left( \frac{I_p}{I_e} \right) \beta_{e^*} \epsilon_e \left( \frac{\bar{\epsilon}_e}{\beta_{e^*}} \right)^{3/2} \left( 1 + \frac{\beta_{e^*}^2 / \beta_p^2}{f_0} \right)^{3/2} \quad (15)$$

The results are shown in Table IV for  $\beta_p^* = \beta_{e^*}$  and  $I_e = 100 I_p$  which we believe to be realistic. We immediately see that relation (14) cannot be satisfied by far for the  $p\bar{p}$ -SSC case, whereas it is satisfied for both the Sp $\bar{p}$ S and Tevatron I. Relativistic electron cooling does not work well for very relativistic energies. For the same reason the technique is quite more effective for the Sp $\bar{p}$ S case than for Tev I. The beam intensities shown in Table IV correspond to the calculated equilibrium normalized emittance  $\epsilon_N$ , also shown in this table, and what is required according to Table II to maintain a luminosity performance as described in Table I. Similarly we show also the beam-beam tune-shift which corresponds to the new configuration. The damping time  $\tau_g$  and  $\tau_p$  due to cooling at the equilibrium is also shown respectively for the betatron oscillations and for the momentum plane.

For Tevatron I the effect of relativistic cooling is significant but not very large. It is possible to reduce the emittance by a factor of four. This will correspond to twice less protons or correspondingly higher luminosity. Moreover the cooling time of 12 hours should lengthen considerably the luminosity lifetime.

For the case of the Sp $\bar{p}$ S the cooling is very effective. In principle the emittance can be lowered by a factor of 200 which would yield a considerable saving on the required number of antiprotons. Nevertheless the beam-beam tune shift is now quite large and it is not clear whether this can be sustained with a damping time of 7 seconds, since this may not be short enough. Obviously there is a draw-back for this significant result: it is required to get to this very small emittance before the cooling becomes that effective. With the initial value of  $18\pi$  mm-mrad the cooling time is a long period of about two hours, still of some practical interest. Of course one could quickly gain on the results by reducing the initial emittance of both beams either with an improved injector and/or more effective stochastic cooling.

#### Fast Momentum Cooling

As shown in Table IV the cooling time on the momentum plane is extremely short for both the Sp $\bar{p}$ S and Tevatron I. We have explained this as due to the relativistic transformation as one can derive by comparing eq. (9a) with eq. (9b), that is a presence of a factor  $\gamma^2$  on the momentum cooling rate. Is there any way that one can find some useful application of this fast momentum cooling? For instance if a device could be inserted that would strongly couple longitudinal and transverse oscillations than it may be possible to cool also betatron oscillations at those large rates.

References

1. C. Rubbia, Proceed. of Workshop on Producing High-Luminosity High Energy Proton-Antiproton Collisions, March 27-31, 1978, Berkeley, California, p. 98.
2. J. Gareyte, 12th Intern. Conf. on High Energy Accelerators, Fermilab Illinois, Aug. 1983, p. 17.
3. Design Report Tevatron I Project, Fermilab, Sept. 1984.
4. A.G. Ruggiero "A Proton-Antiproton Superconducting Super Collider". Paper submitted to the proceedings of the 1984 Snowmass workshop.
5. L. Evans and J. Gareyte, US Particle Accelerator Conference, Santa Fe, March 21-23, 1983.
6. L.R. Evans, 12 Intern. Conf. on High Energy Accelerators, Fermilab, Illinois, Aug. 1983, p. 229.
7. B. Richter. Private Communication, SLAC, Stanford, California, 1980.
8. A. Piwinski, IX Intern. Conf. on High Energy Accelerators, Stanford California, May 1974, p. 405.
9. J.D. Bjorken and S.K. Mtingwa, Particle Accelerators, Vol. 13, p. 115, 1983.
10. M. Martini, CERN PS/84-9 (AA) May, 1984.
11. A.G. Ruggiero, Proceed. of Workshop on Producing High-Luminosity High Energy Proton-Antiproton Collisions, March 27-31, 1978, Berkeley, California, p. 166.

Table I. Proton-Antiproton Colliders

|   | SppS<br>(achieved)    | Tevatron I           | p-p-SSC               |
|---|-----------------------|----------------------|-----------------------|
| Average radius, km                        | 1.1                   | 1.0                  | 104.6                 |
| Energy, max, TeV                          | 0.27                  | 1.0                  | 20.                   |
| No. of bunches/beam                       | 3                     | 3                    | 4428                  |
| No. of p's/bunch                          | $0.15 \times 10^{11}$ | $6 \times 10^{10}$   | $0.77 \times 10^{10}$ |
| No. of p's/bunch                          | $1.4 \times 10^{11}$  | $6 \times 10^{10}$   | $3 \times 10^{10}$    |
| Bunch area, eV-sec                        | 0.5                   | 3.0                  | 4.5                   |
| Momentum spread, $\delta_p$               | $0.8 \times 10^{-4}$  | $1.2 \times 10^{-4}$ | $0.18 \times 10^{-4}$ |
| Normalized emittance<br>$\pi$ mm-mrad     | 18                    | 24                   | 24                    |
| $\beta^*_{H,V}$ , m<br>$\eta^*_{H,V}$ , m | 1.3/0.65 m<br>0.0     | 1.0<br>0.18          | 1.0<br>0.0            |
| Luminosity, $\text{cm}^{-2}\text{s}^{-1}$ | $1.8 \times 10^{29}$  | $1.0 \times 10^{30}$ | $1.0 \times 10^{32}$  |
| Beam-beam tune-shift                      | 0.0045                | 0.0017               | 0.00082               |
| Antiproton Production<br>rate,/sec        | $2.5 \times 10^{-6}$  | $3.5 \times 10^{-7}$ | $8 \times 10^{-8}$    |
| Filling time (p)                          | 24 h                  | 1.5 h                | 12 h                  |

Table II. Collider Performance vs. Emittance

| Normalized<br>Emittance |                 | SppS   | Tevatron I | p-p-SSC |
|-------------------------|-----------------|--------|------------|---------|
| $24\pi$ mm-mrad,        | $\Delta v_{BB}$ | 0.0045 | 0.0017     | 0.00082 |
|                         | N               | 1      | 1          | 1       |
|                         | N/ $\epsilon$   | 1      | 1          | 1       |
| 6                       | $\Delta v_{BB}$ | 0.009  | 0.0034     | 0.00164 |
|                         | N               | 0.5    | 0.5        | 0.5     |
|                         | N/ $\epsilon$   | 2      | 2          | 2       |
| 1                       | $\Delta v_{BB}$ | 0.022  | 0.0083     | 0.004   |
|                         | N               | 0.2    | 0.2        | 0.2     |
|                         | N/ $\epsilon$   | 5      | 5          | 5       |
| 0.24                    | $\Delta v_{BB}$ | 0.045  | 0.017      | 0.0082  |
|                         | N               | 0.1    | 0.1        | 0.1     |
|                         | N/ $\epsilon$   | 10     | 10         | 10      |
| 0.06                    | $\Delta v_{BB}$ | 0.09   | 0.034      | 0.0164  |
|                         | N               | 0.05   | 0.05       | 0.05    |
|                         | N/ $\epsilon$   | 20     | 20         | 20      |
| 0.01                    | $\Delta v_{BB}$ | 0.22   | 0.085      | 0.04    |
|                         | N               | 0.02   | 0.02       | 0.02    |
|                         | N/ $\epsilon$   | 50     | 50         | 50      |

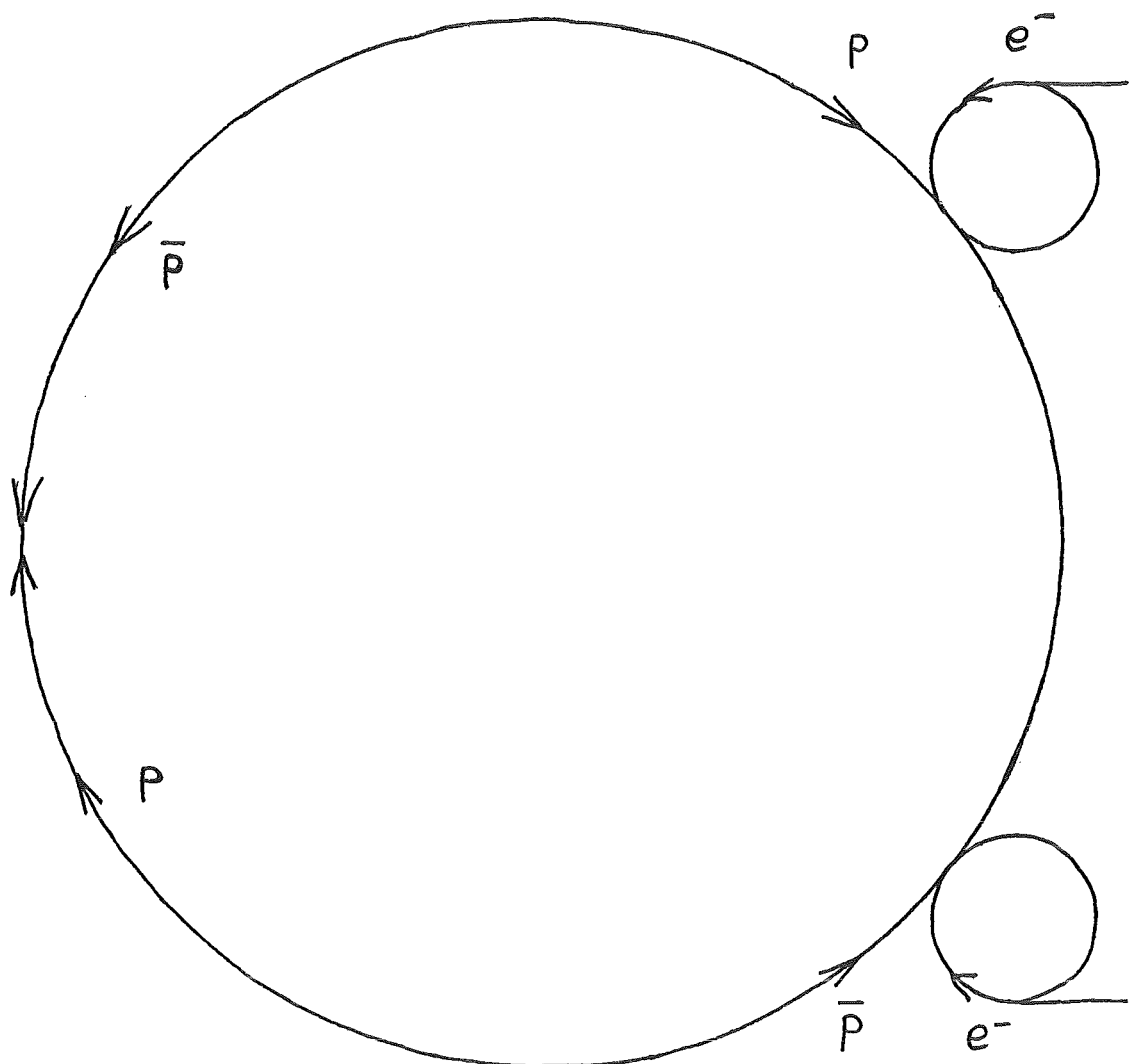
Table III Electron Storage Ring Parameters

|                                  | Sp $\bar{p}$ S          | Tevatron I              | p $\bar{p}$ -SSC        |
|----------------------------------|-------------------------|-------------------------|-------------------------|
| $\gamma$                         | 270                     | 1000                    | 20,000                  |
| Circumference                    | 30 m                    | 50 m                    | 1,000 m                 |
| Bending radius*                  | 1 m                     | 2 m                     | 40 m                    |
| Betatron tune                    | 6                       | 10                      | 200                     |
| Energy loss/turn                 | 30 eV                   | 2.8 KeV                 | 22 MeV                  |
| Damping time, $\tau$             | 450 msec                | 30 msec                 | 15 msec                 |
| rms energy spread, $\delta_e$    | $1.2 \times 10^{-4}$    | $3.1 \times 10^{-4}$    | $1.4 \times 10^{-3}$    |
| $\beta$ -emittance, $\epsilon_e$ | $3.1 \times 10^{-10}$ m | $7.6 \times 10^{-10}$ m | $3.8 \times 10^{-11}$ m |
| $\beta_e^*$ (H and V)            | 70 m                    | 70 m                    | 200 m                   |
| Interaction length               | 10 m                    | 10 m                    | 200 m                   |

(\*)With a bending field of about 10 KG.

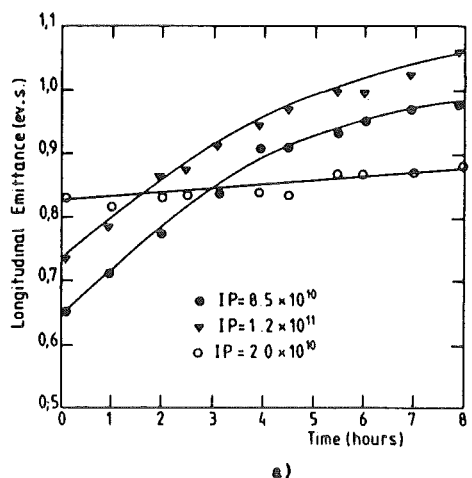
Table IV. Performance with Relativistic Electron Cooling  
( $I_e = 100 I_p$ )

|                           | Sp $\bar{p}$ S        | Tevatron I            | p $\bar{p}$ -SSC       |
|---------------------------|-----------------------|-----------------------|------------------------|
| $\gamma$                  | 270                   | 1000                  | 20,000                 |
| $\epsilon_f^p$            | $6 \times 10^{-11}$ m | $9 \times 10^{-10}$ m | $1.6 \times 10^{-6}$ m |
| $\epsilon_o^p$            | 5                     | 1                     | $2.4 \times 10^{-5}$   |
| $\epsilon_N^N$            | $0.1\pi$ mm-mrad      | $5.4\pi$ mm-mrad      | -                      |
| $N_p^p$                   | $10^{10}$             | $3 \times 10^{10}$    | -                      |
| $I_p^p$                   | 0.5 amp               | 1.5 amp               | -                      |
| $I_p^e$                   | 50 amp                | 150 amp               | -                      |
| $N_e^e$                   | $10^{12}$             | $3 \times 10^{12}$    | -                      |
| $\tau_\beta$              | 7 sec                 | 12 hour               | -                      |
| $\tau_p$                  | 0.2 msec              | 80 msec               | -                      |
| $\Delta v_{BB}$           | 0.05                  | 0.0034                | -                      |
| p $\bar{p}$ -filling time | 2-3 hour              | <1 hour               | -                      |

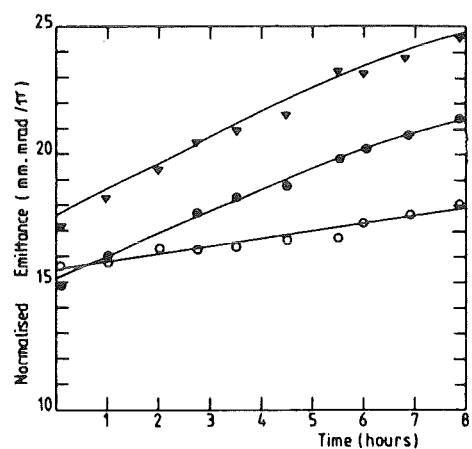


- |                                  |                         |                         |
|----------------------------------|-------------------------|-------------------------|
| 1. S <sub>P</sub> P <sub>S</sub> | $E_p = 270 \text{ GeV}$ | $E_e = 135 \text{ MeV}$ |
| 2. TeV I                         | 1 TeV                   | 500 MeV                 |
| 3. p <sub>P</sub> -SSC           | 20 TeV                  | 10 GeV                  |

Fig. 1 Layout of a  $p\bar{p}$  Collider with  $e^-$  Storage Rings for Relativistic Electron Cooling



a)



b)

**Fig. 2** Longitudinal a) and radial b) emittance growth of three proton bunches with different intensities

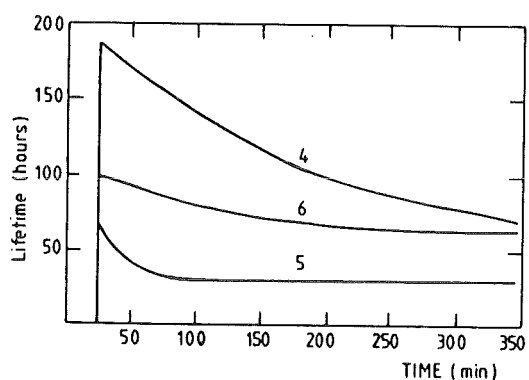


**Fig. 3** Lifetime evolution of three proton bunches with different longitudinal emittance and intensity.

Construction of a 3 MeV  
Ampere-Intensity Recirculating  
Electron Beam System: A Progress Report

National Electrostatics Corp.  
M. Sundquist  
J. Adney

U.S. Department of Energy  
Contract DE-AC02-83ER80074

**Abstract**

Construction of a 3 MeV electrostatic accelerator designed to recirculate DC electron beams with intensities up to 5 A is in progress. The test facility includes a 3 MV, SF<sub>6</sub> insulated vertical accelerator with parallel accelerator and decelerator tubes, diagnostic equipment, and vacuum and beam line components to bend the electron beam 180° and return it to the terminal. Special consideration has been given to cathode, collector, and optical design to allow very high recovery efficiency at any current from 100 μA to 5A.

## Introduction

Two key experiments provided the basis for the accelerator system. The first was the successful adaptation of the NEC 3 MV electrostatic test accelerator for pulsed recirculating electron beams by Elias and Ramian (1). The second was the development of an electron collector system by T. Ellison, et al. at Fermilab with losses less than one part in  $10^4$  (2).

We have based our design in part on the design of Elias and Ramian and will use the same electrostatic accelerator as they used for their initial experiments. Because we require DC operation, however, and far better recirculation efficiency than with a pulsed beam, both the electron gun cathode and the entire electron collector are new designs (3).

### Electron Gun

The electron gun has nearly the same electrostatic geometry as the very low emittance (4) gun of Elias and Ramian but the mechanical construction has been altered to conform to NEC manufacturing practice. The design incorporates the following features (see Fig. 2.1):

1. Three-element (cathode, control electrode, anode) geometry,
2. Disassembly to replace electrodes or cathode requires no welding; reassembly requires no alignment tools,
3. Entire construction is all metal and ceramic, bakeable to 450° C,
4. Cathode flange has a coaxial multipin heater feedthrough and a port for an ion pump,
5. All insulators are shielded from sputtering or beam-induced charging,
6. Cathode element is a dispenser cathode with four independently heated concentric emitting surfaces. These allow operation with space charge limited gun optics over a wide range of beam currents, and make DC operation and adjustment possible with minimum charging current. Anticipated cathode areas and loading ranges are shown in Table 2.1.

Table 2.1

| @0.2 mA Lost Max. |        |                       |           |          |           |           |
|-------------------|--------|-----------------------|-----------|----------|-----------|-----------|
|                   | O.D.   | AREA                  | I<br>MIN* | I<br>MAX | %<br>@MIN | %<br>@MAX |
| Inner Spot        | 0.12mm | 0.011 cm <sup>2</sup> | 1mA       | 11mA     | 80%       | 98.2%     |
| 1st Ring          | 3.0mm  | 0.071 cm <sup>2</sup> | 7mA       | 71mA     | 97.1%     | 99.7%     |
| 2nd Ring          | 8.0mm  | 0.502 cm <sup>2</sup> | 50mA      | 500mA    | 99.6%     | 99.96%    |
| 3rd Ring          | 20.0mm | 3.14 cm <sup>2</sup>  | 315mA     | 3.1A     | 99.93%    | 99.993%   |
|                   |        |                       |           | 5.0A**   |           | 99.996%   |

\*For optics similar to maximum (0.1 A/cm<sup>2</sup>)

\*\*At slightly increased cathode loading of 1.6 A/cm<sup>2</sup>

### Collector

The collector design is patterned after the collector tested at 120keV at Fermilab by F. Mills, et. al. It incorporates entrance electrodes that mirror the electron gun geometry (some parts are common to both) and combines electrostatic electron trapping with space charge neutralization by ions confined in the ion potential well which is located within the collector solenoid (Figures 3.1 and 3.2). The electrons are slowed down to about 1 keV at the bottom of this well then reaccelerated to the collector. Their minimum energy occurs within the cylinder surrounded by the collector solenoid. The Fermilab experiments with this configuration suggest that a plasma is created within this cylinder which helps to prevent blow up of the electron beam.

### Beam Line

The beam line (Figure 4.1) incorporates standard components found on numerous NEC accelerators. In order from the electron gun: NEC High-gradient Accelerating Tube, nine sections, rated at 3MV, pumping tee with 120 1/sec ion pump, NEC High Power Faraday Cup, quadrupole singlet lens, pumping tee with shared 220 1/sec ion pump, NEC Beam Profile Monitor, 90 degree double focusing dipole magnet, and single slit assembly, after which all components repeat in the reverse order.

As discussed in section 5, there are solenoid lenses at one-third the way down the accelerating tube and at its exit, which act to keep the beam size limited to somewhat less than the tube minimum aperture even at the beam current design limit of 5A.

The beam tube diameter is 4 inches wherever possible, but due to tank restrictions the portion of the tube passing through the tank bottom has a reduced diameter as does the tubing within the quadrupole singlets and the dipoles. At no point does the beam size approach the effective aperture of the beam line; moreover, due to distributed pumping, the localized small diameters should have minimal affect on vacuum and beam quality.

- 1) T. Ellison, W. Kells, V. Kerner, F. Mills, R. Peters, T. Rathbun, D. Young, and P.M. McIntyre, "Electron Cooling and Accumulation of 200 MeV Protons at Fermilab", presented at the APS 1983 Particle Accel. Conf. (Santa Fe, Mar 21-23, 1983).
- 2) L.R. Elias and G. Ramian, "Design of the UCSB FEL Electron Beam System", Quantum Institute, University of California-Santa Barbara, QIFEL011/81.
- 3) M. Sundquist and J. Adney, "Design of Components for an Ampere Intensity, MeV Energy, DC Electron Beam System", NEC Report No. 182. (Jan, 1984).
- 4) D.B. Cline, D.J. Larson, W. Kells, F.E. Mills, J. Adney, J. Ferry and M. Sundquist, IEEE Trans. Nucl. Sci., (June 83).

The authors would like to acknowledge the support of the U.S. Department of Energy, and the assistance of F.E. Mills of Fermilab, and D.B. Cline and D.J. Larson of the University of Wisconsin.

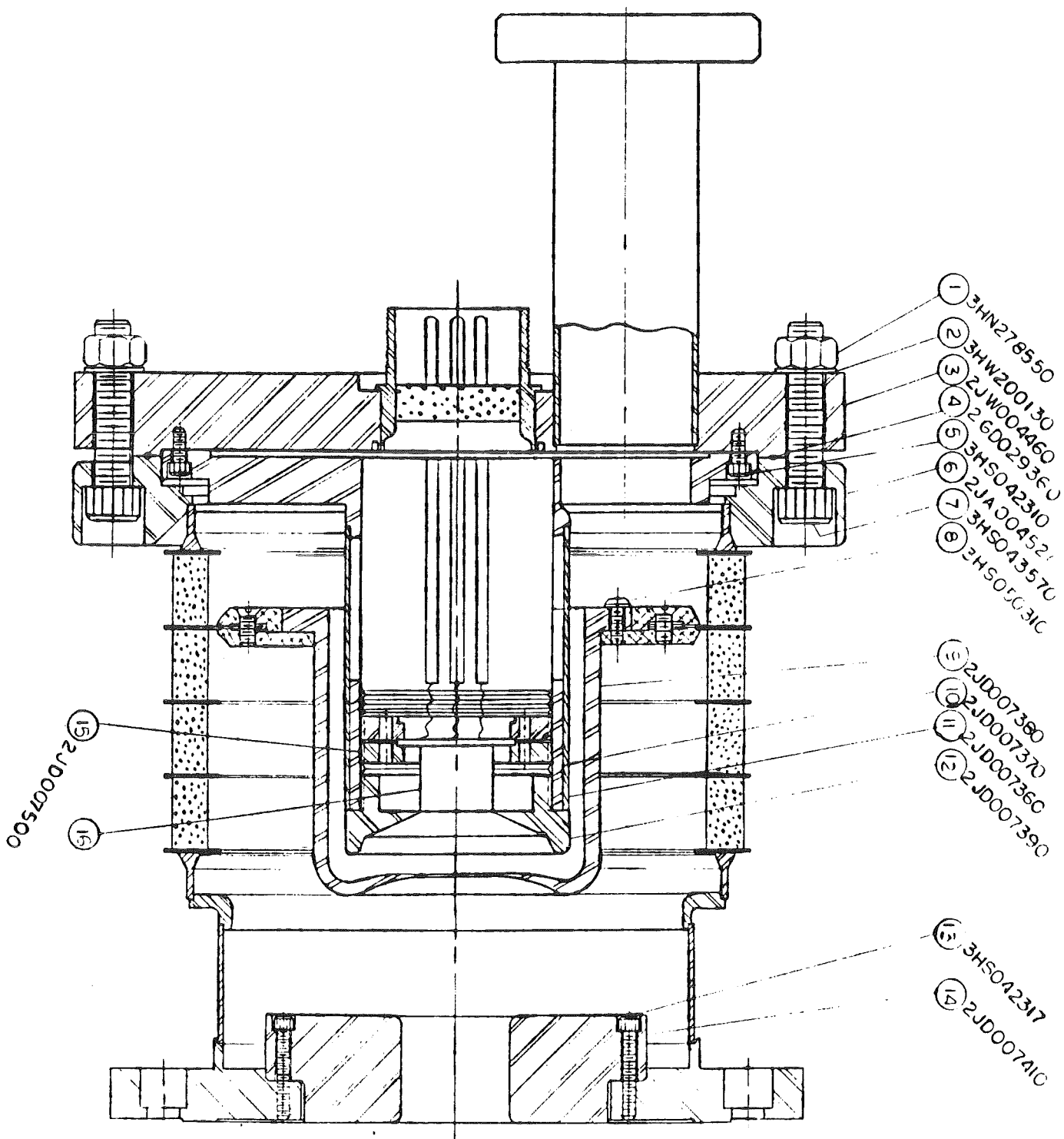


Fig. 2.1 Electron Gun Assembly (NEC Dwg. #11-0-447)

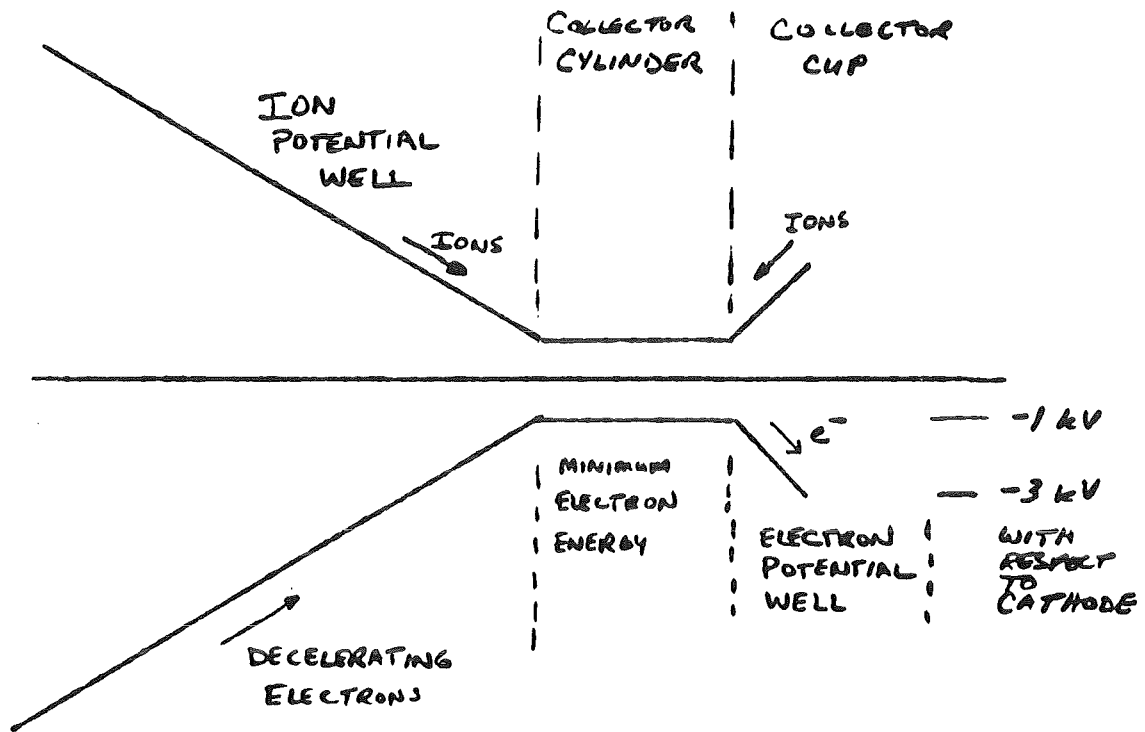


FIG. 3.1

COLLECTOR ENERGY WELLS

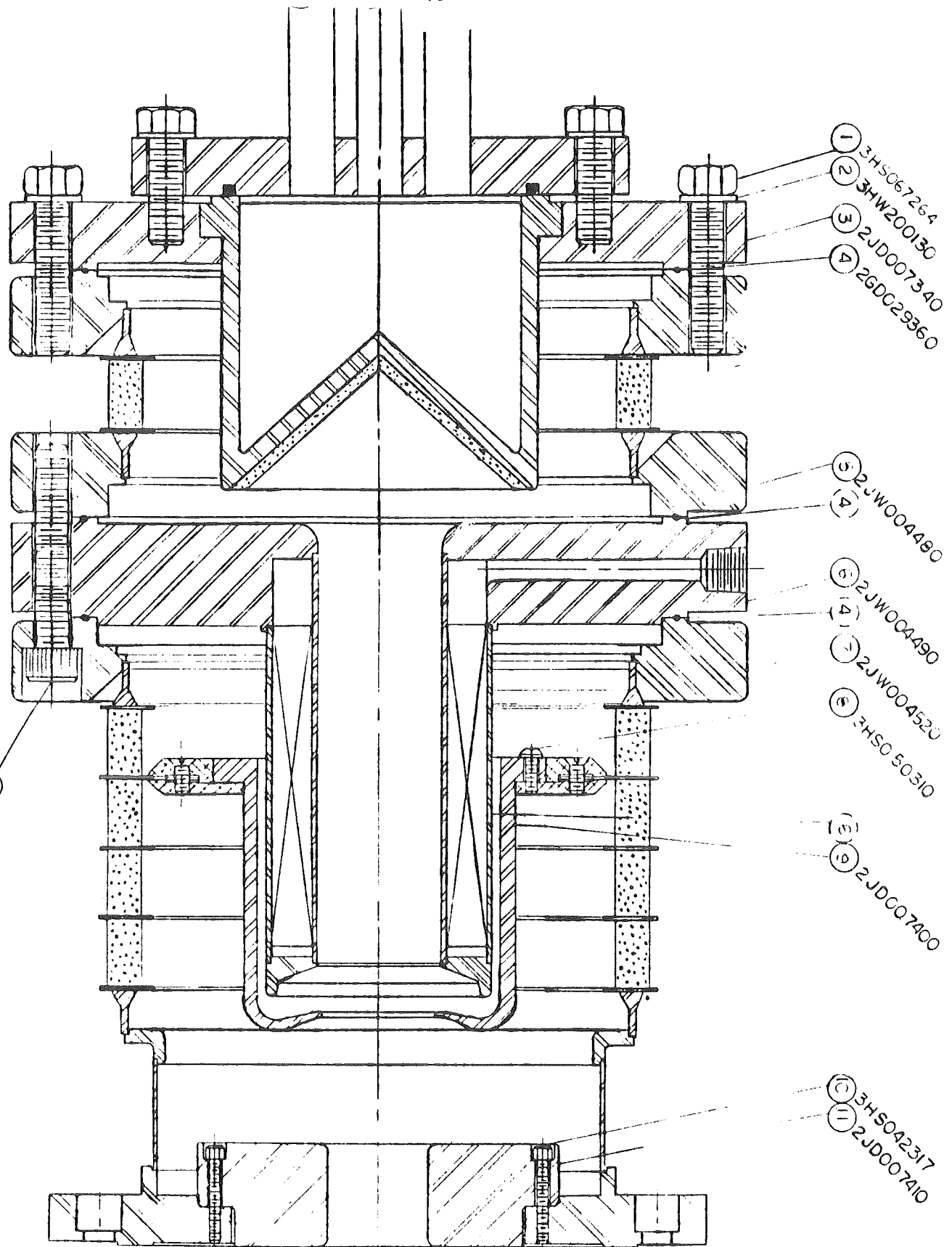


Fig. 3.2 Collector Assembly (NEC Dwg. #11-0-450)

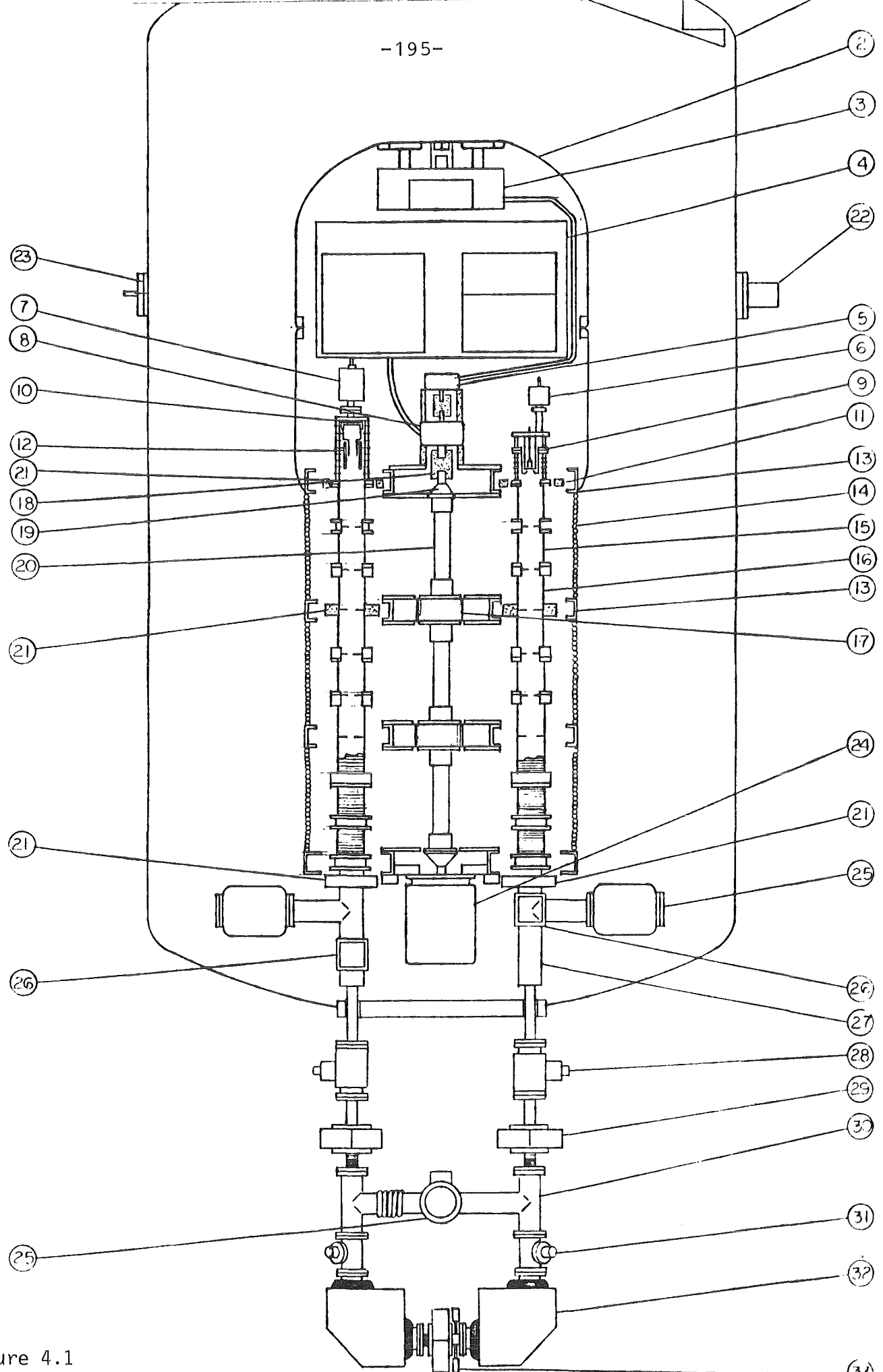
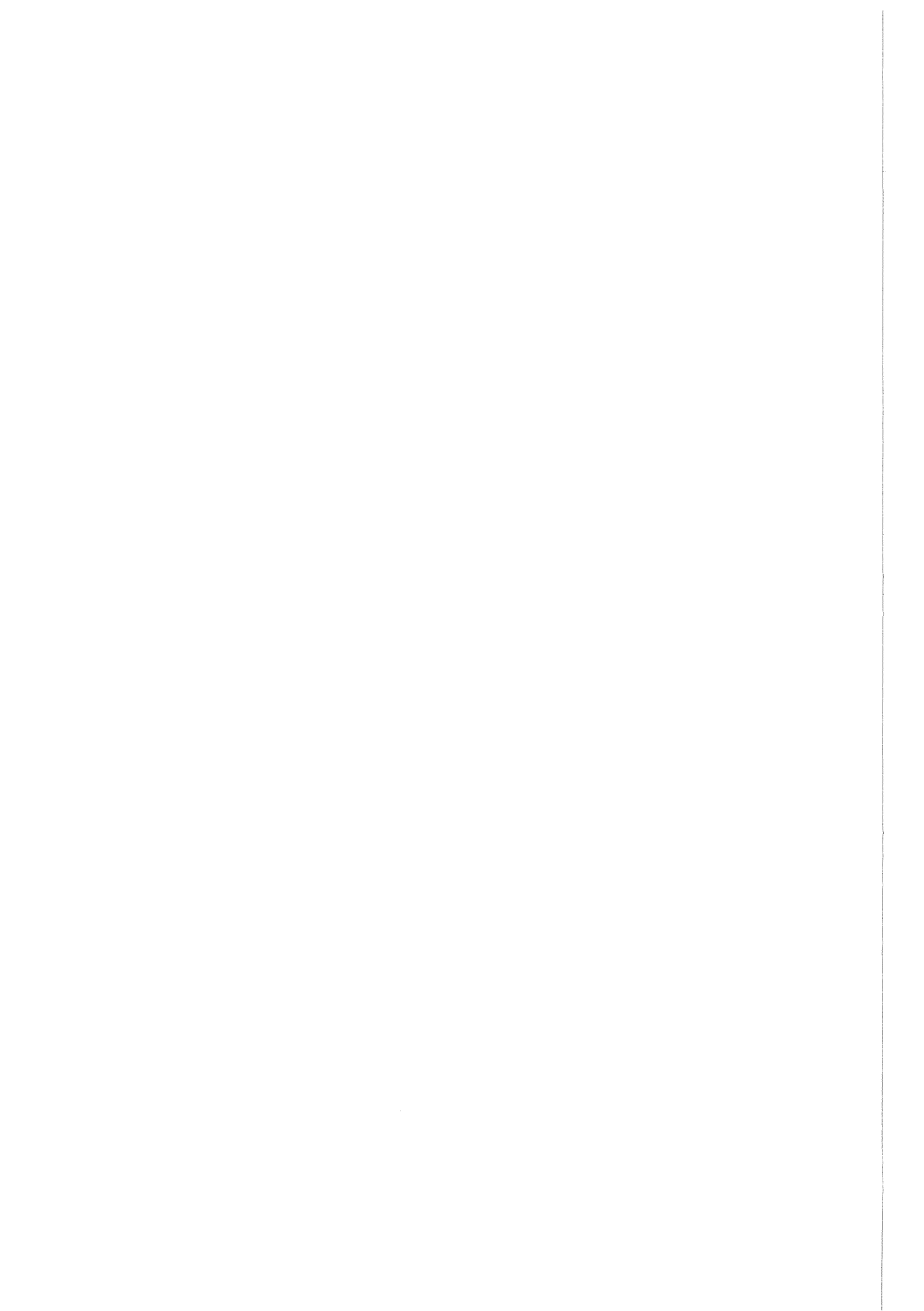


Figure 4.1



High Efficiency Recovery of an Ampere Intensity 3 MeV

Electron Beam

Delbert Larson - University of Wisconsin

Fred Mills and Frank Cole - Fermilab

i) Introduction

Antiprotons are produced in greater numbers as their production momenta is increased<sup>1,2</sup>. Electron cooling of antiproton sources in the several GeV range will require electron beam energies in the range of three to ten MeV in order to match the antiproton velocity. High quality electron beams of this energy range can be produced by Pelletron accelerators manufactured by National Electrostatics Corporation of Middleton, Wisconsin. To obtain currents in the order of amperes highly efficient recovery of the electron beam is required since the charging capability is limited to about 500 microamps. The collection of these nonmagnetized electron beams requires a highly efficient collector just above terminal potential as well as electron optics designed to keep the beam within apertures throughout the system. A schematic of the electron cooler is shown in figure 1. The optics calculations done in this paper are for the recirculating beam test to be done within the next year. In that test, the beam will be sent down the Pelletron, turned around by the two dipoles, and

Schema of Intermediate Energy Electron Cooling Device

-198-

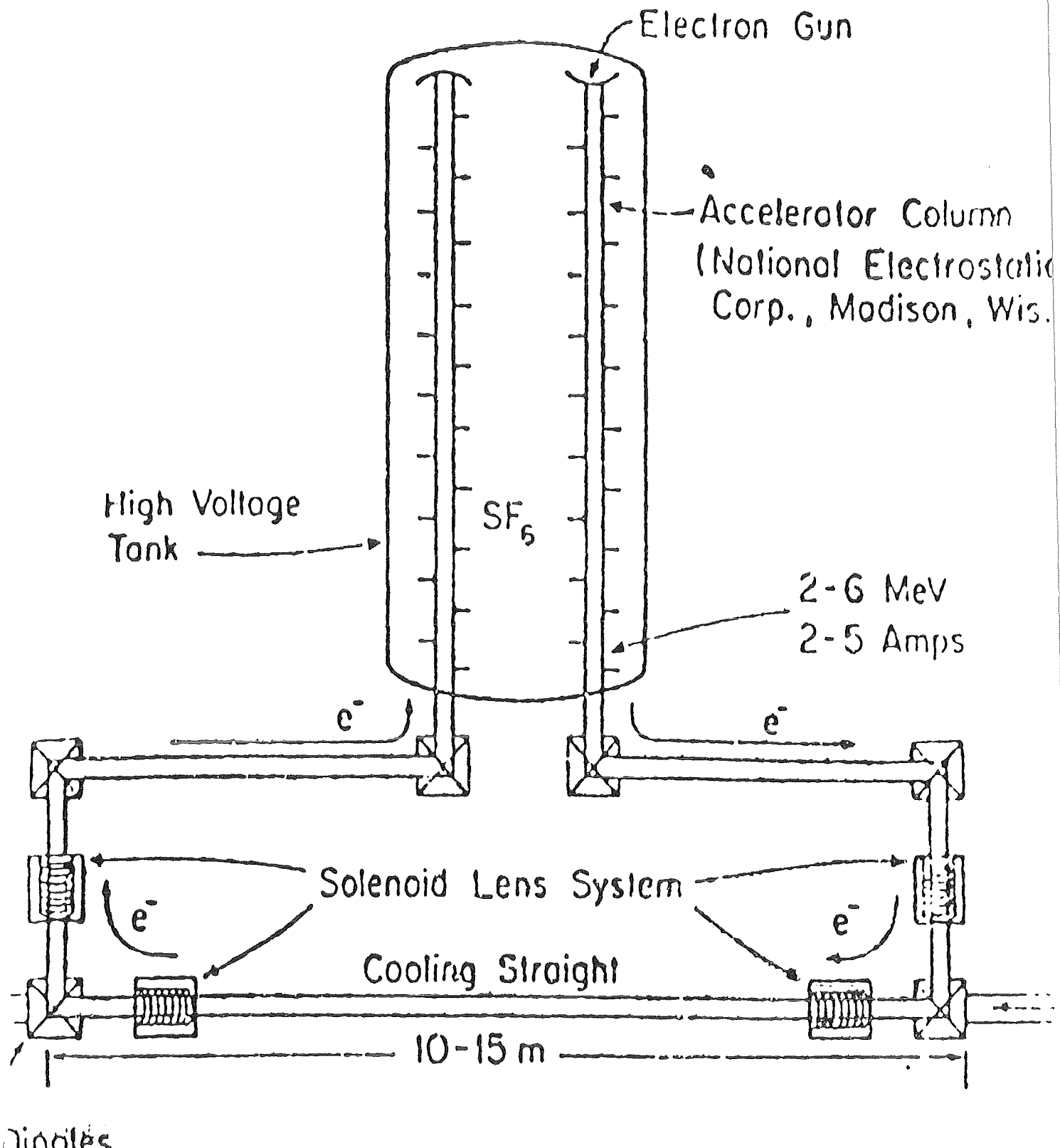


FIGURE 1

recirculated to the terminal (without the rest of the beamline shown in the figure).

I) Electron Optics Studies of a Pelletron Accelerator

A) Electron Gun Optics

The intermediate energy electron cooling effort at the University of Wisconsin began as a collaboration with the University of California - Santa Barbara free electron laser group lead by Luis Elias<sup>3</sup>. Since both efforts require high current low emittance beams, the f.e.l. group agreed to having the U.W. measure the emittance of their test device. The measurement indicated that the optics of the f.e.l. test device was extremely good - there was no emittance degradation throughout the system<sup>4</sup>. For this reason, the electron gun for the electron cooling effort has been designed to be optically identical to the U.C.S.B gun. The original f.e.l. gun was designed to be an optical match to the Pelletron by Bill Hermannsfeldt of SLAC.

One major difference existed between the electron cooling effort and f.e.l. operation, the electron cooling machine must operate in a D.C. mode, while the f.e.l. ran in pulsed mode. Since the collector space charge neutralization region takes a time of about a second to respond (from the Fermilab Electron Cooling experiment<sup>5,6</sup> - also see later calculations) the cathode had to be made so as to be able to slowly turn the current up. The design of the gun has a center spot and three concentric cathode rings, which can all be operated in both

the thermal and space charge limited regimes. By turning on one ring after another the current can be ramped up from one milliamp to 3.9 amperes. Two optics runs have been done on the gun, one at 3.9 amperes, the other at the thermal emission limit of .315 amperes. These calculations were done with all cathodes heated, but due to the radial symmetry of both the space charge and emittance forces the calculations are valid for any cathode radius. The optics program used to investigate the gun behavior is EGUN written by Bill Hermannsfeldt. This program uses the method of finite differences to numerically solve for the fields created by various potential surfaces, and then recursively solves for the electron trajectories. Space charge of the electron beam is included in the problem, but as of yet the finite beam temperature has not been put in (although EGUN allows this to be done). Due to the complicated problem of attempting to do electron optics at the start of the Pelletron accelerating column, the first 120,000 volts of acceleration in the Pelletron is included in the gun optical study. At that point in the Pelletron the electric field no longer has any radial component and another optical treatment of the device is done. Figure 2 shows the electron trajectories calculated for a current of 0.315 amperes, while figure 3 shows the full space charge limited current of 3.962 amps as it is accelerated through the first 170,000 volts (the gun provides 50,000 volts of acceleration).

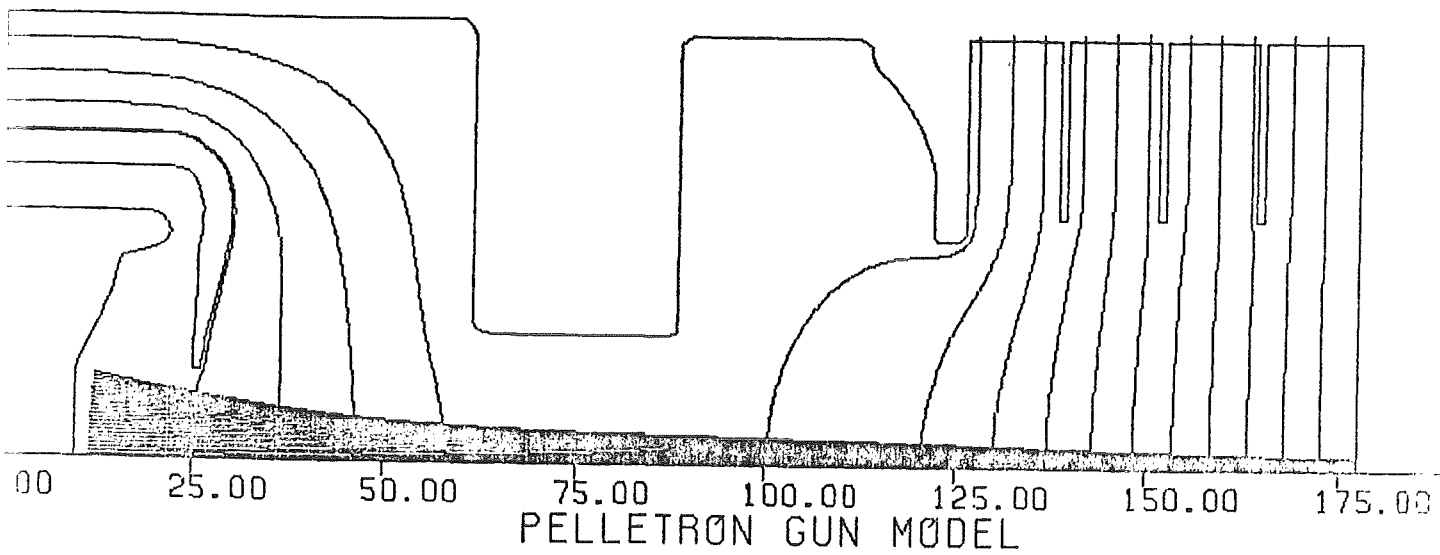


Figure 2 - E-Gun Output for Gun at Thermal Emission Limit

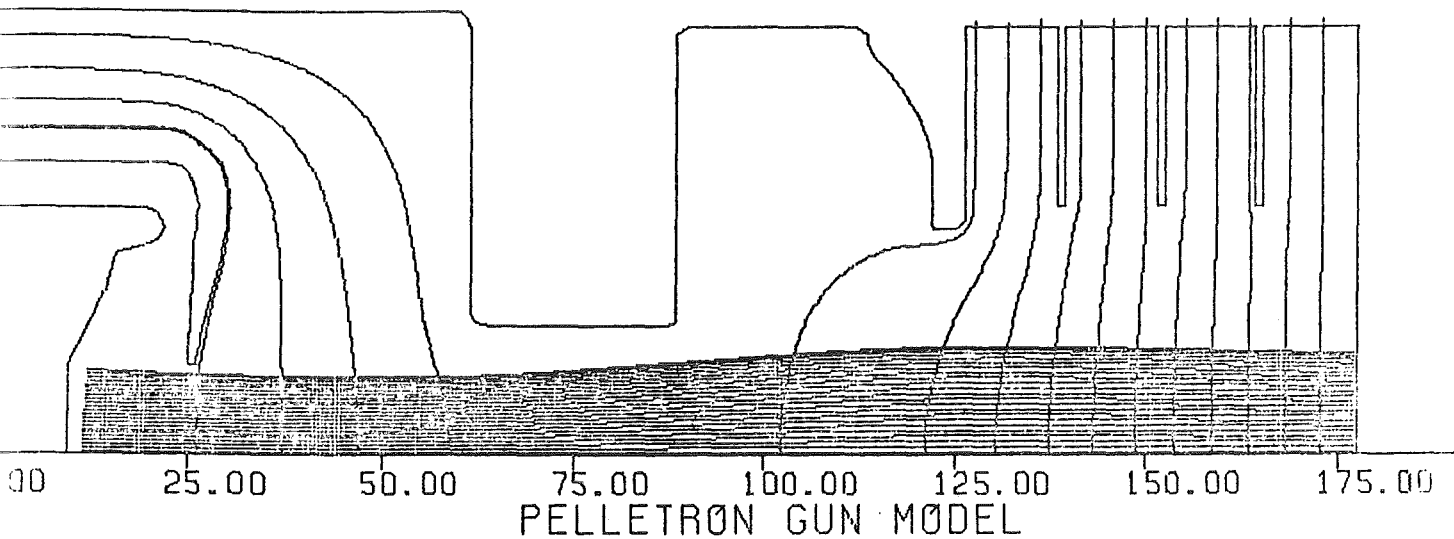


Figure 3 - E-gun output for space charge limit

B) Pelletron Optics

The solution of the Pelletron optics is accomplished by the use of Hamiltonian mechanics combined with a treatment similar to that used by Courant, Livingston and Snyder in their classic treatment of strong focusing synchrotrons<sup>7</sup>. Since the desired quantity is the beam radius as a function of distance along the beamline ( $z$ ) it is reasonable to switch to the coordinate  $z$  as the independent variable in the problem. This is done by means of the generalized Hamilton's principle to obtain the Hamiltonian for the problem,  $G$ .

$$G = -P_z c = -([M_e c^2 + e\phi]^2 - P_r^2 c^2 - [M_e c^2]^2)^{1/2} - eA_z c \quad (1)$$

The space charge effect on the electric potential  $\phi$  can be calculated by Gauss' law to see that the potential at the beam edge is not a function of the size of the beam. The potential is thus given by the voltage of the Pelletron.

$$\phi = \phi_0 + E_0 z \quad (2)$$

Next the increase of the radial momentum with respect to the independent variable can be calculated from Hamilton's equations using the fact that  $A_z$  is much less than  $P_z$ .

$$\frac{dp_r}{dz} = -\frac{\partial G}{\partial r} = -\frac{M_e c^2 + e\phi}{P_z} \cdot \frac{\partial}{\partial r}(e\phi) + e \frac{\partial}{\partial r} A_z c \quad (3)$$

The partial derivative of the electrostatic potential is simply the radial electric field due to the space charge of the beam which can be determined from Gauss' law (for a beam of radius  $a$ ).

$$\frac{\partial}{\partial r} e\phi = -eE = -\frac{eIr}{2\pi\epsilon_0\beta ca^2} \quad (4)$$

The partial derivative of the magnetic vector potential is the azimuthal component of the magnetic field which can be found from Ampères' law.

$$\frac{\partial}{\partial r} eAc = -eB = -\frac{eIr}{2\pi\epsilon_0 ca^2} \quad (5)$$

By noting that  $\frac{M_e c^2}{P_z} + \frac{e\phi}{c} = \frac{1}{\beta_z}$  equations (4) and (5) can be substituted into equation (3) to obtain a numerically integrable relation for  $P_r$ .

$$\frac{\partial P_r}{\partial r} = -\frac{eI \cdot (1 - \beta_z^2)r}{2\pi\epsilon_0 a^2 \beta^2 c} \cdot \Delta z = -\frac{eIr}{2\pi\epsilon_0 a^2 (\beta\gamma)^2 c} \quad (6)$$

By constantly updating the radial momentum in this way it is then possible to obtain the longitudinal momentum from equations (6), (2), and (1).

Numerical integration shows that for space charge limited emission current density the beam profile obtained in this way is an adequate representation of the problem, but for the lowest densities beam expansion due to beam emittance must be included. Inclusion of beam emittance into the Pelletron optics can be done by the WKB method as first done by Courant, Livingston and Snyder. To do this a differential equation for the radial coordinate with respect to  $z$  must be obtained along with equations for  $\beta$  and  $\gamma$  as functions of  $z$ . The values  $\beta$  and  $\gamma$  will be evaluated on the central trajectory of the orbit ( $r = 0$   $P_r = 0$ ).

$$\gamma = \frac{eE_0 z}{M_e c^2} + 1 = \alpha z + 1$$

$$\text{with } \alpha = \frac{eE_0}{M_e c^2} \quad (7)$$

$$\beta = \left(1 - \frac{1}{(1 + \alpha z)^2}\right)^{1/2}$$

The radial momentum can now be expressed as the relativistic mass multiplied by the velocity in the radial direction.

$$P_r = \gamma m \beta r' c \quad (r' = \frac{\partial r}{\partial z}; \quad r'' = \frac{\partial^2 r}{\partial z^2}) \quad (8)$$

In the above equation the radial velocity is written as the z velocity multiplied by the derivative of the trajectory with respect to z. Equation (8) can now be differentiated with respect to z and set equal to equation (6). By rearranging terms a differential equation for r is obtained.

$$r'' + \frac{(\beta\gamma)}{(\beta\gamma)}r' - \frac{k_0}{(\beta\gamma)^3}r = 0 \quad (k_0 = \frac{eI}{2\pi\varepsilon_0a^2c}) \quad (9)$$

In order to apply the matrix techniques used by Courant, Livingston and Snyder the coefficient of the first derivative of r must be zero. Since this is not the case here, another function with a known relationship to r must be found which does satisfy this condition, this is done by means of a canonical transformation using the following generating function.

$$F_2 = f(z)P_xr \quad (10)$$

Applying this generating function to the Hamiltonian of equation (1) the following conjugate coordinate and momentum pair and Hamiltonian are obtained.

$$G^* = G + \frac{f'P_xr}{f} = -[(H - e\phi)^2 - P_x^2f^2c^2 - (mc^2)^2]^{1/2} - eA_zc \quad (11)$$

$$P_r = P_xf; \quad x = fr \quad (12)$$

Next use is made of Hamilton's equations to find the equations of motion for the electrons in the new coordinates.

$$P_x' = - \frac{\partial G^*}{\partial x} = \frac{K_0 x}{(\beta\gamma)^2 f} - \frac{f' P_x}{f} \quad (13)$$

-  $K_0$  is found in equation (9) -

$$x' = \frac{\partial G^*}{\partial P_x} = \frac{P_x f^2 c}{[(H - e\phi)^2 - P_x^2 f^2 c^2 - (mc^2)^2]^{1/2}} + \frac{f' x}{f} = \frac{P_x f^2}{P_z} + \frac{f' x}{f} \quad (14)$$

In equation (14)  $eA_z$  is much less than  $P_z$ . Next the derivative of equation (14) will be taken and the values for  $x'$  and  $P_x'$  will be substituted in. After cancelling terms the following equation is found.

$$x'' = \frac{f'' x}{f} + \frac{K_0 f}{(\beta\gamma)^2 P_z} - \frac{2f' f P_x}{P_z} + \frac{P_x P_z' f^2}{P_z^2} \quad (15)$$

Note that if  $f^2$  is proportional to  $P_z$  the last two terms in equation (15) drop out leaving the differential equation for the function  $x$  without any first derivative in  $x$ . One obvious choice for the function  $f(z)$  is  $f(z) = (\beta\gamma)^{1/2}$ . By making this choice and by recalling the relation for  $P_z$  the equation can be rewritten as follows.

$$x'' + K(z)x = 0 \quad (16)$$

$$\text{with } K(z) = -\frac{f''}{f} - \frac{K_0}{(\beta\gamma)^{5/2} M_e c}$$

$$\text{and } \frac{f''}{f} = -\frac{(\gamma^2 + 2)\alpha^2}{4(\beta\gamma)^4}$$

Since the equation for  $x$  is now in a form identical to that used by Courant, Livingston, and Snyder in their analysis, the differential equations for the Twiss parameters of the beam are the same as shown below.

$$\alpha'_L = K\beta_L - \gamma_L, \quad \beta'_L = -2\alpha_L, \quad \gamma_L = (1+\alpha_L^2)/\beta_L. \quad (17)$$

Numerical integration of these equations can now be done to determine the evolution of the function  $x$ , with  $x = (\beta_L \epsilon)^{1/2}$  and  $\epsilon$  is an invariant of the motion given by the following equation.

$$\epsilon = \frac{\pi}{\beta_L} (x^2 + (\alpha_L x + \beta_L x')^2)$$

By now using the relation between  $x$  and  $r$  the beam envelope equation as a function of  $z$  can be obtained.

C) Transport line optics

Once the beam leaves the Pelletron it undergoes a defocusing due to the change in the electric field. The focal length for this phenomena is given by the following formula.

$$f = \frac{4V}{E} \quad (18)$$

The solution of the beam size as a function of position for the transport line is a numerical integration of equations (17) with the difference that the equations now represent the variable  $r$  directly and  $K(z) = K_0$ .

$$r = \sqrt{\beta_L \epsilon} \text{ (with } \epsilon \text{ the beam emittance)} \quad (19)$$

$$\alpha'_L = K_0 \beta_L - \gamma_L, \quad \beta'_L = -2\alpha_L, \quad \gamma_L = (1+\alpha_L^2)/\beta_L. \quad (20)$$

$$r' = (\epsilon/\beta_L)^{1/2} \cdot \beta'_L = -2\frac{\epsilon}{r}\alpha_L \quad (21)$$

The effect of space charge enters the problem as shown above, but the magnetic fields of beamline components such as magnetic dipoles, quadrupoles, and solenoids must also be included in the calculation. For dipole and quadrupole fields the effect on the beam enters through the parameter  $K = B'/B\rho$  where  $B'$  is the derivative of the magnetic

field with respect to the perpendicular direction, and  $B\rho = \beta\gamma M_e c$  is the measure of the beam magnetic rigidity. The effect of solenoidal focusing is accomplished by reversing (or partially reversing) the value of  $\alpha_L$ .

The complete optics calculation for the Pelletron is shown in figure 4 for a current of .315 amperes. The space charge limited current of 3.962 amps is shown in figure 5. Due to the symmetry of the optics the calculation is identical for the accelerating and decelerating columns and thus the figures show the calculations for just a bit past the point of symmetry.

## PELLETRØN RECIRCULATING E-BEAM

CURRENT OF 0.315 AMPS

RADIUS ØF BEAM (CENTIMETERS)

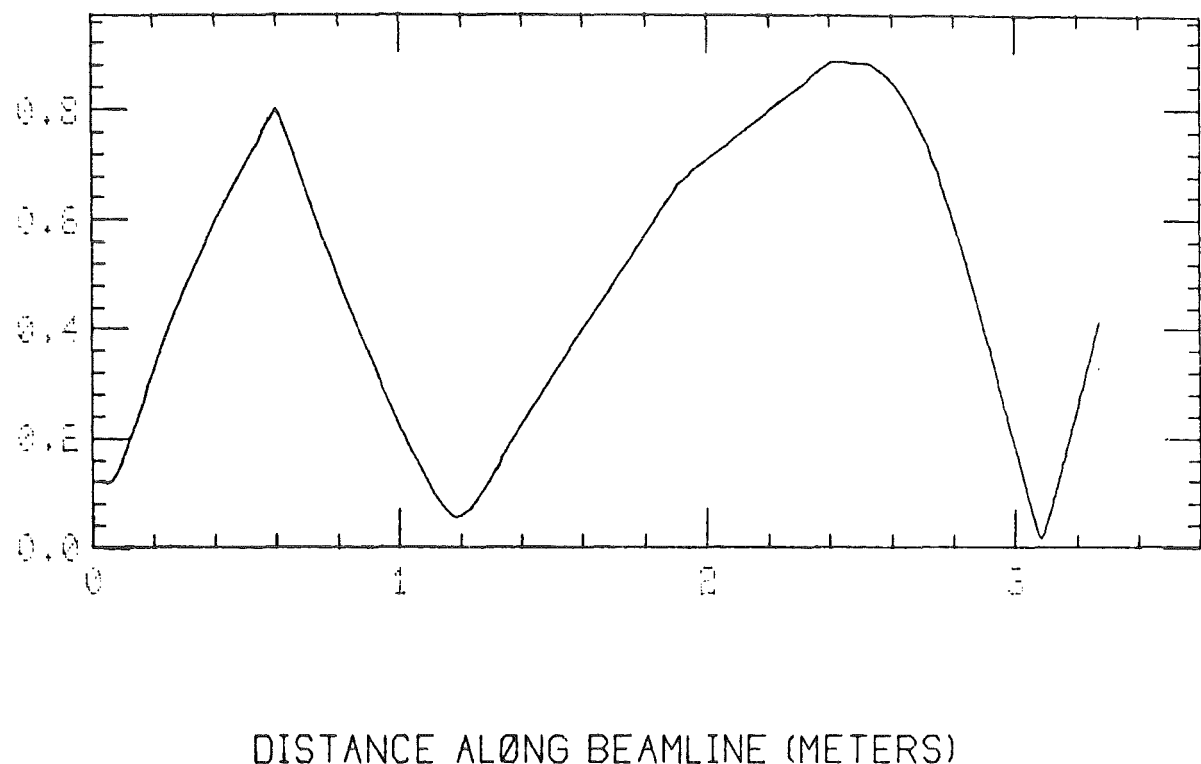
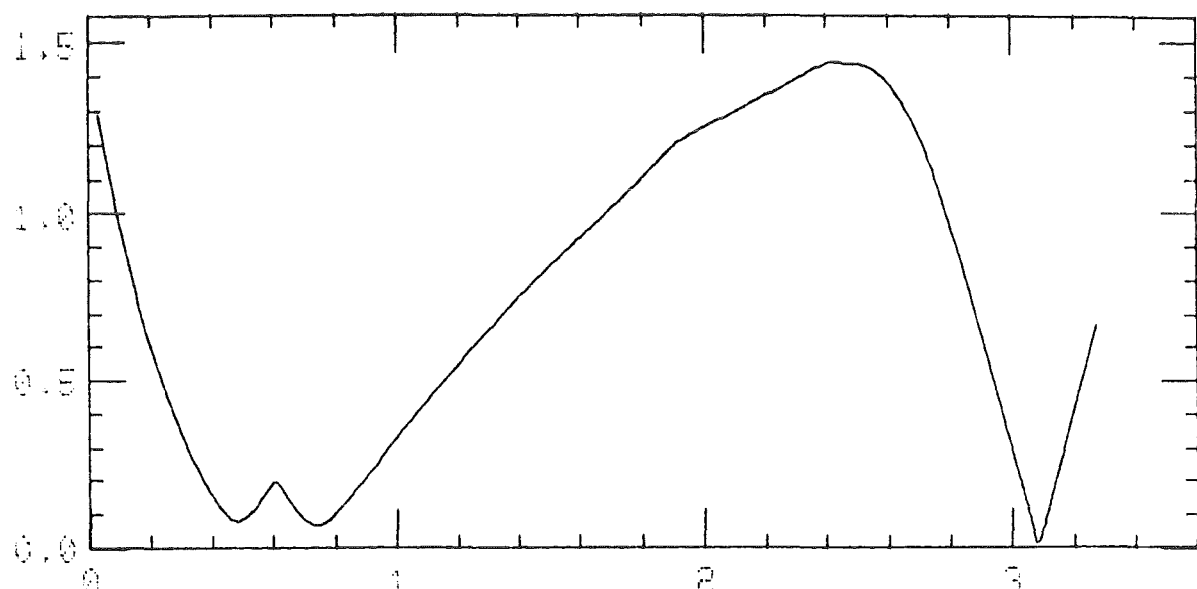


Figure 4- Low Current Pelletron Optics

## PELLETRØN RECIRCULATING E-BEAM

CURRENT OF 3.926 AMPS

RADIUS Ø BEAM (CENTIMETERS)



DISTANCE ALONG BEAMLINE (METERS)

Figure 5 - High Current Pelletron Optics

## II) Collector Design

### A) Introduction

The collector for the intermediate energy electron cooling effort has been designed by following the principles which led to the successful operation of the Fermilab Electron Cooling Experiment<sup>5,6</sup>. In that experiment electron beam recovery was found to be 99.99%. A schematic of the collector planned for this experiment is shown in figure 6. Not shown in the figure is a solenoid just preceding the collector, which focuses the beam. The collector has a Pierce geometry which is used to decelerate the electrons to an energy of about 3 KeV without space charge blowup of the beam. After the final Pierce electrode the beam enters a solenoidal magnetic field region which is space charge neutralized by an ion cloud formed from the ionization of the residual gas as the beam passes through this region. The ions are radially trapped by the solenoidal field, and longitudinally trapped by the electrostatic fields of the collector. The potential wells are shown in figure 7. After the beam leaves the solenoidal field it is accelerated to the collecting surface which is a graphite surface brazed on stainless steel. The remainder of this paper will present calculations done concerning the operation of the collector.

### B) Ion and Electron Gyro-radii in the Solenoidal Field

The formula for the gyro-radius of a particle in a magnetic field is given by the following equation.

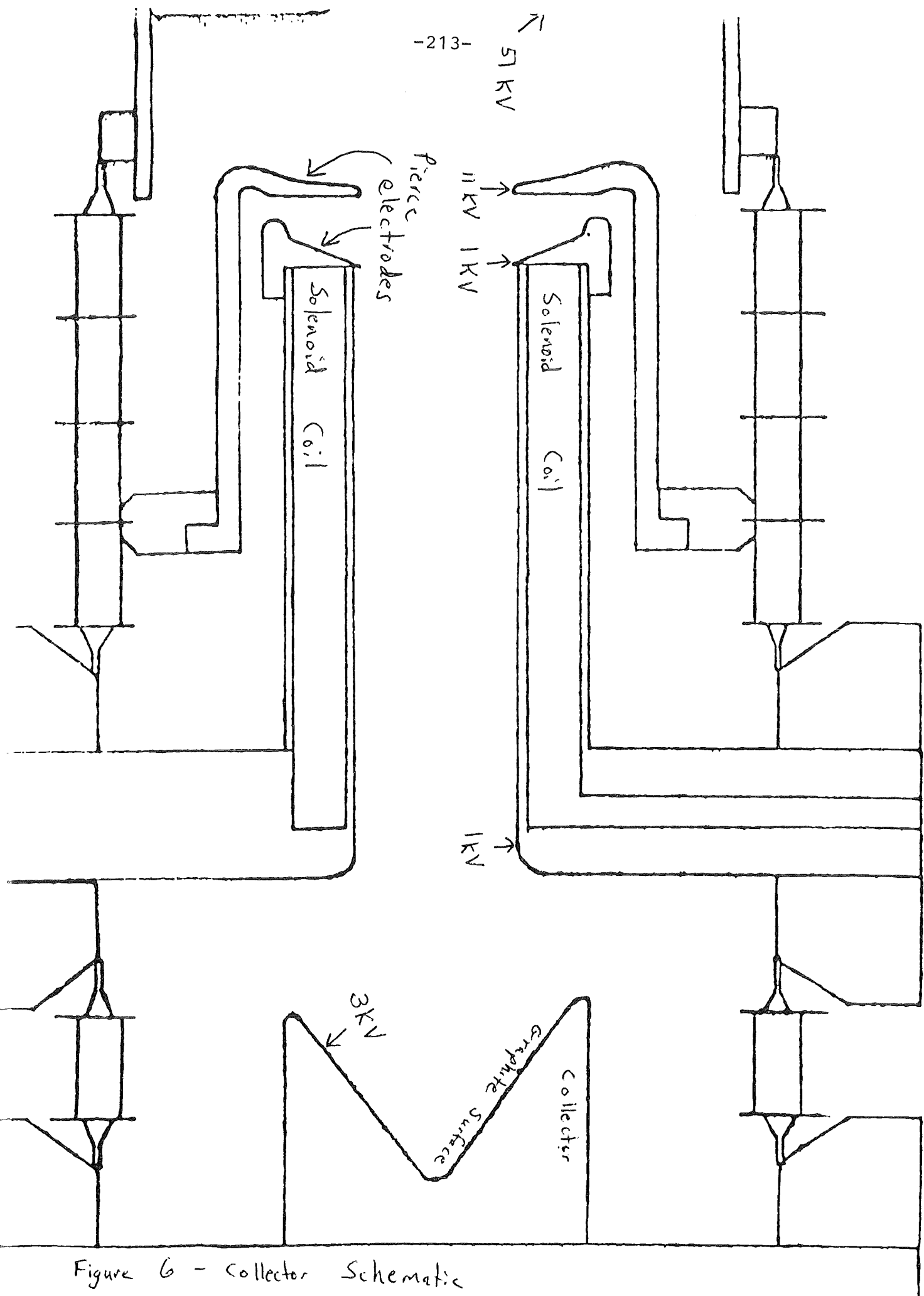


Figure 6 - Collector Schematic

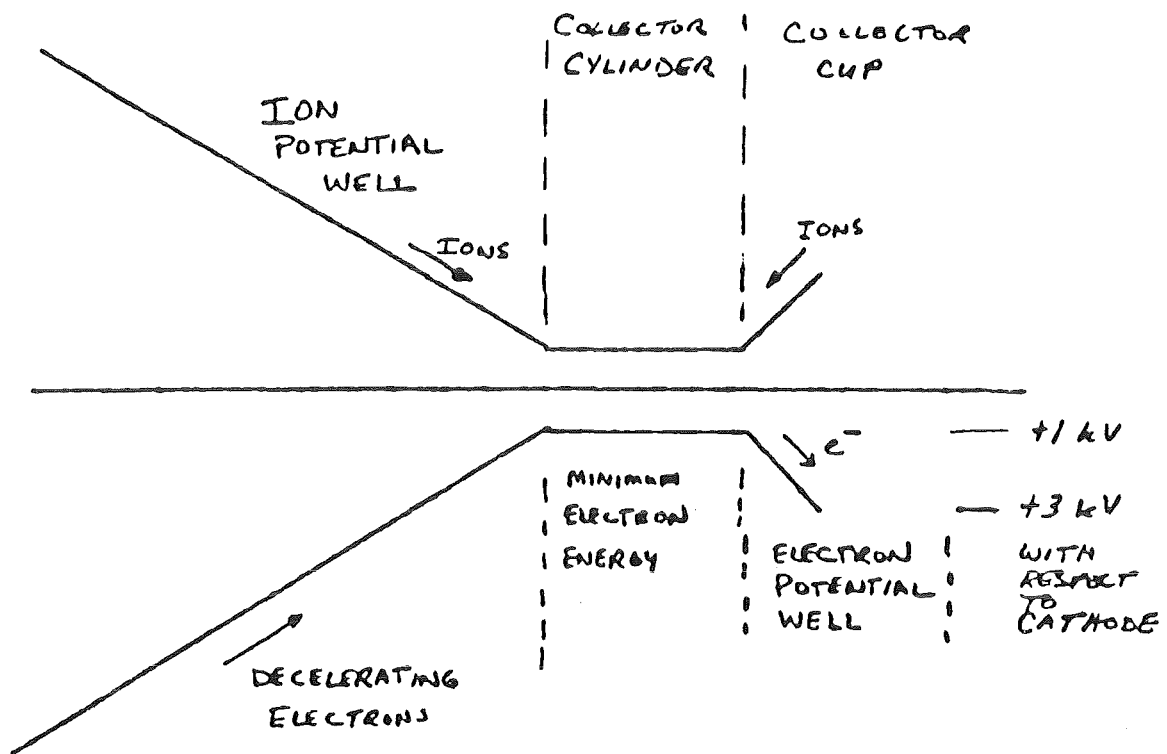


FIG. 7

COLLECTOR ENERGY WELLS

$$r_g = \frac{mv}{eB} \quad (22)$$

Values for the ion and electron gyro-radii are presented in table 1. Since the electron gyro-radius is a strong function of the divergence of the electron beam in the solenoidal region it will vary strongly with that parameter. For the values presented in table 1 a beam divergence of 1% is assumed.

| B(T) | $r_{ion}$ (mm) | $r_{electron}$ (mm) |
|------|----------------|---------------------|
| .025 | .289           | .30                 |
| .015 | .482           | .50                 |
| .005 | 1.45           | 1.5                 |

Table 1) Ion and electron gyro-radii

### C) Production Rate for Ion Cloud Formation

The rate for production of ions is given by the following equation.

$$R = \frac{n \sigma_i I}{\sigma_b} \quad (23)$$

In the above equation n is the number density of neutral hydrogen molecules in the collector due to residual gas,  $\sigma_i$  is the cross section for ionization of the gas, I is the electron beam current, and

$\sigma_b$  is the cross sectional area of the beam in the solenoidal region. Calculations for this design show that  $R = 2.11E-11 \text{ s}^{-1}$ . This results in the time  $\tau$  for complete space charge neutralization of  $\tau = n_e/R = .8 \text{ sec}$ . This result is compatible with the experimentally obtained value in the Fermilab electron cooling experiment.

D) Effect of Solenoidal Field on Azimuthal Beam Momenta

The electron beam will pick up azimuthal momentum as it enters the solenoidal field region of the collector due to Busch's Theorem. The amount of that energy the beam has is given in the following equation.

$$E_{az} = \frac{e^2 r^2 B^2}{2m} \quad (24)$$

| r(m) | .012 | .006 | .003 |
|------|------|------|------|
| B(T) |      |      |      |
| .025 | 7910 | 1979 | 494  |
| .015 | 2850 | 712  | 178  |
| .005 | 316  | 79   | 20   |

Table II) Azimuthal Energy (eV) of outer electrons

The electron beam energy in the solenoidal field can not exceed the energy of the beam as it enters that region, therefore the case of  $r = 1.2 \text{ cm}$ . and  $B = 250 \text{ gauss}$  will cause reflection of part of the beam. In the bench test as well as in the first recirculation tests

the collector parameters will be varied to determine optimum operating conditions.

#### References

1. F. Krienen and J. A. MacLachlan, "Antiproton Collection from a Production Target", IEEE Trans. Nuc. Sci, Vol. NS-28, No. 3, June 1981, 2711-2716.
2. John Peoples, "The Fermilab Antiproton Source", IEEE Trans. Nuc. Sci, Vol. NS-30, No. 4, August 1983, 1970-1975.
3. Luis Elias, "High-Power, cw, Efficient, Tunable (uv through ir) Free-Electron Laser Using Low-Energy Electron Beams", Phys. Rev. Lett., Vol. 42, No.15, 9 April 1979, 977-981.
4. D.B.Cline et.al., "Intermediate Energy Cooling for Antiproton Sources using a Pelletron Accelerator", IEEE Trans. Nuc. Sci, Vol. NS-30, No. 4, August 1983, 2370-2372.
5. T. Ellison et. al., "Electron Cooling and Accumulation of 200-MeV Protons at Fermilab", IEEE Trans. Nuc. Sci, Vol. NS-30, No. 4, August 1983, 2636-2638.
6. W. Kells et.al., "Electron Cooling for the Fermilab  $\bar{p}$  Source", IEEE Trans. Nuc. Sci, Vol. NS-28, No. 3, June 1981, 2583-2584.
7. E.D. Courant and H.S. Snyder, "Theory of the Alternating-Gradient Synchrotron", Annals of Physics, Vol.3, No. 1, 1-48, 1958.



DIAGNOSTICS FOR ELECTRON- AND ION BEAM IN ELECTRON COOLING.

Poul Møller Petersen  
DK-4270 Høng, Denmark

Summary: This paper summarizes some of the diagnostic methods applied on electron- and ion beams in cooling experiments.

1. Diagnostics for the Electron Beam.

1.1 Introduction.

A typical electron cooling installation for production of an intense and monochromatic ( low temperature ) electron beam in the energy range from, say 100 eV to several hundreds of keV consists of mainly three parts:  
a) An electron gun; b) an interaction region; c) a collector.

a) The basic elements of the electron gun are a cathode with thermo-ionic emission and a high voltage acceleration. Frequently the classical Pierce geometry is adopted, which assures that the space-charge limited beam emerges perpendicular to the cathode surface. The cathode is fully immersed in a strong, longitudinal magnetic field, which is much stronger than the one needed just to balance the space-charge force of the beam. The longitudinal, magnetic field extends from the gun into the interaction region and further to the collector, where it is weakened.

b) In the interaction region, the cooling of the circulating beam takes place as a result of repetitive Coulomb-interactions between electrons and the ions.

The simplest formula for the cooling time,  $\tau$  ( i.e. disregarding the effects due to adiabatic collisions with magnetized electrons ) is

$$\tau = \frac{0.6 m M c^4 \beta^4 \gamma^5 e \gamma}{J Z^2 e^4 L_{ei}} \times \begin{cases} \theta_e^3 & \text{for } \theta_e \gg \theta_i \\ \theta_i^3 & \text{for } \theta_e \ll \theta_i \end{cases} \quad (1)$$

where  $m$  and  $M$  are the masses of the electron and ion, respectively, and  $Z$  is the charge state of the ion.  $J$  is the current-density of the electron beam and  $L_{ei}$  is the Coulomb logarithm for collisions between electrons and ions.  $\theta_i$  is the divergence of the ion beam and  $\theta_e (= (2E_{trans}/m)^{1/2}/\beta c)$  is the divergence of the electron beam.  $\gamma$  is the fraction of the storage ring occupied by the cooling system.  $c$  is the speed of light and  $e$  is the elementary charge, whereas  $\beta$  and  $\gamma$  are the usual relativistic factors.

c) In the collector the electron beam is decelerated and the beam-power recuperated. This device is also essential for obtaining a good vacuum pressure.

As may be seen from the formula for the cooling time (1), the following parameters of the electron beam should be known:

- i) Total current.
- ii) Current density.
- iii) Beam position.
- iv) Velocity ( both in magnitude and direction ).
- v) Longitudinal energy spread.
- vi) Transverse energy ( Larmor energy and drift rotational energy ).

It is worthwhile to note, that these parameters vary with radial position, R and quite often also with axial distance, Z along the beam. In the literature, usually only mean values of the parameters are quoted.

When discussing diagnostics for determining the parameters of the electron beam, it is convenient to divide into:

- a) Beam destructive methods.
- b) Non-destructive methods.

## 1.2 Beam Destructive Methods.

A destructive probe inserted to the beam will in most cases immediately melt or evaporate. The current- and power-density load on the probe is for a typical, space-charge-limited electron beam:

$$I(\text{amp}) = 6 \times 10^{-7} V^{3/2}(\text{volt}) \quad \text{and} \quad P(W/cm^2) = 3 \times 10^{-8} V^{5/2}(\text{volt}) \quad (2)$$

This power load may mainly be carried away through conductivity and black-body radiation. However, the best conductivity achieved with water-cooled copper surfaces amounts to  $2\text{kW/cm}^2$ , whereas the radiated power-density for an object at a temperature of 4000 K is  $1.5\text{ kW/cm}^2$ .

Balancing the power load with the radiated or conducted power, the absolute limit in the energy of the electron beam when using beam destructive probes is 20 keV; whereas 10 keV seems to be more realistic. The alternative is to pulse the electron beam, but here the beam-optics may be different, in particular, if a certain amount of space-charge neutralization occurs.

The disadvantages of beam destructive probes may be summarized as:

- i) The probes can only be used for low power-density electron beams ( $< 1\text{ kW/cm}^2$ ); say, for typical electron beams up to 10 keV.

- ii) The probe changes the space-charge fields and self-fields of the electron beam.
- iii) The current intersected by the probe is a load on the high-voltage power supply.

### 1.3 Faraday-cups and scintillator screens.

The beamposition and current-density may be measured as a function of radial position and axial distance by the use of a small, suppressed and water-cooled Faraday-cup. The use of a phosphorus screen surveyed by a TV-camera enables to measure the beam position with axial distance and also to get an impression of the uniformity of the current-density.

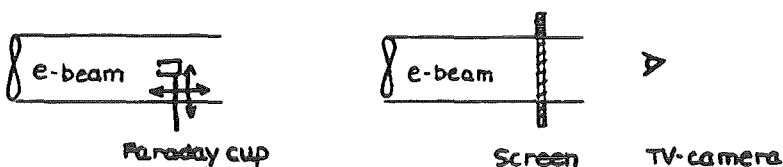


Figure 1.

The disadvantages when applying such methods are, as mentioned, that they are destructive, change the space-charge fields, cause a current load on the HT-supply and can only be used for low power-density beams.

### 1.4 Faraday-cup or scintillator screens with pin-hole collimators.

The principle here is to measure the current to a small Faraday-cup, which is situated behind a movable pin-hole collimator ("pencil beam method"). Instead of a cup, phosphorus screens may be used.

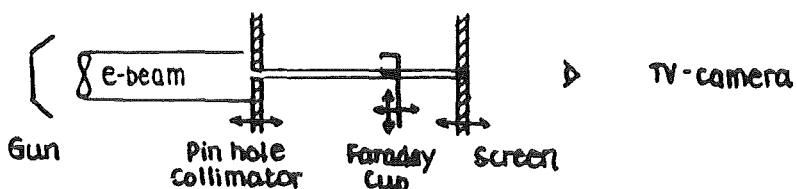


Figure 2.

By this method it is possible to find the current-density and position of the e-beam, but further, also the divergence of the beam as such - which in most cooling devices gives a measure of the straigthness of the guiding magnetic field.

### 1.5 Measurements on beam-ripple.

The cyclotron motion of the electron is superimposed on a slow, drift rotational motion, which is caused by crossed space-charge electric field and longitudinal, magnetic field. These two motions cause the beam radius to oscillate in axial direction with the Larmor wavelength.

When changing the longitudinal magnetic field, the variation in beam radius can be measured as a current to a stationary, iris-shaped colimator or by means of a phosphorus screen.

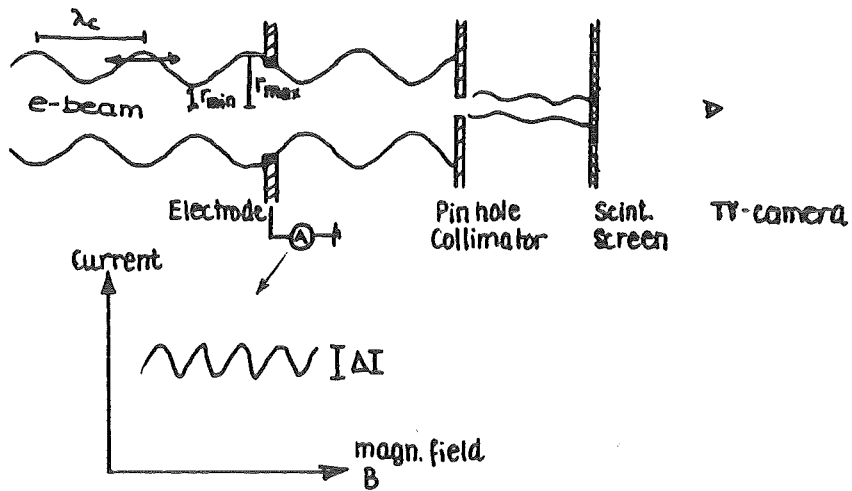


Figure 3.

Since the variation in current is closely related to the Larmor radius,  $r_L$  ( $= \frac{1}{2}(r_{\max} - r_{\min}) = 2\Delta I/I$ ), it is possible to extract the transverse energy of the electron beam,  $E_{\text{trans}} = \frac{1}{2}m(r_L\omega_c)^2$ .

#### 1.6 Cross wires.

The principle here is to insert thin tungsten cross wires ( $\phi = 20\mu\text{m}$ ) into the beam. The parts of the wires intersected by the beam become incandescent and are surveyed by a TV-camera.

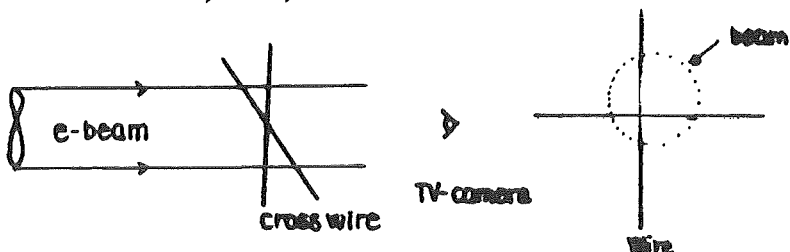


Figure 4.

The beam size and position can be determined in this way, but only for electron beams with low power-density.

#### 1.7 Non-Destructive Methods.

Amongst the non-destructive methods for observation of the electron beam I shall mention the following:

- Current diagnostics and recording of the vacuum pressure.
- Laser beam diagnostics.
- Microwave radiation.
- Pick-up electrodes.

### 1.8 Current diagnostics and recording of the vacuum pressure.

In a high power installation with ultrahigh vacuum such as a cooling device, it is essential that most of the beampower is recuperated by means of a collector. An increasing vacuum pressure is generally interpreted as being due to bad electron beam optics and collection, which then has to be corrected.

To optimize the beam optics and collection it is necessary to measure currents to the various electrodes in the system: i) loss-currents to the vacuum tube, ii) currents to the collector and its various electrodes, iii) the current drawn from the cathode equals the beam current, iv) currents to the anodes of the gun, etc.

Current characteristics for space-charge-limited beam may define the perveance of the gun and reveal the eventuality of space-charge neutralization in the gun. Similar measurements on the collector may also indicate space-charge neutralization, which here could be beneficial. The alignment between gun and magnetic field can be checked by measuring currents to the anodes when exciting dipole fields. In addition, one may find minimum collector potentials, limits for instabilities, etc.

Measurements of currents give an insight in the general behaviour of the beam and is a powerful and necessary method for tuning the installation, even though none of the parameters of the electron beam are directly found.

### 1.9 Laser beam diagnostics.

The principle here is to measure the spectral density of Doppler-shifted, backscattered laser light, which is sent antiparallel to the electron beam.

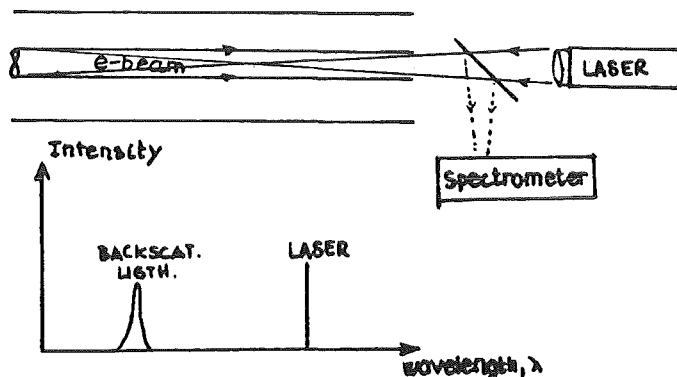


Figure 5.

The scattered laser light is blue-shifted with a reduction in wavelength of typically a factor 2-5, which facilitates detection of the signal far away from the primary laser light. The backscattered light may be ana-

lyzed with a high-resolution Fabry-Perot spectrometer.

Laser beam diagnostics is a rather powerfull method for determining the parameters of the electron beam:

- i) The velocity of the beam can be found from the Doppler-shift in wavelength.
- ii) The longitudinal energy spread can be derived from the width of the backscattered spectrum.
- iii) The current ( number of scatterers ) may be found from the amplitude of the scattered ligh.

For high density electron beams and "good" laser beam optics, where the laser ligh is scanned across the e-beam, it may even be possible to measure the velocity-profiles, velocity spreads and current densities as a function of radial position, and hereby study space-charge neutralization of the electron beam.

#### 1.10 Microwave radiation.

Electrons spiralling around the magnetic field lines emit radiation with a total power, which is proportional to the transverse energy of the electrons. This radiation may be detected with an antenna situated outside the beam. The power spectrum is centered around the cyclotronfrequency,  $\omega_c$ , but is Doppler-broadened with a width from  $\omega_c(1-\beta)$  to  $\omega_c(1+\beta)$ . (see figure 6)

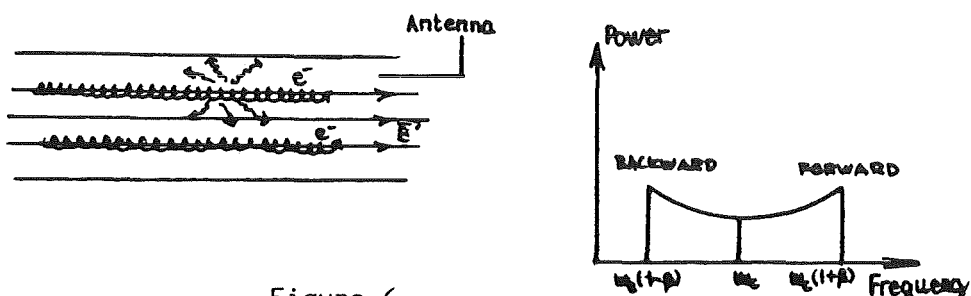


Figure 6.

Even though, the power signal is very small and no absolute measure of the transverse energy seems possible, the main optical parameters like the longitudinal, magnetic field may be optimized by the method.

The detection of microwave radiation may, however, only be possible for high density electron beams.

#### 1.11 Pick-up electrodes.

Cylindrical electrodes or sector-shaped cylinders situated inside the vacuum chambers may serve to obtain information on the electron beam:

- i) DC-beams may be centered in the cylinder.
- ii) For pulsed or modulated beams, the beamposition and beamsize can be

- derived by measuring the voltage-signal to the pick-up electrodes.
- iii) The electrodes may be used for clearing in experiments with space-charge neutralization.

In addition to above mentioned diagnostic methods, the beamsize and position can be found by observing the emission of light when injecting a gas into the beam. Further, electrostatic analyzers may be used for measuring the longitudinal energy-spread of the beam.

The diagnostic methods for the electron beam and their limitations are summarized in Table I.

## 2. Diagnostics on the Ion Beam in Cooling Experiments.

The following parameters of the circulating ion beam may be of interest in cooling experiments:

- i) Beam current ( number of stored particles ).
- ii) Particle momentum ( Energy ).
- iii) Momentum spread of the ion beam.
- iv) Beam position ( position of closed orbit ).
- v) Beam size of the ion beam ( amplitudedistribution of betatron oscillations ).

Furthermore, the diagnostic devices should be able to measure changes in these parameters, which have time constants smaller than the cooling times, i.e., fractions of seconds.

Some of the diagnostic methods, which have been applied in cooling experiments, are summarized in the following sections.

### 2.1 Neutral beam channel.

The principle is to measure the profile and rate of neutral atoms, which are formed by radiative recombinations of electrons and ions in the interaction region ( i.e.  $e^- + p^+ \rightarrow h\nu + H$ , but also other possibilities like  $e^+ + \bar{p} \rightarrow \bar{H} + h\nu$  ). The formed neutral atoms are not affected by the main magnetic field of the storage ring and travel straight towards a detector ( see figure 7 ), which may consist of a Multiwire Proportional Counter (MWPC) or a photographic emulsion to measure profiles and a scintillator with a photomultiplier for determination of the rate.

From the method it is possible to derive the following parameters:

- i) Measurements of the formation rate of neutral atoms in equilibrium between the two beams is a rather powerful method for a determination of the transverse energy of the electron beam.

- ii) The profile and position of the ion beam can be derived from the profile and position of the neutral atom beam.
- iii) Angular deviations between the electron- and ion beam may be corrected on the basis of measurements of the rate and profile of neutral atoms.

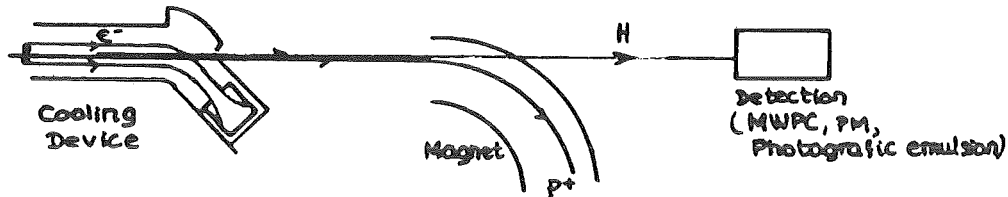


Figure 7.

Since the formation rate is rather small, the device is not fast enough to follow the evolution of the cooling process. However, it has been proposed to enhance the rate by laser stimulated radiative capture. Further, the neutral atoms represent a beam loss, which at conditions with a good vacuum pressure and large acceptances of the storage-ring, may limit the lifetime of the ion beam - in particular, for heavy, highly charged ions.

## 2.2 Scrapers.

The beamposition and the distribution in amplitudes of betatron oscillations can be found by inserting slow moving, destructive probes into the ion beam and recording the decrement in intensity as a function of probe position.

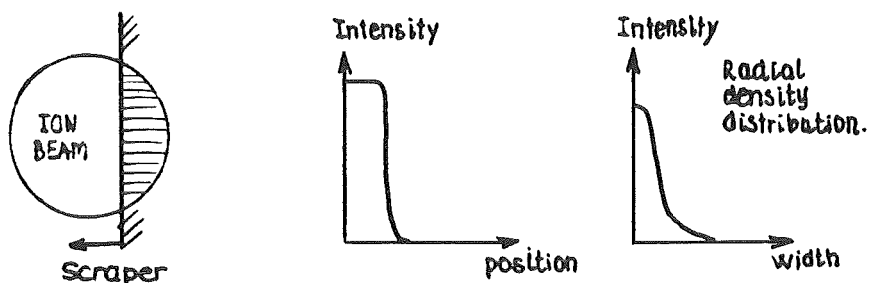


Figure 8.

The advantages of such a system are that it is a simple and reliable method with a good resolution ( $\sim 0.1$  mm), whereas the disadvantages are that it is destructive and relatively slow.

## 2.3 Beam profile monitors.

These devices have shown to be of extreme importance in cooling experiments ( i.e. the Mg-jet at INP, Novosibirsk; the beam profile monitor in the ICE-experiment, CERN and the atomic carbon jet at LEAR, CERN ).

The principle is to measure the profiles of electrons ( also ions may be used ), which are created in ionizing collisions between the circulating ion beam and stationary gas atoms ( vacuum molecules or jets ).

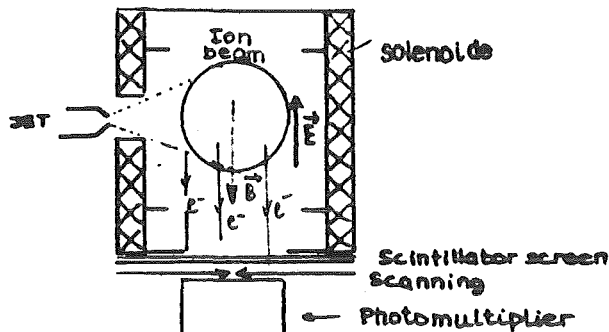


Figure 9.

The ionization induced electrons are accelerated and focussed by means of parallel electric- and magnetic fields. The electrons impinge on a scintillator, which is scanned with a photomultiplier.

By means of these devices the beam profiles can be measured in both transverse planes. Further, the relative intensities of the beam can be found.

Some of the advantages of these devices are that they are non-destructive, fast and have a good resolution. The disadvantages are that the devices require a sufficient "target thickness" of vacuum or jet atoms, and that the magnetic field in the devices causes some distortion of the closed orbit.

In cooling experiments, beam profile monitors are used in measurements of:

- i) Time constants for cooling of betatron oscillations.
- ii) Longitudinal frictional forces ( from rate of horizontal displacement due to the momentum-dispersion of the storage-ring ).
- iii) Beam sizes in equilibrium.
- iv) Beam observation in stacking experiments.

#### 2.4 Schottky scans.

From measurements of the Schottky signal of the beam on a higher order harmonic of the revolution frequency by means of a longitudinal pick-up, it is possible to derive the following parameters of the ion beam:

- i) The absolute momentum of the ion beam,  $p$ .
- ii) The momentum spread of the ion beam,  $\Delta p$ .
- iii) Relative intensities of the beam.

The advantages of this non-destructive method is, that it is fast, has a high sensitivity and a good resolution. However, only momentum

spreads for coasting beams can be measured, and further, is the Schottky signal reduced and distorted in strongly cooled ion beams.

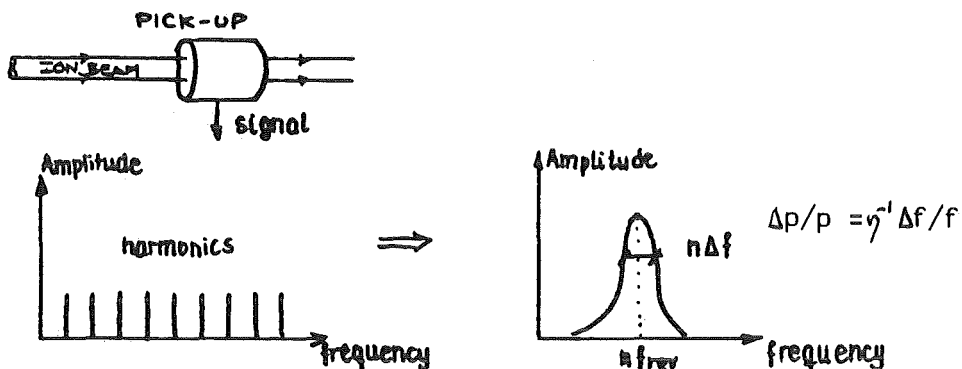


Figure 10.

In cooling experiments, Schottky scans are performed when measuring:

- i) The absolute momentum of the ion beam ( find HT of the e-gun ).
- ii) The momentum spread in equilibrium.
- iii) The time constants for cooling of momentum spreads.
- iv) The longitudinal frictional force ( hereby also the acceleration capability of the cooling process ).

## 2.5 Pick-up stations.

Cylindrical pick-ups with a diagonal cut can be used for measurements of the closed orbit of a bunched beam. In addition, the pick-up stations may be used for a precise determination of the Q-values of the storage-ring, i.e., the frequency of betatron oscillations normalized to the revolution frequency.

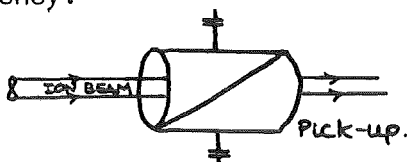


Figure 11.

## 2.6 Scintillator screens.

By means of the scintillator screens, which are inserted to the beam and surveyed by TV-cameras, it is possible to find the position and size of the ion beam.

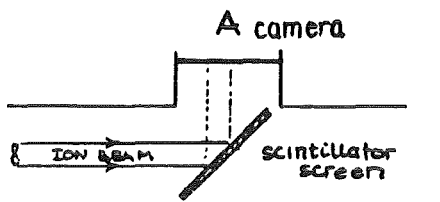


Figure 12.

The advantages of the system is that it is simple and reliable, whereas the sensitivity of this beam-destructive method is rather low.

The mentioned diagnostic devices are summarized in Table II, where also is given the measured parameters of the ion beam as well as some of the advantages and disadvantages of the methods.

3. Conclusion.

As may be seen from the summary given here, there has been a considerable development in diagnostic devices, which have been based on a large variety of physical processes - in fact, the cooling experiments has forced a progress in diagnostics, which may be of great importance for many physicist working with electron- and ion beams.

DIAGNOSTICS ON ELECTRON BEAMS FOR ELECTRON COOLING

| <u>DIAGNOSTIC DEVICE</u>                   | <u>MEASURED PARAMETER OF THE ELECTRON BEAM</u>   | <u>COMMENTS</u>                                  |
|--|--|--|
| Faraday cups                               | Beamsize, beamposition , Current density in (R,Z)  | Destructive, Low energy e-beams, good resolution |
| Screens+Camera                             | Beam size, beamposition in (R,Z)   | Destructive, Low energy beams                    |
| Pin-hole collimator<br>Faraday cup/Screens | Beam position, Current density, Straightness of magnetic field lines.(Pencil beams)  | Destructive, Low energy beams                    |
| Beam ripple measurements                   | Larmour radius (Transverse energy) of mainly peripheral electrons  | Destructive or semidestructiv                    |
| Cross wires                                | Beamsize and Beamposition  | Semidestructive, Low energy beams                |
| Micro-wave radiation                       | Average transverse energy of electron beam,<br>Tuning of main optics   | Nondestructive, High density beams               |
| Laser beam diagnostics                     | Longitudinal velocity spread, total current (evt.<br>velocity profiles, current density with radial position.(investigate space charge neutralization) | Nondestructive, High density beams               |
| Cylindrical Pick-up electrodes             | Beamposition and size (evt. also higher order moments)<br>for pulsed or modulated beams . Also diagnostics for space charge depression.                | Nondestructive, pulsed or modulated beams        |

Destructive: Changes space charge and self fields, current load on HT, only low power density beams ( $P \ll 1 \text{ kW/cm}^2$ )

Semidestructiv: Destorts space charge and self fields, only low power density beams ( $P \ll 1 \text{ kW/cm}^2$ )

TABLE I.

DIAGNOSTICS ON ION BEAMS IN ELECTRON COOLING

| DIAGNOSTIC DEVICE                             | MEASURED PARAMETERS OF THE ION BEAM   | <u>COMMENTS</u>   |
|---|---|---|
| Schottky scans                                | Momentum, Momentum spread, Beam current (calibration)<br>(Nondestructive)                     | fast,good resolution,high sensitivity<br>only coasting beams, signal suppressed<br>in presence of strong cooling          |
| Beam Profile Monitors<br>( BPM, Mg-jet,C-jet) | Beamsize, Beam-position, Intensity (calibration)<br>(Nondestructive)                          | fast, good resolution,sensitivity in-<br>creased by use of jets,bunched and<br>coasting beams, orbitdistortion            |
| Neutral Atom<br>Channel                       | Beamsize, Beamposition, Temperature of electron beam<br>from formation rate. (Nondestructive) | Slow due to low formation rate (may be<br>enhanced by laser), coasting and bun-<br>ched beams; capture may limit lifetime |
| Scrapers                                      | Beamsize, Beamposition ( Destructive )  | Simple and reliable,relatively slow   |
| Pick-up Stations                              | Beamposition for bunched beams, Q-measurements<br>(Nondestructive)                            | Fast  |
| Scintillator<br>Screens                       | Beamposition, Beamsize (Destructive)  | Fast, low resolution and sensitivity<br>Simple and reliable   |
| Beam Transformers                             | Beamintensity (Nondestructive)  | Fast, coasting and bunched beams<br>relatively low sensitivity  |

TABLE II



COMPUTATIONAL CALCULATION OF  
ELECTRON TRAJECTORIES

Miroslav Sedlaček  
Accelerator Technology  
The Royal Institute of Technology, Stockholm

### 1. Introduction

The computation of electron trajectories has relied, since the middle of the sixtieth, very much on the simulation with digital computers. The most known program is the SLAC Electron Trajectory program written by W.B. Herrmannsfeldt (1), but a few other are used too: the Sheffield code (2), the Kirstein-Hornsby code (3), SPCGUN (4), together with different modifications and the programs for simulation of ion sources including trajectory computations, e.g. the BEAM program (5).

All these programs solve the Laplace or Poisson equation by discretization. When the solution of the equation is obtained using the finite difference method (FDM) the particle trajectories are computed and the corresponding space-charge is determined. The process is repeated until the convergence criteria are satisfied.

The electron beam in an electron cooling device must have a very low transverse energy, in the order of 0.1 eV, at the total energy of several hundred keV. When we started the design of the gun for the electron cooling in the CELSIUS ring at the Uppsala University, we therefore decided to check the design by simulation with two programs: the SPCGUN program, written at our institute and with the SLAC electron trajectory program. In the first tests only minor differences were observed, for example the transverse energy, in the order of 1 eV, differed by less than 1 per cent.

In order to achieve operation with voltages between 20 keV and 300 keV a new design of the CELSIUS gun was later started. This gun is based on the work at Fermilab (3). The layout of the rotationally symmetrical gun is shown in Fig. 1.

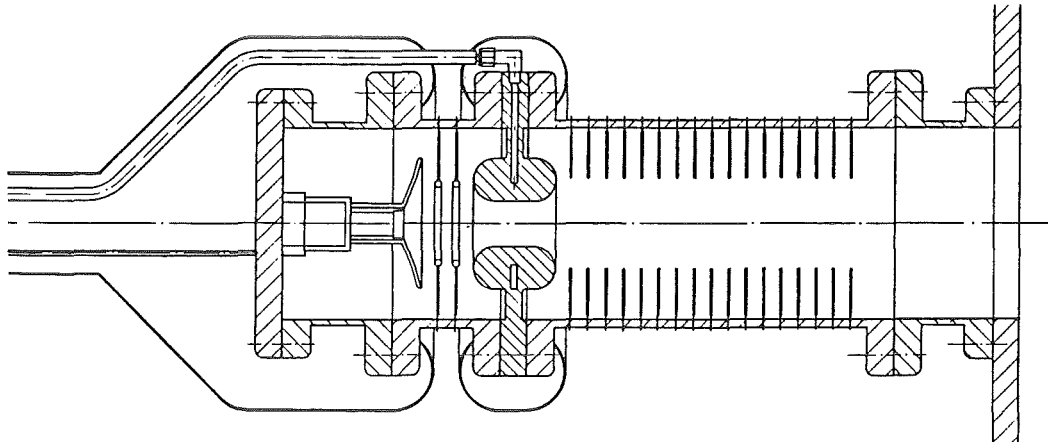


Fig. 1.

It uses an acceleration column to be supplied by National Electrostatic. A homogenous axial magnetic field is assumed. In the simulations a peculiar behaviour of the electron beam near the cathode was observed. With a planar cathode surrounded by a Pierce electrode of conventional design with an opening half-angle of 67.5 degrees, it was expected that the beam would start without any appreciable scallop. However, the orbits computed with either program have near the cathode shown perturbations of the outer trajectories, Fig. 2. This could be explained by two different reasons:

1. Either the shape of the Pierce electrode not being appropriate for a geometry with cylindrical symmetry or
2. There is some error existing in both the programs.

A detailed analysis showed that the largest part of the scallop comes from the chosen shape of the Pierce electrode (7), but also that both programs had errors.

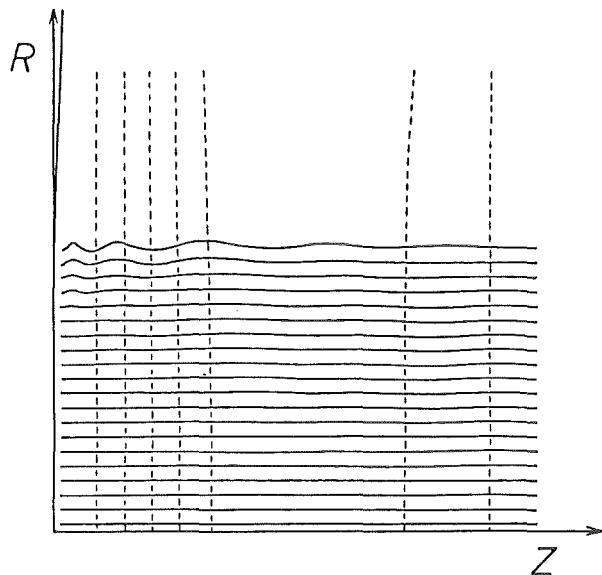


Fig. 2.

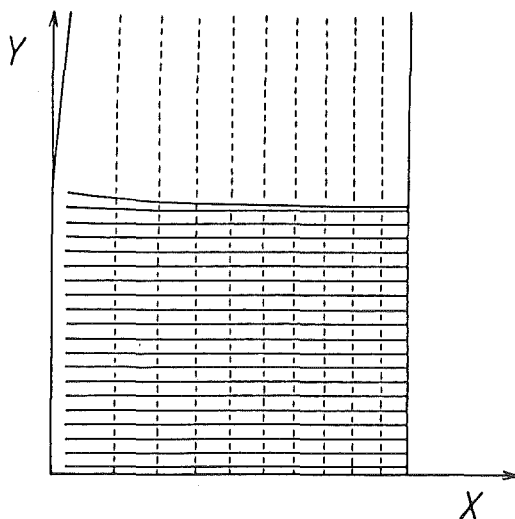


Fig. 3.

## 2. Problems in computer programs

The obvious way to check the programs was starting with the planar Pierce case, where the theoretical result is well known (8). The somewhat unexpected result is shown in Fig. 3.

The electron beam did not behave as expected, i.e. having all trajectories parallel with the axis: the outer trajectory was strongly convergent. One point became clear rather soon. Theoretically, for a constant axial coordinate the potential should not vary in the radial direction across the beam and should be continuous at the edge of the beam. On the edge of the beam the first radial derivative of the potential must be zero and the second derivative discontinuous.

A computed potential distribution in the radial direction near the cathode is shown in Fig. 4. In order to calculate the electron trajectories, a computer program must find the components of the electric field in a point on the trajectory. This means that the program must calculate the derivatives of the potential.

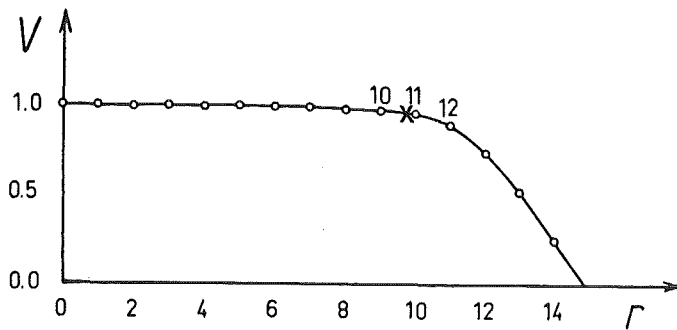


Fig. 4.

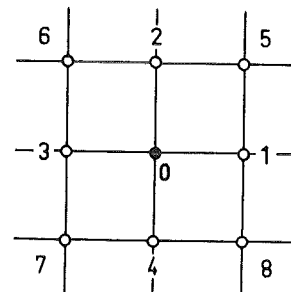


Fig. 5.

In both programs this is done in a conventional way: the nearest node of the superimposed mesh is found (0 in Fig. 5.) From the value of the potential in the surrounding 8 nodes (1-8) the first derivatives are found using the potential at the nodes 1,3 and 2,4. The second derivatives are computed from the potential values at the nodes 1,0,3 and 2,0,4, the mixed second derivatives using the nodes 5,6,7,8. Returning to Fig. 4. one can observe that near the edge of the beam (the outermost orbit crosses the mesh line at X), the derivative in the radial direction must be wrong, if the nodes 10,11,12 are used to obtain its value.

A possible way to avoid this is to use only the nodes inside the discontinuity, i.e. inside the electron beam. In the case of Fig. 4., the first radial derivative of the potential can be computed using only the points 10,11, i.e. the nodes 0 and 4, the second derivative set to zero and the mixed second derivative computed using the nodes 0,3,7,4 or 1,0,4,8 according to the position of the electron. This means, that near the edge of the beam the same approximations are used as in the case of boundary points.

This type of calculation of the electric field was finally adopted in the two programs. The result of a run with the SPCGUN program is shown in Fig. 6. Almost the same result was obtained also with the program SLAC. The radial coordinate of the outermost trajectory at the anode in the SPCGUN program was in error by 0.7, in the SLAC program by 0.6 per cent when compared with the Pierce solution.

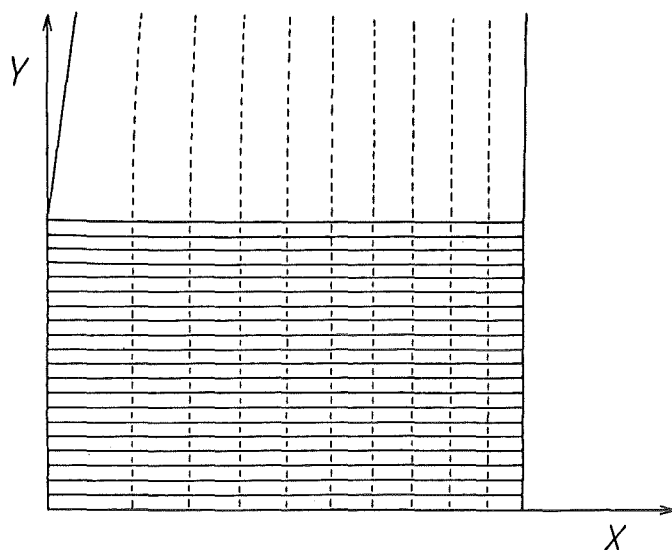


Fig. 6.

The next test was done with a rotationally symmetric geometry. Here, an approximate solution to the Pierce problem (7) in cylindrical geometry was used. The error at the end of the outermost trajectory was 0.6 per cent when computed by the SPCGUN program. The SLAC program, on the contrary, was still wrong by about 3.7 per cent.

The SPCGUN program has an option to printout the space-charge distribution. A similar printout was eventually included also in the SLAC program. While the SPCGUN program printed out a practically constant space-charge distribution across the beam, both in the planar and in the rotationally symmetric geometry, the SLAC program did it only in the planar case. In the rotationally symmetric geometry the space charge was wrong on the axis and in a few rows near the axis. It was therefore clear, that there must be some error in the SLAC program, which must depend on the computation of the space-charge. In the original paper (1) describing the SLAC program a problem was mentioned with cylindrical coordinates: the axial space-charge must be multiplied by an empirical factor of 5.5 in order to obtain a laminar beam.

By checking the space-charge computation in the SLAC program the origin of the error became clear. The program divides the the region of the beam into a certain number of electron trajectories,

the number of which can be decided by the user. For each orbit a current connected to this orbit is computed using the Langmuir-Blodgett factor for a cylindrical cathode (subroutine CHILDA) or for a spherical one (subroutine CHILDB). This means, that initially the computation of the current associated with a trajectory always is made for the rotationally symmetric case, but in case of planar geometry the current of a trajectory is obtained by dividing the initial result by the transverse coordinate at the starting point. If one wants to obtain the current density in the planar case, one has just to check the distance between two successive trajectories, but if only a normalized value is needed, the computed current can directly be used for the computation of the space-charge. The normalization is done in such a way, that the position of the trajectory versus the nearest node is computed. When the axial coordinate of a trajectory reaches a node line, the program notes the intersection of the trajectory with this node line and adds the current connected to the trajectory in relation to the distances to the two nearest nodes (usually in the radial direction; only if the radial velocity is greater than the axial one, the axial nodes will be used), Fig. 7.

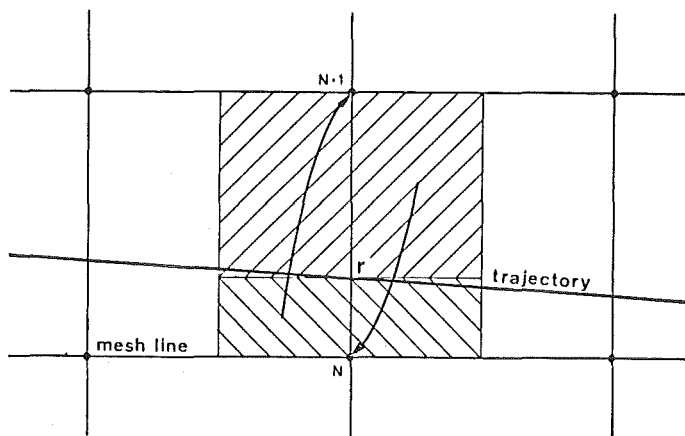


Fig. 7.

In cylindrical coordinates this type of addition of the space-charge to the two nearest nodes works satisfactorily for large distances from the axis. However, for the nodes near the axis, it gives an erroneous result. There it is important to take care of the ratio between the areas enclosed by the circles de-

fined by the intersection of a trajectory with the node line and the nearest two nodes. In the case of the nodes on the axis this gives a factor of 8 by which the computed space-charge must be multiplied.

The necessary changes were introduced into the SLAC program and when the solution of the rotationally symmetric Pierce problem is done the result differs by 0.1 per cent as compared to the SPCGUN program. The computer plotted trajectories are shown in Fig. 8. Fig. 9. shows the complete cathode-anode region.

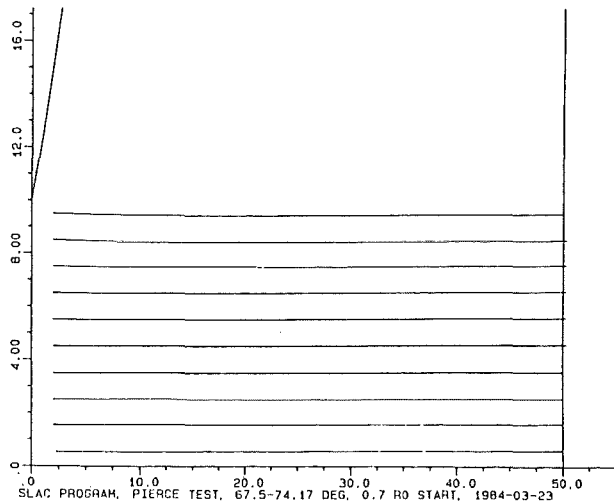


Fig. 8.

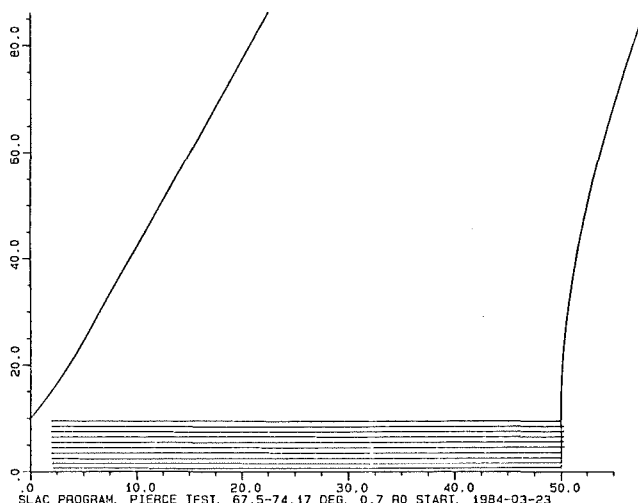


Fig. 9.

There is one more problem which should be mentioned. All potential computations near the boundaries have a small error because of the lower accuracy of the solution when unequal mesh widths are used. For example, the potential in the first node at the beam edge in the planar Pierce problem (independently of the mesh size) is in error by 3.6 per cent. It is important to have this in mind when the calculated potential distribution is used to compute the electric field distribution along the electrodes, especially near sharp corners.

### 3. Conclusions

The correction of the space-charge computation near the axis in cylindrical coordinates in the SLAC program introduces only minor changes in the computed results. The use of a factor of 8 instead of 5.5 on the axis, and a correct treatment of the rows near the axis give a marginal improvement in the computed position and velocity of the particles.

The computation of the electric field components near the beam edge is a more difficult problem. In the original versions of the SLAC and SPCGUN programs the computed results depend on the distance between the outermost orbit and the nearest horizontal mesh line, especially in the region near the emitting surface, and are therefore difficult to predict. The earlier mentioned fix is a good approximation for the Pierce case, where the electron beam has a constant radius in the whole region between the cathode and the anode and where there is no radial component of the electric field inside the beam.

In practice, however, in a real electron gun similar conditions will exist only near the cathode. But near the cathode the space-charge contributes strongly to the solution of the Poisson equation and the potential falls rapidly outside the beam. The proposed fix should therefore be applied only in this region, say up to 5-10 mesh units from the cathode, i.e. in the region where the electric field is practically perpendicular to the cathode.

Taking as an example the CELSIUS gun: The upper curve in Fig. 10. shows the space-charge 2 mesh units and the lower curve 20 mesh units from the cathode. The z-axis length of the problem is 550 mesh units and the cathode-anode distance 90. The potential distributions at the same two distances from the cathode are shown in Fig. 11. By comparing the magnitude of the space-charge and by observing the shape of the potential distribution outside the beam (beam edge at 10 mesh units) it can be seen that the problem of the computation of the electric field components is limited to the

region near the cathode. In this region even the outermost trajectory is well defined.

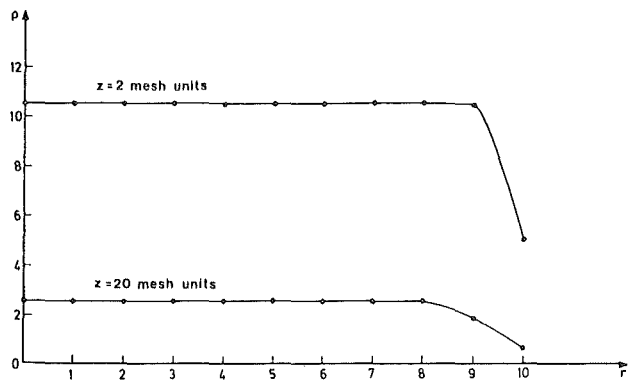


Fig. 10.

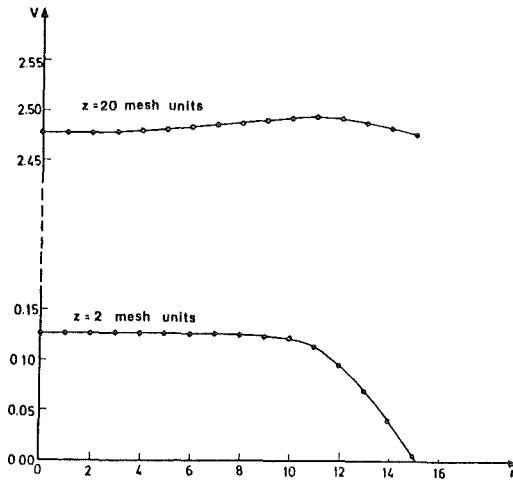


Fig. 11.

It should be pointed out, that in the case of a gun for electron cooling, where the cathode is immersed in a homogeneous magnetic field, the influence of the used fix is very small. In the CELSIUS gun, Fig. 12., for the shown configuration of electron trajectories, the transverse energy of the outermost trajectory differs only by 0.08 eV at 300 keV and by 0.12 eV at 100 keV total energy, when computed by the original and the modified version of the SLAC program. The strong axial magnetic field keeps the electron trajectories almost parallel to the axis of the gun and, if the shape of the Pierce electrode is correct, only small scallops will be observed. In the case of other electron guns, for example guns for klystrons or TWT tubes, the effect can be more pronounced.

The modified SLAC and SPCGUN programs have shown an increase in the computed perveance. In the case of a klystron gun the increase was about 5 per cent. This result is in better agreement with perveance measurements of a few klystron guns made at our institute. The perveance computed with the old version of the SPCGUN program was always too low by 5-10 per cent.

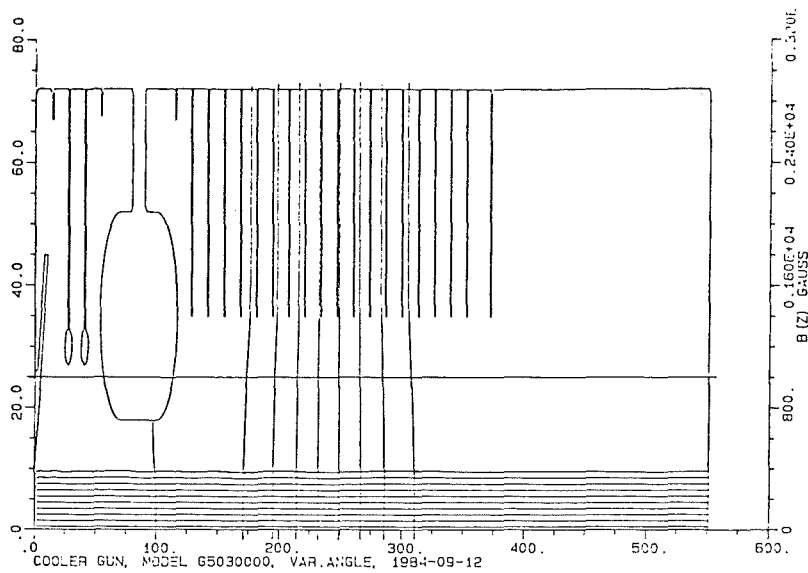


Fig. 12.

The third problem, i.e. the error of the computed potential in a node facing the boundary could introduce additional errors in the position and velocity of a particle on the outermost trajectory. The SLAC program, where the initial position and velocity of the particle is computed at a distance of at least two mesh units from the cathode (or the emitting surface) uses therefore potential values with almost negligible error.

The SLAC program is certainly the most used program for simulation of electron guns. The program has undergone many changes and different features have been added to the program so that it is becoming difficult to understand it and to get out information which is not explicitly printed out. It might, therefore, be a good idea to rewrite the whole program as was done recently, for instance, with the POISSON program for magnetic field computation.

In the following we give a few points that should be discussed and/or included before an attempt to rewrite the program is made:

1. The input should be written in such a way that the user can introduce the boundary in the form of straight lines or simple arcs in units of mm.
2. A decision should be made which method for solving the Poisson (or Laplace) equation to use. In electron optical problems the

FDM (Finite Difference Method) is favoured in comparison with the FEM (Finite Element Method). The reason is that an evenly spaced mesh gives a better approximation when the electric field is computed as the derivative of the potential. However, a variable mesh density should be discussed thoroughly. This is especially true in the regions with high potential gradient or with narrow electron beam.

3. The computation of the trajectories is done with the Runge-Kutta routine. There are several other methods for solving a system of linear differential equations. One should investigate if these methods give a faster code and/or a more correct result.
4. There are two possibilities of computing the space-charge: The current can be associated with a trajectory, as in the SLAC program, or the region between two trajectories can be seen as a current tube. Both methods have advantages and drawbacks.
5. A correct solution of the beam edge problem.
6. In trajectory computations a correction of the particle velocities according to the energy as computed from the potential in the corresponding point can be included.
7. Of the different methods for introducing the magnetic field it should be discussed whether the method using sixth derivatives should remain in the program at all. Even if the magnetic field along the axis or symmetry plane is smoothed by minimizing the sixth differences, the computed field far from the axis can have large errors.
8. A restart option would be useful. Today one can run the SLAC program with, say, 50000 nodes on comparatively small computers provided with virtual memory (VAX). Running times in the order of one hour or more are not uncommon when in the same run solutions with different potentials and magnetic fields are computed.
9. The output should be easy to read. Options to decide which part of the output is desired should be included.
10. All the possibilities which SLAC electron trajectory program already opens should be included.

REFERENCES

1. Herrmannsfeldt, W.B., Electron Trajectory Program  
SLAC-Report-226, Stanford Linear Accelerator Center, 1979
2. Dirkinis, D., PhD Thesis, Sheffield University, 1975
3. Kirnstein, P.T., Hornsby, J.S., IEEE Trans. Electron Dev.,  
196, 1964
4. Nilsson, B.H., Sedláček, M., SPCGUN, a Computer Program for  
Computation of Electron Guns with Space-charge  
Internal report, Dept. of Electron Physics, Royal Institute of  
Technology, Stockholm, 1973
5. Shubaly, M.R., Judd, R.A., Hamm, R.W, BEAM (Beam Extrarction And  
Modeling code), Atomic Energy of Canada, Ltd, Chalk River
6. Oleksiuk, L., Design Study of a 750 kV Electron Gun for Elec-  
tron Cooler, Fermilab P-Note 124, 1981
7. Sedlacek, M., On the shape of the Pierce electrode in rotation-  
al symmetric electron guns and comments on two electron optics  
programs, CELSIUS-Note 84-38, april 1984
8. Pierce, J.R., Theory and Design of Electron Beams  
D.van Nostrand, Princeton, 1954

## PROPOSAL FOR HOLLOW CATHODE ELECTRON GUN FOR ELECTRON COOLING\*

FRANK KRIENEN AND W. B. HERRMANNSFELDT

*Stanford Linear Accelerator Center  
Stanford University, Stanford, California, 94305*

### I. PRINCIPLE

If we consider a magnetic shunt, an iron plate with a hole in it, sandwiched between two solenoids which are polarized in opposite direction, the resulting magnetic field would be as shown in Figure 1.

If we put a voltage between the magnetic shunt and two conducting plates perpendicular to the  $z$ -axis in a symmetric fashion, we would obtain the same shape of the electric field, because both  $E$  and  $B$  may be derived as gradient of a potential. We propose to explore this simple physical system, in which  $E$  and  $B$  are everywhere parallel, to obtain low temperature, magnetically confined electron beams.

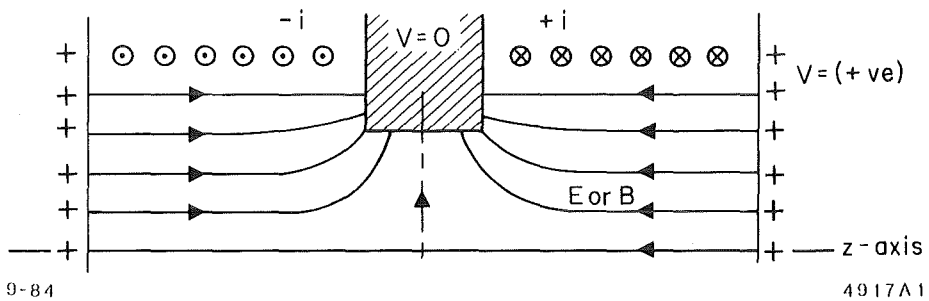


Figure 1. The Principle

\* Work supported by the Department of Energy, contract DE-AC03-76SF00515

We arrange the cathode to lie on an equipotential surface, which could be for the sake of argument, the cylindrical boundary of the magnetic shunt. For a onesided gun, Figure 2, the cathode occupies only half of the magnetic shunt. Electrons are now accelerated by the electric field but stay more or less "frozen" on the magnetic field lines, so that they gain very little transverse energy, i.e. the beam will be cool.

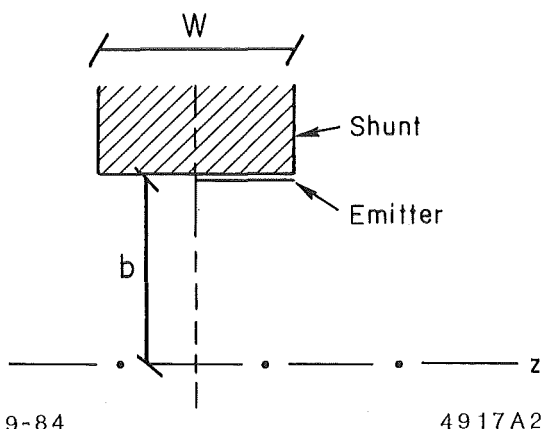


Figure 2. One-sided Gun

## II. FEATURE

The hollow cathode has the feature that the ion beam may pass through it. Indeed the electron cooler could be arranged so that the gun, drift and collector sections are all in line and positioned in the straight section of the ion storage ring. The hollow collector was in principle realized, but not used, in the CERN electron cooler.<sup>1</sup>

One may appreciate the dramatic savings in space and cost if we compare the all-coaxial, in-line system with current electron coolers, Figure 3. Indeed, the two toroids needed there to bend the electron beam in or out, so that it is aligned with the coasting ion beam in the straight section, are costly and require a lot of trim. The in-line system may have the cathode at ground potential, so that the depressed collector potential is only a few kilovolt above ground. Hence we may dispense with the costly high voltage Faraday cage. Also the utilization of the

straight section will be more efficient with the in-line system. For instance, in the CERN 7 m straight section only 3 m was effective for cooling, but the in-line version would need only an estimated 5 m of straight section.

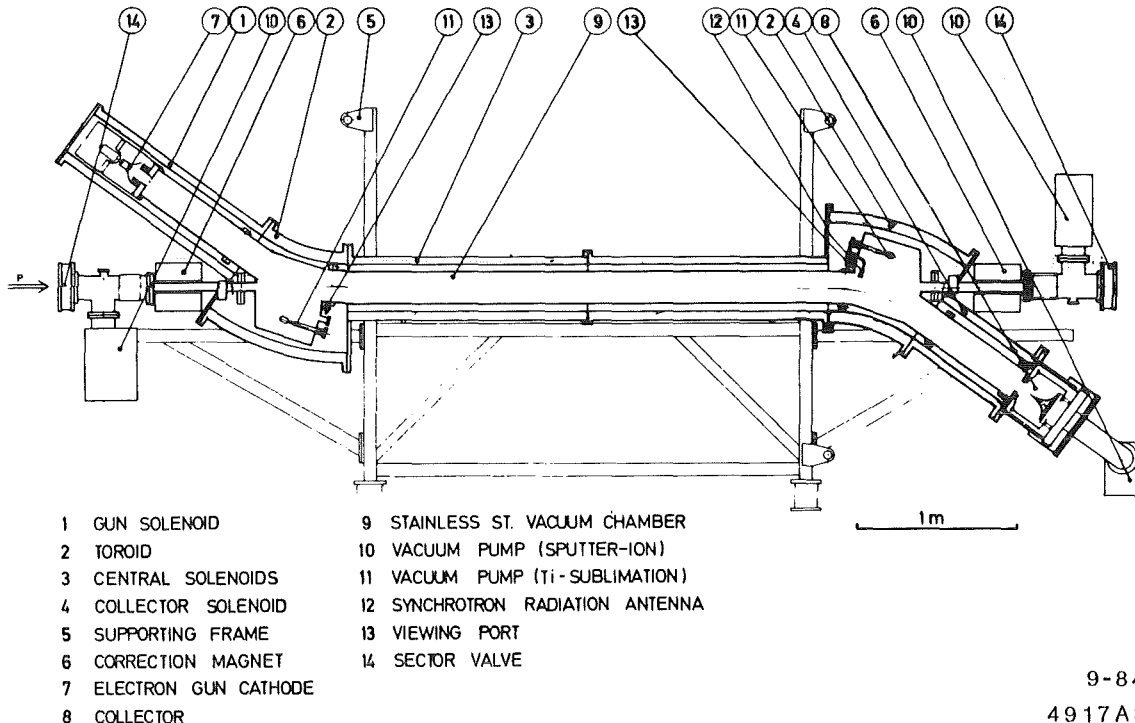


Figure 3. The ICE Electron Cooler

### III. CORRECTIONS

Clearly several corrections have to be made:

Heat shields are needed between shunt and cathode, but the principle remains the same if the emitting surface coincides with a magnetic equipotential, Figure 4(a).

The space charge distortion of the Laplacian electrostatic field will require a focus electrode à la Pierce, to be worked out by trial and error, Figure 4(b).

Presumably the rays near the z-axis will give problems, for the principle of freezing on a magnetic flux line is valid only if the radius of curvature  $R = p/(eBc)$ , ( $p$  in  $eV/c$ ), is small compared to the radius of curvature of the flux

line. Hence it may be better to suppress those rays altogether by reducing the emitting surface of the cathode accordingly, Figure 4(c). The ensuing hole in the electron beam is also an advantage for efficient collection on the depressed collector.

The current density across the beam may be adjusted by shaping the magnetic shunt profile. For instance, a rounded-off shunt, Figure 4(d), will boost the current density of the inner rays. A large aspect ratio of the width and the inner radius of the magnetic shunt will lower the perveance of the gun and reduce the current density of the inner rays, whereas the reverse would diminish the cathode area needed to obtain a given beam radius.

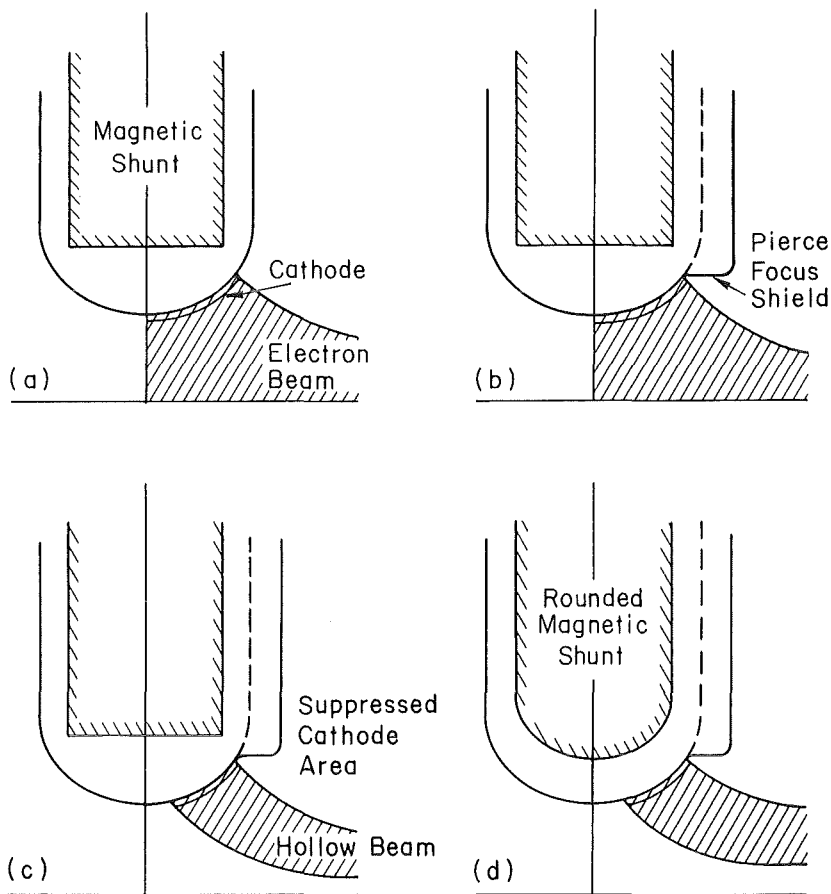


Figure 4. Gun Development

#### IV. OTHER ASPECTS

Unless one wants to make a double sided gun, the plane of mirror symmetry of the magnetic field pre-suppose a set of dummy anodes on the left to obtain parallelism of the  $E$  and  $B$  lines. However, this requirement may be less exacting in view of a) the space charge correction, b) the hollow anode and c) the poor ratio of the curvatures near the axis. Hence it may be possible to simplify somewhat the dummy side of the system, i.e. lower voltages with respect to the cathode. For instance, a hollow beam may be terminated with a low voltage dummy as shown in Figure 5.

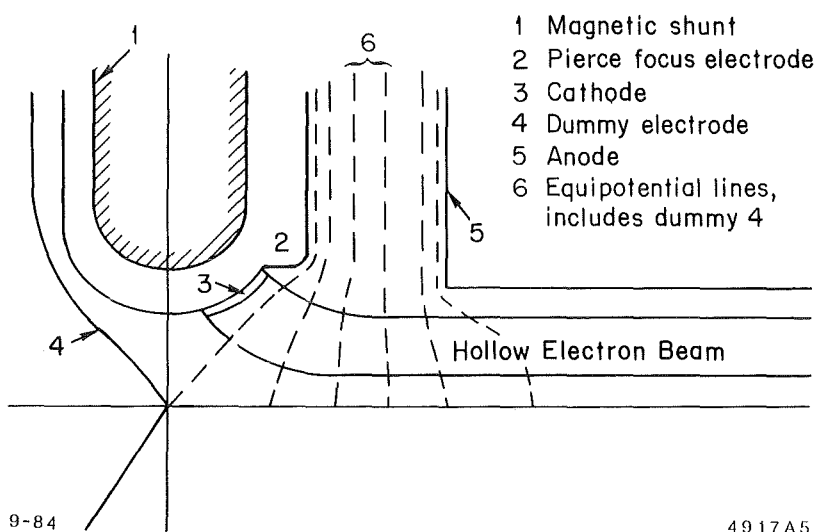


Figure 5. Lowest Voltage Dummy

The temperature may not be equally low everywhere across the beam, however, we may relax considerably on this requirement. In the initial stage of cooling, the average transverse cooling should be comparable to the angular divergence of the coasting ion beam, but if the beam cools and thus shrinks, it should see a progressively better quality electron beam. Thus we arrange the relative position of the two beams so that the ion beam shrinks on the spot where the electron beam is coolest.

The hole in the electron beam may, under some circumstances, prevent cooling part of the coasting ion beam. We would remedy this by having zero dispersion in the straight section, and off-set the electron beam so that the equilibrium orbit coincides with the coolest radius of the electron beam.

Field shaping anodes would be needed to remove the remaining scallops of the electron beam. It may be worthwhile to pursue the finding,<sup>2</sup> that cavities in the drift tube have a weak focusing action, so that one may need fewer anodes.

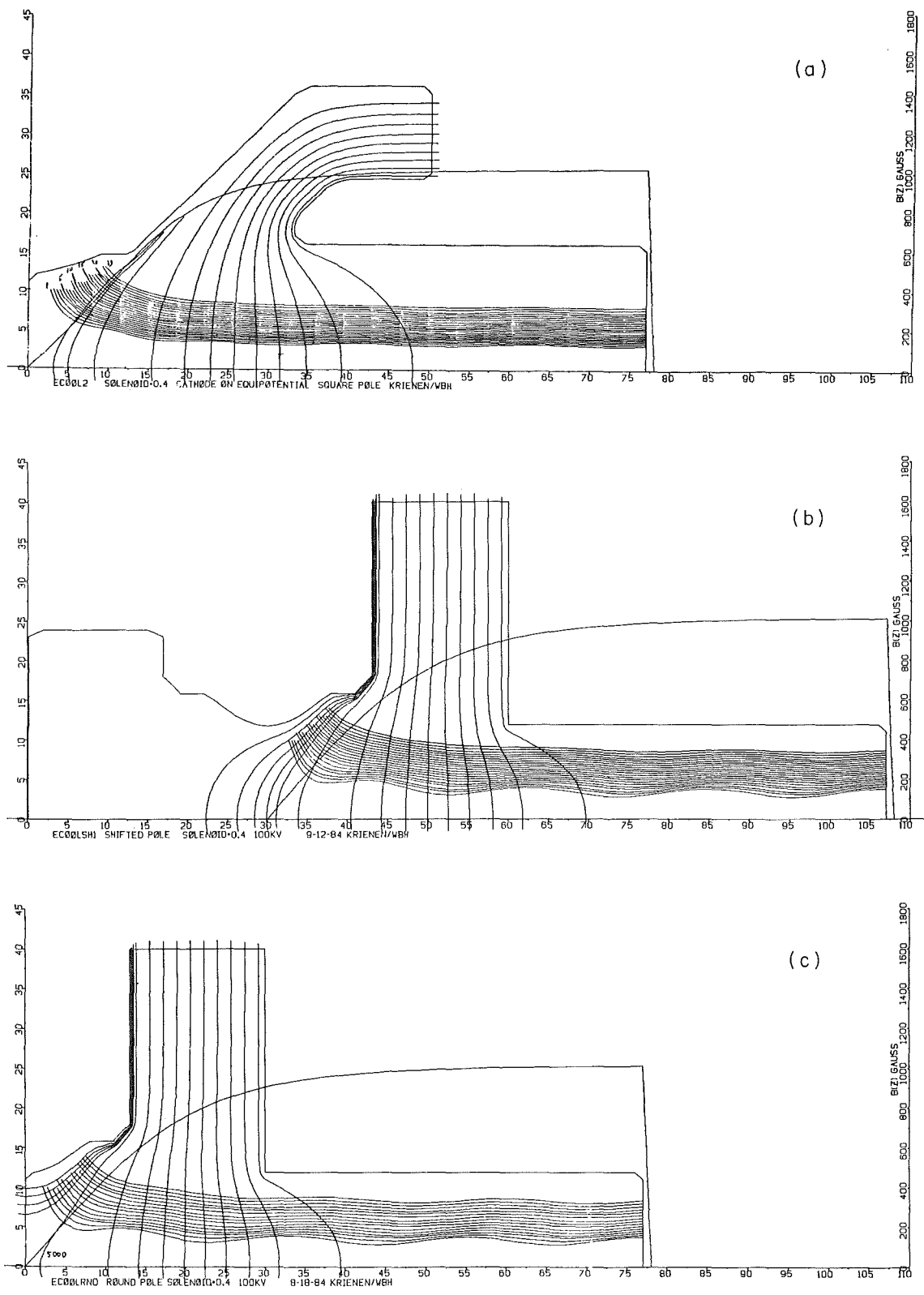
The collection of the hollow electron beam may be done following the CERN ICE cooler,<sup>1</sup> i.e. catch the electron on the same magnetic flux line where it was during its passage in the drift tube. The spike in this design may be suppressed since the beam is hollow, leaving therefore the coasting ion beam free of this obstruction.

## V. PRELIMINARY RESULTS

The magnetic field is calculated on a grid of 4 mesh to the inch. The electric field and the trajectories are calculated on a grid of 8 mesh to the inch. The method is that of Ref. 3. We used an anode voltage of 100 kV and a solenoidal magnetic field of 1000 gauss. We considered only hollow beams with an approximate outer radius of 1 inch and a hole radius of 3/8 inch. Figure 6 shows some preliminary results, which are tabulated below:

| Figure | pole   | micro | $j$ max | Remarks  |
|--------|--------|-------|---------|--|
|        |        | perv. | $j$ min |  |
| 6(a)   | square | .27   | 2.0     | Symmetry in $B$ and $E$  |
| 6(b)   | round  | .77   | 1.6     | Symmetry in $B$ and $E$  |
| 6(c)   | round  | .91   | 2.2     | Symmetry in $B$ only, terminated on the left with cavity at cathode potential. |

Although beam 6(a) is the coolest,  $< 100$  eV average, a lot of optimization has to be done before we can start at the fine trim to reach 1 eV temperature. Upon studying the waviness of the rays, we notice that for a first trial, they run reasonably in phase so that one may expect that the goal is within reach.



9-84

4917B6

Figure 6. Preliminary Results

### REFERENCES

1. M. Bell et al., Nucl. Instrum. Methods 190 (1981) 237.
2. F. Krienen, Karlsruhe Workshop Electron Colling, KfK 2836 (1979) 43.
3. W. B. Herrmannsfeldt, Electron Trajectory Program, SLAC-226 (1979).

ENERGY RECOVERING OF THE ELECTRON BEAM IN  
ELECTRON COOLING DEVICES

I.N.Meshkov, A.N.Sharapa and A.V.Shemjakin

Institute of Nuclear Physics,  
630000 Novosibirsk, USSR

The efficiency of electron cooling is known to sharply increase if the electron beam is magnetized and to possess a specific "flattened" distribution over electron velocities (when the longitudinal-velocity spread of electrons is considerably less than the transverse-velocity spread)<sup>1</sup>. To form such a beam in electron cooling devices at low and average energies of the particles (from 1 MeV to several GeV for protons and antiprotons and, correspondingly, from 0,5 keV to units of MeV for electrons) we have to use a guiding longitudinal magnetic field for the transport of electrons and their electrostatic acceleration. It is the application of the latter which makes expedient to introduce the energy recovering of the "used" electrons in the cases when the reactive power of the electron beam becomes substantial (about tens kilowatts and higher). The paper discusses the possibilities of creating highly-effective recuperators in electron cooling devices.

The power necessary for obtaining the electron beam in such devices is determined by a collector perveance  $P_{col}$  and by an electron loss current  $\Delta I$  at a given energy and electron current:

$$Q = P_{col}^{2/3} I^{5/3} + U_0 \cdot \Delta I , \quad (1)$$

where  $I$  is the beam current and  $U_0$  is the accelerating voltage of an injector. The obvious relation between the collec-

tor and beam perveances can be written as follows:

$$P_{col} = P_{beam} \cdot \xi^{3/2}, \quad \xi = U_0 / U_{col}, \quad (2)$$

where the parameter  $\xi$  is naturally referred to as a deceleration depth and  $U_{col}$  is the collector potential relative to a cathode one.

Minimization of the loss current  $\Delta I$  is required not only to lower the  $P_{active}$  but also to provide the necessary vacuum conditions in the cooling section because the electrons which are not trapped by the collector, arrive, sooner or later, at the vacuum chamber walls and gives rise to gas detachment. It is precisely the achievement of as minimal collector potential as possible (or its maximum perveance) which constitutes the recovering problem.

It would seem, there is an evident solution of this problem enabling the unlimited collector perveance ( $U_{col} = 0$ ) to be obtained; for this purpose, the recuperator should have an electron-optical scheme, mirror relative to the injector. However, the repeated attempts to realize this scheme have failed. This is associated with the secondary electron emission from the accepting surface of the collector, which occurs at any small values of  $U_{col}$ . An attempt to "arrange" the capture of the secondary-emission electrons leads unavoidably to a reduction of the collector perveance. In addition, a recuperator of any construction is subjected to the general regularity, namely: the loss current increases with the growth of the deceleration depth. A specific shape of the dependence  $\Delta I(\xi)$  is determined by the construction of a recuperator.

It is easy to demonstrate the availability of this regu-

larity by means of a recuperator without a guiding magnetic field ("electrostatic" recuperator). To capture the secondary electrons in it there is a single method - the obtaining of a minimum of the potential in the vicinity of the accepting surface, using, for example, a suppressor-electrode as it is shown in Fig. 1. If the configuration of the electrode is conformed with the geometry of the electric field of the beam in the recuperator (the known problem in electron optics), the potential inside the beam has the same value,  $U_{\min}$ , in the middle plane of the suppressor-electrode. The value of  $U_{\min}$ , equal to the suppressor-electrode potential, should be chosen in accordance with the values of  $U_0$  and  $U_{col}$ . In this case, the loss current from the recuperator is

$$\Delta I = I \cdot \int \frac{d\varphi}{dW} \cdot dW , \quad (3)$$

$\frac{eU_{col}}{e(U_{col} - U_{\min})}$

where  $\frac{d\varphi}{dW}$  is the distribution of secondary-emission electrons over the energy of the longitudinal (axial) degree of freedom. This distribution depends only on the energy of the primary electrons at the collector,  $eU_{col}$ , and on the material of collector's accepting surface. Thus, the quantity  $\Delta I/I$  is a rather definite deceleration depth function for the collector which increases with increasing  $\xi$ . Fig. 2 presents the dependence for the given recuperator, which has been obtained experimentally<sup>2</sup>.

It is worth emphasizing that the relation between the loss current and the deceleration depth takes place for any recuperators, including those in which the equipotential ca-

vities ("Faraday cylinders") serve as the collector. In particular, the collector of the recuperator shown in Fig. 1 has no difference, in properties, from a Faraday cylinder if the suppressor potential is equal to a collector one.

In addition, we would like to note the following. If the shape and potential of the suppressor are not conformed with the collector and anode potentials and with the beam current, then the suppressor plane is not an equipotential surface, and the equipotentials near the suppressor are "saddle"-shaped (see, e.g., <sup>3</sup>). It is just this fashion in which the recuperators are arranged with a collector of the Faraday-cylinder type and with a suppressor-electrode at the entrance of the collector <sup>3</sup>.

A guiding magnetic field offers additional possibilities of increasing the effectiveness of the recuperator. First of all, this is the use of a shielded collector with a "magnetic trap" at its entrance <sup>3</sup>.

The systems with a guiding magnetic field are characteristic of one more important feature: at a sufficiently strong longitudinal magnetic field all the secondary electrons leaving the collector pass through the system and, having reflected near the cathode surface, return again at the collector. In this case, the loss current  $\Delta I$  is determined by a slow electron drift across the field and can be considerably lower in comparison with the current of the secondary electrons from the collector. This peculiarity of the guiding magnetic field systems permits one to substantially reduce the suppressing voltage  $(U_{col} - U_{min}) / U_{col}$  at a given level of loss current, i.e. to increase the deceleration depth and, correspond-

dingly, to raise the collector perveance. In the limiting case we obtain a recuperator with a monotonously decreasing distribution of the potential which may be referred to as the "opened" one: this potential does not trap the secondary electrons by its electric field at all and is no sense in the absence of a guiding magnetic field. The experimental study of an "opened" recuperator has been performed at the device whose layout is depicted in Fig. 3. This recuperator has no suppressor-electrode and the collector is made as a Faraday cylinder with magnetic shielding. In this device, we have obtained the collector perveance  $P_{col} \approx 100 \mu A/V^{3/2}$  (at relative current losses  $\Delta I/I \leq 10^{-3}$ ). This is several times better than the similar results for the closed recuperators<sup>3</sup>. The collector perveance can be further increased upon transition from the Faraday cylinder to the plane-shaped collector. However, as the experiments have shown, the realization of an "opened" recuperator presents significant difficulties. First of all, this is the problem of initiating the Penning discharge in the guiding-magnetic-field systems.

The Penning discharge is observed in most of the systems with the straight trajectories of electrons if the magnetic field is rather high (the total Larmor radius of electrons is several times smaller than the aperture). The Penning discharge in the systems with electron energy recovering cause at least two effects:

- a) the current losses grow,
- b) the potential distribution along the electron beam is dramatically changed<sup>4</sup>.

It is apparent that the latter is not intolerable at all

in the electron cooling systems. The experiments have demonstrated that the installation of aperture diaphragms at the end faces of the drift chamber (Fig. 3), which shunt the near-wall layer inherent in the Penning discharge, is referred to the simplest and most effective methods of suppressing this discharge.

In electron cooling devices with curved sections (cooled beam injection-ejection sections) the centrifugal backward electron drift can prove to be sufficient to "clean" the system from the Penning discharge. The vacuum conditions can have a similar influence.

The "freezing-in" of the trajectories can lead also to emerging the coupling between the collector potential and the current in the cathode-collector circuit. A typical dependence  $I(U_{col})$  observed in the opened recuperator (i.e. in the recuperator with a high backward flux of electrons) is presented in Fig. 4. This coupling is caused by the influence of the secondary electrons: these arrive at the gun region and increase the space charge density in it; this gives rise to reducing the current from the cathode. The impact of the secondary electrons becomes more considerable as the potential falls off. One can show that in the limiting case  $U_{col} = 0$ , the current  $I_{col}$  in the cathode-collector circuit is related to the total current  $I_{tot}$  in the chamber (arithmetic sum of the direct and return current) as follows:

$$\frac{I_{col}}{I_{tot}} = \frac{1 - \delta}{1 + \delta}, \quad (4)$$

where  $\delta$  is the total coefficient of secondary emission.

Of course, in this case the  $I_{tot}$  is numerically equal to the maximum beam current <sup>of the gun</sup> according to the Child-Langmuir law. The most serious among the related problems is the stability problem of the electron beam in the presence of the reflected beam.

The capability of the electron cooling device to operate in this mode needs undoubtedly further investigation.

There exists one more direction of development of high-power electron cooling systems - the recuperators with transformation of the electron beam geometry. Reference 5 discuss the possibilities of this method in detail. Transformation of the cylindrical beam to a tube- or disc-shaped one before deceleration at the collector permits the efficiency of the device to be sharply increased. As an illustration of these possibilities, we present the results of the experiments with a recuperator shown in Fig. 5.

|                        |   |
|------------------------|---|
| Electron energy        | 25 keV                                  |
| Electron current       | 4 A                                     |
| Loss current           | 2 mA ( $\Delta I/I = 5 \cdot 10^{-4}$ ) |
| Collector potential    | 400 V                                   |
| Collector perveance    | $500 \mu\text{A/V}^{3/2}$               |
| Reactive beam power    | 100 kW                                  |
| Energy loss power      | 1.6 kW                                  |
| Recuperator efficiency | 98.4%                                   |

To set up the field of opposite direction and to transform the beam geometry, we have used, in the recuperator, a permanent magnet with a 3.6 kGs field at the face; the strength of the guiding magnetic field in its homogeneity region was 500 Gs, the diameter of the cathode was 3 cm, and the average

diameter of the tube beam was 11 cm.

Despite the relative complexity of construction, this type of recuperators seems to be very promising.

Figure captions

- Fig. 1. Electrostatic recuperator and potential distribution in it; 1: cathode, 2: anode, 3: suppressor-electrode, 4: collector.
- Fig. 2. The dependence  $U_o / U_{col}$  from  $\Delta I / I$ .
- Fig. 3. Layout of the opened collector with a guiding magnetic field; 1: cathode, 2: anode, 3: diaphragm to suppress the Penning discharge, 4: shielded collector, 5: solenoid.
- Fig. 4. The dependence  $I_{col}(U_{col})$ .
- Fig. 5. The scheme of transformation of the cylindrical beam into a tube-shaped one; 1: electron gun, 2: collector;  $H_0$  and  $H_1$  are the guiding and opposite-direction fields.

References

1. Skrinsky A.N. and Parkhomchuk V.V. "Methods of cooling the charged particle beams". Elementary particle and nuclear physics, 1981, v. 12, issue 3.
2. Abramjan E.A. and Sharapa A.N. Preprint 6-012. IVTAN, Moscow, 1977.
3. Kudelainen V.I., Meshkov I.N., Parkhomchuk V.V., Salimov R.A., Skrinsky A.N. and Fainstein V.G. ZhTF, 46, No. 8 (1976) 1678.
4. Granovsky V.A. "Electric current in gas". Gostekhizdat, 1952.
5. Kokoulin V.I., Meshkov I.N. and Sharapa A.N. ZhTF, 50, No. 7, (1980) 1575.

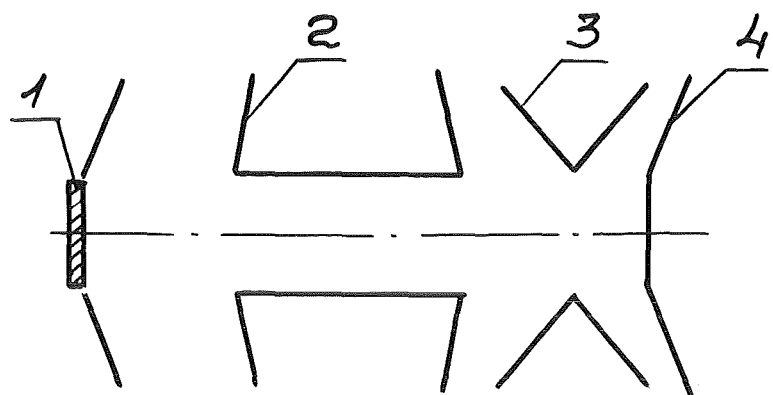


Fig. 1

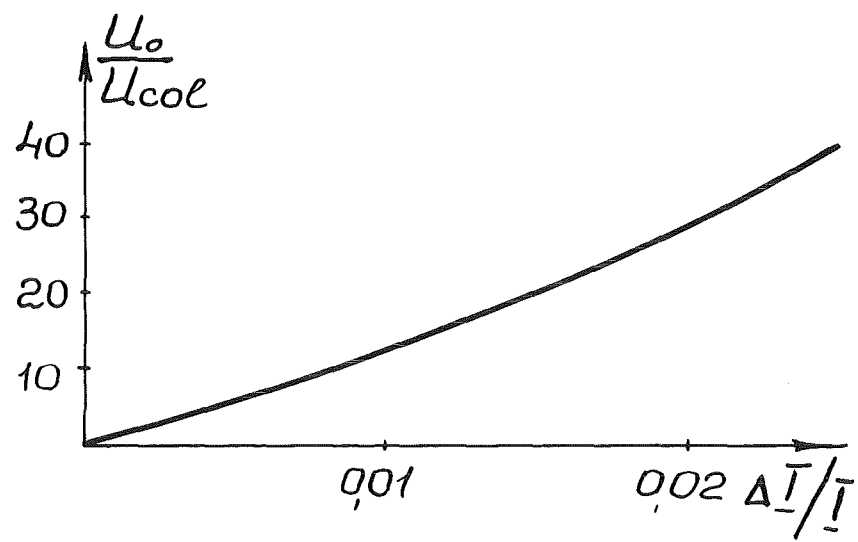
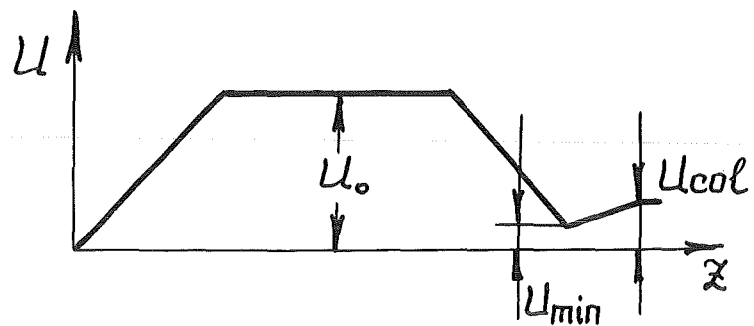


Fig. 2

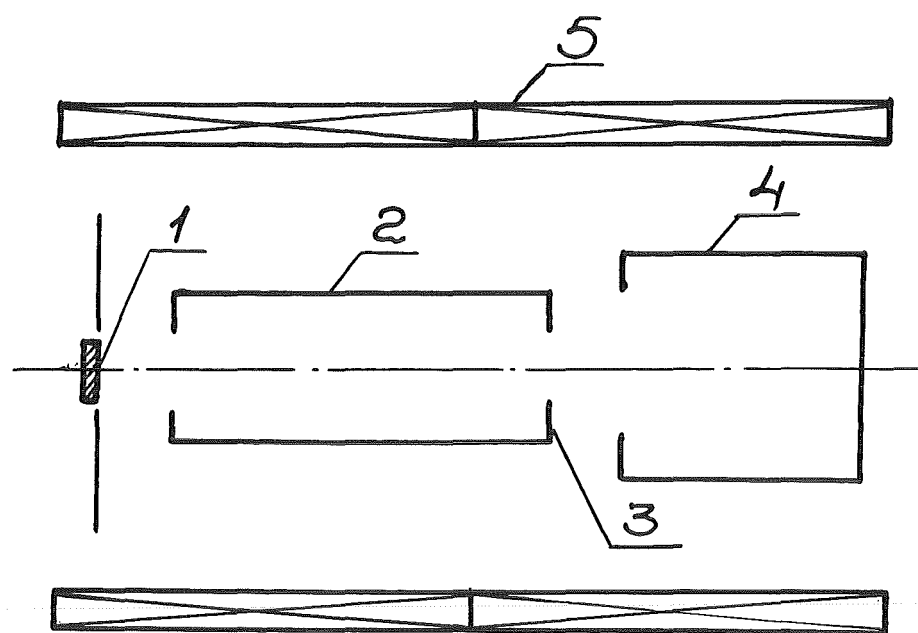


Fig. 3

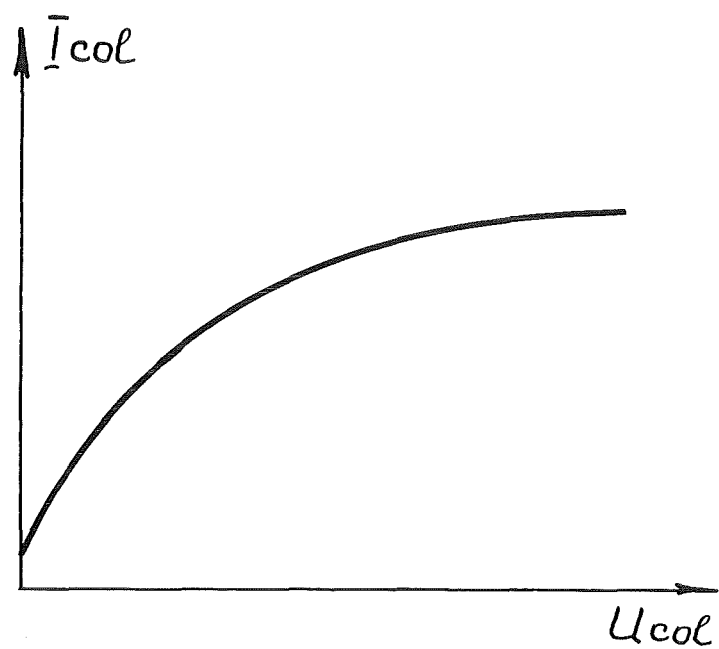


Fig. 4

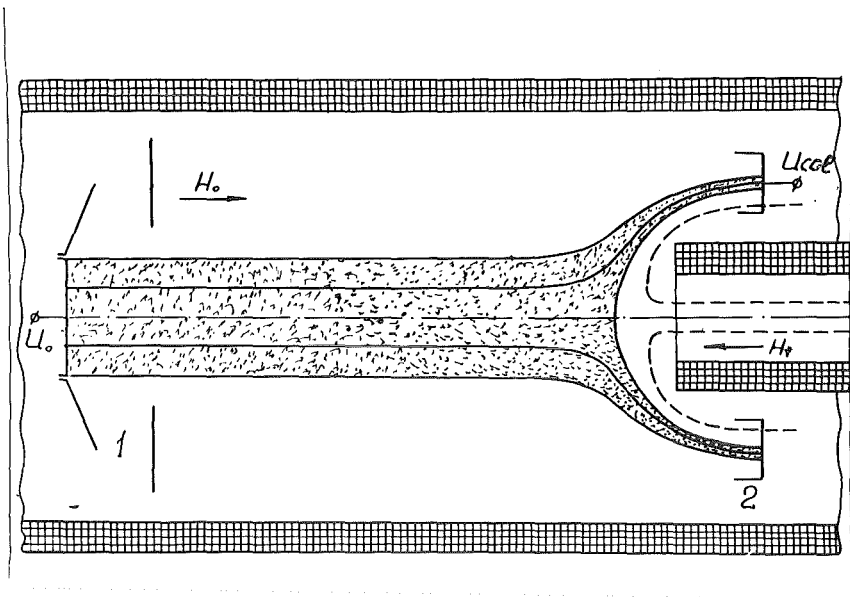


Fig. 5



AN ULTRA-HIGH VACUUM SYSTEM FOR COOLERS

M. Brouet, M. Girardini, A. Poncet and A. Wolf  
CERN, Geneva, Switzerland

L. Hütten, H. Poth and C. Habfast  
Kernforschungszentrum Karlsruhe, Institut für Kernphysik, Karlsruhe, FRG

(Presented by A. Poncet)

1. INTRODUCTION

The rapidly increasing interest in low energy storage rings designed to produce dense ion beams with devices such as electron coolers<sup>1</sup> forces Ultra-High Vacuum (UHV) Technology into the challenge of obtaining extremely low vacua with high gas throughputs. The CERN Low Energy Antiproton Ring (LEAR)<sup>2</sup> provides a number of physics experiments since 1983 with antiproton beams eventually in the range of 0.1 to 2 GeV/c<sup>3</sup>. In order to allow for future operating modes of this machine, mainly experimentation with internal gas targets at low momenta, it will be necessary to use an Electron Cooler<sup>4</sup> to compensate the beam blow-up and energy loss due to repeated passages of the beam through the target. The vacuum requirements for this device are such as to meet the stringent specification of less than  $10^{-11}$  Torr average pressure ( $N_2$  equivalent), as for the rest of the machine<sup>2,5</sup>, despite the high gas load associated with the operation of high power electron gun and collector.

In the following, the technology of the vacuum system for the LEAR electron cooling device is presented, and its preliminary performance is discussed.

2. THE UHV SYSTEM FOR THE COOLER

2.1 Generalities

The LEAR Electron Cooler is shown in Fig. 1. Its detailed design and architecture are the subject of another presentation at this Workshop<sup>1</sup>. Although largely inspired from the ICE experimental set-up<sup>6</sup>, the complete vacuum envelope has been re-designed and built according to UHV recipes, as was applied to the LEAR vacuum system<sup>7</sup>. The different chamber parts and flanges are made of high quality AISI 316LN austenitic stainless steel, and have been vacuum fired in the finished state ( $950^\circ\text{C}$  - 2 hours  $p < 10^{-5}$  Torr), as a final and optimum bulk degassing and cleaning treatment. The system as a whole is designed to be bakeable at  $300^\circ\text{C}$  in situ for 24 hours, and is thus equipped with permanently installed heating jackets providing also the necessary thermal insulation. These jackets during bakeout and pump down are powered individually according to thermocouple readings, as is usual on such UHV systems.

2.2 Choice of the Pumping Principle

The particular UHV problem in an electron cooler is to achieve very low pressures while the gas throughputs and loads are high with the system active. The gas produced results primarily from thermal degassing and chemistry of the hot cathod ( $\sim 1050^\circ\text{C}$ ) of the gun, from the collector, and from impact desorption of gases sorbed on surfaces by lost electrons from the primary beam.

While a careful choice of materials, cleaning and bulk degassing treatments can help, it is yet necessary to provide a very large pumping speed and capacity for the gas species normally desorbed. Moreover, little flexibility exists in the space available for pumping due to the geometrical arrangement, leading eventually to small conductances from the main gas source (gun or collector) to the drift tube where the lowest pressure is required; considerations of electron beam dynamics usually prime over vacuum and fix the design. This same argument of the rigidity of boundaries has some consequences in the choice of the principle of pumping; vacuum proximity between gas source and sinks is not necessarily an easy matter, since this leads to zones of high pressure in the system, thus requiring pumps

having the ability to cover an abnormally wide range of pressure decades down to extremely low pressures. Given these tight conditions, an analysis of the existing pumping principles while designing the LEAR electron cooler led to the choice of the NEG (Non-Evaporable Getter) pump; cryopumping and sputter ion pumps could be ruled out because of space problems, and sublimation pumps (Evaporable Getter) -widely used on the LEAR vacuum system- could not be considered because of their low capacity and narrow practical pressure range.

### 3. THE NEG PUMP

The NEG pumps chosen for the LEAR electron cooler consist of commercially available modules (SAES Getters, Milano, Italy) densely packed with konstantan strips onto which is bonded a powder mixture of Zr 84%-Al 16% alloy known as ST 101. While the detailed functioning and advantages of this getter -also used as the main pumping device for the Large Electron Positron Collider (LEP) under construction at CERN- have been well described in the literature<sup>8</sup>, it is worth recalling briefly here some of its characteristics relevant to the cooler application, for which some specific measurements have been made.

The pumping action of the getter is established by heating at high temperature under vacuum, an operation known as activation. It forms stable components with active gases such as CO, CO<sub>2</sub>, H<sub>2</sub>O while the sorption of H<sub>2</sub> is thermally reversible. The pumping speed for these gases results from a balance between their rate of arrival -i.e. the gas throughput or pressure- and the rate of diffusion of the compounds into the bulk of the getter. This diffusion rate depends strongly on the operating temperature, and consequently so does the pumping speed for a given gas throughput. Therefore, it is important to know in the Cooler UHV pumping application at which temperature has the getter to operate in order to have optimum performance. In particular, it was feared early in the design that if the getter had to operate continuously at a higher than room temperature in order to meet the gas throughput, this would have had uneasy consequences, such as necessity of water cooling of envelopes to reduce thermal degassing and, furthermore, it might altogether have been impossible to meet the design low limit pressure of the system due to higher dissociation pressures of the getter.

Figure 1 shows the disposition of the getter cartridges in the system, essentially split into three units: the gun pump and the two toroid chamber modules (cf Figs 5 and 6).

For evaluation of the getter optimum operating conditions, the gun pump has been chosen -since it has to support the largest part of the gas throughput- and tested with gas injection (H<sub>2</sub>-CO) from a Fischer-Momsen dome as a first step, and subsequently with the hot cathode of the gun itself. Figures 3 and 4 show the results of pumping speed measurements and ultimate performance, as a function of intake gas load. The necessary reconditionings to restore the optimum speed are also marked as milestones. The results clearly indicate the possibility of operating the NEG at room temperature without too frequent conditionings, and yet obtaining the required low pressure. As the hot cathode also produces a little amount of methane (CH<sub>4</sub>), which is not pumped by NEG, the results also show clearly the necessity to provide sputter ion pumping. In the final installation on LEAR, this will be provided by pumps placed adjacent and as close as possible to the electron cooler.

#### 4. PRELIMINARY PERFORMANCE

At the time of this conference, after completion of numerous pre-qualification tests for the NEG pump, the overall performance of the Cooler UHV system has been partly assessed. Figure 8 shows the complete system assembled, with a Fischer-Momsen dome in place of the gun to simulate the cathode throughput. Also shown is the evolution of the pressure and gas composition in different parts of the system, after a 150°C bakeout and NEG activation, for different throughputs and gas loads. Although only 3 out of 5 modules in the gun pump had been activated (cf. § 5), the pressure gradient obtained between the gas source and the toroid chamber is spectacular, peaking at roughly 400 for a CO gas throughput representing several times the normal hot cathode production. For the calculated gas conductance given in Fig. 1, the transmission probability for a gas molecule originated at the cathode to the toroid chamber would be about 30%. The actual transmission probability for the gun pump arrangement (Fig. 5) derived from the pressure gradient and the separately measured pumping speed of the toroid chamber NEG, for the known throughput, is initially between 2 and 4%, i.e. close to the 1.5% minimum theoretically possible<sup>9</sup> that would be approached if a gas molecule entering the NEG module had a 100% chance to be trapped (sticking coefficient of 1). For CO injection, this transmission probability only rises to 11-12% after 0.54 Tl of gas injected, showing the effect of saturation of the gun pump. Knowing the toroid chamber pumping speed, estimated from separate measurements<sup>10</sup>, the pumping speed of the gun NEG pump chamber can as well be deduced from these measurements. With 3 modules active out of 5, it varies for CO from ~900 l/s to 600 l/s after saturation with a load of 0.54 Tl. For H<sub>2</sub>, the pumping speed is still ~1500 l/s after injection of 1.5 Tl.

Indeed, given the space available for pumping and throttling the gas flow, these results show that NEG pumps are probably an adequate answer, while still operating at room temperature. Not until the complete throughput with the gun and collector operating at nominal values is obtained, will it be possible to assess on the frequency of reconditionings. However, there seems to be some safety margin as shown by the graph of pressures vs gas load shown in Fig. 8.

#### 5. TECHNICAL PROBLEMS

Two main technical difficulties have been encountered so far in the operation of the NEG gun pump, which are somewhat linked to the compactness of the geometrical arrangement, namely high electrical current (~90 A) and power (~6.6 kW for 6 modules) necessary for activation at 700°C. The current feedthroughs are not standard, since they have to be as small as possible to fit in the external solenoid and still be able to carry safely 90 A for periods of 15 to 20 minutes. It is not yet known if the actual design has reached the reliability required. The second difficulty arises from the large electrical power during activation. Since there is no thermocouple installed on the NEG, the power is controlled externally on the power supply to give an activation temperature of ~700°C, from separately obtained power temperature calibration values. Due to the proximity of the vacuum envelope, its temperature during activation goes well above the nominal bakeout temperature of 350°C with the getter at 700°C (the getter is activated during the bakeout cycle), which would be detrimental to the system, if applied routinely. Since water cooling is not feasible in the space available, a different activation procedure had to be envisaged, so as to control both

temperatures on the vacuum chamber ( $350^{\circ}\text{C}$ ) and the NEG ( $700^{\circ}\text{C}$ ) with two separate parameters. Preliminary tests done in pulsing the power, with interval between the power pulses chosen in such a way as to limit the temperature on the vacuum envelope at  $\sim 300^{\circ}\text{C}$ , have shown that the activation of the getter could be obtained and still yield near to the optimum pumping speed. Although promising, this technique needs to be further studied, both from the point of view of the reliability of the system and the fine tuning of the pumping parameters.

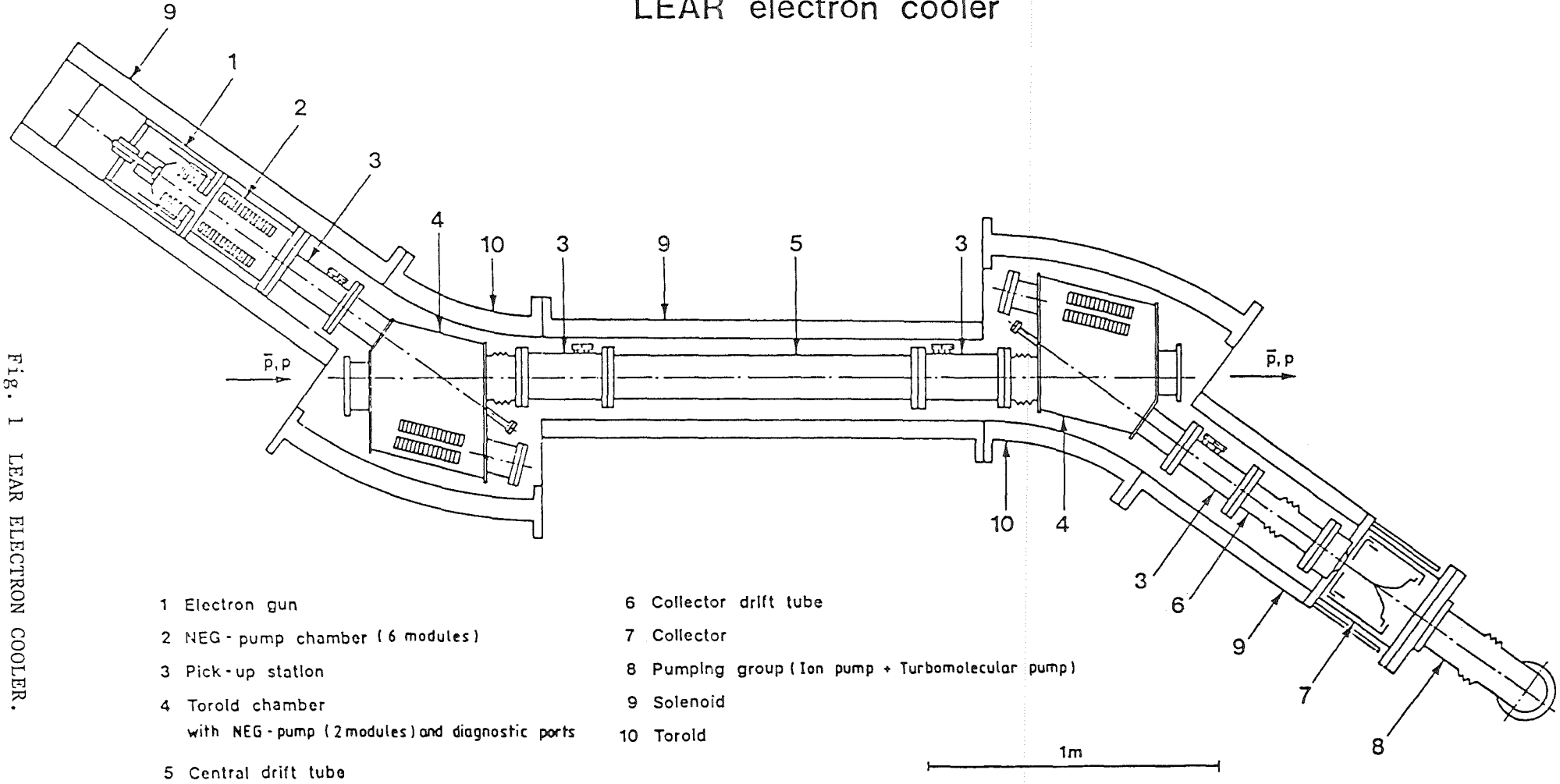
#### 6. CONCLUSION AND FURTHER DEVELOPMENTS

Numerous tests and measurements have shown that the use of NEG pumps can be an answer to the challenge of obtaining extreme vacua with the high gas loads of the future LEAR Electron Cooler. The chosen solution will be tested in the near future in real life with the cooler fully assembled and operating. However, it is felt that further improvements in pumping speed can be obtained, if a low activation temperature getter known as ST 707 (from SAES Getter, Milano, Italy) can be used to provide a pumping wall in the cooler drift tube. Preliminary laboratory tests have shown that this getter can be activated at the normal system bakeout temperature of  $300^{\circ}\text{C}$ , this requiring no external power source, and still provide a low pressure limit compatible with the LEAR machine. Further developments also involve the use of this type of getter in the gun pump, thus avoiding the activation problems, and allowing more flexibility to achieve a geometrical arrangement giving optimum pumping speed and minimum conductance. Finally, little has yet been done on the pumping system of the collector itself, which should give less problems given the space available.

#### REFERENCES

1. H. Haseroth and al., The LEAR Electron Cooler, CERN/PS/84-28, 1984, this Conference.
2. Design Study of a Facility for Experiments with Low Energy Antiprotons (LEAR), CERN/PS-DL/80-7, 1980 (Ed. G. Plass).
3. P. Lefèvre, LEAR, PS/LEA/Note 84-7, 1984.
4. L. Hütten and al., The Status of the Electron Cooling Device for LEAR, CERN/PS-LI/83-38, 1983.
5. M. Giesch and al., Implications of an Internal Target for Antineutron Production in LEAR, PS/DL/LEAR Note 95, 1 September 1981.
6. M. Bell and al., Electron Cooling in ICE at CERN, Nucl. Instrum. and Methods, 190, 237 (1981).
7. M. Brouet and al., The Ultra High Vacuum System for the Low Energy Antiproton Ring (LEAR), CERN/PS-ML/83-42, 1983.
8. C. Benvenuti, A New Pumping Approach for the Large Electron Positron Collider (LEP), CERN/ISR-VA/82-12.
9. G. Smith and G. Lewin, Free Molecular Conductance of a Cylindrical Tube with Wall Sorption, Journal of Vacuum Science and Technology, Vol. 3, no 3, 1965.
10. M. Girardini, Pompe Modulaire insérable à Getter non évaporable. Caractéristiques et vitesse de pompage, CERN/PS/ML Note Tech. 22.4.1983.

## LEAR electron cooler



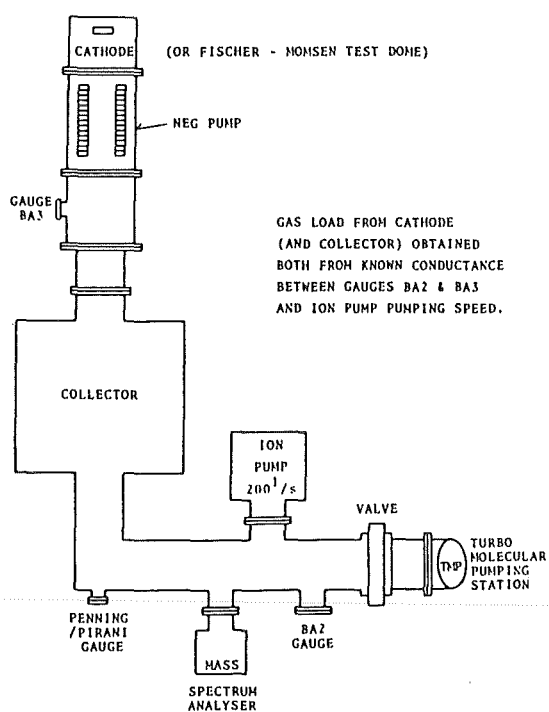


Fig. 2 THE HOT CATHODE GAS LOAD TEST SET UP.

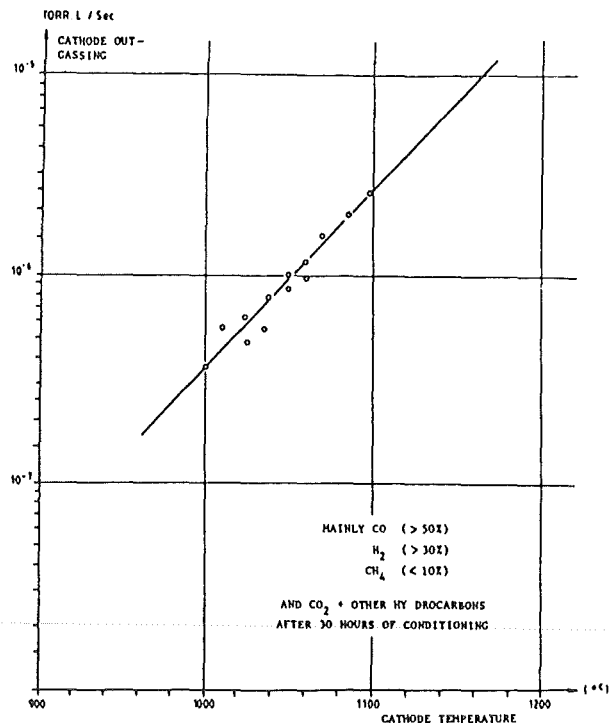


Fig. 4 GAS LOAD FROM HOT CATHODE AS A FUNCTION OF ITS TEMPERATURE.

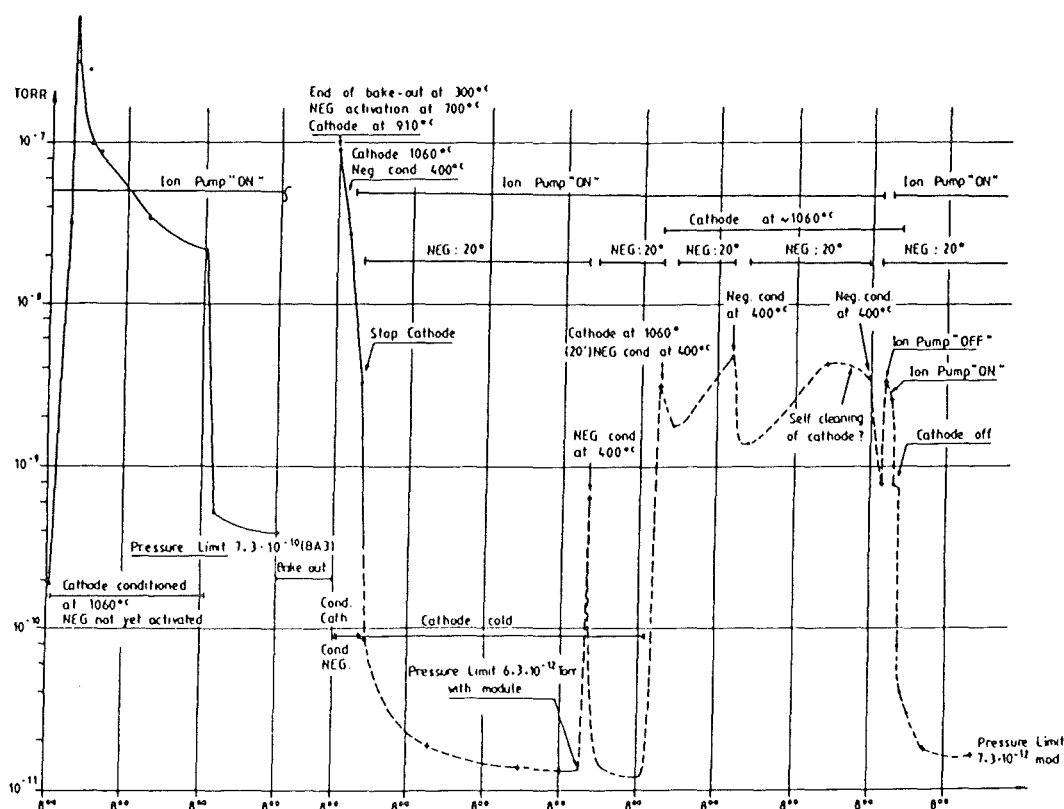


Fig. 3 PRESSURE WITH CATHODE HOT.

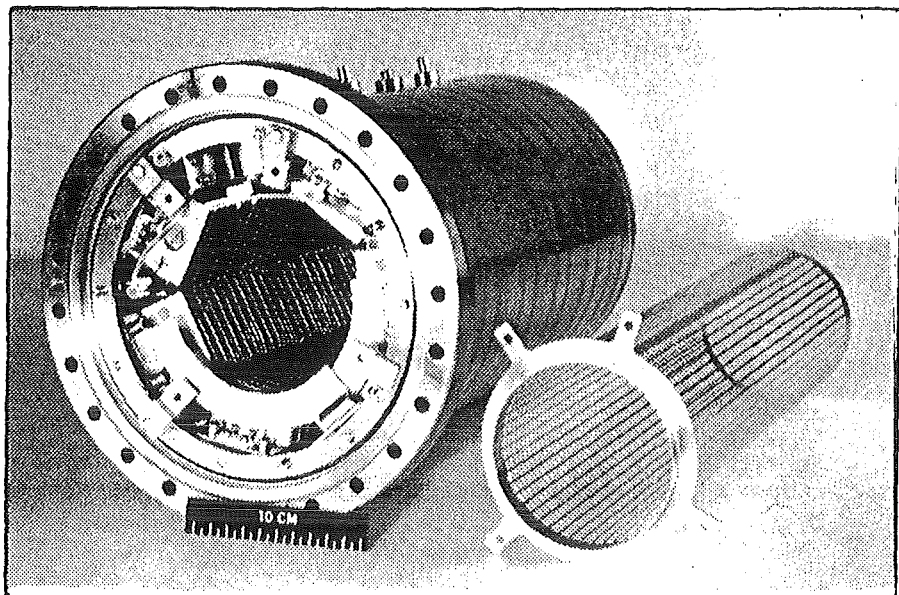


Fig. 5  
THE GUN NEG PUMP.

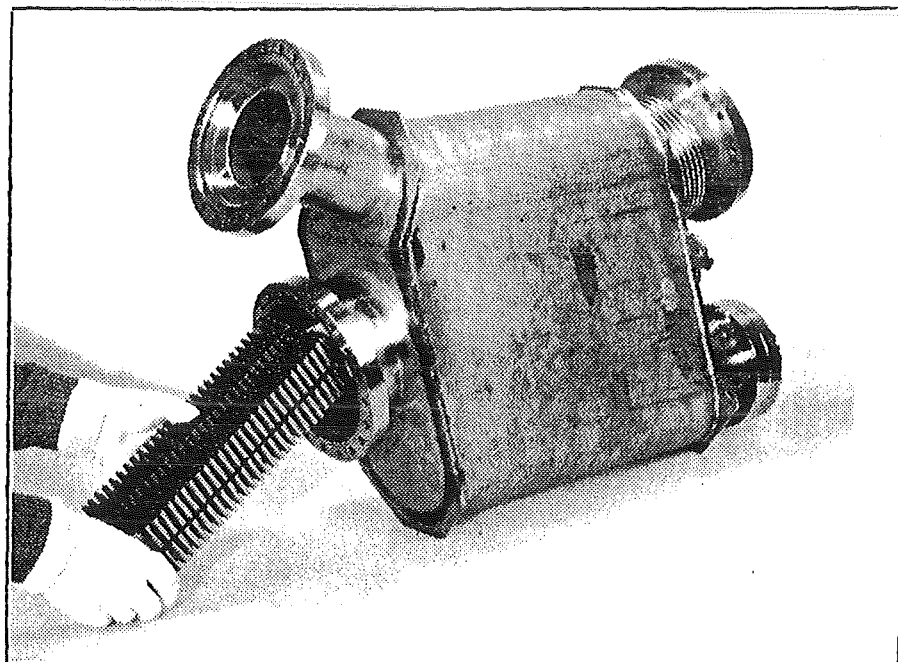


Fig. 6  
THE TOROID CHAMBER  
NEG PUMP.

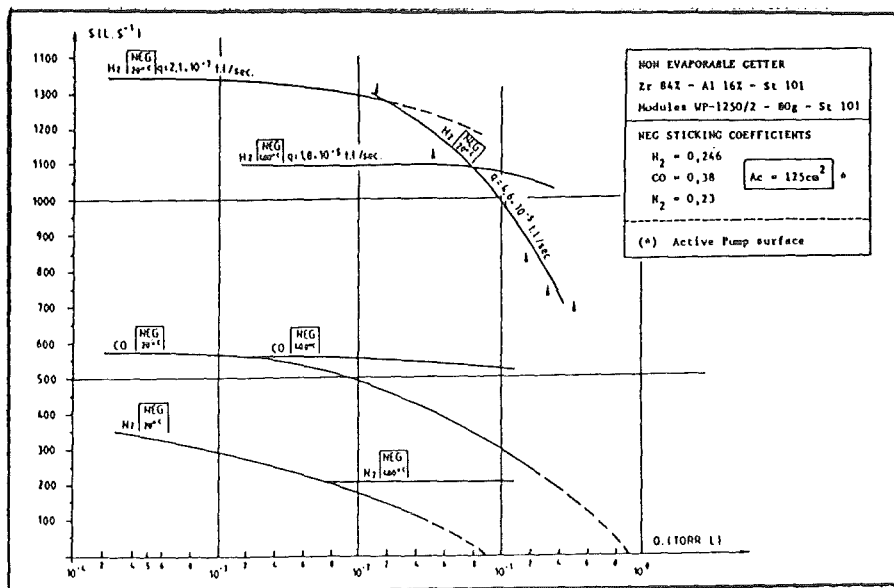
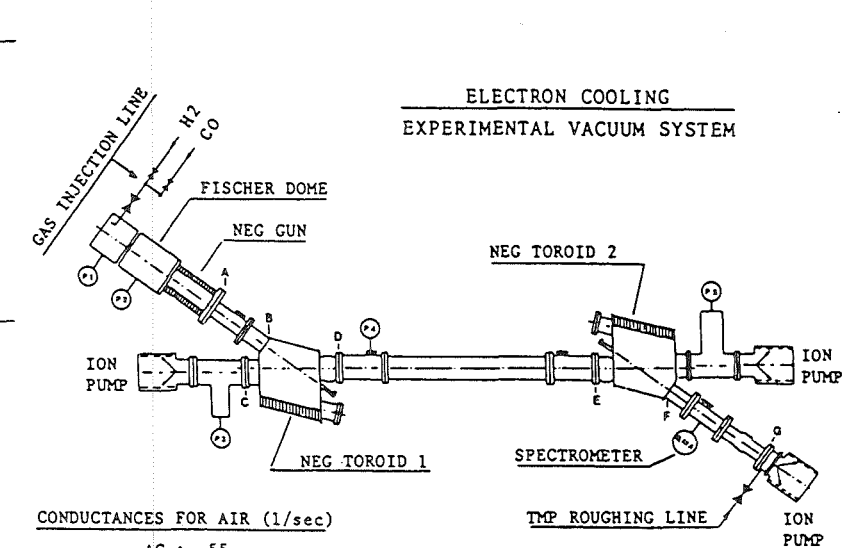
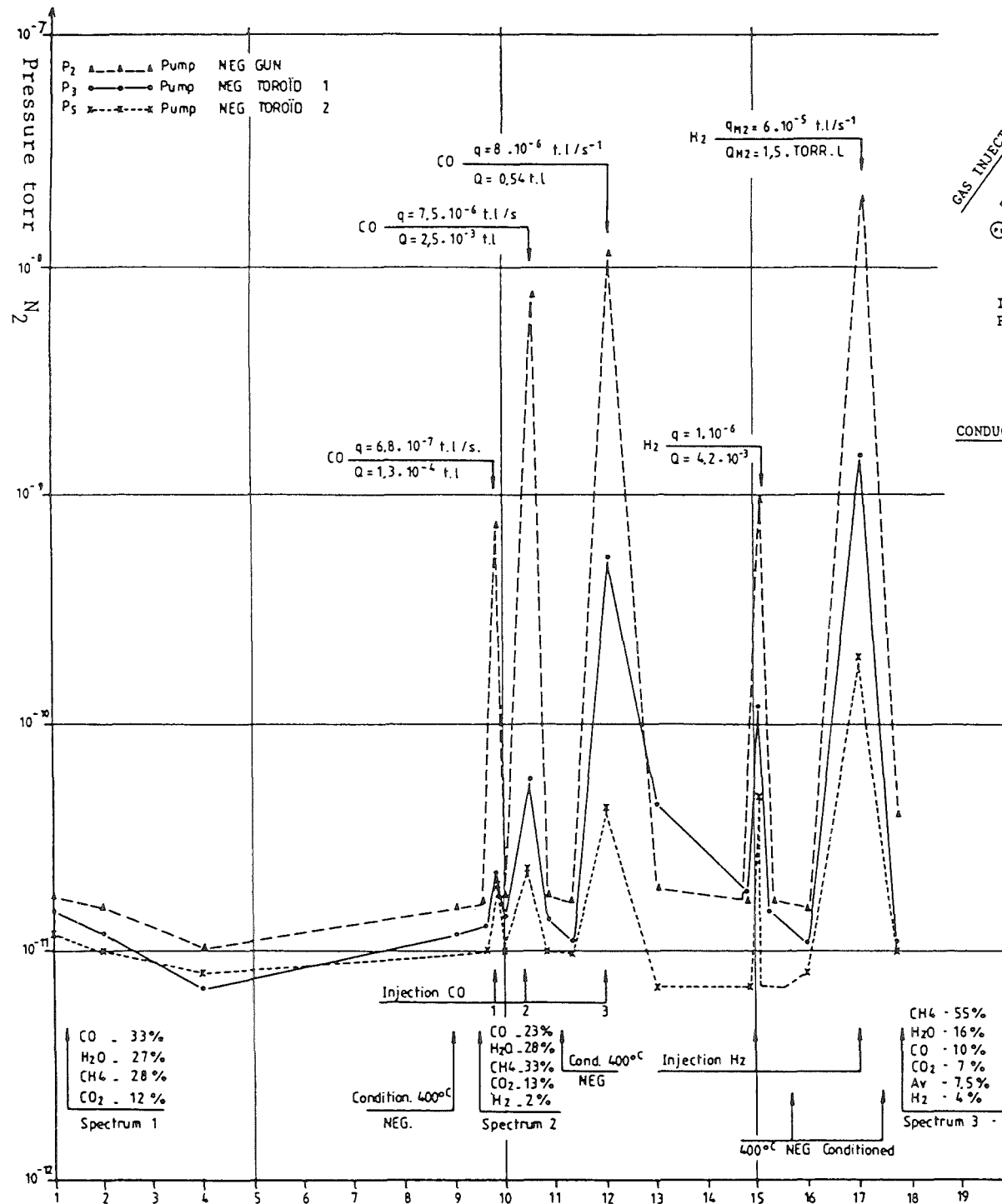


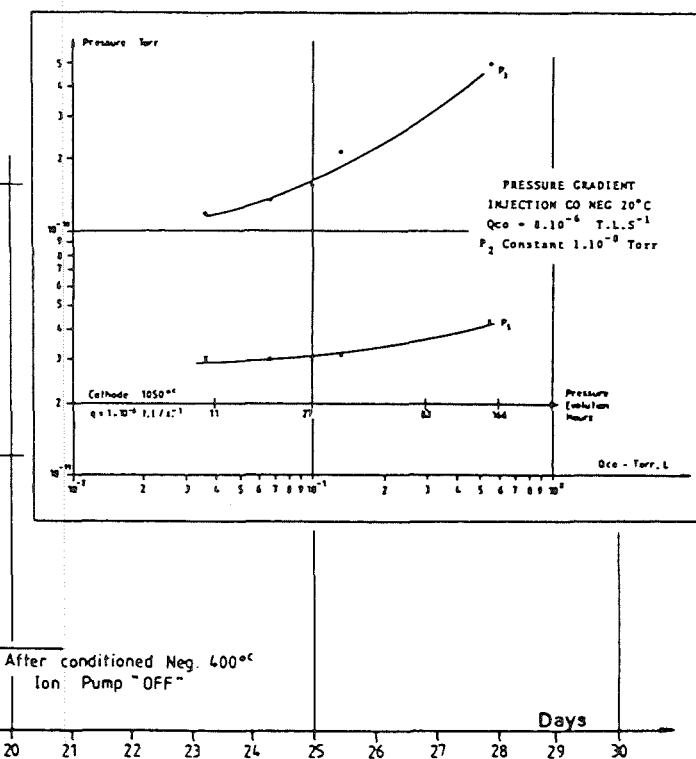
Fig. 7  
NEG PUMPING SPEED.

Fig. 8 EXPERIMENTAL VAC SYSTEM.



CONDUCTANCES FOR AIR (1/sec)

AG : 55  
AB : 300  
DE : 125  
CF : 157  
FG : 126



ORDERING EFFECTS IN COULOMB RELAXATION OF  
A COLD BEAM

N.S.Dikansky, D.V.Pestrikov

Institute of Nuclear Physics, Novosibirsk, USSR

Introduction

The aim of this report is to point out some effects, which are specific for Coulomb relaxation of a cold beam. In a normal beam this relaxation is mainly caused by the well known effect of intrabeam scattering (IBS). Due to undesirable redistribution of partial temperatures this can limit the beam intensity. For a long time /1/ IBS was expected to be responsible for the rise in longitudinal temperature  $\bar{T}$  of the beam with its current  $I$  in a storage ring with electron cooling.

The measurements of  $\bar{T}$ , which have been done at NAP-M /2/, showed, that until  $I \leq 10\mu\text{A}$   $\bar{T}$  does not depend on  $I$  and can be extraordinary small  $\bar{T} \approx 1^\circ\text{K}$ . The rise of  $\bar{T}$  with the beam current was seen after threshold  $I = 10\mu\text{A}$ . These results do not agree with existing theory of IBS /1,3/, which predicts more regular increase in  $\bar{T}$  with the beam current, without any threshold. The same disagreement has been seen in recent measurements of longitudinal temperature of the cooling electron beam /4/.

There are two facts which can explain this disagreement and which were ignored in Refs. /1,3/. The first one is now well known to those, who deal with electron cooling. It is the magnetization of scattered particles (in our case, by focusing fields of a storage ring). If collision times  $\tilde{\tau}_{col}$  become larger than periods of betatron oscillations ( $\sim 1/\omega_b$ )

$$\tilde{\tau}_{col} \omega_b > 1, \quad (1)$$

collisions will not contribute to longitudinal-transverse energy exchange. The main part of collisions in a cold beam

satisfies eq. (1).

Analogous to the magnetized electron beam /5/ we can replace the beam of particles by that consisting of charged disks. Transversal dimensions of these disks are determined by the amplitudes of betatron oscillations. The number of disks coincides with number of particles  $N$ , the temperature - with the longitudinal temperature of the beam  $T$ .

The second important factor is the Landau damping depression of coherent oscillations in a cold beam. When damping time of these oscillations  $\tau_{coh}$  becomes comparable with the relaxation time  $\tau_z$

$$\tau_z \lesssim \tau_{coh} \quad (2)$$

coherent fluctuations can exchange energy with particles. Because of thermal motion, particles excite new oscillations. This energy exchange opens up one more channel for the relaxation, which stops with thermalization of particles and coherent noise of the beam. The average number of coherent modes  $N_{ex}$  excited in this equilibrium is determined by (2) and generally increases with the decrease of  $T$ .

While propagating along the beam, the longlive coherent oscillations produce strong spatial correlations in motion of various particles. So, the presence of coherent background in equilibrium yields the ordering in spatial distribution of particles along the beam. The level of this ordering increases with that of  $N_{ex}$  and can come into crystal ordering provided by  $T$  is small enough.

Therefore, one can expect that collective interaction of particles depresses their longitudinal mobility. Together with the beam magnetization this can cause the depression of IBS\*).

In this report we shall consider the simplest example -- the relaxation of the energy distribution in a coasting nonrelativistic beam without coherent instabilities. This very region of parameters corresponds to that of experiments /2/.

\*) We thank V.Parkhomchuk which drew our attention to this possibility.

### 1. Basic equations

Equations describing the relaxation of energy distribution under condition (2) can be obtained by straightforward statistical approach. This had been done in Refs. /6,7/. Here we shall use simplified but the more descriptive way.

Let us describe the beam by thermodynamical values by longitudinal  $T$  and transversal  $T_{\perp}$  temperatures and by some level of coherent fluctuations. We shall assume, that in a cold nonrelativistic beam the only longitudinal coherent modes can be responsible for the relaxation of the energy distribution. This seems be correct especially for a nonrelativistic beam because of a very fast damping of transversal coherent motion due to frequency spread produced by the Coulomb tune shift  $\Delta\nu \sim N/a^2$  ( $a$  is the beam radius).

The first equation, which can be used a priori with Coulomb interaction between particles is the energy conservation law. Let us introduce the total energy of thermal motion in the beam

$$\begin{aligned} \mathcal{E} &= \frac{NT}{2} + NT_{\perp} + U_N \\ &= \frac{NT}{2} + NT_{\perp} + \sum_n \frac{e^2 \omega_s}{2\pi} \left( \frac{iZ_n}{n} \right) \langle |\delta p_n|^2 \rangle \end{aligned} \quad (3)$$

Here  $\omega_s$  is the revolution frequency;  $e$  is the charge of particles;  $\delta p_n$  is the  $n$ -th harmonic of the fluctuation of the longitudinal beam density

$$p(\theta, t) = \sum_{k=1}^N \delta(\theta - \theta_k(t)) = \frac{N}{2\pi} + \sum_n \frac{\delta p_n(t)}{2\pi} e^{in\theta}, \quad (4)$$

$Z_n$  - is impedance describing the interaction between particles, i.e.

$$\delta E_{n\omega} = \frac{e \omega_s Z_n}{\pi} \delta p_{n\omega}, \quad (5)$$

where  $\delta E_{n\omega}$  is the Fourier amplitude of longitudinal elec-

trical field induced by fluctuation  $\delta\rho_{nw}$ ,  $17 = 2\pi R_0$  is the irbit perimeter. For the Coulomb interaction in a nonrelativistic beam one can use

$$\frac{iZ_n}{n} = \frac{4}{\theta_s} \begin{cases} \frac{1}{2} \ln\left(\frac{2R_0}{n}\right), & n < n_0 = R_0/a \\ (n_0/n)^2, & n > n_0. \end{cases} \quad (6)$$

The energy conservation law ( $dE/dt = 0$ ) yields

$$\frac{dT}{dt} = -2 \frac{dT_L}{dt} - \frac{2}{N} \sum_n \frac{e^2 \omega_s}{2\pi} \left( \frac{iZ_n}{n} \right) \frac{d}{dt} \langle |\delta\rho_n|^2 \rangle$$

or, using (5),

$$\frac{dT}{dt} = -2 \frac{dT_L}{dt} - \frac{2}{N} \sum_n \frac{R_0^2}{n^2 \omega_s} \left( \frac{n}{iZ_n} \right) \frac{d}{dt} \int_{-\infty}^{\infty} d\omega (\delta E_n)_\omega^2 \quad (7)$$

Here

$$(\delta E_n)_\omega^2 = \lim_{\Delta \rightarrow 0} 2\Delta \langle \delta E_{n,\omega+i\Delta}^* \delta E_{n,\omega-i\Delta} \rangle$$

is the spectral density of the field fluctuations.

The first item in r.h.s. of eq. (7) describes the transversal-longitudinal energy exchange. As we mentioned, it is mainly caused by fast collisions. In the adiabatical limit (1)  $dT_L/dt \rightarrow 0$ , and (7) gives

$$\frac{dT}{dt} = - \frac{2}{N} \sum_n \frac{R_0^2}{n^2 \omega_s} \left( \frac{n}{iZ_n} \right) \frac{d}{dt} \int_{-\infty}^{\infty} d\omega (\delta E_n)_\omega^2 \quad (8)$$

i.e. evolution of  $T$  is governed by evolution of the beam noise.

So, we need now equation for  $(\delta E_n)_\omega^2$ . It can be constructed in the following way. Without excitations the longitudinal coherent oscillations of the beam decay due to Landau damping. So one can write

$$\frac{\partial}{\partial t} (\delta E_n)_\omega^2 = -2\lambda_n(\omega) (\delta E_n)_\omega^2. \quad (9)$$

But thermal motion of particles excites new coherent oscillations and this concurrences with considered decay. As a result, the field fluctuations reach the equilibrium level. This can be described by the equation

$$\frac{\partial}{\partial t} (\delta E_n)^2 = -\omega \lambda_n(\omega) \left[ (\delta E_n)^2 - (\delta E_n)^2_{\text{st}} \right]. \quad (10)$$

The equilibrium value  $(\delta E_n)^2_{\text{st}}$  can be calculated using the Callen, Welton formula, which yields

$$(\delta E_n)^2_{\text{st}} = \frac{\omega_s n^2}{R_0^2} \frac{\ell}{\pi} \frac{\varepsilon_n''(\omega)}{|\varepsilon_n(\omega)|^2} \frac{\beta T}{\Delta \omega_n}, \quad (11)$$

where  $\Delta \omega_n = \omega - \hbar \omega_s$  and

$$\varepsilon_n(\omega) = \varepsilon_n'(\omega) + i \varepsilon_n''(\omega) = 1 + \frac{\Omega_n^2}{n \omega_0'} \int dp \frac{\alpha_f / \beta p}{\omega - \hbar \omega_0(p)} \quad (12)$$

is the dielectrical constant of the beam,

$$\Omega_n^2 = n^2 \frac{Ne^2 \omega_s \omega_0'}{17} \left( \frac{i Z_n}{n} \right) \quad (13)$$

is the square of longitudinal coherent tune shift,  $\omega_0' = \frac{\omega_s \gamma}{\beta M \theta_s}$ ,  $\gamma = \frac{1}{J^2} - \frac{1}{J_{\text{trr}}^2}$ ,  $M c^2 J_{\text{trr}}$  is the transition energy of the ring (here  $J < J_{\text{trr}}$ ). If the temperature  $T$  is small enough for all  $\omega$ , except

$$\varepsilon_n'(\omega) = 0 \quad (14)$$

one has  $|\varepsilon_n'(\omega)| \gg |\varepsilon_n''(\omega)|$ . So, eq. (11) can be rewritten as

$$(\delta E_n)^2_{\text{st}} = \frac{n^2 \omega_s}{R_0^2} \left( \frac{i Z_n}{n} \right) \left| \frac{d \varepsilon_n'}{d \omega} \right| \delta [\varepsilon_n'(\omega)] T. \quad (15)$$

Substitution of eq. (15) to eq. (10) completes our construction:

$$\frac{\partial}{\partial t} (\delta E_n)^2 = -\omega \lambda_n(\omega) \left[ (\delta E_n)^2 - \frac{n^2 \omega_s}{R_0^2} \left( \frac{i Z_n}{n} \right) \left| \frac{d \varepsilon_n'}{d \omega} \right| \delta [\varepsilon_n'(\omega)] T \right]. \quad (16)$$

It is more suitable to introduce instead of  $(\delta E_n)^2$

the temperatures of coherent excitations:

$$T_n = \frac{R_0^2}{n^2 \omega_s} \left( \frac{n}{i Z_n} \right) \int_{-\infty}^{\infty} d\omega (8E_n)^2 \quad (17)$$

Then equations (8,16) can be rewritten in the form

$$\frac{dT_n}{dt} = -2\lambda_n (T_n - T) \quad (18)$$

$$\frac{dT}{dt} = \sum_n \frac{2\lambda_n}{N} (T_n - T), \quad (19)$$

where  $\lambda_n = \lambda_n(\omega)$  with  $\varepsilon'_n(\omega) = 0$  ( $\Delta\omega_n \approx \Omega_n$ ). Correspondingly, for  $\mathcal{E}$  one can get

$$\mathcal{E} = \frac{NT}{2} + \sum_n \frac{T_n}{2}. \quad (20)$$

## 2. Relaxation of an uncooled beam

As we found out, the relaxation of the beam without cooling is described by the system of eqs. (18,19). The process looks like a temperature exchange in the mixture of two gases: particles and collective fluctuations. It stops when temperatures of components become equal:

$$T = T_n. \quad (21)$$

The longitudinal temperature itself can be found from the energy conservation law

$$\mathcal{E} = \frac{NT}{2} + \sum_n \frac{T}{2} = \frac{N+N_{ex}}{2} T. \quad (22)$$

The number of excitations can be estimated using condition (2) or (in equilibrium) using thermodynamical consideration. Anyway, it can not exceed  $N$ . So, with an accuracy of factor between 1 and 2 eq. (22) yields

$$T \approx \mathcal{E}/N, \quad (23)$$

where  $\mathcal{E}$  is determined by initial conditions.

One of the important results, which follows from eqs. (18, 19), is the heating of particles if initial level of coherent noise of the beam exceeds the equilibrium one. This can be, for instance, while the beam unbunching. Let the initial spatial distribution in the bunch have the Gaussian form

$$\rho(\theta, t) = \frac{N}{\sqrt{2\pi} \theta_0} \exp\left(-\frac{\theta^2}{2\theta_0^2}\right)$$

Then

$$\begin{aligned} \mathcal{E} &= \frac{N T_i}{2} + \frac{1}{2} \sum_n \frac{e^2 \omega_s}{2\pi} \left( \frac{i z_n}{n} \right) \left| p_n \right|^2 \\ &= \frac{N}{2} \left( T_i + \sum_n \frac{N e^2 \omega_s}{2\pi} \left( \frac{i z_n}{n} \right) e^{-2n^2 \theta_0^2} \right), \end{aligned}$$

where  $T_i$  is initial value of  $T$ . Assuming  $\theta_0 n_0 \gg 1$ ,  $\theta_0 < \pi$  and  $(iz_n/n) = \text{const}$  when  $|n| < n_0$ , we shall get from (23)

$$\begin{aligned} T_f &\approx T_i + \sum_n \frac{N e^2 \omega_s}{2\pi} \left( \frac{i z_n}{n} \right) e^{-2n^2 \theta_0^2} = \\ &= T_i + \frac{N e^2 \omega_s}{\sqrt{2\pi} 2\theta_0} \left( \frac{i z_n}{n} \right). \end{aligned} \tag{24}$$

Using  $T = R_0 \Delta \omega^2 / \omega_0'$  (where  $\Delta \omega$  is the revolution frequency spread) we can rewrite eq. (24) as

$$\begin{aligned} \Delta \omega_f^2 &= \Delta \omega_i^2 \left( 1 + \frac{1}{\theta_0} \left. \frac{R_n^2}{(n \Delta \omega)^2} \right|_{n < n_0} \right) \\ &= \Delta \omega_i^2 \left( 1 + \frac{1}{\theta_0} \frac{N}{N_c} \right). \end{aligned} \tag{25}$$

Here we introduce

$$N_c = \frac{4\omega^2/\pi}{e^2\omega_s\omega'_o} \left( \frac{n}{iz_u} \right)$$

the threshold number of particles for the effect of the noise suppression /8/. One can see that heating can be significant provided initial temperature is small

$$\frac{N}{N_c} \gg \theta_o \quad (26)$$

For long bunches ( $\pi < \theta_o < 2\pi$ ) the energy of coherent motion in  $\mathcal{E}$  decreases  $\theta_g/\theta_o$  ( $\theta_g = 2\pi - \theta_o$ ) times.

Then

$$T_f = T_i + \frac{\theta_g}{\theta_o} \cdot \frac{Ne^2\omega_s}{\sqrt{2\pi}} \left( \frac{iz_u}{n} \right)$$

and condition (26) becomes more stronger

$$\frac{N}{N_c} \gg \frac{\theta_o^2}{\theta_g}, \quad \theta_o > \theta_g \quad (26.a)$$

This heating of a beam by nonequilibrium coherent noise is not specific for Coulomb interaction only. The same formulae are valid for any interaction (electrodes and so on), which do not produce coherent instabilities, provided, certainly, that dissipation is negligible.

Another important result can be obtained by calculation of relaxation time. It is given by eq. (19)

$$N\lambda_o = \sum_n \lambda_n. \quad (27)$$

In the l.h.s. we have the sum of decrements for beam particles and it is equal to the same of coherent modes. This is, so-called, the theorem of the sum of decrements of coherent oscillations. Formerly this was established in ref. /9/ for the beam without frequency spread. Eq. (27) generalize this statement for beams with non-zero frequency spreads.

From general point of view, eq. (27) allows one to estimate the ability of the particular cooling system to cool down the intense beams. By the order of value

$$\lambda_n \simeq \frac{N}{N_{ex}} \lambda_0$$

and in order to provide coherent stability of the beam this should be less than revolution period  $2\pi/\omega_s$ :

$$\frac{N\lambda_0}{N_{ex}} < \frac{\omega_s}{2\pi}$$

So, the cooling will be not accompanied by coherent instabilities, if

$$N < \frac{N_{ex} \omega_s}{2\pi \lambda_0} = W \tilde{\epsilon}_{cool}, \quad (28)$$

where  $W$  is the cooling system "bandwidth". Formerly the same limitation was obtained in Ref. /10/ for stochastic cooling systems.

We should now return back to Coulomb interaction. Let us estimate  $\lambda_0$  for this case. For the Gaussian energy distribution the decrement of Landau damping has the form

$$\lambda_n = \sqrt{\frac{\pi}{2}} \frac{\Omega_n^4}{|n\Delta\omega|^3} \exp\left(-\frac{\Omega_n^2}{2n^2\Delta\omega^2}\right). \quad (29)$$

Substituting this in eq. (27) we shall get

$$\lambda_0 = \sqrt{\frac{\pi}{2}} \frac{1}{N} \sum_{n=1}^{N_{ex}/2} \frac{\Omega_n^4}{|n\Delta\omega|^3} \exp\left(-\frac{\Omega_n^2}{2n^2\Delta\omega^2}\right). \quad (30)$$

For the beams cold enough,  $N_{ex}$  can be very high (see section 4). Therefore we can replace the summation over  $n$  in eq. (30) by integration and  $N_{ex}$  - by infinity. This yields

$$\lambda_o = \frac{\Delta\omega}{N} \sqrt{\frac{\pi}{2}} \left\{ \frac{n_o^2}{2} \left( \frac{N}{N_c} \right)^2 \exp\left(-\frac{N}{2N_c}\right) + \right. \\ \left. + n_d^2 \left( 1 - \exp\left[-\frac{n_d^2}{2n_o^2}\right] \right) \right\},$$

where

$$n_d^2 = \left. \frac{\Omega_n^2}{\Delta\omega^2} \right|_{n>n_o} = \frac{2Ne^2R_o}{\pi a^2 T} \simeq n_o^2 \frac{N}{N_c} \quad (32)$$

is a harmonic number corresponding to Debye radius  $\chi_d = R_o/n_d$ . But in cold beams  $N \gg N_c$  and so,  $n_d \gg n_o$ . Under these conditions, eq. (31) can be simplified and rewritten as

$$\lambda_o \simeq \frac{n_d^2 \Delta\omega}{N} \simeq \frac{e^2}{a^4 p} \quad (33)$$

where  $\Delta p$  is momentum spread in the beam.

It is interesting to note the formal coincidence of eq. (33) for  $\lambda_o$  with the asymptotical expression for the cooling rate of a cold beam in stochastic cooling method /10/.

$$\lambda_{st. cool} \simeq \frac{W \omega_s^2}{N}, \quad (34)$$

where  $W \omega_s / 2\pi$  is the bandwidth of the cooling feed-back system. The value of  $W$  is determined by parameters of the feedback and is constant while cooling. For Coulomb interaction the analogous value  $n_d$  increases like  $1/(a\Delta\omega)$  during cooling and can be very high. Anyway,  $W \leq n_o$ , so we can write

$$\lambda_o \gg \lambda_{st. cool} \quad (35)$$

In practice, the value of  $\lambda_o$  can be not small. Say, for parameters of NAP-M /2/:  $a = 0.01$  cm,  $\Delta p/p \simeq 10^{-6}$  (with the beam current  $I \leq 10 \mu A$ ) eq. (33) gives

$$\lambda_o = 10^5 / \text{sec.}$$

The dependence of  $\lambda_o$  on  $\Delta p$  corresponds to the friction force

$$|F_n| \approx \frac{e^2}{a^2}$$

independent of particles velocities, which is specific for the so-called "dry friction".

### 3. Equilibrium temperature of cooled beam

Let us consider now the current dependence of  $\bar{T}$  for the beam in the storage ring with electron cooling. This time eq. (19) should be modified:

$$\begin{aligned} \frac{dT_n}{dt} &= -2\lambda_n (T_n - T), \\ \frac{dT}{dt} &= \sum_n \frac{2\lambda_n}{N} (T_n - T) - 2\lambda \bar{T} + d + \left(\frac{dT}{dt}\right)_{fast} \end{aligned} \quad (36)$$

where  $\lambda$  and  $d$  are cooling and diffusion rates, produced by cooler,  $(dT/dt)_{fast}$  - describes the contribution from fast collisions.

System (36) also has an equilibrium. In adiabatical limit [ $(dT/dt)_{fast} \rightarrow 0$ ] the equilibrium temperature is given by

$$T = T_n = T_0 = \frac{d}{2\lambda} \quad (37)$$

and does not depend on  $N$ . Since cooling down, the interaction energy is distributed between new collective modes.

If the contribution from fast collisions is not small,  $\bar{T}$  will increase with the beam current. So, let us estimate the region of parameters, which corresponds to adiabatical collisions. Representation of a beam as that consisting of disks with constant transversal energy ( $M\omega_b^2 a^2$ ) will be valid until for any couple the time, taken to pass average distance between particles  $\bar{l}/N$ , will exceed the periods of betatron oscillations:

$$\frac{N}{\bar{N}} \frac{\omega_b}{\omega'_b R_0 \Delta p} > 1,$$

or (38)

$$N < N_{tr} = \frac{\pi \nu_b}{\gamma (\Delta P/P_s)}.$$

Thus, we can summarize the current dependence of  $\bar{T}$  in a cooled beam. If  $N < N_{tr}$ , the equilibrium temperature of the beam does not depend on  $N$ . For  $N > N_{tr}$ ,  $\bar{T}$  will increase with  $N$  due to fast collisions of particles. Such depression of IBS in a cold beam was seen experimentally at NAP-M [2]. Estimation of  $N_{tr}$  for NAP-M parameters yields  $N_{tr} \approx 3 \cdot 10^7$ , which agree with results of these measurements.

#### 4. The crystallization of a cold beam

An increase in a specific heat (see eq. (22)) and depression of IBS in a cold beam mean that at low temperatures the properties of the beam should be close to that of a crystal. The last ones are mainly determined by significant spatial ordering of particles placement along the beam.

In nonrelativistic beams the transversal ordering can be hardly expected due to high betatron frequencies spreads. On the contrary, the revolution frequency spread is small, when the beam is cooled down. Thus, the presence of a numerous collective oscillations in equilibrium amplifies the correlations in spatial longitudinal distribution of particles along the beam.

Thermodynamical properties of the beam in equilibrium can be described using the statistical sum. In adiabatical limit (38) it is given by

$$\mathcal{Z}_N = \int d\Gamma_N f_N = \int \left( \frac{dp d\theta R_0}{2\pi\hbar} \right)^N \frac{f_N}{N!} \quad (39)$$

Here  $2\pi\hbar$  is Planck constant;

$$f_N = \exp \left[ - \sum_{k=1}^N \frac{p_k^2}{2\mu T} - \sum_{k,j}^N \frac{U_{kj}}{2T} \right]$$

is  $N$ -particles distribution function,  $\mu^{-1} = R_0 \omega'_0$  is the effective mass of longitudinal motion;

$$\frac{U_{kj}}{2T} = \sum_n \xi_n \exp(i n [\theta_k - \theta_j]), \quad (40)$$

$$\xi_n = \frac{e^{i\omega_s}}{4\pi T} \left( \frac{iZ_n}{n} \right) = \frac{1}{2N} \begin{cases} \frac{N}{n}, & |n| < n_0 \\ \left( \frac{n_0}{n} \right)^2, & |n| > n_0 \end{cases} \quad (41)$$

Let us rewrite  $Z_N$  in the form

$$Z_N = Z_N^0 \exp \left( \sum_n N \xi_n \right) Q_N, \quad (42)$$

where

$$Z_N^0 = \frac{1}{N!} \left( \frac{R_0}{\hbar} \sqrt{2\pi\mu T} \right)^N$$

is the statistical sum of the ideal gas and

$$Q_N = \frac{\int d\theta_1 \dots d\theta_N}{(2\pi)^N} \exp \left( - \sum_n \xi_n |\rho_n|^2 \right) \quad (43)$$

with

$$\rho_n = \sum_{k=1}^N e^{-in\theta_k}$$

$n$ -th harmonic of the beam density.

Below we shall calculate thermodynamical values, which are determined by free energy  $F$  and by its derivatives over temperature. Free energy itself is given by

$$F = -T \ln Z_N$$

or, omitting the items independent on  $T$

$$F = -T \ln \bar{Z}_N^0 - T \ln Q_N = F_0 + \Delta F. \quad (44)$$

The way of calculation of  $Q_N$  depends on ratio between  $N$  and  $\kappa_d$ . If  $N \gg \kappa_d$ , it is convenient to use

$$\begin{aligned} \langle |\rho_n|^2 \rangle &= \int \frac{d\Gamma_N}{\bar{Z}_N^0} |\rho_n|^2 f_N = \frac{1}{Q_N} \int \frac{d\theta_1 \dots d\theta_N}{(2\pi)^N} |\rho_n|^2 \exp(-\sum_n \bar{\xi}_n |\rho_n|^2) \\ &= - \frac{\partial}{\partial \bar{\xi}_n} \ln Q_N \quad , \quad Q_N (\bar{\xi}_n = 0) = 1. \end{aligned} \quad (45)$$

The l.h.s. of eq. (45) provided by  $N \gg \kappa_d$  can be obtained from eq. (11) (see also /8/):

$$\langle |\rho_n|^2 \rangle = \frac{N}{1 + N \bar{\xi}_n}.$$

Integration of eq. (45) over  $\bar{\xi}_n$  yields

$$Q_N = \prod_n \frac{1}{1 + N \bar{\xi}_n}$$

and, so

$$\Delta F = -T \ln Q_N = T \sum_n \ln (1 + N \bar{\xi}_n). \quad (46)$$

Due to fast convergence the summation over  $n$  in eq. (46) can be expended over  $|h| < \infty$ . Eq. (46) corresponds to calculation of  $Q_N$  in the so-called "ring approximation".

Making summation over  $n$ , with additional condition  $\kappa_d \gg \kappa_0$ , yields

$$\Delta F = 2\pi \kappa_d T. \quad (47)$$

This gives for energy  $\mathcal{E}$ , specific heat and entropy of the beam following expressions:

$$\mathcal{E} = -T^2 \frac{\partial}{\partial T} \left( \frac{F}{T} \right) = \frac{NT}{2} \left( 1 + \frac{2\pi \kappa_d}{N} \right), \quad (48)$$

$$C = \frac{\partial \mathcal{E}}{\partial T} = \frac{N}{2} \left( 1 + \frac{2\pi n_d}{N} \right), \quad (49)$$

$$S = -\frac{\partial F}{\partial T} = N \ln \left( \frac{e R_0}{N h} \sqrt{2\pi \mu T} \right) + \frac{N}{2} \left( 1 - \frac{2\pi n_d}{N} \right), \text{ here } (50)$$

In these formulae the interaction of particles is described by ratio  $2\pi n_d/N$  - of average distance between particles to sheelding radius  $1/n_d$ . One can see, that approaching of  $n_d$  to  $N/2\pi$  leads to significant decrease of entropy and to duplication both of  $\mathcal{E}$  and  $C$ :

$$\mathcal{E} \rightarrow NT, \quad C \rightarrow N. \quad (51)$$

Such variation of thermodynamical values is caused by significant ordering of relative motion of particles inside beam produced by collective interaction. Comparison of eqs. (48,49) and (22) yields the average number of excitations in equilibrium

$$N_{ex} = 2\pi n_d < N \quad (52)$$

It increases towards  $N$  since cooling down the beam.

Equations (46)+52) become not valid provided by  $n_d \gg N$ . In this region  $\rho_N$  can be calculated assuming that  $\theta_k$  are close to points  $2\pi k/N$ :

$$\rho_n \approx -i\hbar \sum_{k=1}^N \zeta_k \exp\left(-\frac{2\pi i k n}{N}\right), \quad \theta_k = \frac{2\pi k}{N} + \zeta_k, \quad (53)$$

$$|\zeta_k| \ll \frac{2\pi}{N}.$$

Substitution of eq. (53) into  $f_N$  gives

$$\exp\left(-\sum_n \zeta_n |\rho_n|^2\right) = \exp\left(-\sum_n \zeta_n n^2 \sum_{kj} \zeta_k \zeta_j \exp\left[\frac{2\pi i n}{N}(k-j)\right]\right).$$

Omitting here the values of the order of  $(n_d/N) \ll 1$ , this can be replaced by

$$\exp\left[-\frac{n_d^2}{2} \sum_{k=1}^N \zeta_k^2\right],$$

or

$$f_N = \exp \left[ - \sum_{K=1}^N \frac{\rho_K^2}{2\mu T} - \frac{\kappa_d^2}{2} \sum_{K=1}^N \left( \theta_K - \frac{2\pi K}{N} \right)^2 \right], \quad (54)$$

which agree with localization of particles near equilibrium points  $2\pi K/N$  with dispersion

$$\langle \zeta_K^2 \rangle = \frac{1}{\kappa_d^2} \ll \left( \frac{2\pi}{N} \right)^2 \quad (55)$$

We should underline that eq. (54) corresponds to very strong collective correlations in the beam, which can not be calculated in quasilinear approximation. The physical meaning of a parameter  $\kappa_d$  also changes. It is no more the shielding radius, but the average amplitude of oscillations of particle near equilibrium points  $2\pi K/N$ .

Calculation of thermodynamical values of the beam with distribution function (54) is trivial and leads to well known expressions /11/

$$F = -N \ln \frac{T}{\hbar \omega_1}, \quad S = N \left[ \ln \frac{T}{\hbar \omega_1} + 1 \right] \\ E = NT, \quad C = N, \quad (56)$$

which coincide with that of a onedimensional crystal at high temperatures ( $T \gg \hbar \omega_1$ ,  $\omega_1$  - is plasma frequency of the beam).

So, we can write down the criterion for transition of a cold beam into crystal (or exactly ordered /11/) state

$$\frac{2\pi \kappa_d}{N} \geq 1. \quad (57)$$

It is not surprising that transition to crystal state is not accompanied by critical phenomena. Due to longrange interaction between particles the state of the beam with a reasonable temperature is the mixture of ordered and random phases. The variation of the beam temperature changes the

ratio between both components of this mixture.

The amplification of ordering effects, when cooling down the beam, justifies the choice of  $\pi/N$  as a spatial parameter in adiabaticity condition (38). The longitudinal mobility of particles inside the beam is depressed by their collective interaction.

We thank V.Parkhomchuk and A.N.Skrinsky for encouraging discussions.

---

References

1. V.V.Parkhomchuk, D.V.Pestrikov. Preprint IYaPh N77-31, Novosibirsk 1977.
2. E.N.Dementiev et al. J.T.Ph., 50, N 8, 1717, 1980.
3. A.Piwinski. Proc. of the IX Intern. Conf. on High Energy Accelerat., p. 405, Stanford, 1974.
4. V.I.Kudelainen et al. JETPh, 82, N 6, 2056, 1982.
5. Ya.S.Derbenev, A.N.Skrinsky. Preprint IYaPh N 79-87, Novosibirsk 1979.
6. U.L.Klimontovich. Statistical theory of nonequilibrium processes in plasma. MGU: 1964.
7. N.S.Dikansky, D.V.Pestrikov. Preprint IYaPh N 84-48. Novosibirsk 1984.
8. V.V.Parkhomchuk, D.V.Pestrikov. JTPh 50, N 7m 1411, 1980.
9. Ya.S.Derbenev, N.S.Dikansky, D.V.Pestrikov. Proc. of the II USSR Nation. Accelerat. Conf. Moscow, 1970, Moscow: Nauka 1972.
10. V.V.Parkhomchuck, D.V.Pestrikov. Preprint IYaPh N 80-170, Novosibirsk 1980.
11. L.D.Landau, E.M.Lifshitz. Statistical physics. Moscow 1964.

A COMPARISON BETWEEN ELECTRON COOLING AND STOCHASTIC COOLING

D. Möhl  
CERN, CH-1211 Geneva, Switzerland

1. Introduction

The two cooling methods<sup>1-7</sup> have been compared in a number of papers<sup>7-10</sup>. Most authors agree that stochastic and electron cooling are complementary in their dependence on many of the basic machine and beam parameters. There is little to be added to this general finding.

In the present talk, I will try to illustrate the complementary character in some detail for the specific case of transverse cooling in a hypothetical "model ring". To do so, I invite you to go through some simplified, and hence very approximate, design considerations for a cooling system of either kind. During the course of this exercise, some points of comparison will hopefully emerge.

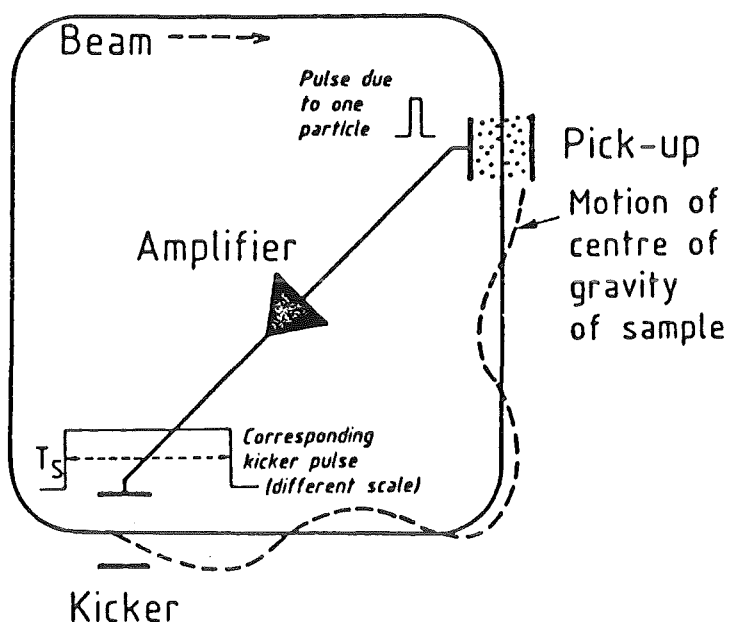
2. The stochastic cooling system

Fig. 1 : The principle of horizontal stochastic cooling

The pick-up measures horizontal deviation; the kicker corrects angular deviation. They are spaced by a multiple plus one quarter of the betatron wavelength. A position error at the pick-up transforms into an error of angle at the kicker. This angular error is corrected. For a beam of many particles, the system corrects the centre of gravity of successive beam samples. The sample length  $T_s = 1/(2W)$  is the time interval during which the kicker pulse due to each single particle is present. It is given by the bandwidth  $W$  of the system. Due to momentum spread, particles migrate between samples and this mixing continuously exchanges the sample populations.

Assuming that you are familiar with the principles (Fig. 1), let us start by writing down the simplified equation for the cooling rate of betatron amplitude :

$$\frac{1}{\tau} = \frac{W}{2N} [2g(1 - \tilde{M}^{-2}) - g^2(M + U/Z^2)] \quad (1)$$

coherent effect (cooling)      incoherent effect (heating)

N : number of particles in the beam

W : cooling system bandwidth

g : "gain" parameter ( $g < 1$ )

M : desired beam mixing on the way kicker to pick-up ( $M > 1$ )

$\tilde{M}$  : undesired beam mixing on the way pick-up to kicker ( $\tilde{M} > 1$ )

U : noise to signal ratio ( $U > 0$ ) for (anti-)protons

Z : charge number of particle.

"Optimum" conditions are reached when the gain is chosen such that the term in the square bracket is maximum. The corresponding g and  $1/\tau$  are:

$$g_0 = (1 - \tilde{M}^{-2})/(M + U/Z^2)$$
$$\frac{1}{\tau_0} = \frac{W}{2N} [(1 - \tilde{M}^{-2})^2 / (M + U/Z^2)] \quad (2)$$

This choice of g will be assumed throughout in what follows. All that remains to be done then is to pickup values for N, Z, W, M,  $\tilde{M}$  and U.

We take it that the number of particles and their charge state are given by the peculiarities of our cooler ring. To be specific, let us assume  $N = 10^9$ ,  $Z = 1$ . As to the bandwidth, looking at what has been achieved (see Table 1), we take  $W = 0.5$  GHz as a well established state of the art figure. The two mixing factors to be discussed next are closely related to W. In fact, we may interpret M, the number of turns for mixing, in terms of the "migration"  $\Delta T = |\eta|T \Delta p/p$  of a typical off-momentum particle with respect to the nominal particle ( $\Delta p = 0$ ). Here  $\eta = 1/\gamma_{transition}^2 - 1/\gamma^2$  is the off-momentum function of the storage ring, and T the revolution time. We expect good mixing if this migration is comparable to a sample length  $T_s = 1/2W$ .

Table 1

Effective bandwidths used or proposed

|                               |        |      |     |
|-------------------------------|--------|------|-----|
| ISR                           | (1975) | 0.1  | GHz |
| ICE                           | (1976) | 0.25 | GHz |
| AA (precooling)               | (1980) | 0.5  | GHz |
| Fermilab                      | (1986) | 2    | GHz |
| ACOL                          | (1986) | 2    | GHz |
| Source for<br>20 TeV collider | ( ? )  | 5    | GHz |

Hence, we put

$$M \propto \frac{T_s}{\Delta T} = (2 |\eta| T W \frac{\Delta p}{p})^{-1}$$

All the finer peculiarities are hidden in the proportionality constant. We avoid going into a painful discussion of details by assuming  $M = 1$  for  $\Delta p/p = 10^{-2}$ .

In a similar way, the unwanted mixing is given by the time lag  $\Delta T_{PK}$  of a typical off-momentum particle with respect to the cooling signal on the way from pick-up to kicker. In a regular lattice, this lag is proportional to the migration per turn  $\Delta T$ . To work out  $M$ , we compare  $\Delta T_{PK}$  to the useful width  $T_c$  of the correction pulse due to a single particle. This pulse width is in turn proportional to the sample length. Hence, we may write:

$$\tilde{M} \propto \frac{T_c}{\Delta T_{PK}} \propto \frac{T_s}{\Delta T} \propto M$$

Again, to avoid lengthy details, we fix fairly arbitrarily :

$$\tilde{M} = 2 \cdot M$$

We note, in passing, the importance of a good choice of transition energy: for a given bandwidth and given  $\Delta p/p$ , we get too much mixing ( $M \approx 1$ ) if  $|\eta| T W \Delta p/p$  is considerably larger than 1 and not enough mixing ( $M \gg 1$ ) in the opposite limit. Extreme bandwidth only pays if  $|\eta| T \Delta p/p$  is small enough.

The final parameter to be fixed is the noise to signal power ratio  $U$ . The noise is determined by the characteristics of the amplifier system whereas the signal depends on a variety of parameters, among them the beam intensity, the number and the sensitivity of the pick-ups and - most important in the present context - the ratio of "plate spacing to beam size" for the case of position sensitive electrodes. All we want to retain is this proportionality of the signal power with the square of the beam size  $a$ : Hence we take

$$U \propto \frac{1}{a^2} \propto \frac{1}{E} \quad (3)$$

Here  $E$  is the beam emittance. In writing down (3), we assume fixed pick-up plates. If, instead, the plates are moved mechanically to stay always close to the beam edge, then  $U$  is independent or only weakly dependent on beam size and good conditions ( $U \lesssim 1$ ) can be maintained as cooling proceeds. Such movable pick-ups will be used in the  $\bar{p}$  accumulator ACOL !

Basing our considerations here on fixed pick-ups, we will assume that good signal to noise ratio ( $U = 1$ ) is reached for an emittance of  $100 \pi \text{ mm.mrad}$ . We thus arrive at the model parameters summarized in Table 2.

Table 2

Parameters assumed for stochastic cooling

|             |                               |
|-------------|-------------------------------|
| $N$         | $10^9$                        |
| $W$         | 500 MHz                       |
| $M$         | $10^{-2}/(\Delta p/p)$        |
| $\tilde{M}$ | 2M                            |
| $U/Z^2$     | $(100 \pi \text{ mm.mrad})/E$ |

Resulting cooling times are compiled in the first part of Table 3 where from one column to the next, we half both the momentum spread and the emittance.

Table 3

Comparison of stochastic ( $\tau_s$ ) and electron ( $\tau_e$ ) cooling.  
Time constant  $\tau$  as a function of beam emittances

|                      |     |    |      |      |     |     |      |      |                       |
|----------------------|-----|----|------|------|-----|-----|------|------|-----------------------|
| $E_H$                | 100 | 50 | 25.0 | 12.0 | 6.0 | 3.0 | 1.5  | 0.75 | $\pi \text{ mm.mrad}$ |
| $\frac{\Delta p}{p}$ | 10  | 5  | 2.5  | 1.2  | 0.6 | 0.3 | 0.15 | 0.07 | $\times 10^{-3}$      |
| $\tau_s$             | 14  | 18 | 33   | 65   | 128 | 256 | 512  | 1024 | s                     |
| $\tau_e$             | 64  | 25 | 10   | 5    | 3   | 2   | 1.3  | 1.2  | s                     |

### 3. The electron cooling system

As we have been very qualitative with stochastic cooling, we feel free to be approximate with the electron system as well. We take the cooling time given by <sup>4)</sup>

$$\tau = \frac{k e}{r_p r_e L_c} \frac{\beta^4 \gamma^5 (\theta_e^2 + \theta_p^2)^{3/2}}{J \eta_c} \quad (4)$$

$k = 0.16 - 0.6$  form factor (0.16)

$\theta_e \approx v_{e\perp} / \beta c$  electron beam divergence ( $2 \cdot 10^{-3}$ )

$$\theta_p = \left[ \frac{E_h}{\pi \beta_H} + \frac{E_v}{\pi \beta_V} + \left( \frac{1}{\gamma} \frac{\Delta p}{p} \right)^2 \right]^{1/2}$$

$\beta_H, V$  horizontal and vertical focusing function of storage ring at cooling section ( $\beta_H = 2 \text{ m}$ ,  $\beta_V = 5 \text{ m}$ )

$E_{H,V}$  horizontal and vertical beam emittance ( $E_H = 2 \text{ E}_V$ )

$j$  electron beam current density ( $0.25 \text{ A/cm}^2$ )

$L_c$  Coulomb logarithm (10)

$$\begin{aligned} \eta_c & \quad \text{cooling length/circumference (0.02)} \\ e & = 1.6 \times 10^{-19} \text{ As} \quad \beta = v/c \quad (0.3) \\ r_e & = 2.8 \times 10^{-13} \text{ cm} \quad r_p = 1.5 \times 10^{-16} \text{ cm} \end{aligned}$$

In practical units (taking  $\tau$  in s,  $j$  in Amp/cm<sup>2</sup> and  $\theta$  in mrad):

$$\tau = 0.06 \frac{\beta^4 \gamma^5}{j \eta} \left( \frac{\theta_e^2}{e} + \frac{\theta_p^2}{p} \right)^{3/2} \quad (4a)$$

Using the "model parameters" given in parenthesis under eq. (4), we may write

$$\begin{aligned} \tau &= 0.12 \left( 4 + \frac{\theta_p^2}{p} \right)^{3/2} \\ \theta_p &= \sqrt{0.6 \frac{E_h}{\pi} + \left( 0.95 \frac{\Delta p}{p} \right)^2} \quad (\text{in mrad}) \end{aligned} \quad (4b)$$

We can then complete Table 3 to include the electron cooling times

Several remarks concerning eq. (4) are now in order. We have taken  $k$  to be constant ( $k = 0.16$ ) independent of  $\theta_p$  and  $\theta_e$ . For large proton angles  $\theta_{p//} \approx \theta_{p\perp} > \theta_e$ ,  $k$  may be larger and eq. (4b) may then underestimate the cooling time. We have also assumed overlap of electron and ion beam, even for very large emittance. Thus, we are optimistic for large beams. On the other hand, we have neglected many details, especially the effect of the magnetic field<sup>3, 4</sup> which can increase the cooling speed for the small beam. Thus, the increase of cooling time with beam size may be more pronounced than observed from Table 3.

### 3. Comparison and conclusion

The behaviour of the two cooling time constants with beam size ( $E_h$  and  $\Delta p/p$ ) is illustrated in Fig. 2 which clearly indicates the efficiency of electron cooling for the cold and of stochastic cooling for the hot beam. This behaviour (sketched in Fig. 3) very naturally suggests combining core cooling by electrons with stochastic pre-cooling and cleaning of the beam halo.

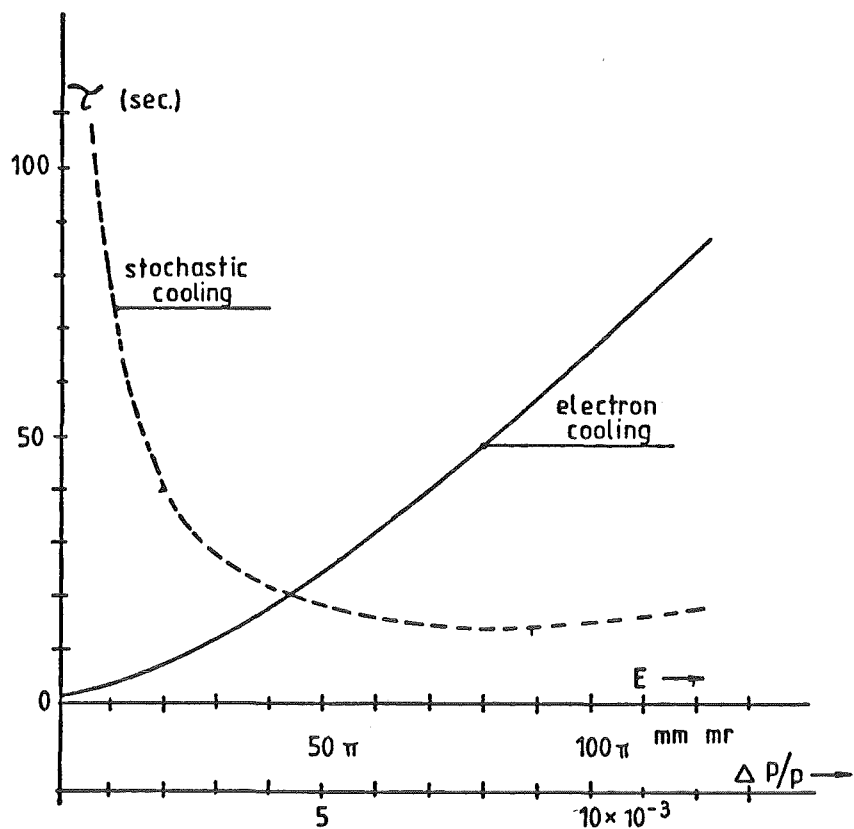


Fig. 2 : Stochastic and electron cooling time as a function of beam emittance.

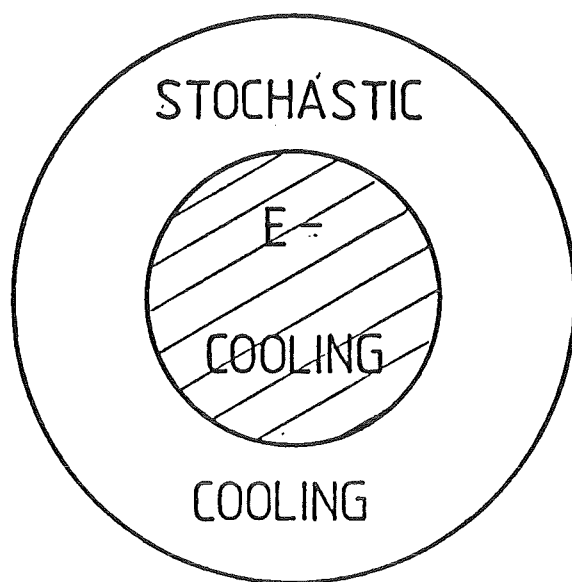


Fig. 3 : Sketch of beam cross-section to indicate regions where one of the two cooling methods is most efficient. The combination of "core cooling" by electrons with "halo cooling" by the stochastic method is capable of taking advantage of both of them.

Clearly, the detailed comparison depends very much on the exact parameters of the cooling ring and more precise design equations have to be taken for a real machine. Yet, I hope that our example has correctly illustrated one of the trends. The more general comparison and the conclusions which have been drawn many times before may be summarized as:

1. Stochastic and electron cooling are largely complementary:

- Stochastic cooling works well for large emittance beams.
- Electron cooling works well for beams which are already very cool.
- Stochastic cooling is therefore well adapted to the accumulation of rare particles, ~~the compensation of large blow-ups~~, the recuperation of large amplitude particles.
- Electron cooling is ideal to provide highly monochromatic sharply collimated beams and to keep the beam centre cool.
- Stochastic cooling depends strongly on particle number and weakly on energy.
- The inverse is true for electron cooling (but it has never been tested for more than  $10^9$  particles, so far!).
- Stochastic cooling needs many pieces of straight section space and a separate system for each - horizontal, vertical and momentum - cooling.
- Electron cooling needs one relatively long piece of space; it works simultaneously in all three planes.

2. The combination of stochastic and electron cooling will open new possibilities in LEAR and could also be very handy in other accumulation and cooling rings.

REFERENCES

1. G.I. Budker, Atomnaya Energiya (Sov. I. of Atom. Energy) 22 p. 346 (1967); see also in: International Symposium on Electron and Positron Storage Rings, Saclay 1966.
2. S. van der Meer, Stochastic damping of betatron oscillations, CERN Int. Report ISR-PO/72-31 (1972).
3. G.I. Budker, A.N. Skrinsky, Sov. Phys. Usp. 21, p. 277 (1978).
4. G.I. Budker et al., Studies on electron cooling ... CERN Report 77-08.
5. F. Sacherer, Stochastic cooling theory, CERN Int. Report ISR/TH 78-11 (1978).
6. D. Möhl, G. Petrucci, L. Thorndahl, S. van der Meer, Phys. Rep. 58, p. 75 (1980).
7. F.T. Cole, F.E. Mills, Ann. Rev. Nucl. Part. Sci. 31, p. 295, (1981).
8. A.N. Skrinsky, W.V. Parkhomchuk, Sov. J. Part. Nucl. 12 (3), p. 223 (1981).
9. D. Möhl, in Proc. of the Workshop on Physics at LEAR..., Erice 1982 (Plenum Press, London, 1984), p. 27.  
K. Kilian, D. Möhl, in Proc. Symp. on Detectors in Heavy Ion Reactions, Vol. 178 of Lecture Notes in Phys., Springer Verl, Berlin, 1982, p. 220.
10. L. Tecchio, in Proc. of Beam Cooling Workshop, Stoughton, Univ. of Wisconsin, Madison, 1982).

Further references on stochastic cooling are given in the Proceedings of the CERN Accelerator School on Antiprotons for Colliding Beam Facilities, CERN 84-15; and in: S. van der Meer, Stochastic cooling and the accumulation of antiprotons (Nobel Lecture in Physics, 1984), CERN preprint PS 84-32 (AA).



## COOLING OF HEAVY ION BEAMS

B. FRANZKE, GSI - Darmstadt, West Germany

### Abstract

This note discusses typical requirements for beam cooling in heavy ion storage rings. By comparison with the cooling of proton beams problems related especially to heavy ions are reviewed. A brief description of the experimental storage ring (ESR) project of GSI-Darmstadt, designed for accumulation and cooling of highly or fully ionized ions up to uranium, is given.

### 1. Typical requirements for heavy ion beam cooling

The progress in beam accumulation and cooling techniques at high energy proton rings is increasingly stimulating the interest of nuclear and atomic physicists in heavy ion storage rings. This is demonstrated by a series of cooler ring projects presented in the past few years in different countries. Extreme angular and energy resolution in atomic and nuclear spectroscopy as well as totally new types of experiments using circulating cold beams are expected. The ring projects cover a wide range of specific energies and ion masses. The ESR (GSI-Darmstadt), for instance, is designed to accept highly or fully ionized beams up to uranium after acceleration to 556 MeV/u in the planned heavy ion synchrotron SIS 18 and should be able to decelerate down to 10 MeV/u. Other rings behind electrostatic machines or cyclotrons (e.g. HSR/Heidelberg) will work typically in the 1-10 MeV/u range or even below 1 MeV/u (CRYRING/Stockholm). All plans for heavy ion cooler rings are based on experimental results<sup>1'2'3</sup> for electron cooling of proton beams in the range 1.4 MeV (Novosibirsk) and 200 MeV (Fermilab) or the practical experience with stochastic high energy antiproton cooling gathered mainly at CERN<sup>4</sup>.

High cooling rates as well as - in principle - extremely small equilibrium values of momentum spread and emittances speak clearly well for the application of electron cooling in heavy ion storage rings. Extrapolations of electron cooling results of the Novosibirsk-group<sup>1</sup>, applied to totally ionized uranium at 50 MeV/u, give rise to expect cooling times in the ms-range, provided the initial temperature of the ion beam is not much higher than that of the electron beam ( $\leq 0.5$  eV) times the ion to electron mass ratio  $A_m/m_e$ . At higher

ion beam temperatures stochastic cooling will compete with electron cooling, if the number of circulating ions is below the band-width of the cooling system.

a) Improvement of primary beam quality

In most cases, the beam intensity in heavy ion rings has to be accumulated by means of radial or longitudinal stacking methods which reduce the phase space density of the injected beam. The application of beam cooling simultaneously to the stacking process will save ring acceptance or enable to attain higher beam currents. The phase space density limit for a given number of stored ions or is determined by space charge forces increasing  $\propto q^2/A$  with the mass number A and the charge state q of the ion. An incoherent betatron tune shift  $\Delta Q_{\perp} \approx -0.05$  due to transverse space charge forces seems to be tolerable in storage rings. The reduced ion number  $N_r$  listed in the following table together with some typical initial and desired beam parameters is related only to this  $\Delta Q_{\perp}$  - limitation, and has to be multiplied by  $\beta^2 \gamma^3 A/q^2$ :

| Beam                                | initial                 | cooled                | cooled                |
|-------------------------------------|-------------------------|-----------------------|-----------------------|
| Transv. emittances ( $\pi$ mm mrad) | $\leq 20$               | $\approx 1$           | $\approx 0.1$         |
| Momentum spread $\Delta p/p$        | $\leq 5 \times 10^{-3}$ | $\approx 10^{-4}$     | $\approx 10^{-5}$     |
| $N_r$ (d.c.)                        | $2.7 \times 10^{13}$    | $1.35 \times 10^{12}$ | $1.35 \times 10^{11}$ |

Other effects - e.g. the longitudinal instability limit, which is proportional to  $(\Delta p/p)^2$  - could set even stronger limits to the allowed number of circulating ions, though, for intermediate or low energies ( $\beta < 1$ ), estimates by means of the Keil-Schnell criterion should be used with caution.

b) Compensation for beam heating

The cooled beam will be heated by scattering processes between circulating ions and atoms at rest either concentrated in an internal target of typically  $1 \text{ ng/cm}^2$  thickness (gas jet or atomic beam) or, at pressures as low as  $10^{-11} \text{ mbar}$  negligible, distributed in the vacuum chamber. Energy loss, small angle scattering, and momentum scattering (energy straggling) will reduce the beam quality and consequently also the efficiency for in-ring experiments. Compensation for this beam heating could be achieved by simultaneous electron cooling. The beam life would then be mainly influenced by charge changing processes in the internal target, by radiative capture of cooling electrons or by large angle scattering. Variable electron beam intensity would be desirable, for instance, to optimize between cooling rate and radiative capture rate. In ring designs for large momentum acceptance and

vanishing dispersion at the position of target and cooling, one will be able to tolerate higher charge change rates by means of a multi-charge operation.

If the circulating beam is bunched, compensation for the mean energy loss is easily done by means of an rf-cavity. In this case, if not disallowed by too high charge changing or large angle scattering rates, the application of larger target thickness up to  $1 \mu\text{g}/\text{cm}^2$  may come into question.

Additional sources of beam heating are intra beam scattering and - mainly incoherent - longitudinal and transversal space charge forces. So far, there are no quantitative estimates to what extend electron cooling could be used as compensation for those effects.

### c) Accumulation of radioactive beams

The ESR-ring described below, operated in the accumulator mode, is able to accept beams with transverse emittances between  $20$  and  $50 \pi \text{ mm mrad}$  and momentum spread up to  $1\%$ . The corresponding beam temperatures are in the order of  $10 \text{ MeV}$ . If the available phase space of the storage ring could be repeatedly made free by sufficiently fast beam cooling, the accumulation of radioactive beams - produced by fragmentation of fast heavy projectiles - to comfortable intensity and brightness should be possible. The radioactive beams are initially very hot with velocity spreads in the order of  $0.01 c$ .

At high relative velocities between ions and cooling electrons ( $\beta_{\text{rel}} \geq 1\%$ ) the electron cooling rates are drastically reduced, and one may attain higher rates by the stochastic cooling method. Therefore, similar to the cooling of antiprotons in the AA-ring at CERN, the application of a two stage cooling method suggests itself. Fast stochastic precooling of the injected turn - before moving it towards the stack - could be combined with consecutive electron (in AA-ring stochastic) cooling of the stack in order to reach excellent beam quality. Assumed a band-width of  $1 \text{ GHz}$  for the pick-up and kicker systems and  $10^7$  to  $10^8$  fragment ions circulating on the injection orbit, cooling times and, correspondingly, accumulation step periods close to or even below  $1 \text{ s}$  should be attained.

## 2. Comparison between proton and heavy ion cooling

### a) Cooling rates

Under identical conditions the electron cooling rates for ions  $R_i$  are, in a good approximation, determined by the proton cooling rate  $R_p$  multiplied by  $q^2/A$ . For instance, the following partially stripped ions will be cooled approximately as fast as protons:  $\text{Ne}^{5+}$ ,  $\text{Ar}^{6+}$ ,  $\text{Kr}^{10+}$ ,  $\text{Xe}^{12+}$ , and  $\text{U}^{16+}$ . For fully ionized ions the cooling rates are increased by the following factors: 5 (Ne), 8.1 (Ar), 15.4 (Kr), 22.1 (Xe), and 35.6 (U).

Stochastic heavy ion cooling works faster than proton cooling only in the amplifier noise limited range, i.e. at very low beam currents ( $10^6$  to  $10^7$  circulating ions at  $v=c$ ) and/or high beam temperature, where it takes profit from the large signal power ( $\propto q^2$ ) of highly charged ions. However, the effective gain in the cooling rate is modest, if low beam temperatures have to be reached, and the cooling time is determined by the increasing number of revolutions needed for the development of totally new mixtures of particle samples. It should be mentioned that - compared to proton cooling - the optimal amplifier gain must be variable according to the mass to charge ratio of the ion.

### b) Beam loss

The beam loss rate due to charge changing collisions between heavy ions and residual gas molecules is determined by the product  $\beta\sigma_t\rho$  ( $\sigma_t$  is the total charge changing cross sections and  $\rho$  the mean gas density in the ring). Experimental cross section data for partially stripped heavy ions - the worst case - are available below 10 MeV/u. Semi-empirical extrapolations of the low energy data for several charge states of uranium ions are plotted in Fig. 1. Two points for  $\text{U}^{91+}$  and  $\text{U}^{92+}$  on carbon recently measured at 437 and 962 MeV/u behind the Bevalac<sup>6</sup> are found to be lower by more than two orders of magnitude.

The following (charge state) survival times of partially and fully ionized uranium ions at a pressure of  $10^{-11}$  mbar are deduced from Fig. 1 and should be strongly underestimated at least for  $\text{U}^{92+}$  at 550 MeV/u:

|                  | 30 MeV/u | 200 MeV/u | 550 MeV/u |
|------------------|----------|-----------|-----------|
| $\text{U}^{78+}$ | 150 s    | 1500 s    | 0.75 h    |
| $\text{U}^{92+}$ | 140 s    | 2.2 h     | 22 h      |

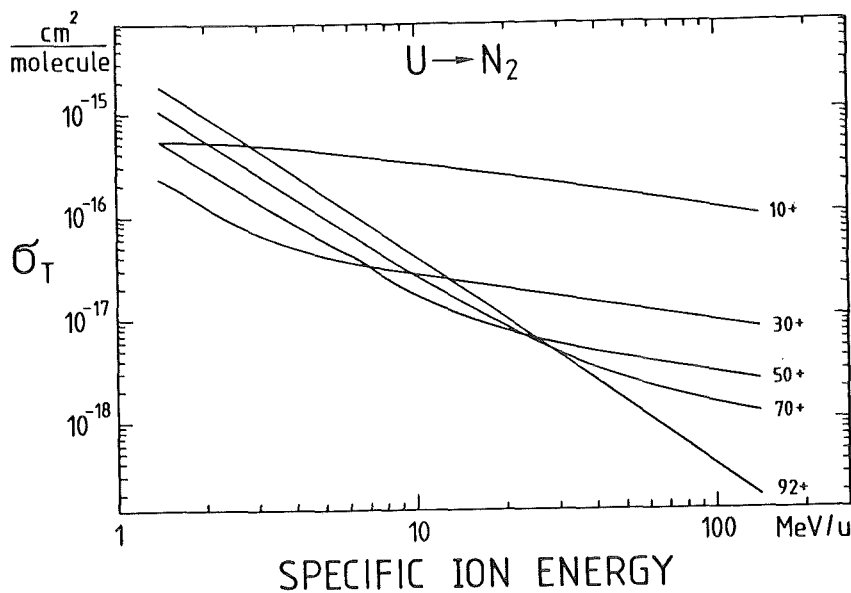


Fig. 1: Total charge changing cross sections<sup>5</sup> for several charge states of uranium incident on nitrogen vs. specific kinetic energy. The curves describe semi-empirical estimates deduced from experimental data below 10 MeV/u.

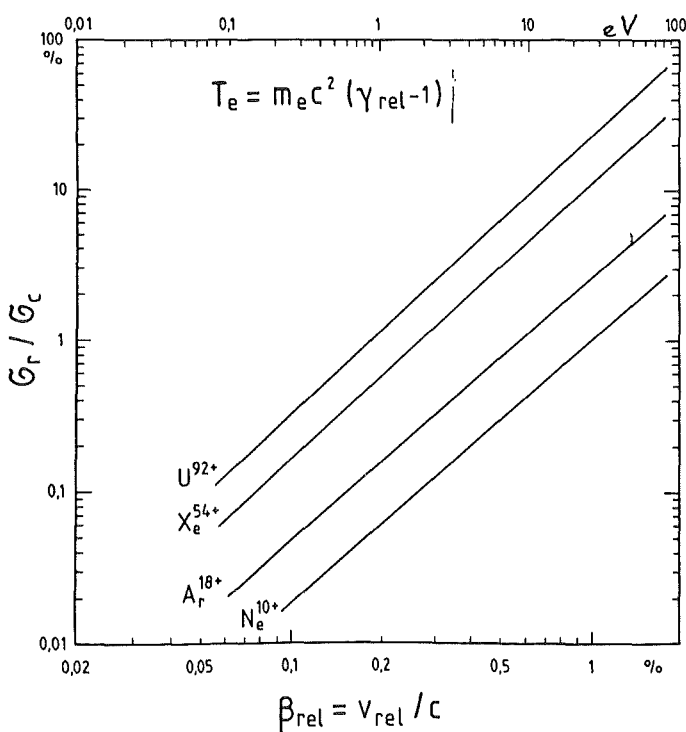


Fig. 2: Ratio of cross sections for electron cooling and recombination  $\sigma_c / \sigma_r$  vs. relative velocity  $\beta_{rel}$  between ions and electrons. At the beginning of the cooling procedure, the mean initial values for the equivalent electron energy  $T_e$  (upper scale) range typically from a few eV (SIS 18-beam) to more than 10 eV (projectile fragment beam). The electron beam 'temperature' is below 0.5 eV.

A more serious problem is the radiative recombination of cooling electrons with the highly ionized ions. The most important quantity is the ratio of recombination<sup>7</sup> to cooling<sup>1</sup> cross sections  $\sigma_r/\sigma_c$  which theoretically turns out to be independent of the ionic charge state and to increase linearly with the ionic mass number. Its quadratic dependence on  $\beta_{\text{rel}}$  is illustrated in Fig. 2. During the cooling process beam losses are expected to be tolerable even for the most massive ions, provided the initial mean  $\beta_{\text{rel}}$  (beam temperature) is not too high. The recombination time of a cold uranium beam interacting continuously with cooling electrons of  $4 \times 10^8/\text{cm}^3$  density over 1 % of the orbit length is estimated to be 11 s. This value seems not to be very comfortable. Therefore, one should, if possible, reduce the electron current density which just avoids beam heating. Anyway, the duration of experiments with the circulating ion beam needing simultaneous electron cooling will be limited to several seconds, at least in the worst case of a highly ionized uranium beam.

c) Ionisation of the residual gas

The ionization power of highly charged ions grows proportionally to  $q^2$ . Hence,  $10^9$  fully stripped uranium ions circulating with 2 MHz in a ring will produce nearly as much secondary ions per meter as a 3 A-electron beam at the same velocity would do, but - in the average - the charge state of secondary ions produced by the ion beam will be much higher<sup>8</sup>. The increased presence of positive charge in the electron cooling section could additionally give rise to instabilities of both the electron and the ion beam. On the other hand, there is some hope, that a compensation for the negative space charge of the electron beam could be advantageous.

d) Diagnostics for beam temperatures

Temperature measurements at both the electron and the ion beam seem to be of essential importance to achieve high performance in cooler ring operation. For heavy ion cooling, in particular, one should look for new methods, making use of the high recombination, ionization and excitation cross sections of highly charged ions. Spectral analysis of radiation emitted during radiative capture of cooling electrons, for instance, could possibly give some valuable information: the width of spectral lines is correlated with the distribution of relative velocities between ions and electrons, i.e. with the temperatures in both the electron and ion beam. If one of the temperatures is known or extremely low, the other could be deduced from the spectral line profile. The recombination rate may be enhanced by suitable laser radiation (laser induced capture).

e) Limits of cooling

The equilibrium phase space density of heavy ion beams will be influenced by space charge effects already at relatively low numbers of circulating ions. Compared to proton beams, the stability or tolerable tune shift limit is reduced by the factor  $A/q^2$ . Intra-beam scattering effects are increased even by the factor  $q^4/A^2$ . At 500 MeV/u the following limits for a fully stripped uranium-beam are estimated:  $3 \times 10^{10}$  for the incoherent tune depression of 0.05 and beam emittances of  $1 \pi \text{ mm mrad}$  in both planes;  $1 \times 10^9$  longitudinal instability limit (Keil-Schnell) for  $\Delta p/p = \pm 1 \times 10^{-4}$  and a vacuum chamber impedance of  $10 \Omega$ . By means of strong (electron) cooling it should be possible to work to some extend against the dilution effects. A quantitative theoretical or simulative, numerical treatment of electron cooling in the presence of the different counteracting dilution effects would give better information about the performance limits of heavy ion cooler rings.

### 3. The Experimental Storage Ring (ESR) project<sup>9</sup>

The ESR is designed for the maximum ion stiffness of 10 Tm and is able to accept  $U^{92+}$  up to 556 MeV/u,  $Ne^{10+}$  up to 834 MeV/u and protons up to 2.2 GeV. The motivation for the ring (Fig. 3) is to provide the following novel facilities for atomic and nuclear studies

- Accumulation of fully ionized ions up to uranium to the highest possible phase space density using various cooling techniques.
- Accumulation and cooling of radioactive ion beams produced by fragmentation or fission of fast heavy projectiles.
- Experiments with circulating beams at energies variable from 10 to 556 MeV/u (uranium) using internal targets, electrons or laser beams as interacting media.
- If feasible, experiments with two colliding beams, co-circulating in the ESR on different closed orbits due to different rigidity (see Fig. 4). Atomic collisions between two highly or fully ionized heavy systems could be studied at collision energies near the Coulomb barrier.
- Quality and energy enhancement of the beams accelerated in the heavy ion synchrotron SIS 18. Slow extraction out of ESR enables to stretch the SIS beam pulse to macroscopic duty factors close to 90 %. In the scheme of further acceleration of totally stripped heaviest ions - for  $U^{92+}$  from 1.0 to 1.35 Gev/u - the ESR plays the role of an intermediate storage and cooler ring.

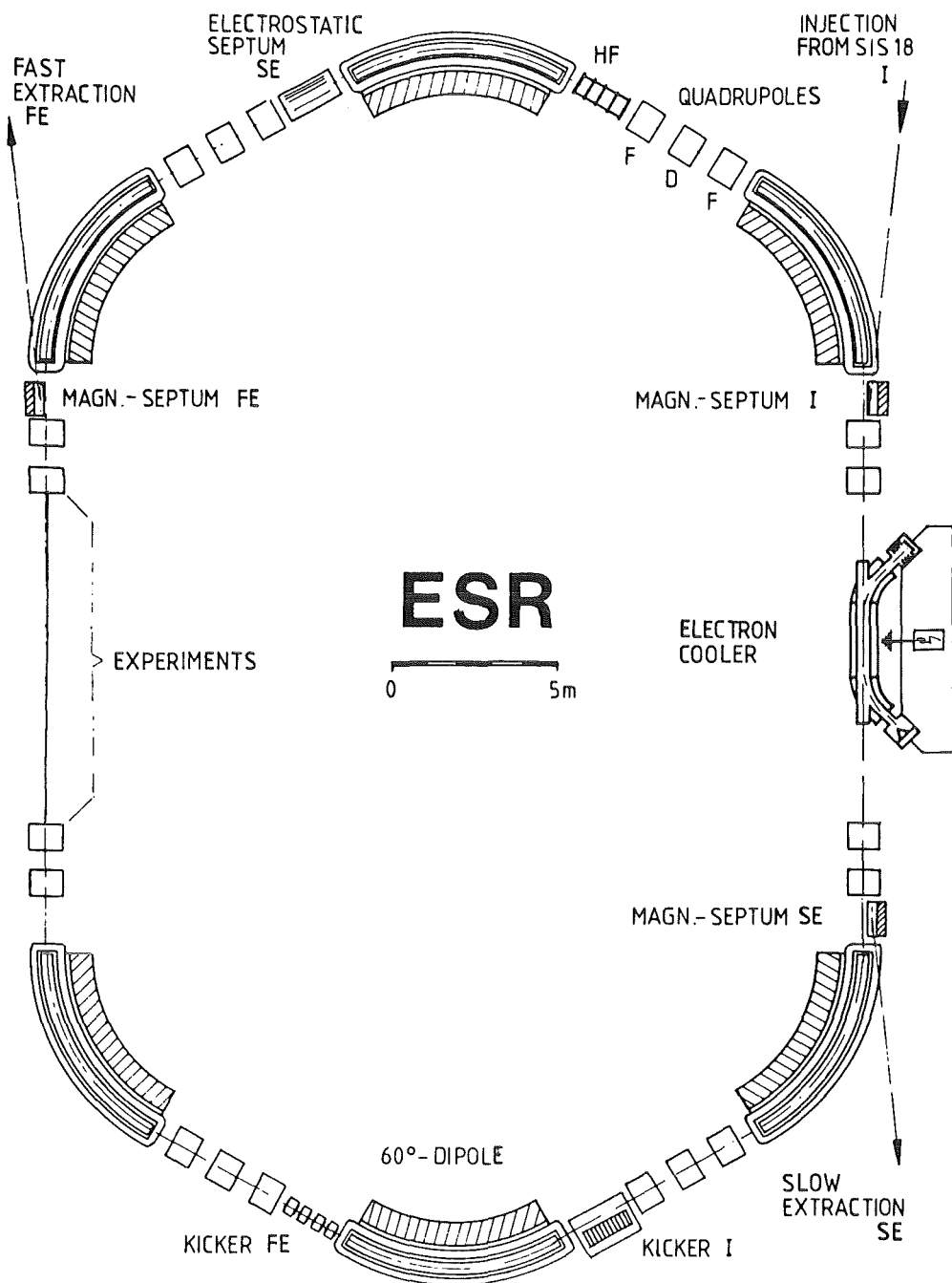


Fig. 3: The Experimental Storage Ring ESR at GSI-Darmstadt.

The circumference of the ESR is 103.2 m. Two 9.5 m long straight sections are provided for the installation of in ring experiment and electron cooling equipment. The magnet structure of ESR enables to match the ion optics to special requirements for electron cooling, internal targets, crossed beams, etc. by means of variable tunes (typically between 2 and 2.5) and variable dispersion function. Elements for injection, fast and slow extraction and an

r.f. cavity will be placed into four 2.5 m and two 1.50 m long straight sections. The smaller gaps between the magnets will be used for higher order corrections, beam diagnostics and stochastic cooling.

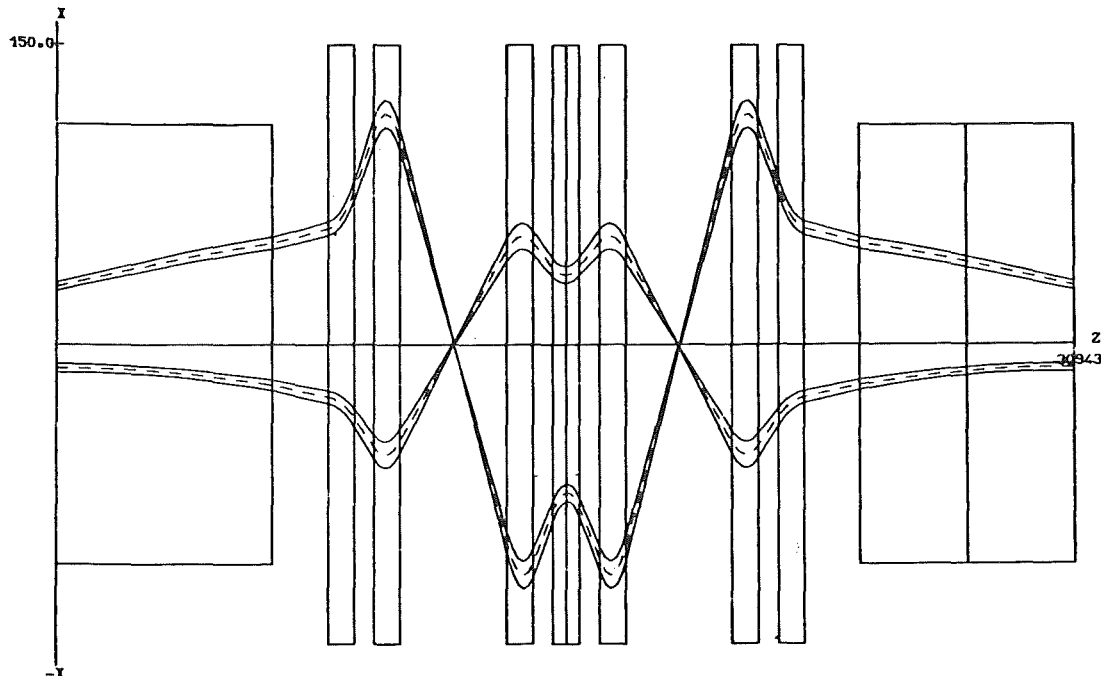


Fig. 4: First approach to the crossing of two cold ( $1 \pi$  mm mrad) beams co-circulating in the ESR. The crossing angle is 100 mrad, the relative momentum difference 1 %. With uranium ions at energies of 550.6 MeV/u and 559.7 MeV/u the same c.m. energy is obtained as by 7.2 MeV/u-uranium impinging on an uranium nucleus at rest. With  $3 \times 10^{10}$  ions in each of the beams one would obtain luminosities of approximately  $5 \times 10^{23} /(\text{cm}^2\text{s})$ . The estimate is based on a incoherent detune limit of 0.05 and  $\Delta p/p = 0.0005$  in each beam without regard to beam-beam effects.

The most important (tentative) parameters of the electron cooling section for the ESR are:

|                                     |              |
|-------------------------------------|--------------|
| Range of specific ion energy        | 10-560 MeV/u |
| Working range for the electron beam | 5-310 keV    |
| Electron current                    | 1-10 A       |

|                                     |                           |
|-------------------------------------|---------------------------|
| Current density $j_e$               | 0.1-1.0 A/cm <sup>2</sup> |
| Electron beam diameter              | 35 - 50 mm                |
| Cathode temperature                 | 0.1 eV (1100 K)           |
| Effective length of cooling section | 2.00 m                    |
| Installation length                 | 4.50 m                    |
| Beam pipe aperture (horiz.)         | 250 mm                    |

Presently, feasibility studies on the desired parameter set for the electron cooling section have been started. The technical design of main components of the ESR (dipoles, quadrupoles, r.f. cavity) is underway. Simultaneously, the beam dynamics calculations are being extended to higher orders to determine the requirements for chromaticity correction and, eventually, for counter-balance of the most severe (high order) magnet imperfections over the large operational range from 0.5 to 10 Tm.

#### REFERENCES:

1. G.I. Budker et al., 5th Nat. Conf. on Particle Accelerators, Dubna/USSR 1976, Proceedings, p. 236 (1976)  
Report on the VAPP-NAP-Group, CERN 77-08 (1977)
2. M. Bell et al., Phys. Letters 87b, 275 (1979)
3. R. Forster et al., IEEE Trans. NS 28.3, 2386 (1981)
4. S. van der Meer, D. Moehl, G. Petrucci, and L. Thorndahl, Phys. Rep. 58, 73 (1980)
5. B. Franzke, IEEE Trans. NS 28.3, 2116 (1981)
6. H. Gould et al., Phys. Rev. Letters 52, 180 (1984)
7. H.A. Bethe and E.E. Salpeter, Quantum mechanics of one and two electron atoms, Springer, Berlin (1957)
8. S. Kelbch, R. Mann, P. Richard, H. Schmidt-Böcking, T. Ullrich, GSI Scientific Report 1983, GSI 84-1, p. 162 (1984)
10. B. Franzke, H. Eickhoff, B. Franczak, B. Langenbeck, GSI-SIS-INT/84-5 (1984)

## STORING AND ELECTRON COOLING OF POLARIZED IONS

E. Steffens

Max-Planck-Institut für Kernphysik, D-6900 Heidelberg,  
Federal Republic of Germany  
and visiting scientist at PS Division, CERN, CH-1211 Geneva,  
Switzerland

### ABSTRACT

Storing and synchrotron acceleration of medium energy polarized ions like protons is reviewed. For short storage times of the order of seconds to minutes the present experience from high energy proton synchrotrons indicates that little depolarization has to be expected. No experiments have been done so far to study depolarization rates for storage times of several hours as well as for simultaneous strong heating and cooling of the beam. Finally it is shown that hyperfine interaction between circulating ions and cooler electrons does not cause depolarization.

## INTRODUCTION

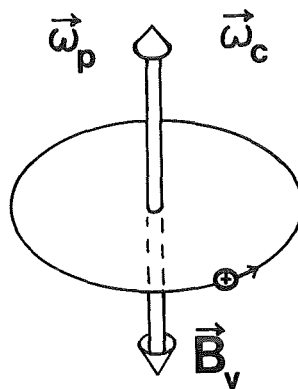
Experiments with stored beams aim at obtaining new experimental information by the improved angular and energy resolution possible in such an arrangement. Using internal polarized targets new observables like the so-called "analyzing power" could be measured. Another class of new observables, e.g., "spin correlation coefficients", becomes accessible, if the circulating beam is polarized, too. Therefore, storing and electron cooling of polarized ions, like proton and deuterons, has been proposed so far for the cooler ring projects at IUCF<sup>1</sup>, Uppsala (CELSIUS)<sup>2</sup> and Jülich (COSY)<sup>3</sup>. In this paper, the problems related to the acceleration of polarized ions are reviewed and the solutions found for high energy machines are presented. Finally, the depolarization caused by the electron cooler is discussed.

Experiments in a storage ring can be performed either using a thin internal target or operating the ring as a collider. The storage times required depend on the availability of the ions to be injected and on other constraints imposed by the experiment. For the IUCF storage ring working with light ions frequently injected from a cyclotron short cycling times of the order of seconds are anticipated. In order to achieve high luminosities internal targets of  $10^{-9}$  g/cm<sup>2</sup> in density and more together with permanent electron cooling will be used. This mode is characterized by short storage times with strong heating and cooling of the beam. For antiprotons circulating in a storage ring it has been proposed<sup>4</sup> to polarize them by an internal polarized hydrogen target (thickness of the order  $10^{-11}$  to  $10^{-10}$  g/cm<sup>2</sup>) which acts as a filter for one substate. In this case storage times of the order of a day, i.e., very low depolarization rates in the presence of moderate heating and cooling are required.

## SPIN RESONANCES IN CIRCULAR MACHINES

In the following, only heavy particles like protons are considered where no self-polarizing and self-cooling occurs in contrast to electrons or positrons. The conditions to conserve polarization during synchrotron acceleration and short flat-tops have been studied extensively<sup>5,6,7,8,9</sup>. No storage ring with polarized protons or heavier ions is working up to now. Therefore, the problems of long storage times or simultaneous heating and cooling of a polarized beam have not been studied experimentally.

Fig. 1 : Orientation of the precession vector  $\vec{\omega}_p$  for a positive ion with  $G > 0$ .



We start our discussion by considering the effect of the vertical guiding field on the spin motion. We write (see fig. 1):

$$\frac{d\vec{S}}{dt} = \frac{e}{\gamma mc} [1 + \gamma G] \vec{S} \times \vec{B} = \vec{\omega}_p \times \vec{S}$$

$$\frac{d\vec{\omega}_p}{dt} = -\frac{e}{\gamma mc} [1 + \gamma G] \vec{B} = \frac{\omega_c}{c} [1 + \gamma G] \hat{y} \quad (1)$$

$$\text{with } \frac{\omega_c}{c} = \frac{eB_v}{\gamma mc}$$

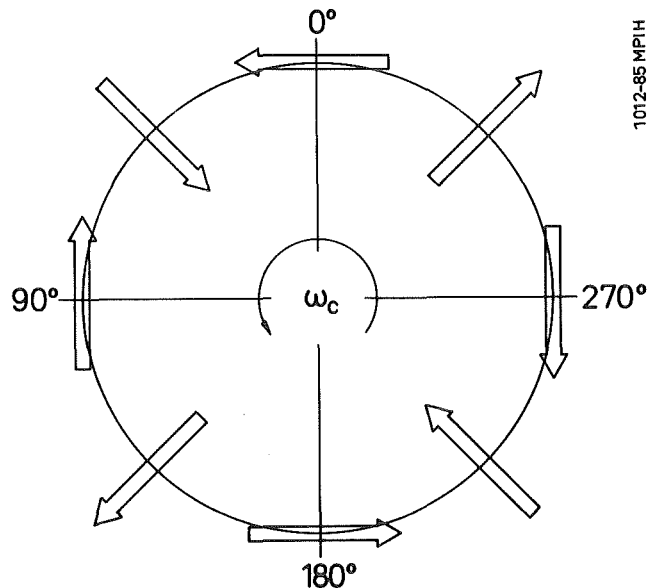
Here  $\vec{S}$  is the spin vector in the rest frame,  $\vec{B}$  is the magnetic field strength in the laboratory frame and  $G = (g - 2)/2$  the gyromagnetic anomaly (see Table 1). For a vertical orientation of  $S$  the spin is stationary; otherwise, the horizontal component precesses with angular frequency  $\vec{\omega}_p$ , which can be expressed as a multiple of the revolution frequency  $\omega_c$ . For

example, protons of 108 MeV ( $\gamma G = 2$ ) perform three spin rotations per turn, protons of 631 MeV ( $\gamma G = 3$ ) four rotations, etc. The situation for  $\gamma G = 2$  is sketched in fig. 2.

| Ion   | Gyromagnetic anomaly<br>G | Number of spin<br>rev. per turn<br>( $\omega_p - \omega_c$ ) | Lowest imperfection res. |       |
|---|---------------------------|--|--------------------------|-------|
|   |                           |  | n                        | T/GeV |
| p   | .793                      | few ( $> 2$ )  | 2                        | 0.108 |
|   |                           |  | 3                        | 0.631 |
| d   | -0.143                    | fewer  | -1                       | 11.25 |
| paramagnetic ion<br>$\mu \approx \frac{1}{2}$ Bohr<br>$m \approx m_p$ | $\approx 10^3$            | $\geq 10^3$<br>( $\rightarrow$ depol.)                       | -                        | -     |
| e, $\mu$  | $1.16 \times 10^{-3}$     | $\approx 0$  | 1                        | 0.440 |

Table 1: Some parameters relevant for storage of polarized ions

Fig. 2 : Precession of the horizontal spin component for  $\gamma G = 2$  (e.g. protons of 108MeV).



In a real machine, there are radial and longitudinal components of the magnetic field from the focussing and stray fields, and from magnet imperfections. We refer the generalized precession frequency ( $\vec{\omega}_p$ )<sub>rot</sub><sup>7</sup> relative to the frame rotating with  $\omega_c$ :

$$(\vec{\omega})_{\text{rot}} = - \frac{eB_v}{\gamma mc} \left[ (1 + G) \frac{B_{||}}{B_v} + \gamma G \frac{\vec{B}_r}{B_v} + \gamma G \hat{y} \right] \quad (2)$$

The main sources of these fast-varying fields are field errors leading to vertical closed orbit distortions ("wave number"  $n=\text{integer}$ ) or vertical betatron oscillations ("wave number" of the corresponding field distortion:  $kP \pm Q_v$ ;  $P$  = machine periodicity,  $Q_v$  = vertical betatron tune).

Under most conditions, the spin precession caused by horizontal field components averages to zero and the vertical spin direction would still be quasi-stationary. Only if the wave number  $\gamma G$  of the vertical precession comes close to one of the horizontal wave numbers, these small horizontal precession angles add up coherently and a sizeable spin precession arises<sup>5</sup>.

This is illustrated in fig. 3 for the lowest order  $\gamma G = 2$  is represented by localized field components which cause the spins to precess by a small angle  $\Delta\theta$ . Due to the resonance condition the kicks add up to  $4\Delta\theta$  per revolution.

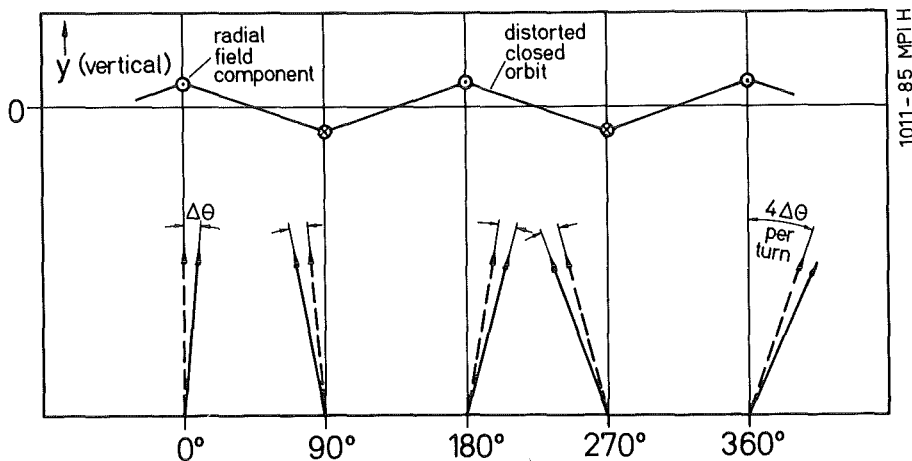


Fig. 3 : (see text)

In general, depolarizing resonances occur under the following conditions (for more general conditions, see ref. 8):

$$(i) \text{ imperfection resonances: } \gamma G = n \quad (3a)$$

$$(ii) \text{ intrinsic resonances: } \gamma G = kP \pm Q_V \quad (3b)$$

Imperfection resonances are fixed in energy, whereas the position of intrinsic resonances depends on the betatron tune of the machine. The location of the lowest imperfection resonances for some typical ion species are given in Table 1.

#### STORAGE AND ACCELERATION

If we inject a polarized beam with vertical spin, i.e. parallel to the bending field, at a certain energy  $\gamma_0$  well separated from depolarizing resonances and if this beam is stored, no depolarization would be expected in first approximation. Of course resonances might have tails which stretch out to the energy at which the beam is stored. Other factors like residual gas scattering or interaction with a colliding beam or an internal target may cause additional depolarization.

To my knowledge, only one experimental study has been done so far on this problem. At the ZGS, using an extended 21 s flat-top at 3.25 GeV/c, an upper limit for the depolarization rate of 0,025% per second was found<sup>10</sup>. This value corresponds to a 1/e polarization life time of more than one hour, which is much more than the cycling times envisaged for proton storage rings<sup>3,11</sup>. Therefore, even if one admits the influence of other neighbouring resonances, the depolarization of the stored beam due to spin resonances should be negligible, at least under the condition of the ZGS experiment. But depolarization rates in a proton storage ring with strong cooling by a cooler and simultaneous strong heating by an internal target have not been studied yet. It was pointed out in ref. 12 that depolarization away from resonances requires the simultaneous presence of scattering and

damping processes. This led to the conjecture<sup>13</sup> that polarized proton beams simultaneously heated and cooled would be subject to depolarization, by a process similar to that of quantum fluctuations and radiation damping in electron storage rings. This would suggest a polarization lifetime of the order of the beam lifetime without cooling, but requires a more specific calculation for this situation.

If the particle energy in the cooler synchrotron is varied, the left hand side of eq. (3) changes and the resonance condition may be fulfilled. In their pioneering paper<sup>5</sup>, Froissart and Stora obtained the following formula for the polarization  $P_f$  after having crossed an isolated resonance:

$$P_f/P_i = 2 \exp [-\pi \epsilon^2/2\alpha] - 1 \quad (4)$$

with

$P_i$  = initial polarization

$\epsilon$  = strength of the resonance

$\alpha$  = parameter which describes the speed of the resonance crossing

(e.g.  $\alpha = \gamma G/\omega_C$  for an intrinsic resonance).

The relevant parameter is  $\epsilon^2/2\alpha$ . The two limiting cases are:

(i)  $\epsilon^2/2\alpha \ll 1$ . This means a weak resonance and/or fast crossing and we

obtain:  $P_f \approx P_i$

(ii)  $\epsilon^2/2\alpha \gg 1$ . Here we have a strong resonance and/or slow crossing

speed, which results in  $P_f \approx -P_i$ , that means a complete spin flip will take place.

A better account for the resonance strength of a given lattice can be obtained by using the computer program "DEPOL" written by E.D. Courant<sup>14</sup>. In addition, the simple picture of resonance crossing is strongly modified by the presence of synchrotron oscillations, which cause multiple resonance crossing<sup>5,10</sup>.

For a small storage ring with synchrotron acceleration, where the number of resonances is small, it is not necessary to device elaborate techniques like pulsed quadrupoles or Siberian snakes, which are used or proposed for the big accelerators<sup>15,9</sup>. As for Saturne II, it seems possible to cross the weak resonances quickly without change and the strong ones slowly to perform a proper spin flip<sup>16</sup>. Therefore, a flexible system of ramping the magnets of different velocity is required. Using the correction dipoles, the strength of an imperfection resonance can be modified by correcting or amplifying closed orbit distortions in order to optimize the conditions for resonance crossing<sup>16</sup>.

Finally, we want to emphasize that for deuterons, there are no depolarizing resonances in the relevant energy range (see Table 1), as the gyromagnetic anomaly is about 12 times smaller than for protons.

#### ELECTRON COOLING

Two effects may cause depolarization of the circulating ions by the electron cooler:

- a) spin precession in the longitudinal field  $B_{||}$  of the Solenoid;
  - b) hyperfine interaction (hfi) with the cooler electrons.
- a) The spin precession angle is given by:

$$\theta_{||} = \theta_0 \frac{B_{||}}{T} \frac{L}{m} \frac{1}{\beta\gamma} \quad (5)$$

where  $B_{||}$  is the axial field, L the length and  $\theta_0$  (prot.) =  $51.2^\circ$ ,  $\theta_0$  (deut.) =  $7.9^\circ$  etc. For  $B_{||} \times L$  equal to 0.2 Tm we get in the case of 100 MeV protons a precession angle of  $21.6^\circ$  per passage for the transverse polarization component. This would destroy the polarization completely, but it can be easily compensated by additional solenoids with opposite field direction, as it has been proposed for the IUCF

cooler ring<sup>1</sup>. Small compensation errors give additional contributions to the imperfection resonances which have to be avoided or suppressed anyhow.

- b) The question whether significant depolarization due to hfi between electron and ion takes place, is related to the very interesting problem whether circulating ions can be polarized using polarization transfer from polarized electrons<sup>16</sup>. In contrast to the case of a bound system we have to consider hfi between ions like protons or antiprotons and scattered electrons from an electron gas of typical density  $n_e = 3 \cdot 10^8 / \text{cm}^3$  and temperature of the order of 1 eV, which is at rest with respect to the ions.

Due to the  $r^{-3}$  dependence of the dipole-dipole interaction only collisions with small impact parameter contribute to hfi. As an estimate, we obtain for the rates of close collisions:

$$\dot{N}_{cc} \approx 3 j_x \sigma_{cc} \quad (6)$$

$$\text{with } j_x = n_e v_x \quad \text{and } \sigma_{cc} = \pi a_0^2$$

$$(a_0 = \text{Bohr radius})$$

With the above numbers for  $n_e$  and  $T_e$  we obtain:

$$\dot{N}_{cc} \approx 3 / \text{s}$$

Now we estimate the amount of hfi which takes place during each close collision.

The problem of angular momentum transfer from the nucleus to the electrons is well known from studies on perturbed angular correlations<sup>17</sup>. Nuclear and electron spins are coupled by the hyperfine field for a short time  $\tau$  which is the life time of the electron state with strong hfi (hyperfine frequency  $\omega$ ). The attenuation coefficients  $G_k^{17}$  can

be interpreted as the ratio of final and initial nuclear polarization of rank k. Thus  $G_1$  gives the attenuation for vector polarization we are interested in.  $G_1 = 1$  corresponds to vanishing hfi.

In the special case of  $J = 1/2$  (spin of the electron state), which corresponds to the  $1\ s_{1/2}$  state with maximum hfi, the attenuation coefficient  $G_1$  takes the simple form<sup>18</sup>:

$$G_1 = 1 - \frac{1}{2} \cdot \frac{(\omega\tau)^2}{1 + (\omega\tau)^2} \quad (7)$$

$$\text{with } \omega = \frac{\mu_k}{h} g (2I + 1) H(0)$$

$\mu_k$  is the nuclear magneton, g the magnetic moment of the ion in units of  $\mu_k$ , I the spin of the ion and  $H(0)$  the magnetic field produced by the 1s electron at the nucleus. For a proton in the field of 1 MGs we get:

$$\omega = 2.7 \cdot 10^{10} \text{ s}^{-1}$$

For  $\tau$  we take a typical time for a close collision:

$$\tau = 2\alpha_0 / v_x \approx 10^{-16} \text{ s}$$

For the product  $\omega\tau$  we get:

$$\omega\tau \approx 3 \cdot 10^{-6} \ll 1$$

which means very weak hfi. Using equ. (7) we obtain for the attenuation collision:

$$G_1 = 1 - 4 \cdot 10^{-12}$$

With the above value for  $N_{cc}$  we get:

$$P(t) = P(0) | 1 - n \cdot 1.2 \cdot 10^{-11} t/\text{s} | \quad (8)$$

( $n = L_{\text{cooler}}/C \approx 3\%$ ). The 1/e polarization life time  $\tau_p$  is of the order:

$$\tau_p \approx 2 \cdot 10^{12} \text{ s}$$

From this extremely long life time we conclude that depolarization due to hfi with the cooler electrons is completely negligible. On the other hand it can be stated that polarizing circulating ions using polarized electrons is not feasible. Only in the case of circulating paramagnetic ions (that is ions with an uneven number of electrons) one might take advantage of the large spin-exchange cross sections<sup>19</sup>. But it seems doubtful whether the polarization of paramagnetic ions (see tab. 1) can be conserved in a storage ring for a sufficiently long time.

#### Acknowledgement

I wish to thank B.W. Montague for pointing out the possibility of polarization life time limitations for simultaneous cooling and heating of the beam and D. Möhl for encouragement and guidance in the preparation of this talk.

REFERENCES

1. The IUCF cooler-tripler proposal, IUCF, December 1980.
2. A. Johansson, CELSIUS-Note 83-1, 1983
3. COSY-Studie, JüI-Spez-242, February 1984
4. K. Kilian and D. Möhl, Proc. Workshop on Physics at LEAR ..., Erice (1982), p. 701
5. M. Froissart and R. Stora, Nucl. Instr. Meth. 7 297 (1960)
6. J. Kho et al., Part. Accel. 6, 213 (1975)
7. L.C. Teng, in: High Energy Physics with Polarized beams and targets (Argonne 1978); G.H. Thomas (Ed.), AIP Conference Proceedings 51, p. 248 (1979)
8. R.D. Ruth, in: High Energy Spin Physics (Brookhaven 1982); G.M. bruce (Ed.), AIP Conference Proceedings 95, p. 378 (1983)
9. B.W. Montague, Physics Report 113, 1 (1984)
10. Y. Cho et al., IEEE NS24, 1509 (1977)
11. R.E. Pollock, IEEE NS30, 2056 (1983)
12. Ya. S. Derbenev and A.M. Kondratenko, Sov. Phys. JETP 35, p. 230 (1972)
13. B.W. Montague, in: High Energy Polarized Proton Beams (Ann Arbor 1977), A.J. Krisch and A.J. Salthouse (Ed.), AIP Conf. Proceed. 42, p. 46, and private communication (1984)
14. E.D. Courant, in: High Energy Polarized Proton Beams (Ann Arbor 1977), A.D. Krisch and A.J. Salthouse (Ed.), AIP Conference Proceedings 42, p. 94
15. L.G. Ratner, IEEE NS30 (1983) 2690
16. E. Grorud et al., High Energy Spin Physics, Brookhaven (1982), AIP Conf. Proc. 95, p. 407
17. H. Frauenfelder, R.M. Steffen, in:  $\alpha$ ,  $\beta$  and  $\gamma$  Spectroscopy, K. Siegbahn (Ed.), Amsterdam (1974), p. 997
18. M. A. Faessler, B. Povh and D. Schwalm, Ann. of Phys. 63 (1971) 577
19. E.W. Otten, Workshop on the Physics with Heavy Ion Cooler Rings, Heidelberg (May 1984).

LATTICE DESIGN FOR COOLER RINGS

D.E. Johnson

Fermi National Laboratory, Batavia, Ill.

(Copy of transparencies)

LATTICE DESIGN FOR COOLER RINGS

Past and present examples and  
experience from Fermilab

D. E. Johnson

Fermilab

"Users" of cooling rings are very demanding. They often request many things of a lattice that are very *hard* to supply:

- Do not use many magnets
- Do not make too big
- Do not spend much money
- Give machine strange lattice parameters
- Make machine very versatile
- Etc.

Let the designer beware!

## FERMILAB ELECTRON COOLING

### Initial Requirements

- \* 200 MeV protons (antiprotons)
- \* Cool at a rate of 15 Hertz
- \* Be able to accumulate  
 $10^{10}$  antiprotons in  $\sim 3$  hours.

### Electron Gun Requirements

- \* 26 Amps
- \* 25 cm $^{\star\star}2$  beam
- \* 110 kV
- \*  $T_{electron\ beam} \leq 1eV$
- \*  $L(gun)/L(ring) = 0.05$

Such an electron gun will produce the desired cooling rate. The problem is now to design a high-quality storage ring to accomodate it.

Requirements on storage ring

- \* must be able to inject at 15 Hz  
and accumulate for several hours
- \* must have low proton temperature  
in the cooling region
- \* must be small -  $\eta = .05$   
 $L(\text{electron beam}) \leq 5 \text{ meters}$   
 $C(\text{ring}) = 135 \text{ meters (for 1 gun)}$
- \* must be able to run with gun off,  
protons with gun on,  
antiprotons with gun on.

linear tune shift due to 26 Amp and  
5 meter electron beam:

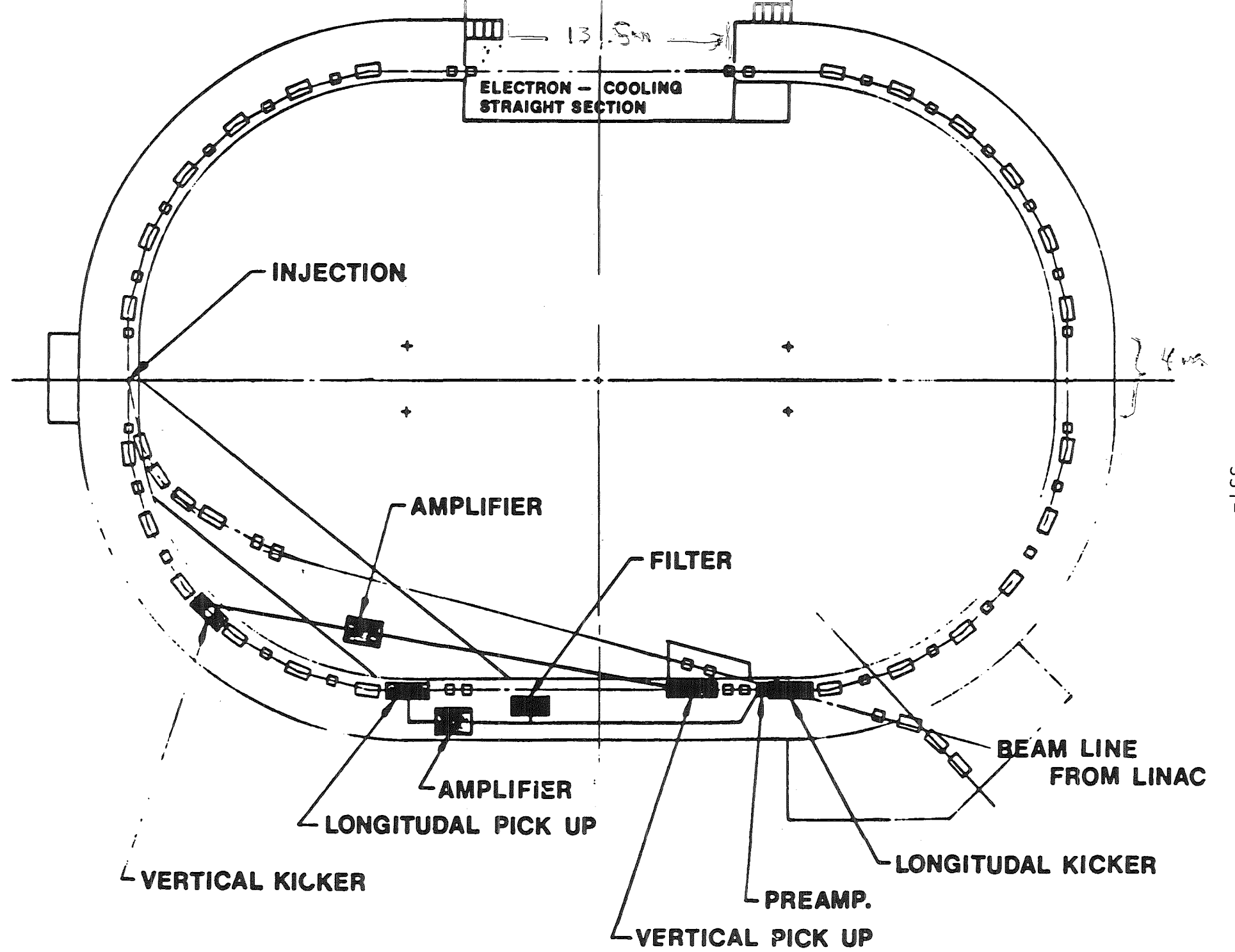
$$\Delta v = 0.13!$$

This tune shift must be locally  
corrected in order to preserve storage  
ring design for rest of machine.

- injection. sextupole corrections. etc

### Final Ring Design

- racetrack design
- two short straight sections for injection and abort
- two long straight sections for cooling. Only one for electrons initially.
- momentum stack with full aperture kickers, no shutters.
- injected beam  $E(h) = 40\pi \text{mm mrad}$   
 $E(v) = 20\pi \text{mm mrad}$   
 $\Delta p/p = \pm 0.15\%$
- total momentum aperture as small as possible.



Machine Design Problems

- Injection straight: large dispersion, small betas
- Cooling straight: zero dispersion, large betas

$B = 40m \Rightarrow \Theta(h) = 1.3 \text{ mrad}$

$\Theta(v) = 0.9 \text{ mrad}$

$T(\text{proton}) = T_{\parallel} + T_{\perp} < 1.7 \text{ kV}$

- Not enough room for "standard" dispersion killers  $\Rightarrow$  do it with quadrupoles.
- Cooling straight section must be easily adjustable for protons, protons + electrons, antiprotons + electrons

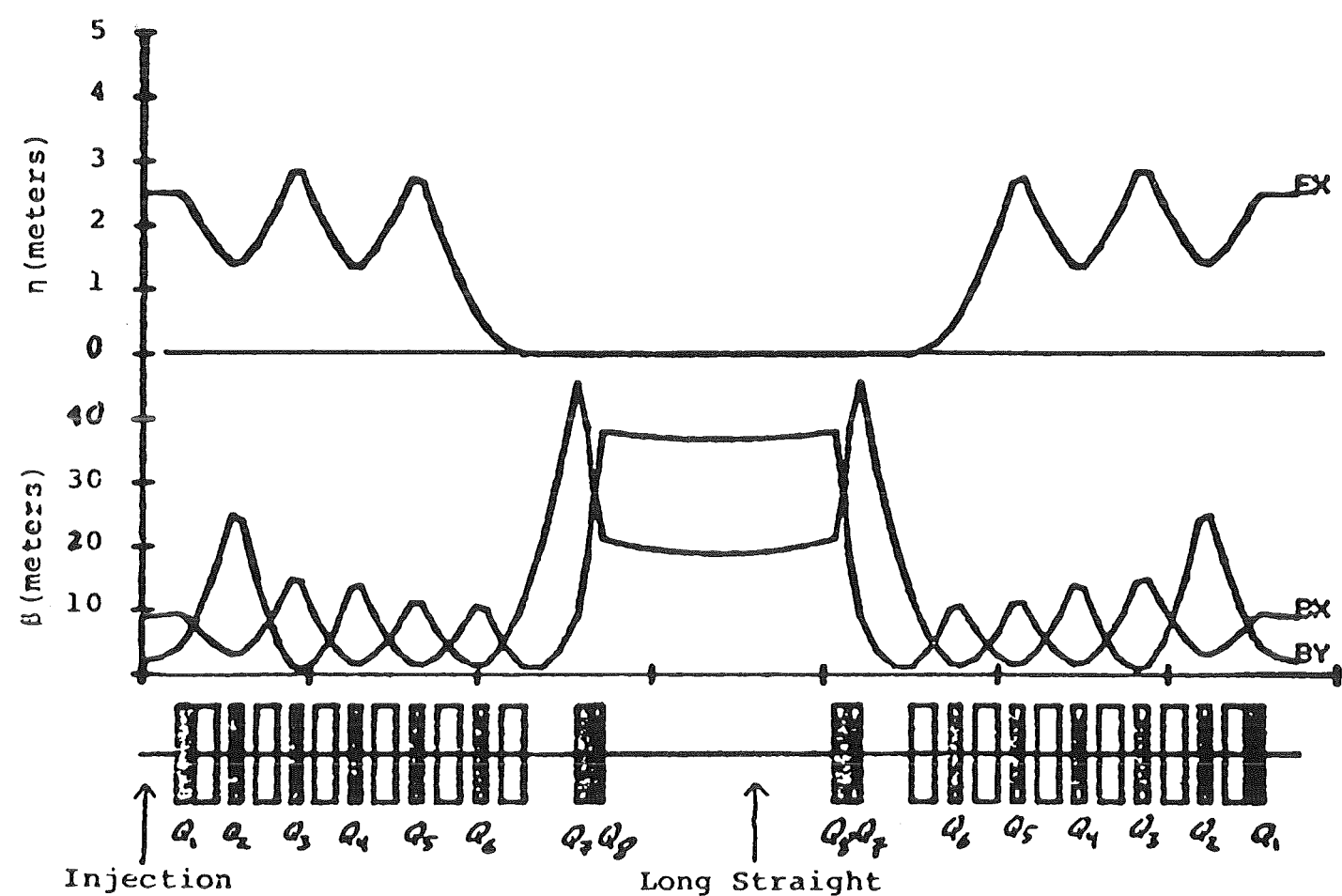


Figure 2 Racetrack Superperiod

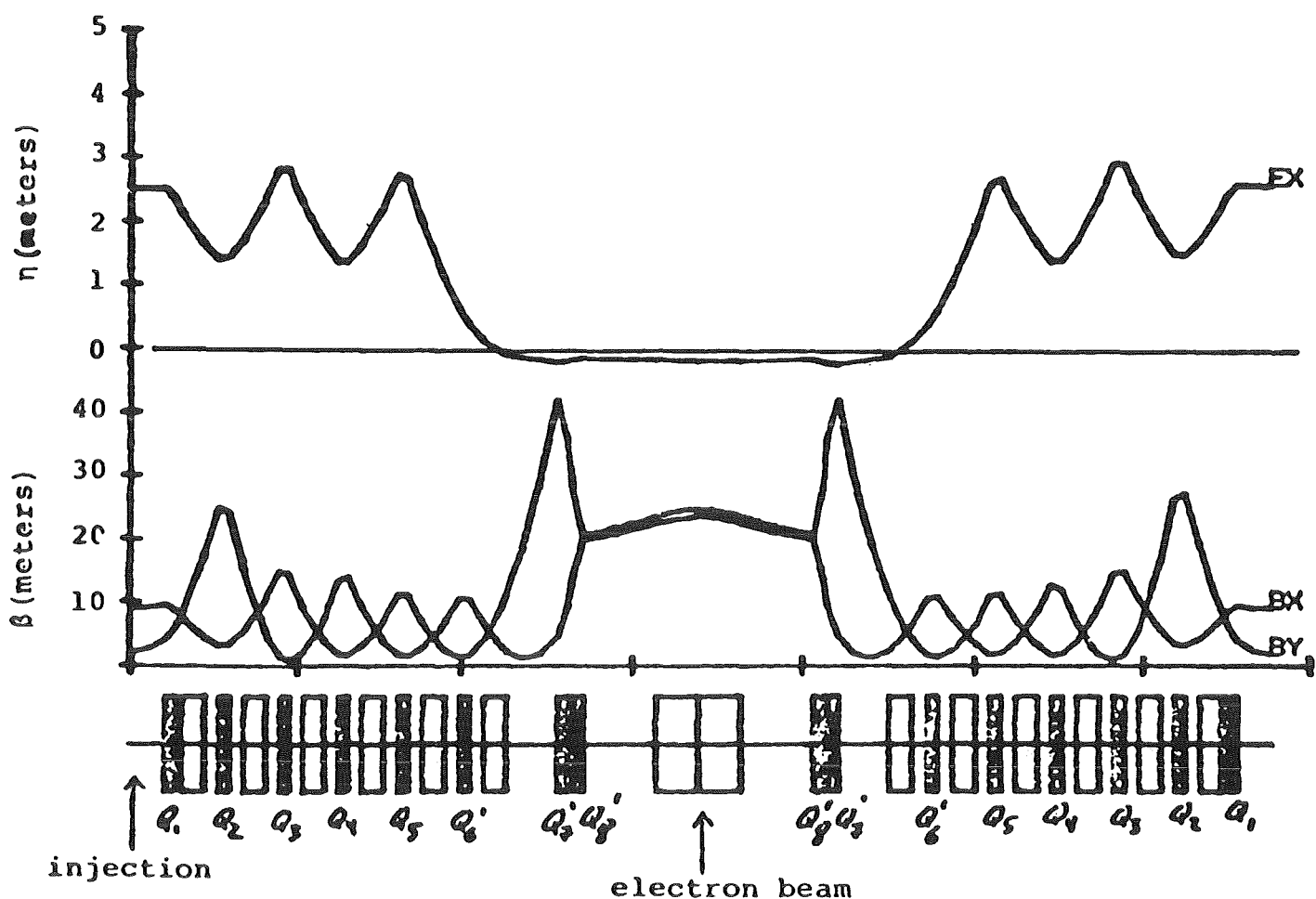
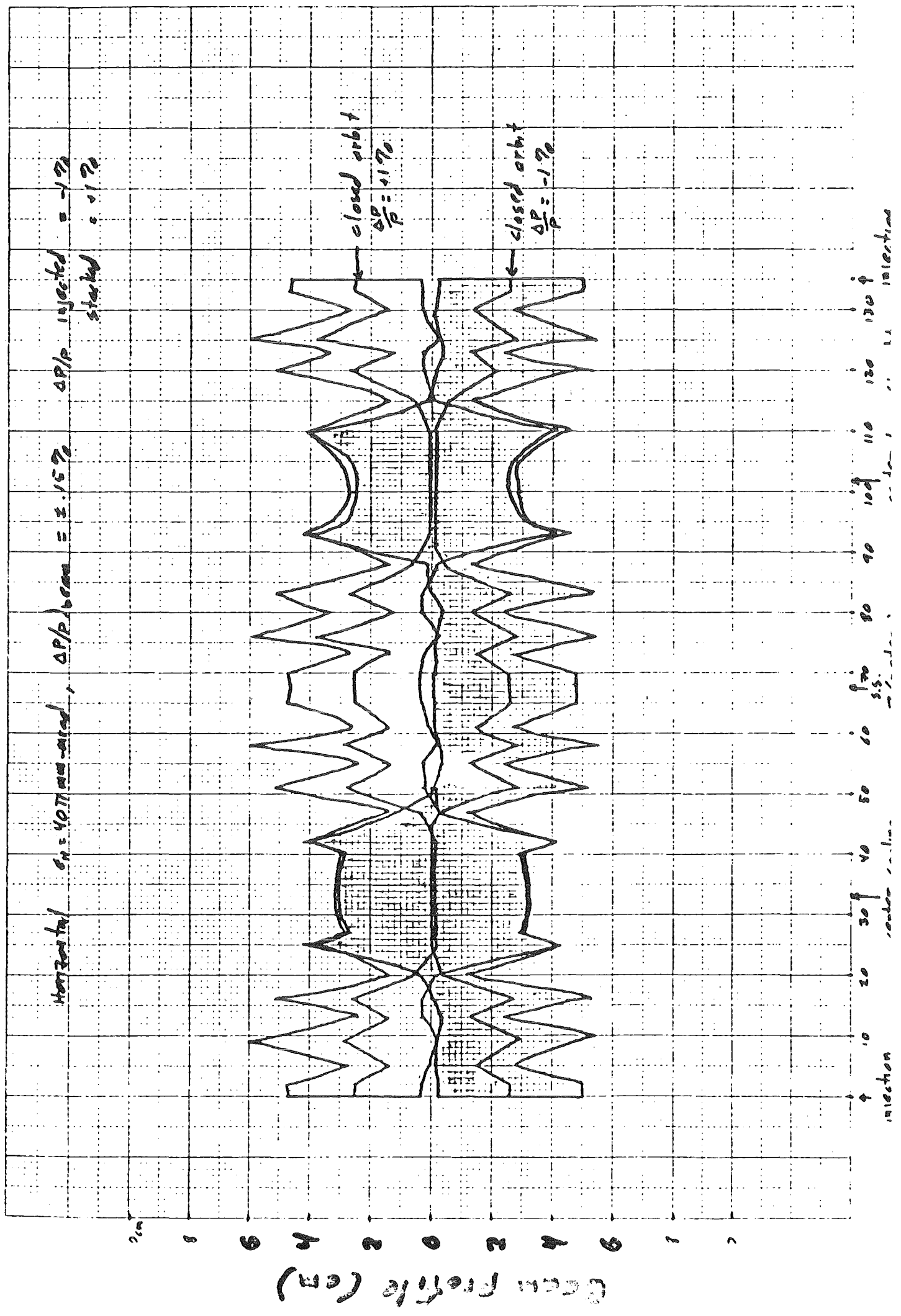


Figure 3 Half racetrack with cooling straight section

Proton Cooling Ring injected and stacked beams with e<sup>-</sup> beam  
12/12/72

-335-

Figure 4



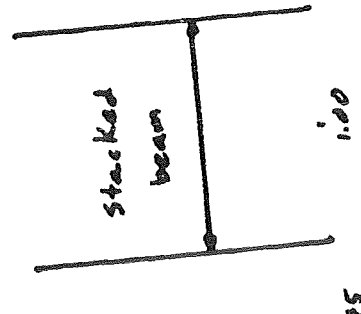
Tune vs.  $\Delta P/P$  with electron beam



-336-

June 17, 1961

-5.36



.50

.25

$-\frac{1}{2} \Delta P/P / \eta_{c1}$

-.50

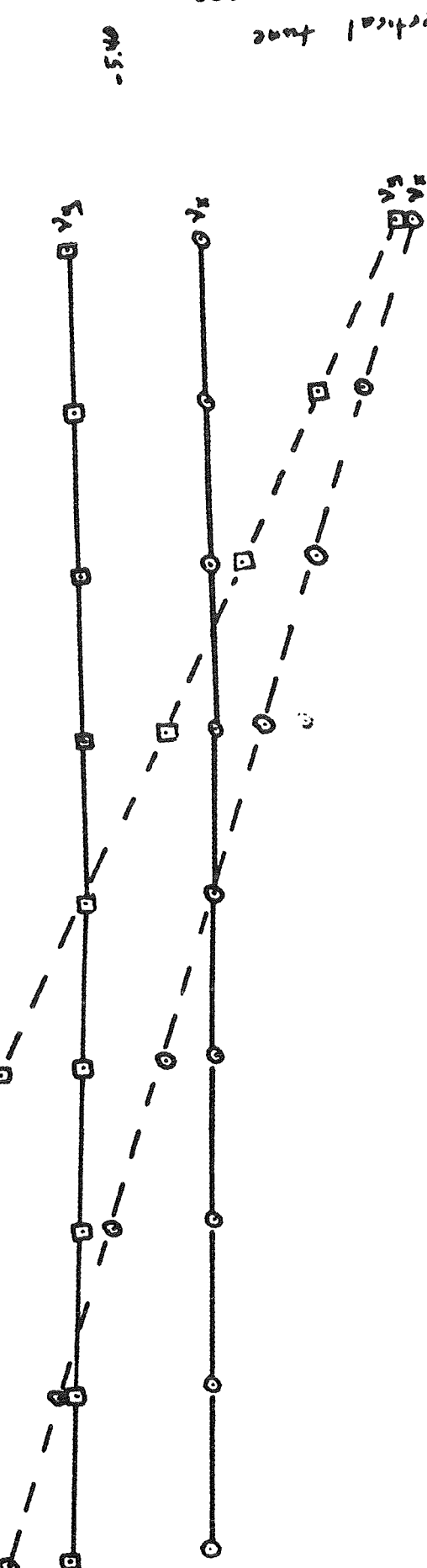
.25

-.50

-.75

-1.00

Harmonic tune



3.00 -

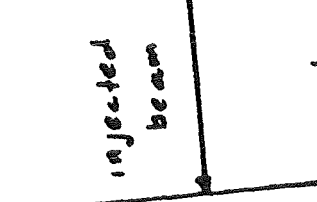
3.20 -

Harmonic tune

1.40 -

1.20 -

1.00 -



This machine worked as it was intended, however, it was hard to operate. For example there were 11 separate quadrupole power supplies=> most operators did not know how to change the beam properties or tunes in a simple manner

The natural chromaticities were easily linearly corrected with two sets of sextupoles. Again, however, if the machine parameters changed it was hard for operators to re-establish correction.

-Doing any form of cooling - electron or stochastic - is very difficult.

-Lattice design should be as simple as possible so that all attention can be given to cooling problems not to understanding the machine.

## Antiproton Source Design

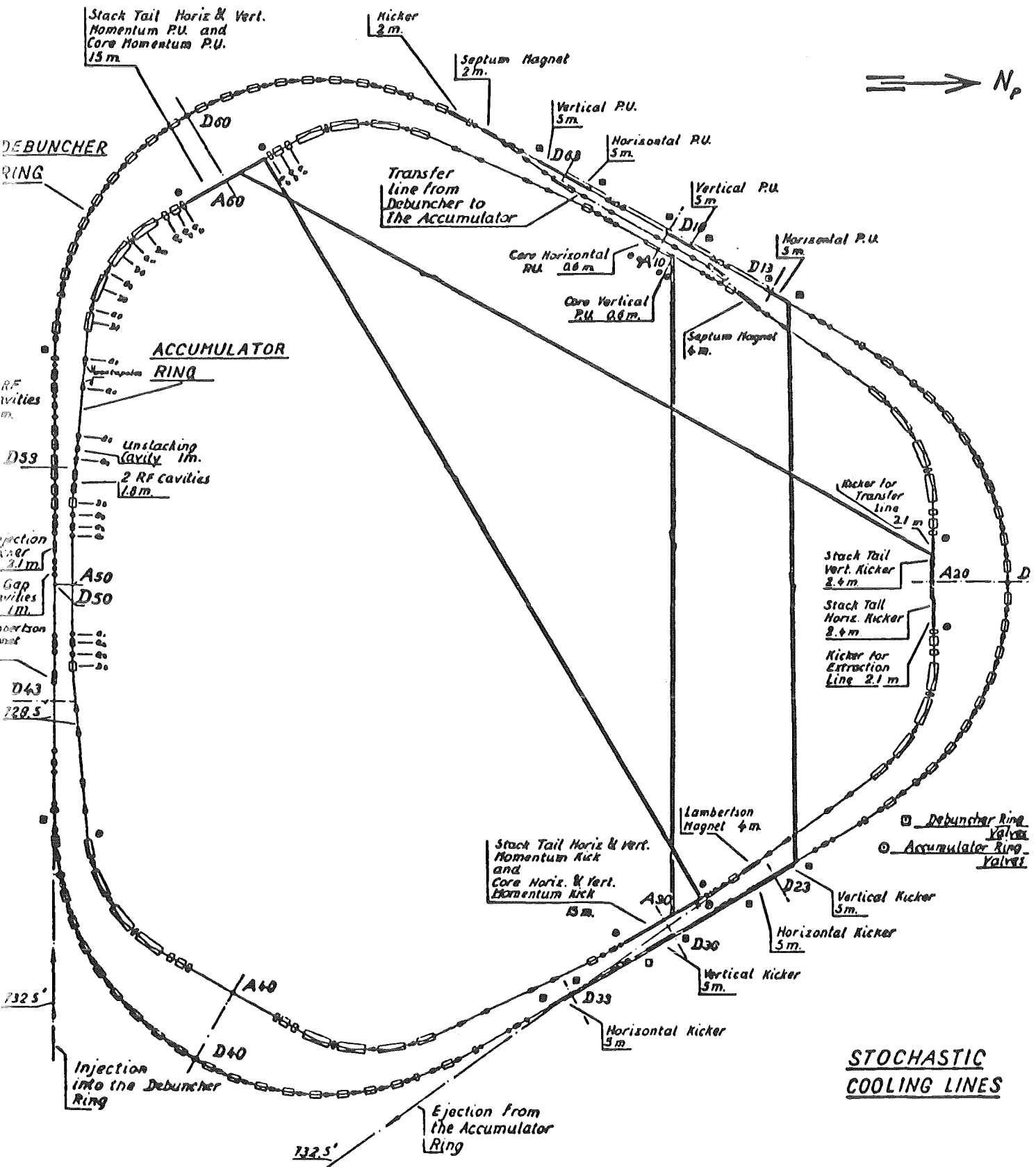
Two machines: Debuncher,

Accumulator

Design philosophy:

make the machines as simple  
as possible + still be able  
to cool and store.

This can be done for debuncher, cooling  
requirements are not hard. An early  
version, specialized for cooling showed  
chromatic sextupole problems. Present  
design 60° cells with missing dipoles  
for 3 straight sections.



Debuncher must work . . . . .

there will be enough problems elsewhere.

### ACCUMULATOR

Cooling requirements very tough:

6 straight sections

3 with  $B \sim 7m$

$\alpha = 0$

3 with  $B \sim 7m$

$\alpha = 9m$

$$n = 1/\gamma^2 - 1/\gamma_t^2 = 0.02$$

Design exists and seems to be allright.

## CONCLUSIONS

Debuncher problems found by tracking have been fixed. It will be a nice machine.

Accumulator will be harder to operate but should work.

Machine designs should be as simple as possible.

Stability should be checked analytically or with tracking.

Good looking designs may be deceiving!



## LATTICE DESIGN OF TARN II COOLER RING MODE

A. Noda, N. Takahashi, T. Tanabe, T. Katayama and Y. Hirao

Institute for Nuclear Study, University of Tokyo  
Midori-cho 3-2-1, Tanashi-city, Tokyo 188, Japan

M. Takanaka

National Institute of Radiological Sciences  
Anagawa 4-9-1, Chiba-city, Chiba 260, Japan

### Abstract

As the improvement project of TARN, a ring with radius of ~12 m (TARN II) is under construction. It is designed to be able to operate as a synchrotron which accelerates ions with  $\epsilon$  of 1/2 up to 450 MeV/u and proton up to 1300 MeV (Synchrotron Mode). The ring is also to be operated as a cooler ring which utilizes electron beam and stochastic cooling (Cooler Ring Mode). Both modes are designed to be operated either as separated ones or as ones which can be moved between each other without change of operation point.

### Introduction

At TARN (Test Accumulation Ring for NUMATRON project), a variety of accelerator developments related to a storage ring have been studied<sup>1)</sup>. The combination of multi-turn injection into transverse phase space and RF-stacking into longitudinal phase space has attained the intensity increase of ~300 times compared with a single turn injection although the phase space densities are diluted by factor 2 and 1.8 in transverse and longitudinal phase spaces, respectively. Recently, the stochastic momentum cooling has also been successfully applied to 7MeV protons at TARN. The fractional momentum spread of the stacked beam as large as 1.4 % has been reduced to 0.5 % with cooling time of ~20 sec. as shown in Fig. 1. The cooling parameters at TARN is given in Table 1. Our result is given on the chart given by D. Möhl<sup>2)</sup> in Fig. 2.

Recently the necessity of high-energy heavy-ion synchrotron such as NUMATRON has been increasing more and more not only for nuclear physics but

also for other applications as medical use. Further, interest has been increasing in high-resolution experiment with use of a cooler ring which realizes high-quality circulating beam with electron cooling<sup>3,4,5</sup>).

However, the present TARN is rather small to fulfil the above requirement. DC characteristics of dipole magnets in the TARN make developments related to synchrotron acceleration out of our scope. The limited length of the long straight section (1.8 m) prevents us from installation of equipments for beam extraction and electron cooling.

Considering such situation, TARN is decided to be improved to the larger one (TARN II). Its mean radius is almost twice as large as TARN (~12 m) and it is designed to be able to accelerate proton up to 1300 MeV and ions with  $\epsilon$ (charge to mass ratio) of 1/2 up to 450 MeV/u.

As the injector of TARN II, the SF cyclotron at INS with K-number of 68 is assumed for the time being. Layout of TARN II is shown in Fig. 3 overlapping with that of the present TARN and its transport system from the cyclotron. Although the SF cyclotron has accelerated various heavy ions up to  $^{132}\text{Xe}^{6+}$ <sup>6</sup>), ions up to Ne are to be injected into TARN II considering the peak intensity necessary for beam handling during synchrotron acceleration process. In Table 2, ion species from the SF cyclotron to be accelerated at TARN II are listed up.

Space charge limit at TARN II for these ions are calculated as given in Table 3. The expected output intensities of TARN II with the SF cyclotron as an injector are also given in the Table. So as to reach the space charge limit, the injector linac system, which is now partially under construction, is needed<sup>7</sup>). The linac system will provide ions up to Xe with energy of ~5 MeV/u with higher intensity.

So as to fulfil the necessary characteristics for beam cooling and internal target experiment, TARN II ring is designed to provide doubly achromatic long straight sections together with ones of large dispersion allowing reduction of superperiodicity from 6 to 3.

### Lattice Design

TARN II lattice is designed to be able to operate with two different excitation modes. One of which aims at large intensity multiplication and higher maximum energy attainable in the limited site (Synchrotron Mode). The other provides doubly achromatic long straight sections needed for cooler equipments so as to be free from the transverse emittance blow up

due to momentum correction during the cooling process (Cooler Ring Mode)<sup>8</sup>).

The lattice is based on a simple FODO structure. With Synchrotron Mode, intensity increase of 20 times by the multi-turn injection into horizontal transverse phase space is assumed, which is anticipated to lead to emittance increase about ~40 times. So the maximum value of  $\beta_H$  is suppressed at rather smaller value (~10 m) by taking higher superperiodicity of 6. In Fig. 4, beta and dispersion functions of Synchrotron Mode are shown for a unit cell, which is composed of a single FODO cell and a long straight section of 4 m in length. So the superperiod coincides with the unit cell, which is the same as the present TARN.  $v$ -values are chosen at ~1.75 both in horizontal and vertical directions.

#### Cooler Ring Mode Lattice

On the basis of the arrangement of magnet elements described above, Cooler Ring Mode is studied to provide necessary characteristics for beam cooling with only the change of excitation currents of focusing elements. For Cooler Ring Mode, as well as doubly achromatic long straight section, one with large dispersion is also needed if an internal target experiment with cooled beam and dispersion matched spectrograph is considered<sup>9</sup>). So the structure where every second long straight section is made doubly achromatic and other long straight sections have rather larger dispersion (~5m) is adopted. From the above condition, constraints to be imposed on field gradients of quadrupole magnets are obtained by multiplication of transfer matrices for the arrangement of magnet elements symmetric with respect to the point B in Fig. 5. If the transfer matrix from point A to B is denoted as

$$M = \begin{pmatrix} a & b & c \\ d & e & f \\ 0 & 0 & 1 \end{pmatrix}, \quad (1)$$

the constraint to realize doubly achromatic long straight sections just outside of points A and C in Fig. 5 is given by

$$f = 0. \quad (2)$$

The dispersion function at the point B,  $n_0$ , can be given by

$$n_0 = c . \quad (3)$$

The numerical calculation of Twiss parameters and dispersion is executed with use of computer code SYNCH<sup>10</sup>). The main parameters of magnetic focusing system of TARN II is given in Table 4.

For the electron cooling section, rather smooth  $\beta$ -functions are preferable from the point of view of reducing the transverse temperature of the circulating ion beam<sup>11</sup>). However this condition leads to rather larger  $\beta$ -value at the cooler section. The size of  $\beta$ -function should be suppressed at moderate value so as to keep the ion beam size inside the electron beam size. For the internal target position (point B) low  $\beta$  is needed to focus the beam size. In Fig. 5, beta and dispersion functions are shown for the Cooler Ring Mode with  $v$ -values 1.75 and 1.25 in horizontal and vertical directions, respectively. The superperiodicity of this mode is 3 and one third of the circumference is shown in the figure. For these  $v$ -values,  $\beta$ -functions at the target position are made to be 1.50 m and 2.60 m in horizontal and vertical directions respectively, but this structure has such demerit as  $\beta$ -functions at electron cooler section becomes considerably larger ( $\sim 36$  m and 19 m for  $\beta_H$  and  $\beta_V$ , respectively), which leads to larger tune shift due to the effect of the focusing force originated by electron beam as is described later. The structure with  $v$ -values of 2.25 and 1.25 in horizontal and vertical directions, respectively has smooth  $\beta$ -functions with moderate size ( $\beta_H \sim 16$  m,  $\beta_V \sim 11$  m) at the electron beam section, but  $\beta$ -functions at the target position are not so small as the one above described (Fig. 6). For the purpose of test experiment of electron cooling system itself without internal target, the latter tune might be preferable.

#### Effect of Existence of the Electron Beam

The existence of the high-intensity electron beam on the ion beam orbit causes additional focusing force. For the condition where electron cooling proceeds, velocities of electron and ion are well adjusted and the equation of motion of the ion in electron beam is written as

$$\frac{d^2r}{ds^2} - \frac{qe_{j0}}{2Am_0c^2\epsilon_0\beta^3\gamma^3c} r = 0 , \quad (4)$$

where  $r$ ,  $j_0$  and  $\epsilon_0$  are the distance of the ion beam from the center of the electron beam, current density of the electron beam and dielectric constant in the air, respectively. In the numerical calculation, current density,  $j_0$  as is given in Fig. 7 is assumed<sup>12)</sup>. Tune shift due to this focusing force is evaluated by insertion of equivalent focusing element at the electron beam position. The effect of self force between ion beams is not included, because it is considered to be quite small. The intensity of the circulating ion beam is more than two order smaller compared with space charge limit as is known from Table 3. The results are listed up in Table 5 for cases of  $(\nu_H, \nu_V) = (1.75, 1.25)$  and  $(2.25, 1.25)$ . The shift for tune of  $(1.75, 1.25)$  is almost twice as large as that of  $(2.25, 1.25)$  reflecting the fact that for the former  $\beta$ -values at electron beam section are almost twice as large as the latter. The beta functions are modified slightly as shown in Fig. 5 even for the case of largest tune shift with electron beam of 60 keV and  $0.5 \text{ A/cm}^2$ .

For the condition where the ion beam is injected at lower energy, the equation of motion of the ion is given by

$$\frac{d^2r}{ds^2} - \frac{qe j_0 (1 - \beta_e \beta_i)}{2A m_0 c^2 \epsilon_0 \beta_i^2 \gamma_i \beta_e c} r = 0 , \quad (5)$$

where  $\beta_i$  and  $\beta_e$  are  $\beta (=v/c)$  for ion and electron, respectively. At the injection time,  $\beta_i$  is smaller than  $\beta_e$ , so the effect of the focusing force becomes larger and for heavier ions as Ne which is injected at relatively lower energy, the betatron oscillation becomes even unstable if such a high intensity electron beam exists at injection time. So it is inevitable to put the electron beam off at injection and after rising up to the flat top, turn it on with good quality (low temperature).

#### Possibility of Transition from Synchrotron Mode to Cooler Ring Mode

Synchrotron and Cooler Ring Modes have been so far considered as entirely separate ones which are used independently, because their operating points are different. It is needed to go across the half integer resonance ( $\nu_V = 1.5$ ) to move from Synchrotron Mode to Cooler Ring Mode with operating point of  $(1.75, 1.25)$  and almost all beams are anticipated to be lost by such a transition with circulating beams in the ring. For Cooler Ring Mode, three degree of freedom ( $G_F$ ,  $G_{F1}$  and  $G_D$ ) are available.

Two of them are used for adjustment of horizontal and vertical tunes and the other is used for the condition of doubly achromaticity given by Eq. (2). So if we take off the doubly achromatic condition, one freedom is left without changing the operating point. In reality, a variety of sets of parameters are found to realize the same operating point (1.75, 1.25) as is shown in Fig. 8. At the point A in the figure, where  $G_{F1}$  is set to the value which satisfies the doubly achromatic condition, Cooler Ring Mode is realized, while the point B with the same value of  $G_F$  and  $G_{F1}$  realizes Synchrotron Mode with superperiodicity of 6. In Fig. 9, dependences of maximum values of  $\beta_H$ ,  $\beta_V$  and  $\eta$  on  $G_{F1}$  are given. It is seen that continuous movement from Synchrotron Mode to Cooler Ring Mode is possible without increase of maximum sizes of  $\beta$ -functions compared with those of Cooler Ring Mode, although the maximum value of dispersion becomes a little larger meanwhile. Considering the fact that the momentum spread of the injected beam is about 0.1% for the case of TARN II, such small increase of dispersion is to be well managed if the transition from Synchrotron Mode to Cooler Ring Mode is applied after acceleration to a certain energy level where adiabatic damping has already reduced the momentum spread.

One of the purpose of such a transition is to increase the machine acceptance for cooling experiment. Owing to the fact that maximum value of  $\beta_H$  is much larger for Cooler Ring Mode ( $\sim 36$  m) compared with that of Synchrotron Mode ( $\sim 10$  m), the acceptance for Cooler Ring Mode is anticipated to be much smaller (70 mm·mrad) compared with that of Synchrotron Mode (400 mm·mrad). If multi-turn injection and following RF acceleration is applied with Synchrotron Mode and then after decrease of unnormalized beam emittance, the lattice structure is moved to Cooler Ring Mode for cooling experiment, the intensity increase by multi-turn injection is expected to be so much improved.

Another merit of such transition is to remove the problem related to the acceleration across the transition energy<sup>13)</sup> for the case of proton. Due to the fact that average value of dispersion throughout the whole circumference for Cooler Ring Mode is almost half of that of Synchrotron Mode, the transition energy of Cooler Ring Mode is much higher (1850 MeV) than the maximum energy of TARN II (1300 MeV). If the structure of magnetic focusing is shifted from Synchrotron Mode to Cooler Ring Mode after acceleration until just below the transition energy of Synchrotron Mode (810 MeV), the acceleration through this energy region can be made with usual manner without such complicated technique as  $\gamma_t$ -jump.

The scheme that RF acceleration is applied only by Synchrotron Mode with superperiodicity of 6 is also preferable from the point of view of single particle resonance. If the operating point is chosen around (1.75, 1.25), it is rather close to the sum resonance  $v_H + v_Y = 3$  as shown in Fig. 10, which is structure one for Cooler Ring Mode with superperiodicity of 3, while it is not structural for Synchrotron Mode. Somewhat larger excursion of the real operating point from the designed one is anticipated during acceleration process because of tracking errors between dipole field and field gradients of quadrupole magnets. So it seems to be safer to use the mode free from structure resonance during acceleration.

### Conclusion

TARN II lattice can provide the necessary structure as doubly achromatic straight section and low beta large dispersion point needed for cooling section and internal target position, respectively by rather simple structure based on FODO lattice with three parameters. Because of the rather larger beam emittance to be handled at TARN II compared with other cooler rings, it seems to be dangerous to use such superperiodicity as 1 and three-fold symmetry is imposed even on Cooler Ring Mode. Reflecting this restriction, our structure has somewhat larger  $\beta$ -values at doubly achromatic cooling section, if we want to realize low  $\beta$  point with high dispersion at the same time. However simple structure will help us to concentrate our efforts to beam cooling experiments rather than the study of lattice characteristic itself<sup>14)</sup>. The possibility of raising up the transition energy will also make the proton acceleration up to maximum energy much easier.

### References

- 1) A. Noda, Proc. of INS Kikuchi Winter School on Accelerators for Nuclear Physics (1984) 367.  
N. Tokuda et al., Proc. of the 5th Symp. on Accel. Sci. & Tech., KEK, Tsukuba (1984) 265.
- 2) D. Möhl et al., Phys. Rep. 58, No. 2 (1980) 73.
- 3) B. R. Karlsson and G. Tibell, Contributions to the Workshop on the Physics Program at CELSIUS (1983).
- 4) R. E. Pollock, IEEE Trans. on Nucl. Sci. NS-30, No. 4 (1983) 2056.

- 5) G. Berg et al., Studie zum Bau eines kombinierten Kuhler-Synchrotron-Rings an der Jülich (COSY-Studie) (1984).
- 6) Y. Sakurada et al., Proc. of the 5th Symp. on Accel. Sci. & Tech. KEK, Tsukuba (1984) 28.
- 7) N. Ueda et al., Proc. of the 1984 Linear Accel. Conf. GSI, Darmstadt (1984) 71.
- 8) A. Noda et al., Proc. of the 5th Symp. on Accel. Sci. & Tech. KEK, Tsukuba (1984) 268.
- 9) H. Ikegami, Proc. of Workshop on Electron Cooling and Beam Circulation, RCNP, Osaka (1983) 2-1 (in Japanese).
- 10) A. A. Garren and J. W. Eusebio, Lawrence Radiation Laboratory Report UCID-10153 (1965).
- 11) H. Herr, CELSIUS-Note 83-2.
- 12) T. Tanabe et al., Contribution to this Workshop.
- 13) B. Franczak, K. Blasche and K. H. Reich, IEEE Trans. on Nucl. Sci. NS-30, No. 4 (1983) 2120.
- 14) D. Johnson, Talk at this Workshop.

Table 1

Parameters of Stochastic Momentum Cooling for  
7 MeV Proton at TARN

|  |                           |
|--|---------------------------|
| Number of Particles (N)                                | $10^8$                    |
| Fractional Momentum Spread ( $\frac{\Delta p}{p}$ )    |                           |
| Initial  | + 0.7 x 10 <sup>-2</sup>  |
| Final  | + 0.25 x 10 <sup>-2</sup> |
| System Band Width (W)<br>(System Pass Band)            | 90 MHz<br>20 ~ 110 MHz)   |
| Number of Harmonics in the Pass Band (n <sub>g</sub> ) | 80                        |
| Circulating Current (I)                                | 18 μA                     |
| Schottky Current per Band (I <sub>S</sub> )            | 2.56 nA                   |
| Ratio of Thermal Noise to Schottky Noise (n)           | 3.56                      |
| Mixing Factor (M)                                      | 2.17                      |
| Single Particle Cooling Time ( $\tau_0$ )              | 9.5 sec.                  |
| Cooling Time for Optimum Gain ( $\tau = 2\tau_0$ )     | 18.9 sec.                 |
| System Gain for Optimum Cooling Rate (K)               | 105.3 dB                  |
| Correction Voltage for Optimum Gain ( $\Delta V_C$ )   | 9.1 mV                    |
| Schottky Noise Power (P <sub>b</sub> )                 | 7.18 mW                   |
| Total Power (P <sub>tot</sub> )                        | 32.72 mW                  |

Table 2

Ions from the SF cyclotron to be injected at TARN II

| Ion                            | Harmonic<br>Number | Kinetic Energy | Extracted Beam Current |
|--------------------------------|--------------------|----------------|------------------------|
|                                |                    | (MeV/u)        | (eμA)                  |
| p                              | 1                  | 20             | ~ 100                  |
| <sup>3</sup> He <sup>2+</sup>  | 1                  | 30             | ~ 30                   |
| <sup>4</sup> He <sup>2+</sup>  | 1                  | 16.75          | ~ 30                   |
| <sup>6</sup> Li <sup>2+</sup>  | 1                  | 6.67           | ~ 10                   |
| <sup>7</sup> Li <sup>2+</sup>  | 3                  | 4.57           | ~ 10                   |
| <sup>11</sup> B <sup>3+</sup>  | 3                  | 4.18           | ~ 10                   |
| <sup>12</sup> C <sup>4+</sup>  | 1                  | 7.08           | ~ 15                   |
| <sup>14</sup> N <sup>5+</sup>  | 1                  | 8.21           | ~ 10                   |
| <sup>16</sup> O <sup>5+</sup>  | 1                  | 6.56           | ~ 5                    |
| <sup>19</sup> F <sup>6+</sup>  | 3                  | 3.37           | ~ 5                    |
| <sup>20</sup> Ne <sup>6+</sup> | 1                  | 5.80           | ~ 10                   |

( Extracted beam current is estimated with pulse arc mode  
with duty factor of 3 % ). )

Table 3

Space charge limit and expected output intensity of TARN II

| Ion                    | Space Charge Limit   | Expected Output Intensity (p.p.p) |
|------------------------|----------------------|-----------------------------------|
| p                      | $3.4 \times 10^{12}$ | $2 \times 10^{10}$                |
| $^4\text{He}^{2+}$     | $2.8 \times 10^{12}$ | $3 \times 10^9$                   |
| $^7\text{Li}^{3+}$     | $5.9 \times 10^{11}$ | $5 \times 10^8$                   |
| $^{12}\text{C}^{6+}$   | $3.9 \times 10^{11}$ | $3 \times 10^8$                   |
| $^{14}\text{N}^{7+}$   | $3.9 \times 10^{11}$ | $2 \times 10^8$                   |
| $^{16}\text{O}^{8+}$   | $2.7 \times 10^{11}$ | $1 \times 10^8$                   |
| $^{19}\text{F}^{9+}$   | $1.3 \times 10^{11}$ | $1 \times 10^8$                   |
| $^{20}\text{Ne}^{10+}$ | $8.9 \times 10^{10}$ | $2 \times 10^8$                   |

Table 4

Magnetic focusing system of TARN II

|   |                          |      |
|---|--------------------------|------|
| Maximum Magnetic Rigidity                   | 68.75 kG.m               |      |
| Average Radius                              | 12.03 m                  |      |
| Circumference                               | 75.60 m                  |      |
| Radius of Curvature                         | 3.82 m                   |      |
| Focusing Structure                          | FBDBFO                   |      |
| Repetition Rate                             | 1/2 Hz                   |      |
| Maximum Field of Dipole Magnet              | 18 kG                    |      |
| Maximum Field Gradient of Quadrupole Magnet | 70 kG/m                  |      |
| Number of Dipole Magnets                    | 24                       |      |
| Number of Quadrupole Magnets                | 18                       |      |
| Length of Dipole Magnet                     | 1.00 m                   |      |
| Length of Quadrupole Magnet                 | 0.20 m                   |      |
| Superperiodicity                            |                          |      |
| Synchrotron Mode                            | 6                        |      |
| Cooler Ring Mode                            | 3                        |      |
| Transition Gamma                            |                          |      |
| Synchrotron Mode                            | 1.86                     |      |
| Cooler Ring Mode                            | 2.97                     |      |
| Betatron Tune Value                         | Horizontal      Vertical |      |
| Synchrotron Mode                            | 1.75                     | 1.75 |
| Cooler Ring Mode                            | 1.75 or 2.25             | 1.25 |

Table 5

Tune shift due to existence of high current electron beam

| Tion (MeV/u) | Te (keV) | j <sub>o</sub> (A/cm <sup>2</sup> ) | Tune Shift                                 |       |  |       |
|--------------|----------|-------------------------------------|--|-------|--|-------|
|              |          |                                     | v <sub>H</sub> =1.75, v <sub>Y</sub> =1.25 |       | v <sub>H</sub> =2.25, v <sub>Y</sub> =1.25 |       |
| 40           | 21.8     | 0.1                                 | 0.046                                      | 0.024 | 0.020                                      | 0.013 |
| 110          | 59.9     | 0.5                                 | 0.047                                      | 0.025 | 0.021                                      | 0.014 |
| 200          | 108.9    | 0.5                                 | 0.018                                      | 0.009 | 0.008                                      | 0.005 |

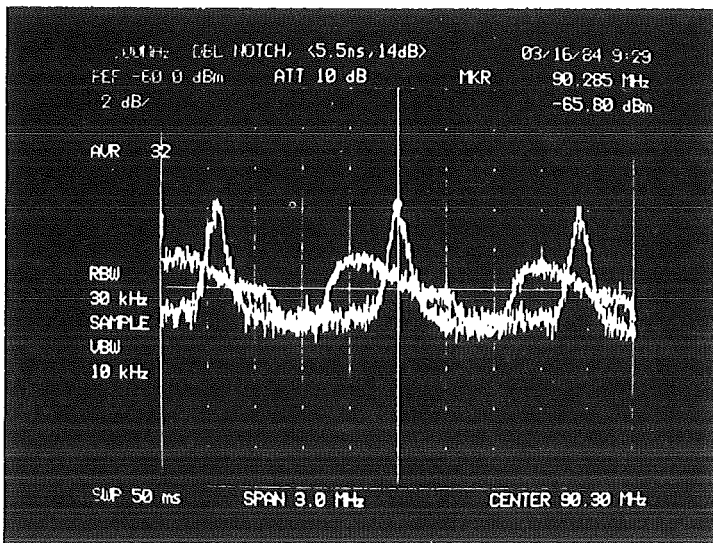


Fig. 1 Typical example of Schottky signals observed at TARN before and after the stochastic cooling process. Fractional momentum spread is reduced from 1.4% to 0.5% in  $\sim 20$  sec.

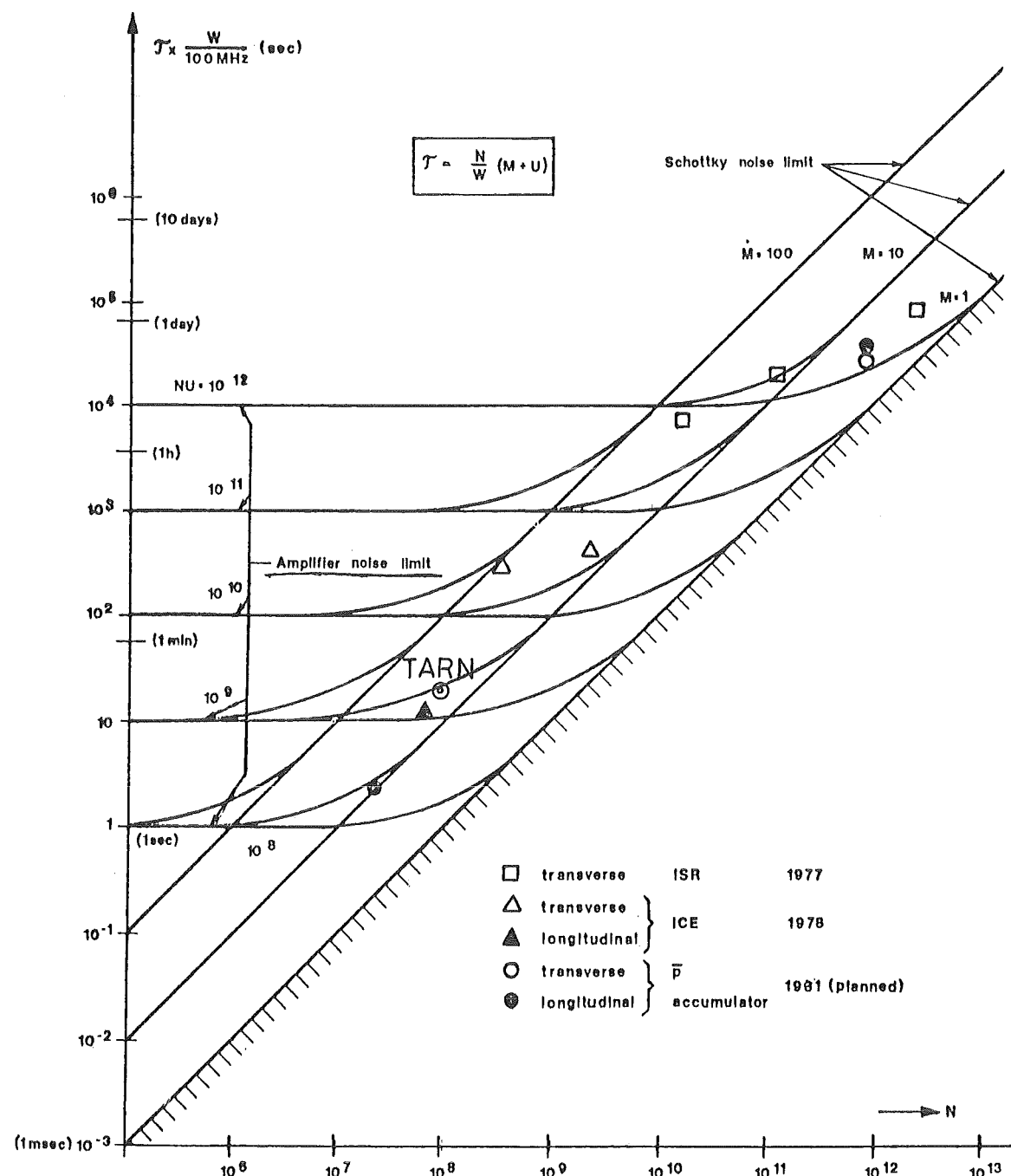


Fig. 2 Cooling result at TARN plotted on the chart of cooling time versus intensity borrowed from Ref. (2).

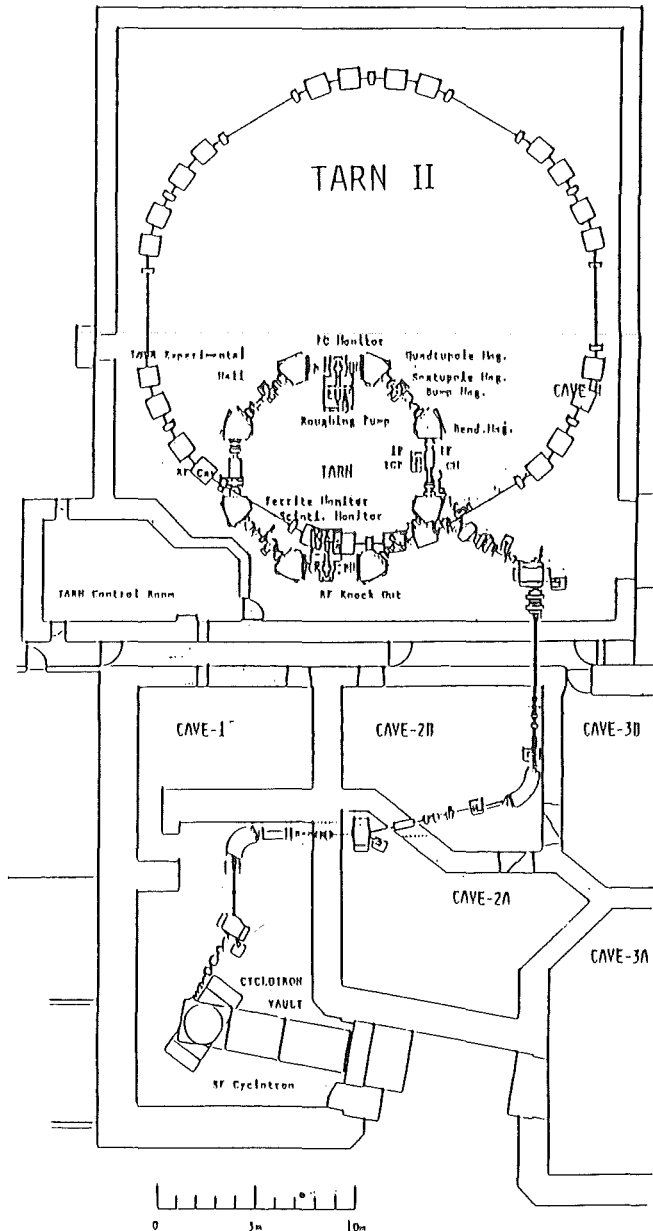


Fig. 3 Layout of TARN II.

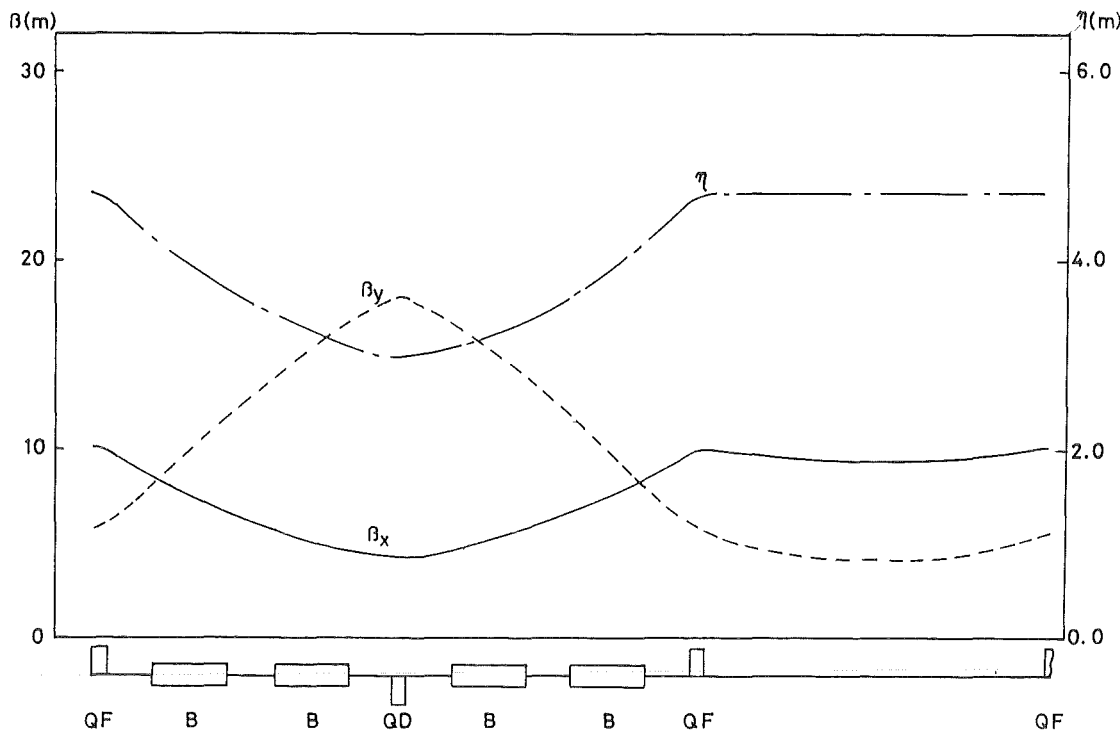


Fig. 4 Beta and dispersion functions of TARN II Synchrotron Mode. Tune values are chosen at 1.75 both in horizontal and vertical directions.

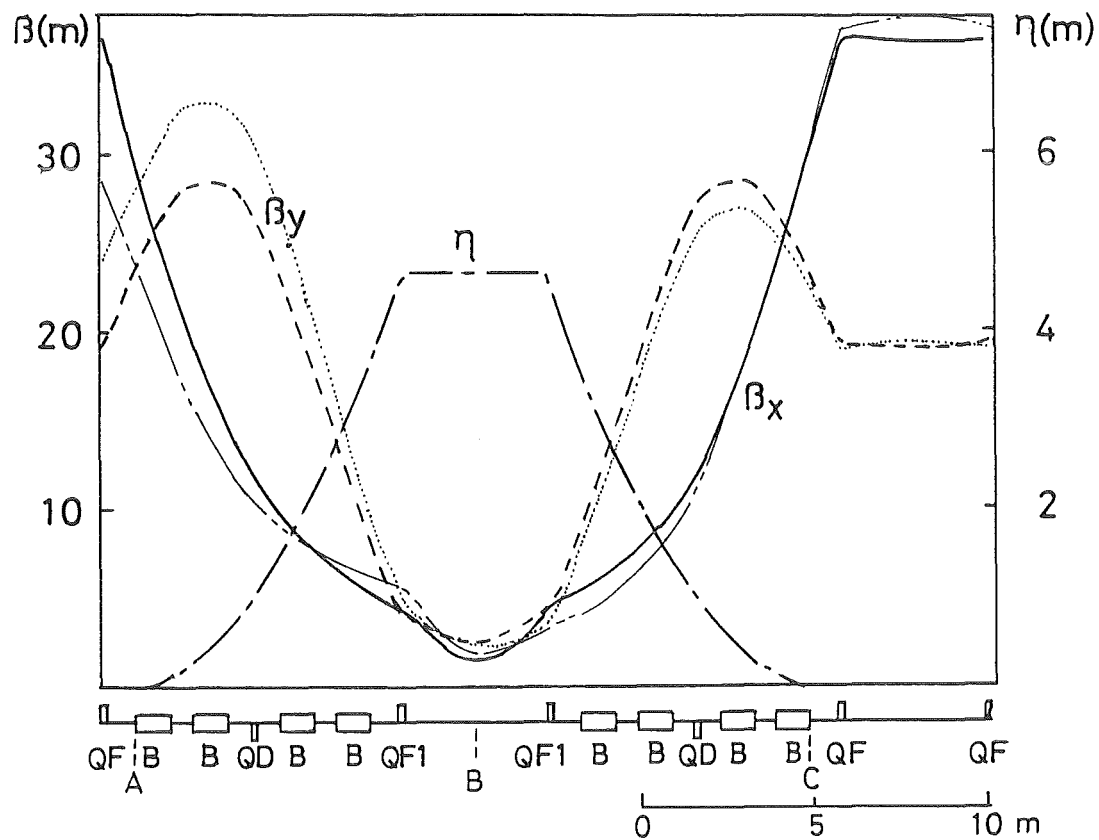


Fig. 5 Beta and dispersion functions of TARN II Cooler Ring Mode with  $v$ -values of 1.75 and 1.25 in horizontal and vertical directions, respectively. Dotted line and dash double dotted line show modified beta-functions with the effect of electron beam.

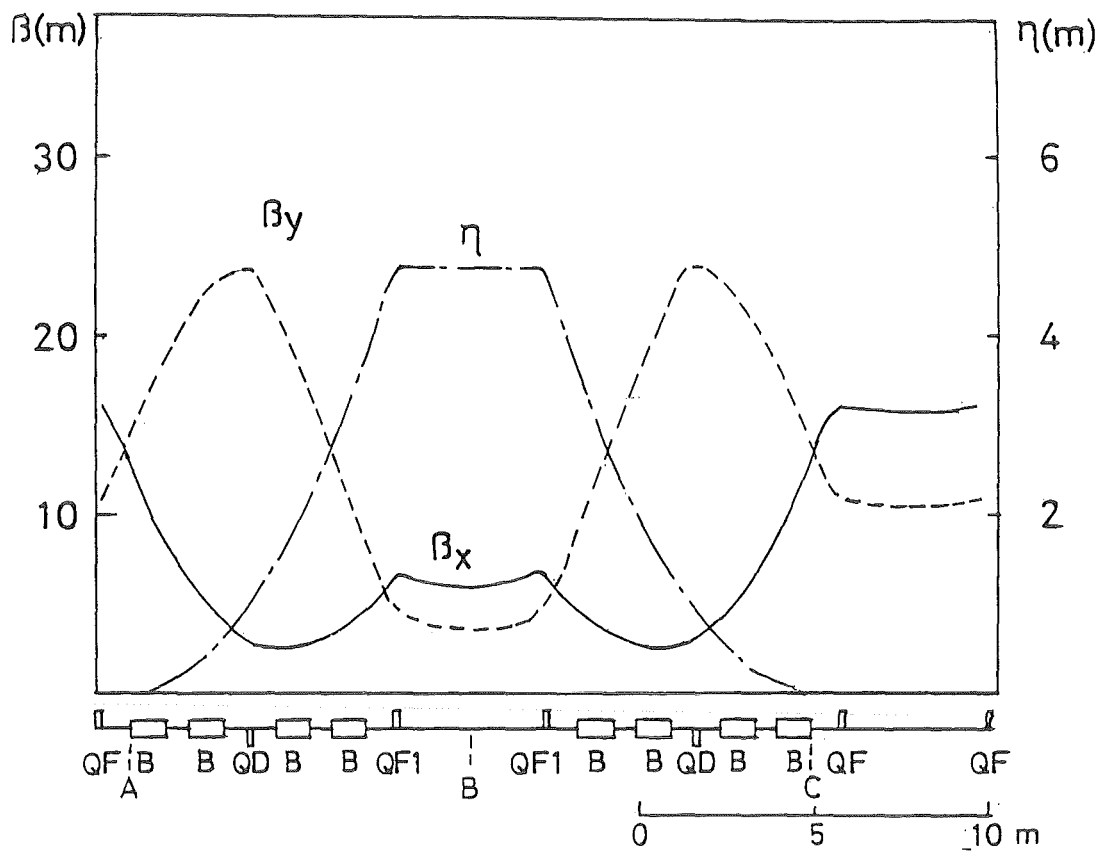


Fig. 6 Beta and dispersion functions of TARN II Cooler Ring Mode with  $v$ -values of 2.25 and 1.25 in horizontal and vertical directions, respectively.

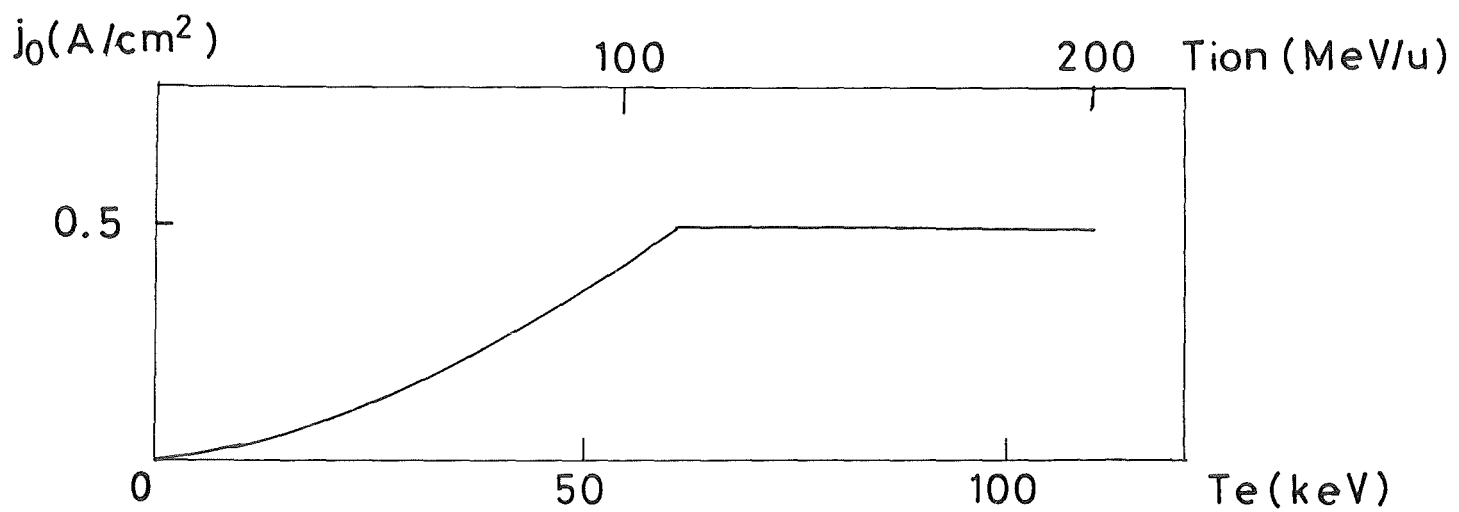


Fig. 7 Assumed current density of the electron beam system for TARN II.

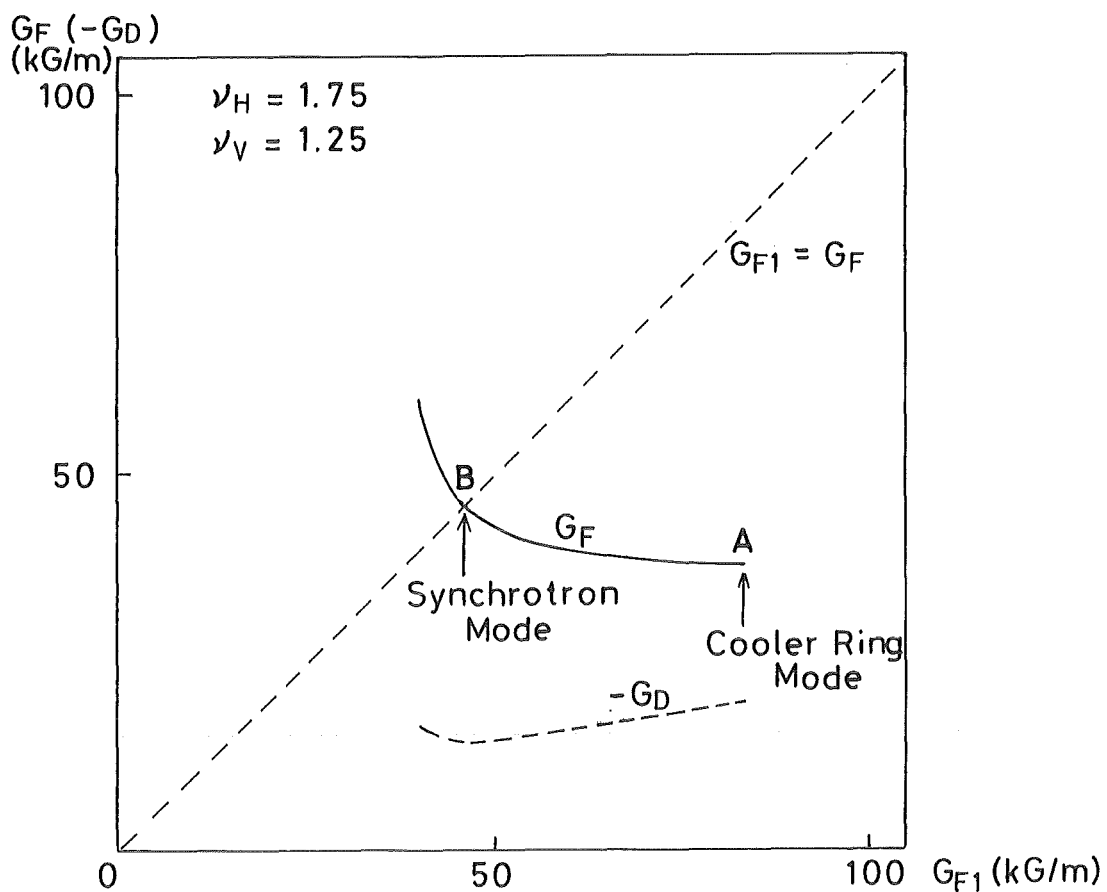


Fig. 8 A variety of parameter sets ( $G_F$ ,  $G_{F1}$ ,  $G_D$ ) to attain  $\nu_H = 1.75$  and  $\nu_V = 1.25$ . The point A realizes Cooler Ring Mode with three doubly achromatic sections, while the point B corresponds to Synchrotron Mode with superperiodicity of 6.

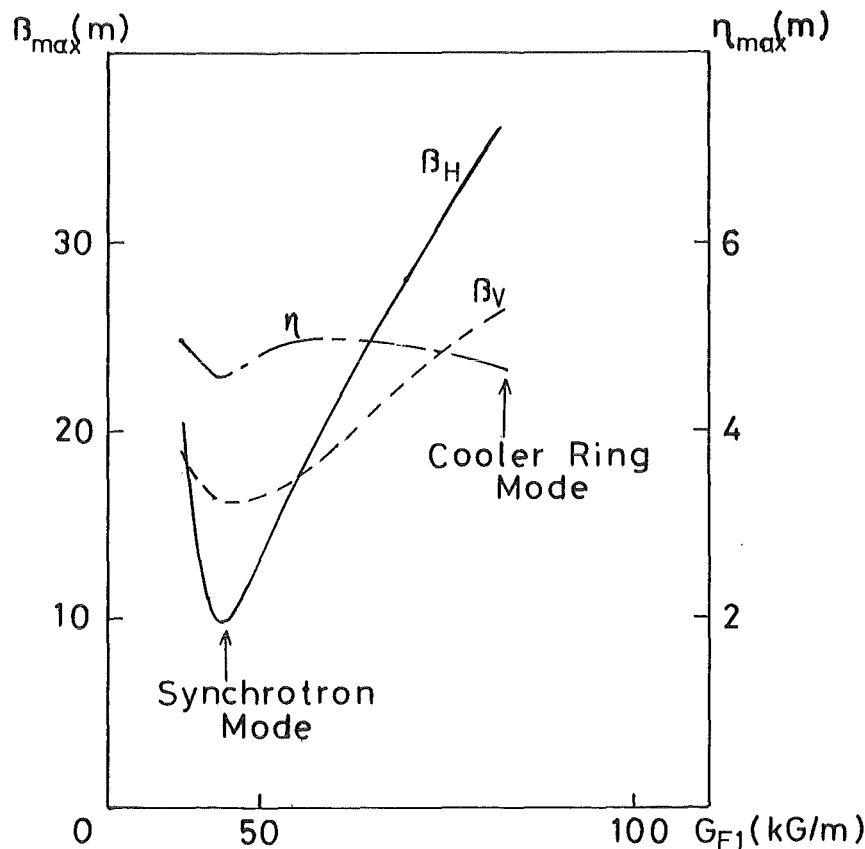


Fig. 9 Dependences of maximum values of  $\beta_H$ ,  $\beta_V$  and  $\eta$  on the parameter  $G_{F1}$  for the condition to fix the operating point to  $(1.75, 1.25)$ .

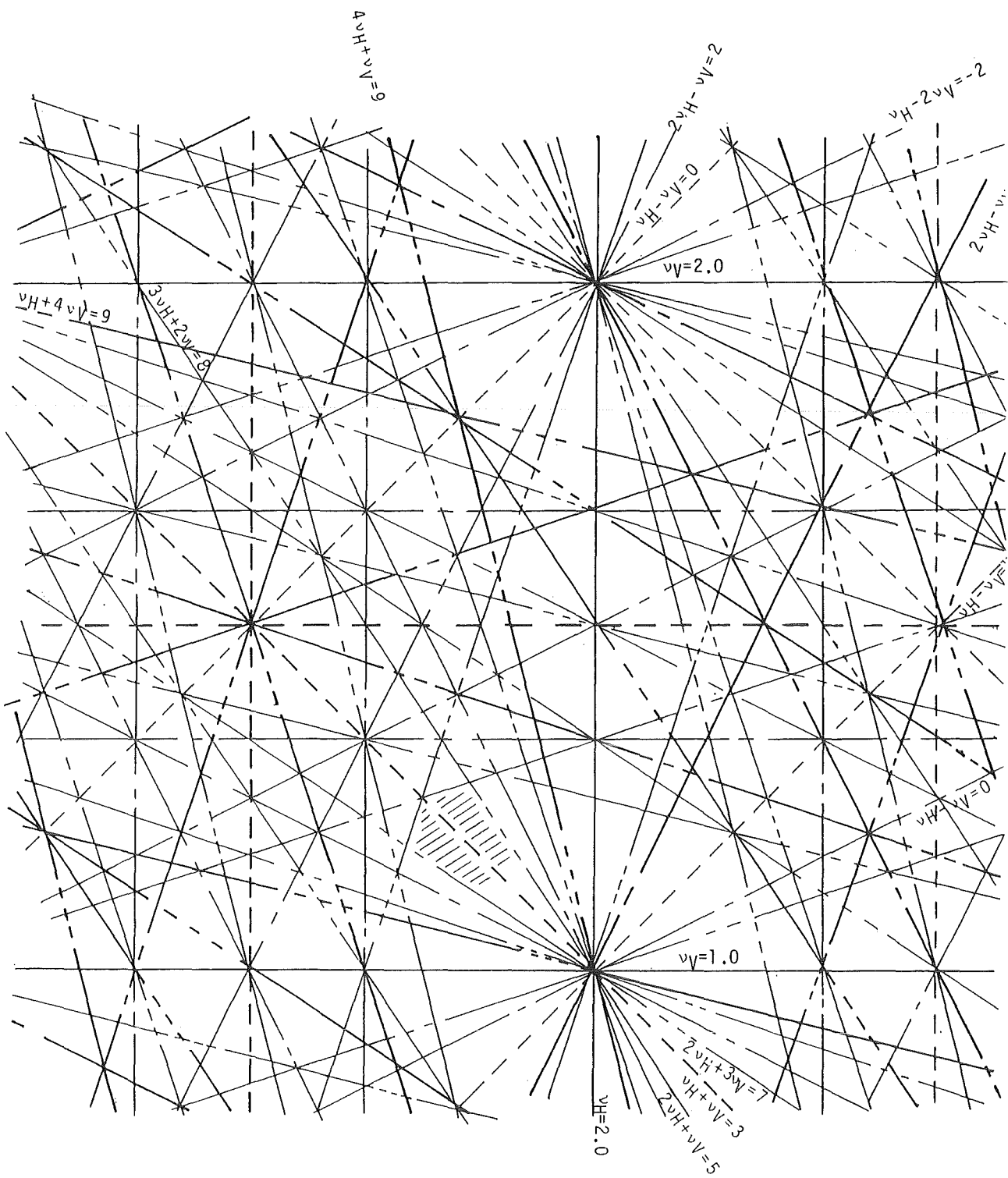
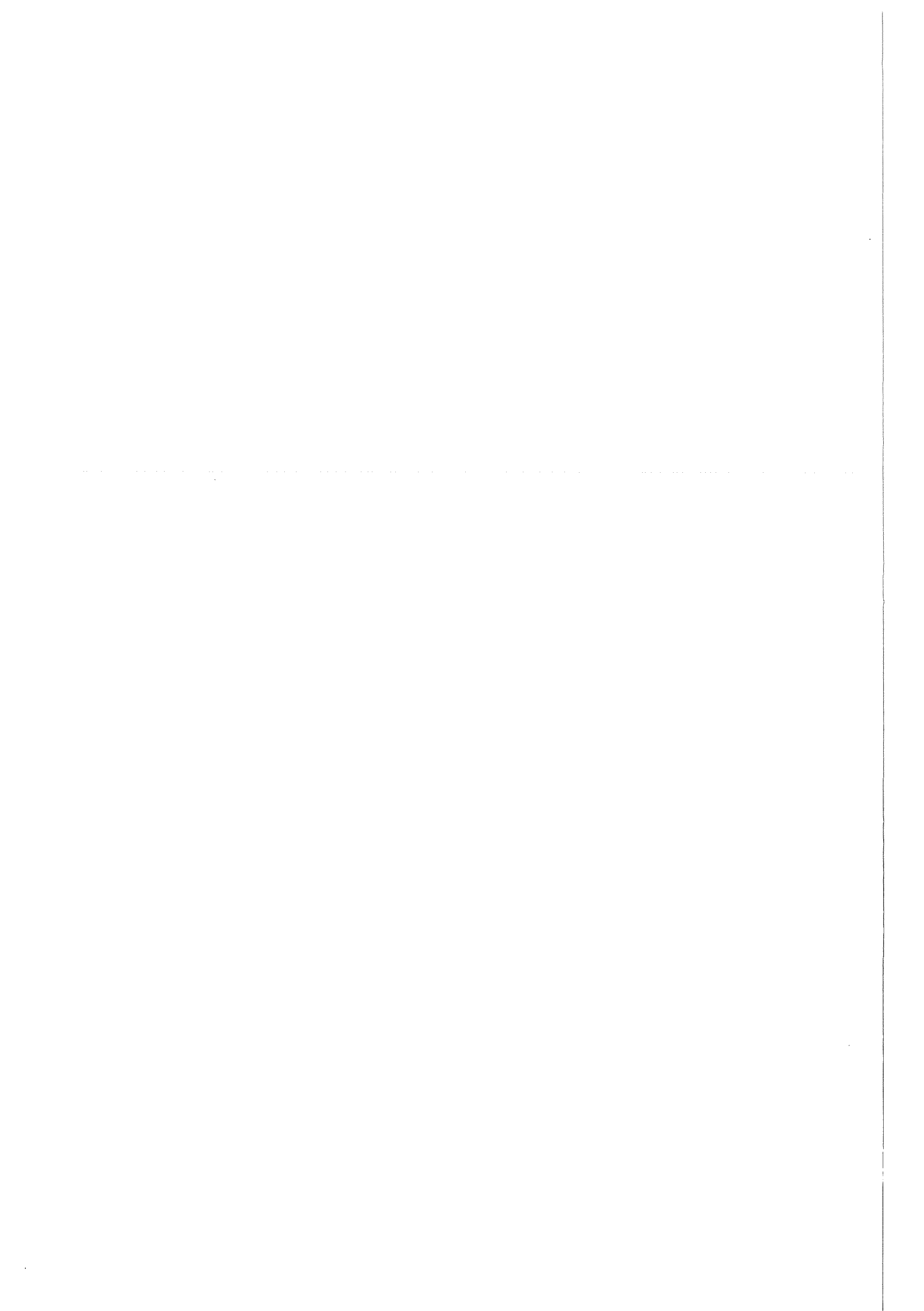


Fig. 10 Resonance lines and assumed region for the operating point of TARN II (shaded area). The region is rather close to the sum resonance,  $v_H + v_V = 3$ , which is structural one for Cooler Ring Mode but is not for Synchrotron Mode.



NEW POSSIBILITIES WITH ELECTRON COOLING  
IN ATOMIC, NUCLEAR AND PARTICLE PHYSICS

K. Kilian

CERN, Geneva Switzerland

(Copy of transparencies)

NEW POSSIBILITIES WITH ELECTRON COOLING  
IN ATOMIC, NUCLEAR AND PARTICLE PHYSICS

K. Kilian  
CERN, Geneva, Switzerland

(Copy of transparencies)

- \* Electron cooling is fast. It allows to balance emittance blow up especially at low energies.
- \* It gives particularly good ultimate beam quality.
- Provides time to perform manipulations on stored particles.  
Internal targets; beam-beam interactions; change of duty cycle;  
bunching; e-capture; ionization; photon-ion interactions;  
mass-frequency measurements; beam diagnostics; ...

Many new possibilities have been discussed at this workshop:

Internal targets, high resolution nuclear physics, storage + cooling of heavy ions and polarized particles. Electron capture processes also with laser charge transfer.

I want to restrict to some few (arbitrary) examples:

(mass measurements,  
electron capture,  
"EBIS")  
(threshold reactions)  
Polarization by filtering (polarized  $\bar{p}$  ?)  
Production + storage of rare particles ( $\bar{d}$ )

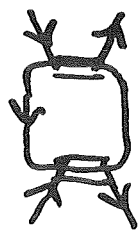
The ultimate beam quality is normally limited by intrabeam scattering  
Inelastic intrabeam scattering of partially ionized ions might be a  
new type of phase space-cooling which could be studied with the dense  
beams obtained with electron cooling.

## Storage Synchrotron with electron cooling

Basic fixed target operation      double ring beam-beam experiment  
 single ring with e cooling      external - internal - antiparallel - parallel



Single ring with e cooling



?

just RF  
 $\frac{\Delta m}{m} = \eta \frac{\Delta f}{f}$   
 intrabeam scattering  
 excites ions  
 photon-emission

capture cools

Electron capture + excitation + ionization of ions

laser induced e capture

Fully stripped heavy ions

recillas production

Mass measurement  
 $\frac{\Delta m}{m} = \eta \frac{\Delta f}{f}$   
 scattering  
 excites ions  
 photon-emission

capture cools

Electron capture + excitation + ionization of ions

laser induced e capture

Fully stripped heavy ions

recillas production

cooling compensates beam blow up →  
 ← Optimally economic use of particles →  
 BETTER - ULTIMATE energy resolution  
 ("Landau") (pure two body systems)  
 Ion-Ion collisions

Production and accumulation  
 of rare nuclei (Reactions with  
 unstable beams?)

Polarization filter?

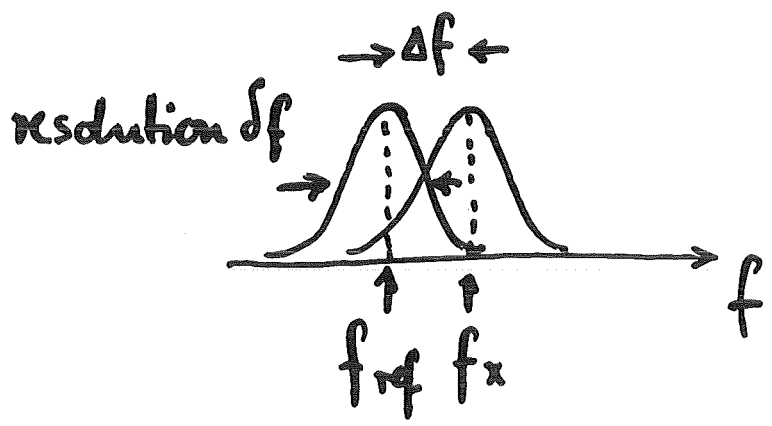
antiproton physics LEAR type →  
 pstop experiments! p and pp react. →  
 ← pstop experiments! p and pp react. →  
 compensation with extreme step density  
 Thresholds and Coulomb slabs



## Mass measurement (comparison)

H. Poth CERN EP/82-56  
also NIM

$$\frac{\Delta f}{f} = \eta \frac{\Delta p}{p} = \eta \frac{\Delta m}{m}$$

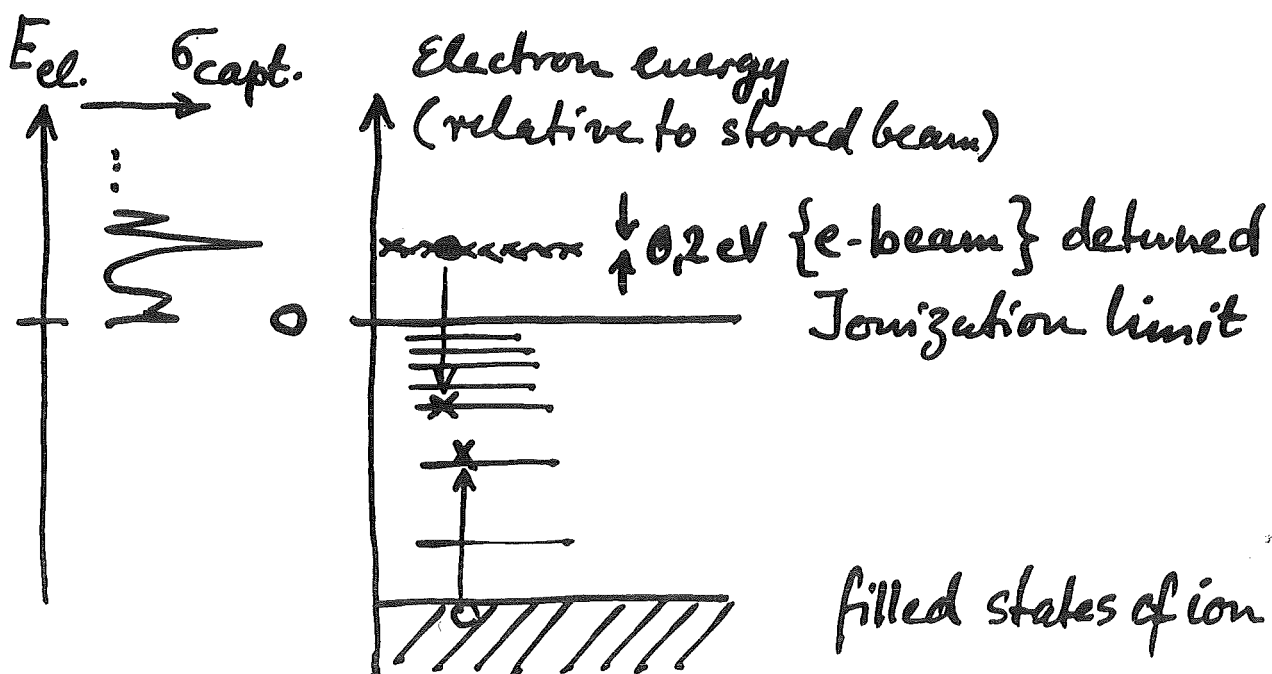


$\Delta f$  and therefore  $\Delta m$  can be measured quite accurately (better than  $\delta f$ )

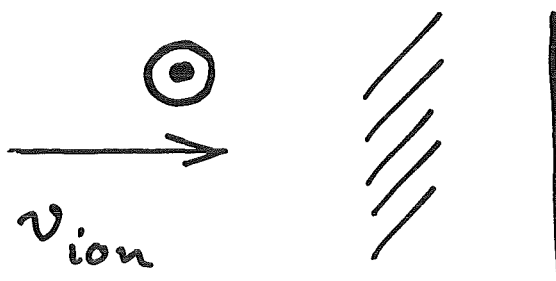
$\delta f$  can be reduced by electron cooling.

## Dielectrowe electron capture with variable electron energy

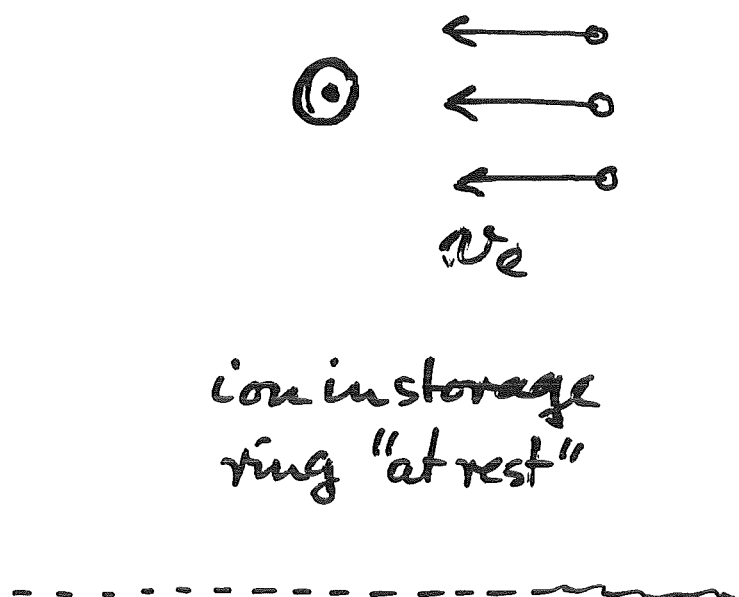
S. Datz  
Kreis proceedings



## Fully stripped heavy ions



Electrons in  
stripperfoil  
at rest



ion in storage  
ring "at rest"

$$v_{\text{ion}} \gtrsim v_{1s}$$

$$v_e \gtrsim v_{1s}$$

For U

$$\Rightarrow E/A \approx 0.4 \text{ GeV}/A$$

For U

$$T_{\text{electr.}} \approx 200 \text{ keV}$$

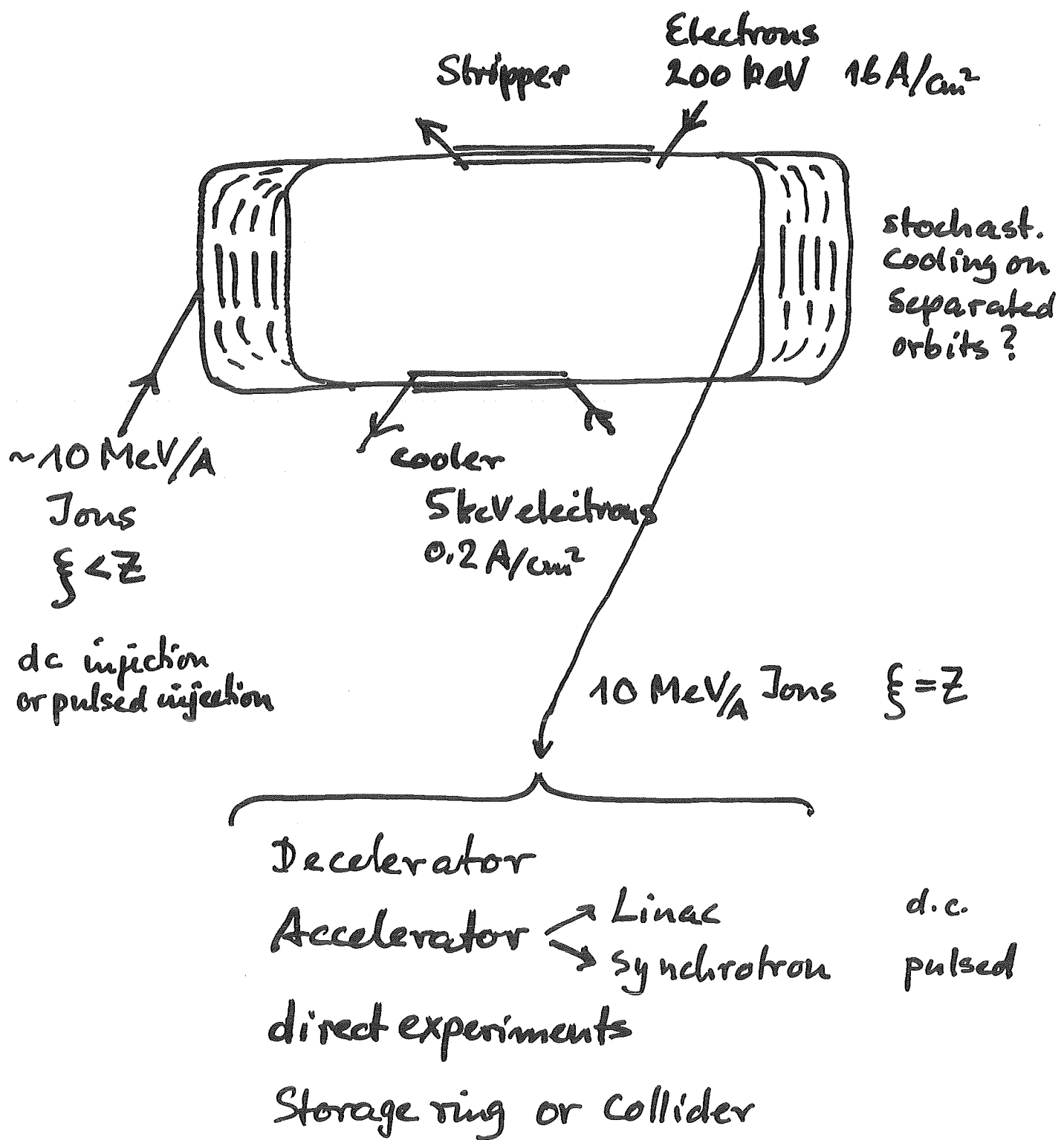
↑  
expensive!

can be achieved with an  
electronbeam overlapping  
the stored ions

(compare EBIS)

J. Möhl + K. K. CERN EP/82-214  
also in  
Lecture Notes in physics Vol 178  
(Springer) 1982 p. 220

# Stripping with electronbeam in cooler ring



Order of magnitude of the time constant for ionization of inner shell electrons in U by an electron current density of  $16 \text{ A/cm}^2$  (over 5 m length and 200 keV energy)

| $i \rightarrow i + 1$ |    | $\tau_{i \rightarrow i+1}$ |
|-----------------------|----|----------------------------|
| 88                    | 89 | $6.3 \cdot 10^2 \text{ s}$ |
| 89                    | 90 | $1.3 \cdot 10^3 \text{ s}$ |
| 90                    | 91 | $1.8 \cdot 10^4 \text{ s}$ |
| 91                    | 92 | $3.6 \cdot 10^4 \text{ s}$ |

$$(\sigma_{91 \rightarrow 92} \sim 10^{-23} \text{ cm}^2)$$

Example

$10^8 \text{ U}^{88+}$  stored  $\rightarrow 1.6 \cdot 10^5 \text{ U}^{89+}$  per sec.

after a breeding time of  $\sim 6$  hours there would be  
 $\rightarrow > 10^3 \text{ U}^{92+}$  per sec

These fluxes of highly ionized heavy ions could be accumulated or extracted continuously for experiments e.g. for  $\beta^+$  experiments (vacuum dissociation) with minimal background.

Here K shell vacancies will have very high probability !

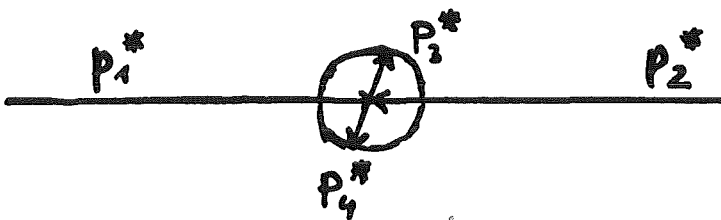
## Close to thresholds

-368-

The kinetic excess energy  $E$  of the particles  $3 + 4 + \dots$  in the c.m. system is small.

C.m. situation

$$(p_3^* = p_4^* = p^* \text{ for 2 body prod.})$$



$$E = \sqrt{S} - (m_3 + m_4) = \frac{(p_3^*)^2}{2m_3} + \frac{(p_4^*)^2}{2m_4}$$

### Consequences

#### PHYSICS

Low relative velocities

Particles stay close to each other for a long time

#### Strong FSI effects

"Known" angular momentum

#### EXPERIMENT

Small transverse momenta in the Lab system ( $\leq p^*$ )

Large longit. momenta in the Lab. System (sums up to  $p_1^*$ )

Particles confined in a narrow forward cone

100% acceptance with small detectors. Low background.

Example:  $p + p \rightarrow d + \pi^+$



$$p_{th} = 788.8$$

| $\Delta p = p - p_{th}$      | 0 | 1   | 2    | 3    | 4    | 10    |
|------------------------------|---|-----|------|------|------|-------|
| $E$ (MeV)                    | 0 | 0,3 | 0,6  | 0,9  | 1,2  | 3,005 |
| $\Theta$ in $m\pi$ {<br>max} | 0 | 12  | 17   | 21   | 24   | 38    |
| $P_3^* = p_4^*$ (MeV/c)      | 0 | 8,8 | 12,5 | 15,3 | 17,7 | 28,1  |

For threshold studies one really needs good energy and angular resolution.

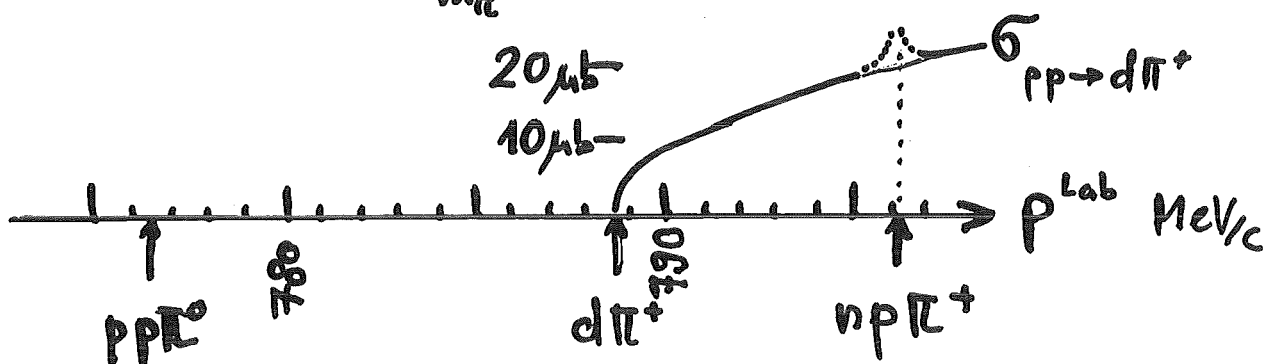
(The missing mass technique does not help if one wants to measure excitation functions)

$$\delta E = \delta \sqrt{S} = \frac{\delta p}{p_{\text{beam}}} \frac{m_{\text{tgt.}} \cdot \beta_{\text{beam}}}{\sqrt{S}}$$

in PP at pion threshold }  $\rightarrow \frac{\delta p}{p} = 10^{-5}$  gives  $\delta E \approx \underline{2.5 \text{ keV}}$

extrapolated (from Crawford + Stevenson P.R. 97(55)1305

$$\sigma_{pp \rightarrow d\pi^+} \approx C \cdot (0.14 \text{ mb} \cdot \frac{p^*}{m_\pi})$$



## Thresholds in $\bar{p}p$ reactions

e.g.



$$P_{th} \sim 100 \text{ keV}_c (\sim 5 \text{ keV})$$



$$P_{th} \sim 1435 \div 1898 \text{ MeV}_c$$

$$\sigma_{\bar{p}p \rightarrow \bar{n}n}$$

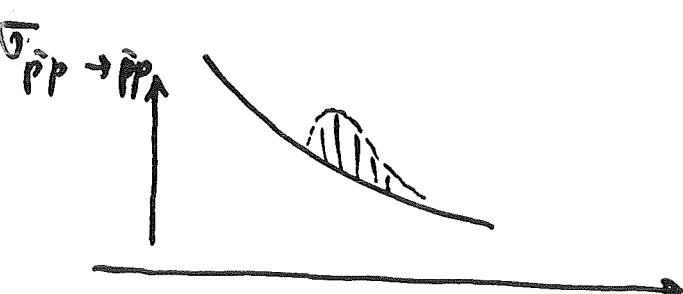
losses via FSI

0

$P_{\bar{p}}$   $\text{keV}_c$

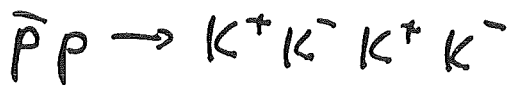
$$\sigma_{\bar{p}p \rightarrow \text{annih}}$$

cusps



low energy  $\bar{n}n$  annihilation may be studied in FSI effects ( $\rightarrow$  cusps)

Exotic example:



$$P_{th} \approx 646,853$$



$$P_{th} \approx 646,901$$

$$\Delta P_c < 10^{-4}$$

Antiproton stop experiments

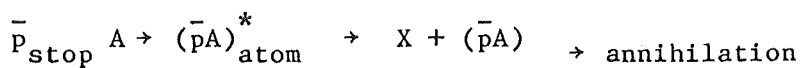
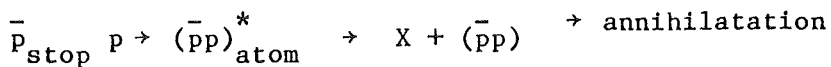
$\bar{p}$  stop distribution is blown up by  
angular straggling : transversly  
energy straggling : longitudinally

Both these unwanted effects can be strongly reduced if one can make a  
high quality low energy  $\bar{p}$  beam  $\rightarrow$  Electron cooling !

| $\bar{p}$ momentum<br>in MeV/c | Range curve width in $\lambda H_2$<br>in g/cm <sup>2</sup> (only straggling) |
|--------------------------------|--|
| 100                            | $3.5 \cdot 10^{-4}$  |
| 300                            | $14 \cdot 10^{-3}$   |
| 900                            | $3.5 \cdot 10^{-1}$  |

$\leftarrow 50\mu \lambda H_2$

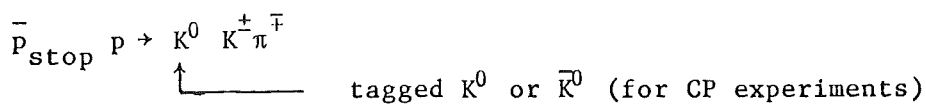
\* The tiny  $\bar{p}$  stop volume is an important experimental advantage !



.

.

.

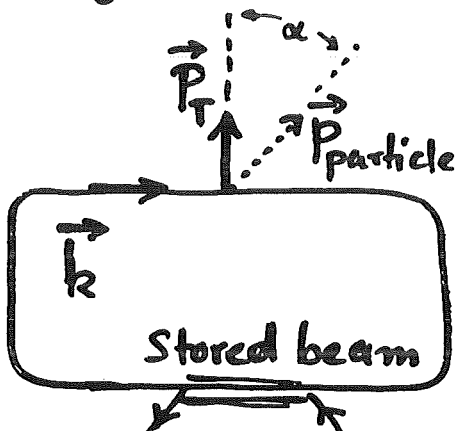


# Polarized $\bar{p}$ stored in LEAR? "Spinfilter"

for  $\bar{p}$  with cooling

K.K + D. Möhl LEAR work-shop Erice 1982

Pass an initially unpolarized beam ( $\uparrow, \downarrow$ ) through an internal ~100% transversely pol. jet target ( $\uparrow$ ). If e.g.  $\sigma_{\uparrow\uparrow} < \sigma_{\downarrow\uparrow}$ , then in the stack of particles which have not interacted a polarization  $\uparrow$  will be enriched on the expense of intensity



$$\sigma_t = \sigma_0 + \frac{\Delta\sigma_T}{2} \vec{P}_b \vec{P}_T + \underbrace{\sigma_2(\vec{P}_b \cdot \vec{k})(\vec{P}_T \cdot \vec{k})}_{=0}$$

$$\frac{I(t)}{I_0} = e^{-\sigma_0 d \nu t} \frac{2 \sinh(\frac{\Delta\sigma_T}{2} d \nu t)}{\Delta\sigma_T d \nu t}$$

typical time

$$\tau_0 \sim \frac{1}{\sigma_0 \nu d}$$

$$P(t) = \coth\left(\frac{\Delta\sigma_T}{2} d \nu t\right) - \frac{2}{\Delta\sigma_T d \nu t}$$

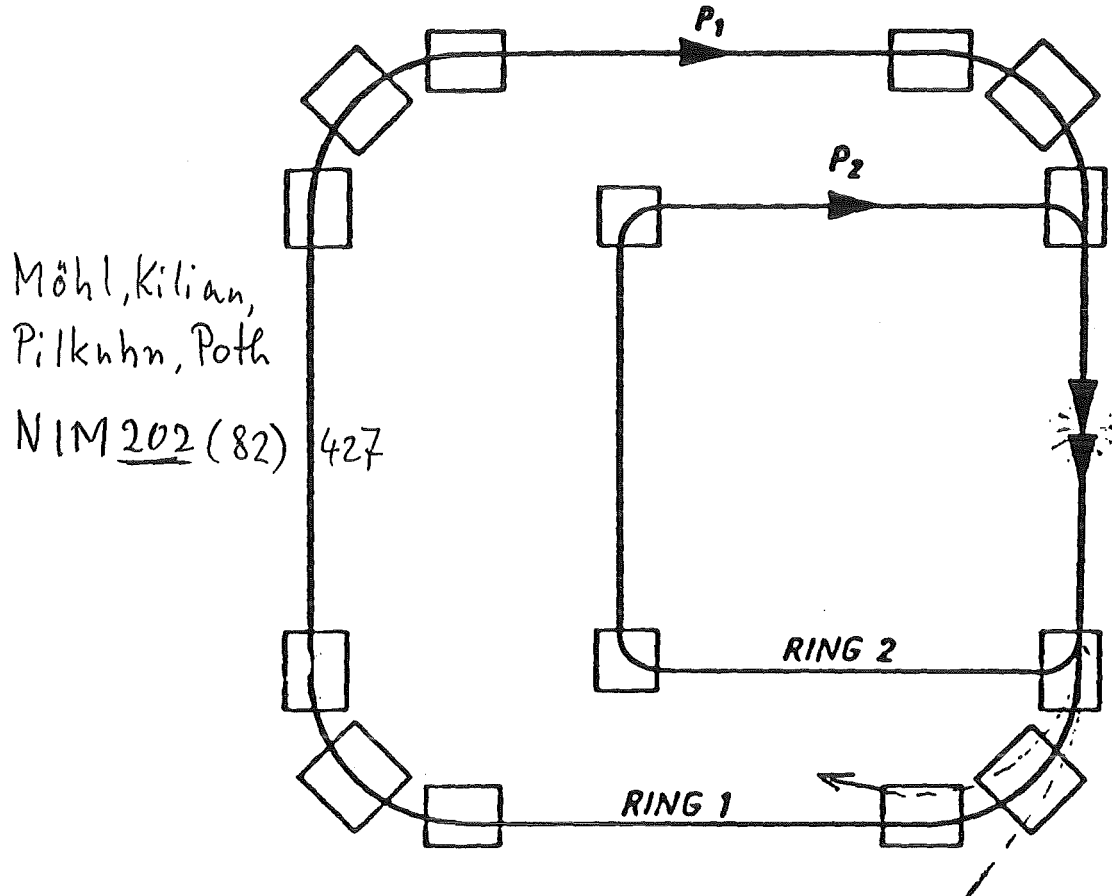
| $t/t_0$ | $\frac{\Delta\sigma_T}{\sigma_0} = 0,2$ |     |         | $\frac{\Delta\sigma_T}{\sigma_0} = 2/3$ |     |         | $\frac{\Delta\sigma_T}{\sigma_0} = 2$ |     |         |
|---------|---|-----|---------|---|-----|---------|---------------------------------------|-----|---------|
|         | $\frac{I}{I_0}$                         | $P$ | $P^2 I$ | $\frac{I}{I_0}$                         | $P$ | $P^2 I$ | $\frac{I}{I_0}$                       | $P$ | $P^2 I$ |
| 1       | .37                                     | .03 | .4%     | .38                                     | .11 | .45%    | .43                                   | .31 | .42%    |
| 2       | .14                                     | .07 | .6%     | .15                                     | .21 | .6,6%   | .24                                   | .53 | .6,9%   |
| 3       | .05                                     | .10 | .5%     | .06                                     | .31 | .5,6%   | .16                                   | .67 | .7,3%   |

Need cooling

$\Delta\sigma_T$  unknown

$\tau_0 \sim 10^4 \text{ s} \leftrightarrow 5 \cdot 10^{-9} \text{ g/cm}$   
pol. "filter" formed

# Antiproton collider to produce antideuterons



In ring 1       $10^{11} \bar{p}$       2 GeV/c  
 In ring 2       $2 \cdot 10^{10} \bar{p}$       0.52 GeV/c

with  $\Delta Q \lesssim 5 \cdot 10^{-3}$

$$L \sim 1.6 \cdot 10^{-28} \text{ cm}^{-2} \text{ s}^{-1}$$



$10^3$  interact./s

$$\gamma = \frac{\frac{d\sigma}{d\Omega}(ppd\Omega) \cdot \Delta \Omega}{(G_t + \Delta G_{cl})}$$

with  $\theta \leq 1^\circ$  and

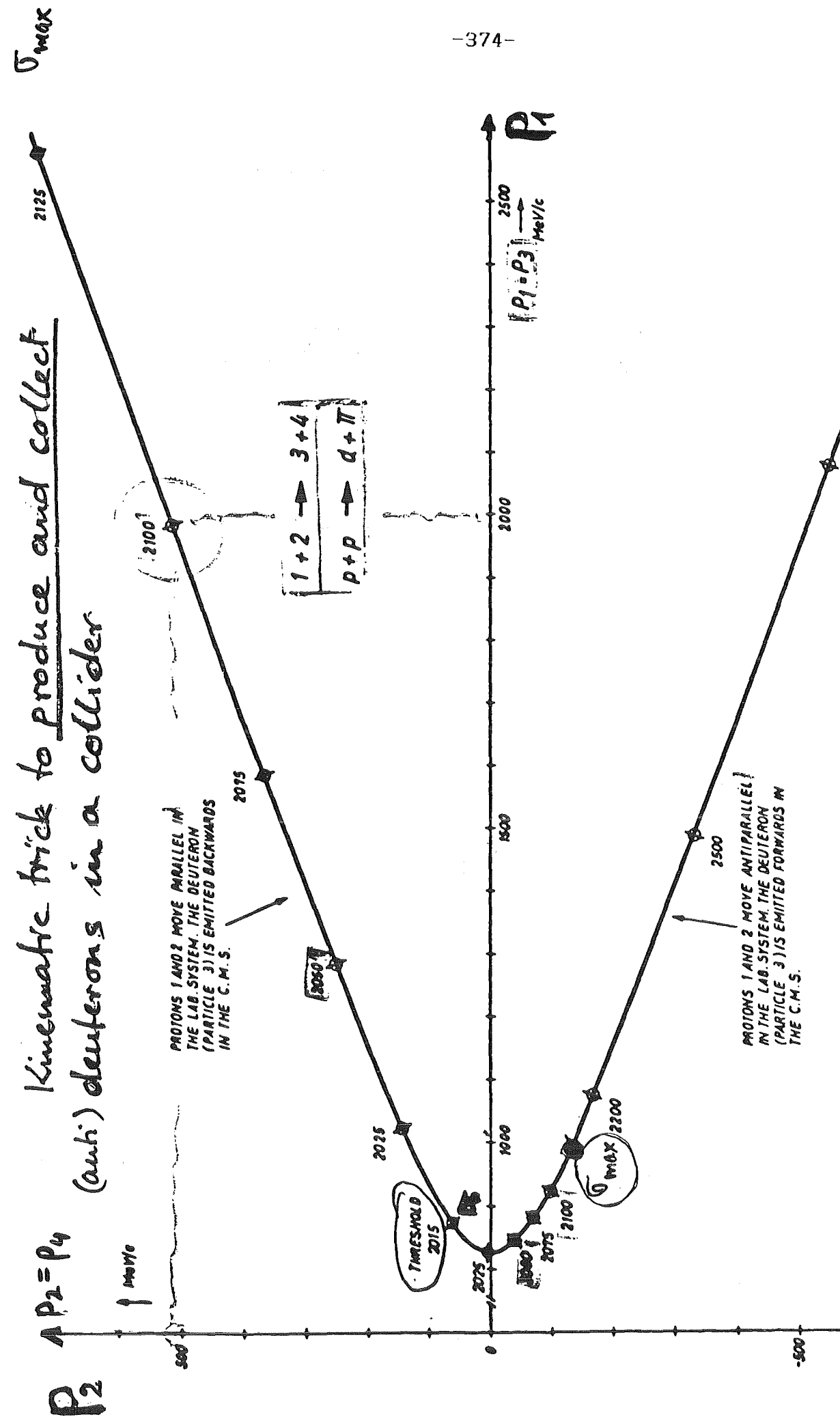
$$\frac{dp/p}{p} \leq 10^{-3} \text{ (for d)}$$



$$\gamma \sim \frac{1}{2} 10^{-3} \frac{d}{(\bar{p}_{\text{used}})}$$

0.5  $\bar{d}$  per second

( $4 \cdot 10^4$  / day)



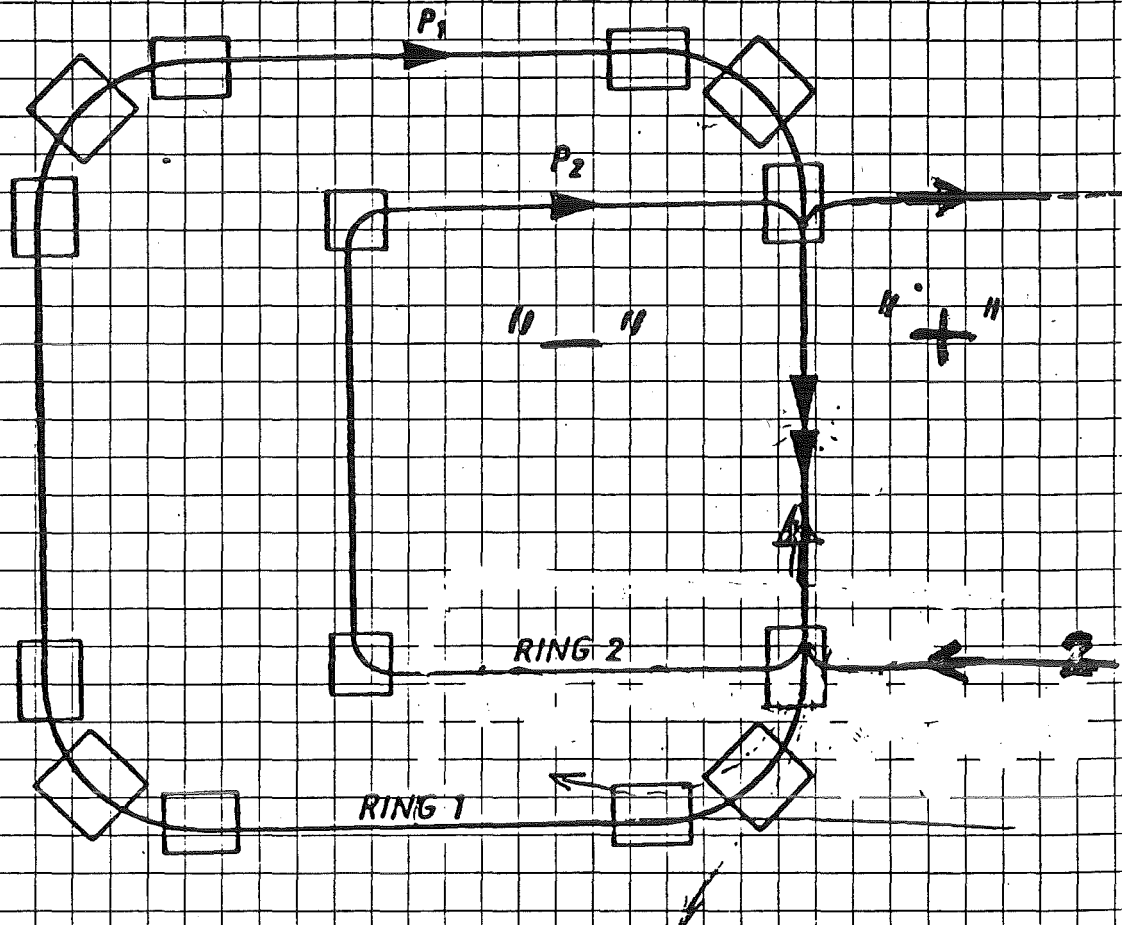
Combinations of  $P_1$  and  $P_2$  which are on the curve give reaction products with

$$P_1 = P_3 \quad \text{and} \quad P_2 = P_4$$

By moving on the curve one can change the invariant mass  $\sqrt{s}$

# Ion Collider parallel (" - ") or antiparallel (" + ")

Accumulation and experiments with unstable isotopes ( $\beta$ )



Produced ions will be accepted in rings 3 if  
in reaction



$$\frac{P_1}{Z_1} = \frac{P_3}{Z_3} \quad \text{or} \quad \frac{P_2}{Z_2} = \frac{P_4}{Z_4}$$

Kinematics:

$$S_{12} = m_1^2 + m_2^2 + 2(E_1 E_2 - \vec{p}_1 \cdot \vec{p}_2)$$

In parallel mode ( $\theta_{12} = 0^\circ$ )

$$\text{Kin. En. : } E = (\sqrt{S} - m_1 - m_2) \approx \Delta p \frac{(\beta_1/\beta_2 - 1) p_2}{\sqrt{S}}$$

Radiative cooling of (partially ionized) stored ions

K.K. CERN EP internal report 84-05

Idea:

- \* Intrabeam scattering excites (partially ionized) ions
  - \* Radiative de-excitation then removes energy
  - \* Relative motion of ions is damped (bunched beam)
- Avoid charge changing collisions

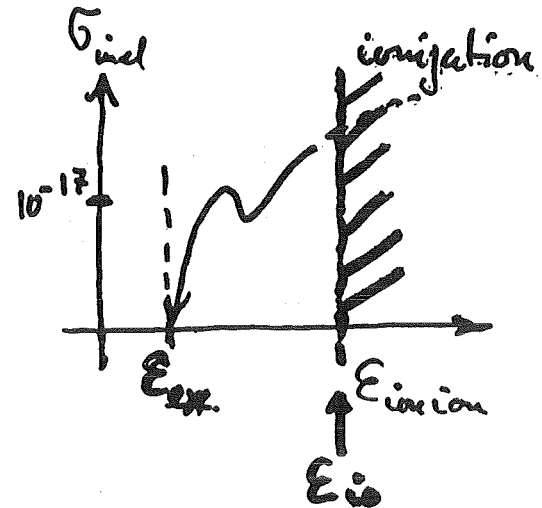
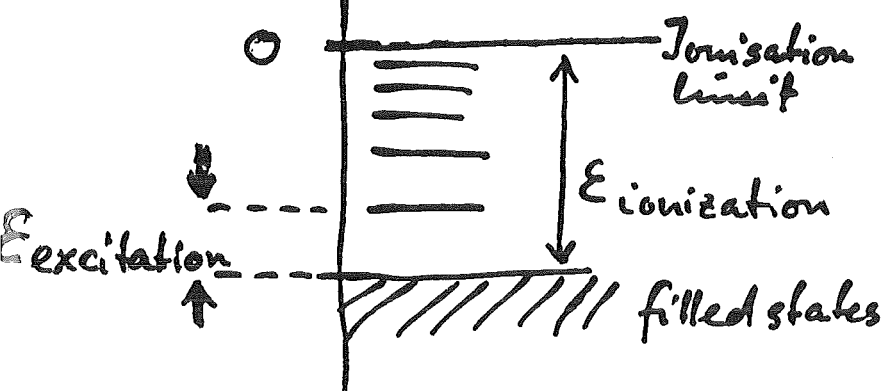
$$\text{Keep } \varepsilon_{\text{coll}} < \varepsilon_{\text{ioniz.}}$$

- Provide enough collision energy

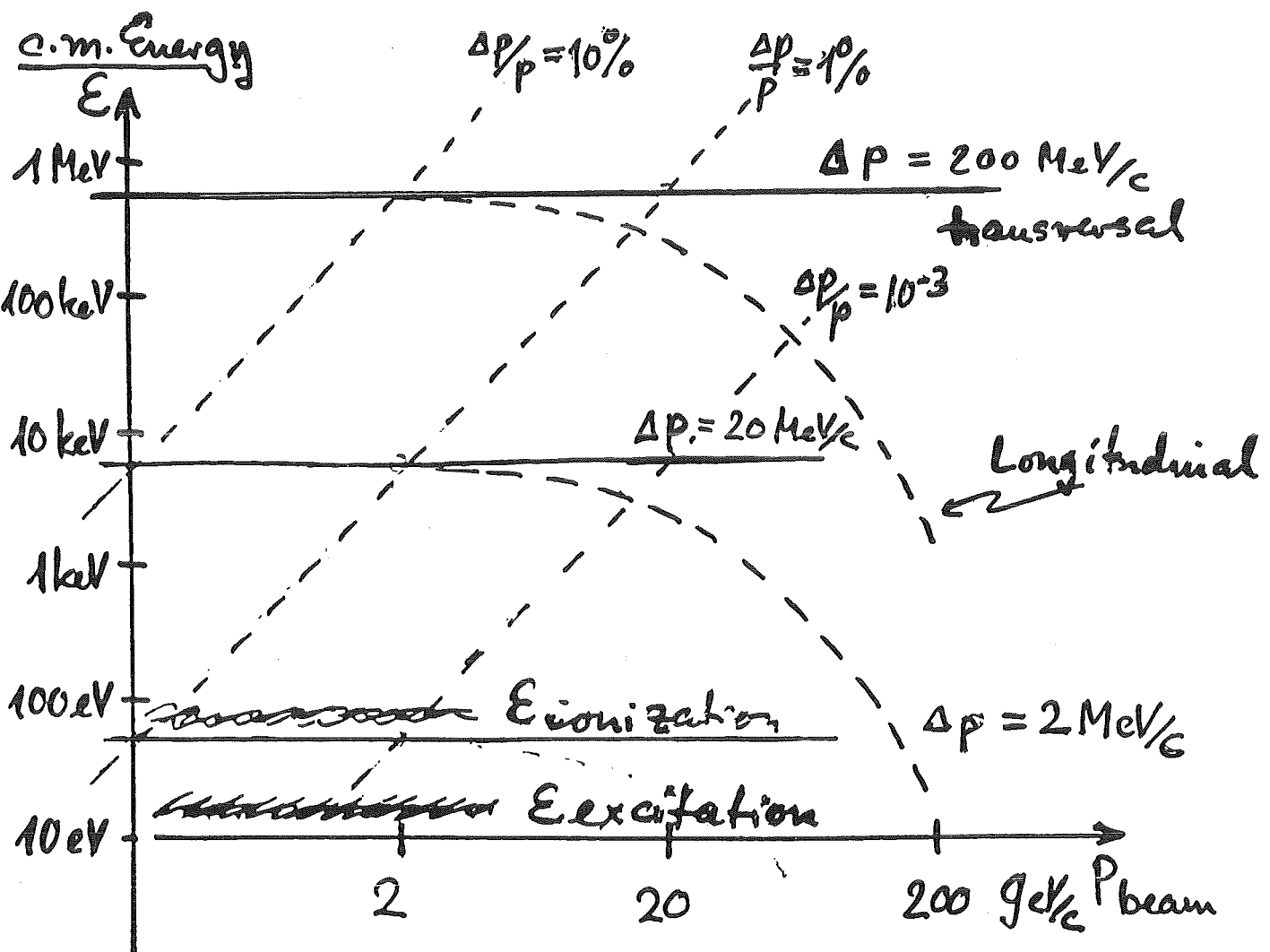
$$\text{Keep } \varepsilon_{\text{excit.}} < \varepsilon_{\text{coll}}$$

The cooling process reduces  $\varepsilon_{\text{coll}}$ . An increase of RF voltage allows to increase  $\Delta p$  in turn and  $2 \cdot \varepsilon_{\text{coll}} \sim (\Delta p)^2 / 2 m_{\text{ion}}$  so that cooling can go on. Longitud. emittance :  $\Delta p \cdot \Delta \phi = \text{const.}$  (if no cooling) and  $\Delta p \propto \sqrt{U_{\text{RF}}}$ .

By continuously increasing  $U_{\text{RF}}$  one keeps  $\Delta p$  at an optimum. The radiative damping leads to a continuous reduction of the bunch length  $\Delta \phi$ . Finally an adiabatic reduction of  $U_{\text{RF}}$  reduces  $\Delta p$  on the expense of increased  $\Delta \phi \rightarrow$  cool beam (compare adiabatic demagnetisation)



$\{^{20}\text{Ne} + ^{20}\text{N}_2\}$  Intra beam scattering



- Provide high enough collision rate

$$\tau_{\text{coll}}^{-1} \approx \sigma \cdot L_1 \approx \sigma \cdot \frac{1}{4} \frac{N}{L} \frac{1}{A} c \cdot \Delta\beta$$

Example:

$$N \approx 10^{11} \text{ ions}$$

$$L \approx 5 \text{ m bunch length}$$

$$A \approx 1 \text{ cm}^2 \text{ beam } \phi$$

$$\Delta\beta \approx 1.4 \cdot 10^{-4} \quad \leftarrow \Delta p/p = 10^{-3} \text{ for } {}^{20}\text{Ne } 2 \text{ GeV/c}$$

$$\sigma_{\text{excit}} \approx 10^{-17} \text{ cm}^2 \quad \leftarrow \text{atomic cross section}$$

$$\tau_{\text{coll}}^{-1} = 2 \cdot 10^{-3} \text{ s}^{-1}$$

$$\frac{1}{2} \tau_{\text{coll}} \sim 500 \text{ s} \gg \tau_{\text{rad}}$$

Process is determined by

collision rate alone and not by  
radiative de-excitation

- Features of ion cooling by photon emission

- \* works with partially stripped ions
- \* each ion has its own optimal  $\Delta p$  range
- \* better with higher beam density
- \* needs bunching; gives short bunches

#### COMPARISON OF COOLING METHODS

|  | Electron       | Stochastic       | Photon<br>(if it works) |
|--|----------------|------------------|-------------------------|
| high density<br>large $\Delta p$<br>technical effort | 0<br>-<br>high | -<br>+<br>medium | +<br>tunable (+)<br>low |

Note: This cooling method can be best studied with dense beams  
 → use electron cooling as a first step.

**Electron Capture.**

Mary Bell, CERN.

In electron cooling of a proton beam, a proton sometimes captures an electron, with radiation of a photon and formation of a hydrogen atom. We summarize here simple approximate formulae for capture cross section and recombination rate [1]. To cover the case of bare nuclei other than the proton, the nuclear charge will be taken as  $Z_e$  in what follows, with  $Z=1$  for proton.

The capture cross section in nonrelativistic dipole approximation is [2]:

$$(1) \quad \sigma = (E_0/E) A s$$

where

$$A = \pi 2^5 3^{-3/2} (h/(2\pi m_e c)) (e^2/m_e c^2) = 2.105 10^{-22} \text{ cm}^2$$

$$h/(2\pi m_e c) = \text{electron Compton wavelength} = 2.818 10^{-13} \text{ cm}^2$$

$$(e^2/m_e c^2) = \text{classical electron radius} = 3.862 10^{-11} \text{ cm}^2$$

$E$  = electron kinetic energy in nucleus rest system

$E_0$  = ground state binding energy of hydrogenic atom =  $13.61 Z^2 \text{ eV}$

and

$$(2) \quad s = \sum_1^{\infty} g_n / (n + n^3 E/E_0)$$

where the  $g_n$ , functions of  $E/E_0$ , are the 'Gaunt factors'. The terms in the summation refer to the various energy levels in which the atom can be formed.

The Gaunt factors can be expressed in terms of hypergeometric functions, and the series summed numerically. Results for  $\sigma$  are quoted by Bates et al. [3] and by Nieminen [4]. (Actually Nieminen considers the capture of electrons by positrons; the above formulae apply with  $m_e$  replaced by the reduced mass  $m_e/2$ ; then  $A = 8.421 \cdot 10^{-22} \text{ cm}^2$  and  $E_0 = 6.80 \text{ eV}$ ). In Table 1 columns 3 and 4 give values of  $s$  extracted from these results.

We are interested in simple approximate formulae which can be readily averaged over electron velocity distributions. Asymptotic expansions of the  $g_n$  [5] indicate that they become unity for small  $(E/E_0)$  and large  $n$  (at fixed  $n^2 E/E_0$ ). Then for small  $E/E_0$  we expect

$$s \approx \sum_{n=1}^{\infty} (n + n^3 E/E_0)^{-1}$$

$$\approx \int_{1}^{\infty} (n + n^3 E/E_0)^{-1}$$

$$\approx \int_{1}^{N} dn/n$$

(with  $N = \sqrt{E_0/E}$ )

$$= \ln \sqrt{E_0/E}$$

Taking account [5] of the next terms in the expansion gives the improved approximation

$$(3) \quad s = \ln \sqrt{E_0/E} + .1402 + .525(E/E_0)^{1/3}$$

Numerical values of (3) are given in column 2 of the Table . The top few entries are those of most interest for electron cooling. The approximate formula (3) agrees there with the two sets of accurate numerical results about as well as they agree with one another...to about one percent. The approximate formula is still within two percent of Niemenin at  $E = E_0$  and within twenty percent at  $E = 3E_0$ . Above that (3) becomes rapidly much too large.

The recombination rate per proton is

$$\alpha_r n_e$$

where  $n_e$  is number of electrons per unit volume, and

$$\alpha_r = \langle V_e \sigma \rangle$$

where  $\langle \rangle$  denotes averaging over electron velocity  $V_e$ .

In [1] we averaged, with the approximation (3), over Maxwellian and 'flattened' Maxwellian distributions:

$$\text{Maxwell: } f(V_e) = (m_e/(2\pi kT))^{3/2} \exp(-E/(kT))$$

$$\text{flattened: } f(V_e) = (m_e/(2\pi kT))\delta(V_{ex})\exp(-E/(kT))$$

The results are

$$(4) \quad \alpha_r(\text{Max.}) = B\sqrt{E_0/kT} [\ln\sqrt{(E_0/kT)} + .429 + .469(kT/E_0)^{1/3}]$$

$$(5) \alpha_r(\text{flat.}) = (\pi/2)B\sqrt{(E_0/kT)}[\ln\sqrt{(E_0/kT)} + 1.122 + .334(kT/E_0)^{1/3}]$$

where

$$B = c\sqrt{(8/\pi)}\sqrt{(E_0/m_e c^2)}A = 5.20 \times 10^{-14} \text{ cm}^3/\text{sec}$$

Numerically, with  $kT$  in electron volts,

$$(6) \alpha_r(\text{Max.}) = 1.92 Z^2/\sqrt{(kT)}[\ln(5.66Z/\sqrt{(kT)}) + .196(kT/Z^2)^{1/3}] 10^{-13} \text{ cm}^3/\text{sec}$$

$$(7) \alpha_r(\text{flat.}) = 3.02 Z^2/\sqrt{(kT)}[\ln(11.32Z/\sqrt{(kT)}) + .140(kT/Z^2)^{1/3}] 10^{-13} \text{ cm}^3/\text{sec}$$

Formula (4) is equivalent to one given by Seaton [5] (his (36)). In fact the coefficients in (3) were chosen to this end. According to Seaton the formula should be accurate to a few percent for  $(kT/Z^2) < 1\text{eV}$ . It agrees within one percent with results quoted by Massey et al. [6] (their table 14.4) for  $.02\text{eV} < kT/Z^2 < 5\text{eV}$ . We suppose (7) to be of similar accuracy.

Simple approximations to (6) and (7) are

$$(8) \alpha_r(\text{Max.}) = 3.79 (Z^2/kT)^{678/1000} 10^{-13} \text{ cm}^3/\text{sec}$$

$$(9) \alpha_r(\text{flat.}) = 7.88 (Z^2/kT)^{645/1000} 10^{-13} \text{ cm}^3/\text{sec}$$

These reproduce (6) and (7) to within one percent for

$$.07 < kT/Z^2 < .07$$

and to within ten percent for

$$01 < kT/Z^2 < 3.0$$

with  $kT$  always in electron volts.

We retained the factor  $Z$  above, to cover not only the proton case, but also that of other fully stripped nuclei (with  $Z \ll 137$ , so that the nonrelativistic approximation is good). For nuclei which retain some electrons, the formulae do not apply. The states already occupied must be excluded from the summation defining  $s$ . Even for unoccupied states, the hydrogenic wavefunctions are not quite correct. And there are processes in which the electron cloud becomes excited.

We worked above in the common rest system of nucleus and electron gas. With the  $\alpha_r$  so calculated, and with  $T$  still defined in the rest system of the electron gas, the capture rate per proton in the laboratory system is

$$(10) \quad \alpha_r n_e d \gamma^{-2}$$

where

$n_e$  = electron density in lab. system

$\gamma = (1 - V_0^2/c^2)^{1/2}$

$V_0$  = mean electron velocity, and nucleus velocity, in lab.

$c$  = velocity of light

$d$  = fraction of ion orbit to which cooling is applied

REFERENCES.

- [1] M. Bell and J.S. Bell, Particle Accelerators 12(1982)49
- [2] L. Spitzer, Physics of Fully Ionized Gases (Interscience, New York 1956)
- [3] D. R. Bates et al., Proc. Roy. Soc. A170(1939)322
- [4] I. Nieminen, Arkiv for Fysik 35(1967)1
- [5] M. J. Seaton, Mon. Not. Roy. Ast. Soc. 119(1959)81
- [6] H. S. W. Massey, E. H. S. Burhop, and H. B. Gilbody, Electronic and Ionic Impact Phenomena (Oxford 1969) Vol. 2, ch. 14

Table: Reduced capture cross sections  $s$  according to approximation (3) compared with accurate numerical calculations of Nieminen and of Bates et al.

| $\sqrt{E/E_0}$ | $s(3)$ | $s(\text{Nieminen})$ | $s(\text{Bates et al.})$ |
|----------------|--------|----------------------|--------------------------|
| .05            | 3.207  | 3.185                | 3.23                     |
| .07143         | 2.870  |                      | 2.88                     |
| .1             | 2.556  | 2.577                | 2.55                     |
| .1429          | 2.229  |                      | 2.23                     |
| .2             | 1.929  | 1.955                |                          |
| .3             | 1.579  | 1.603                |                          |
| .4             | 1.342  | 1.362                |                          |
| .5             | 1.164  | 1.180                |                          |
| .6             | 1.025  | 1.036                |                          |
| .7             | .911   | .918                 |                          |
| .8             | .816   | .817                 |                          |
| .9             | .735   | .730                 |                          |
| 1.0            | .665   | .655                 |                          |
| 1.5            | .423   | .394                 |                          |
| 2.0            | .280   | .250                 |                          |
| 2.5            | .191   | .166                 |                          |
| 3.0            | .134   | .115                 |                          |
| 4.0            | .077   | .062                 |                          |
| 5.0            | .066   | .037                 |                          |
| 7.0            | .115   | .016                 |                          |
| 10.0           | .274   | .006                 |                          |

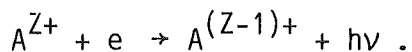
Laser Induced Electron Capture and  
Related Physics

R. Neumann

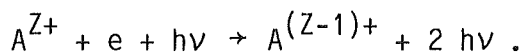
Physikalisches Institut der Universität Heidelberg  
Federal Republic of Germany

### 1. Introduction

The concept of induced transitions between bound atomic states in the presence of a resonant radiation field can be immediately extended to radiative electron-ion recombination, i.e. the capture of a continuum electron into a bound state, connected with the emission of a photon. Spontaneous radiative electron capture by ions of charge  $Z+$  can be written as



For low electron densities, this is the only way how electrons and bare nuclei, especially protons, but also electrons and positrons can recombine. Additional irradiation of an intense light beam should enhance the recombination process via stimulated emission of a photon as described by



The enhancement of positronium formation under the influence of a strong light field, travelling in opposite direction to overlapping beams of electrons and positrons, was proposed and discussed in ref. 1. Laser-induced electron-ion recombination was treated theoretically (2-4), but has not yet been demonstrated experimentally.

This report deals with various aspects of laser-enhanced radiative capture of cooling electrons by charged particles stored in a ring, like protons and heavy ions. After a brief review of basic ideas, conceivable applications are considered, namely beam diagnostics of the electron cooling device, production of antihydrogen atoms, and preparation of Rydberg states, i.e. states with large principal quantum number  $n$ , of highly charged heavy ions.

## 2. Radiative electron-ion recombination

### a. Electron cooling

Let us consider the following specific configuration: Ions with mass  $m_i$  and charge  $Z+$  which could also be bare nuclei, are stored in a ring. A merging electron beam overlaps the ion beam in a straight section of the ring. Ions and electrons travel in the same direction with the same average velocity  $\bar{v}_i = \bar{v}_e = \bar{v}$ . This is provided by an electron cooling device, inserted in the ring, as was discussed in several contributions to this conference.

The respective spreads of kinetic energies of the two particle beams can be characterized by two temperatures  $T_i$  and  $T_e$ . In a reference frame moving with the velocity  $\bar{v}$  in which ions and electrons are at rest with respect to their average velocity  $\bar{v}_i = \bar{v}_e$ , these temperatures are related with velocity distributions

$$\Delta v_i = \sqrt{2kT_i/m_i} \text{ and } \Delta v_e = \sqrt{2kT_e/m_e}.$$

In case the ions have a larger energy spread than the electrons, they transfer energy to the electrons by collisions, until thermal equilibrium is reached. This is expressed by the equation

$$(m_i/2)\Delta v_i^2 = (m_e/2)\Delta v_e^2 \text{ or } \Delta v_i = \sqrt{m_e/m_i} \Delta v_e.$$

The average relative velocity between ions and electrons is thus dominated by the electron velocity spread, and the ions can be considered to be at rest in the electron gas.

The electrons populate a continuum energy band of width

$$kT_e = (m_e/2)\Delta v_e^2$$

immediately above the ionization limit of the ions of charge Z-1 or of the atoms, if singly charged ions are investigated. During the cooling process spontaneous capture of an electron by an ion can occur via the emission of a photon with energy  $h\nu$ . The photon carries away the sum of the ionization energy of the electronic state in which the captured electron was bound, and of the kinetic energy of the electron (5).

When electron cooling was developed in Novosibirsk and applied to stored protons, one observed the production of hydrogen atoms, and used them as a diagnostic tool (6). The same phenomenon was observed in 1979 with the ICE ring at CERN (7).

### b. Spontaneous recombination

This section treats radiative recombination of protons and electrons during the cooling process in a storage ring. As was said before, the electrons populate an energy band of width  $kT_e$  right above the ionization limit of hydrogen. This is illustrated in Fig. 1. The cross section for capture of an electron into the electronic state with

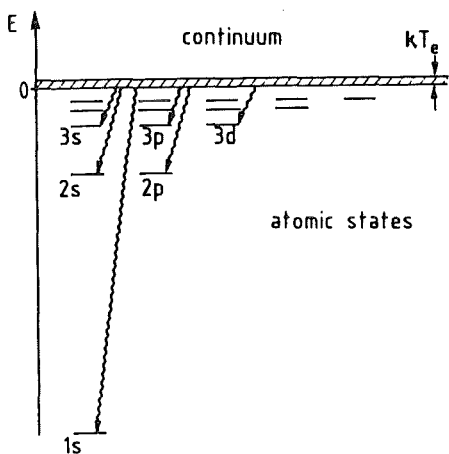


Fig. 1. Energy level diagram of hydrogen illustrating the continuum electron band, as seen in the proton-electron rest frame.

principal quantum number  $n$  is given by the analytical expression (8)

$$\sigma_n = 1.96\pi^2 \alpha \lambda_e^2 \frac{E_0^2}{n E_e (E_0 + n^2 E_e)} = 2.11 \cdot 10^{-22} \cdot \frac{E_0^2}{n E_e (E_0 + n^2 E_e)} \text{ cm}^2 .$$

$E_0$  is the ground state binding energy,  $E_e$  the kinetic energy of the electrons,  $\alpha$  the Sommerfeld fine structure constant, and  $\lambda$  the electron Compton wavelength. For  $E_e \ll E_0$  the equation simplifies to

$$\sigma_n \approx 1.96\pi^2 \alpha \lambda_e^2 (E_0 / n E_e) .$$

More refined calculations for  $\sigma_n$  can be found in ref. 9. The spontaneous capture rate per proton in the proton rest frame is

$$r^{\text{spon}} = n_e \int \sum_{n=1}^{\infty} f(\vec{v}_e) v_e \sigma_n(v_e) d\vec{v}_e = n \alpha_r .$$

Here  $n_e$  is the electron density,  $f(\vec{v}_e)$  the normalized distribution function of the electron velocities, and  $\alpha_r$  the recombination coefficient.

Immediately after emission, the electrons exhibit a Maxwellian velocity distribution, imposed by the temperature of the electron gun cathode. In the direction of electron acceleration a reduction of the initial velocity spread occurs. Thus, the longitudinal velocity distribution  $\Delta v_{||}$  can become much narrower than the transverse distribution  $\Delta v_{\perp}$  which remains unaltered. Rate equations for spontaneous radiative recombination have been developed by various authors (10,11). The expression from ref. 11 for a flattened longitudinal velocity distribution provides

$$\alpha_r^{\text{flat}} = 2.2 \cdot 10^{-12} \text{ cm}^3 \text{s}^{-1}$$

for a transverse electron energy of  $kT_{\perp} = 0.2$  eV where  $T_{\perp}$  is the temperature related with the transverse velocity spread  $\Delta v_{\perp}$ . For 0.2 eV a value of

$\alpha_r = 2.26 \cdot 10^{-12} \text{ cm}^3 \text{s}^{-1}$  was found (12) experimentally in Novosibirsk (13), a result which supports the concept of a flattened distribution.

### b. Laser-induced recombination

Spontaneous capture populates all electronic levels, though with different probabilities. Light irradiation of appropriate wavelength and sufficient intensity should enhance the capture rate to a specific energy level. The recombination process must fulfill energy conservation according to

$$mv^2/2 + E_0/n^2 = hv .$$

This means, that the photon energy  $hv$  must be equal to the sum of  $E_{\text{kin}} = mv^2/2$  of the electrons and the ionization energy  $E_0/n^2$  of the final state with quantum number  $n$ . The emitted photon coherently joins the light wave. From the above formula follows

$$\Delta v = (h/mv)\Delta\nu .$$

$\Delta\nu$  is the combined spectral width of the light field and the final bound state. Thus, only electrons within the velocity band of width  $\Delta v$  will be captured. It is supposed, that the proton velocity distribution can be neglected in comparison to that of the electrons.

In an atomic nondegenerate two-level system, consisting of a higher-lying initial level  $i$  with population number  $N_i$  and a lower-lying final level  $f$ , the number of spontaneous transitions per second from  $i$  to  $f$  is

$$R_{if}^{\text{spon}} = A_{if} N_i = r_{if}^{\text{spon}} N_i .$$

$A_{if}$  is the Einstein coefficient for spontaneous emission. In the presence of a light field with the spectral energy density  $u(\nu)$ , the number of induced transitions per second from  $i$  to  $f$  is

$$R_{if}^{ind} = u(v) B_{if} N_i = r_{if}^{ind} N_i.$$

$B_{if}$  is the Einstein coefficient for induced or stimulated emission. The ratio of induced to spontaneous recombination rates of electrons in the velocity band  $\Delta v$  into the electronic state  $n$  therefore is

$$g = \frac{r_n^{ind}(\Delta v)}{r_n^{spont}(\Delta v)} = u(v) \frac{B_{if}}{A_{if}}.$$

On the other hand, A and B are connected via

$$A = 8\pi \frac{h\nu^3}{c^3} B.$$

The spectral energy density  $u(v)$  per frequency interval  $\Delta v$  in a light beam of power  $P$  and geometrical cross section  $F$  can be written

$$u(v) = \frac{P}{cF\Delta v}.$$

From the three preceding equations follows

$$g = \frac{Pc^2}{8\pi F\Delta v/v^3}$$

The ratio of induced recombination rate per proton from the electron velocity band  $\Delta v$  into a state  $n$ , and of the total spontaneous recombination rate per proton into all states, represents the total enhancement factor

$$G = \frac{r_n^{ind}(\Delta v)}{r_n^{spont}} = g \cdot \frac{r_n^{spont}(\Delta v)}{r_n^{spont}}.$$

Evaluation for a spherical and a flattened velocity distribution (14)

gives

$$G_{\text{spher}} = \frac{P\pi^2 n^5}{F_c} \left( \frac{\hbar c}{E_0 + n^2 m v_0^2 / 2} \right)^3 \cdot \frac{1}{T_\perp} \cdot \frac{1}{2.54} \quad \text{and} \quad G_{\text{flat}} \approx \frac{2}{\pi} G_{\text{spher}} \frac{\Delta v_\perp}{\Delta v_\parallel} .$$

Calculation for protons with a flattened electron distribution  $\left( \frac{\Delta v_\perp}{\Delta v_\parallel} \geq 30 \right)$ , final state  $n = 2$ , and  $kT_\perp = 0.2 \text{ eV}$  provides

$$G_{\text{flat}} \geq \frac{6I}{\text{MWatt} \cdot \text{cm}^{-2}} .$$

With a light intensity of  $I = 18 \text{ MW/cm}^2$  follows  $G_{\text{flat}} \geq 110$ . This quantitative consideration shows quite clearly that pulsed high-power lasers are the only useful light sources for this purpose.

Competing processes to laser-induced capture are photoionization and free-free transitions. The latter means acceleration of a continuum electron by absorption of a photon rather than recombination. These processes are discussed in ref. 14. Photoionization sets an upper limit of useful light intensity of about  $18 \text{ MW/cm}^2$ .

### 3. Conceivable applications of laser-induced electron-ion recombination

#### a. Electron beam diagnostics

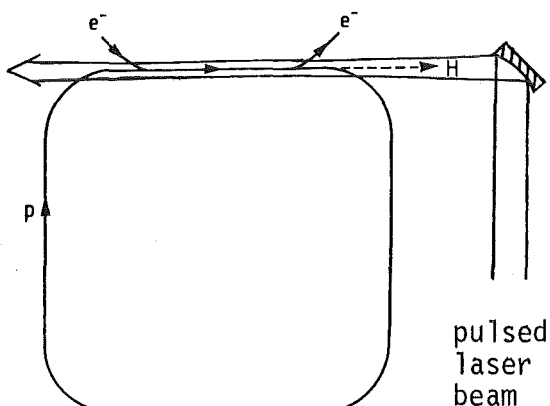


Fig.2. Schematic of electron cooling of stored protons and laser-enhanced recombination

As is shown in Fig. 2, a pulsed laser light beam propagates in opposite direction to proton and electron beams. The protons and electrons see the laboratory laser wavelength  $\lambda_{\text{lab}}$  Doppler-shifted to

$$\lambda = \lambda_{\text{lab}} \frac{1-v/c}{[1-(v/c)^2]^{1/2}} .$$

Taking as an example  $v/c = 0.4$ , the laboratory wavelength  $\lambda_{\text{lab}} = 557 \text{ nm}$  is needed to induce the transition from the ionization limit to the  $n = 2$  state of hydrogen with  $\lambda = 365 \text{ nm}$ . Light with  $\lambda_{\text{lab}} = 557 \text{ nm}$  can be easily produced at high intensity with a dye laser, pumped by an excimer laser.

Hence, the velocity profile of the electron beam in a cooling device - e.g. the one under construction for LEAR - can be investigated by measuring the production rate of hydrogen atoms as a function of laser wavelength or of  $v/c$  during the time intervals of light irradiation. This should be possible since the total enhancement factor  $G$  is connected with  $\Delta v_{||}$  and  $\Delta v_{\perp}$ . The technique may also allow to measure the proton velocity very accurately via the laser wavelength. The spontaneous hydrogen production rate is

$$R = n_e \alpha_{\text{spon}}^{\text{flat}} \cdot \frac{1}{1/(1-(v/c)^2)} \cdot n N_i = 4 \cdot 10^4 \text{ s}^{-1},$$

with  $n_e = 10^8 \text{ electrons/cm}^3$ ,  $\alpha_{\text{spon}}^{\text{flat}} = 2.2 \cdot 10^{-12} \text{ cm}^3 \text{s}^{-1}$ ,  $v/c = 0.47$ ,  $N_i = 10^{10}$  protons, homogeneously distributed in the ring, and with an overlap region of proton and electron beams which is a fraction  $\eta = 0.02$  of the total ring circumference.

Irradiation of dye laser light pulses with 20 ns length and a repetition rate of 250 Hz may be considered. In order to obtain the induced production rate of hydrogen atoms, the spontaneous rate within the 250 time windows per second has to be calculated. This rate is 0.2 atoms/s.

With a total enhancement factor  $G = 100$  for stimulated recombination to the state with  $n = 2$ , there follows an induced rate of 20 atoms/s. Higher electron recombination rates can be expected in near future, since commercial excimer lasers, and dye lasers pumped with excimer lasers with larger puls power and repetition rate are being developed. The hydrogen atoms leave the ring tangentially with proton velocity, and are ionized when passing a thin foil. The protons could then be monitored in a wire chamber.

b. Production of antihydrogen atoms

The idea to form a bound atomic system out of an antiproton and a positron (6) has been discussed already in more detail in two earlier publications (14,15). Only the case of a pulsed positron beam structure will be considered here, and a conceivable way of  $e^+$  bunch creation is sketched briefly: The electron beam of a LINAC is converted to positrons in a target. The positrons leaving the target are moderated in a copper or tungsten single crystal. The thermalized  $e^+$  beam is focused, bunched to pulses to fit the laser puls length, and accelerated to the same velocity of the stored antiprotons. The following numbers are supposed:

number of stored antiprotons  $N_p = 5 \cdot 10^{11}$ ;  
number of positrons/bunch  $N_{e^+} = 10^7$ ;  
bunch cross section  $F = 0.1 \text{ cm}^2$ ;  
overlapping fraction of total ring circumference  $\eta = 0.06$ ;  
number of positron pulses  $f = 100$ ;  $\beta = v/c = 0.3$ ;  
spontaneous positron-antiproton recombination coefficient  
 $\alpha = 2.2 \cdot 10^{-12} \text{ cm}^3 \text{ sec}^{-1}$ .

The detailed calculation is performed in ref. 14 and gives a total spontaneous rate of antihydrogen atoms

$$R_H \approx 0.06 \text{ H sec}^{-1}.$$

With a laser enhancement factor  $G = 100$  a few H atoms per second with a pulsed beam structure will leave the ring. It should be mentioned, that there is encouraging progress concerning the production of positron pulses with higher intensities and repetition rates (16,17).

Antihydrogen would be the first antiatom ever produced and give the opportunity to investigate (by comparison with hydrogen data) questions related to matter-antimatter symmetries, in particular tests of QED in a system of bound antiparticles. A conceivable experiment is to measure the 2s-2p Lamb shift. Antihydrogen atoms leaving an antiproton storage ring in their ground state are excited to the metastable  $2^2S_{1/2}$  state by a pulsed dye laser via two-photon absorption. Clearly the laser pulses must be synchronized with the  $\bar{H}$  beam pulse structure. The antiatoms then pass a microwave cavity where 2s-2p magnetic dipole transitions are induced. Atoms in the 2p state (lifetime  $\tau \approx 2\text{ns}$ ) undergo a fast decay to the 1s ground state. A continuous-wave laser excites the remaining excited atoms to the 4p state from where they can be easily ionized in a motional electric field. The  $e^+$  and  $\bar{p}$  particles are counted.

### c. Preparation of Rydberg states of stored highly-charged heavy ions

The application of laser-induced electron capture to highly-charged heavy ions was proposed in ref. 18. As an example bare  $S^{16+}$  nuclei stored in a heavy-ion storage ring are considered. The number of circulating ions be  $10^{10}$ , with  $10^9$  ions in the electron beam overlap region. For  $kT = 0.2$  eV the calculation of the recombination coefficient gives  $\alpha_r^{\text{flat}} = 2.2 \cdot 10^{-12} \text{cm}^3 \text{s}^{-1}$  in the case of protons. Supposing that  $\alpha_r$  scales with  $z^2$ , a value of  $\alpha_r^{\text{flat}} = 4 \cdot 10^{-10} \text{cm}^3 \text{s}^{-1}$  results for  $S^{16+}$ , providing a spontaneous capture rate  $R = n_e \alpha_r N_i = 4 \cdot 10^7 \text{s}^{-1}$  for  $n_e = 10^8 \text{cm}^{-3}$ . Though laser enhancement seems to be superfluous with a spontaneous rate of that size, let us consider induced capture to the state with  $n = 30$  of hydrogen-like  $S^{15+}$ . This state has an ionization potential of 4 eV and an energy separation of 0.27 eV from the adjacent states with  $n \pm 1$ . On the basis of an enhancement factor  $G = 10$ , irradiation

of 250 laser pulses per second, each of 20 ns length, results in 2000 induced captures to  $n=30$  within the 250 time windows of altogether  $5 \cdot 10^{-6}$  s.

The question arises whether these highly-excited  $S^{15+}$  ions can pass the bending magnet of the storage ring without loosing again the outer electron. One finds that the  $n = 30$  state of  $S^{15+}$  survives a magnetic field of 15 kG for a kinetic energy of the ions of 8 MeV/nucleon and  $v \perp B$ . Selective production of  $S^{15+}(n = 30)$  ions could be monitored by ionizing the  $n = 30$  Rydberg state in a static electric field. A field strength of  $4 \cdot 10^5$  V/cm is necessary.

#### 4. Summary

The interest for electron cooling of stored particles is not limited to the cooling process itself and to the improvement of beam characteristics, but increasingly includes also side effects occurring in the overlap region of stored particle and electron beams. Such an effect is radiative electron-ion recombination. After a brief review of spontaneous radiative capture the present report dealt with the concept of laser-induced enhancement of the process. Only pulsed high-power lasers are useful for this purpose. Since laser-induced capture should increase the electron-proton recombination, i.e. production of hydrogen atoms considerably, the use of this technique for electron beam diagnostics can be envisaged. The production of antihydrogen atoms through laser-stimulated positron-antiproton recombination is another conceivable application. Antihydrogen would be the first antiatom ever produced and would open up interesting spectroscopic perspectives.

Keeping in mind that heavy ion storage rings are under construction or in preparation in several countries, the concept of laser-enhanced electron-ion recombination may provide a way to prepare hydrogen- or helium-like heavy ions in Rydberg states of well-defined principal quantum number  $n$  and angular momentum  $l$ . This is a difficult goal, but if it will be

reached, a wealth of new physics may arise.

Acknowledgement. The author thanks H. Poth and A. Wolf for helpful discussions and reading of the manuscript.

### References

- 1 L.A. Rivlin: Sov. J. Quantum Electron. 9, 353 (1979)
- 2 F.H.M. Faisal, A. Lami, N.K. Rahman: J. Phys. B. 14, L 569 (1981)
- 3 B. Ritchie: Phys. Rev. A 30, 1849 (1984)
- 4 A. Lami, N.K. Rahman, F.H.M. Faisal: Phys. Rev. A 30, 2433 (1984)
- 5 H. Poth, A. Wolf: Phys. Lett. 97A, 135 (1983)
- 6 G.I. Budker, A.N. Skrinsky: Sov. Phys. Usp. 21, 277 (1978)
- 7 M. Bell, J. Chaney, H. Herr, F. Krienen, P. Møller-Petersen, G. Petrucci: Nucl. Instr. Meth. 190, 237 (1981)
- 8 H. Bethe, E. Salpeter: Quantum mechanics of one- and two-electron atoms. In: Handbuch der Physik, vol. 35, p. 88. (Springer-Verlag, 1957)
- 9 M. Stobbe: Ann. Phys. 7, 661 (1930)
- 10 L. Spitzer: Physics of fully ionized gases. (Interscience, 1956)
- 11 M. Bell, J. Bell: Part. Accel. 12, 49 (1982) and references therein
- 12 V.V. Parkhomchuk: Private communication
- 13 G.I. Budker, N.S. Dikansky, V.I. Kudelainen, I.N. Meshkov, V.V. Parkhomchuk, D.V. Pestrikov, A.N. Skrinsky, B.N. Sukhina: Part. Accel. 7, 197 (1976)
- 14 R. Neumann, H. Poth, A. Winnacker, A. Wolf: Z. Physik A 313, 253 (1983)
- 15 H. Herr, D. Möhl, A. Winnacker, in: Physics at LEAR with Low-Energy Cooled Antiprotons. Edited by U. Gastaldi and R. Klapisch. p. 659. (Plenum Publishing Corporation, 1984)
- 16 G. Gräff, R. Ley, A. Osipowicz, G. Werth, J. Ahrens: Appl. Phys. A 33, 59 (1984)
- 17 A. P. Mills, Jr., in: Positron Scattering in Gases. Edited by J.W. Humbertson and M.R.C. McDowell. p. 121. (Plenum Publishing Corporation,

1984)

- 18 A. Winnacker, in: Workshop on the Physics with Heavy Ion Cooler Rings,  
Report C9. Heidelberg, May 29-30, 1984. Collected material, printed  
and distributed by the Max-Planck-Institut für Kernphysik in Heidel-  
berg



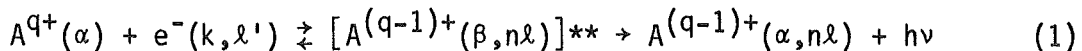
## DIELECTRONIC RECOMBINATION MEASUREMENTS IN A SINGLE PASS EXPERIMENT

S. Datz, P. F. Ditttner, P. D. Miller, and P. L. Pepmiller

Oak Ridge National Laboratory  
Oak Ridge, TN 37831 USA

Much current interest in the area of atomic collision physics centers on interactions of multiply charged ions. Aside from strong intrinsic interest in this field, knowledge obtained from such work has application in modeling high temperature plasmas such as those found in stellar coronae and controlled fusion devices.

Electron-ion collisions can lead to ionization, excitation, or recombination. Here we center on recombination. When an unbound electron recombines the gain in potential energy must be removed in some way. Two processes are known to be important in recombination: radiative recombination (RR) in which a photon is released whose energy is exactly equal to the potential energy gain, and dielectronic recombination (DR) in which a continuum electron excites a previously bound electron and in so doing loses just enough energy to be captured into a bound state ( $n\ell$ ). The latter process results in a doubly excited ion in the next lower charge state which may either auto-ionize or emit a photon resulting in a stabilized recombination. Thus, for an ion A of charge state q in initial state  $\alpha$  the process may be written:



Since the DR cross section is made up from a set of resonances and the radiative recombination cross section falls rapidly with increasing relative energy, it is clear that there should be a peak in the energy dependence of the relative importance of DR vis-a-vis RR for a given ionic species.

The simplest theory which has been used to generate DR rates is that due to Burgess and Merts and may be summarized as follows. We start with a description of the cross section in terms of  $\Gamma_r$  the radiative rate for stabilization via  $\beta \rightarrow \alpha + h\nu$  and  $\Gamma_a(n, \ell)$  the autoionizing rate

$$\sigma = \pi/k^2 \sum_{n\ell} (2\ell+1) \frac{\Gamma_r \Gamma_a(n\ell)}{(E-E_{n\ell})^2 + 1/4[\Gamma_r + \Gamma_a(n\ell)]^2} \quad (2)$$

where E is the relative energy, and  $E_{n\ell}$  is the position of the resonance. Folding in the Maxwell-Boltzmann distribution of  $E_{rel}$  gives the rate

$$R = CT^{-3/2} \sum_{n\ell} (2\ell+1) \frac{\Gamma_a(n\ell)}{\Gamma_r + \Gamma_a(n\ell)} e^{-E_{n\ell}/T} \quad (3)$$

Until 1983 the only experimental information on DR had come from spectroscopic observations of plasmas from which only thermally averaged rates may be inferred. In 1983-84 four groups reported DR cross section measurements. A group at the Joint Institute for Laboratory Astrophysics (JILA) measured the DR cross section for  $Mg^+$  using crossed ion-electron beams and recording coincidences between recombined Mg atoms and stabilizing photons from the collision region.<sup>1</sup> A similar experiment was carried out by Williams for  $Ca^+$ .<sup>2</sup> Two groups used merged electron-ion beam methods (i.e. similar in geometry to electron beam cooling systems). One experiment at the University of Western Ontario<sup>3</sup> used a tenuous; emission limited, highly monoenergetic electron beam merged with a 450 keV  $C^+$  beam to reach the requisite collision energies of a few eV; (the signal levels here were very low). At Oak Ridge National Laboratory (ORNL) we wish to work with multiply charged ions and we have chosen to use a compressed space charge limited electron beam.<sup>4</sup>

We chose a merged beam approach to take advantage of our ability to produce high charge state, MeV/amu ions and a high current, high energy (1-3 keV) electron beam. The merged beam apparatus (outlined in Fig. 1) is constructed such that in the interaction region, the ion beam is coaxial with and embedded within the electron beam for a distance of 84 cm.

ORNL-DWG. 84-10367

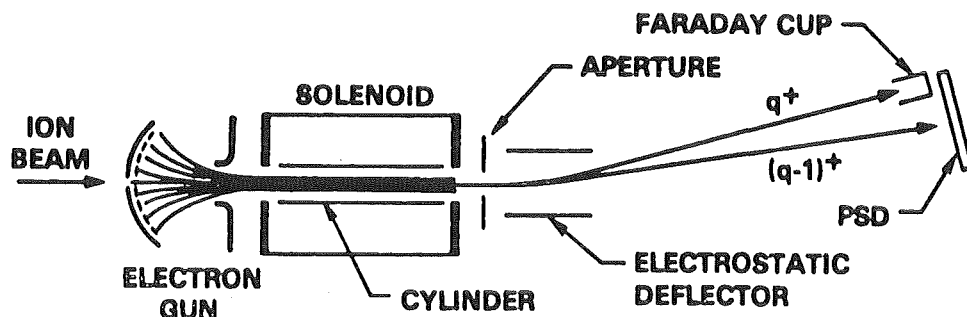


Fig. 1. Schematic Diagram of Merged Beam Apparatus

The ion beam from the ORNL EN-tandem accelerator enters the interaction region through an axial, 0.64 mm diameter hole in the cathode of the electron gun. After exiting the interaction region, the ion beam is subjected to charge analysis. In our earlier work, we used magnetic deflection and in our more recent efforts, we use electrostatic deflection (see below). The initial charge state of the ion beam,  $q^+$  is deflected into a Faraday cup. The cup is connected to a current integrator and the output pulses are counted by a scaler. Ions that have picked up an electron (charge =  $(q-1)^+$ ) are deflected onto a solid state position sensitive detector (PSD). The ions having charge  $(q-1)^+$  arise from electron pickup of the  $q^+$  ions from the residual gas molecules, slit edge scattering and the sought after effect, DR.

The source of the electron beam is a doubly gridded Pierce-type high intensity electron gun which is designed to produce a convergent, laminar electron beam. The gun was operated in the space charge limited mode where the space charge limited current,  $I_c$ , is given in terms of the cathode to anode voltage,  $V_c$ , by  $I_c = PV_c^{3/2}$ . The constant  $P$  (the "perveance") is determined by the electrode geometry and here equals  $10^{-6}$ . The electron gun is magnetically shielded from the solenoidal field of the interaction region. The emerging electron beam comes to a focus  $\sim 7$  mm from the anode where it has a diameter (containing 95% of the beam) of 3.15 mm. It enters a coaxial solenoidal magnetic field which is adjusted to establish Brillouin flow (e.g.  $\sim 0.18$  T for 1 keV electrons) in which the beam radius stays constant and the beam rotates as a solid of revolution about its axis with the Larmor frequency,  $\omega_L$ . Under Brillouin flow, the longitudinal velocity of an electron is independent of radius, the radial velocity is zero and the azimuthal velocity is equal to  $\omega_L$  times the radial position of that electron. Surrounding the electron beam is a coaxial cylinder 84 cm long having an inside diameter of 7.9 mm which is normally electrically grounded. Following the interaction region, defined by the length of the coaxial cylinder and the solenoidal field, the electrons expand due to space charge repulsion and strike the chamber walls.

The experimental procedure consisted of optimizing the electron beam, at a particular  $V_c$ , and counting the  $A(q-1)^+$  and  $Aq^+$  beams while stepping through the relative energies of interest by changing the energy of the ion beam. This optimization was carried out by adjusting the orientation of the solenoid and the cylinder and making small adjustments to the solenoidal field such that the current to the cylinder was a minimum ( $<0.01 I_c$ ). It was then verified by observing the position spectrum while switching the electron beam on and off that the electrostatic field, due to the electron space charge, produced no steering of the ion beam. We believe that minimum ion beam steering indicates minimum misalignment between the ion and electron beams. The deviation of the ratio,  $R$ , of  $(q-1)^+$  ions to  $q^+$  ions from a monotonic trend with ion beam energy gives a measure of the DR cross section. In Fig. 2 we plot this ratio for two ion energy "sweeps" of a  $B^{2+}$  beam (14-18 MeV) merged with the electron beam. In the first sweep  $V_c = 1022$  V (solid squares) and the second sweep  $V_c = 1079$  V (open circles). The lines through the data in Fig. 2 are to guide the eye. It can be seen that

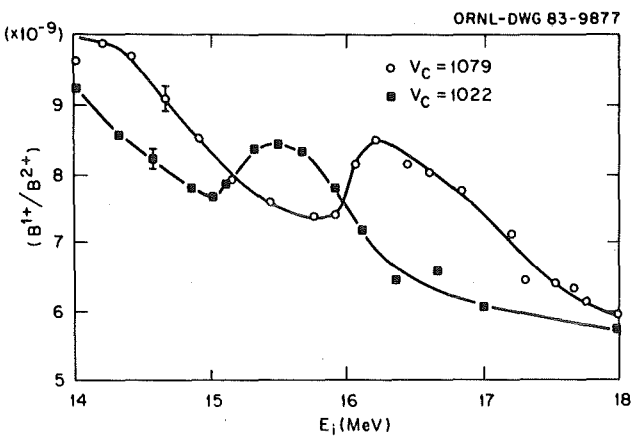


Fig. 2. Ratio,  $B^{1+}/B^{2+}$ , as a function of  $B^{2+}$  ion energy for  $V_c = 1022$  V (solid squares) and  $V_c = 1079$  V (open circles).

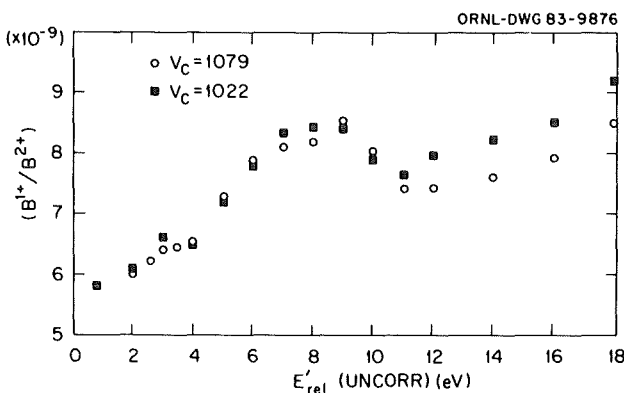


Fig. 3. Ratio,  $B^{1+}/B^{2+}$ , vs. relative energy. For potential drop correction to the relative energy scale, see Ref. 4.

the DR signal shifts to higher ion energies as the electron energy is increased, i.e. the signal depends on the relative energy. To emphasize this point further, we plot this ratio, in Fig. 3, for the two  $B^{2+}$  sweeps vs. the relative energy,  $E'_{rel}$ . In Fig. 4 this ratio is plotted for a  $C^{3+}$  beam (17.5 - 23 MeV) merged with an electron beam at  $V_c = 1079$  V. The background ratio,  $R_B$ , can be fitted by a monotonic trend line as in Fig. 4. Subtracting  $R_B$  from  $R$  yields the signal ratio  $R_s$ .  $R_s$  is related to the DR cross section  $\sigma$ , by

$$R_s = (\iint \sigma(v_r) \rho_e(v_r) \rho_i d v_r d V) / \int \rho_i v_i d A$$

where  $\rho_e$  is the electron density,  $\rho_i$  is the ion density,  $v_r$  is the relative velocity,  $v_i$  is the velocity of the ions, and  $V$  and  $A$  are the volume and cross sectional area of the interaction region, a cylinder whose radius is that of the ion beam  $r_i$ , and having the length of the electron beam,  $L$ ;

ORNL-DWG 83-9875

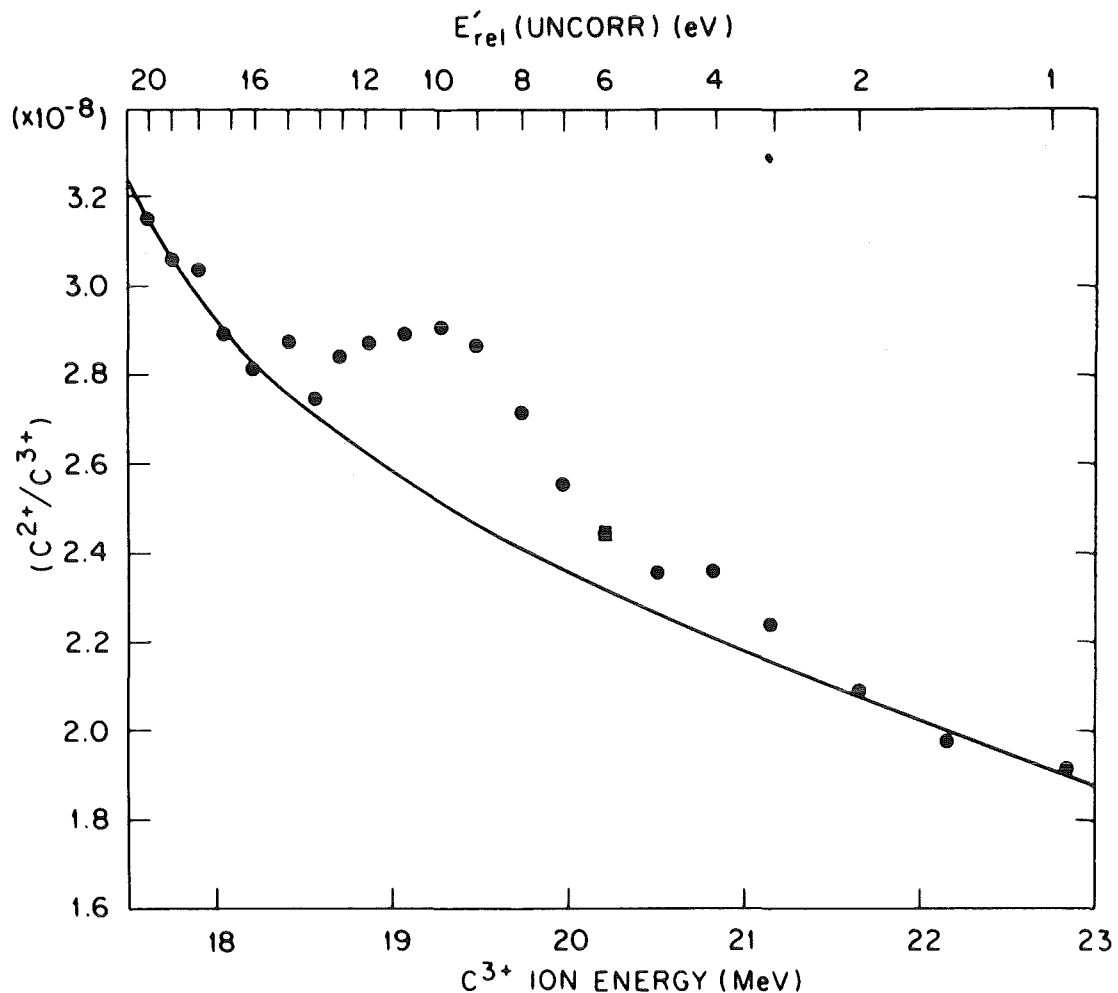


Fig. 4. Ratio,  $C^{2+}/C^{3+}$  as a function of  $C^{3+}$  ion energy for  $V_C = 1079$  V. For potential drop correction to the relative energy scale, see Ref. 4.

since  $\rho_i$  and  $v_i$  are constant within  $V$ , the ion current  $I_i = \int \rho_i v_i dA = \rho_i v_i A$ . Approximating  $\rho_e$  by an average electron density  $\bar{\rho}_e$ , times a distribution in relative velocities  $f(v_r)$ , both being independent of position within  $V$ , we can write that,  $R_s = (\bar{\rho}_e L / v_i) \langle v_r \sigma \rangle$ , where the triangular brackets denote the average over  $f(v_r)$ . Thus, from the measured quantities we can calculate  $\langle v_r \sigma \rangle$  at every ion energy or relative energy, i.e.,  $\langle v_r \sigma \rangle = R_s v_i / \bar{\rho}_e L$ .

The best possible resolution in relative energy for this cathode configuration would be  $\sim 2$  eV; about 0.5 eV arising from the non-zero radius of the ion beam in the space charge limited electron beam and  $\sim 2$  eV from the cathode temperature ( $\sim 1400^\circ\text{K}$ ) coupled with a compression factor of  $\sim 16$ .

In our first reported measurements<sup>4</sup> we arrived at our signal level by simply subtracting a smooth extrapolated background drawn under the resonance region. This treatment indicated a resolution of  $\sim 3$  eV, but subsequent improvements in measuring technique have shown this to be overly optimistic.

Our gun contains a gridded cathode; the initial idea was to modulate the electron beam to determine the background. This technique did not prove feasible because turning the electron beam on and off modulated the background gas density and gave rise to a large spurious signal even at energies where signals were not physically possible.

An alternative scheme has proved more successful. Here we modulate the voltage applied to the guide tube surrounding the merged beam region. For half the time the tube is grounded and for the other half the tube is raised in voltage such that the electron beam energy is shifted to be off resonance. The result of such an experiment is shown for  $S^{5+}$  in Fig. 5. Several jumps appear in the data which are much beyond the range of statistical error. These jumps probably occur because of slit edge scattering which may vary somewhat with ion beam steering at different energies. (Note that in our configuration the ion beam may be scattered at the narrow

ORNL-DWG 84-17888

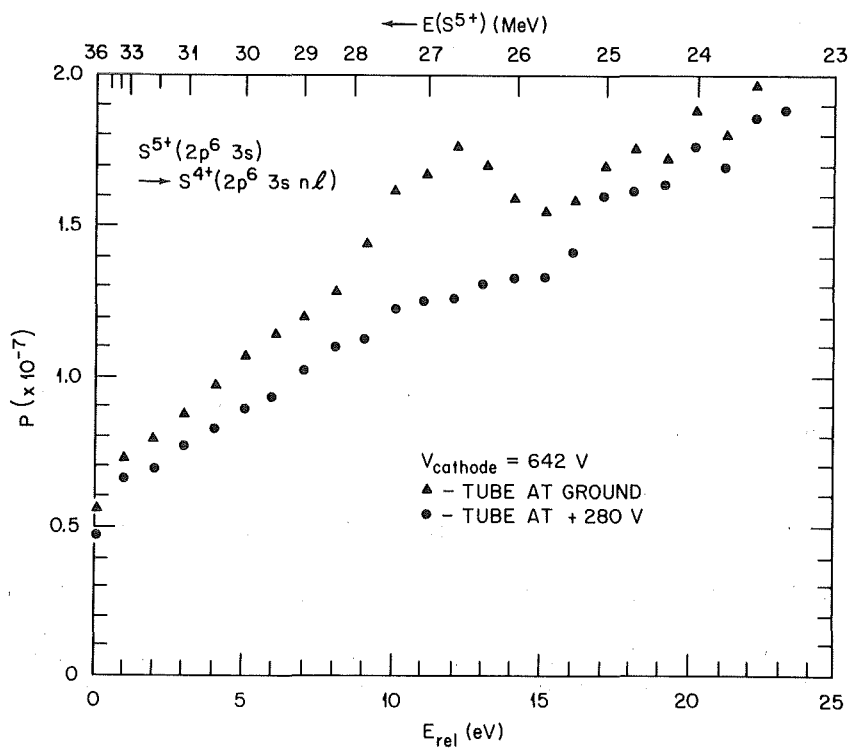


Fig. 5. Ratio ( $S^{4+}/S^{5+}$ ) as a function of  $S^{5+}$  ion energy (top) and relative energy (bottom) for a 617 eV merged electron beam. Lower curve shows effect of offset electron beam energy at same ion energy.

entrance aperture in the cathode.) These "jumps" disappear when we plot the difference signal as in Fig. 6. The effect of some residual background modulation is seen in the non-zero level in the 16 to 24 eV region and this may be subtracted to give the final signal values. The consistency of this method may be seen in Fig. 7 where we have plotted the rates  $\langle v\sigma \rangle$  derived from such measurements for  $C^{3+}$  ions. The round points were determined with an electron beam moving slower than the ion beam (lab system), the square points from measurements where the electron beam was moving faster than the ion beam (lab system). Here, the observed peak is asymmetric with a full width of  $\sim 6$  eV (+2, -4). For  $C^{3+}$ , we expect a very sharp peak (almost a  $\delta$  function on our scale) at 7 eV.<sup>5</sup> The observed spread around 7 eV is due to electron beam energy resolution. Using a 2 parameter fit, one describing the longitudinal and the second the transverse distribution, we find we are able to fit the rates. The same two parameters fit for all the ions used ( $C^{3+}$ ,  $O^{5+}$ ,  $P^{4+}$ ,  $S^{5+}$ , and  $Cl^{6+}$ ) thus giving us some confidence that we have now characterized our electron beam.

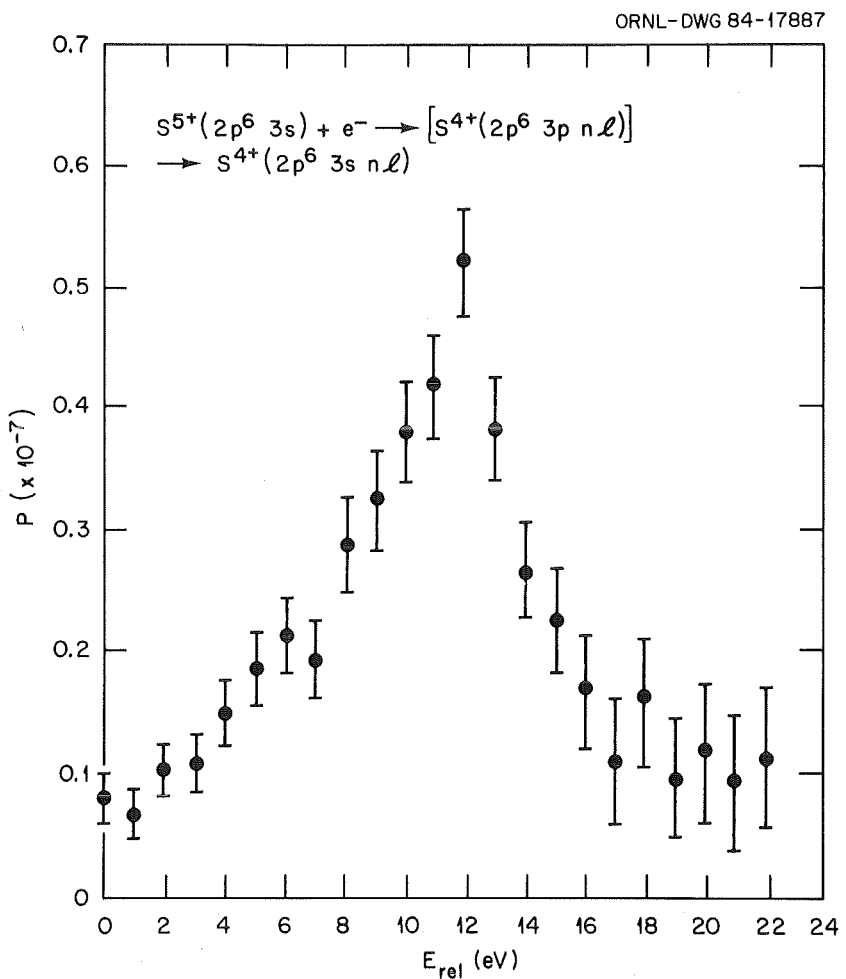


Fig. 6. Difference signal of  $(S^{4+}/S^{5+})$  ratio from Fig. 5.

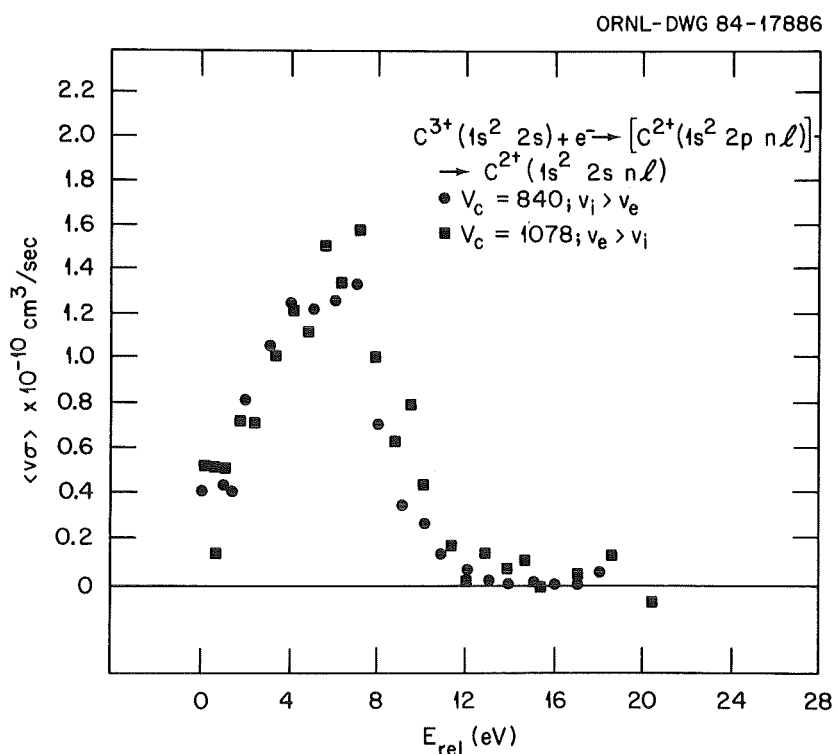


Fig. 7. Measured rates ( $\langle v\sigma \rangle$ ) for  $C^{3+}$  DR as a function of relative energy for: ■ ion velocity greater than electron velocity, and ● ion velocity lower than electron velocity.

The theoretically predicted probability of recombination observed in these experiments depends on the electric fields present in two regions; first, the electron-ion interaction region and second, the charge analysis region.

The electric fields in the charge analysis region can Stark strip Rydberg states formed in the electron-ion interaction. The maximum  $n$  state that can survive these fields is given by

$$n_{max} \approx (6.43 \times 10^8 q^3/E)^{1/4}$$

where  $q$  is the core charge and  $E$  is the field in volts per cm. In our first experiments<sup>4</sup> we used a magnetic field of 0.1 T to separate the charge states of ions moving at  $\sim 2$  MeV/u. This corresponds to a field of  $\sim 40$  kV/cm so that for  $C^{3+}$  the highest surviving  $n$  is  $n_{max} = 26$ . Our more recent experiments use electrostatic deflection fields of  $\sim 4$  kV/cm corresponding  $n_{max} = 44$  and indeed we observe a factor of 1.8 increase in  $C^{2+}$  signal at the peak under these conditions.

Less well understood is the effect of small fields in the interaction region which mix  $\ell$  states for a given  $n$  and increase the DR cross section. This is illustrated in Fig. 8 for  $B^{2+}$ .<sup>6</sup> The upper left portion of the figure shows the autoionizing,  $A_a$ , and radiative rates,  $A_r$ , for  $n=20$  as a function of  $\ell$ . The radiative rate is  $\sim$  independent of  $\ell$ . Since the DR cross section

$$\sigma_{DR} \propto A_r A_a / [A_r + A_a]$$

it can be seen that low values of  $\ell$  will be favored. In the approximation that only values of  $\ell$  which give  $A_a > A_r$  contribute to  $\sigma_{DR}$  we weight each contributing  $\ell$  by  $2 \times (2\ell + 1)$ , and we assign a total weight of 128 to the  $n=20$  state. If, on the other hand, we have an electric field present which gives complete Stark mixing, the picture changes to that shown in the upper right portion of Fig. 8. We now deal in the Stark representation where  $n$ ,  $k$ , and  $m$  are good quantum numbers. The parameter of the curves is the magnetic quantum number  $m$ , and each point for  $m>0$  counts for two states. Using the same criterion as in the upper left the total weight is 404, hence a gain of 3.2 in the DR cross section for  $n=20$ . The same treatment in the lower portion of Fig. 8 shows a gain of 6.8 for  $n=40$ . The big question then is how much Stark mixing is there for a given field at the interaction region? The question is still open.

In our work we find that for the Na-like ions  $P^{4+}$ ,  $S^{5+}$ , and  $Cl^{6+}$  the measured rates are intermediate between the no mixing and total mixing predictions while for the Li-like  $C^{3+}$  and  $O^{5+}$  complete mixing seems a better fit.

Thus far, we have dealt with  $\Delta n=0$  transitions of alkali-like ions where the spectra should be relatively simple. If we chose more complex ions there should be a wide spectrum of discrete energies which give DR. For these experiments, it will be necessary to have better energy resolution and thus there is a direct connection to the technologies which have been developed for electron beam cooling.

This research was sponsored by the U. S. Department of Energy, Division of Basic Energy Sciences under Contract No. DE-AC05-84OR21400 with Martin Marietta Energy Systems, Inc.

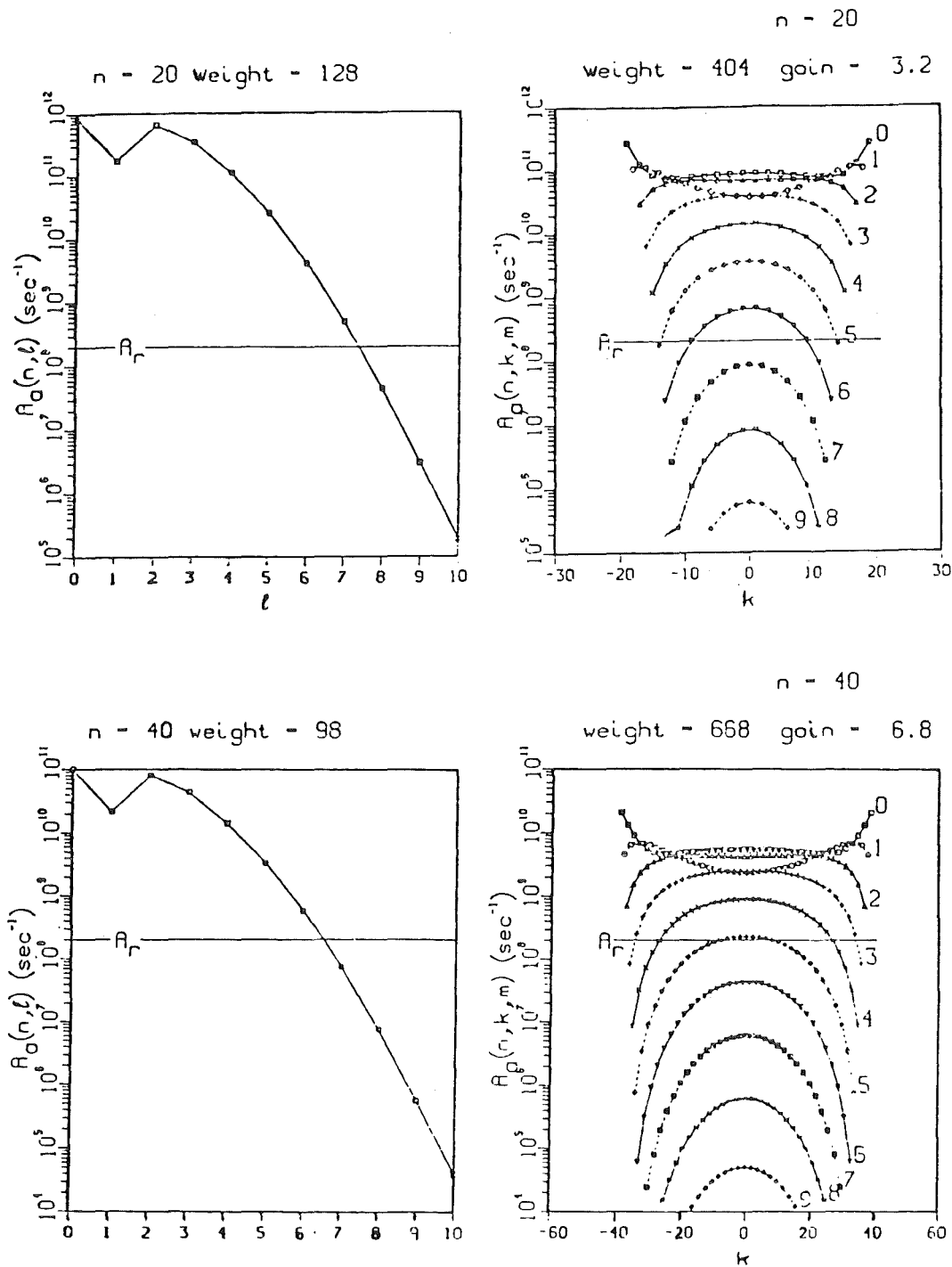


Fig. 8. Autoionizing and radiative ( $2p \rightarrow 2s$ ) rates for  $B^2+(1s^2 2pn\ell)$  without Stark mixing and with complete Stark mixing for  $n=20$  and  $n=40$ .

### References

1. D. S. Belić, G. H. Dunn, T. J. Morgan, D. W. Mueller, and C. Timmer, Phys. Rev. Lett. 50, 339 (1983).
2. J. F. William, Phys. Rev. A29, 2936 (1984).
3. J.B.A. Mitchell, C. T. Ng, J. L. Forand, D. P. Levac, R. E. Mitchell, A. Sen, D. B. Miko, and J. W. McGowan, Phys. Rev. Lett. 50, 335 (1983).
4. P. F. Dittner, S. Datz, P. D. Miller, C. D. Moak, P. H. Stelson, C. Bottcher, W. B. Dress, G. D. Alton, and N. Nesković, Phys. Rev. Lett. 51, 31 (1983); Electronic and Atomic Collisions, Eichler, Hertel, and Stoßterfoht, eds., North-Holland Press, 1984.
5. D. McLaughlin and Y. Hahn, Phys. Rev. A27, 1389 (1983); Phys. Lett. 88A, 394 (1981); Phys. Rev. A28 (1983), In press.
6. M. Pindzola, D. Griffin, and C. Bottcher, Private Communication.



AN ION BEAM LAMP FOR MONOCHROMATIC X-RAYS

---

H. PILKUHN and H. POTH

Institut für Theoretische Kernphysik  
and Kernforschungszentrum - Karlsruhe

(presented by H. Pilkuhn)

Last year, Poth and Wolf [1] pointed out that the capture of cooling electrons on fully stripped ions can be used as a tunable X-ray source, as most of the electrons are captured into the ionic ground state. The energy resolution is estimated to be of the order of  $10^{-4}$ , the intensity of the order of  $3 \times 10^9$  fotons/s. It should also be possible to steer the capture into highly excited ion states by means of a laser. Then one can use the subsequent deexcitation as an X-ray source, which improves the energy resolution roughly by a factor  $\beta$  (for  $\beta \ll 1$ ), say to  $\sim 10^{-5}$ .

Meanwhile, it seems possible to improve the energy resolution by another factor 100 [2]. There exists presently no tunable X-ray source of comparable precision, to our knowledge. The idea is to manipulate the metastable triplet states of two-electron ions by an optical laser. The ion ring is filled with one-electron ions ( $B^{4+}$ ,  $C^{5+}$ ,  $N^{6+}$  ...) and cooled with electrons. After induced electron capture, many of the ions will deexcite to the metastable tripled S-state with a statistical weight of 3/4. The lifetimes of these metastable states are 149, 20.4, and 3.9 ms for the above three ions. During these times, one can laser excite the triplet S-state to the triplet P-state of  $J = 1$  (fig.1), which then decays to the singlet ionic ground state with a sufficiently large branching ratio, within a fraction of a microsecond. As the natural line width is negligible, the width of the X-rays is solely determined by the laser width. Their energy varies between 203 eV for B and 420 eV for N, plus or minus the Doppler shift.

For a Doppler width of  $10^{-5}$  and a laser width of  $10^{-7}$ , the laser cuts a slice of thickness  $10^{-2}$  into the ionic momentum distribution. If it does so in one  $\mu s$ , it will need 100  $\mu s$  for eating the whole cake. In principle, even a laser of width  $10^{-8}$  could eat the cake before it decays.

In that case, the metastable ions must circulate a few thousand times through the lamp.

In conclusion then, the  $3 \times 10^9$  fotons/s now come in bursts of a few milliseconds, with a frequency width of the order of  $10^{-7}$ .

The tuning of the X-ray source by Doppler shift has a great disadvantage : the lamp shines in different direction with different frequencies. For a lamp length of 30 cm, one can only use the forward and background emitted X-rays within a 1cm disk at 5m distance (for  $\beta=0.1$ ). Although adjacent disks do see adjacent frequencies, the frequency resolution deteriorates for positions seeing the lenght of the lamp. For the same reason, focussing seems pointless. If one is content with  $\Delta\nu/\nu = 10^{-5}$ , one can replace the ion ring by a simple linac. In this case, the metastable ions are provide directly by the ion source, or by foil excitation and their lower abundance (a few percent) is overcompensated by a large ion flux. The ion ring must be viewed as a precision instrument, not as a powerful lamp. The induced ionic X-ray emission could also be used for hyperfine studies.

#### REFERENCES

1. H. Poth and A. Wolf, Phys.Letters 94A, 135 (1983)
2. H. Pilkuhn and H.Poth, KfK Bericht 3764 (Kernforschungszentrum Karlsruhe, 1984).

THOMAS PEAK MEASUREMENT IN BEAM RECIRCULATION RING

I. Katayama  
RCNP, Osaka University, Ibaraki, Osaka 567, Japan

**Abstract** A stringent test of recent theories on electron capture (charge transfer) processes at asymptotically high energy is to measure the differential cross sections and their velocity dependence. A possibility of the experiment in a beam recirculation ring is discussed.

An epoch-making experiment in electron capture or charge transfer collisions was recently made by Horsdal-Pedersen, C.L. Cocke and M. Stockli at Kansas Univ.<sup>1)</sup>. They observed a peak at  $\theta_L = 0.027^\circ$  (Thomas peak) in the differential cross section of  $P + He \rightarrow H^0 + He^+$  using 7 MeV protons. Table 1 gives a brief summary of the historical progress of the study of electron capture reactions at high energy<sup>2,3)</sup>. Thomas proposed a model which is called double scattering model<sup>4)</sup>. In this model the capture process is explained to proceed as follows; the electron which is scattered in the  $60^\circ$  direction to the beam acquires the same velocity with that of the projectile. The electron, if scattered again by the target nucleus into the beam direction, is captured in the projectile atomic orbit. In the first collision, the projectile receives a recoil momentum and is scattered by an angle of  $(\sqrt{3}/2) (me/M_p)$ , which is exactly the angle where Horsdal-Pedersen et al. observed a peak in the yield of hydrogen atoms. Drisko has shown that the second order Born calculation has a close connection to this classical model by Thomas<sup>5)</sup>. Electron capture at high energy is a three body problem of Coulomb interaction. This is the reason why so many approximations have been proposed so far. Present

Table 1 History of electron capture at high energy

|      |                                 |   |
|------|---------------------------------|---|
| 1923 | Hederson                        | ${}^4He^{2+} \rightarrow {}^4He^{1+}$ observed in air |
| 1928 | Thomas                          | Double scattering model                               |
| 1930 | Oppenheimer                     | OBK Born calculation                                  |
| 1931 | Brinkman-Kramers                |   |
| 1952 | Jackson-Shiff<br>Bate-McCarroll | Bate Born calculation                                 |
| 1958 | Drisko                          | 2nd order Born calculation                            |
| 1978 | Shakeshaft-Spruch               | Quantum mechanical picture of Thomas model            |
| 1983 | Horsdal-Pedersen-Cocke-Stockli  | First observation of Thomas peak                      |

status of the theories and their relations have been discussed in refs. 6 and 7. It has been pointed out that a stringent test of theories is to measure angular distributions and their dependences on the projectile velocity<sup>3,8)</sup>. Although several theories predicted the right location of the peak as observed by Horsdal-Pedersen et al., they were not able to reproduce the cross section as well. It is extremely valuable to extend the differential cross section measurements to much higher energies than that in Kansas experiment.

The experimental difficulty is clear from the small angle of the Thomas peak. Horsdal-Pedersen et al. used a double slits of 0.3mm×0.1mm and 0.2mm×0.05mm in dimensions with a spacing of 5m to get a pencil beam with 0.058 mrad at FWHM. If one employs this straightforward method for the beams from a cyclotron, the available fraction of the beam extracted from the cyclotron will be about  $1 \times 10^{-6}$  on a target. The total cross sections are roughly  $1.2 \times 10^{-2}$ ,  $2.1 \times 10^{-4}$  and  $1.2 \times 10^{-6}$  b at proton energies of 10, 20 and 50 MeV, respectively for  $P + He \rightarrow H^0 + He^+$  reactions<sup>9)</sup>. The small values of the cross sections together with the requirement for the small beam emittance show how this kind of measurement is difficult to perform in the cyclotron laboratories. The most important is to increase the brightness of the beam on the target. The brightness is defined as a ratio of the beam intensity over the beam emittance. Let us think about the situation for the beam recirculation ring. In the Kansas data of angular spreading of the beam penetrating the target, we notice that the multiple scattering effect is only observed at the tail of the spectrum and the FWHM of the beam is not affected by the multiple scattering<sup>10)</sup>. The width of a Gaussian curve which fits the tail component was 0.16 mr which is compatible with the prediction of 0.10 mr from a multiple scattering formula<sup>11)</sup>. The intensity of the tail part was a few percent of the total intensity. This implies that the most part of the beam could be used again to irradiate the target. By recirculating the beam, one can increase the brightness by a factor given as

$$f = (A + c)/c - (A + c)^2/(nc^2) \quad (1),$$

where  $A$  is the acceptance of the storage ring,  $c$  the increase in beam emittance due to multiple scattering and  $n$  the number of turn in the ring. The acceptance of the ring is determined by a beam collimator in the ring, by which the emittance of the beam on the target is kept constant in such a way that the growing part of the beam in angle by the multiple scattering in the target is stopped by the collimator. It is also important that the injection of the beam in the ring should not induce any betatron oscillation. This will be possible by a longitudinal stacking which, however, results in a deterioration of the beam energy resolution. It is, therefore, important that the ring should be operated so as to give zero

dispersion at the target position. Note that the position of the Thomas peak is constant irrespective of the beam energy. Making use of the data by Kansas and injection method being considered at Indiana, we can estimate the factor of eq.(1) to be around 10. How does the electron cooling work? In this case, the the  $H^0$  beams from the radiative capture process in the electron cooler section can be used to monitor the emittance of the beam. If the ring is used in the cooling mode, it has an effect of increasing the brightness of the beam. The beam luminosity is, however, by an order of magnitude less than that of a single pass mode. It is, therefore, not clear that the cooling mode can improve the feasibility of the experiment. Taking advantage of the increase in the brightness of the beam by beam recirculation as given above, we can expect to perform the measurement at 10 to 20 MeV of proton energies. The experiment at much higher energies, however, still remains not simple without introduction of a break-through technique in the injection method.

It is to be mentioned that even at the energy of Kansas experiment, if the beam spreading can be reduced further by a factor of several by the beam recirculation there will be no need to convolute the theoretical curve with the experimental angular resolution of the beam. This allows us to test the theory in much clear way.

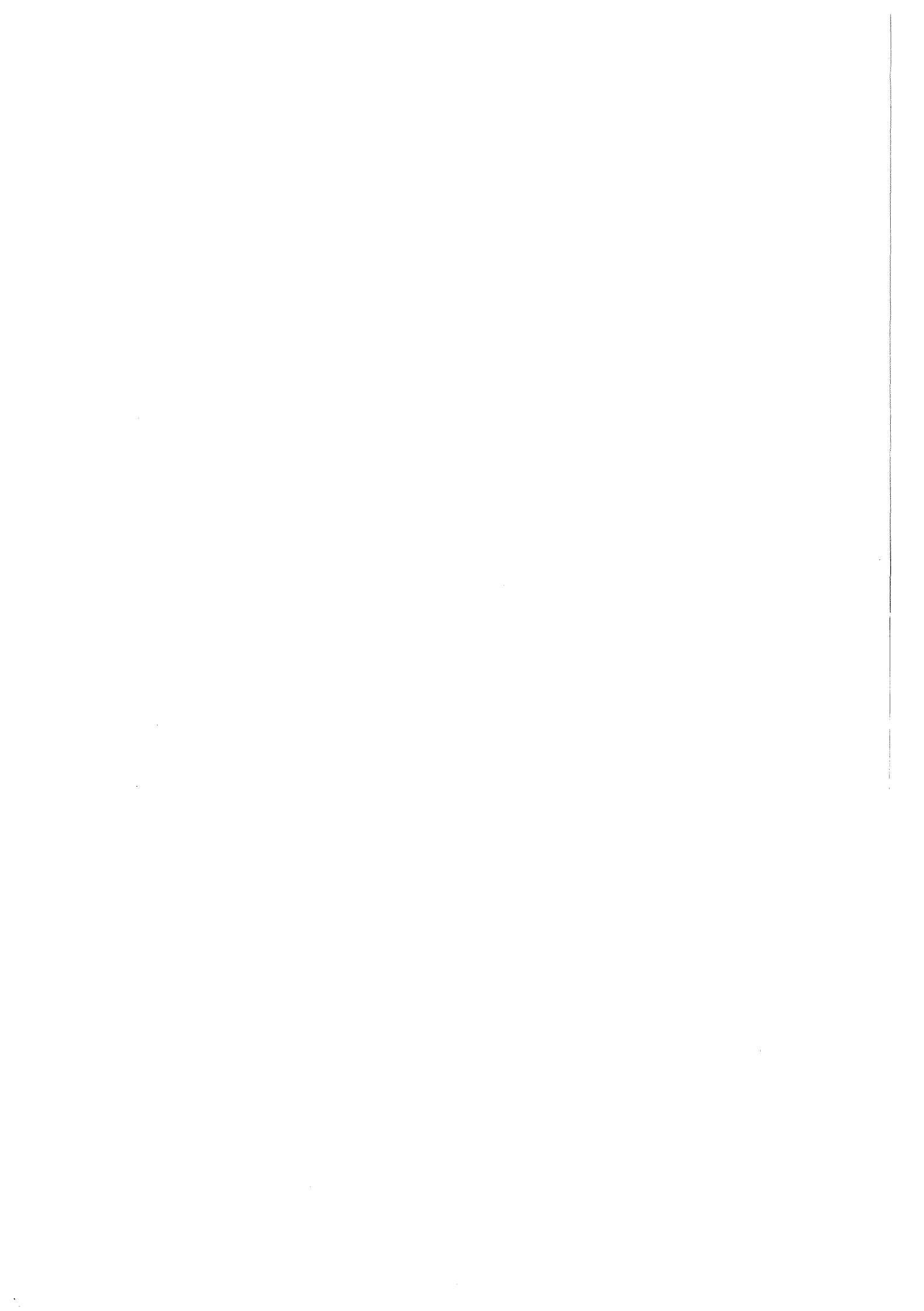
The author wishes to thank Drs. S. Morinobu, O. Schult and E. Horsdal-Pedersen for their comments.

#### References

1. E. Horsdal-Pedersen, C.L. Cocke and M. Stockli, Phys. Rev. Lett. 50 (1983) 1910.
2. M.R.C. McDowell and J.P. Coleman, Introduction to the Theory of Ion-Atom Collision (A North-Holland, 1970) ch.8.
3. R. Shakeshaft and L. Spruch, Rev. Mod. Phys. 51 (1979) 369.
4. L.H. Thomas, Proc. R. Soc. 114 (1927) 561.
5. R.M. Drisko, Ph. D. Thesis Carnegie Inst. of Tech. (1955).
6. J. Briggs, J. Macek, and K. Taulbjerg, Comments on At. Mol. Phys. 12 (1982) 1.
7. J. Macek, Proceedings on 13th ICPEC (1983, Berlin) p.316.
8. J. Briggs, P.T. Greenland, and L. Kochbach, J. Phys. B15 (1982) 3085.
9. Estimated by Drisko's result (ref. 5)

$$\sigma_c = \sigma_{OBK} (0.293 + 2^{-11} 5 \pi (Z_p + Z_t)^{-1} v_1^{-1})$$
$$\sigma_{OBK} = 5^{-1} 2^{11} z_p^5 z_t^5 v_1^{-12} a_0^2$$

10. J.H. McGuire, M. Stockli, C.L. Cocke, E. Horsdal-Pedersen and N.C. Sil, Phys. Rev. A30 (1984) 89.
11. Particle Properties Data Booklet 1980, ed. CERN (1980) 81.



# ELECTRON COOLING ANTI PROTONS TO THERMAL ENERGIES IN A PENNING TRAP

William Kells\*, Gerald Gabrielse, and Kristian Helmerson

Department of Physics, FM-15  
University of Washington  
Seattle, WA 98195

## I Introduction

Precision "Geonium" studies of a single antiproton in a Penning trap would be a natural continuation of such studies on more readily available particles<sup>1</sup>. At the University of Washington, single electrons and positrons have been trapped for precision g-value measurements<sup>2</sup> and small numbers of protons have been trapped to measure the ratio of the proton and electron masses<sup>3</sup>. The major new challenge offered by antiprotons is in getting them from the high energies at which they are produced down to the very low energies where trapping can be carried out. Once a small cloud of antiprotons is trapped (and eventually just a single antiproton), a logical first experiment is to measure the antiproton mass and then to measure the ratio of the proton and antiproton masses by measuring the cyclotron frequencies of these particles in the same trap. The properties of the trap can be well established ahead of time via studies with protons. Long trapping times have already been repeatedly demonstrated (eg. greater than 9 months for a single electron by us<sup>4</sup>) so that an antiproton lifetime greater than the existing 32 hours<sup>5</sup> would be soon established. Many other studies would also be possible.

The most direct approach to trapping antiprotons requires several stages of deceleration and cooling in progressively smaller "rings", with the minimum cooled phase space density ultimately determined by space charge limitations. Space charge directly limits the number of cooled  $\bar{p}$ 's available in a given ring at low energy via the intrabeam scattering mechanism (IBS)<sup>7</sup>. The cooling mechanism of choice at the lowest  $\bar{p}$  energies would be electron cooling, since it is energy tunable and very compact. On the other hand space charge limits the current in a low velocity  $e^-$  beam consistent with low electron temperature. Therefore beam storage/cooling is not possible at the lowest energy stage ( $\leq 100$  KeV  $\bar{p}$  kinetic energy). One method would be direct, transient, deceleration from the last storage/cooling stage at a few hundred KeV. Unfortunately such a scheme still requires an auxiliary ring to bridge the gap, at LEAR for instance, from 5-10 MeV

\* On leave from Fermi National Accelerator Laboratory

to several keV to allow trapping. The direct approach might allow the trapping of very large number of antiprotons in one filling of the trap<sup>8</sup>.

The current state of proton/electron trapping sensitivity at Washington; however, requires only small numbers ( $\leq 100$ ) of trapped  $\bar{p}$  in order to achieve high signal to noise ratios. We therefore investigate here a  $\bar{p}$  trapping scheme based on stopping foils which, in the simplest case, require no auxiliary decelerator/cooler past a LEAR (or equivalent) stage. Cooling of the trapped particles could be accomplished via the damping provided by an external resistor as in all of the other experiments<sup>8</sup>. The rate for this cooling would be rather low, even in the most ideal case<sup>8</sup>, and likely would be much lower when the electrostatic anharmonicity of such a trap is realistically considered. We therefore identify electron cooling with a cold electron gas cloud as a very attractive alternate method. Cloud/trap parameters already achieved give cooling times of a few seconds.

## II $\bar{p}$ Facility Requirements

We discuss trapping  $\bar{p}$ 's in the context of working at LEAR, in order to use its well defined beam parameters. We use the lowest energy LEAR  $\bar{p}$  energies (5–10 MeV) with beam parameters in Table I<sup>9</sup>.

TABLE I

Assumed LEAR Parameters

|                    |                          |
|--------------------|--------------------------|
| $\bar{p}$ momentum | 141 mev/c                |
| $\Delta p/p$       | $\pm 0.8 \times 10^{-3}$ |
| $\epsilon_H$       | 7 mm mrad                |
| $\epsilon_v$       | 3.5 mm mrad              |

It seems likely, however, that the  $\approx 30$  Mev kinetic energies already realized at LEAR would be sufficient. Such parameters are modest in the sense that only the initial (600 mev/c) stochastic cooling is called upon.  $N_{\bar{p}}$  is kept well below any limit where IBS becomes significant. We calculate the IBS total emittance blow up time<sup>7</sup>,  $\tau$ , to be much larger than one hour for  $10^7$ – $10^8$   $\bar{p}$  for the parameters of Table I. After cooling at 600 mev/c the beam is decelerated to 141 mev/c and a longitudinal segment is fast ejected. No further cooling is required (although the scheme can, of course, be improved upon — as we discuss later) and the enhancement which would be offered by RF bunching is not required.

Since any one LEAR  $\bar{p}$  batch can load our trap the only "beam time" requirement is for tuning. After loading the experiment could be removed from the beam

line.

### III Antiproton Trap Loading

The Penning trap used for load antiprotons is represented in figure I and Table II. For the most precise experiments, a small number of antiprotons would be transferred to a second smaller trap which is specifically designed for optimal anharmonicity reduction<sup>10</sup>. The initial electrostatic well for the loading trap is considerably deeper than usual (2 KeV) in order to trap a significant energy bite of the  $\bar{p}$  "beam". Consequently the trap dimensions are also larger. After the injected  $\bar{p}$ 's are cooled the well potential would be reduced to  $\leq 100$  volts to accomodate the standard cell potential source necessary for precision work. Injection into the trap is accomplished by keeping the injection endcap electrode at ground until  $\bar{p}$ 's from the head of the  $\bar{p}$  bunch have completed one full cycle (axially) through the trap ( $\leq 130$  ns). The injection cap electrode is then stepped down to -4 KV, thus trapping all  $\bar{p}$ 's which exited the degrader with  $2 \text{ KeV} \leq E_{K,z} \leq 4 \text{ KeV}$ . Notice that the 130 ns transit time  $\equiv \tau_I$  sets the required LEAR bunch length (= 5.9 meter at 141 mev/c or 7.4% of LEAR circumference).

TABLE II Trap Parameters

|   |               |
|---|---------------|
| Axial Half Height ( $z_0$ )               | 1 cm          |
| Radial Half Height ( $\rho_0$ )           | 1 cm          |
| Endcap - Ring Potential Diff.             | 4 KV          |
| $\bar{p}$ "Beam" Entrance Aperture Radius | 1 mm          |
| Magnetic Field                            | $\approx 6$ T |
| $\nu_z (\bar{p})$                         | 11.4 MHz      |

Table II lists the nominal parameters of the trap we envision using.  $\bar{p}$ 's are degraded from 10 meV to mean zero energy in the surface layer of the injection endcap electrode.  $\bar{p}$ 's emerging into the trap volume with an axial kinetic energy between 2-4 KeV will be trapped. We note that the Larmor radius for 4 KeV (worst case)  $\bar{p}$ 's in 6 Tesla is 0.5 mm, so that the final trapped  $\bar{p}$  distribution radial extent is determined entirely by the spot size on the degrader (thin target — see section IV).

Degrading the  $\bar{p}$  energy at the last possible instant serves two important purposes. First, we take full advantage of the radial containment of the magnetic field. Second we can maintain the "sealed trap" concept which has proven so successful in Seattle single particle studies. A slight alternative would be a *flat* degrader followed immediately by a mesh electrode face. The combined requirement of

UHV seals and of an electrically floating endcap electrode makes the construction somewhat more complex than in usual practice. We note, in this respect, that the endcaps could be at ground while the ring electrode would pulse positive. This would result in  $\tau_f$  being reduced by approximately  $\frac{1}{2}$  while the accepted axial kinetic energy slice would be 0-2 KeV (see section V).

The  $\bar{p}$  capture cross section<sup>11</sup> determines the vacuum we must achieve in our trap. For instance  $\sim 1 \times 10^{-11}$  torr will give a capture rate of one per day for 5°K thermalized Helium. The quiescent pressure expected from the sealed type trap of figure 1 submerged is  $<< 10^{-14}$  torr<sup>13</sup>. No evidence of collision is detected in the existing vacuum<sup>14</sup> enclosures used now for the precision single particle experiments. However surface perturbing action such as  $e^-$  impact from the field emission point or ionizing radiation from  $\bar{p}$  annihilation or the accelerator environment must be taken into account.

#### IV Beam Optics and Trapping Efficiency

In order to concentrate the initially trapped  $\bar{p}$ 's as much as possible to allow fast electron cooling (section VI) we choose a  $\bar{p}$  spot size on degrader as small as possible compatible with LEAR transverse emittance. Injection must be precisely along the trap solenoid axis. We assume that a minimum separation of 2 m must be maintained between trap and the last focusing beam line element. Probably this spacing can be reduced since only precision studies are sensitive to magnetic perturbation. (Alternatively, electrostatic lenses are possible here. Clearly a precision servoed beam line is required to aim down the magnet axis.

For a 1 mm radius degrader aperture the emittances of table I indicate a 4 cm diameter beam at the 2 meter distant last focus elements. The horizontal plane will be twice as spread out: half the beam is lost. However the solenoid fringe field provides a significant focusing itself, full benefit from which depends on accurate entrance beam alignment. Several low pressure proportional chambers could be included to servo in the beam alignment (in conjunction with fast electrostatic steering elements).

The degrader will be of a high purity low Z material to minimize induced radioactivity and multiple scatter. Figure I indicates a monolithic degrader/endcap. Though simplest, this is not essential and may change after detailed fabrication and material property consideration. For Aluminum the range is about  $250\mu$ , enough for sturdy mechanical design. Apparently little is known about the stopping power for negative massive charges below  $v_{ion} \approx \alpha c$ ; while for 3 KeV  $\bar{p}$ 's  $v_{\bar{p}} = 0.22\alpha c$ . Within mechanical tolerances, uncertainty in this very low energy range of stopping powers does not alter the gross range predicted (or measured) for protons. On the other hand the details of energy loss from  $\approx 100$  KeV to  $\approx 3$  KeV (last  $\approx 1\mu$  of range) could conceivably lead to unexpected  $\bar{p}$  yields. For instance it is clear that by the time  $\bar{p}$ 's reach velocities  $\lesssim \alpha c$  their velocity distribution must

essentially be isotropic. No notion of "beam" will hold, and an anomalous number will be lost to capture. We will allow for this by incorporating an additional factor 2 dilution in estimates of the final trapped number of  $\bar{p}$ 's. Notice that  $0.22\alpha c > \alpha c\sqrt{m_e/m_p}$  which is the threshold for significant capture cross section<sup>11</sup>.

The longitudinal emittance (Table I) translates to a  $\bar{p}$  energy spread of 950 KeV at the degrader. The spread due to straggling is about  $\frac{1}{8}$  this<sup>12</sup>. Therefore our 2 KeV acceptance slice represents a dilution of 475. Table III summarizes the loss fractions we assume starting from a coasting LEAR beam (Table I).

TABLE III  $\bar{p}$  Loss Factors

|  |                   |
|--|-------------------|
| LEAR Revolution period / $r_I$ at 10 MeV | = 14.5            |
| Accepted energy slice: 960 KeV / 2 KeV   | = 480             |
| Isotropic Degraded Distribution          | $\approx 2$       |
| Transverse Acceptance Match              | 4                 |
| Net Dilution                             | $4.4 \times 10^5$ |

Thus for  $\lesssim 2 \times 10^7 \bar{p}$  coasting in LEAR at 10 mev we expect to trap  $\approx 20 \bar{p}$ , a quite adequate number. Nonetheless, the trapping is inefficient: most of the  $\approx 10^7 \bar{p}$  will be captured in the trap electrodes. One advantage of a phase space conserving deceleration scheme would be to greatly increase this efficiency<sup>8</sup>. The total induced radioactivity will be negligible since the total number of stopped  $\bar{p}$ 's for a complete experiment will be small. Single charges are routinely kept in our traps indefinitely. Therefore the bulk of the  $\bar{p}$  dose will accrue during tuning.

Many features of the  $\bar{p}$  transfer from LEAR to trap are improved if further cooling processes and/or steps become available at LEAR. In particular a LEAR low energy *electron* cooling stage helps us three ways. First, the  $\bar{p}$  beam phase space density is considerably increased. Second, entrainment of the  $\bar{p}$ 's by the *highly stable* electron beam allows for stable beam tuning (both in energy *and* position). This would greatly simplify tuning the exact range through the necessarily *fixed* degrader. Alignment of the beam line down the solenoid axis would be more reproducible. Third, the momentum spread in LEAR would be so small ( $\lesssim 10^{-4} \Delta p/p$ ) that tight bunching with still small energy spread is possible. These improvements could reduce the net dilution to only  $\sim 250$ !

## V Electron Cooling

In principal the  $\approx 2$  KeV trapped  $\bar{p}$ 's could be cooled for precision work by external resistor damping as has been demonstrated in the previously mentioned

experiments and recently calculated in some detail<sup>14</sup>. We investigate here the possibility of attaining much faster damping via collisions with a cold electron cloud introduced by standard methods into the center of the trap after a potential well is established. This electron cloud would serve only as an electron cooler. After the  $\bar{p}$ 's cool, these electrons would be ejected (by R.F. excitation) from the trap.

Thus we consider the properties of such a cloud in the 2 KeV potential well (Table IV).

TABLE IV Cold Electron Cloud Parameters

|                            |                             |
|----------------------------|-----------------------------|
| cloud radius               | $\approx 2\text{mm}$        |
| cloud density              | $2 \times 10^7/\text{cc}$   |
| maximum space charge field | 720 volts / meter           |
| Debye length               | $4 \times 10^{-3}\text{cm}$ |
| $\eta$                     | 0.18                        |
| fast Coulomb log           | 9.2                         |
| electron temperature       | $\approx 5^\circ K$         |

The cloud radius is determined by the  $\bar{p}$ /degrader spot size to be  $\approx 2\text{ mm}$ . This radius is maintained by the standard "magnetron cooling techniques"<sup>15</sup>. Electrostatic considerations show that the shape will be approximately spherical for the symmetric trap we consider here. Then the maximum electron density  $n_e$  is constrained such that the space charge field  $\ll$  trap field. Choosing  $n_e = 4 \times 10^7/\text{cc}$  gives a worst spacecharge to trap field ratio of  $\lesssim 1\%$ . Such a density for electrons thermalized in the usual way<sup>16</sup> gives a Debye length  $\lambda_D \lesssim 4 \times 10^{-3}\text{ cm} \ll$  cloud radius. This insures a well defined cloud edge.

We avoid the issue of "adiabatic"  $\bar{p}-e^-$  coulomb collisions by estimating the electron cooling time solely on the basis of the "fast" collisions (impact parameter  $/ v_{\bar{p}} \lesssim e^-$ -cyclotron period)<sup>17</sup>. This criteria is a stronger limit on the maximum impact parameter than  $\lambda_D$ , so we use it to arrive at a ("fast") coulomb logarithm  $L = 9.2$ .

The electron cloud is very cold so that we have the "classic" electron cooling situation  $v_{e^-} \ll v_{\bar{p}}$  for which the damping rate formula<sup>18</sup>:

$$\lambda = -8\pi c r_e r_p L n_e \eta \beta_{\bar{p}}^{-3}$$

may be employed ( $\eta$  being the fraction of time the  $\bar{p}$ 's spend in the cloud during their axial oscillation). The values summarized in Table IV then yield  $\lambda = 0.18/s$ .

Proven sideband cooling techniques can be used to insure that the unstable magnetron motion of the  $\bar{p}$  does not increase in radius because of the collisions to

the point where antiprotons are lost from the trap. Moreover we observe that an electron cloud which does not entirely fill the trap cannot drive the antiprotons entirely out of the trap. In more detail, although each  $e^- - \bar{p}$  collision reduces the  $\bar{p}$  kinetic energy, the *angular* deflection of the scattered  $\bar{p}$  allows significant *diffusion* of the magnetron orbit radially out from the center of the trap. Since the magnetron energy is  $\ll$  the cyclotron energy (initially  $r_m \approx 1$  mm,  $r_c \approx 0.45$  mm while  $E_m \approx 0.08$  ev and  $E_c \approx 3$  KeV) the magnetron motion will not be initially cooled. In the transverse plane (cyclotron plane) a  $\bar{p}$  will suffer "multiple" scattering:

$$\theta_{rms}^2 = 8\pi r_p^2 L n_e \beta_{\bar{p}}^{-4} l$$

where  $l = \bar{p}$  path length segment and  $L$  is the *same* Coulomb Log used for  $\lambda$ . Let  $l \equiv \eta v_{\bar{p}}/\lambda$ , yielding  $\theta_{rms}^2 \equiv m_e/m_{\bar{p}}$ . The net diffusion of  $r_m$  will then be:

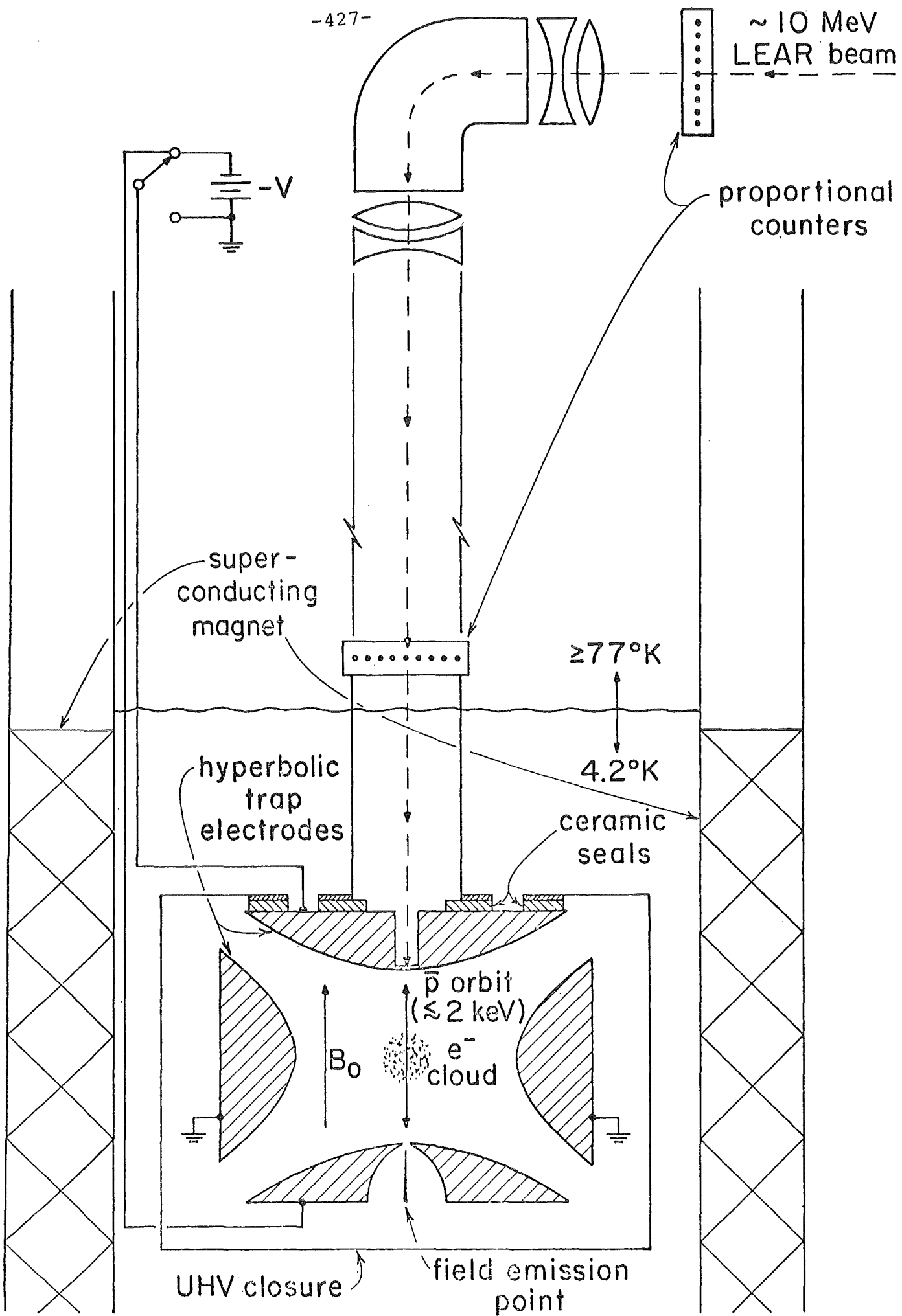
$$\Delta r_m \equiv r_c \theta_{rms} \sim 0.01 \text{mm}$$

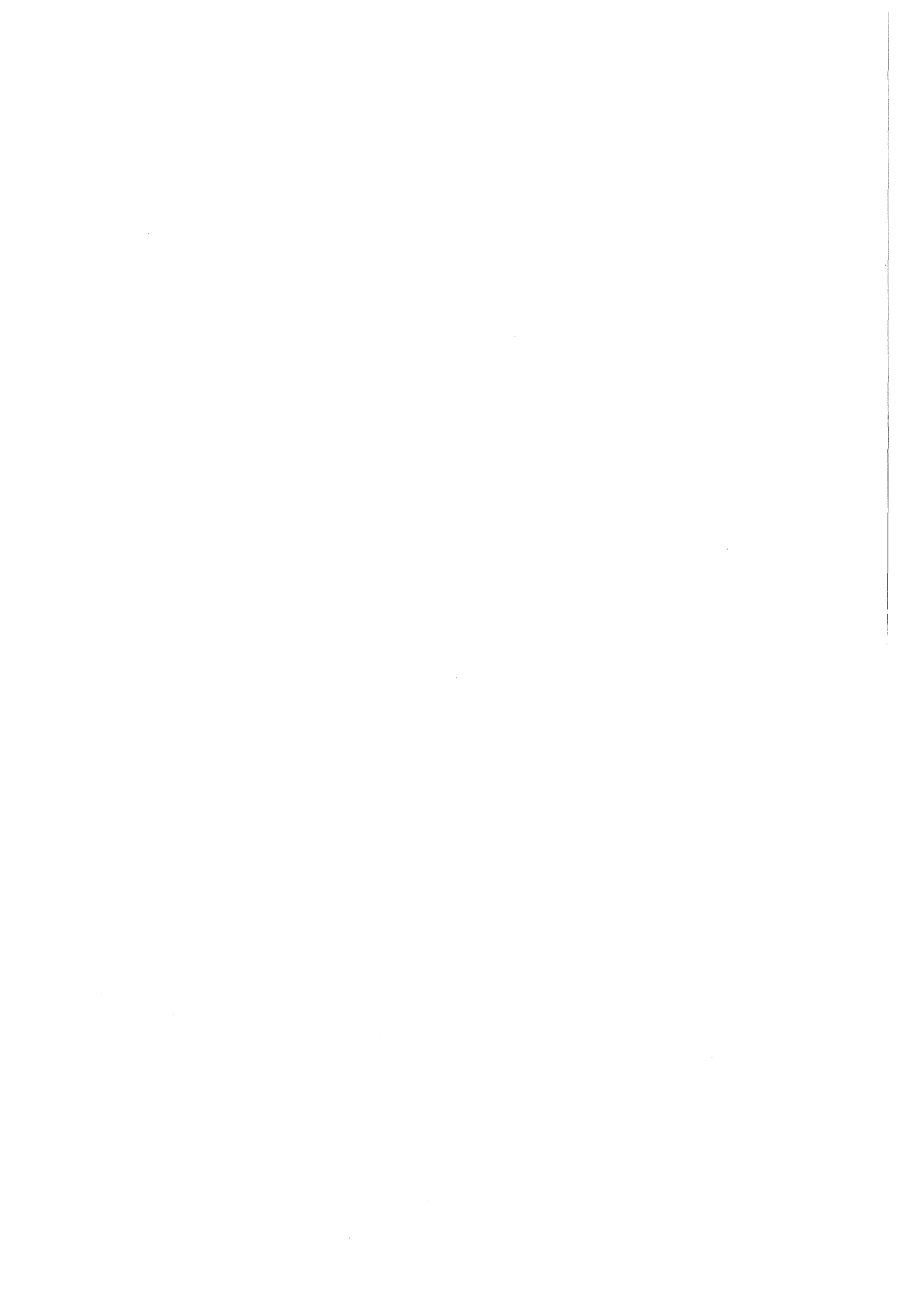
Since  $r_c$  progressively shrinks as the cooling progresses the total diffusion of  $r_m$  is not qualitatively larger than the above.

#### References

1. See, for example, H.G. Dehmelt, R. Van Dyck, Jr., P. Schwinberg and G. Gabrielse, *Bull. Am. Phys. Soc.* **24**, 757 (1979).
2. P. Schwinberg, R. Van Dyck, Jr. and H. Dehmelt *Phys Rev Lett.* **47**, 1879 (1981).
3. R. Van Dyck Jr., F.L.Moore, D.L. Farnham and P. Schwinberg in Proceedings 9<sup>th</sup> ICAP B87, (1984)
4. G. Gabrielse, W. Kells and H. Dehmelt, in Proceedings 9<sup>th</sup> ICAP B88 (1984).
5. M. Bregman, et. al. *Phys. Lett.* **78B**, 174 (1978).
6. A review of such facilities and ideas related to those presented here are contained in *Physics at LEAR with Low Energy Cooled Antiprotons*, U. Gastaldi and R. Klapisch, Eds. (Plenum, 1984)
7. S. Mttingwa and J. Bjorken, *Fermilab Pub 82/47-THY*, 1982.
8. N. Beverini et. al. in Reference 6
9. D. Möhl in Reference 6
10. G. Gabrielse. *Phys Rev.* **A27**, 2277 (1983)

11. L. Bracci et. al. *Phys Lett.* **85B**, 280 (1979)
12. See standard nuclear physics stopping power compendia and W. Eyrich and A. Hofmann in Reference 6.
13. W. Thompson and S. Hanrahan, *J. Vac. Sci. Tech.* **14**, 643 (1977).
14. G. Gabrielse, *Phys. Rev. A* **29**, 462 (1984).
15. R. Van Dyck, Jr., P. Schwinberg and H. Dehmelt in *New Frontiers in High Energy Physics*, edited by B. Kursuhoglu, A. Perlmutter and L. Scott (Plenum, New York, 1978).
16. D. Wineland, and H. Dehmelt. *J. Appl. Phys.* **46**, 919 (1975).
17. Y.S. Derbenev and A.N. Skrinsky, *Part. Accl.* **8**, 235 (1978).
18. F.T. Cole and E.E. Mills *Ann. Rev. Nucl. Sci.* 1981, 31:295.





CRYRING, a small storage and acceleration ring for heavy ions

C.J. Herrlander and A. Bárány

Research Institute of Physics, S-104 05 Stockholm, Sweden

CRYRING, which was proposed in October 1983, aims at a facility for performing experimental atomic, molecular and nuclear structure physics using very heavy, highly charged ions. In particular the possibility to study the interaction between a circulating heavy ion beam ( $\sim(1-5) \cdot 10^9$  ions) and beams of ions, electrons or photons is foreseen. An extracted beam (10 Hz, 30 % duty cycle,  $\sim(1-5)$  pnA) with an energy around or slightly above the Coulomb barrier will allow experiments in atomic and nuclear structure physics.

The name CRYING, which originally was just a working name, should be interpreted as "CRYebis connected to a small synchrotron RING". CRYEBIS is an electron beam ion source for producing highly charged heavy ions<sup>1)</sup>. It is presently being tested and is planned to be in operation in the beginning of 1985. The CRYEBIS is a pulsed ion source and with the given electron beam energy (10 keV) and anticipated current density ( $\sim 10^4$  A/cm<sup>2</sup>) the repetition frequency will be  $10-10^4$  Hz. For the longest confinement times, 100 ms, the source is expected to give in the order of  $10^{10}$  ions per pulse (see Table 1). In the future a new electron gun will be installed allowing higher electron beam energy and intensity. The CRYEBIS will be coupled to an injector isotope separator system which will be an improved version of the system used at LNS, Saclay<sup>2)</sup>. This will allow the source to deliver isotopically well defined ions, which is of great importance for the planned physics program. Thus, the injector will allow separation of ions with similar Q/A like  $^{129}\text{Xe}^{43+}$  and  $^{132}\text{Xe}^{44+}$ , and also the possibility to accelerate rare isotopes (1-10 %) with highest possible intensity is foreseen.

Originally the plans put CRYEBIS on a 600 kV platform to reach an ion energy of a few hundred keV/A before injection into the storage and acceleration/deceleration ring. Inspired by the successful tests of LITL at

INS, Tokyo<sup>3)</sup>, and similar experiences at LNS, Saclay<sup>4)</sup>, demonstrating the possibilities to build an RFQ-linac for a wide spectrum of charge-to-mass-ratios, studies on the possibilities to replace the HV-platform with an RFQ were initiated. The results reported by the RFQ-group at IAP<sup>5)</sup> in Frankfurt have finally changed the design and calculations and test experiments have now started with the aim of designing an RFQ-linac as injector to the ring. It is foreseen to accept ions with  $0.1 < Q/A < 0.5$  and accelerate them from 5 keV/A to an output energy of 250-300 keV/A. The injection energy of the RFQ is in accordance with the 50 kV acceleration than can be achieved at the output of CRYEBIS.

The various components discussed are indicated in Fig. 1, which gives the lay-out of CRYRING. The ring in its present configuration has a circumference of about 30 m and is split in four superperiods. Each superperiod has two homogenous field, 45°, dipoles, seven quadropoles and four sextupoles. The dipoles have a radius of 1.1 m and a gap of 7-8 cm. To simplify the construction of the dipoles 22.5° edge focusing is assumed. The present design parameters for CRYRING are summarized in Table 2.

The relatively large number of magnetic elements are chosen to obtain a high flexibility: the ring is planned to work both as a low-energy storage ring and a fast cycling accelerator.

In the fast cycling mode the frequency 10 Hz is chosen in accordance with the repetition rate of CRYEBIS in producing the highest charge states. The extraction will be made with a "slow" resonance system giving about 30 % duty cycle. The beam will then be brought 20-25 m away from the ring to an experimental area mainly equipped for nuclear structure and atomic physics research.

The straight sections of the ring are 2.2 meters each. Their different functions are indicated in Fig.1. The lattice calculations<sup>6)</sup>, which are performed using the MAD program<sup>7)</sup>, have taken the various working modes into consideration. Because of the different demands the ring in the storage mode is considered having two superperiods. The results of the lattice-studies are demonstrated in Fig. 2. It should be mentioned that the injection/extraction system as it is shown in Fig. 1 is a copy of a preliminary lay-out of a design-study for the ELENA-project at CERN<sup>8)</sup>. For several reasons a closer study of the present project might result in separated injection and extrac-

tion systems. One of the reasons is to allocate proper laboratory space for experiments on the ion beam for CRYEBIS when not injected into the ring. The demand for a well defined beam for experiments implies an electron cooling system working down to 100 keV/A or less. An electron gun working in the range of the corresponding electron energies is reported at this conference<sup>9</sup>.

The original plans for CRYRING emerged from wishes to study atomic collisions at very low energies in a merged beam system, utilizing the unique properties of a cooled recirculating beam of highly charged ions. The ideas are indicated in Fig. 1 as a second beam from a conventional ion source on an HV-platform injected colinearly with the circulating beam along the experimental straight section. Such a system is now being studied in detail, but experiments in this section might also involve collision and spectroscopy studies using laserphotons and crossed atomic or electron beams.

An interesting question relates to electron cooling and recombination of highly charged heavy ions. Most feasibility studies are done with fully stripped ions where the only recombination channel (the radiative one) can be shown to be unimportant. Going to partially stripped ions the picture is different, since then dielectronic and higher order recombination processes can occur. Cross sections are largely unknown, but are probably strongly dependent on the actual electronic structure of the ions. It seems very plausible, though, that the cross sections are small enough at the relevant energies for a wide class of ions. This should in particular include highly charged ions having rare gas electronic configurations, such as Kr<sup>34+</sup> and Xe<sup>44+</sup> (cf. Table 1).

It is also tempting to mention that to our knowledge no other storage ring is planned to-day where this recombination phenomenon could be studied systematically. Because of the easiness to change ion charge stepwise in CRYEBIS, CRYRING would be a very powerful tool for studying the low-energy interaction between partially stripped heavy ions and electrons as the problem is encountered in a cooling device.

The present report is for obvious reasons very brief. Different study programs are presently running to achieve a more definite design of the ring. Besides those already mentioned, the most important program is the building up of an UHV test facility. When going to low energy heavy ions, the

interaction cross section with the rest gas of the vacuum system becomes very high and if such ions are going to be stored in the ring for a period of tenths of seconds to minutes, a vacuum of  $10^{-12}$  torr is desirable. Such a vacuum is to-day a "standard" planned to be used in several storage rings. But these rings are normally intended for protons, and an increased knowledge in the case of rings connected to heavy-ion sources is needed. Also, there is a connection between these studies and experiments with a rapid cycling magnet and the beam tube in such a magnet. Optimizing the vacuum and accessibility with minimized eddy currents effects and financial input certainly need more detailed studies. For that reason a magnet in what is supposed to be half scale is presently assembled.

The project has received some support for these different studies. If funded in the summer of 1985 it is planned to be operational in 1989 with full availability for experiments in 1990.

## REFERENCES

1. E.D. Donets, *Physica Scripta* T3 (1983) 11.  
J. Arianer, C. Collart, Ch. Goldstein, H. Laurent, and M. Malard,  
*Physica Scripta* T3 (1983) 35.
2. J. Faure, B. Feinberg, A. Courtois, and R. Gobin, *Nucl. Instr. and  
Meth.* 219 (1984) 449.
3. N. Ueda, T. Nakanishi, S. Arai, T. Hattori, T. Fukushima, Y. Sakurada,  
T. Homma, N. Tokuda, S. Yamada, M. Takanaka, A. Itano,  
A. Mizobuchi, and Y. Hirao, *IEEE Trans. Nucl. Sci.* NS-30 (1983) 2975.
4. M. Olivier, J. Faure, J.L. Laclare, J.M. Lefebvre, G. Leleux, A. Ropert,  
A. Tkatchenko, and M. Tkatchenko, *IEEE Trans. Nucl. Sci.* NS-30,  
(1983) 1463.
5. A. Schempf, P. Junior, H. Klein, M. Daehne, M. Ferch, K. Langbein,  
and N. Zoubek, *IEEE Trans. Nucl. Sci.* NS-30 (1983) 3536.  
H. Klein, *IEEE Trans. Nucl. Sci.* NS-30 (1983) 3313.
6. P. Heikkinnen (to be published).
7. F.Ch. Iselin, The MAD Program, CERN, LEP div.
8. P. Lefèvre and D. Möhl (private comm.).
9. H. Herr (private comm. and this conference).

TABLE 1

Examples of ions with maximum final energies  
to be reached in CRYRING.

---

|                    |       |                 |                 |                 |                 |
|--------------------|-------|-----------------|-----------------|-----------------|-----------------|
| A                  | =     | Ar              | Kr              | Xe              | Pb              |
| Q                  | =     | 18 <sup>+</sup> | 34 <sup>+</sup> | 44 <sup>+</sup> | 60 <sup>+</sup> |
| Q/A                | =     | .45             | .40             | .33             | .28             |
| E/A <sub>max</sub> | =     | 17.2            | 13.6            | 9.2             | 6.6             |
|                    | (MeV) |                 |                 |                 |                 |

TABLE 2

Design parameters for CRYRING (preliminary data)

|                                     |  |                                |
|-------------------------------------|--|--------------------------------|
| Energy region                       | (80 $\frac{Q}{A}$ ) <sup>2</sup> MeV/A | ~30 keV/A - 20 MeV/A           |
| Momentum region                     |  | 15 - 400 MeV/c                 |
| Injection energy (RFQ)              |  | 300 keV/A                      |
| Circumference                       |  | 30 m                           |
| Straight sections                   |  | 4 x 2.2 m                      |
| Magnets (laminated, 0.5 mm sheets): |  |                                |
| Dipoles, r = 1.1 m                  |  | 8 units, 0.04 T < B < 1.3 T    |
| Q-poles                             |  | 4 x 7 units, $\lesssim 10$ T/m |
| Sextupoles                          |  | 4 x 4 "                        |
| Pulsing frequency                   |  | 10 Hz, 0.15 T < B < 1.3 T      |
| $Q_x$                               |  | 2.34                           |
| $Q_z$                               |  | 3.76                           |
| $\beta_x$                           |  | 0.4 $\beta_x < 16$             |
| $\beta_z$                           |  | 0.5 $< \beta_z < 2.6$          |
| Vacuum system                       |  | $\sim 10^{-12}$ torr           |
| Baking temperature                  |  | $\gtrsim 300^\circ\text{C}$    |
| RF system:                          |  |                                |
| Frequency range                     |  | 10 - 80 MHz                    |
| Harmonic numbers                    |  | 1 and 3                        |
| RF voltage                          |  | ~500 Volts                     |

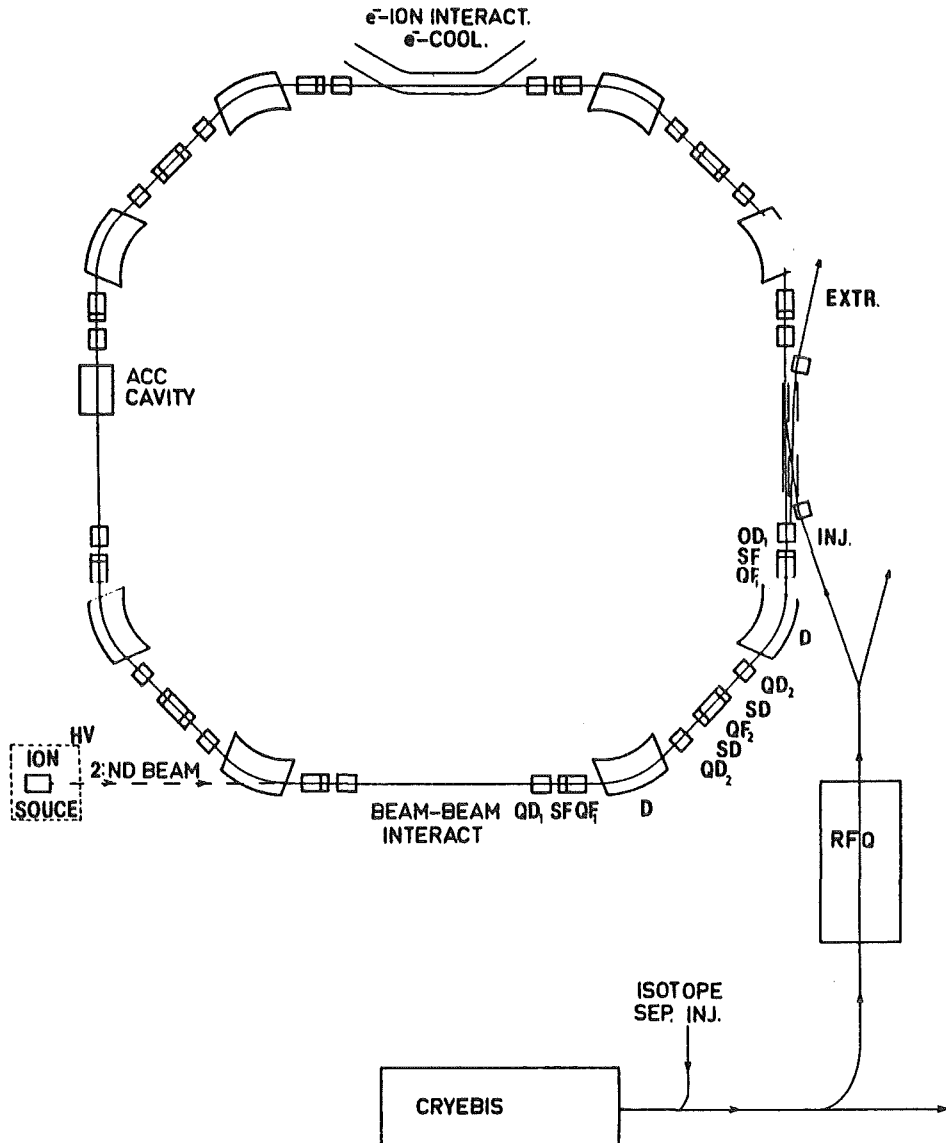


Fig. 1 Tentative lay-out of CRYRING.

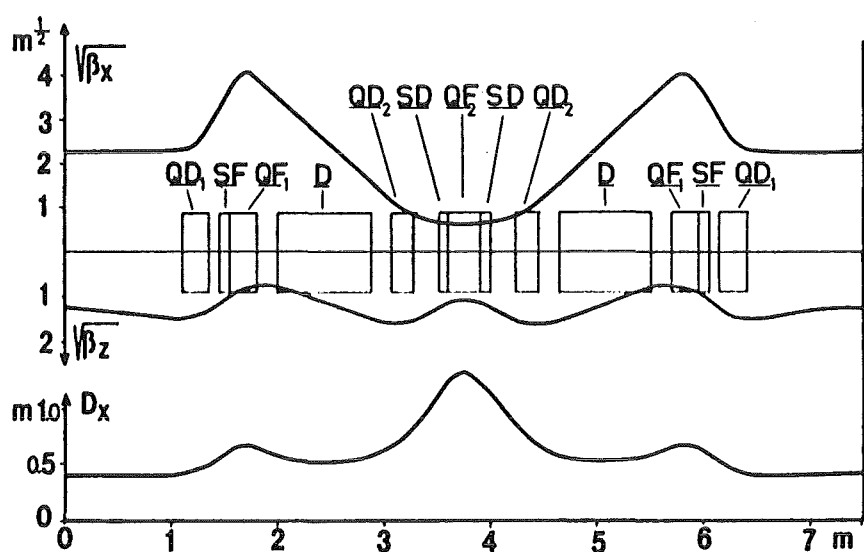


Fig. 2  $\beta$ -functions and dispersion of CRYRING (accelerating mode).





LIST OF PARTICIPANTS

1. N. Angert, GSI Darmstadt
2. A. Bárány, Res. Inst. of Phys., Stockholm
3. R. Becker, Uni Frankfurt
4. M. Bell, CERN
5. J.S. Bell, CERN
6. G. Berg, KFA Jülich
7. P. Blatt, Uni Heidelberg
8. K. Bongardt, KFA Jülich
9. R. Calabrese, Inst. of Phys. Ferrara
10. A. Citron, KfK/Uni Karlsruhe
11. D. Cline, Univ. of Wisconsin and Madison
12. S. Datz, Oak Ridge Nat. Lab.
13. U. Diehl, KfK/Uni Karlsruhe
14. W. Eyrich, Physikal. Inst. Uni Erlangen
15. B. Franzke, GSI Darmstadt
16. S. Galster, KfK Karlsruhe
17. H.J. Gils, KfK Karlsruhe
18. C. Habfast, KfK Karlsruhe
19. D. Habs, MPI Heidelberg
20. W. Hennerici, MPI Heidelberg
21. H. Herr, CERN
22. C.J. Herrlander, Res. Inst. of Physics, Stockholm
23. Ch. Hill, CERN
24. F. Hinterberger, Uni Bonn
25. A. Hofmann, Uni Erlangen
26. I. Hofmann, GSI Darmstadt

27. S. Hultberg, Res. Inst. of Phys. Stockholm
28. L. Hütten, KfK Karlsruhe
29. M. Inoue, KFA Jülich (Osaka-Univ.)
30. E. Jaeschke, MPI Heidelberg
31. E. Jennewein, Uni Frankfurt
32. A. Johannsson, Tandem Lab. Uppsala Schweden
33. D.E. Johnson, Fermilab, Batavia, Ill.
34. I. Katayama, RCNP Osaka University
35. K. Kilian, CERN
36. M. Kleinod, Uni Frankfurt
37. W. Klose, KfK Karlsruhe
38. P. Klumpp, Bad Wimpfen
39. M. Köhler, KFA Jülich
40. F. Krienen, Stanford Univ. Cal.
41. V. Lallemand, KfK/Uni Karlsruhe
42. D. Larson, Fermilab, Batavia, Ill.
43. S. Martin, KFA Jülich
44. J. Meissburger, KFA Jülich
45. H.O. Meyer, Indiana Univ. Bloomington
46. F. Mills, Fermilab, Batavia Ill.
47. D. Möhl, CERN
48. P. Møller-Petersen, Aarhus, Denmark
49. R. Neumann, Uni Heidelberg
50. A. Noda, Inst. for Nucl. Study, Uni Tokyo
51. V.V. Parkhomchuk, INPh, Novosibirsk

52. Passoni, SAES Getters S.p.a. Milano
53. S. Penselin, Uni Bonn
54. F. Petrucci, Inst. of Physics, Ferrara
55. D.V. Pestrikov, INPh. Novosibirsk
56. H. Pilkuhn, Uni Karlsruhe
57. R.E. Pollock, Indiana Univ., Bloomington
58. A. Poncet, CERN
59. H. Poth, KfK Karlsruhe
60. H. Rebel, KfK Karlsruhe
61. D. Reistad, Tandem Acc. Lab., Uppsala
62. R. Repnow, MPI Heidelberg
63. M. Roge, KFA Jülich
64. S. Rosander, Acceleratorteknik, Stockholm
65. P. v. Rossen, KFA Jülich
66. A.G. Ruggiero, Fermilab. Batavia Ill.
67. M. Savrié, Inst. of Physics, Ferrara
68. M. Sedlacek<sup>V</sup>, Acceleratorteknik, Stockholm
69. B. Seligmann, KfK Karlsruhe
70. A. Sørensen, CERN
71. P. Spädtke, GSI Darmstadt
72. M.L. Sundquist, Electrostatics Int., Madison, Wisconsin
73. G. Schatz, KfK Karlsruhe
74. U. Schmidt-Rohr, MPI Heidelberg
75. R. Schuch, Uni Heidelberg
76. H. Schweickert, KfK Karlsruhe

77. E. Steffens, CERN/MPI Heidelberg
78. R. Stensgaard, University of Aarhus, Denmark
79. T. Tanabe, Uni. of Tokyo
80. L. Tecchio, Uni. of Turin
81. G. Tranquille, CERN
82. P. Turek, KFA Jülich
83. J.-L. Vallet, CERN
84. G.-J. Wagner, Uni. Tübingen
85. Ch. Wiedner, MPI Heidelberg
86. A. Wolf, CERN
87. B. Wolf, GSI Darmstadt